NADC-SIRLAB-1089

PROCEEDINGS OF THE 1989 TRI-SERVICE CONFERENCE ON CORROSION

Vinod S. Agarwala
Editor

Naval Air Development Center
Warminster, PA 18974-5000

NADC-SIRLAB-1089

PROCEEDINGS OF THE 1989 TRI-SERVICE CONFERENCE ON CORROSION

Editor
Dr. Vinod S. Agarwala
Surface Interactions Research Laboratory
Naval Air Development Center

17-19 October 1989
Atlantic City, New Jersey

Sponsored by
The Tri-Service Committee on Corrosion
The Department of Defense

Organized by
Naval Air Development Center
Warminster, PA 18974

ACKNOWLEDGMENT

This publication is a consequence of exchange between scientists and engineers working very diligently and sincerely to combat corrosion and corrosion assisted failures in the military. The technology provided in these pages are contributions of the authors listed in the Table of Contents. The contributing organizations are R & D laboratories of the departments of Navy, Air Force and the Army, and their contractors. The editor is grateful to the authors for their contribution, and the members of the Conference Committee and the Naval Air Development Center for their support.

****

****

CONFERENCE COMMITTEE

Conference Chairman
Dr. Vinod S. Agarwala
Naval Air Development Center

PLANNING COMMITTEE

AIR FORCE

Mr. Richard Kinzie
Warner-Robins Air Logistic Center

Mr. Fred H. Meyer, Jr.
Wright Research & Development Center

ARMY

Dr. Saul Isserow
Army Materials Technology Laboratory

Dr. Robert R. Reeber
Army Research Office

NAVY

Dr. Vinod S. Agarwala
Naval Air Development Center

Ms. Denise Aylor
David Taylor Research Center

Dr. Jack F. McIntyre
Naval Surface Warfare Center

Dr. A. John Sedriks
Office of Naval Research

Mr. David A. Vaughn
Amphibian Warfare Technology Directorate

Administrative Assistant

Mr. Lee A. Biggs
Naval Air Development Center

PREFACE

This conference is the 11th in the series of Tri-Service Conference on Corrosion since its inception in 1967. Over the years, these conferences have proved their usefulness and endured the test-of-time in serving the present and future needs of the military. Considering the global environment as the theater of operation for the services, which is not only highly corrosive to the military hardware but also extremely demanding (stressful) under combat conditions, prevention and control of corrosion become a never ending task.

The purpose of this conference is to develop new directions, and highlight the awareness that the problems of corrosion in the military are far from over. There is a serious need for new approaches, methods and products for our aging weapon systems, and even current acquisitions. As we step into the twenty first century, new concepts will have to be devised to protect materials of the future. We will have to seek out new ways to maintain the structural and functional integrity of all naval, ground, air and space weapon systems. The concepts like smart coatings, materials with artificial intelligence, sensors and electric field or electronic barriers for corrosion protection, which are in their infancy now, will become the technology of tomorrow. Conferences like this provide an excellent forum for a free exchange of ideas and cultivate an interservice coordination of current and future research.

There is still a great need for more implementation of the existing technology into our fleets and commands, and for transitioning the state-of-the-art in solving problems relating to corrosion and corrosion assisted failures. This requires an active participation of all levels of technical and maintenance support personnel of the DOD and its contractors. The forums like this are ideal for preparing new technical manuals, training courses, etc. for experts from the government, industry and academia are available to provide valuable guidance and assistance. The theme is to disseminate the latest information available in the services as soon as possible.

The papers published in this proceeding cover a wide variety of topics such as organic and inorganic coatings, inhibitors, environmental assisted cracking, new materials, electronics and EMI corrosion, measurement techniques, sensors and corrosion monitors, tribology, failure analysis, lessons learned, and others of general interest. Keywords:

(Corrosion inhibition; Resistance; Ceramic coatings; Military aircraft/airframes; Military equipment finishes; Corrosion/synthesis; Anti-barrier; Aerospace; Paint/servicing; Metal coating; Plating/Naval; Tribology; Stress; Hydrogen embrittlement; Superalloys; High temperature; Gas turbines; Stress corrosion; Avionics; Monitors; Electromagnetic interference/pulses. (EDC)

Finally, I would like to conclude by expressing my sincere thanks to Lee Biggs and Chris Dickey in helping prepare this final manuscript for publication before the conference.

Vinod S. Agarwala

FORWARD

The 1989 Tri-Service Corrosion Conference continues the tradition of conferences held on this important topic by the three services since the 60's. The purpose of the conference is to focus attention on the state-of-the-art, as well as the research and development efforts of corrosion control of military equipment within the Department of Defense. Both DoD personnel and contractors must become more aware of the cost, both in dollars and in readiness, the "corrosion tax" is imposing on all aspects of our national defense. Additionally the products, procedures and techniques of corrosion control pioneered by the services can be of a more general benefit to the nation in transitions to the private sector. Thus, this conference endeavors to provide a forum for exchange of the latest information to minimize the ravages of corrosion to our national assets.

JOHN J. DE LUCCIA
Manager, Aerospace Materials Division
Naval Air Development Center

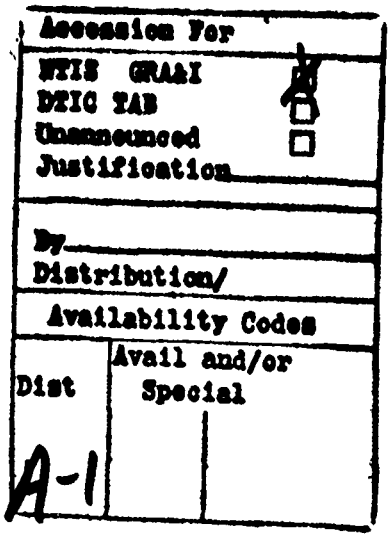

TABLE OF CONTENTS

CORROSION ENGINEERING IN THE 90s

T.S. Lee
NACE
P.O. Box 218340
Houston, TX 77218 USA

ABSTRACT

Demands and opportunities face the entire engineering community as we approach a new decade. This paper explores several areas where corrosion engineers can focus their individual and collective attention to contribute to society and to enhance their position in the technical community.

INTRODUCTION

Today the corrosion engineering profession faces a critical period but also we are presented with an opportunity to positively influence the future. The time is critical because we have seen the recent dismantling of research labs and customer technical service groups by some industries with a resultant upheaval and early retirement of many senior professionals.

By contrast, however, there appears to be some growing evidence of recognition by public officials and some industries that technology is important to the future economic health of industrialized countries. This presents our profession with an opportunity to impact future policy decisions and enhance the importance of the corrosion engineering profession.

We know that corrosion is important economically and represents a significant cost to an industrialized nation. Based on the well known NBS-Battelle study conducted at the request of US Congress in the mid 1970s, it is estimated that 3-5% of the US gross national product is the annual cost of corrosion. This is an amount almost equivalent to the annual US federal budget deficit in recent years and may indeed be just as difficult a cost to control in its entirety as the deficit has proven to be. However, there is a component of this annual corrosion cost that was estimated in the study to be avoidable through the proper application of existing technology. Estimated at 15% of the annual cost, this represents almost $20 billion a year.

To realize these savings and to develop or refine the technology to properly control some of the remaining 85% of the annual cost, we must have skilled and knowledgeable corrosion engineering professionals properly influencing industry and government leaders in their policy decision making.

This is not easily accomplished for two reasons. First, corrosion is not recognized as a specific engineering discipline. The corrosion engineer is a unique individual who develops a special skill which requires a working familiarity with many disciplines. The result is that corrosion engineers do not have the recognized identity and influence that civil, mechanical, electrical, or chemical engineers do. The second reason for the difficulty faced by corrosion engineers in

influencing policy is that our profession is rather inconspicuous when we are doing a good job of corrosion control. It is very easy for the unenlightened to view corrosion control as an avoidable cost when no material or system failures occur. The situation is somewhat analogous to saving costs by eliminating security at airports since hijacking incidents are no longer commonplace. It is only with a disaster that the effective control techniques and personnel are missed.

However, despite these difficulties, it is possible for corrosion professionals both as individuals, and collectively through organizations such as NACE, to properly exert influence in an effective manner.

ENGINEERING PRIORITIES

Before reviewing specific actions which can be taken, a review is in order of some items which have been targeted by the American Association of Engineering Societies (AAES) as priority issues[1] and which may help place the concerns of the corrosion engineering community in a more global perspective.

A first priority of AAES is the comprehensive review of US technology policy undertaken by The Committee on Science, Space and Technology of the US House of Representatives. This study is intended to complement a similar recent policy report on the sciences and will cover topics such as patent policy, intellectual property rights, antitrust laws, research, education, and international competitiveness. This policy review is a promising step toward recognition of the importance that a coherent national technology policy has on our national and international economic well being.

As an example of the link between technology and economic strength, Congressman George Brown of California in a speech to AAES[2] noted that economists have estimated that nearly 50 percent of the growth of the American economy in the last century was derived from new technology. Even with technology serving as the biggest contributor to economic growth, Congressman Brown marveled that the annual economic report by the Council of Economic Advisors never mentions the impact of science and technology on economic policy.

To further elucidate the role of technology in fostering economic strength, Congressman Brown referred to a National Academy of Sciences report which compared the US and Japan economies in terms of technology investments. He reported that in Japan each manufacturing worker is backed by $48,000 in technology and capital investment, in contrast to a $32,000 per worker investment in the US. To achieve equivalency to Japan, it was estimated that an investment in industrial plants and equipment of about $320 billion would be required for the 20 million manufacturing workers in the US.

Brown also pointed out that, unfortunately, the disparity is growing rather than diminishing as reflected by a report by the President's Commission on Industrial Competitiveness. This report noted that from 1960 to 1982, Japan invested 32% of its GNP in fixed capital versus only a 10% investment by the US. During that same period Japanese productivity increased an average of 5.9% annually versus only a nominal 1.2% annual increase in the US.

With this potentially critical situation faced by the engineering community, there is a need to assess our future ability to retain technological strength. Clearly, we are in an age of information and technology that requires a highly skilled and well educated work force to retain a competitive position. Thus, the AAES has identified engineering and science education as another of its priority issues. The goal is to increase standards for elementary and secondary education and to enhance emphasis on math, science and technology in schools. The importance of these goals is very evident in a recent report by Dr. Erich Bloch,[3] the Director of the National Science Foundation, in which he reviewed recent trends in education and demographics as they reflect our ability to produce scientists and engineers to effectively handle future technological needs.

Dr. Bloch noted that in the last decade, the employment of scientists and engineers increased three times faster than total US employment and twice as fast as total professional employment. He also noted that the total number of scientists and engineers engaged in research and development increased by almost 60% from 1973 to 1985.

However, he observed that over the last 20 years there has been no increase in the proportion of US scientists and engineers engaged in research and development. In contrast, other industrialized countries are rapidly gaining in their research and development work force. Japan, for example, in 1982 produced more engineers in absolute numbers than did the US with only half the overall population total. Developing nations also are positioning themselves to be more effective international competitors as evidenced by India's tenfold increase in scientists and engineers in the last two decades.

These numbers reflect an apparent continuing need for educated and skilled scientists and engineers, yet our trend in the universities has been in the opposite direction with science and engineering degrees representing a smaller fraction of total degrees awarded by US colleges and universities than was evident in the mid-60's.

Further, Dr. Bloch pointed out the increasing dependence that the US faces on foreign nationals to provide necessary skills in some science and engineering disciplines. In recent years more than half of the new engineering PhD's have been foreign nationals. Obviously, many of these graduates remain in the US and make valuable contributions to research, education, and the economy. However, it does reflect a recent trend of decreased interest of US students in science and engineering and further reinforces the reality that the US is one of many increasingly equal partners in the global technology base.

In light of this situation, what can we as corrosion engineering professionals do to positively impact future developments? There are numerous possibilities but I would like to focus on the four areas of communications, education, productivity, and globalization.

COMMUNICATIONS

First, we must communicate more effectively with different constituencies than we have traditionally. All too frequently, we as corrosion professionals talk only with our peers. However, we must reach out and interact with other groups if we expect to influence decision making. Some specific steps we can take individually and collectively include making conscious attempts to talk with management and financial personnel in industry and government to better educate

them on matters related to corrosion control and materials. We should meet with civic groups to better educate local civic leaders on the importance of materials and their performance in hostile environments. We also should meet with other local societies and trade groups and provide technical speakers on corrosion control at their local meetings and at national conferences.

Your corrosion society, NACE, also should continue to participate with other engineering societies in groups such as the Federation of Materials Societies where a collective voice can be raised over materials policies. NACE also maintains contacts in Washington DC to provide insights on opportunities for NACE members to contribute input on proposed government studies, legislation, and regulations. Through this arrangement, it is hoped that NACE will better be able to have appropriate representations from our membership on various advisory panels, which will result in more technically enlightened government action.
All of these steps at communicating with different constituencies serve to elevate the visibility of corrosion engineering. This can have only positive benefits to the profession and to society in general since there are major issues facing the US and the world that involve materials performance and corrosion and for which industry and government leaders and the general public have a concern.

For example, economic considerations are dictating that many utilities and process industry plants are operating beyond their original design lives. In many cases this is successfully occurring due to effective corrosion monitoring and control. The result is that the public benefits directly by lower costs through avoiding additional capital investments and by experiencing a safe environment made possible by proper containment of potentially hazardous process environments.

Another example of concern to the public is the situation with the nation's infrastructure. Our highways, bridges, and municipal water and wastewater facilities have, in many cases, exceeded their original design lives. Good corrosion control technology will play a key role in the rehabilitation and rebuilding of much of this infrastructure. The public and government should be made aware of this role since the overall effort will be of enormous economic impact to the US--estimated at $400 billion to $3 trillion over the next 10 to 20 years.

EDUCATION

The second area where our profession can have a positive impact is in education. Individually and collectively we can influence education programs to rejuvenate the sciences and engineering.

At a local level, each of us can become more involved with school boards and attempt to establish a renewed emphasis on math and science. We can become more proactive with math and science teachers in our junior and senior high schools and provide them with assistance in lectures, field trips, and equipment. As individuals and through local NACE sections, we should support these programs and help motivate young people to complete their schooling, to acquire a proficiency in science and math, and to pursue careers in engineering or the sciences.

In parallel to these efforts, we also should encourage development of a proper balance of skills to assure that well rounded engineers result with good communication skills and exposure to

civics, politics, law, and economics. After all, these are critical survival skills for engineers in today's society.

In the colleges and universities, an effective dialogue must develop between industry and the educators to assure that students are provided with a proper balance of theoretical and practical knowledge. It is in everyone's best interest for students to enter industry prepared to contribute rather than requiring deprogramming and retraining.

We can impact this issue in at least three ways. First, by offering opportunities for students to work in our industries on a "co-op" basis, we provide an invaluable training ground to the student and hopefully provide equal benefit to industry. Second, interaction between corrosion professionals and local university engineering students and educators fosters a critical dialogue which can be sustained by involvement of students in student sections of professional societies or in existing local sections. NACE members also can lend their support to university programs through lectures, field trips, and donations of supplies and equipment. And third, as individuals and through professional associations, we must redouble our efforts to integrate an undergraduate corrosion and materials performance course in all engineering curricula. All engineering graduates should have at least a rudimentary knowledge of corrosion for their ultimate cost effective performance in industry.

Beyond the area of formal education, we must also recognize the value of continuing education in this world of rapid technology advancement. To retain our competitive edge and to survive technically, we must continue to pursue new knowledge through participation in special conferences, through reading of technical journals and books, and through specialized education and training courses. It is through professional associations like NACE that many of these continuing education needs can be served.

PRODUCTIVITY

A third area which will impact the future role of the corrosion engineering profession is our ability to enhance our productivity. This obviously is a difficult thing to quantify, but it has been estimated in a number of surveys that technical professionals spend about one-half of their time doing jobs that do not require the level of talent that the professional possesses. In today's bottom-line business climate, it behooves us to maximize our contributions and somehow increase our efficiency in use of our technical skills.

In this case, the answer is probably not to work harder but rather to work smarter. We must efficiently use information sources available to us and apply the benefits of prior experience. There are many traditional information sources such as periodicals, books, standards, and vendor literature which are invaluable. Also critical is the network of peers with whom we consult and with whom we work in various technical committees. The knowledge of who to call for help is often 90% of the battle of solving a materials problem in a timely and cost effective manner.

A final information tool of obvious increasing importance is computer software. Many packages are available and NACE is actively developing a variety of computer tools for corrosion professionals including personal computer application packages; an evaluated, comprehensive database of materials performance information; expert systems software to aid the novice and experienced corrosion professional; and text retrieval packages for convenient access to literature.

GLOBALIZATION

The final area of which we should be increasingly conscious is the need to think on a global scale. Our ability to function effectively while oblivious of international technology developments is in the past. We must recognize that there are indeed technological developments overseas which can help all of us in our professional duties and we must effectively engage in two-way dialogues with our international partners.

The US engineering community has traditionally paid little attention to foreign technical literature while our US technical journals are regularly translated and eagerly read by our overseas counterparts. We must reverse that trend and pay close attention to technical developments from outside the US.

NACE can aid in these efforts to broaden our international perspective through its functions as an international professional association. With 20% of our membership, or about 3000 members, residing outside of the US, we have a reasonable base from which to grow and further enhance the proper two-way exchange of technology. This responsibility is recognized by NACE leadership and is a high priority issue.

CONCLUSION

In summary, this paper has presented a few thoughts on how NACE corrosion engineering professionals can become more visible partners in shaping the future of our society. There are numerous other approaches and our collective and individual goal should be to pursue the opportunities which present themselves and positively impact the future of the world in which we live.

REFERENCES

1. "Public Policy Perspectives and Positions", American Association of Engineering Societies, Washington, DC, January 1988.
2. "Speech to American Association of Engineering Societies Government Affairs Conference", Congressman G. B. Brown, Jr., March 1987.
3. "Human Talent for Competitiveness", National Science Foundation, Washington, DC.

CORROSION CONTROL AND PREVENTION ON AGING COMMERCIAL AIRCRAFT

J. A. Marceau, Corrosion Control Specialist
The Boeing Company, Seattle, Washington

R. G. Caton, Manager Metals Unit,
The Boeing Company, Seattle, Washington

This paper describes types and causes of corrosion in aging commercial aircraft. Areas of concern, corrosion detection and prevention, design philosophy and preventive maintenance will also be described.

INTRODUCTION

As commercial jet aircraft age, the normal signs of extended use are usually wear and fatigue, both of which are predictable and repairable in a timely manner to maintain airworthiness of the aircraft. Corrosion is another form of deterioration which may occur, but one that is not predictable nor easily detectable in many instances. Consequently, the insidious nature of corrosion may degrade structure such that fail-safe and/or load carrying capability may be lost unless the operator continually takes corrective action through a good corrosion control program.

In the airline industry, economic and market conditions are resulting in the use of airplanes beyond their original economic design life objective. Because of this situation, Boeing initiated a program in July 1986 to assess aging airplane structures and systems. Figure 1 shows the Boeing fleet status as of September 1988 illustrating the number of airplanes of each model approaching and exceeding their design objective. Over 70 airplanes which had exceeded at least 75% of their economic design objective were surveyed. The results of this survey were used to support actions necessary to ensure safe and economic operation of aging airplanes and to promote improved design of new airplanes. The presence of corrosion was one of the more significant findings of this program and its severity varied considerably depending upon the effectiveness of the operator's corrosion control program.

The following discussion is intended to provide an awareness of the many facets of potential corrosion problems in commercial jet aircraft from their design through their years of commercial service. It is a basic fact that the structural materials available for aircraft design have a potential for corrosion. Therefore, operators still must establish and maintain an effective corrosion control program on new airplanes as well as the old.

CAUSES OF CORROSION

There are many contributing causes for corrosion in commercial aircraft as shown in Figure 2. The process starts with the initial design. Corrosion

prevention is influenced by the selection of materials, processes, finishes and the details of the structural configuration. It is important to consider not only the mechancial properties but also corrosion resistance properties when selecting the optimum material for design and to develop a structural configuration with good drainage, as well as the elimination of crevices in corrosion prone areas by faying surface sealing.

The next potential source for corrosion problems lies in the manufacturing process. Processing for the various finish systems is crucial because protection of metal details is almost entirely dependent on the finishes applied. The most important processing combination which influences corrosion performance is the metal surface treatment and the organic (paint or adhesive) primer applied afterwards. The system must offer the long term durability needed to prevent separation of the organic material from that surface which often may result in corrosion.

Once airplanes are in the hands of the operators many conditions exist which may cause deterioration of the protective finishes, e.g., general use resulting in damage to the finishes, environmental conditions within the airplane (for example from cargo), the aircraft operational environment (Figure 2), accidental contamination (e.g., lavatory and galley spillage), and maintenance practices.

These contributing causes of corrosion either create the water (electrolyte) necessary for corrosion to occur or the condition for the electrolyte to be trapped. Water will always be present in and around an operational airplane, therefore, elimination of water sources (or electrolyte) is not possible and other means of combating corrosion must be taken. The influence these electrolytes have on potential corrosion problems is greatly influenced by the operators corrosion control plan and his effectiveness in implementing such a plan. One of the most significant observations from the Aging Fleet Survey conducted by Boeing during 1987 and 1988, reference 1, was the effectiveness of the operator's corrosion control program regardless of his geographic locations or aircraft utilization. The following discussion on types of corrosion, areas of concern, design philosophy, preventive maintenance and detection is primarily based on the corrosion of aluminum alloys since these alloys comprise approximately 80% of the aircraft structure.

TYPES OF CORROSION

Corrosion manifests itself in many different forms although there are only a few basic mechanisms. Following is a brief description of some of the most common forms seen in aicraft structure. Exfoliation corrosion and stress corrosion cracking (SCC) are the two most destructive forms of corrosion found. Stress corrosion cracking is a rapid stress and environmentally induced reaction which follows the grain boundaries in a single plane for aluminum causing rapid loss of load carrying capability. Exfoliation corrosion follows grain boundaries of the metal alloy at a fairly rapid rate but involves multiple planes causing a leaf like separation with very slow corrosion of the grains themselves, Figure 3. This results in a rapid loss of structure with relatively little loss of metal. General surface corosion,

on the other hand, consumes metal at a relatively slow uniform rate over large areas taking much longer to reduce the load carrying capability of the structure. However, when general corrosion is allowed to proceed unchecked, it can develop pits which then become stress risers allowing fatigue cracks to develop in the structure.

Crevice corrosion is the most common form of corrosion found in airplanes and occurs whenever water (electrolyte) is trapped between two confinements, e.g., under loose paint, a delaminated bondline, a poorly protected joint, to name a few. It can occur either on a macro scale or a micro scale and can quickly develop into pits or exfoliation, depending on the alloy involved.

Pitting corrosion is another form of crevice corrosion, where a localized area starts corroding more rapidly than the surrounding area to form a pit. This then becomes self-contained, like crevice corrosion, by creating its own aggressive environment. Pits are generally not as destructive as exfoliation, but quite often result in a stress riser which may reduce the fatigue life of the part.

Filiform corrosion most commonly occurs under exterior decorative paints. It is also a form of crevice corrosion, but takes on the appearance of little filaments growing under the paint film, Figure 4. Filiform corrosion occurs only when the relative humidity is between 65% and 95%. Normally it is an aesthetic problem, but may develop into a structural problem if ignored developing into pits and/or exfoliation corrosion.

Galvanic corrosion results when two galvanically dissimilar metals are electrically connected in the presence of an electrolyte. This can occur on a macro scale, e.g., stainless steel attached to aluminum, or on a micro scale, e.g., an alloying constituent in an aluminum alloy forming a bimetallic precipitate at the surface. The localized anode and cathode will cause galvanic corrosion under the right conditions and subsequently develop into a pit.

AREAS OF CONCERN

As a result of many years of service experience, plus information gained from the aging fleet survey, certain areas present more problems because of their function and location in the aircraft. The most common problem areas on older aircraft have been floor structure under lavatories and galleys, Figure 5, and around entry areas, Figure 6. The bilge always sees the worst environments, so structure (e.g., stringers, frame shear ties, fittings and extrusions against the skin) suffer.

Adhesive bonding of structure on early aircraft resulted in mixed performance creating a major portion of skin related corrosion problems. Some early aircraft have experienced delamination of these bonds. The reason some bonds have delaminated was found to be a process deficiency of the metal surface treatment not identifiable using technology available at the time the processes were established by the aircraft industry. The problems have since been corrected on aircraft manufactured since the mid-1970's and today Boeing

uses a phosphoric acid anodize process for all structural bonding. A delaminated bond in the bilge, Figure 7, and a delaminated longitudinal lap splice, Figure 8, will generally result in more severe corrosion because of a more aggressive environment than a bond delamination in the interior of the crown which by comparison is very mild environment, Figure 9.

Wing and empennage structure have had their share of corrosion problems also, although to a much lesser degree than the fuselage. Bond delamination of honeycomb sandwich trailing edge components has contributed to many of these early problems. However, most problems have been in faying surfaces, most commonly the spar buildup and of fittings.

Fittings in older model aircraft exhibited a high incidence of stress corrosion cracking, primarily because of a materials problem. The aluminum alloy used, 7079-T6, had excellent mechanical properties for many structural applications. The phenomenon of stress corrosion cracking was known and laboratory tests of this material were conducted in accelerated environments to validate the use of this material. Based on these test results the material appeared reasonable for use and was selected for design. However, after exposure to airplane service environments, it was found that 7079-T6 was more susceptible to real time exposure. Since then all aluminum alloys have had extended seacoast SCC testing before being used.

DESIGN PHILOSOPHY FOR CORROSION PREVENTION

Many material compromises go into the design of an airplane and are based on weight, cost, function and reliability. Aluminum and low alloy steels are the two groups of metals most susceptible to corrosion problems. Therefore, the first step in designing corrosion prevention into an airplane is to select the alloys which are least prone to corrode and still meet the requirements of the design, for instance, 7075-T6 aluminum alloy is susceptible to exfoliation corrosion, whereas 7075-T73 while it will not exfoliate does pit and suffers a reduction in strength properties. A new heat treatment -T76 is much less subject to exfoliation than the -T6 condition and gives good pitting resistance while resulting in only a minor weight penalty.

Once the structural materials have been selected, there are basically four additional design considerations which will significantly reduce corrosion during the service life of the airplane. These are:

1. Effective drainage of all structure is vital to prevent entrapment of any fluids. This may be accomplished by providing cross-drainage of fuselage stringers allowing all liquids to effectively find their way into the bilge where through hull drains are located. Wherever water can be trapped, the design must provide for drainage pathways to the through hull drains. Figure 10 shows the results of poor cross drainage. Good drainage is particularly important with the new high recirculation air-conditioning systems which increase the humidity level in the aircraft.

2. The finish system is required to protect the metals. A system consists of a specific surface treatment process and a specific paint compatible with that surface. This results in an environmentally durable system that won't chip, delaminate or otherwise form a crevice between the metal surface and the paint.

3. The elimination of crevices in joints is required by faying surface sealing all joints with a chromated polysulfide sealant in known corrosion prone areas, e.g., skin/stringer/shear tie joints below passenger floor, fittings, wing/empennage spar web to chord to skin joints, wheel well structure and nonaluminum fastener installation.

4. Corrosion inhibiting compounds need to be applied in the final assembly of models to all corrosion prone areas of the structure, e.g., inside the fuselage crown and lower lobe, pressure bulkheads, pressure deck, under lavatories and galleys, wheel wells, wing/empennage cove areas, dry bays, empennage torque box interiors and under fairings.

These are only the major considerations in designing corrosion prevention into an airplane. Examples of corrosion improvements implemented into the production of one of the Boeing models over the years is shown in Figure 11. Today's aging fleet is represented by those airplanes manufactured over 15 years ago, whereas the newer designs of the 757/767/737-300, 400 and 500/747-400 models represent the bulk of corrosion improvements. Based on today's knowledge of corrosion prevention, tomorrow's aging fleet should have far fewer corrosion problems than those now being experienced.

PREVENTIVE MAINTENANCE

Airlines have become increasingly aware of the significance their maintenance programs can have on corrosion. Operators can significantly reduce its occurrence and severity by using a good corrosion prevention program. The specifics of each individual operator's plan will differ depending on his experience, maintenance program and operational environment. However, corrosion is always a potential threat because of the many factors pointed out in Figure 2. There are several significant factors which should be common among operators because of their impact on corrosion control:

- Personnel training
- The continual use of corrosion inhibitors
- Planning for corrosion and factoring in the time to clean up corrosion early during "C" and HMV checks
- Accessibility to the structure

Personnel training can be a significant impact on the repair of corrosion once it is discovered. The restoration of a good, durable finish is very important if recurrence of corrosion is to be eliminated. It is necessary to remove all evidence of corrosion, treat the surface with an approved chemical (e.g., Alodine 1200) to produce a conversion coating (cleanliness is extremely

critical to insure good paint primer adhesion) and apply one or two coats of an approved corrosion inhibiting primer. Figure 12 shows an example of poor surface treatment of a previously repaired stringer area. Application of a corrosion inhibiting compound may have prevented the corrosion from reforming or at least slowed it down significantly.

Washing exterior surfaces of an airplane will help reduce corrosion if done intelligently. Washing will remove dirt deposits which are sites for retaining water (electrolyte) which then can lead to corrosion. However, the operator must understand that washing areas, e.g., wheel wells, landing gear and wing cove areas, corrosion inhibitors previously applied will be removed as well as some of the grease in lubricated joints. These areas are normally washed less frequently than aerodynamic surfaces and, when washed, the corrosion inhibitor must be reapplied followed by greasing all lubricated joints. Avoid removal of materials such as grease and fay seals by high pressure.

CORROSION DETECTION

Corrosion detection is most effectively achieved by visual inspection and touching. The effectiveness of the inspector is entirely dependent on his skill which is a function of his training, experience and knowledge of the structure. A good inspector is like a detective. He not only looks for the obvious and known problems, but is wary of possible new problem areas. Visual inspection and touching accounts for more than 90% of detection. Equipment necessary for visual inspection is relatively simple and consists of a flashlight, long handle mirror, magnifying glass, plastic scraper for probing and removing loose paint and work stands and ladders. Other methods include dye penetrant, eddy current, ultrasonic and X-ray procedures for specific applications.

All corrosion problems start out as small, seemingly insignficant problems. The chipped paint around the fastener heads in a wing spar cove area present a small problem but, if ignored, may develop into a major/costly repair.

Corrosion in faying surfaces such as body skin lap splices, skin doublers, skin stringers, wing spar chord/skin or webs are difficult to detect until some additional evidence is apparent. Bulging of body skins between fasteners is a telltale sign of corrosion in the joint. If not repaired in a timely manner signficant structural degradation may occur; fastener heads may become distressed or cracks in the skin may develop as shown in Figure 13. The presence of blind fasteners in this example indicates that previously distressed fasteners existed, but were replaced with blind fasteners. The operator in this case failed to recognize and correct the basic source of the problem.

A lack of easy accessibility to the structure sometimes results in corrosion initiation without detection in its early stages. The stringer flange corrosion in the fuselage crown area, Figure 14, is often not found in its early stages because airlines don't get into these areas very often. Since the environment in the crown is rather benign, there has been less tendency to be

concerned with corrosion compared to areas below the passenger floor. However, an increase in interior crown corrosion incidences in older aircraft was evident from the aging fleet survey.

The effectiveness of feeling as well as seeing is illustrated in Figure 15 where corrosion occurred under a spar chord-to-wing skin joint. This could be difficult to see unless the light and shadowing was right, but was easily detectable by running a hand along the surface and feeling the discontinuity.

In some situations where a costly teardown would be necessary to gain inspection access to the structure, eddy current, ultrasonic or X-ray may help determine if significant corrosion exists. It should be noted that these techniques have limitations in detecting corrosion, and their success is highly dependent on the skill and training of the operator.

SUMMARY

Corrosion of aging airplanes is the combined effects of materials selection, design, finishing, processing details, maintenance programs and operational environments. Airplanes manufactured today are expected to have fewer corrosion problems 20 years from now than the current aged fleet because of significant design and corrosion protection improvements and the increased awareness operators have of their role of preventive maintenance in corrosion control. However, maintenance and corrosion control programs will still play a major role in the control of corrosion as the airplanes age.

The most significant factors in controlling corrosion have been drainage, sealing faying surfaces in corrosion prone areas, the finish systems used to protect the metals, the liberal use of corrosion preventive compounds and a good corrosion control maintenance program.

REFERENCE

U. G. Goranson and M. Miller, "Aging Fleet - Aging Fleet Evaluation Program," Airliner, Oct.-Dec. 1987.

MODEL	INITIAL SERVICE DATE	ACTIVE FLEET * (TOTAL) NUMBER OPERATORS	ACTIVE FLEET * (TOTAL) NUMBER AIRPLANES	ECONOMIC DESIGN LIFE OBJECTIVE	AIRPLANES EXCEEDING GIVEN % OF DESIGN OBJECTIVE 75%	100%
707	Sep. 1958	80	206 (729)	20,000 Flights 60,000 Hours 20 Years	167 148 189	64 52 147
720	Jul. 1960	6	12 (153)	30,000 Flights 60,000 Hours 20 Years	12 12 12	5 5 12
727	Feb. 1964	124	1,653 (1,821)	60,000 Flights 50,000 Hours 20 Years	199 825 836	7 389 510
737	Feb. 1968	128	1,503 (1,567)	75,000 Flights 51,000 Hours 20 Years	61 258 296	1 43 69
747	Jan. 1970	65	593 (629)	20,000 Flights ** 60,000 Hours 20 Years	83 225 197	5 73 0

* Airplanes known to have flown during the past 12 months.

** Special design life objectives have been established for -SP and -SR derivatives.

Figure 1. Fleet status of Boeing commercial jet airplanes for September 1988.

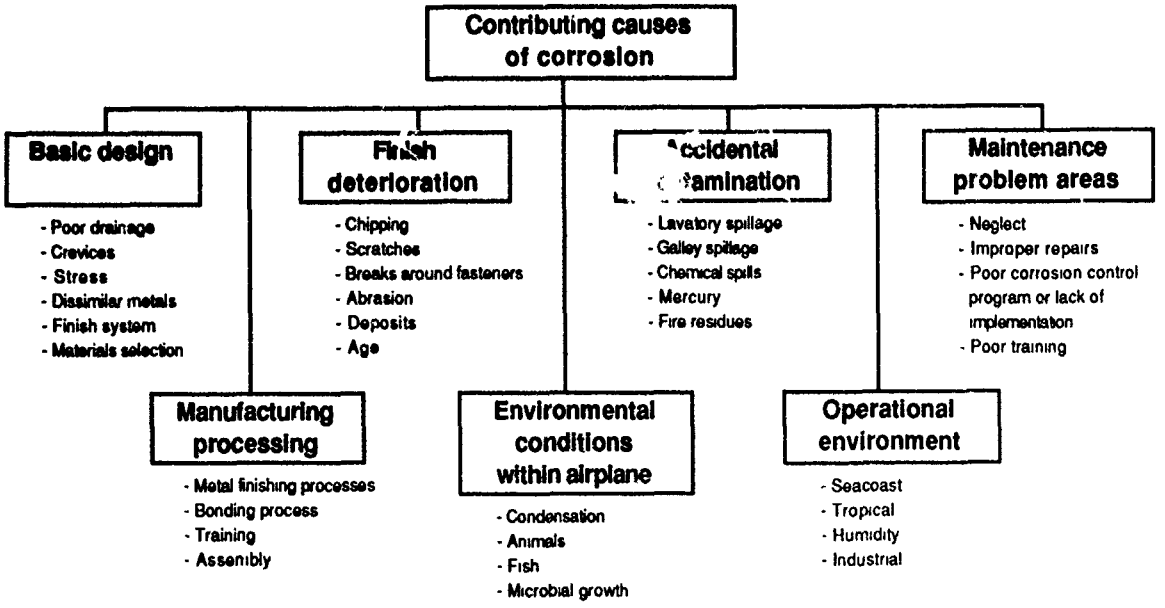

Figure 2. Contributing causes of corrosion.

Figure 3. Seat track exfoliation corrosion (aluminum alloy 7178-T6) located under galley.

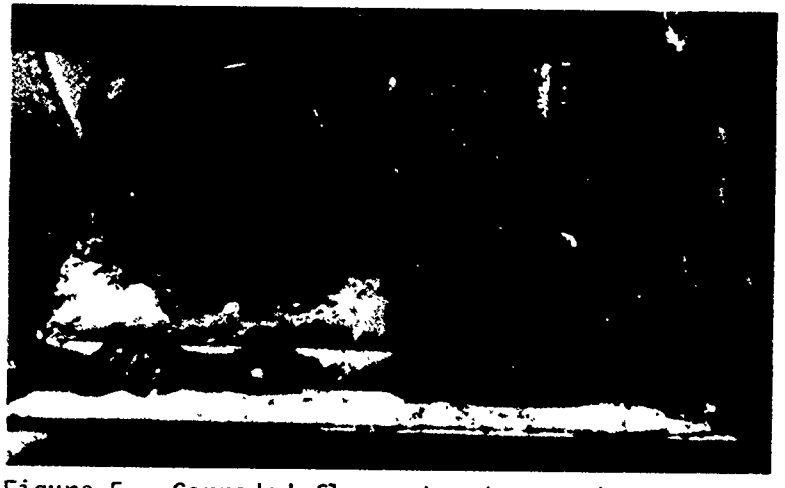

Figure 5. Corroded floor structure under lavatory.

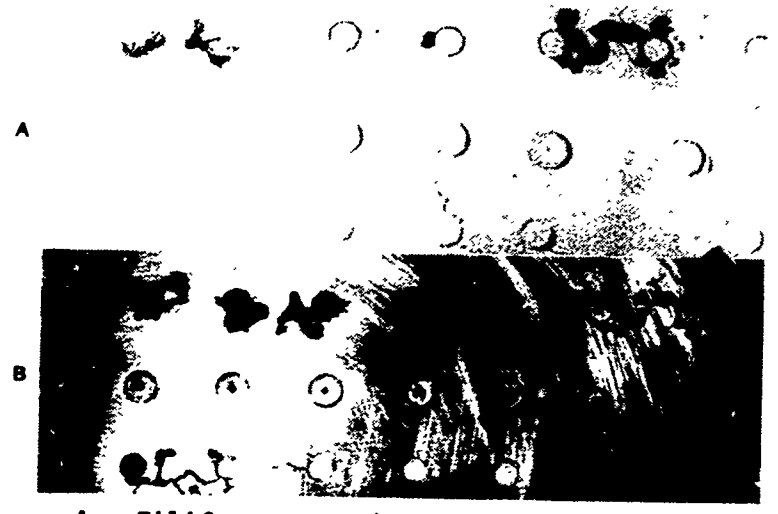

Figure 4. Filiform corrosion around fastener heads in a fuselage skin. (a) As the corrosion appears under the paint as small filaments. (b) After removal of the paint.

Figure 6. Corroded frame around cargo door entry at sill.

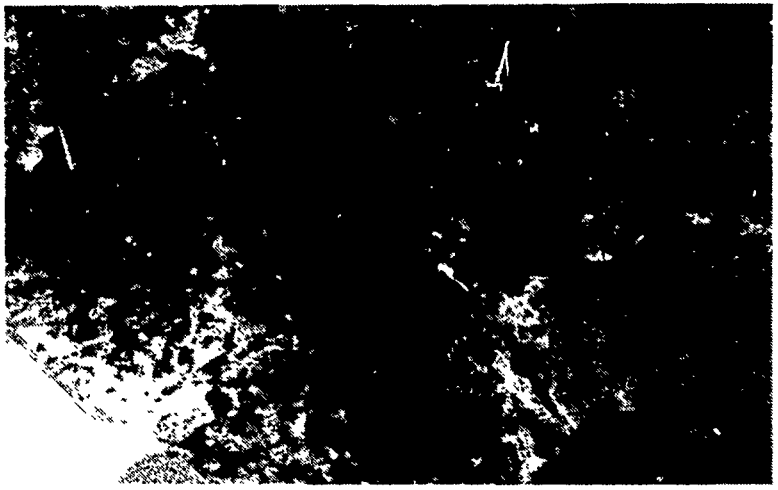

Figure 7. Typical results of crevice corrosion in a delaminated bondline located in the bilge.

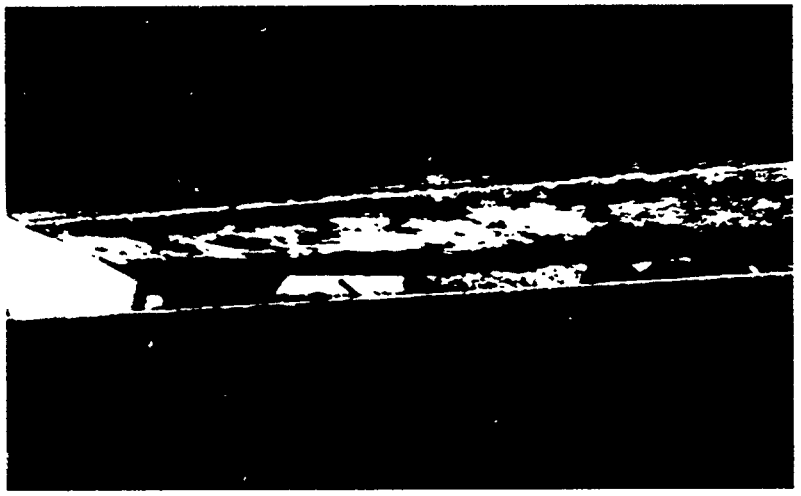

Figure 8. Typical corrosion in a delaminated longitudinal lap splice.

Figure 9. Delaminated tear strap under a frame in a fuselage crown with insignificant corrosion.

Figure 10. Poor cross drainage in bilge. Note center bay with drain is dry and each adjacent bay is filled with water.

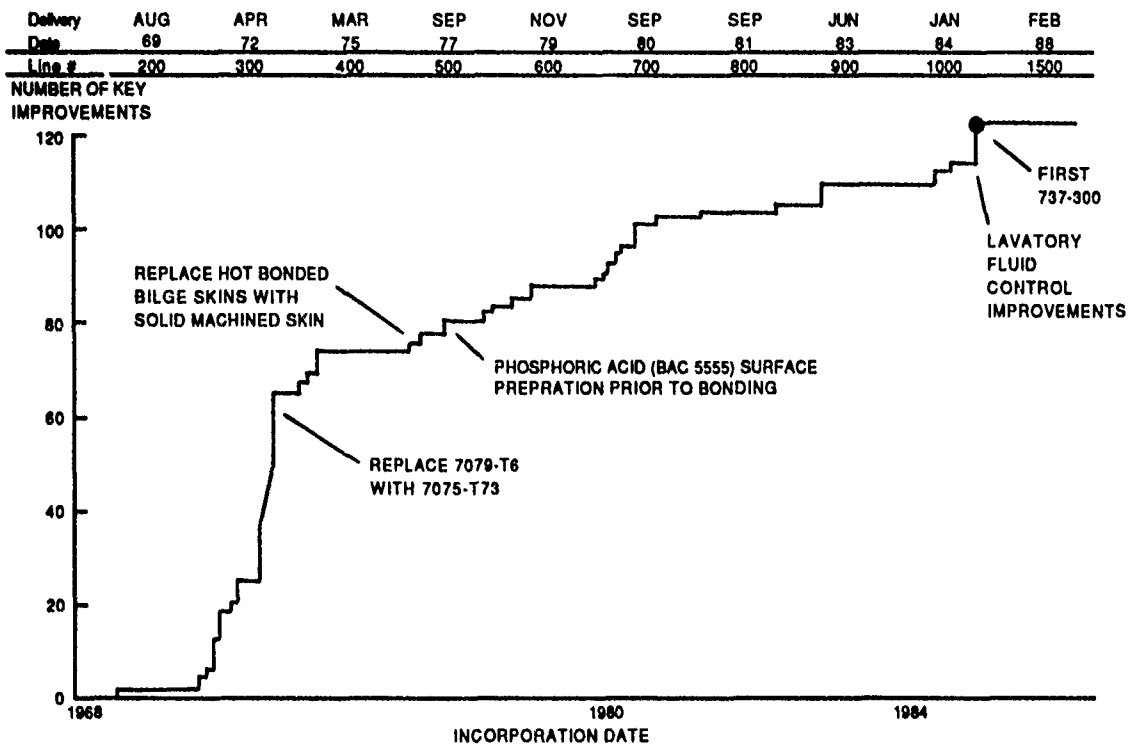

Figure 11. Corrosion improvements implemented on the 737 model and typical of others.

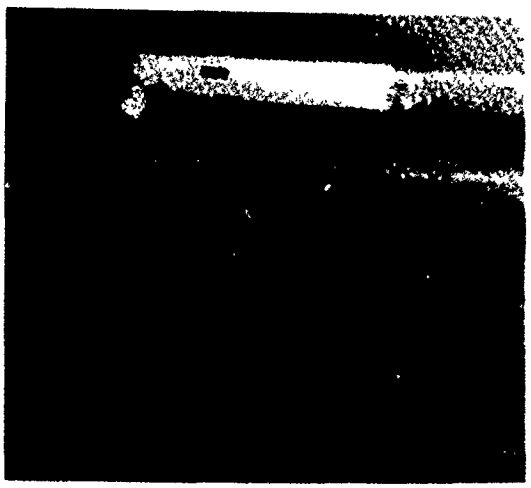

Figure 12. Corrosion of a previous repair because of inadequate corrosion removal, poor surface treatment or improper repair materials.

Figure 13. Bulging of skin between fasteners due to corrosion causing distressed fastener heads plus stress corrosion cracking of the skin.

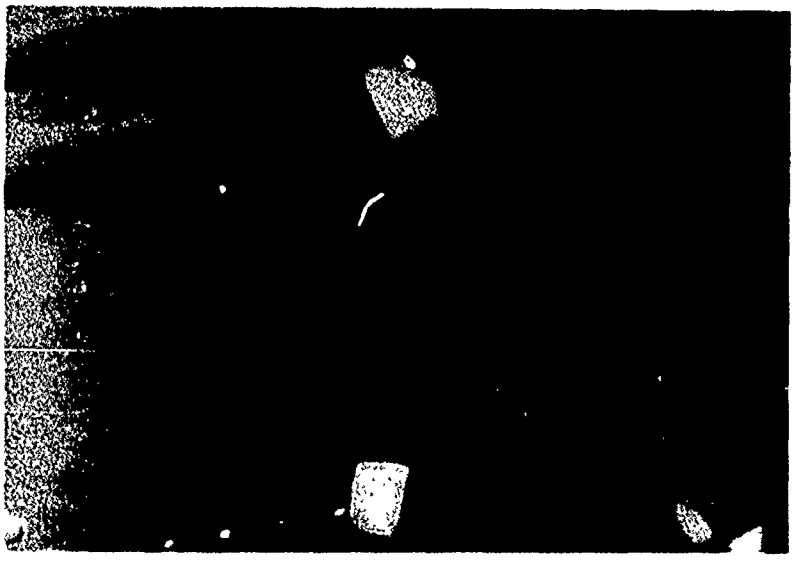

Figure 14. Stringer flange corrosion in the crown of an aged airplane.

Figure 15. Slight lifting of spar chord due to corrosion underneath which is not easily felt.

PRESERVING UNSHELTERED EXHIBIT AIRCRAFT

Robert C. Mikesh
Senior Curator
Aeronautics Department

National Air and Space Museum
Smithsonian Institution
Washington, DC 20560

Abstract: This paper describes the problems of protecting museum aircraft from corrosion resulting from outdoor display environments. The approach adopted by the Swiss Transport Museum is presented, together with a description of other measures taken to extend the life of these aircraft in order to preserve their technology. Recommendations are made to show how other museums can adopt similar programs for displaying aircraft in outdoor, corrosive environments.

We deplore it! We search for alternate solutions -- but in time, nearly every air museum is faced with the realization that a large aircraft essential to the collection may have to be exhibited outside the museum building. This has only one advantage, and that is to save for study and exhibit a particular aircraft that would otherwise be rejected and, in a short time, cut up for scrap.

To collect and display selected aircraft is the purpose of air museums in the first place. However, the disadvantages of exhibiting them outdoors become overwhelming if the exhibit is not realistically planned in advance. Recognizing and facing the problems at the very beginning, before accepting an aircraft, are often obscured by the allure and excitement of acquiring the magnificent airplane that is being offered. Within a few short years, the wisdom of having accepted such a large aircraft that is beyond the capability of the museum staff and volunteers to maintain is often questioned. As a result, they must watch the elements overtake and produce a shabby, rust-streaked aircraft exterior that has anything but a pleasing and inviting appearance. Such airplanes soon become a liability to the museum, not an asset.

There are solutions, if the problems are properly addressed in a methodical, well-planned program for each aircraft. The cost can be high and much time can be consumed, and this must be recognized early. Airplanes have never been inexpensive, including those that cost the museum nothing to acquire. So often it is not its initial cost to be considered, even when the airplane is free, but the continual up-keep required to maintain and support them.

One measure of the professionalism and maturity of a museum is how this difficult problem is managed.

Perhaps only portions of the plan described here can be managed by most museums, but at least this description will address the issues to be considered. These actions divide into four distinct phases that can be addressed separately in aircraft planning considerations. These phases include the acceptance transactions, aircraft moving, exhibit positioning, and reccurring maintenance. If each of these major phases is adequately solved, the airplane and the museum have a chance at a long and pleasant relationship.

One museum that has attained near perfection in outdoor preservation of an aircraft is the Swiss Transport Museum in Luzern. The Museum acquired a Convair 990 Coronado from Swissair in 1975 and moved it to the Museum grounds. It was placed in the courtyard of the Museum, and even today it looks as new as the day it arrived. The years of exposure to the country's extreme seasonal temperatures and conditions show little effect because of proper care. The air in Luzern has a high content of carbon and sulfur dioxides and nitrogen oxide, combined with high and low humidities depending upon the time of year and wind direction.

Despite these problems, the Museum intended to have the airplane in an open environment, flanked by some of the support equipment associated with passenger transports, as aircraft of this size are seen. Had they elected to house this airplane in a building, it would not have blended well with the other buildings or the openness they desired. One can wonder, however, which avenue, outdoor maintenance costs or building costs, would have been the least expensive to follow. Based upon the experience gained by the Swiss Transport Museum, here then, are some factors and guidance to consider before acquiring an aircraft for outdoor exhibit.

The acceptance transaction is always the first issue to be considered, but perhaps it is not always addressed with the museum's best interest in perspective. If the airplane in question is an air transport being acquired directly from a major airline, the problems can be less cumbersome than if it is accepted after several users. Nevertheless, the benefits of enlisting the help of an airline that once used the type as an active and supportive sponsor, should be recognized by both the sponsoring company and the museum. In the case of the Coronado, this airplane represents Swissair, the flag carrier of Switzerland. The company was proud of this airplane and its service, and now it has high visibility in the company colors and the bold name on its fuselage that is seen by countless visitors to the museum.

It is essential to work out mutual agreements with the sponsoring company early in the acceptance phase. Preparation and maintenance support can most efficiently be done by the company rather than by the museum staff, which is always limited in number. During this early, pre-acceptance phase, try to work out a written agreement concerning periodic support that the company will give to the airplane and the museum. Identify recurring work to be

performed by the company. Set a time limit for this support, such as five years. This would be much easier for its management to accept than an open-ended agreement. If the museum exhibits this aircraft in that company's markings, a satisfied company would probably renew its agreement rather than see the airplane deteriorate with its name on it. Whenever possible, enlist the help of the airline's maintenance facility to prepare the airplane before it is delivered to the museum. The importance of this was not recognized until after the Convair 990 was in place at the Swiss Museum. It then became the responsibility of the airline technicians to accomplish the entire project while working out of tool boxes in the open museum location. It was estimated that sixty percent of the preparation work could have been done at the maintenance facility under much easier, and less costly, conditions.

The airline's maintenance facility is the best place to check for, and to remove, corrosion. This is a must in any case in order to enhance the life expectancy of the airplane, a task which the maintenance facility is well equipped to accomplish. Replacement with worn parts just because this airplane will not fly after its ferry flight is false economy. Those parts will not last as long, so their purpose is defeated. The airplane should be delivered in first-class condition, as the airline wishes it to represent its company.

The interior can be brought up to exhibit standards and configuration while at the maintenance facility. This is important if museum visitors will be permitted to enter the cabin, especially since this is an important feature in the preservation of air transports. While some museums have resorted to placing plexiglass walls along the aisle to keep visitors away from seats, this portrays a false, confining interior. Much depends upon the museum's location and its visitors, but a more aesthetically pleasing method is to have heavy clear mylar covers for the seats along the aisle to protect them from hands as visitors move through the cabin. These protective covers will not last indefinitely, so a continuing source for replacements must be available.

Other work to be done at the maintenance facility will become evident, depending upon the aircraft type. The next phase, aircraft moving will be a problem that can only be addressed on an individual basis, but exhibit placement is a factor needing considerable pre-planning. A major reason for the Swiss Museum's continuing success in preserving the Coronado is that ground support equipment is close at hand and has been dedicated to it. Not visible to visitors is an underground room below the airplane, hidden beneath the surface of the exhibit grounds. An air conditioner with a 500 cu/m/hr capacity is in this well lighted and ventilated basement. The outlet for this unit is connected unobtrusively to the airplane at the normal connecting point for a ground equipment air conditioning unit. This permanent installation maintains the aircraft cabin between 18 to 20 degrees C (65 to 69 degrees F).

This feature not only makes it pleasant for visitors walking through the museum aircraft, especially on a hot summer day, but is important for other reasons as well. During the hours that the cabin doors are closed and air

flow is restricted, the exhausted air is forced through the structural parts of the airplane, i.e. wings and fuel systems, cabin wall interiors, lower fuselage cargo compartment, empennage, etc. With the Coronado, the fuel purge-and-dump system is used to direct low humidity air through the fuel cells and wing structure. Openings were made through closed parts of the structure to allow this gentle passage of air to take place. As a result, daily condensation and damaging moisture is prevented at all points of the structure's interior by the flow of cool dry air.

Also contained in the basement below the aircraft is a heavy duty air compressor. When maintenance work requires compressed air, which is often needed with any aircraft, the source is readily available. Concealed in this way, the resounding noise that the air compressor generates is muffled and therefore not offensive to museum visitors, and is certainly less tiring for technicians working on the aircraft.

While considering these major expense items for the well-being of the airplane, a water line to the aircraft site should be included. An airplane needs exterior washing frequently to keep it in exhibitable condition; therefore, the convenience of available water should be addressed early in the planning phase.

Where and how to locate the airplane is more of an exhibits design function, but other factors should be considered as well. When making this selection, it should be looked upon as a permanent fixture. Placement of the underground support equipment for an aircraft, for example, is a major consideration. This might be determined by the predicted direction of strong winds. Pointing the nose into the wind is normal in positioning aircraft, but if wind is not a factor, consider the direction of sun exposure. Sunlight has a damaging effect upon the outside finish of an aircraft, and will effect one side more than the other. The angle at which the aircraft will generally be viewed by visitors may warrant some inflexibility in positioning.

How an aircraft rests on its landing gear should be an important element for special attention. While viewed at distances that outdoor exhibits can provide, an airplane does not look right if the landing gear strut travel is bottomed out, or worse if one or more tires are flat. The best solution is to place a spacer within each landing gear strut that will support the weight of the aircraft and maintain proper strut extension. Make certain not to insert a material that will rust or corrode and therefore cause damage. A correctly sized phenolic bar insert would be best, but a properly treated metal bar that will not rust would suffice. To disassemble a landing gear strut is a heavy equipment operation, and to avoid this, some museums fabricate a split collar to go around the strut extension. This is the next best solution, but the strut does not look normal when viewed closely, and the sleeve can damage the sliding surface of the strut over time.

Landing gear jacks are essential for taking the weight of the aircraft off the tires. These must be custom made for the height of the jack support point of the strut, allowing about one inch of tire-to-ground clearance. If

securely anchored, these jacks can also serve as points at which to secure the airplane to the ground. This avoids the ugliness of tie-down cables. Once in place, this all but eliminates the endless need to re-inflate tires as their air slowly seeps away.

Some museums prefer to mount an aircraft in some attitude other than as it would normally rest on the ground. This introduces a new set of problems. An example is the Douglas DC-3 at the Swiss Transport Museum. The designers of this airplane took into account that while at rest, rain water would surely seep into the aircraft in varying degrees, and they provided water drain holes at low points throughout the structure. With the aircraft mounted at a level flight attitude, for example, moisture pools appeared in unexpected places and new avenues for water to escape had to be created.

With the airplane established on the museum grounds, the recurring maintenance phase begins by preparing the exterior to endure the rigors of outdoor exposure in the years ahead. Again, the technicians of Swissair are to be complimented for mastering the many problems encountered. Following their plan, once the airplane is initially prepared, a periodic process of attacking certain areas of the aircraft surface in greatest need of attention begins. The side facing the sun will require the most repeated attention. For the Coronado, Max Widmer from the Swissair Technical Department has all but taken this reccurring project as a personal undertaking. It shows by his workmanship. Each spring, at the end of Switzerland's winter snow, Widmer and an assistant depart the airline maintenance facility in Zurich for a ten- to fifteen-week stay at Luzern. Their time is devoted to accomplishing many things that would have been best accomplished originally at the maintenance facility and, more visibly, with working on areas of the aircraft needing painting or repairs. What they cannot accomplish in this time must be left until the following year. Nevertheless, this ongoing maintenance program is rigorously followed, and the excellent condition of the airplane shows this.

Max Widmer has a simple and logical checklist for these functions which he can recite from memory. This forms the basis for any portion of the airplane being worked on.

1. Clean by generally washing the airplane.
2. Remove any corrosion.
3. Paint inside surfaces with primer (the National Air and Space Museum, on the other hand, recommends a clear coating if not painted originally by the factory) and paint outside surfaces with appropriate color.
4. Apply corrosion prevention material on the inside of the structure.
5. Clear all cracks and crevasses that are not securely filled, and seal all skin-line seams on the top and sides of the structure, leaving lower seams open.
6. Ventilate structure where possible.
7. Inspect from time to time and prevent damage before it occurs.
8. Repair as needed.

Understanding most of these steps is rather straightforward, but some need

further explanation. This airplane is washed religiously twice a year, in the spring and fall. Natural rain will not handle the situation as well as it used to in earlier years. Not all the unsightly rust stains will wash off. To prevent them from recurring, steel items which cause rust stains are removed. Where possible on the Coronado, steel fasteners have been replaced with titanium hardware of the type used on Swissair DC-10s. When suitable replacement items cannot be found, the fasteners are removed and sandblasted for rust removal. This is followed by a normal galvanic treatment such as cadmium plating. Uncoated steel parts are coated the same day after cleaning with NOVEROX, a rust converter primer (Material Note 1). Otherwise they would begin rusting overnight in Switzerland's humid night air, which is not unlike conditions at many places in the United States. When installed they are coated with a wet, putty-like material, PR1422B2 (Material Note 2), which seals them in place and prevents water entry under the taper screw head and threads. Residue is removed with acetone and a cotton towel. The heads are painted again to match the surrounding area, which is normally covered using a paint roller. Cross point screw slots that are missed are paint-filled with a small brush. This material does not permanently fix the screws in place, for they can be removed. All this is painstakingly time consuming work, but the results are gratifying.

To help cut down on water streak lines on the lower surfaces of the aircraft structure, an area easily examined by visitors, artificial dams made with aluminum tape have been strategically placed. Rather than having a run of water go the entire length of a surface, leaving a telltale streak, the tape causes water to drip off at the point of contact. This is also used to divert water and its associated streaks so that it will drop from the lower surface of the aircraft at an earlier point.

Any access panels within the area worked on are opened for interior inspection. After corrections are made, a coating of LPS3 is sprayed over the interior (Note 3). This product is recommended by Boeing as a preservative for the interior of aircraft structures. There are other products that can be obtained for this purpose, such as Bilstein R-2000 (Note 4). These materials have a property which neutralizes electrolysis action, or provides a thin self-healing coating that displaces moisture for the prevention of corrosion. They can be expected to last from three to five years. LPS3 remaining on outer surfaces or closing edges must be removed before the access panels are closed. Since this material creeps very well, as it is designed to do, it would otherwise serve as a barrier preventing sealing these edges.

Properly sealing the upper and side surfaces of the aircraft from water is of prime importance. Not only does this prevent trapped moisture from causing corrosion and related deterioration, it also prevents water streaks from entering skin openings. This is a laborious, but rewarding, operation.

First, the skin mating line is cleaned, using a tow-scraper to loosen embedded dirt and deteriorated caulking material. Then it is cleared with air pressure from the air compressor previously described. When cleaned and dried, both sides of the seam are masked with masking tape, right at the

edge. Using a caulking gun, sealer such as PR1422B2 (Note 2) is forced into the crevice. A putty knife (a steel rod, of 1/4 to 3/8 inch diameter, bent to a spoon-like profile), or a more suitable trowel, smooths the seam surface, and the masking tape is then removed. What is seen just within the skin line is a very fine black line (white or other colors are available) that detracts in no way from the aesthetic appearance of the airplane. Initially this can be slow work, but in the case of the Coronado, Widmer and his helper Fritz Zaugg sealed 110 windows of this aircraft in four days. Once finished, it gives a crisp appearance, and also keeps water stain lines from reappearing under window frames after the stains have been removed.

Upper skin lines often overlap the lower surface. These must not be overlooked since, through capillary attraction, water does run uphill. To prevent moisture from entering these seams, they must be filled and smoothed as well. By masking the seam edge to be filled, the fill-line need not be any wider than one-and-one-half times the thickness of the lapped skin edge itself. Filled seams of this type, using the material described, can last from six to ten years. But since climate conditions vary, they must be inspected at least annually for cracking and tightness.

Some cracks cannot be filled with putty, such as gaps between flaps, ailerons, and spoilers on the wing, and between the elevator and the horizontal stabilizer. These are bridged with 3M aluminum tape in widths of 1 inch, 2 inches, 3 inches, and 120 mm. One-inch aluminum tape is also used to close gaps around hatches and removable access panels, such as cowlings. This is applied like roof tiles, starting at the lowest edges and the next applied tape overlapping the lower one, and so on. Once all the areas are sealed, a final one-inch save-tape prevents the upper-most seal tape from being forced away by ice and snow as it slides down the wings, stabilizer, and engine cowlings. Tape ends are always smoothly cut with scissors, and all tapes are pressed into place with plastic-smoothers.

Normally, this tape will last for one year through the Swiss seasons, but the operation moves quickly once the skill of application is learned. It is essential that earlier tape residue is completely removed with white-spirit, nylon brush, and cotton cloth, and then degreased with acetone or chloroethene, before new tape is applied. The residue must be removed carefully and not accidentallly distributed over the adjacent area. This is confirmed with the bare hand, for if residue remains on the aircraft skin, the surface feels sticky. This prevents corrosion and improves the adhesive qualities of new tape.

Repainting is a routine process and must be done for appearance's sake, before it is needed. While red is an exciting color on almost any vehicle, it is the most difficult color to maintain. In the case of the Swissair Coronado, the red fuselage stripe on the southern side needed repainting after three years because of white paint run-off that would not wash off. On the shaded side, the same red paint has been in place for ten years and is still in good condition. This illustrates that, by concentrating on selected sections of the aircraft exterior rather than the nearly impossible task of addressing the entire airframe while at the museum, no more than necessary

work need be undertaken.

The unpainted skin on the Coronado is taking on a leadened appearance rather than the once shiny aluminum surface. Good results were obtained over a test section of the fuselage on the shaded side. This test area was prepared by first applying an acid treatment to the metal skin, then treated with Flex Coat (Note 5), followed by Metaflex FCR Wash-Primer (Note 6) and Aerodur Primer S15/90 (Note 7). The final coatings consisted of Aerodur C12/100 (Note 8) and Aerodur Clear Coat UVR (Note 9) applied with a spray gun. This is a clear polyurethane lacquer. When conditions prevent spraying, a paint roller has been used. From close-up inspection, rolling gives an uneven surface, somewhat like that of an orange skin, but it is not noticeable at any normal viewing distance. Max Widmer refers to this clear coated surface as the "wet look." At this point, it is noted that the glossy surface requires more frequent washing than bare metal, but the improved appearance makes it worth the effort.

Sun radiation through windows is another consideration, especially for cockpits, with their larger glassed areas. It is best to totally paint the windows to keep the temperature lower for the interior aircraft components. However, this gives a very artificial appearance. A reflective, yet transparent, window tint film has been applied to the cockpit windows of the Swiss Transport Museum's Coronado 990 and DC-3. Widmer reports a marked reduction of heat in the un-air-conditioned DC-3 cockpit after the window film was applied, from an average 55 degrees C (132 F) to 35 degrees C (95 F) over a one-week period.

The main problem with applying window tint film to aircraft windows is that it will not adhere as well to these acrylic surfaces as it will to auto glass, for which it was designed and is marketed. It will adhere to aircraft windows initially, but over time it will begin to bubble because of the breathing qualities of acrylic surfaces used for aircraft windows. Where the situation warrants, remove the window frame and place the tint film, cut to extend beyond the window area, on the window surface, without removing the clear adhesive barrier. Reinstall the window frame, which now holds the film in place. As an alternate method, adhesive tape has been used to hold the film in place, but it releases the film over time because of the heat and the smooth film surface.

There are three or more types of reflective film available through auto window tinting companies. Of the Matico window tint films on the market, the most reflective mirror-like finish prevents 79 percent of the sun's heat from passing through. This is the best, but it gives an unnatural appearance. For automobiles, RG-210, an almost black film through which the car occupants cannot even be seen, reflects 75 percent of the heat. The best appearing film is RG-321, described as smoke or gray. It reflects 71 percent of the heat. A combination of these films might be used, such as black for covering cabin windows where light is seldom seen from ground level through the cabin, and gray for cockpit windows which often show light from the opposite side. This material costs approximately $1.25 per square foot. Although expensive, there is not all that much window area in an airplane and the benefits gained

through heat reduction would be appreciable.

The visible results of the many phases of preserving the Swiss Transport Museum's Coronado, which have been in place since 1975, are impressive, to say the least. But all good things must come to an end sometime, and when that end will come remains to be seen. Dr. Alfred Waldis, President of the Swiss Transport Museum when the Coronado was accepted, was asked when he would expect that the maintenance of this airplane would be overtaken by outdoor deterioration. He replied that he would be satisfied if this airplane could serve as an exhibit for a period of thirty-five to fifty years. To do so would make all this effort worth while. After that time, a newer generation airplane would be worthy of this exhibit location. With the removal of the 990, the cockpit and other technical components may be retained as separate, and more easily managed, indoor exhibit items.

"This is not a bright future for such an airplane when other museums plan in terms of hundreds of years," according to Waldis. "But this is better than other alternatives, such as letting it deteriorate at its own natural rate or not having the airplane at all."

Materials:

Note 1.
Rust converter primer

NOVEROX
SFS Stadler Inc.
Building 1, Box 9392
McArther Road, Route 183
Reading, Pennsylvania 19605

Note 2.
Airplane putty as PR1422 types

Product Research & Chemical Corporation
Burbank, California
or
410 Jersey Ave
Glouchester City, New Jersey 08030

PR1422B2 = thick viscosity, 2-hours working time
PR1422B1/2 = thick viscosity, ½ hour working time
PR1422A2 = thin viscosity, 2-hour working time
PR1422A1/2 = thin viscosity, ½ hour working time

Note 3.
LPS3 conforms to MIL-Spec. C23411, C16173D, SAE AMS-3066
Boeing Material Standard 3-23D

LPS-Research Laboratories Inc.
4647 Hugh Howell Road
Tucker, Georgia 30084
(404) 934 7800

Note 4.
Bilstein R-2000 Anti-Rust Compound

S.E. Waxoyl
6001 F Georgia Ave.
West Palm Beach, Florida 33405

Note 5.
Flex Coat for surface preparation.

B & B Chemical Company Inc.
Miami, Florida 33266-0796
Telex 51-4794

Note 6.
Metaflex is a European product. Equivalent to
PPG Industries DX1791/1792

PPG Industries
19699 Progress Drive
Strongsville, Ohio 44136

Note 7.
Aerodur is a European product. Primer S15/90 is equivalent to
PPG Industries DPU 35/301
(See address above)

Note 8.
Aerodur C12/100 is equivalent to
PPG Industries Durethane

Note 9.
Aerodur Clear Coat UVR is equivalent to
Ditzler Delclear

Ditzler Automotive Finishes
P.O. Box 5090
Seven Oaks Station
Detroit, Michigan 48235

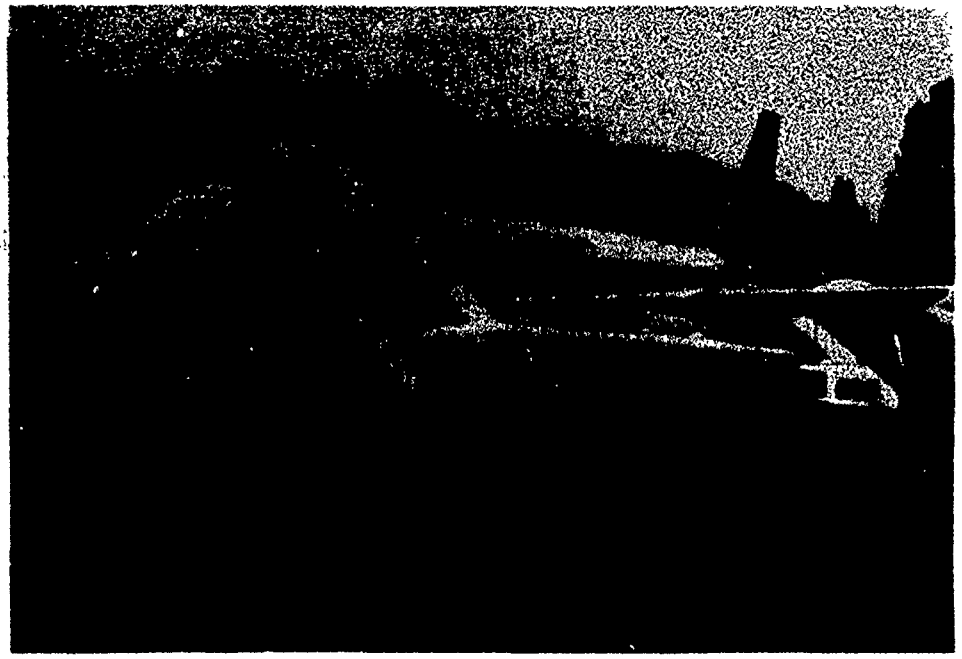

CONVAIR 990 CORONADO has been on outdoor exhibit at the Swiss Transport Museum in Luzern since 1975. Having had proper care over the years, it is a handsome center-piece in its normal setting. Condition and appearance remain near perfect.

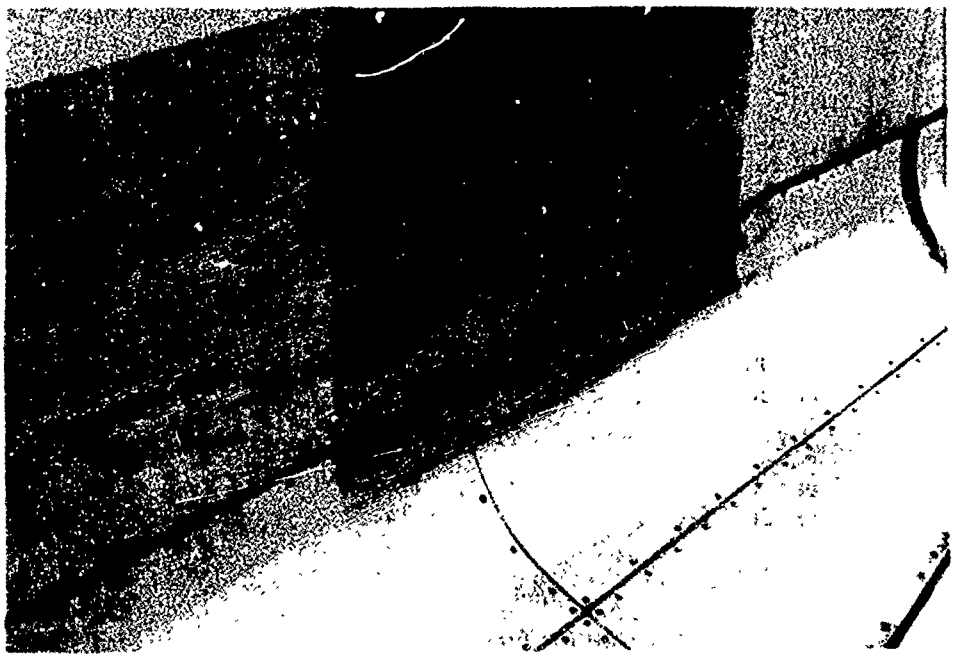

TEST PANEL of outer skin has been coated with polyurethane lacquer to test its protective quality. This has proven successful and also gives a like-new appearance. Unprotected areas to the left and right show water streaks more readily.

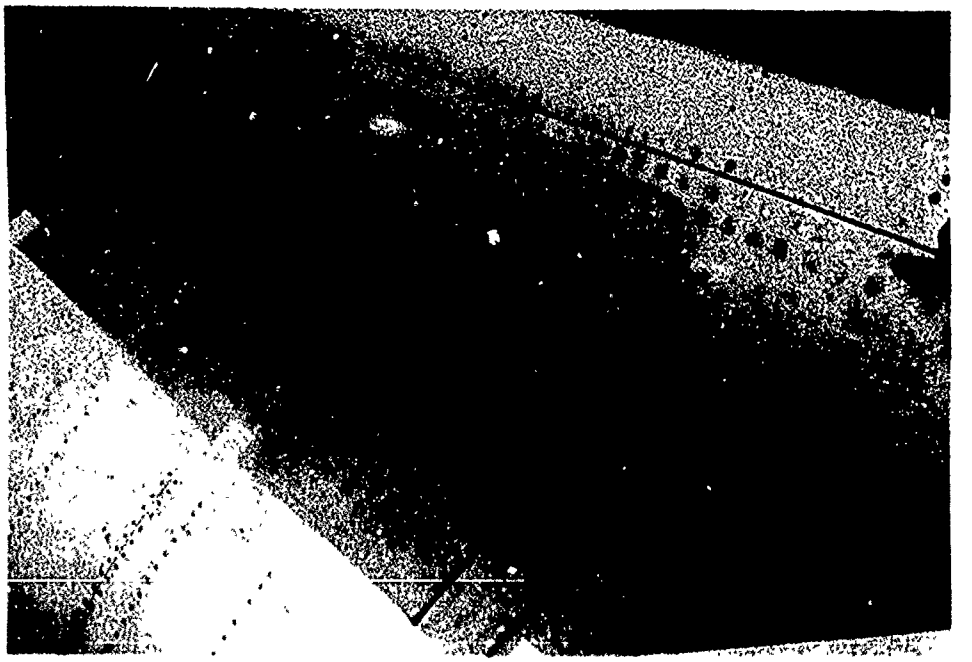

SEALING MATERIAL (black caulking) has been used to fill all seams that would allow water to enter the structure. Steel screws in this engine pylon have been freed of rust and coated with a putty-like material for a tight, waterproof seal.

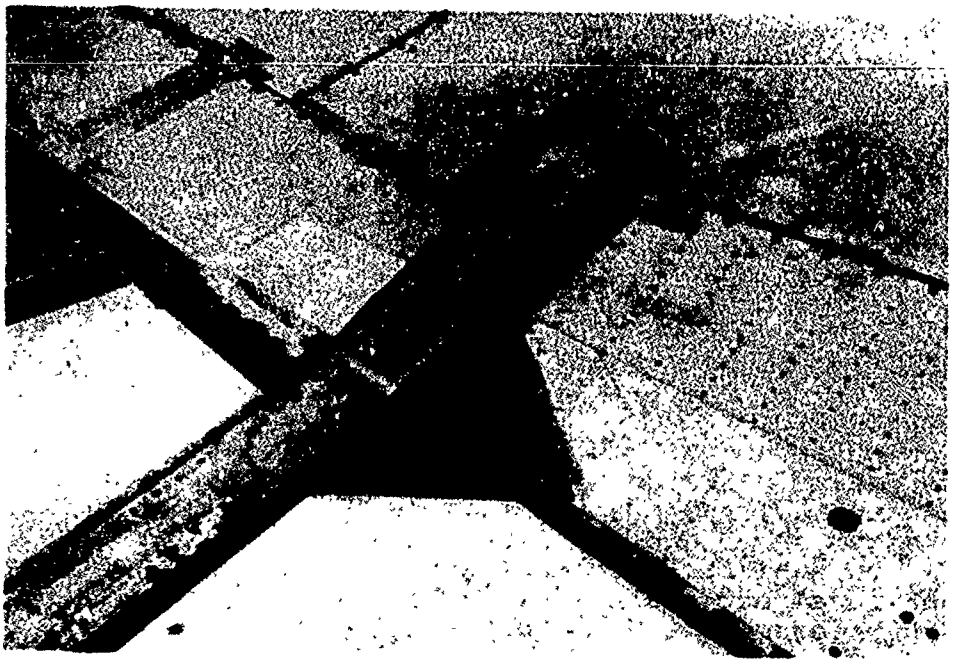

POOLING OF WATER is prevented by this build-up of black sealing compound where an external wing spar stiffener would otherwise prevent water runoff. Note aluminum sealing tape at left which covers the gap between the wing and the landing flap.

MICROENCAPSULATED DNBM QUATERNARY AMMONIUM CORROSION INHIBITORS

L. J. Bailin
Research & Development Division
Lockheed Missile & Space Company, Inc.
Palo Alto, CA 94304-1191

and

V. S. Agarwala
Naval Air Development Center
Warminster, PA 18974-5000

ABSTRACT

The microencapsulation of kilogram quantities of DNBM (dichromate, nitrite, borate, and molybdate) quaternary ammonium corrosion inhibitors for use in anticorrosion primers, paints, and polymers has been performed by spray drying an oil-in-water emulsion of the DNBM in aqueous methyl cellulose. An organosilane, methyltrimethoxy silane, was applied to render the shells impermeable to the solvents in the test formulation during cure. The microcapsules produced were principally in the 5-50 μm particle size range. The capsules contain up to 78% core (payload), and increased levels to 85-90% are expected during scale-up. The inhibitor DNBM was developed to retard corrosion fatigue and stress corrosion cracking, as well as general corrosion, in high strength steels and aluminum alloys. The test results for the materials in varied configurations have been presented.

INTRODUCTION

The catastrophic damage that is caused by environmentally related failures of naval aircraft parts made from high strength steel and aluminum alloy has long been recognized as a major material problem. Several compounds in combination that have been successful in retarding corrosion fatigue and stress corrosion cracking in these materials are described in a recent report on corrosion inhibition of aerospace components in naval environments (1). The inhibitors are abbreviated DMBM, which is an acronym for a dark brown, high viscosity, 100 percent mixture of neat quaternary ammonium

dichromate, nitrite, borate, and molybdate. The functional properties of these compounds are:

a) Inhibition of moisture entry at a crack tip, thereby inhibiting corrosion;
b) Modification of the interfacial chemistry, wherein atomic hydrogen is removed rapidly, thereby impeding its entry into the metal;
c) Creation of a chemical barrier (passive film) at the crack surface; and
d) Maintenance of a uniform pH at the crack tip by means of buffer reactions.

EXPERIMENTAL AND RESULTS

DNBM Materials Development

The D, N, and M inhibitors have been prepared in kilogram quantities by double exchange reactions of a quaternary ammonium methylsulfate with alkali metal dichromate, nitrite, and dimolybdate salts. The borate quaternary was commercially available in development quantities. The choice of the sulfate salt as a starting material rather than the chloride quaternary was based on the desirability to maintain chloride levels as low as possible. A block diagram of the dichromate synthesis is shown in Figure 1.

The current DNBM mixture is prepared by adding equal molar quantities of $Cr_2O_7^{--}$, MoO_4^{--}, NO_2^-, and $B_4O_7^{--}$ as quaternary ammonium salts to aromatic or aliphatic solvents, followed by solvent evaporation in a vacuum oven at 70-80° C. In the presence of toluene, reduction of Cr(VI) to Cr(III) can occur in bright light to form benzoic acid, benzaldehyde, and benzyl alcohol, as detected in the illuminated solution by GC-MS, and is illustrative of the oxidative activity of the dichromate quaternary salt. Of direct consequence to the performance of the inhibitor are the following observations:

a) The salt is insoluble in distilled (ion free) water;
b) The addition of quaternary starting material does not cause any change in solubilization in distilled water; and
c) The addition of aqueous sodium chloride or other water soluble ions causes an orange color, Cr(VI), to appear.

This evidence supports the concept of reversibility of exchange equilibria, as well as the integrity of the quaternary functionality as shown in Figure 1. The probable mechanism for DNBM corrosion inhibition is therefore release of the inorganic inhibitor anions in the presence of seawater, which, under adverse conditions, will make its way to the substrate that is to be protected. In addition to the dissociation reactions, there will form free quaternary ammonium cations that can act as a barrier at aluminum or steel substrates. Non-dissociated DNBM can also serve as a barrier film. Information on the pH of DNBM mixtures in seawater has been reported elsewhere (2).

- **BASIC EXCHANGE EQUILIBRIA**

$$2[CH_3(C_8 - C_{10})_3N \cdot CH_3SO_4] + Na_2Cr_2O_7 \underset{XS\ NaCH_3SO_4}{\overset{XS\ Cr_2O_7^{2-}}{\rightleftharpoons}} \underset{\text{QUATERNARY AMMONIUM DICHROMATE}}{[CH_3(C_8 - C_{10})_3N]_2^+ \cdot Cr_2O_7^{2-}} + 2\,NaCH_3SO_4$$

- **PROCESS**

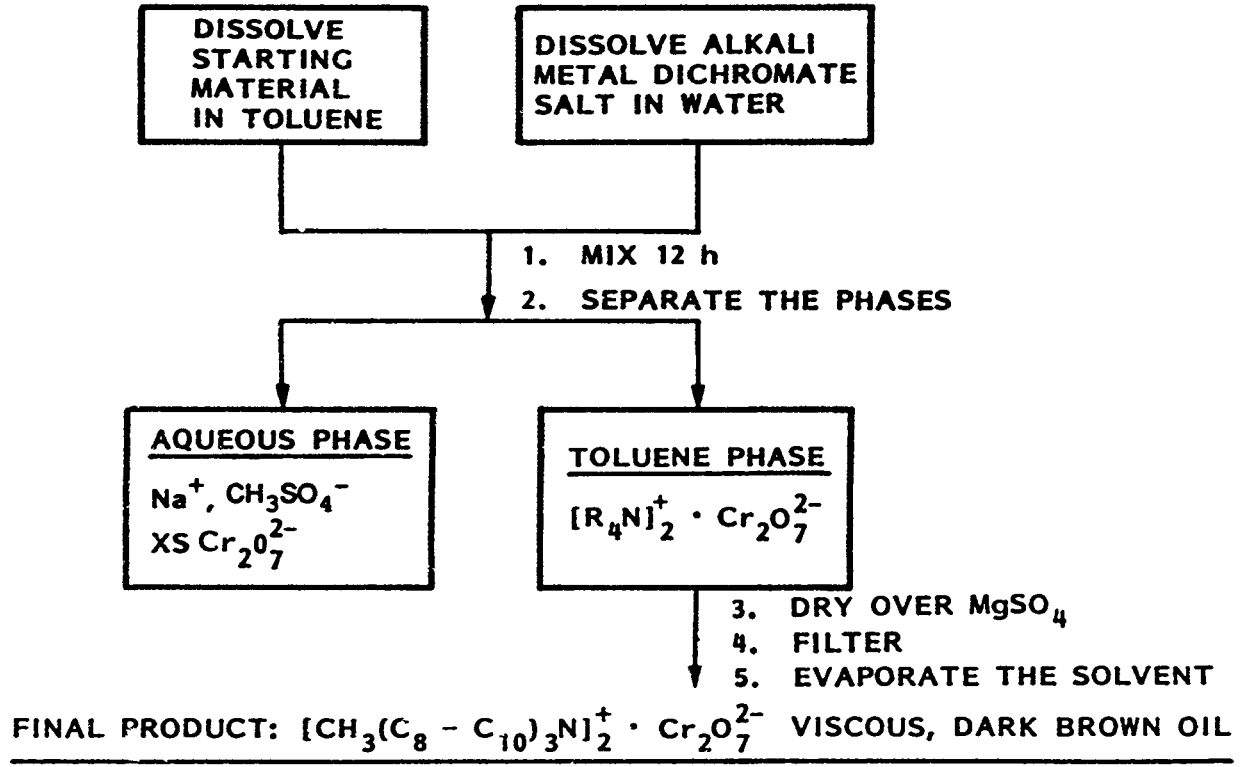

FIGURE 1. SYNTHESIS OF QUATERNARY AMMONIUM DICHROMATE "D"

Packaging of DMBM for Primer Application

The purposes of packaging DNBM into microcapsules are quite specific. The DMBM inhibitor must be prevented from contacting the solvents of the epoxy or other polymer systems with which it is formulated. The DMBM mixture is thereby held in reserve in the primer coat such that when called for, e.g., as the result of environmental effects, the mixture is released into the damaged area. At the same time, the shell of the microcapsule must be sufficiently hydrophilic and susceptible to Cl^- such that when seawater penetrates the primer, the shell will allow passage of salt water, thereby releasing the DNBM inhibitor from the capsules. Since the capsule shell characteristics must be controlled, a shell surface treatment is necessary to accommodate the different penetration/ release rates required of the microcapsules. The criteria used for selection of the microcapsule shell polymers are:

a) Insoluble in coating solvents;
b) Non-reactive with DNBM or coating components;
c) Well-established polymer properties; and
d) Amenable to commercial formulation and production with the DNBM.

The principal solvents that are used in epoxy polyamide coatings, for example, are general solvents. These include methyl ethyl ketone, isopropyl alcohol, isobutyl alcohol, butyl cellosolve, and cellosolve acetate. The MIL-T-81772, Type II (epoxy) diluent contains methyl ethyl ketone, methyl isobutyl ketone, and ethylene glycol monoethyl ether or propylene glycol monomethyl ether. The coating polymers that are insoluble in these solvents and that are also water soluble/dispersible belong to the family of cellulose ethers. Of these, methyl cellulose and hydroxypropyl methylcellulose were the principal test candidates. Polyvinyl alcohols, derived from hydrolyzed polyvinyl acetate, have similar properties and were also included.

Microencapsulation Process

The basic microencapsulation process involves several steps, and are described as follows for the DNBM-cellulose ether system. The initial step is formation of a stable oil-in-water emulsion of DNBM in an aqueous colloidal solution of the cellulose ether. Methyl cellulose is first dissolved in deionized water to form a stable colloidal solution. Next, core material is added, and high shear high speed mixing is applied to disperse the DNBM. It was noted experimentally that excess ionic salt impurities (e.g. chloride, sulfate, acetate, etc.) in the polymer materials, particularly the polyvinyl alcohols, were detrimental to the stability of the emulsions; this was observed when the DNBM mixture, reacting prematurely with the impurities, produced yellow-colored aqueous solutions of Cr(VI) ion with a corresponding loss in stability of the colloid.

The success of the microencapsulation step depended largely on the stability of the micro-emulsion. An example of the emulsification step is given as follows; in this instance, the quaternary ammonium dichromate was used to test the stability of the emulsion in a laboratory run:

To 500 mL of a 5% methyl cellulose colloidal solution, 29% (based on weight of total solids) quaternary ammonium dichromate salt was added. The weight of "D" was 10.0 g. The dispersion was prepared under shear at ~18,000 rpm in a commercial Oster blender. After 10 minute mixing, during which the temperature of the mixture increased to approx. 70° C, the dispersion was centrifuged to separate the foam from the liquid phase. The size of the emulsion particles was between 1 and 20 μm, and remained constant without settling or agglomerating for over four weeks. To prepare large quantities of the emulsion, a Gifford-Wood homogenizer was used to prepare multigallon quantities of DNBM foam-free colloid in which the particle sizes were somewhat larger than that produced in the laboratory unit.

The objective at this juncture was to separate the water layer from the colloid dispersion. Following preliminary coacervation and phase separation experiments, which were only partially successful (cf. Reference 3), spray drying techniques were applied. These were found to provide reproducible results under defined conditions of nozzle size, flow rate, core content, and concentration of the shell polymer. Initially, a laboratory spray dryer was utilized to show feasibility. Following the success of these trials, an Anhydro spray dryer was used to prepare the microcapsules; this is shown in Figure 2. Following a multiplicity of runs, the range of particle sizes obtained was 5-50 μm, with a few capsules as large as 100 μm. In order to compress the range to 20-45 μm for compatibility with current epoxy and polyurethane formulations, air classification will be used for control in future runs. In a recent series from the Anhydro dryer, the following conditions were applied, which are typical of the process:

Nozzle size	0.120 in. (3 mm)
Feed rate	65 g/min
Atomizing air	40 psi
Inlet temperature	190-200° C
Outlet temperature	100-110° C
Yield (recovery)	53%

The microcapsules were examined for their size and roundness by scanning electron microscopy as shown in Figure 3. Their payload was analyzed for chemical content through atomic absorption analysis and compared with the initial Cr and Mo concentrations for the starting DNBM. The results are reported in Table 1. Based on dry weight correction, the average payload of microcapsules was found to be 78.6% DNBM.

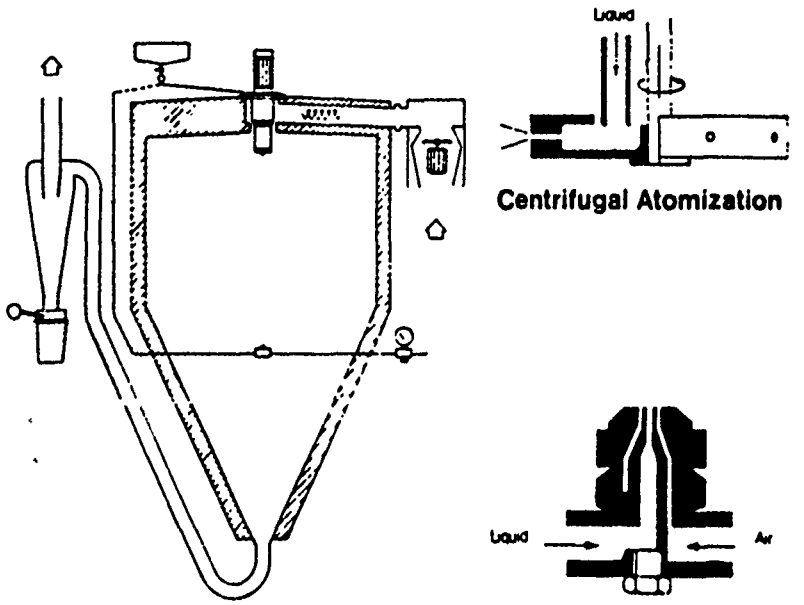

Figure 2. The schematic / flow diagram of Anhydro spray dryer

Table 1. The chemical analysis of microcapsule core for DNBM content (payload)

Sample	%Cr	%Mo	%H2O	Core Load %DNBM (Calc from)
Neet DNBM 11048-29	2.44	4.19	---	----
Microcaps. 8-530	1.76	3.08	7.32	77.8 (Cr data) 79.3 (Mo data)

Microcapsule Surface Treatments

To prevent uncontrolled diffusion of the primer/coating solvents through the methylcellulose shell of the microcapsules during paint formulation, a means to treat the shell surface was developed. Alkoxy silanes were applied by a vapor deposition process. Satisfactory solvent hold-out was achieved when the treated microcapsules were mixed with the epoxy diluent used to formulate commercial MIL-P-23377 epoxy polyamide coatings. The process involves exhausting the silane by means of a low vacuum, 10-100 Torr, through the capsules contained on a stainless steel screen. The liquid silane is contained below the screen in a reservoir, and the excess unreacted silane is trapped in front of the mechanical

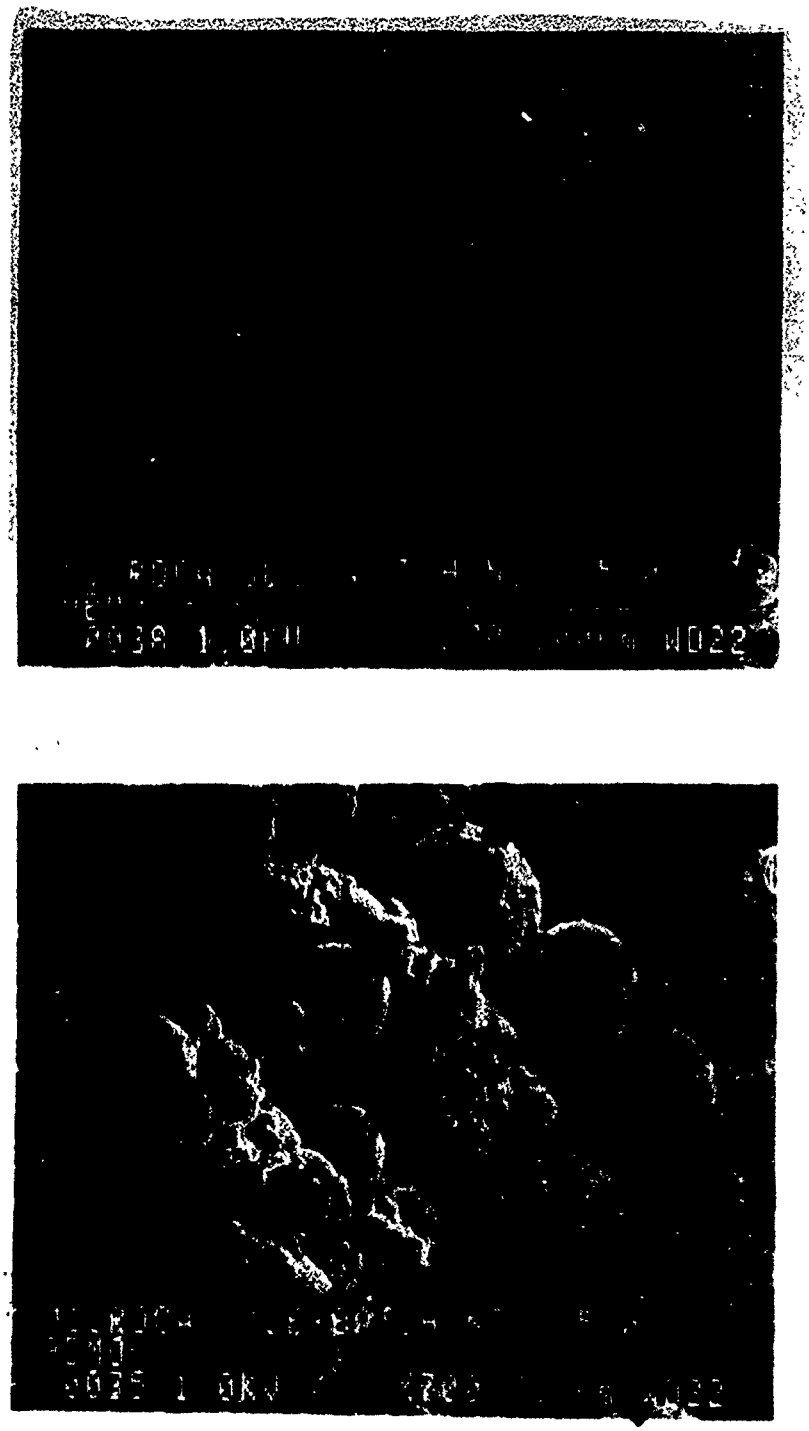

FIGURE 3. SEM PHOTOGRAPHS OF MICROCAPSULES CONTAINING 76% CORE LOAD OF DNBM.

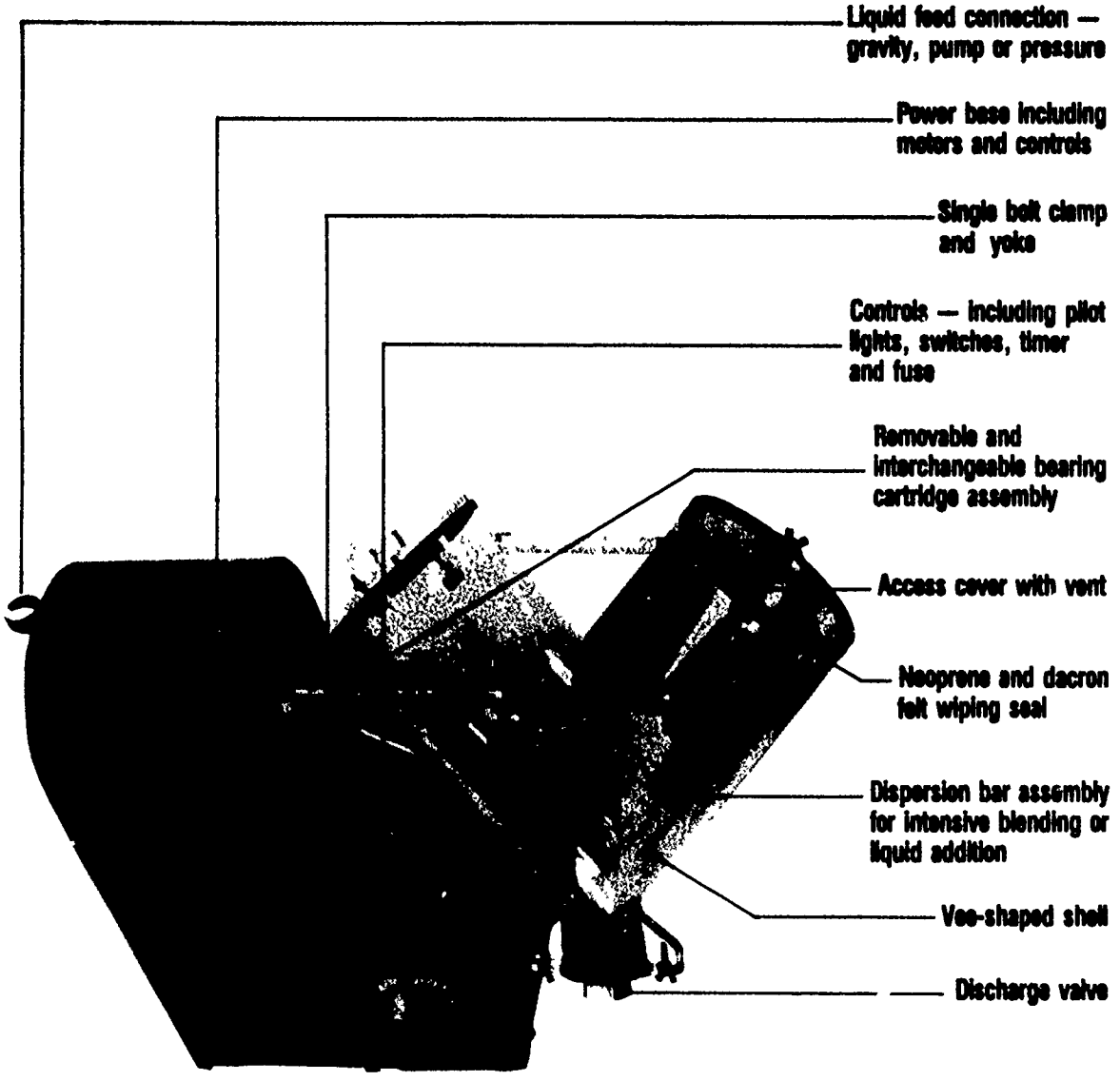

FIGURE 4. TWIN SHELL BLENDER WITH INTENSIFIER BAR FOR MICROCAPSULE SURFACE TREATMENTS

pump using liquid nitrogen. After 2-3 hours of contact in which the silane reacts principally with the absorbed moisture on the surface of the capsules, the reactor is opened to air and allowed to further hydrolyze overnight. The product is then sieved through a 240 mesh screen to break up agglomerates. The principal silanes evaluated were methytrimethoxysilane, hexamethyldisilazane, and trimethylmethoxysilane. Of the series, the first candidate was most successful in achieving a solvent resistant barrier.

The silanized capsules were then used for laboratory preparation and evaluation in the epoxy polyamide coatings. However, because of particle-to-particle contact during the silanization process, which results in incomplete coating of the microcapsules, a series of three separate treatments were required for the laboratory process. A simplified single-stage method was therefore required for use in scale-up. The method that was designed utilizes a twin shell blender (or dual cone blender) that maintains the microcapsules in continuous motion during the silane contact period. The silane is introduced as a gas via an inert gas bubbler through the intensifier bar into the blender which also rotates at a controlled rate, see Figure 4. This is a standard process for treating powders with liquids and gases.

Because of the residual water present on the microcapsules following the spray dry process, the resultant powder is always strongly flocculated. To change the properties of the capsules to a dispersed state, a fumed silica commodity was added. The addition resulted in a significant fluid-like change in flow properties such that the powder will be able to be airclassified efficiently as well as treated uniformly in the twin-shell blender. To test the compatibility of the fumed silica addition, it was determined experimentally that the presence of the silica did not adversely change the reaction of the silane with the microcapsules that contained the SiO_2.

DNBM in Epoxy Polyamide Primer

To establish the effectiveness of DNBM as a general corrosion inhibitor a base-line test was designed using neat DNBM (100%) directly on steel surfaces. The DNBM mixture was spray applied from a solvent solution in toluene onto 1010 steel panels that had been sand blasted to white metal. The calculated weight of DNBM was based on the amount of microcapsules that was designed to take the place, weight for weight, of the strontium chromate in the MIL-P-23377 epoxy polyamide primer. For a 4 in x 6 in x 1/8 in 1010 steel panel, 0.3 - 0.4 g DNBM was deposited directly onto the bare steel surfaces, which was followed after evaporation of the solvent, by deposition of both chromate-free and chromate-containing epoxy layers. A similar quantity of methyl sulfate quaternary (starting material for the DNBM quaternary salts) was also deposited to serve as controls. Clear epoxy

PANEL 74 - 1000 HOURS

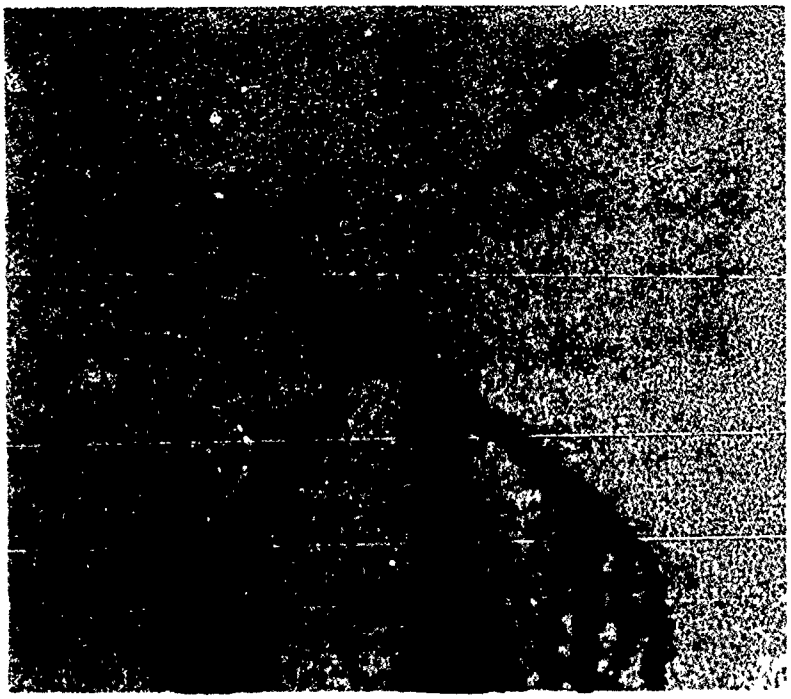

MINUS $SrCrO_4$

PANEL 77 -1000 HOURS

Mil-P-23377

FIGURE 5a. SALT SPRAY EXPOSED PANELS OF 1010 STEEL COATED WITH MULTILAYERS OF DNBM/EPOXY. [Note bleed-through of DNBM unaffected by salt]

PANEL 83 -144H

MINUS $SrCrO_4$

PANEL 85 -72H

Mil-P-23377

FIGURE 5b. SALT SPRAY EXPOSED PANELS OF 1010 STEEL COATED WITH METHYL SULFATE CONTROL QUATERNARY/EPOXY. [Note excessive blistering]

PANEL 88 -24H

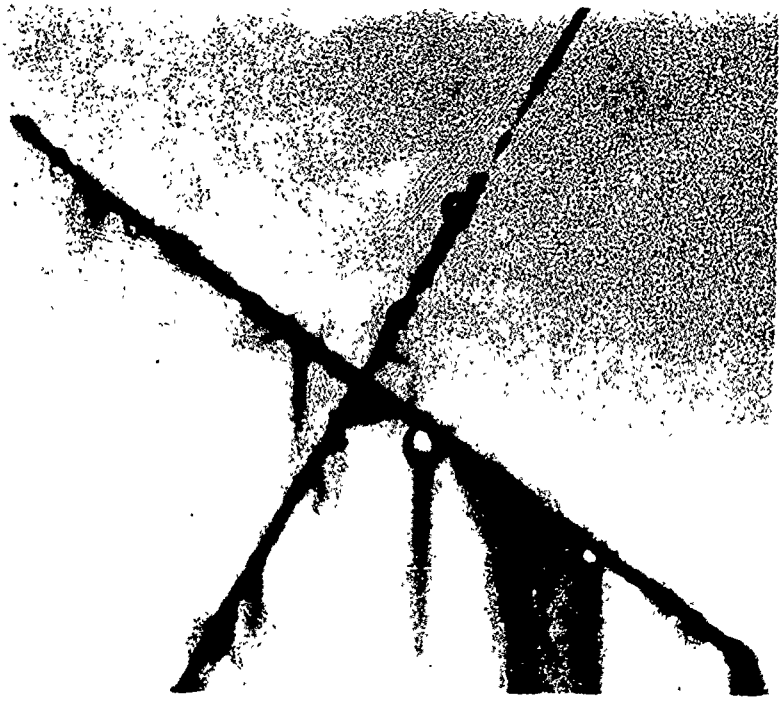

MINUS $SrCrO_4$

PANEL 90 -1000H

Mil-P-23377

FIGURE 5c. SALT SPRAY EXPOSED PANELS OF 1010 STEEL COATED WITH EPOXY AS CONTROL.

was applied last, since some DNBM was observed to have bled-through into the first epoxy layer before cure was complete. Following seven days of room-temperature cure, diagonal scribe lines were drawn on the panels according to ASTM Method D-1654, using a tungsten carbide tip, style E, with 1/64 inch nose radius.

The coatings were exposed to an ASTM Standard B-117 salt spray environment, and the test was run for 1000 hours. Salt spray effects were observed at the scribe lines or within the coatings depending on the formulation and type of inhibitor. Table 2 lists the observed corrosion results. Photographs of the corrosion areas are shown in Figure 5a through 5c. The effects of corrosion inhibition by the DNBM materials are clearly evident.

Table 2. Corrosion Resistance of Multilayer DNBM/Epoxy Coating of 1010 Steel After 1000 Hours of Salt Spray Testing.

Coating Number	Coating System	Time-to-Failure Hours	Mechanism of Corrosion
74 (4)	DNBM/epoxy/Clear (No Cr)	1000	Blisters
77 (3)	DNBM/epoxy/Clear (Includes Cr)	1000	Blisters Lifting
83 (3)	CH_3SO_4 Quat / Epoxy / Clear (No Cr)	144	Excess Small Blisters
85 (2)	CH_3SO_4 Quaternary/ Epoxy /Clear (Includes Cr)	72	Excess Small Blisters
88 (2)	Epoxy /Clear (No Cr)	240	Large Blisters
90 (3)	Epoxy /Clear	1000	Undercutting Lifting

Numbers in parentheses indicate the number of test panels.

Microencapsulated DNBM in Epoxy Polyamide Primer

The first formulations of the microencapsulated DNBM inhibitors were prepared by adding the capsules to mixed Parts A and B of the MIL-P-23377 epoxy polyamide primer. The catalyst remained the same as the standard Part B; however, the Part A contained no strontium chromate but all other fillers, such as titanium dioxide, silica, etc. Because of

the limitations in the method of deposition of the siloxane on the surface of the capsules, which increases the surface area, a maximum of 70% of the replaceable $SrCrO_4$ could be added without exceeding the binder demand of the total pigment content. Thus, 1010 steel panels were coated with this non-$SrCrO_4$ primer but containing 5% microcapsules with two levels of DNBM core loading. In Figures 6 and 7, panels B and C represent the 30% and 55% core load of DNBM in microcapsules, respectively; panels A represent the control, i.e. standard primer with $SrCrO_4$ for comparative evaluation. The panels were tested in the 5% salt spray chamber for up to 36 days. The results can be best described by examining the scribed areas of the test panels shown in Figures 6 and 7 . It can be easily concluded that the severity of corrosion and blistering in the scribe region decreased from Panel A to C, indicating an improvement in the corrosion resistance behavior by the microencapsulated DNBM over the standard primer. Of course, the magnitude of corrosion increased after 36 days of exposure; however, the relative performance did not change. It can be also noted that between Panels B and C an increase in core load with DNBM had improved the corrosion resistance significantly. Thus, it is anticipated that at higher core load, 76% DNBM, the effects may be even more pronounced.

DISCUSSION AND CONCLUSIONS

In an earlier study (4) it was determined that the chemical system DNBM exhibited nearly eight fold increase in the corrosion fatigue or stress corrosion cracking life of a high strength 4340 steel in high humidity (moist) chloride environments. The DNBM is a liquid mixture of quaternary ammonium complexes of dichromate, nitrite, borate and molybdate in an aprotic solvent. In this phase they have performed synergistically and effectively as corrosion inhibitors and crack arrestment compounds. For their application in coatings, the DNBM was packaged into microcapsules so that its multifunctional properties were preserved, and at the same time, are available whenever required to provide protection. Thus, a method was developed to microencapsulate the DNBM for formulation in primers or paints. Methyl cellulose was used as a polymer and alkoxy silane as post treatment to protect the outer shell of the capsules. Specifically, the purpose of microencapsulation was to protect the DNBM from contact with the solvents and uncured polymers of the epoxy system. In microcapsules, the DNBM mixture would be held in reserve in the primer coat until required due to environmental and service damages. The shell of the capsule is held sufficiently hydrophilic so that when seawater seeps through the primer or cracks, the walls of the microcapsule could release the DNBM inhibitor. To date, capsules of 5-50 μm have been successfully fabricated with nearly 78% DNBM core load. The painted panels of steel

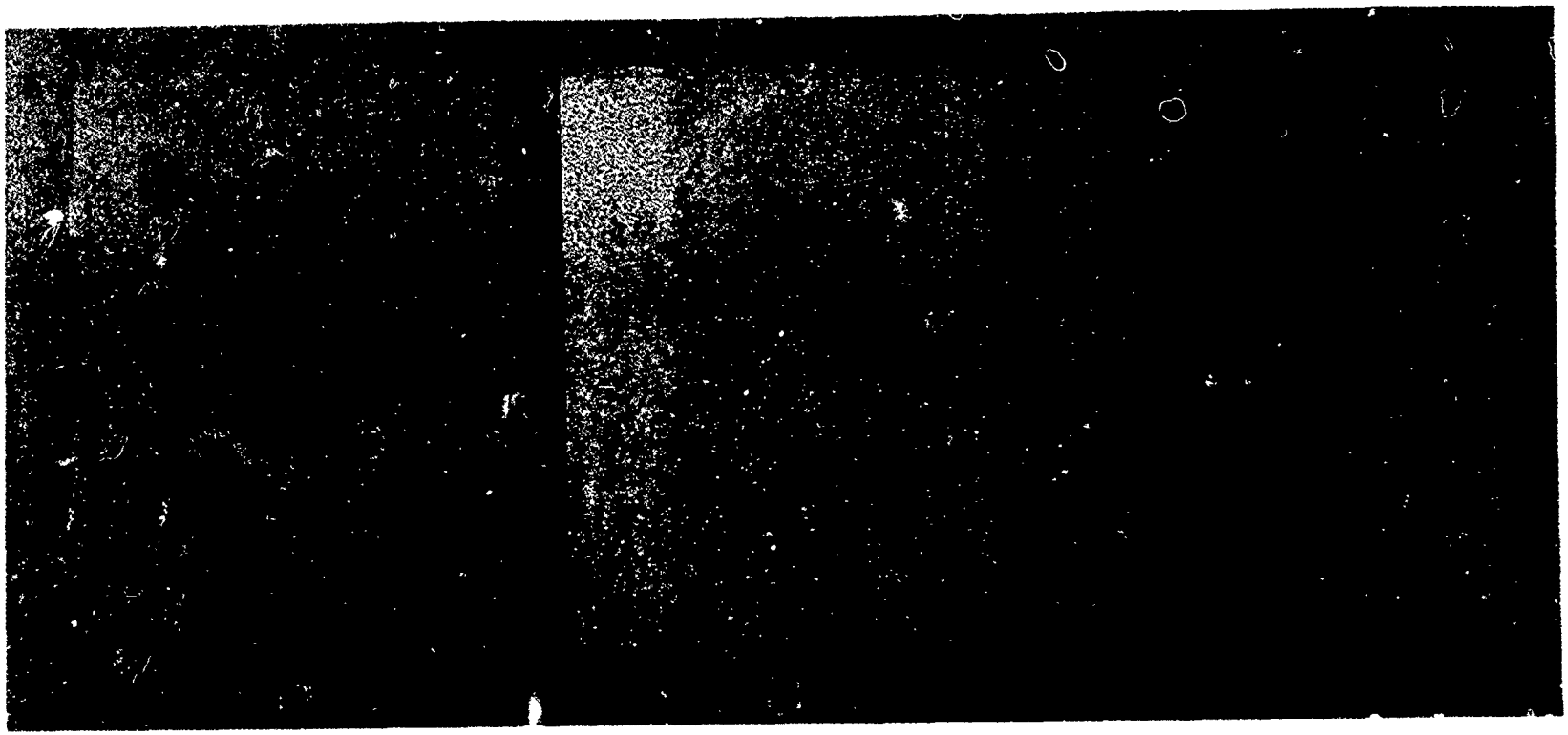

FIGURE 6. PHOTOGRAPHS OF 15 DAY EXPOSED STEEL PANELS COATED WITH STANDARD PRIMER: (A) CONTROL, WITH $SrCrO_4$; THE PRIMER ON PANELS (B) AND (C) CONTAIN NO $SrCrO_4$ BUT 5% MICROCAPSULES CONTAINING DNBM AT 30% AND 55% CORE LOAD, RESPECTIVELY.

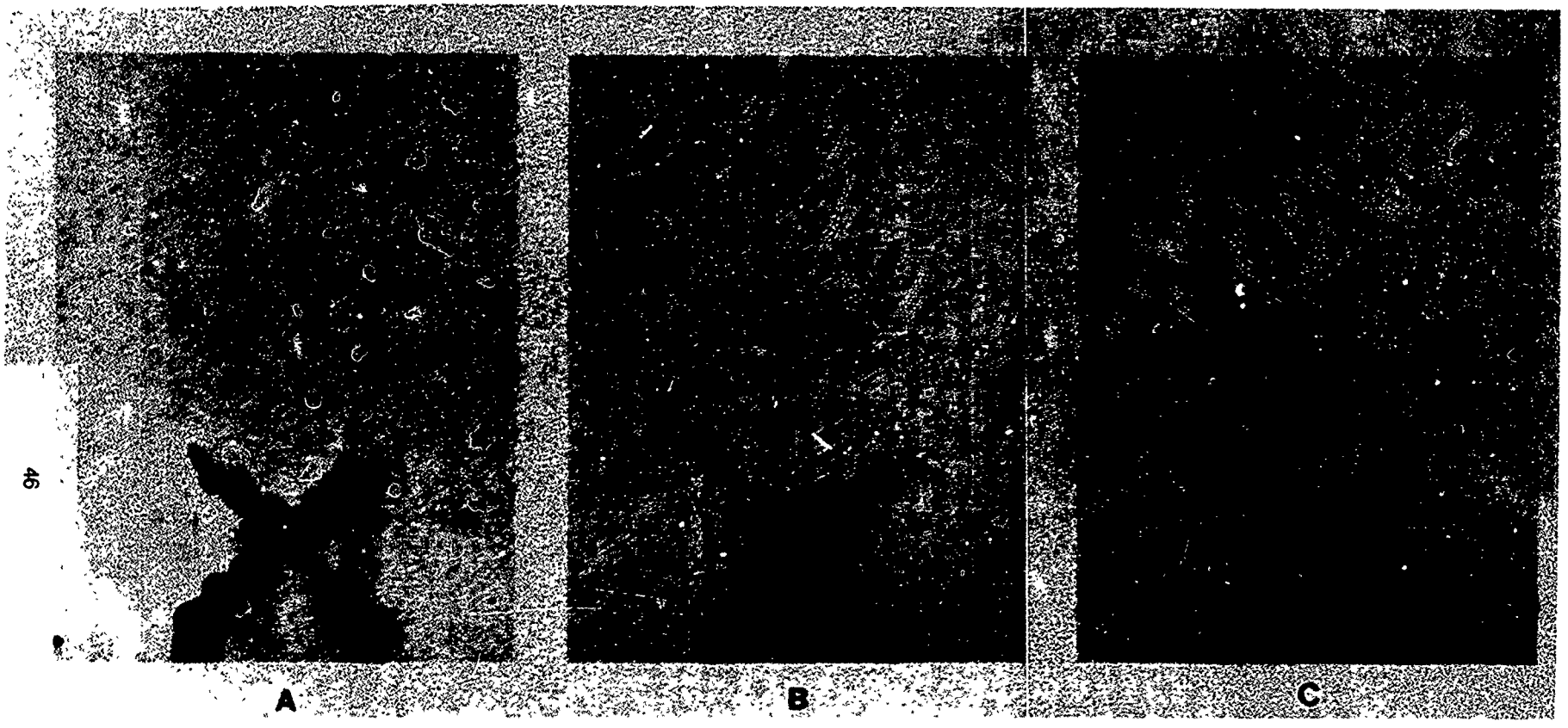

FIGURE 7. PHOTOGRAPHS OF 36 DAY EXPOSED STEEL PANELS COATED WITH STANDARD PRIMER: (A) CONTROL, WITH $SrCrO_4$; THE PRIMER ON PANELS (B) AND (C) CONTAIN NO $SrCrO_4$ BUT 5% MICROCAPSULES CONTAINING DNBM AT 30% AND 55% CORE LOAD, RESPECTIVELY.

with less than 5% of microcapsules (with DNBM) in primer were tested in 5% salt spray chamber for up to 36 days. Their corrosion resistance was superior to that of the standard MIL-P-23377 primer with $SrCrO_4$.

The basic mechanism by which DNBM inhibits corrosion and cracking is that it releases the inorganic (inhibitor) anions in the presence of sea-water, which, under adverse service conditions, will make its way through the coating to the metal substrate that is to be protected. The solvent in the DNBM quaternary complexes serves as a wetting agent and carrier of inhibitor ions, thus enhancing their mobility to reach highly restricted geometries such as fine cracks or crevices.

On-going formulation and salt spray tests include primers that contain fumed silica silane-treated microcapsules and those that are not silica treated. These tests are being performed currently at both Lockheed, Palo Alto, and the Naval Air Development Center. Efforts are under way to up-scale the fabrication of microcapsules to about 25 pounds by 1990.

ACKNOWLEDGMENT

This work has been supported by Materials Block Program of the Naval Air Development Center and the Office of Naval Technology. The authors appreciate the interests of Dr. John J. De Luccia and Mr. Irving S. Shaffer.

REFERENCES

1. Agarwala, V. S.,"Multipurpose Corrosion Inhibitors for Aerospace Materials in Naval Environments", Naval Air Development Center Report, NADC-87034-60, June 1987.

2. Bailin, L. J. and Agarwala,V. S.,"Development of Micro-Encapsulated DNBM Quaternary Ammonium Inhibitors for Paints", Tri-Service Conference on Corrosion, U.S. Air Force Academy, Colorado Springs, CO, AFWAL-TR-87-4139, Vol. II, 111-27, May 1987.

3. Patwardhan, S. A. and Das, K. G.,"Microencapsulation," Ch.5, in Controlled Release Technology, ed. K. G. Das, Wiley-Interscience, 1983.

4. Agarwala, V. S.,"Modification of Crack-Tip Chemistry to Inhibit Corrosion and Stress Corrosion Cracking in High Strength Alloys," in Embrittlement by the Localized Crack Environment, R.P. Gangloff, Ed., AIME Publication, pp.405-519, 1984.

USE OF PLASTIC MEDIA BLAST (PMB) ON COMPOSITE SURFACES

Presented at U. S. Department of Defense
Tri-Service Corrosion Conference
Atlantic City, New Jersey, 17-19 Oct 1989

Robert Pauli
President
Pauli & Griffin Company
907 Cotting Lane
Vacaville, California 95688

and

Charles Owens
United Airlines (retired)
28 Spinnaker Place
Redwood City, California 94065

ABSTRACT
Conventional paint strippers cannot be used on composite surfaces without damage to the substrate. Current practice is the use of hand sanding for paint removal from these surfaces. Plastic Media Blast (PMB) offers a more economical means of paint removal. In this paper, it is our intent to provide data supporting PMB as a viable process for paint removal from composite surfaces. The PMB process eliminates health hazards associated with chemical stripping and reduces hazardous waste. Plastic media dust is classified as a hazardous waste only if the paint system being removed contains sufficient quantities of hazardous ingredients

PMB applications for composites is based solely on economic justification. Methylene chloride, the major ingredient in chemical strippers, attacks the resin binder and gel coats used in composites. Current airframe manufacturer recommendations only approve hand sanding for paint removal from composite surfaces. Hand sanding is a laborious, time consuming process that in itself can also damage the substrate. Airline technical process people can confirm considerable substrate damage resulting from their use of hand sanding.

It is extremely difficult to equate economic advantages due to variance in processing requirements and basic pay rate. However, estimates of reduced man hours should enable any interested facility to calculate their own savings. Examples cited below are taken from AVIATION EQUIPMENT MAINTENANCE (ref. #1) and unpublished United Airlines data (ref. #2). CFMI authorized an evaluation of plastic media blasting to strip CFM56 spinner cone. The General Electric representative examined the test cones and granted final approval to United Airlines to strip these cones using PMB. PMB takes about 25 minutes as opposed to the 3 to 3.5 man hours for chemical stripping. A scrap B-747 wing panel was used to simulate PMB stripping. Polyurethane topcoat removed from a one-square foot area without removing the black conductive coating. In one test area, the conductive paint removed to expose the fiberglass surface. A circular test disc of fiberglass was removed ,exposing honeycomb substrate. Under 40X magnification, small craters were observed where plastic media impinged on the fiberglass, but damage was far less than usually experienced when hand sanding. (The fact that PMB is less damaging than hand sanding is further supported by references #11 & 12.) Recommended policy is removal of polyurethane topcoat only, leaving black conductive coating intact. Estimated man hour savings for PMB versus hand sanding is 75 man hours per B-747 rudder. One side of a B-737 rudder was test stripped using PMB.

Using PolyPlus 30-40 at 48 psig nozzle pressure, three foot standoff distance and 75 degree nozzle angle to the surface, one side of the rudder was completely stripped in about 35 minutes. Surface completely acceptable for reapplication of conductive coating and polyurethane paint system. Use of PMB versus hand sanding saved approximately 34 man hours per B-737 rudder.

A graphite/epoxy composite section, as supplied by Boeing with a 1-mil bondable interior Tedlar coating, was test stripped. PolyPlus 30-40 at 47 psig nozzle pressure (3 feet distance at 75 degrees) removed the Tedlar film. A circular disc, exposing the honeycomb substrate, was examined under 40X magnification. Voids noted were believed to be present in new composite. A very few broken fibers were also noted, but damage is far less than from sanding. PMB used to remove the exterior topcoat paint, leaving primer to assure that the graphite/epoxy substrate is undamaged. Based on test work with the B-747 wing panel, the B-737 rudder, and the graphite/epoxy test panel, United Airlines estimated that an annual savings of over $125,000 could be realized by using PMB processing in lieu of hand sanding of composite surfaces. This was a rough estimate based on work done in 1985. Current estimates may well alter these figures, but the U.S. dollar savings will be greater, not less.

U.S. Naval Air Rework Facility (NARF) Alameda, California, (ref. #3) states that PMB can be used on epoxy cast fiberglass/laminate composites, polyester fiberglass laminates, and graphite/epoxy composites without damaging the surface. Work done at Alameda (ref. #4) on painted graphite/epoxy panels used PolyPlus and PolyExtra 20/30 at 40 psig nozzle pressure. Paint coatings easily removed by both media. PolyExtra yielded a smoother finish. Microscopic examination of stripped graphite/epoxy surface indicated only superficial isolated surface graphite fiber breakage. It was uncertain if this fiber breakage was due to PMB or defects already present. Fiber breakage was so minor that no significant loss of mechanical strength would be realized.

Further testing at NARF North Island, California, (ref. #5) supported the conclusion that PolyExtra is the preferred material for paint/primer removal from graphite/epoxy substrates. Overall mechanical effects were insignificant. Interlaminate shear (ILS) and flexural bending tests, which evaluate interply strength and maximum fiber strain respectively, were run. Specimens were loaded with affected surfaces in tension and in compression. Comparison of ILS strength indicated less than 7% difference in strength values between controls (12 specimens) and test (24 specimens). PMB paint stripping exhibited varying degrees of surface damage, depending upon media hardness and dwell time. Test specimens evaluated for mechanical properties indicate no significant changes in mechanical values, even though in some cases surface deterioration occurred in the first ply of the graphite/epoxy. Damage to the epoxy surface would be minimized if there were no requirement to strip past the primer layer.

Boeing Commercial Airplane Company (ref. #6) states that PMB, under select operating conditions, can efficiently strip protective coatings from fiberglass, graphite and Kevlar substrates without sustaining fiber breakout or visible surface damage. Media recommended is PolyExtra 30/40 at 30 psig nozzle pressure using 1/4 inch nozzle, 45 degree incidence angle, and 4 to 12 inches nozzle distance from substrate. Boeing Vertol (ref. #7) states that the paint can be removed from fiberglass without damage, if their standard procedures are enforced. Media is applied at a 60 degree impingement angle at 30 inches from substrate. Additionally, honeycomb panels (fiberglass and aluminum outer skins) showed no evidence of delamination after PMB.

NARF Cherry Point, North Carolina, (ref. #8), using PolyPlus 30/40 at 20-40 psig nozzle pressure, saw no evidence of delamination and very little disturbance of the epoxy matrix for graphite/epoxy composites. Examination of composite structure revealed very few, very small areas of fiber exposure and occasional broken fiber. These incidences were considered minimal and not as extensive as with hand sanding.

Graphite/epoxy test panels were PMB stripped of polyurethane top coat and epoxy primer by Pauli & Griffin for the U.S. Air Force Wright Aeronautical Laboratories at Wright-Patterson Air Force Base using various mesh sizes of PolyExtra, PolyPlus and Type III media (ref. #9). For summary of test results see summary sheet Exhibit A. Test panels were examined both visually and using scanning electron microscope (SEM) with photomicrographs taken of each test area. Breakthrough or removal of gel coat is considered damaging. Note that on Panels 3, 4, 6, 7, 8, 11 & 12, topcoat removed without completely removing the primer or damaging the substrate. Panel #1 shows complete paint removal without damage in spite of a 10 minute dwell time; panel #2 acceptable with only slight breakthrough of gel coat. Appendix A consists of 7 pages of photomicrographs corresponding to summary Exhibit A.

Data covered in the preceding paragraph was partially the basis for the Air Force Wright Aeronautical Laboratories (AFWAL) Letter of June 2, 1988, to the FAA (ref. #10). In their opinion, research has shown that surface of a composite panel may be left intact during a PMB paint removal process providing excessive pressures, long dwell times, and close standoff distances are not used. Typical safe parmeters (after microscopic examination and nondestructive inspection) are: 90 degree angle, 12-18 inch standoff distance, 30 psi, 3.5 mohs hardness media, 30/40 mesh media. Other sets of parameters are being investigated.

The Systems Support Division of the Materials Laboratory (AFWAL/MLSE), Wright-Patterson AFB, conducted three studies in 1988 to investigate using PMB to remove polyurethane paint (MIL-C-83286) from graphite/epoxy composites (ref. #11). Nondestructive evaluation (NDE) and mechanical testing were performed on stripped and baseline test panels. In no case did NDE show any non-visible damage caused by the PMB process. On comparing the effects of "hand" sanding to PMB, "hand" sanding was found to cause severe degradations in tensile strength. Damage levels were visible to the naked eye. Using 3.0 mohs hardness media and various PMB parameters, tensile and interlaminar shear tests showed no degradation caused by the PMB process. On the average, no harmful effects from PMB were discovered when investigating the effects of nine separate sets of PMB parameters on unidirectional graphite/epoxy. An important criteria is using the primer coast as a "flag". This technique limits dwell time of the blast pattern on any one area of the test panel and thereby reduces chances for damage. Based on their tests, AFWAL/MLSE recommended to HQ Air Force Logistics Command that PMB be approved for use on composites providing: "primer as flag" criteria is used in all operations; System Program Managers for each aircraft also approve the process.

The Naval Air Development Center (NADC) assessed the microstructure of unidirectional graphite/epoxy laminates after paint removal with plastic media blasting (PMB) (ref. #12). Five independent process variables were investigated: media material, media size, nozzle pressure, angle of attack and standoff distance. Any damage to the microstructure was evaluated using ultrasonics, optical microscopy and scanning electron microscopy. Conclusions are:

1. One cycle PMB paint removal can be performed on graphite/epoxy with only minor surface abrasion to the resin. This was demonstrated with a variety of process conditions using both polyester (Type I) and urea formaldehyde (Type II) media.
2. Type I media caused less damage to graphite/epoxy microstructure than the Type II media. Increasing the dwell time to five times the coating removal duration caused severe damage with the Type II media. Little change in the microstructure was seen after extended dwell exposure with the Type I media. This indicates that the Type I media is less sensitive to operator error than the Type II media.
3. All of the Phase I PMB process conditions that were investigated resulted in a surface erosion effect on the graphite/epoxy materials without causing subsurface damage. Paint removal on panels that were hand sanded was non-uniform. The samples had areas of complete coating removal and other areas with primer remaining. Extensive fiber damage resulted and release ply pattern was no longer visual.

4. Minor surface damage was observed in the composite materials after four paint/blast cycles. One condition was found to cause only resin abrasion and no fiber abrasion damage after four paint/blast cycles. However, the use of both Type I and Type II media caused small surface cracks in the resin after four paint/blast cycles. These cracks did not extend past the resin rich surface of the composite. In fact, less damage was caused to the substrate than by hand sanding a single time.
5. Little difference was seen between AS4/3501-6 and IM6/3501-6 graphite/epoxy composite materials. Other materials may be more susceptible to damage. For instance, bismaleimide resins used for higher temperature applications have lower fracture toughness properties and may require less aggressive blast conditions.

CONCLUSIONS

In the past four years considerable testing and actual application of PMB processing have been accomplished. Although reports do exist disclaiming the advantages of PMB, we believe that the preceding data is more than adequate to establish that PMB is both an economic and viable tool for stripping paint from composites. Pauli & Griffin Company is striving to become a leading depository of technical information on PMB. We will gladly furnish you with a copy of the references cited herein and assist you in your confirmation of the economic benefit of PMB for stripping composites. Please remember that only adequately trained personnel should use PMB on composites or damage can and will result. With our equipment, we have available a training package to assure that your people can successfully do the job.

REFERENCES

1. STRIPPED CLEAN AND DRY, Karl D. Forth, Associate Editor, Aviation Equipment Maintenance, October 1985 Issue.
2. Work done by Charles E. Owens, Staff Engineer, United Airlines, before his retirement May 1, 1986. Present contact for information on PMB applications on composites is: Tony Seidl, Staff Technician, Components Engineering, telephone 415/876-3160 or telex SFOEGUA.
3. NARF Alameda Laboratory Report #286-016, PLASTIC MEDIA BLASTING.
4. NARF Alameda Memorandum, Progress Report No. 2 on PLASTIC BLASTING MEDIA, March 22, 1984.
5. NARF North Island PRELIMINARY REPORT ON PLASTIC MEDIA PAINT STRIPPING FROM GRAPHITE/EPOXY SURFACES, March 19, 1984.
6. Boeing Manufacturing Development Report #6-35081, COMPOSITE PAINT STRIPPING DEVELOPMENT, MAY 1985.
7. AM TECH '87 Presentation, Dallas, Texas, March 1987, by Bruce Thompson, Boeing Vertol. (Verbal presentation; not published.)
8. NARF Cherry Point Materials Engineering Division Laboratory Report No. 2218-86, October 31, 1986.
9. Pauli & Griffin Company paper. Acknowledgement given to Russ Wong, Metallurgist, United Airlines, for assistance in reviewing test panels prior to submission to Wright-Patterson AFB and to 1st Lt. Butkus of Wright-Patterson AFB for final evaluation.
10. Letter from U.S. Air Force Wright Aeronautical Laboratories (AFSC), Wright-Patterson Air Force Base, Ohio, to FAA, Aircraft Engineering Division, Airworthiness Staff (AWS-103), Washington, D.C. dated 2 June 1988.
11. PMB PAINT REMOVAL FROM COMPOSITE MATERIALS, 1st Lt. Larry Butkus, AFWAL/MSLE, Wright-Patterson Air Force Base, presented at DOD/Industry Coatings Removal Conference, Ft. Walton Beach, FL, April 11-13, 1989.
12. MICROSTRUCTURAL EFFECTS OF PLASTIC MEDIA BLASTING ON GRAPHITE/EPOXY COMPOSITES, Joseph Kozol, Steven Thoman and Kenneth Clark, Naval Air Development Center, SAE Paper #890928, presented at the 25th Annual Aerospace & Airline Plating & Metal Finishing Forum, New Orleans, LA, March 27-30, 1989.

EXHIBIT A

Graphite Epoxy Panel Testing for 1st Lt. Butkus
U.S. Air Force Wright Aeronautical Laboratories
November 1987
SUMMARY OF PARAMETERS
PMB machine used: Pauli & Griffin PRAM 31 Cabinet
Nozzle used: Pauli & Griffin PTX 1/4" venturi
Panel size: 20 square inches

Exh.A Photo#	Media	Nozz. Angle	Nozz. Dist.	Nozz. Press.	Dwell Time		AFWAL/ML Findings (verbatim)
1.	PolyExtra 30-40	60-80°	12-18"	25 psi	10 min	*1	No visible damage; no damage shown on SEM
2.	PolyExtra 30-40	45°	12-18"	40 psi	2 min	*2	No visible damage; slight breakthrough of "gel coat" on SEM
3.	PolyExtra 30-40	45°	18"	25 psi	2 min	*3	Primer intact visibly and on SEM. No visible damage
4.	PolyExtra 20-40	30°	18"	40 psi	2 min	*4	Same as # 3
5.	PolyPlus 30-40	30-90°	12-18"	20 psi	2 min	5	Faint 'gel coat' pattern remaining. Examination under visible and SEM show almost total lack of gel coat. Damage to surface is apparent
6.	PolyPlus 30-40	45°	12"	20 psi	1 min	*6	Primer and some paint remaining: no visible damage
7.	PolyPlus 40-60	30°	18"	40 psi	1 min	*7	Same as # 3
8.	PolyPlus 40-60	60°	18"	25 psi	1 min	*8	Same as # 3
9.	Type III 20-40	45°	18"	20 psi	1 min	9	Same as # 5
10.	Type III 20-40	30°	18"	40 psi	1 min	10	Same as # 5
11.	Type III 20-40	60°	12"	20 psi	1 min	*11	Primer and some paint remaining. No visible damage
12.	Type III 30-40	30°	18"	40 psi	1 min	*12	Primer generally intact: no visible damage
13.	Type III 20-40	45°	18"	50 psi	20 Sec	13	Extreme damage (total gel coat erosion) visible and SEM
14.	Type III 20-40	45°	18"	60 psi	20 Sec	14	Same as #13

*** NO HARM TO SUBSTRATE**

APPENDIX A - Photomicrographs of U.S. Air Force graphite epoxy panels after dry paint stripping with plastic media blast (PMB) using a Pauli & Griffin PRAM 31 Cabinet PMB system. Photomicrographs and scanning electron microscope analysis by the U.S. Air Force Wright Aeronautical Laboratories (AFWAL), Wright Patterson Air Force Base, Ohio, November 1987.

P&G/AFWAL #1

P&G/AFWAL #1

P&G/AFWAL #2

P&G/AFWAL #2

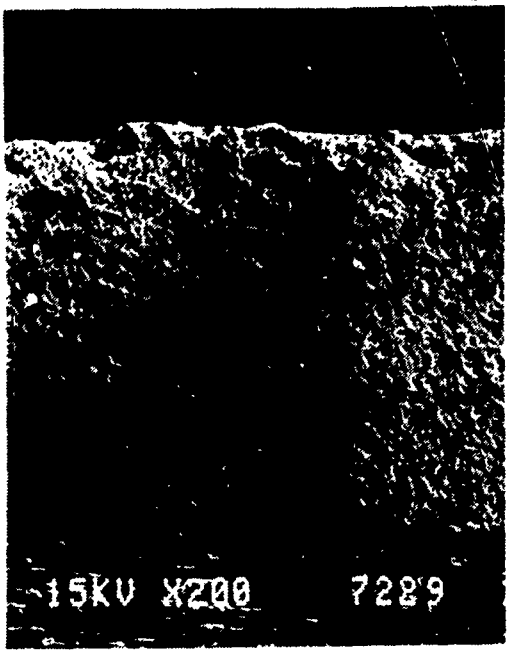

APPENDIX A - Photomicrographs of U.S. Air Force graphite epoxy panels after dry paint stripping with plastic media blast (PMB) using a Pauli & Griffin PRAM 31 Cabinet PMB system. Photomicrographs and scanning electron microscope analysis by the U.S. Air Force Wright Aeronautical Laboratories (AFWAL), Wright Patterson Air Force Base, Ohio, November 1987.

P&G /AFWAL # 3

P&G /AFWAL # 3

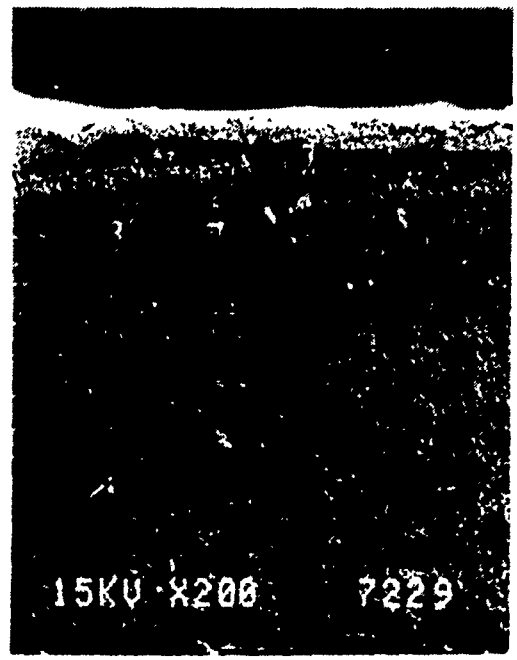

P&G /AFWAL # 4

P&G /AFWAL # 4

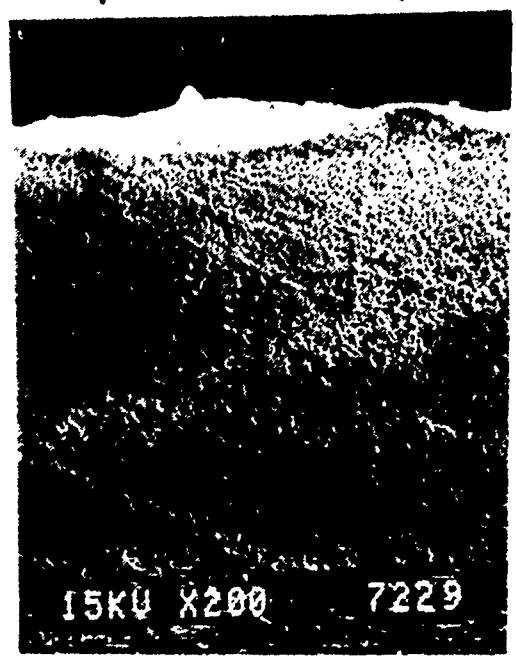

APPENDIX A - Photomicrographs of U.S. Air Force graphite epoxy panels after dry paint stripping with plastic media blast (PMB) using a Pauli & Griffin PRAM 31 Cabinet PMB system. Photomicrographs and scanning electron microscope analysis by the U.S. Air Force Wright Aeronautical Laboratories (AFWAL), Wright Patterson Air Force Base, Ohio, November 1987.

P&G / AFWAL #5

P&G / AFWAL #5

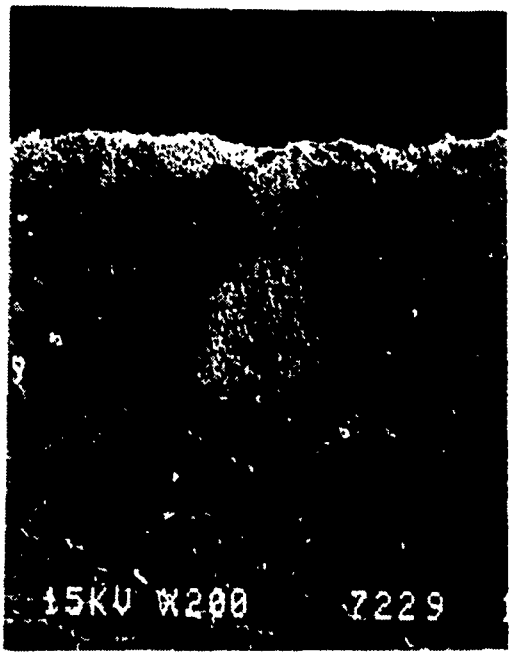

P&G / AFWAL #6

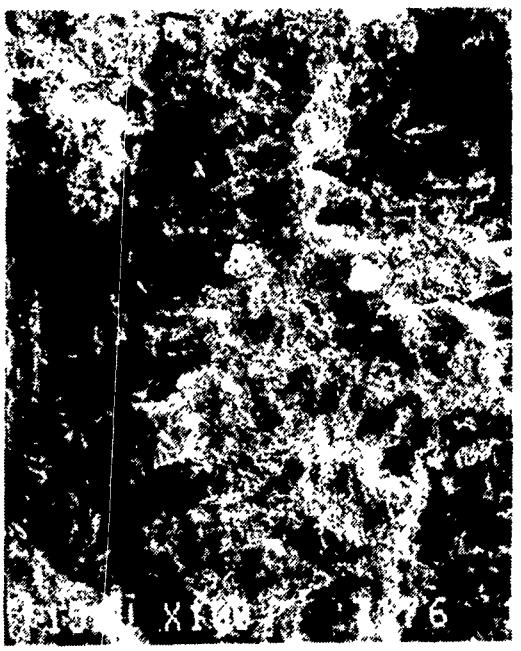

P&G / AFWAL #6

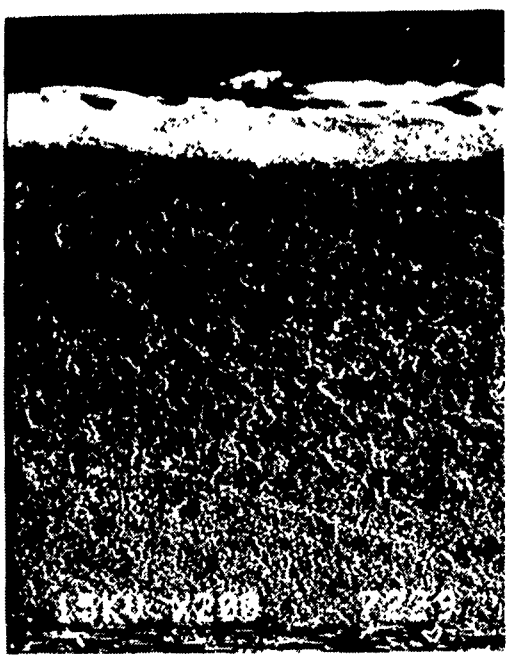

APPENDIX A - Photomicrographs of U.S. Air Force graphite epoxy panels after dry paint stripping with plastic media blast (PMB) using a Pauli & Griffin PRAM 31 Cabinet PMB system. Photomicrographs and scanning electron microscope analysis by the U.S. Air Force Wright Aeronautical Laboratories (AFWAL), Wright Patterson Air Force Base, Ohio, November 1987.

P&G / AFWAL #7

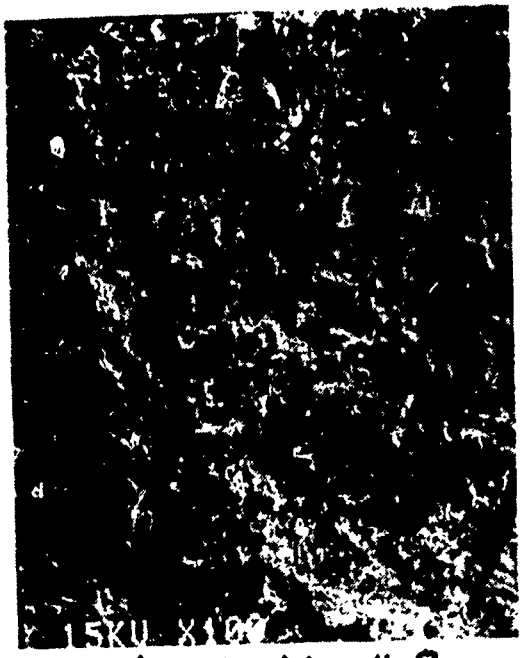

P&G / AFWAL #7

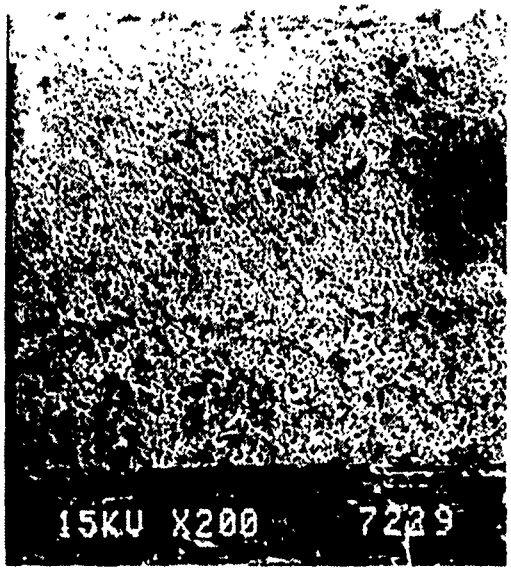

P&G / AFWAL #8

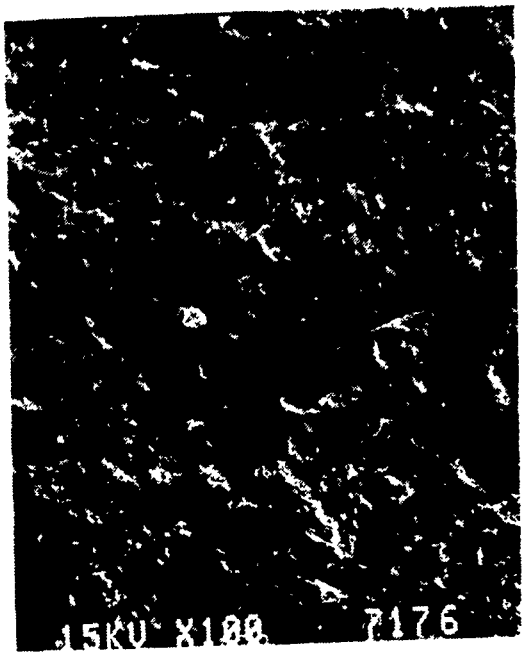

P&G / AFWAL #8

APPENDIX A - Photomicrographs of U.S. Air Force graphite epoxy panels after dry paint stripping with plastic media blast (PMB) using a Pauli & Griffin PRAM 31 Cabinet PMB system. Photomicrographs and scanning electron microscope analysis by the U.S. Air Force Wright Aeronautical Laboratories (AFWAL), Wright Patterson Air Force Base, Ohio, November 1987.

P&G / AFWAL #9

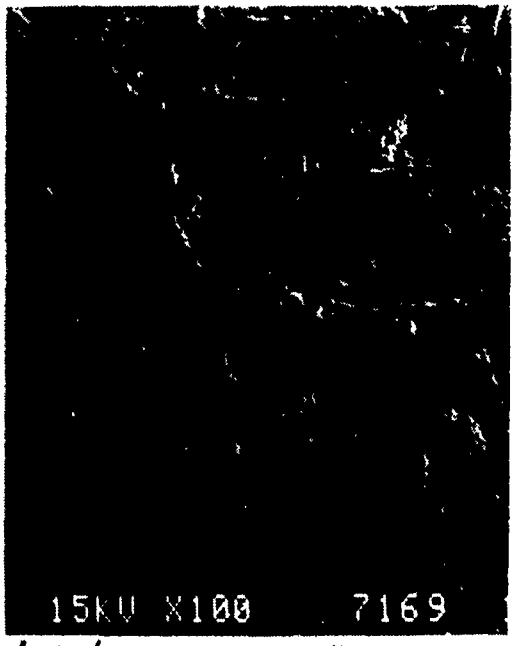

P&G / AFWAL #9

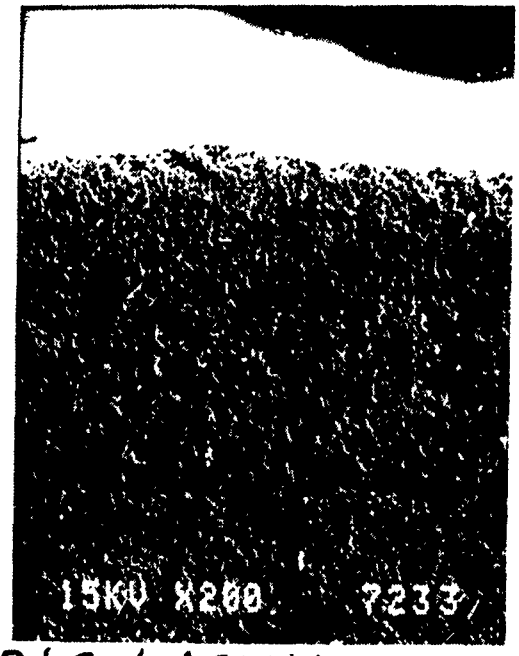

P&G / AFWAL #10

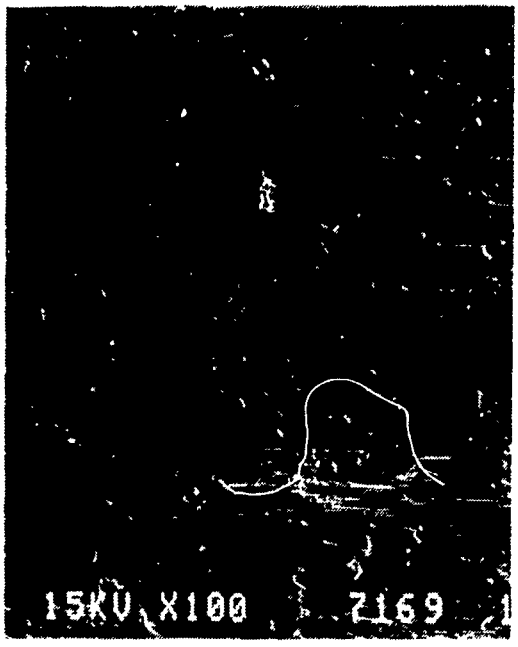

P&G / AFWAL #10

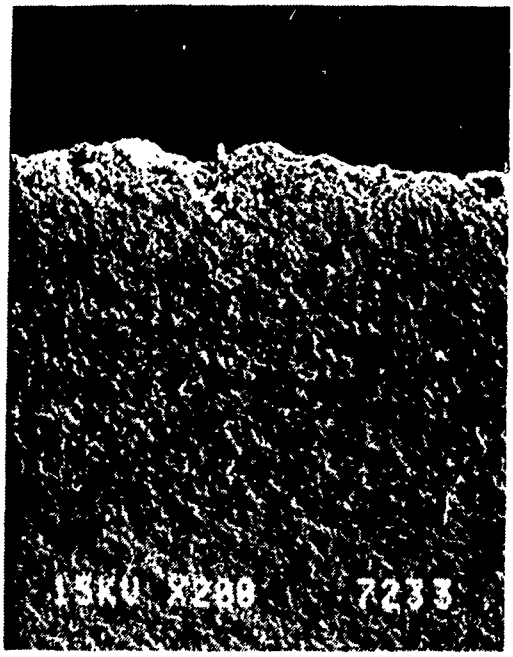

APPENDIX A - Photomicrographs of U.S. Air Force graphite epoxy panels after dry paint stripping with plastic media blast (PMB) using a Pauli & Griffin PRAM 31 Cabinet PMB system. Photomicrographs and scanning electron microscope analysis by the U.S. Air Force Wright Aeronautical Laboratories (AFWAL), Wright Patterson Air Force Base, Ohio, November 1987.

P&G / AFWAL # 11

P&G / AFWAL # 11

P&G / AFWAL # 12

P&G / AFWAL # 12

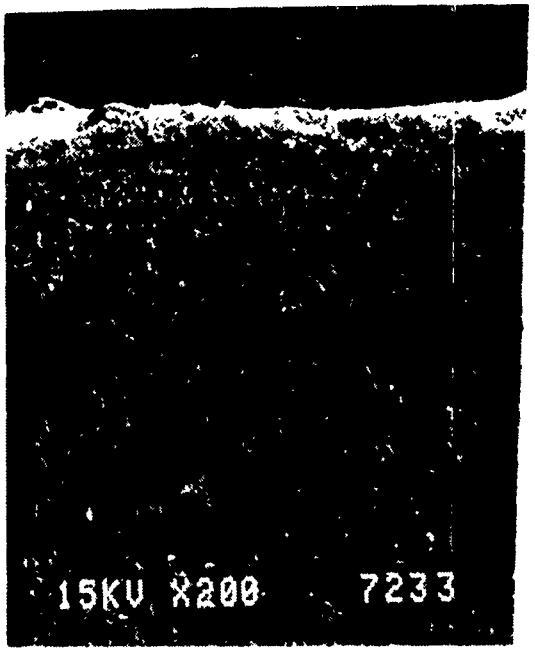

APPENDIX A - Photomicrographs of U.S. Air Force graphite epoxy panels after dry paint stripping with plastic media blast (PMB) using a Pauli & Griffin PRAM 31 Cabinet PMB system. Photomicrographs and scanning electron microscope analysis by the U.S. Air Force Wright Aeronautical Laboratories (AFWAL), Wright Patterson Air Force Base, Ohio, November 1987.

P&G / AFWAL # 13

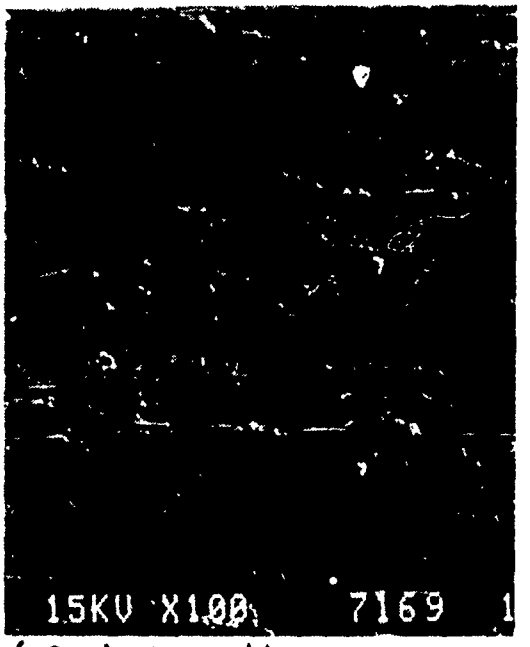

P&G / AFWAL # 13

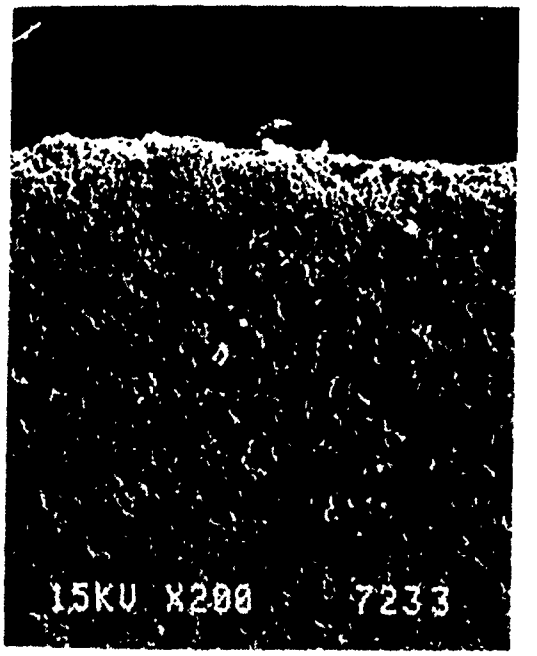

P&G / AFWAL # 14

P&G / AFWAL # 14

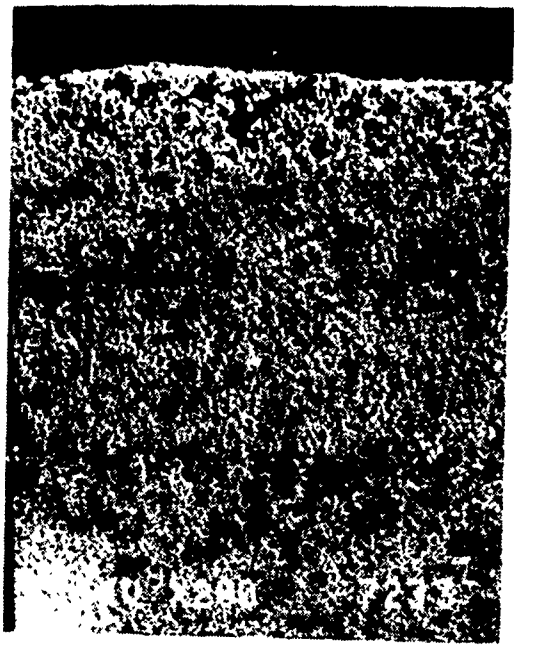

ROBOTIC DRY STRIPPING OF AIRFRAMES: PHASE II

by

Robert A. Pauli
President
Pauli & Griffin Company
Vacaville, California 95688

and

Art M. Wittenberg, Manager
Materials & Process Engineering
Air Canada
Quebec H4Y 1C2, Canada

ABSTRACT

At the U.S. Department of Defense Tri-Service Advanced Coatings Removal Conference, Orlando, Florida, March 1-3, 1988, we presented information on Air Canada's interest in the development of a dust-free, automated, plastic media dry stripping system. This included a description of semi-automated equipment under development for this project based on Air Canada's stationary/simulator configuration experience. Phase I of their program was to build a prototype of the proposed robotic arm, and it's dust enclosure to: prove basic automation concepts; show reasonable paint removal rate from a curved surface; and, establish that process is dust-free and recovers media in a closed-cycle fashion. Phase I was successfully completed by the March 1988 date of the first paper, except for the determination of optimum blasting parameters. This paper contains Air Canada's calculations on the effect of different blasting parameters in order to determine optimum values required for completion of Phase I. Also included is progress into Phase II. Phase II is to prove the total concept by building and demonstrating the capability of a complete system, i.e., with the robotic arm/blast enclosure mounted on the arm of a motorized man-lift/platform.

Air Canada shares the various concerns expressed so far about the dry stripping process (effect on fatigue life, crack propagation, control of blasting operation/parameters to prevent deformation/buckling of aluminum skins and aggressive clad removal, contamination risk for the media, need for adequate/consistent operator training, etc.). Yet, once acceptable

blasting parameters are determined for various substrate materials, structures, etc., control over the execution of the "job" will still be in the hands of the operator. Air Canada does not believe this is acceptable, but does believe PMB will be a viable method of paint removal on their aircraft if the process is automated. After reviewing Republic Airlines' operation in Atlanta, Air Canada concluded that, due to the dust generated by the process, most airlines could not adopt the process, as they cannot afford the luxury of a dedicated dry stripping facility. The only answer to Air Canada would be to use a large blasting enclosure to ensure closed-cycle recovery of plastic media and dust without permitting them to escape into the hangar atmosphere. They were able to prove this concept three years ago by using a small blasting enclosure of their own design and an off-the-shelf Pauli & Griffin PRAM 45 Vacuum Return Unit. However, a larger "blasting enclosure" would be needed to achieve minimum acceptable production (removal) rates. This concept would only be feasible if automated.

Shortly after reaching the above conclusions, Air Canada personnel observed a completely automated blasting operation which used a dedicated booth and was for depainting railcars and locomotives. It appeared that the concept could be transferred and upgraded for use on their aircraft. Air Canada has since agreed to participate in a program with Compustrip Systems Ltd. The program entails the development of an automated, dust-free, dry stripping system meeting Air Canada's minimum requirements. The program has two basic phases:

Phase I: Build a prototype of the proposed robotic arm, and it's dust enclosure, to:

1. Prove the basic automation concepts;
2. Show it is possible to remove paint from a curved surface at a reasonable rate;
3. Prove the process does not generate dust, but recovers the media in a closed-cycle fashion.

Phase II: Prove the total concept by building and demonstrating the capability of the complete system, i.e., with the robotic arm/blast enclosure mounted on the boom of a motorized man-lift/platform.

Phase I was successfully completed in November 1987, except for the determination of optimum blast parameters. To complete Phase I, Air Canada is calculating the effect of different blasting parameters (pressure, angle, media mass flow, media types and sizes, and travel speed) to determine their optimum values for their paint schemes. That is, which parameters give the highest removal rate with the least effect/disturbance of alclad surfaces (alclad removal and surface roughness). This is being done using the "simulator" configuration discussed later on in this paper. Findings so far are:

1. Optimum blast angle: 75 degrees (see Attachment A)
2. A lean flow rate of 7 pounds per minute produces a significantly higher removal rate than a 10 pounds per minute flow rate.
3. Moving up or down the test panel produces little or no significant difference in removal rate.
4. The normal 2.5 to 3.0 mil coatings are easily removed at travel speeds of 8 to 9 feet per minute (maximum for "simulator") and nozzle pressures of 20-25 psi. To obtain complete removal of the 6 mil coating (Red over White) at the same travel speed requires blast pressures some 5 to 10 psi higher (see Attachment B).
5. With pressures in the 15-30 psi range and travel speeds of 5-9 feet per minute, surface roughness is in the 205 to 360 micro-inch range when using PolyPlus 20-40.
6. Varying mass flow rate between 7 and 13 pounds per minute at given pressures and angles produces variations in average surface roughness of 15-20 micro-inches. The leaner flow rates tend to give a slightly rougher surface.
   NOTE: All test panels are .050" 2024-T3 Alclad Aluminum in 2 ft. x 4 ft. sizes. They are painted and cured as complete 4 ft. x 12 ft. sheets and then cut to size. Curing is at room temperature for 7 days, followed by 96 hours at 140 degrees F.

In response to Air Canada's interest in the development of a dust-free, automated, dry-stripping system, Compustrip Systems Ltd. of Montreal proposed the concept shown in Figure 1. It has been named the "Compustrip VR-2000 System." "VR" stands for "vacuum return" and 2000 indicates a two nozzle system designed to fill needs into the next century. The Compustrip VR-2000 System is a semi-automated system in that:

1. It must be positioned manually for access to the different areas of a large aircraft;
2. For each designated section of a specific airframe, it is preprogrammed to execute the dry-stripping operation automatically, using specific blasting parameters (nozzle pressure and angle, media mass flow rate, and travel speed).

Blast distance is fixed at three feet as determined by the depth of the blast enclosure.

It is important to note that Compustrip Systems do not use any vision-type feedback information to alter blasting parameters. The system supervisor, therefore, has to select an initial "travel speed" (the inverse of dwell time) capable of completely removing the coating system using the pre-programmed blasting parameters. This is accomplished manually by testing first the highest possible "travel speed" and then falling back to slower "available" speeds in a step-by-step fashion until satisfied with the visually observed result. That selected speed is used to dry-strip the rest of the specific airframe section. If/when incomplete coating removal is observed, the system supervisor inputs "location data" into a simplified keyboard for

selective re-execution. A line on the hangar floor, illustrated on the right-hand side of Figure 1, represents a portion of the "guidance system" needed to ensure proper travel along the fuselage, wing, etc. A sensor placed under the motorized man-lift completes this guidance system.

Figure 1 shows the four major sub-systems that make-up the complete Compustrip VR-2000 Systems. These are:

1. Motorized man-lift (platform) adapted for this application and mounted on a 45 foot or 65 foot boom, depending upon the size of the aircraft to be stripped. This unit provides all vertical and horizontal axis mobility for the system. The basket will be removed and replaced by the robotic arm, and it's enclosure, for the dry-stripping operation.
2. Custom-built two-nozzle Pauli & Griffin PRAM dry stripping, media recovery, and reclamation system.
3. Four stage telescopic arm and blasting enclosure for a two nozzle operation, each nozzle being 1/2 inch bore, long venturi design. The nozzles are mounted on a turret for precise selection and control of blast angle. Proximity-type sensors mounted at the mouth of the enclosure provide instant feedback to the computer to ensure proper force is exerted against the aircraft fuselage to maintain an adequate "seal" at all times.
4. "Equipment Carriage" with computer console and Pauli & Griffin blast, recovery, and reclamation system.

A prototype of this robotic-arm and blast enclosure, Figure 3, was fabricated and mounted on a stationary column in a "simulator" configuration for use on a simulated DC-9 fuselage half. This took place at Air Canada in June of 1987. A hydraulic system powers this "simulator" robotic arm, which is programmable for motions about five axes:

1. Arm travel "up and down" column.
2. Arm "angle" to column.
3. Arm extension ("in and out")
4. Enclosure angle (180 degree mobility from vertically upward to vertically downward).
5. Nozzle angle of impingement (variable between 65 and 90 degrees in the current enclosure model).

The simulator was built to:

1. Optimize design of the robotic arm and the blast enclosure.
2. Develop basic software to operate the system in the "automatic" mode.
3. Provide a "tool" to Air Canada for experimentation and selection of optimized blasting parameters.

Following the successful November 1987 demonstration of the capability of the system in this stationary/simulator configuration (automated, dust-free paint stripping on a mock-up of a DC-9 fuselage section), Air Canada has:

1. Included the possible acquisition of two Compustrip VR-2000 Systems in their new aircraft dry stripping and repainting facility to be operational in Toronto by the end of 1989.
2. Funded a portion of the fabrication cost for a production model of the Compustrip System for demonstration and acceptance testing.
3. Acquired an "adapted" motorized man-lift for this demonstration/acceptance testing program. Pauli & Griffin is providing the custom-built, two-nozzle PRAM dry stripping system.

This final development and acceptance testing program was scheduled to start in mid 1988 at Air Canada in Montreal. Current plans call for initial testing to be conducted on a life-size mock-up of the aft section of a B-747 fuselage and tail. Further testing will be done on an out-of-service DC-8 prior to moving on to an in-service aircraft demonstration.

In the interim, Air Canada M & P Engineering is conducting a blast parameter evaluation and optimization program, using the Compustrip simulator still in their Montreal facility. Air Canada's production goal is to achieve a net average coating removal rate of 4 sq. ft. per min. with each of the two Compustrip Systems they may acquire.

Air Canada's inspired program to have an automated, dust-free dry stripping operation in place by the end of 1988 has been slightly delayed due to equipment problems. A new production version of the Compustrip VR-2000 was delivered to Air Canada Montreal on September 22, 1988 for on site hardware and software fine-tuning. The current schedule is to demonstrate a fully-automated, production ready system by mid 1989. Prior to this time, Air Canada will have completed calculating the effect of different blast parameters to determine their optimum values for their paint schemes. Air Canada further hopes to put their VR-2000 Compustrip System into service in Toronto in early 1989.

Phase II, so far, has resulted in the following major areas being up-graded from the original stationary simulator prototype:

1. The new/up-graded robotic-arm is now mounted at the end of the boom of a modified 60 foot Simon man-lift. This will permit complete mobility required to access any portion of Air Canada's aircraft.
2. Previous electro-magnetic relay based control panel replaced by independent I/O (input-output) computers for all three major sub-systems (man-lift, robot-arm, blast/reclaim system).
3. The master computer, located at the operator control station will initiate all automated process sequences and will constantly monitor the proper operation of all sub-system components/sensors. Selected failures, disallowed actions and diagnostic information will be provided to the operator via computer screen. The original simulator prototype had none of this on-line feed-back capability.

4. The last/final stage of the three-section hydraulic cylinder of the telescopic robotic arm is now totally independent from the first two stages. Only the former will be used for fine adjustment of arm extension against the aircraft surface.
5. The speed of extension or retraction of the arm is now automatically adjusted to the rate of change in compression/pressure as the blast enclosure travels on the aircraft. This feature combined with the one in (4) above will result in much smoother travel along curved surfaces (while maintaining a "seal").
6. Air pressure transducers located at the blast nozzles will provide on-line feedback and adjustment/shut-down capability within pre-selected ranges of pressure.

To review, the major benefits associated with automated dry-stripping are:

1. All the benefits of manual PMB (better paint adhesion, faster turn around time, less composite damage, no hydrogen embrittlement, high return on investment (ROI)).
2. Consistent effect on substrate (not operator dependent).
3. Reduction in operator training costs (skills development and maintenance).
4. Improved productivity.
5. Reduced labor cost (maximum 3 persons for 2 systems).
6. Records exact process parameters in video, print or disc format. Yields improved QA (quality assurance).

The above benefits are applicable, as well as some valuable additional benefits when the automated system has a dust-free/vacuum return capability, as does the Compustrip VR-2000.
These are:

1. No dust in the work environment.
2. Reduced media contamination risk.
3. Reduced media loss rate.
4. Reduced media inventory requirement.

ATTACHMENT A

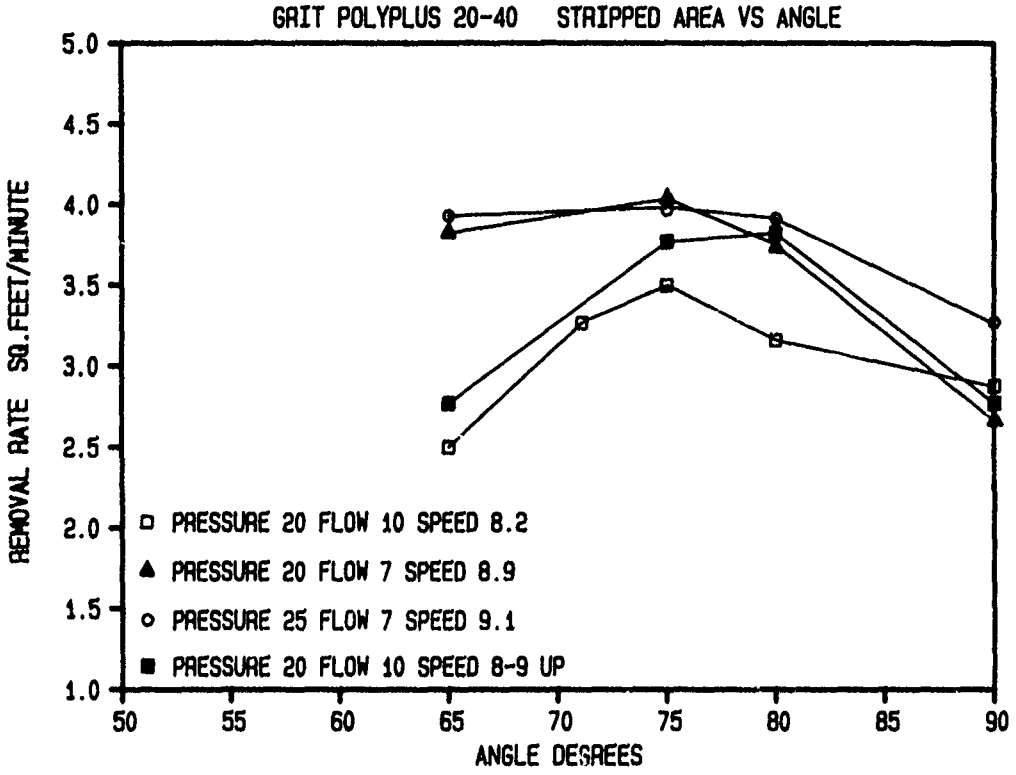

ATTACHMENT B

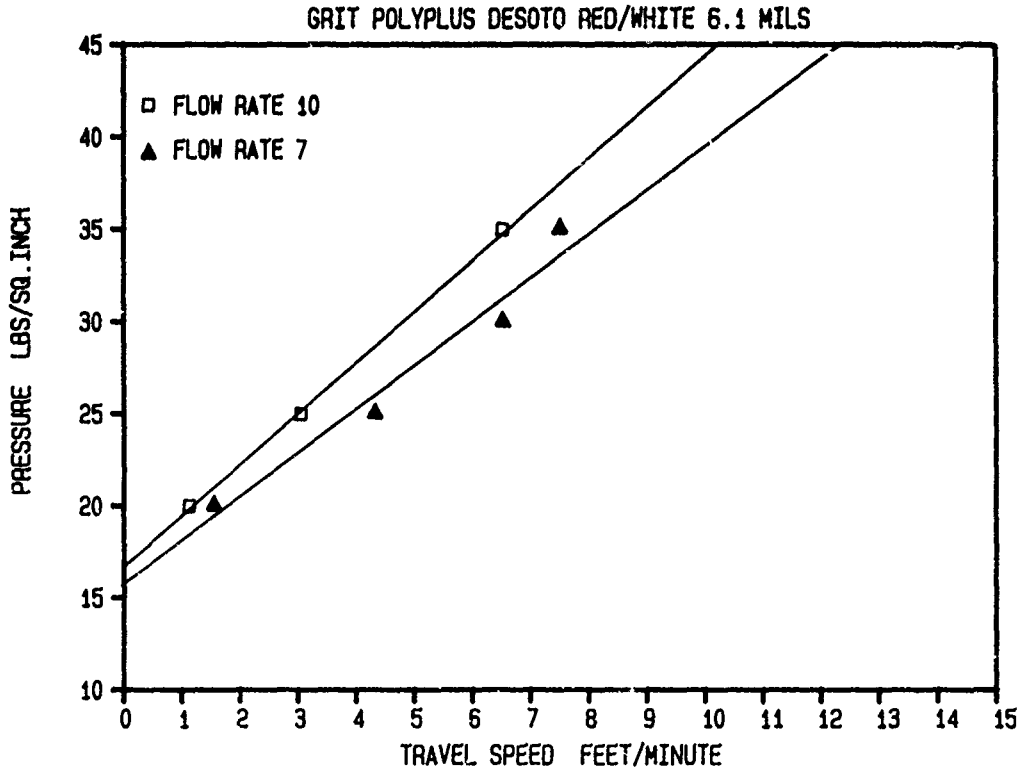

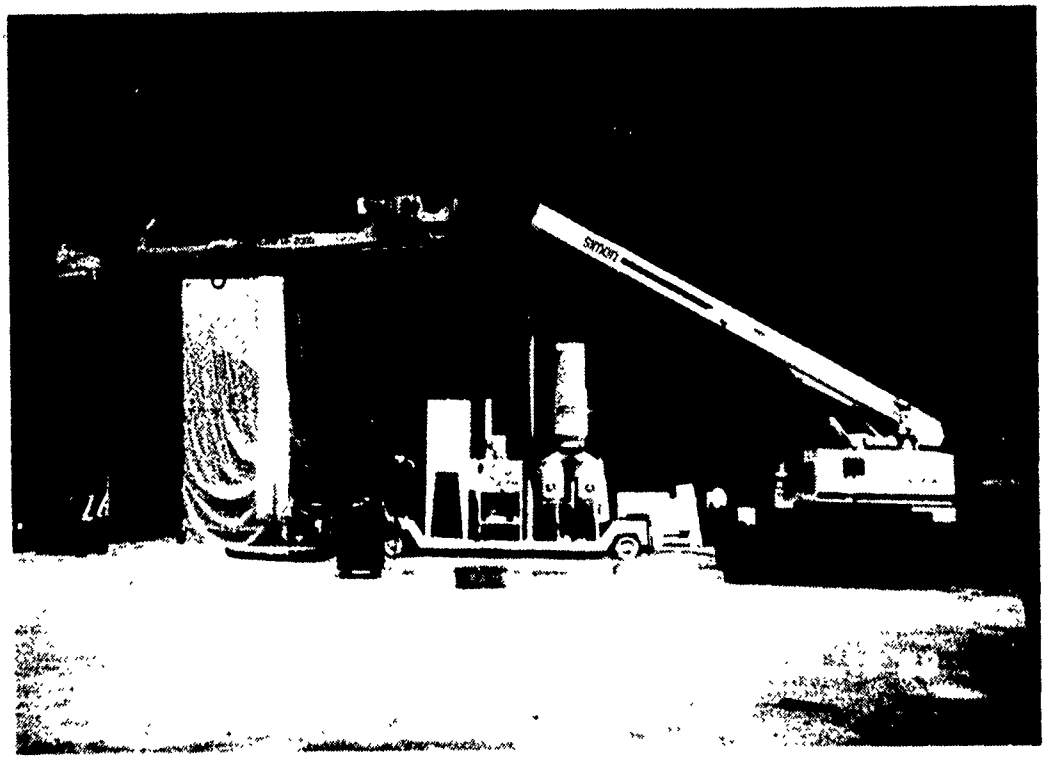

FIGURE 1

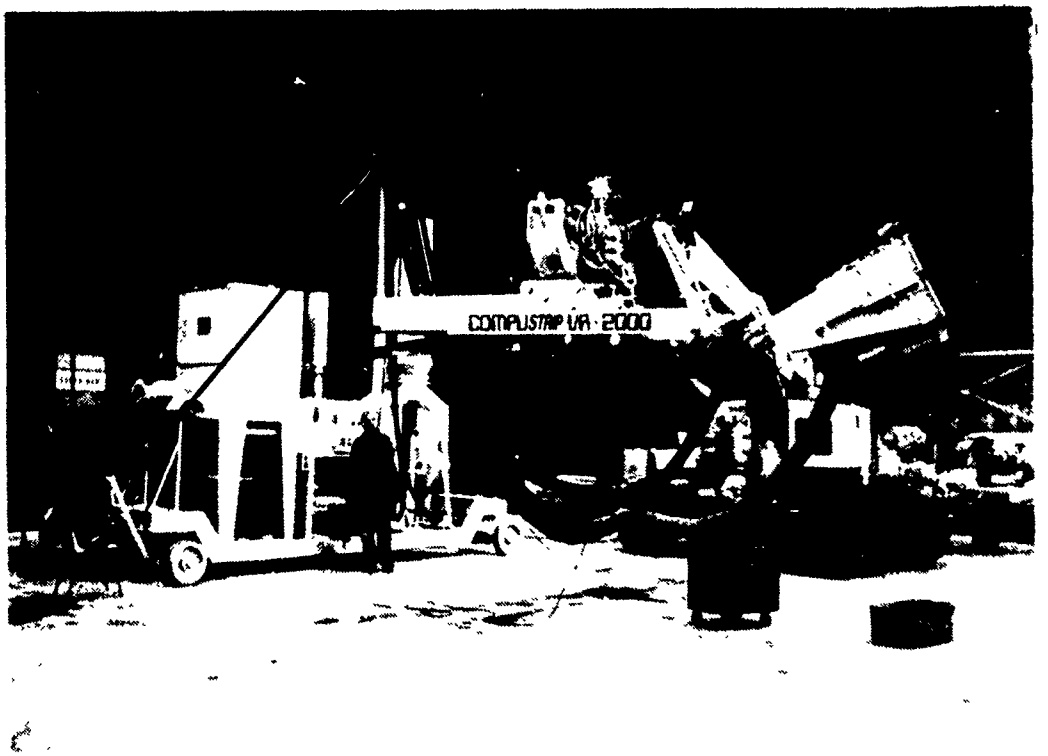

FIGURE 2

FIGURE 3

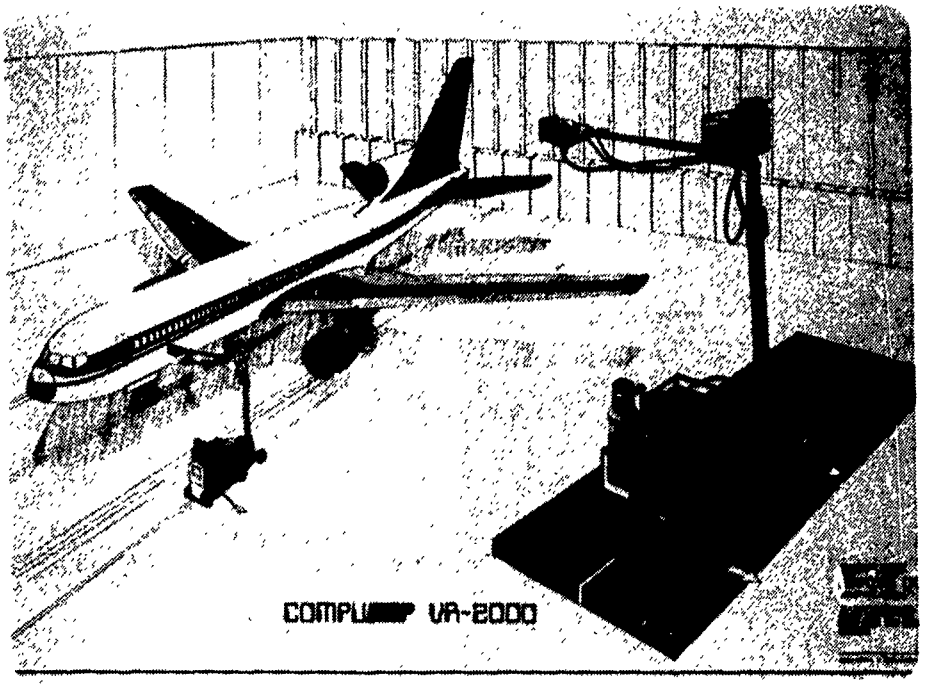

FIGURE 4

IMPROVED NAVY SHIPBOARD ANTICORROSIVE PAINT SYSTEMS

Stephen Hobaica
David Taylor Research Center
Annapolis, MD 21402

ABSTRACT

The many different severe environments aboard Navy ships that corrode metal components have led to the need for new or improved anticorrosive paints. These environments are characterized by high humidity, temperature extremes, and exposure to chemicals and other conditions deleterious to paint. Shipboard areas included are bilges, sanitary tanks, salt water tanks, and machinery spaces. A standard Navy epoxy polyamide paint series, F150 described in MIL-P-24441 is currently used in bilges and tanks. Low temperatures in the bilge, as low as 40°F create poor conditions for application and curing of the F150 series paints. Metal surfaces are wet due to condensation and cure rate is severely decreased. Conversely, sanitary tanks experience elevated temperatures and may contain harsh chemicals from galley waste and detergents. Yet another environment is present in saltwater tanks where paints must resist the effects of cathodic protection and cyclic immersion and drying. The significantly different requirements for each shipboard area results in marginal performance of the F150 series paints, which were not originally formulated for these extreme conditions. Various paints formulated to perform in these environments are being evaluated. Paints for shipboard machinery and components (e.g. hatch and equipment covers) is another area requiring improved anticorrosive paint systems. Currently, F111, a light gray enamel described in MIL-E-15090, is used. Powder coatings and flame spray aluminum topcoated with a powder coating are far superior to conventional liquid paints. For components which can be removed for coating, flame spray aluminum and electrostatic powder coatings are being evaluated. Paints which are easy for the crew to apply and maintain are being investigated for shipboard components which cannot be removed for painting. General requirements for all paint systmes are VOC (volatile organic content) compliance, closed cup flash point greater than 100°F, and that the paints shall not contain carcinogens or toxic materials. The present goal of the Navy is for a VOC of less than 340 g/L.

[Manuscript Not Available at the Time of Printing]

RINSING EFFICIENCY

Albert M. Pradel
U.S. Army Tank-Automotive Command
ATTN: AMSTA-TMC
Warren, Michigan 48397-5000

Rinse water efficiency: ways to improve, ways to trouble-shoot, ways to test. This paper discusses the importance of rinsing in all surface preparations. The role of rinsing will be stressed. Simple rinsing, compound rinsing and counter-flow rinsing will be detailed, with diagrams and mathmatical rinsing efficiency relationships. Examples of industrical installations will be quoted with water cost information. Several very simple methods and tests will be included, which can be used for problem-solving situations, routine process controls, and preventive maintenance.

Corrosion of U.S. Army tactical vehicles' metal components is a perennial problem, with monumental costs. Total U.S. Army "cost of corrosion" is estimated at $2 to $3 billion dollars per year. Metal components, of cold rolled steel, galvanized steels and aluminum are finished with primers and top coat paints. Approximately 70% of the corrosion related failures in U.S. Army tactical vehicles are traceable to improper or inadequate metal surface preparation. This is fact.

But let's think about a typical cross section of a vehicle's finished metal components. This would include any painted part. The metal, typically gets precleaned, cleaned, rinsed, sometimes twice-rinsed, conversion-reaction coated, rinsed, acid rinsed and, on some, rinsed with deionized water. All of this happens before priming, drying, cooling, (some call it prime coating), primer flash-off and/or primer baking, and then, finally, the application of one or more layers of top coat paint. Looks like we have quite a combination of many surface preparations. If the total system is to perform on U.S. Army vehicles in providing corrosion protection, EACH surface must be prepared and maintained properly and completely to assure that our field personnel can depend on top quality and READINESS. The total painted metal system is only as good as its weakest surface. Sound familiar? Of course! Our Navy and Air Force personnel know all about weak chains, we are all in the same boat .... Involvement in the prevention of corrosion. Seems that we have painted multi-faceted corrosion prone systems. Now, why should WE be concerned about RINSING? Better yet - Why not?

Industry had, for many years, wasted more rinse water than was used efficiently. Efficiency involves what? Effective use of time, personnel, material, equipment, and MONEY!! But, with the advent of E.P.A., OSHA, competitive pressure, design changes, vehicle marketing and other factors, improvements in handling vehicular components and the vehicles themselves,

had to be made. These pressures resulted in manufacturers having to pay for water into their factories and processes, and in some areas, effluent or discharge water leaving the plant. The environmental impact of various contaminants in our country's air and water are widely publicized, if not totally known and/or understood. We are building up to the point that we, via exchange of technology with industry, can benefit.

Rinsing is as important as any of the many above steps, processes, and materials, along with process-parameters. The parameters include time, temperature, concentration, pH, type of chemical, work energy, via agitation/immersion or mechanical, sheer, energy. Within the processes we and industry had always thought, and referred to the active steps: The cleaning/cleaner, the etching/etchant, the surface conversion/conversion coatings, such as chromate conversion coatings, iron phosphate coatings, zinc phosphate coatings, with or without calcium modification, and acidulated seal rinses, chromated or non-chromated.

Industry found that we all have to pay more attention to detail. It was long overdue to look at the key surface preparation problems, how to improve ALL surface conditions prior to, within each step, during the time between steps, on and on. Keep in mind all the above process steps!

Rinsing's job is to remove the material of the previous process step and render the work surface ready to receive, accept and retain the next one.

Rinsing is a DILUTION PROCESS. It's efficiency has next to nothing to do with the size of the rinse tank, regardless of the rinse method employed. It has to do with the rate of dilution. Let's look at Figure One, which shows one stage of SIMPLE RINSING. These figures are only schematics. This one shows just the first three steps in a prepaint treatment process. The RINSE, Step two, is to remove, by dilution, the cleaning material, usually alkaline, from the metal surface so that it can accept the phosphate or chromate conversion coating of Step three. Consider the metal parts' surfaces carrying one gallon of liquid per hour. The DRAG-IN/DRAG-OUT RATE is One Gallon per hour, 1-GPH. Fresh tap water enters the rinse stage at the rate of 100 gallons per hour, 100-GPH. The figures are just relative numbers, the mathmatical significance is their ratio. The overflow is maintained constantly. The dilution ratio attained and maintained is one hundred to one, (100:1). O.K.! One stage of Simple Rinsing.

Figure 1

SIMPLE RINSING ONE STAGE

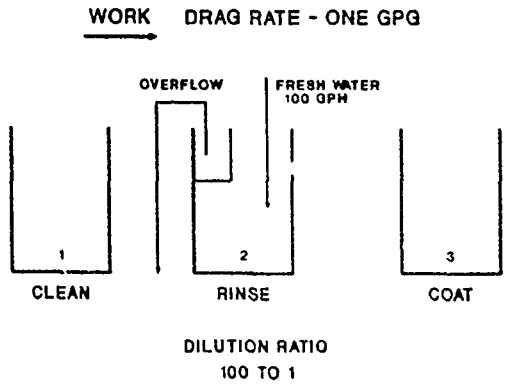

Figure 2

SIMPLE RINSING - TWO STAGES

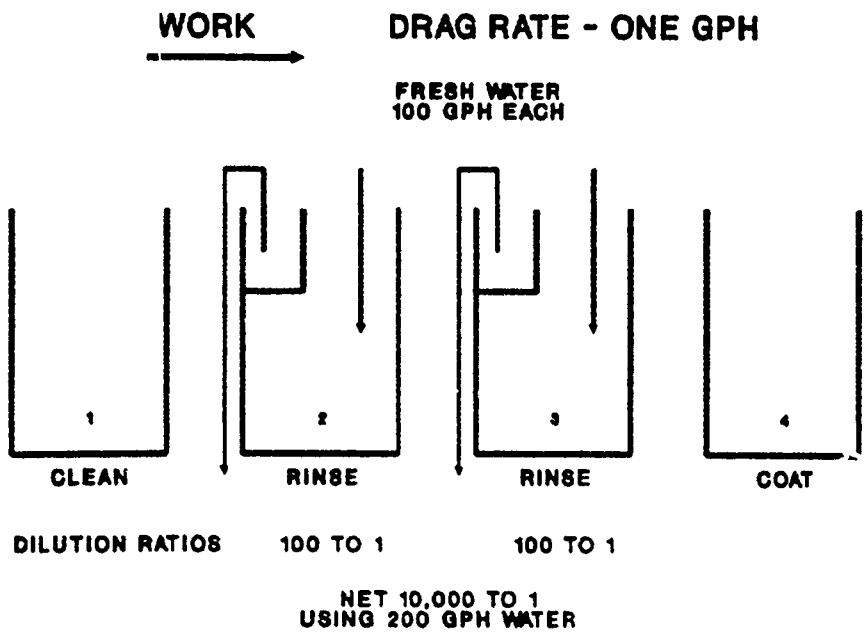

In Figure Two, an improvement is made by using two stages of simple rinsing, stages two and three. The dilution ratio is increased to ten thousand to one. Remember, the Drag-Out/Drag-In rate is the same. But the water feed rate has been doubled, two hundred gallons per hour of fresh water versus one hundred in Figure One. TWICE the water RATE.

Figure 3

COUNTER FLOW RINSING - TWO STAGES

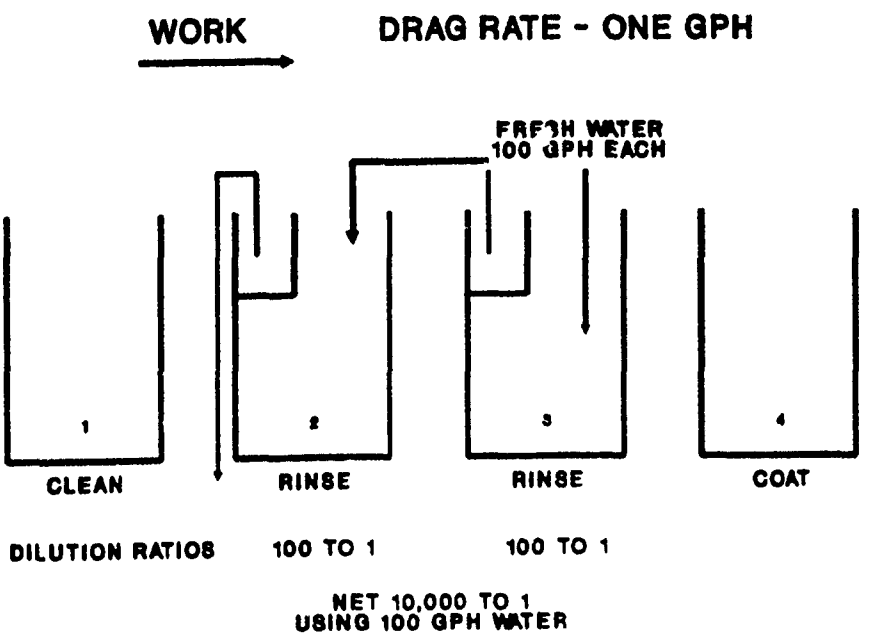

Figure Three is titled Counter Flow Rinsing, Two Stages. The contaminated overflow water from Stage Three is directed back to Stage Two and overflowed from it. The rinse water flow is counter-to, opposite, that of the metal parts, or work in these Figures. With the same drag-out/drag-in rate of one GPH, now only one hundred GPH of fresh tap water, the effected dilution ratio is ten thousand to one. In Figure One we had 100 to 1, with 100 GPH drag-out/drag-in. Here we have the dilution ratio of 10,000 to 1 with the same rate of 100 GPH of rinse water. We have cut from 200 GPH to 100 GPH fresh water, increased the rinse water dilution efficiency to a ratio of 10,000 to 1. Now the metal work surfaces are more ready to accept the material to be developed/deposited/reaction-formed, in Stage Four.

The surfaces are cleaner than those generated with one stage of Simple Rinsing. Industry had to do this, improve product quality, reduce costs within the same process time(s), and conserve water. A large industrial, aluminum extrusion factory retrofitted their process line with counter-flow rinsing in 1979. Their products are used in making storm windows and doors.

Their line includes: (1) Clean (2) Rinse (3) Rinse (4) Etch (5) Rinse (6) Deoxidize (7) Rinse (8) Rinse (9) Deionized water rinse (10) Electrocoat Paint. A very large system. The extrusions are 18-20 feet long. The process containers, tanks, hold 8500 gallons each. They had been paying money for water into and out-of their factory. At the end of the first year following retro-fitting for counter-flow rinsing, their water bill was reduced by $29,000 dollars. A Fact! This is a large system, but the concept can be applied to any size system. Industrial plating factories have used counter-flow rinsing for 50 years. Electrocoat painting is the same as electro plating.

Figure Four shows a take-off on counter-flow rinsing. It is titled COUNTER FLOW RINSING AND NEUTRALIZING. It shows all six functional steps clean, rinse, rinse, coat, rinse, and seal rinse. It could be called Modified Counter-flow Rinsing.

Figure 4

COUNTER FLOW RINSING AND NEUTRALIZING

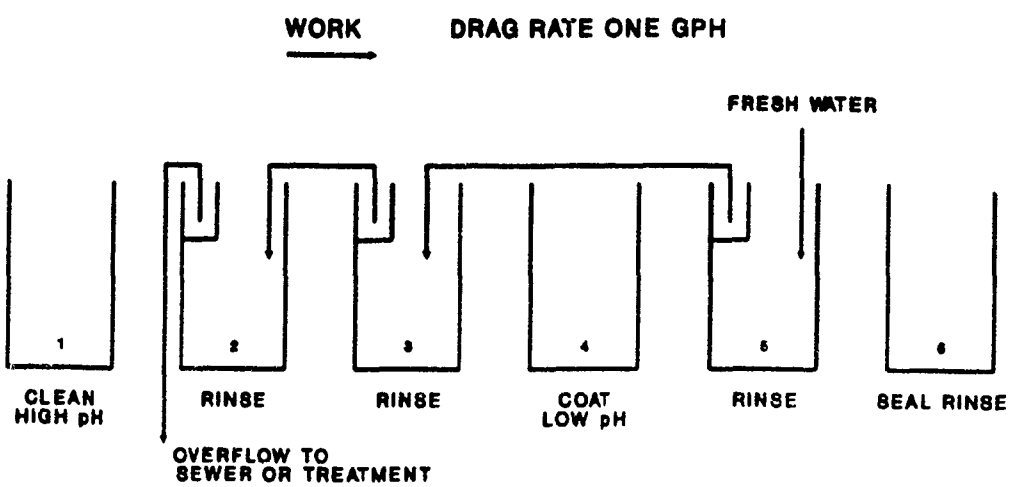

Another function variation that industry has proven successful involves a four, five, or six stage iron phosphate process, via tank immersion or spray. Here they put the same material in two tanks. This is a cleaner-iron phosphate type. They gain more cleaning power and life. In the first tank increased cleaning power is effected by adusting the pH to 5.0 to 5.5. Normal range for this type material is pH 4.0 to 5.5. In the second tank, pH is adjusted to the low end 4.0 to 4.5, to provide maximum iron-phosphating power. The system is cost effective. Naturally, with time the first tank becomes saturated with soils, and adding more fresh cleaner chemicals is not effective. The first tank is dumped, material in the second tank is pumped to the first. The second tank is then recharged with fresh iron phosphate. Some minor adjustments are made to reset the operating parameters for each tank.

In processing aluminum extrusions with a chromate conversion coating, another successful approach has been the use of acidic type cleaning. This is done by some industrial companies who produce to the Architectural Aluminum Manufacturer's Association (AAMA) specifications. They eliminate the problems inherent to drag-out/drag-in of typical alkaline cleaners to the acidic chromate conversion coating tank. The acidic cleaner must be controlled very carefully as to temperature, pH, concentration and time of contact with the aluminum parts.

Industry has had to get more involved with water and how best to use and conserve it. Analysis of the water used is required. The chemical and physical characteristics of water varies considerably throughout the United States and throughout the world.

Think of how many ways water is used, in making parts for U.S. vehicles, aircraft and ships. Cleaning materials, etchants, deoxidizers, pickling acids, neutralizers, conversion coatings, lubricants, stamping compounds. This list could go on for several more pages.

We know that metal treatment chemical companies, who supply the industrial companies, are capable of supplying metal forming compounds that are, indeed, easier to remove. The dissolved solids in water itself can become corrosion sites under the primer/paint, on all vehicles, of all types. Dissolved solids include carbonates, chlorides, oxides, among many others.

Under the various hostile environments that all U.S. Air Force, Navy and Army vehicles must perform, these materials can and do cause corrosion-related failures.

Lets review. Back to the chain and its links---the marriage of metal, coatings, primers, and paint. Our vendor's paint suppliers provide them with paint characteristics, proper application methods, and paint performance requirements. None of us want to waste taxpayers money on top quality paints applied over corrosion-inducing materials. Industry's and our demand for UNIFORMITY gets a bit closer to attainment, when we combine our talents and experiences.

Most first step cleaners are alkaline, pH above 7. Actually, for metal cleaning of our types of metals, pH is between 11 and 14. Conversion coatings are acidic: for ferrous metals these include iron phosphate and zinc phosphate; for non-ferrous metals, magnesium, aluminum, and their alloys, these include chromate conversion coatings, such as chrome-chromate, and chrome-phosphate. All contain hexavalent and tri-valent chrome and fluorides.

The modification is this: The primary fresh tap water enters Stage Five, the overflow water is counter flowed back, to enter Stage Three. Stage Three overflow feeds Stage Two and overflow from Stage Two goes to the sewer or an effluent treatment facility. A further modification, where needed, is to add a low rate water feed to Stage Three. The various prepaint treatment factories and products vary, enough, to cause the need for specific figures and equipment. In addition to increasing rinse water efficiency, this system provides built in neutralization, an added benefit, more mileage out of the same water. The dragont liquid from Stage Four is acidic, that from Stage Two, and less so, from Stage Three, will be alkaline. Neutralization on the fly, built in. Industry learned that much of this information had been known but not applied. They, and we can learn also, look at ways and tools to use in getting the data needed in making decisions. Here are some: (1) Titate the rinse water for presence of the material in the previous stage. Care must be taken in selecting the sample site, (2) Check the pH and Total Dissolved Solids (TDS) on the rinse water. Remember, one percent by weight is 10,000 parts per million, (3) Check pH, TDS and titration of a sample of drippings from the work metal, (4) Check pH, with paper, on the wet surface of the work metal, part, (5) Know the analysis of the water used in the factory. From industry we can also learn ways to improve rinsing efficiency: (1) Put the fresh water entry across the bottom of the rinse tank---with drilled holes every 3-4 inches. This requires installation of an anti-siphon valve.

The most common error made at rinse tanks is location of the fresh water entry too close to the overflow trough. Most of the water is wasted. The across the bottom entry pipe causes all the water to work at providing uniform purge and movement of the entire rinse water volume, (2) The overflow trough should be located along the longest side of the tank. This effects maximum flow efficiency in cleaning the rinse water, (3) In a spray washer, use fresh water in an additional pair of risers---one each side of the rinse stage, at the exit end. This way, fresh water is the last to rinse the work, before it leaves. This water becomes part of the circulated rinse water, (4) Use VEE-JET nozzles for maximum work energy with the highest pressure you can tolerate, (5) Also in spray washers---use misting nozzles in the vestibule areas. This keeps the parts wet and prevents premature dry down providing improved rinse water efficiency AND prevents inter-stage corrosion; rust on ferrous metals and/or other oxidation products on non-ferrous metals, (6) As discussed above, multipe rinse stages and/or (7) Counter-flow Rinsing.

Advantages gained by improving rinse water efficiency are: (1) Reduction in cross contamination---the drag-out/drag-in problem, (2) Reduction in chemical use, (3) Increase in coating integrity, (4) Increase in coating performance and therefore, vehicle performance, (5) Reduction in END COSTS!

If we plot quality versus TIME, and get a saw tooth profile, the system is out of control. Not uniform! If we control as many parameters, tools and materiel as possible, the curve can be flattened. Make it approach horizontal at a level above Q.C. acceptance.

Draw your own curve---plot quality as cleanliness, coating weights, cross-hatch adhesion compliance, salt spray performance - whatever - versus TIME. If the curve is saw-toothed, there are may improvements possible. Problems are solved by making decisions to do something-only when the data has been analyzed. Like the one that says BEFORE WE SOLVE A PROBLEM, WE MUST FIRST DEFINE IT.

CORROSION OF M299 IGNITION CARTRIDGE BODIES IN THE M374A3 81mm MORTAR

J. Senske and C. Manning
SMCAR-AET-M
Picatinny Arsenal
New Jersey 07806-5000

ABSTRACT

Misfires of M374A3 81mm mortars at Ft. Hood, Texas have been traced to the build-up of corrosion in the M299 ignition cartridge body. Corrosion products have been identified in the cavities between the black powder pellet and primer and the black powder pellet and flash tube. A review of the mortar design indicates that the combination of high internal moisture levels, graphite in the black powder pellets and weaknesses which may have contributed to the corrosion problem. Sulfuric acid anodizing and duplex corrosion resistance of ignition cartridge bodies compared to chromate conversion coating after salt spray and temperature -humidity cycling tests. Cost impact on the M374A3 mortar has been minimal.

[Manuscript Not Available at the Time of Printing]

MICROBIOLOGICALLY INFLUENCED CORROSION (MIC) OF 4140 STEEL BY FACULTATIVE ANAEROBIC MICROORGANISM COATING

Joanne M. Jones and C.M. Dacres
Biotechnology Group (Code R301)
Naval Surface Warfare Center
Silver Spring, MD 20903-5000

ABSTRACT

Marine and atmospheric marine corrosion is a potential hazard for metals, alloys and composites that come in contact with the sea or salt spray. A large part of marine corrosion may be initiated or influenced by the attachment and growth of bacteria and other marine organisms. Metal interfaces in aquatic systems are sites of intense microbial activity and can harbor complex communities of bacteria, protozoa and algae. The problem of corrosion in real-life environmental situations is extremely complex and there may be more than one mechanism for biocorrosion operating. In a biofilm, there is the potential for both aerobic corrosion mechanisms involving oxygen concentration cells and anaerobic corrosion from microbes such as sulfate reducers growing in the anodic region. MIC studies have been undertaken to evaluate the corrosivity of coated steel in a marine environment. The coatings are suspected to be breached by microbes which create a freshly exposed steel surface that is further attacked by chloride ions or microorganisms. The corrosion caused by this marine incursion appears to be significant enough to be of concern.

EXPERIMENTAL

The coupons were fabricated from steel alloy 4140 and were zinc plated. They were coated with grey 2770 epoxy, grey 17104 epoxy or black 3147 nylon. These polymeric coatings were electrostatically applied to the metallic coating of zinc in order to improve the corrosion life of the underlying steel. Epoxy coatings are widely used as heavy-duty moisture and chemical resistant coatings and linings in immersion and atmospheric marine environments. Nylon is used because of its strength, low coefficient of friction and wear resistance.

The coated steel coupons were exposed to the marine

environment at NSWC/Ft. Lauderdale. Several forms of corrosion (crevice corrosion, cavitation, pitting and intergranular attack) were observed. Microbial sampling of coupons from the constant immersion flume tank yielded mixed cultures of facultative anaerobic microbes (sulfate reducers and non-sulfate reducers). The three mixed cultures were tested at NSWC/WO for MIC of bare 4140 steel using an accelerated corrosion test: (1) one mixed culture gave a mpy value similar to that of the controls (sterile 4140 steel coupon; sterile coupon + sterile culture medium); (2) one mixed culture gave twice the accelerated corrosion value (mpy) as the controls; and (3) one mixed culture gave an 8-fold decrease in the accelerated corrosion value (mpy) as the controls. Due to the different corrosion rates obtained for the three mixed cultures, it will be important to isolate pure cultures (identify to genus and species) from these mixed cultures and to further study the interactions between the microbes and the coated metals, coatings alone and the bare 4140 steel.

Scanning electron micrographs of the bare 4140 steel and the coated 4140 steel show that the surfaces are heavily fouled with the facultative microbes. In comparing the EDAX (energy dispersive X -ray) spectra for the controls (sterile coupon + sterile medium; no bacteria) versus the experimental samples (bacteria present), one sees a high peak of sulfur in the experimental samples due to the presence of sulfate reducing bacteria. Both the epoxy and nylon coated 4140 steel show a breaching of the coating in the presence of facultative microbes with both iron and zinc from the substrate steel present in the EDAX spectra.

Many investigators have suggested that metal ions attract marine microbes and that biofilms varied for different metals and alloys. Graphite (pure carbon) disks in the constant immersion flume tanks (NSWC/ Ft. Lauderdale) did have a biofilm of facultative anaerobes but sulfate reducing bacteria were not isolated from that biofilm. It will be important to study the epoxy and nylon coatings on graphite or glass to determine if sulfate reducing bacteria are attracted to the protective coatings or if these bacteria are attracted to metal ions leaching through the coatings.

CONCLUSION

We postulate a synergistic effect between the microorganisms in the biofilm and various seawater parameters that results in the degradation/deterioration of the epoxy and nylon coatings as an initial process to the intense corrosion of the substrate material (steel). A detailed knowledge of biocorrosion processes is necessary for developing methods to minimize or inhibit the biodeterioration of metals, coated metals and alloys, and composite materials exposed to the marine environment.

(This page is left intentionally blank.)

CORROSION INHIBITION BY PORPHYRINS AND PHTHALOCYANINES

V. S. Agarwala
Naval Air Development Center, Warminster, PA

and

S. Hettiarachchi
SRI International, Menlo Park, CA

ABSTRACT

The general consideration of the geometrical structure (spatial arrangements) and the chemical properties of porphyrin and phthalocyanine molecules suggest that they could be capable of strong chemisorption at metallic surfaces. Thus, a number of different porphyrins and their metallo-derivatives were synthesized and studied. The corrosion and electrochemical studies showed their excellent potential for corrosion inhibition. The current studies have shown that the "tailor-make" approach, through modification of chemical structure, could transform them into most efficient corrosion inhibitors. The inhibition improves as the parent groups of either porphyrin or phthalocyanine are enhanced in their chelating and pi-bonding properties with the metal substsrate, and as the size of the molecule is enlarged.

INTRODUCTION

Generally most corrosion inhibitors are no custom made items. Classically, the development of the largest class of corrosion inhibiting substances was based on their molecular size which allows them to adsorb on the metal surface and suppress metal dissolution and reduction reactions. Now, it is accepted that the effectiveness of inhibitors is better predicted by the nature of chemical bonds than by the mere sizes of the molecule and their adsorption characteristics. Since porphyrins were discovered as a potential source for corrosion inhibitors (1-4), a considerable amount of interest has been generated in the family of such macrocyclic compounds (5,6). In addition to porphyrins, phthalocyanines also open up an excitingly new field in corrosion inhibition. Structurally, both of these parent compounds are similar with some subtle differences. The macrocyclics of these types are extremely stable, highly planar and possess high electron density in the pi-orbital system of the molecule for strong interactions with the conduction band of the surface metal

atoms (7-12). Their generalized structures are as shown in Figure 1.

The Concepts of Corrosion Inhibition

The mechanism of corrosion inhibition by the porphyrins or phthalocyanines, called macrocyclics, is mostly considered due to strong chemisorption onto the metal surface such as those suggested on the basis of Lewis acid-base and the charge transfer theories (10-12). Further, the chemical structures of porphyrins and phthalocyanines suggest that their strong interaction with a metal surface would involve: (i) chelation of the surface atoms by the four inner nitrogen atoms (1); (ii) coordination of the surface atoms by the peripheral polar substituents of the macrocycle (7-9); (iii) coordination of a surface atom to the central metal of a metallo-macrocycle; (iv)"sitting-atop" complex formation involving the porphyrin and surface metal ions (9-11); and (v) interaction of the pi-molecular orbitals of the macrocycle with the d-orbitals of the metal (12). Despite the likely ability of these compounds to strongly interact with metals, forming a stable surface film, relatively few studies have been conducted with some limited success resulting in potential corrosion inhibitors. The attempts reported here were made to synthesize these compounds with varying degree of complexity, in order to keep the structure rigidly planar and stable in the presence of acid-chloride environments (2-4, 13-14). Theoretically, planar molecules are expected to provide a high degree of coverage and hence a higher corrosion inhibition efficiency. Metallo-derivatives of porphyrins and phthalocyanines have been synthesized by adding transition metal ions in the center of the macrocyclic ring, in order to incorporate redox character in the chemisorbed surface films. A number of metalloporphyrins have been reported in literature which show photoactive electrochemical behavior (15-17). The literature data on phthalocyanine films have been shown to demonstrate photovoltaic, photoconducting and catalytic applications (18-20). The use of phthalocyanines in lubricant systems dates back to the fifties (21-22). Their thermal stability and planar stacking ability make them quite unique in reducing corrosion and wear.

The Parent Structure

Porphyrins and phthalocyanines are analog structures with well defined planar configuration as shown in Figure 1. They are tetradentate ligands containing four pyrrole subunits linked together by unsaturated bridges allowing a full aromatic conjugation throughout the macrocyclic structure. The differences in the bridging groups of the pyrrole subunits make them different macrocyclics. Porphyrins are typically identified with -CH= , and phthalocyanines with -N= bridging groups. These structures can be synthetically

altered by substitution and addition. Depending on the substitution in the pyrrole rings (positions R_1 - R_8) and in the meso (R_α- R_ξ positions) in Figure 1, a range of properties of importance can be designed. With metal insertion into the macrocyclic center, a number of compounds can be formed which can be responsive to electrochemical redox processes, and can be thermally stable. This paper reports a review of such work done on the two macrocyclics, porphyrins and phthalocyanines, as possible corrosion inhibitors. The synthetic steps involved in the preparation of basic, polymeric and metallo-compounds of either macrocycle have been omitted in this paper for brevity and thematic reasons; they have been discussed elsewhere (23-27).

Porphyrins

In the work reported by Longo and Agarwala (3), a number of porphyrins were synthesized and studied. The water soluble porphyrins were prepared by making them ionic or polar through methylation to yield cationic tetramethyl-porphin, called TMP. The counter anions were iodide, chloride, benzoate, sulfate or toluenesulfonate (TS). Several metallo-derivatives of TMP or tetramethylpyridylporphin [TMPyP].TS containing central metal ions of Cr(III), Fe(III), Co(II), Ni(II), Cu(II), Mo(II) and Zn(II) were synthesized (27). Although a number of parent porphyrin compounds are available commercially, most compounds studied by Longo, et al. were synthesized to develop tailor-made structures. For corrosion studies, the water soluble compounds were studied directly by using 1 mM concentration in 1% NaCl solution. The mass-loss results of this study on Armco iron showed some corrosion inhibition (cf.Table 1). It was observed that the inhibition by 5,10,15,20-tetra-4-methyl-pyridylporphin [TMPyP] was most affected by the nature of the polar group (anion) present. For example, the compounds of TMPyP containing toluene sulfonate (also called sultone, TS) and iodide showed higher inhibition efficiencies compared to other polar groups or anions (see Table 1).

Several water soluble metallo-derivatives of TMPyP.TS were also prepared and tested as potential inhibitors in 1.0% NaCl. These results are reported in Table 2. Compared to the results obtained with metal-free porphyrins in Table 1, the mass loss rates for metallo-porphyrins were generally lower, i.e., metallo-porphyrins show higher inhibition efficiencies than their metal-free counterparts. In aqueous systems, the bonding of porphyrin occurs as the metal corrodes, and the surface metal atoms lose their electrons which are then picked up by either the polar group of the porphin ring or the central metal ions of the metallo-porphyrin. Since metallo-porphyrins were more efficient than the metal-free, perhaps the latter mechanism is preferred. The effects of pH and porphyrin concentration on mass-loss rates of iron specimens were also studied. Although, the data for [TMPyP]-

iodide in Table 3 show no significant inhibitor concentration effect in either salt or acid solutions, no genralization could be made at this time. Why only water showed a four-fold decrease in mass-loss rates is not understood.

The study of insoluble porphyrins, listed in Table 4, was made by dissolving them in benzene or N,N-dimethyl formamide (DMF). The test specimens of Armco iron were pretreated with these porphyrins by refluxing at 50° C. According to Longo, et al. (2), the so treated insoluble porphyrins did appear to exhibit a higher degree of corrosion inhibition than the water soluble porphyrins; the experimental data showed a lack of reproducibility. Thus, the results were not reported. However, when vapor deposition method was used the results were highly encouraging. Table 4 summarizes the results of these studies on (iron) specimens which were prepared by vapor deposition of various porphyrins and metallo-porphyrins. It was noted that the metal-free porphyrins showed least mass-loss rate, or inhibition efficiency of 90% or higher (cf. Table 4). Although metallo-porphyrins by vapor deposition also decreased the corrosion rate of iron, but not to same significant level. Probably, thermal treatment provides enough activation energy for a metal-free porphyrin to form a metallo-derivative or complex with the atoms of the iron surface. The fluorescence studies in the near UV region seem to confirm this conclusions (27).

The potentiodynamic polarization studies on Armco iron in 1% NaCl at pH 2 containing porphyrins and metallo-porphyrins (1.0 mM) generally showed mixed, anodic and cathodic, polarization behavior. A typical behavior for a water soluble porphyrin, TMPyP.TS, was as shown in Figure 2 (curves B); here the curves A represent the control, a behavior without porphyrin. However, when TMPyP was vapor deposited before testing in 1% NaCl (pH 2), a further shift in the curves as indicated in Figure 2, curves C, was exhibited. The shifts of curves to lower current densities are direct indications of greater porphyrin effect, and hence higher inhibition efficiency. According to Agarwala and Longo (4), the effects of water soluble compounds were shown to be concentration dependent as they also affected polarization shifts to lower current densities.

Among water soluble compounds, the effects of polarization by metallo-porphyrins were much more significant than their counterpart metal-free porphyrins. The typical behavior of these compounds were as illustrated in Figure 3 for Cu(II)-TMPyP.TS and Fe(III)-TMPyP.TS. The shifts of the anodic and cathodic polarization curves with the inhibitors were much greater than without the inhibitor (control curves A). The anodic curve for Fe(III)-TMPyP.TS exhibited a small passive potential region which was not displayed by metal-free porphyrins. Generally, most metallo-derivatives of TMPyP.TS, including VO(II, Cr(II), Co(II), Ni(II), Mo(II), Ru(II),

Rh(II) and Ag(II), exhibited anodic inhibition. The inflections in the cathodic curves were not due to reduction of oxygen or the porphyrins themselves; solutions which were purged with argon for periods as long as 2 h exhibited these inflections, and spectro-photometric analysis of these solutions showed that the porphyrin were unchanged.

As with the mass-loss studies, the most promising results were obtained when Armco iron specimens, treated with metal-free and water insoluble porphyrins by vapor deposition, were examined. In these cases the cathodic currents were reduced by several factors relative to the cathodic current observed for untreated electrodes (2). In addition, there was a significant decrease in the anodic current. Of the several porphyrins examined, the most effective and efficient corrosion inhibition was achieved by tetraphenylporphin [TPhP]. It is also the least expensive of the porphyrins. Compared to the conventional organic inhibitors, porphyrins, at present, are more expensive. However, porphyrins provide a greater surface coverage therefore, might be comparable in cost. Implications regarding the state of the metal surface after porphyrin treatment came from an examination of the fluorescence produced when treated specimen interface was exposed to near UV radiation (4000 A). Free-base porphyrins will produce a brilliant red fluorescence (6500 A and 7200 A) under these conditions, whereas iron porphyrins and other transition metal porphyrins will not (35). In the case of iron specimens treated with tetraphenyl porphin, TPhP, the specimens prepared by vapor deposition did not fluoresce, whereas those prepared with the benzene solutions fluoresced brilliantly. This suggests that the porphyrin definitely forms some kind of an iron complex during vapor deposition, whereas treatment with organic solutions results in simple, physical deposition of the porphyrin on the iron surface. The same conclusion was reached by electron paramagnetic resonance techniques which are sensitive to a depth of 100 nm; an appreciable decrease in the ferromagnetism with a concomitant appearance of a paramagnetic resonance signal, from what was presumed to be an iron-porphyrin moiety, was observed. Generally, it was concluded by Agarwala and Longo (3) that inhibition by the free-base porphyrins occurs by forming some kind of complexes with the metal atoms of substrate, whereas by the metalloporphyrins primarily by precipitation or chemisorption through oxides or oxygen atoms of the metal surface.

Phthalocyanines

The study of Hettiarachchi, Chan, Wilson and Agarwala (14, 26) was directed to explore the phthalocyanines or polyphthalocyanines as acid corrosion inhibitors for steel. They believed that phthalocyanines would be more effective as corrosion inhibitors compared with porphyrins because of the almost rigid planarity of the phthalocyanine molecule (28-

32). In addition to the chemisorption pathways described earlier, a higher degree of planarity is expected to increase the interaction between the pi-electron system of the phthalocyanine with the conduction band of the metal. Furthermore, the more planar the molecule, higher will be the degree of coverage and, hence, the inhibition efficiency. According to Snow and Jarvis (12) the planarity and electron density in the pi-system of macrocyclics affect their surface adsorption properties and that the phthalocyanine compounds are specifically useful for the formation of stable films.

The study of polyphthalocyanines was considered even more useful than their monomers since the polyphthalocyanines could form an entirely new class of inhibitors because of their high electronic conduction (13, 26). An important feature here is that the polyphthalocyanines, while inhibiting corrosion, are capable of retaining an important property which is only expected of metals, i.e., its electrical conductivity. This suggests some tremendously useful military applications of the material in future.

The synthesis of phthalocyanines and polyphthalocyanines was carried out by conventional chemical routes described elsewhere (26). First, the water soluble compounds were tested to determine if they might be as effective as porphyrins in their inhibitor efficiency. Hettiarachchi, et.al. (26) synthesized highly water-soluble tetrasulfo-phthalocyanines [TSPC], both metal-free and, with a variety of metal ion centers: Co(II), Co(III), Fe(II), Fe(III) and Vanadyl. Although these phthalocyanines satisfied the planarity and the water solubility requirements, they failed as effective inhibitors. Hence water soluble phthalocyanines were eliminated from their investigations. Among the water insoluble compounds, tetraamino [TAPC] and tetracarboxy [TCPC] derivatives based on Co(II), Co(III) and Fe(III) centers were synthesized. The study on metal-free insoluble phthalocyanines was also eliminated as they offered no advantage over their metallo-derivatives. The polymeric phthalocyanine TCPCs were synthesized using Co(II) and Fe(III) as centers.

In the case of water-soluble phthalocyanines, the compounds were directly dissolved in 1% NaCl solution to make it 1 mM with respect to the phthalocyanine before testing. When the phthalocyanine was water-insoluble, the polished steel specimens were immersed in a 1 mM solution of the TCPC compound in dimethylsulfoxide (DMSO) over a period of 13 h, washed with DMSO and dried at 100^{o} C before testing.

The polyphthalocyanines coatings on steel surface were prepared by dissolving Co(II)-TCPC or Fe(III)-TCPC in dimethyl sulfoxide (DMSO) and immersing the polished and degreased metal sample in this solution for 12 h. The metal sample was then removed from the coating solution and

introduced into an oven sparged with argon gas. The sample was then heat treated at 450T^{O} C in the inert atmosphere, during which process an adherent and stable phthalocyanine polymer coating was formed.

The in-situ polymerization of TCPC was first observed by Achar et. al.(25). The polymerization process is not a typical condensation reaction as it occurs with the loss of H_2O, CO, and CO_2. This process (polymerization) is a multistep reaction; loss of water produces the anhydride as an intermediate which, then, thermally decomposes to give the polymeric product where the molecules of phthalocyanines are linked by a covalent bond between benzene rings. Hettiarachchi, et al. (26) adapted this method to polymerize monomeric TCPC adsorbed on a metal electrode surface. In the case of Fe(III)-TCPC polymer coatings, the concentration of the phthalocyanine solution was increased to minimize the porosity of the polymer coating. Some experiments were performed with multiple coatings as well as afte pre-etching the sample in 1% NaCl solution of pH 2 before phthalocyanine treatment.

The effectiveness of phthalocyanines as acid corrosion inhibitors for steel was studied by conventional electrochemical dc and ac techniques. The details of these tests, potentiodynamic polarization and ac impedance spectroscopy, have been reported elsewhere (33-34). A rotating disk electrode at 1800 RPM (30 Hz) has been used for the polarization measurements. Water soluble TSPC derivatives with metal centers exhibited poor corrosion inhibition (14), see Table 5. Water insoluble TAPC derivatives served as better corrosion inhibitors than their water soluble counterparts when the metal surface was coated with an adsorbed layer of the compound. The polarization plots (E vs.log i) showed no significant differences in the presence or absence of phthalocyanines. A summarized view of the electrochemical parameters is reported in Table 5, indicating the influence of these monomers. Compared to Co(II)-TAPC, Fe(III)-TAPC showed higher degree of corrosion inhibition, however, the inhibitor efficiency was still far too low to be of any significance. Thus, the investigators opted to concentrate on the formation of stable polymeric phthalocyanine coatings on the metal surface (14).

To study polyphthalocyanine coatings for corrosion inhibition, the electrochemical testing was performed with a rotating cylinder electrode instead of using a rotating disk arrangement (26). This change was deemed necessary because it was not possible to heat treat the phthalocyanine coated metal disk at 450 C due to the inability of the Teflon mount to withstand such temperatures. The problem was overcome by using a removable cylinder electrode. Additionally, since the rotating cylinder electrode renders much faster mass transfer rates at reasonably slow rotational speeds, all the

experiments with polyphthalocyanine coatings were performed with a rotating cylinder electrode at a rotational speed of 255 RPM. The results of the potentiodynamic polarization measurements for the mild steel in 1% NaCl solution (pH 2) with and without polymeric coatings were as shown in Figure 4. The number of distinct features noted from this figure are: (i) the corrosion potential shifted to more positive values with the polymer, Fe(III)-TCPC showed the most positive shift; (ii) both the anodic and cathodic polarization curves shifted to lower current densities; and (iii) the anodic reaction rates (polarization curves) were reduced by almost two orders of magnitude with the coatings. The results of these studies are summarized in Table 6.

The ac-impedance studies were also performed on the above polymeric coatings at the free corrosion potential by holding the potential at this value, using a PAR Model 173 potentiostat. The impedance measurements over a wide frequency range (1 kHz to 10 mHz or less) were made with the help of a Solartron Model 1250 Transfer Function Analyzer. The amplitude of the ac signal used was 8 mV. Evaluation of the corrosion behavior of a polymer-coated metal, such as that used in this case, was made possible by the wideband ac impedance measurements, which provided information on both the resistive and the capacitive behavior of the interface. The results of these experiments were shown as Nyquist plots [Re(Z) vs. Imag.(Z)] of the interfacial impedance as a function of frequency, as in Figure 5. The curves, slightly suppressed semicircles, show the characteristics of steel in chloride solutions with and without the presence of polyphthalocyanines The polarization resistance (R_p) values, calculated from these impedance spectra, were determined from the intercepts (lengths of the diameters) of the suppressed semicircles along the [Re(Z)] axis. According to Hettiarachchi, et al. (see Table 6), the R_p values increased 3 and 6 folds when three coatings of polymeric Co(II)-TCPC and a single coat of Fe(III)-TCPC were applied on the steel surface, respectively; the corresponding calculated inhibitor efficiencies were approximately 68% and 83%, respectively. Pre-treatment of the metal surface, such as etching, did not improve the bonding of the polymer Fe(III)-TCPC, Table 6. The suppressed nature of the semi-circle still remains with the center below the real axis, indicating that the interfacial impedance is a result of more than one electrochemical process. However, neither the Nyquist plot nor the Bode plot provided the necessary resolution to permit the separation of the multiple electrochemical processes involved.

The water insoluble polymeric phthalocyanine coatings based on Fe(III) centers gave inhibitor efficiencies as high as 83%, as confirmed by both slow potentiodynamic technique and the AC-impedance analysis (Table 7). The polymerization was achieved by simple dip coating followed by heat treatment of

the coated surface at 450° C in an inert atmosphere. The resulting coating was shown to be adherent and electrically conducting, thereby providing a unique set of conducting polymer inhibitors that can be used in acid environments. High void fraction in the polymer were considered possible limitations in the achievement of higher inhibition efficiency. Hence, some studies were conducted to develop polyphthalocyanines with very low void fractions. Thus, polymer coating of Fe(III)-TCPC containing p-hydroxy pyridine groups as shown in Figure 6 were synthesized and tested (26). Contrary to the expectations, the inhibition efficiency did not improve, it went down (cf.Table 7). The authors attributed this to poor surface coverage by the polymer during its derivatization on the metal surface. The alternatives suggested were to overcome this problem by first synthesizing the p-hydroxy pyridine derivative of the monomer and then polymerize it on the metal surface. Currently, this work is being carried out at by the author.

The effects of incorporating long chain aliphatic hydrocarbon groups in the phthalocyanines were also investigated. Particularly, the two groups studied were carboxy-aminoundecanoic acid and carboxy-aminocaproic acid. Hettiarachchi, et al. (26) prepared and studied Fe(III) and Co(II) tetrakis (N-carboxy-12-aminoundecanoic acid) phthalocyanine [TCAUPC], and Fe(III) and Co(II) tetrakis (N-carboxy-6-aminocaproic acid) phthalocyanine [TCACPC] compounds. The results, in Table 7, indicated a significantly high corrosion inhibition. The inhibitor efficiencies of up to 88% were realized by these molecules, whereas with the polyphthalocyanines 83% was the best.

SUMMARY AND CONCLUSIONS

The parent structures of the porphyrins and phthalocyanines, were considered to be unique for the development of new corrosion inhibitors for iron and steel. The "tailor-make" approach, to build on the basic structure through synthetic steps, was found very successful in enhancing the inhibition efficiency. One of the prime considerations in this study was to keep the structure spatially flat and rigid. Several approaches were taken whereby a macrocycle could be anchored to the surface atoms of the test metal. Macrocyclics were weighted down by the addition of heavy groups to the ring structure so that when adsorbed, they could provide high surface coverage, or linked with surface active groups or high valent metal ions for chemisorption.

Corrosion studies were performed with water soluble, insoluble and metallo-derivatives of porphyrins on Armco iron through several methods of application. Among the soluble type, metallo-derivatives with sultones or iodide as counter anion were highly efficient (90%). The best corrosion

inhibition was accomplished with those which were metal-free and vapor-deposited in vacuum. The insoluble porphyrins and metallo-porphyrins were ineffective when applied from organic solutions even at reflux temperatures (80 C or 140 C). These observations imply that the porphyrins can react and bond to metal surface at the higher temperatures as with vapor deposition. The fact that the free base porphyrins are more effective than the metallo-porphyrins suggests that the reaction mechanism involves bonding of surface metal atoms to the inner nitrogen atoms of the porphyrin molecule.

The study on phthalocyanine, a structural analog of porphyrin, was primarily performed by Hettiarachchi and co-workers (14, 26). They synthesized a number of metallized and metal-free derivatives of phthalocyanines with the intent that their basic interactive character and spatial arrangements would remain intact. The water soluble quaternized (tetrasulfo- and tetraamino-) phthalocyanines complexes with Co(II) and Fe(III) showed no significant corrosion inhibition of mild steel when tested in 1% NaCl solution at pH 2. Apparently, these complexes did not adhere well or adsorb on the surface effectively. A number polymeric coatings of the phthalocyanine and derivatives of phthalocyanines which contained long alkyl chains to increase adsorption were also prepared and tested. The polymeric coating of iron(III)-tetracarboxy-phthalocyanines, [Fe(III)-TCPC], was able to provide up to 83% inhibition efficiency. These were sheet polymers of graphite-type structure, containing voids between the phthalocyanine units. Attempts to fill these voids through formation of p-hydroxy-pyridine derivatives were unable to improve corrosion inhibition efficiency. Primarily because these steps were taken after the polymerization, and therefore, could not fill the void. A better alternative would be to syntheize the monomer with p-hydroxy pyridine groups first, a course of action to be pursued next. In comparison with the polymers, the long alkyl-chain substituted phthalocyanines exhibited more promising results (26). It was determined that the length of the alkyl chain and the nature of the central metal ion are important in providing higher inhibition efficiency. For example, a ten carbon chain tetracarboxy-aminoundecanoic acid phthalocyanines [TCAUPC] with Fe(III) and Zn(II) as central metal ions showed inhibition efficiencies of 88% and 87%, respectively. But when the alkyl chain of five carbon atoms was used, as in the case of tetracarboxyaminocaproic acid phthalocyanine [TCACPC] with the same central metal ions, the observed inhibition efficiencies were lower. The substitution of central metal ion with Co(II) or Si(IV) also decreased the inhibition efficiency.

In general, this review has indicated that the macrocyclics of the porphyrin and phthalocyanine type offer an excellent promise as corrosion inhibitors for iron and steels. In particular the "tailor-make" approach has demonstrated that a

number of types of these new classes of compounds can be systematically synthesized to produce successful inhibitors, and that they can be applied to other metallic substrates.

ACKNOWLEDGMENT

The author expresses his gratitude to his co-investigators, Drs. F. R. Longo, S. Hettiarachchi, and R. B. Wilson, Jr. for their innovative contributions in this work. Both the in-house and contractual supports for this work were provided by the Naval Air Systems Command and the Offices of Naval Research and Technology. The author also expresses his thanks to Dr. J.J. De Luccia and Mr. I.S. Shaffer for their support and enthusiasm.

REFERENCES

1. J. Assour, J. Chem. Phys., Vol. 43, 2477 (1965).
2. F. R. Longo, J.J. De Luccia and V.S. Agarwala, Proc. 6th European Symposium on Corrosion Inhibitors, Univ. of Ferrara, Ferrara, Italy, pp.155-166, September 1985.
3. V.S. Agarwala, Proc. International Congress on Metallic Corrosion, Toronto, Canada, Vol.1, p. 380, June 3-7, (1984).
4. V. S. Agarwala and F.R. Longo, "Porphyrins: A New Class of Corrosion Inhibitors" in Surfaces, Inhibition and Prevention, eds., E. McCafferty and R.J. Brodd, The Electrochemical Society Publication, Vol.86-7, pp.56-68, 1986.
5. K. Rajan, Natl. Intelligence. Serv., AD 720384, U.S. Department of Commerce, Washington, DC (1970).
6. K. Rajan, Final Technical Report, IITRI-C6202-6, Contract No. N00019-70-C-0180, Washington, DC (1970).
7. E.B. Fleischer and J.H. Wang, J. Am. Chem. Soc., Vol.82, 3498 (1960)
8. B.F. Burnham and J.J. Zuckerman, J. Am. Chem. Soc., Vol.92, 1547(1970).
9. K. Letts and R.A. McKay, Inorg. Chem., Vol.14, 2993 (1975).
10. W.G. Rau and F.R. Longo, Inorg. Chem., Vol.16, 1372 (1976).
11. M. Zerner and M. Gouterman, Theor. Chim. Acta., Vol.4, 44 (1966).
12. A. Snow and N. Jarvis, J. Am. Chem. Soc., Vol.106, 4706 (1984).
13. S. Hettiarachchi, Y.W. Chan and R.B. Wilson, Jr., "Define Corrosion Inhibitors for Metals in A Naval Environment', Naval Air Development Center Contract No. N62269-85-C-0290; SRI International Annual Report No. PYU-1178, October 1986.
14. S. Hettiarachchi, Y.W. Chan, R.B. Wilson, Jr. and V.S. Agarwala, Corrosion, Vol.45(1), 30-33, 1989.

15. H.F. Schaefer, III, Accounts of Chem. Res., Vol.10, 287 (1977).
16. P. Sayer, M. Gouterman and C.R. Connel, Accounts of Chem. Res., Vol.15, 73 (1982).
17. Yoshio Umazawa and T. Yamamura, J. Electrochem. Soc., Vol. 126(4), 705 (1978).
18. J.H. Sharp and R.1. Miller, J. Phys. Chem., Vol.72, 3335 (1968).
19. M.A, Barrett, Z. Borkowska, M.W. Humphret and R. Parsons, Thin Solid Films, Vol.28, 289 (1975)..
20. P. Vincent, Z.D. Popovic and L. McIntyre, Thin Solid Films, Vol.82, 357 (1981).
21. C.M. Allen, L.B. Silbey and S. Cosgrove, 14th Annual Meeting of the ASLE, Buffalo, NY, Paper No. 59AM, April 1959.
22. V.G. Fitzsimmons, R.L. Merker and C.R. Singleterry, Naval Research Laboratory Report No. 3672, May 1950.
23. A.D. Adler and Longo, F.R., J. Org. Chem., Vol.32, 376 (1967).
24. L.R. Nudy, H.G. Hutchinson, C. Schieber and F.R. Longo, Tetrahedron, Vol.40, 2359 (1984).
25. B.N. Achar, G.M. Fohlen and J.A. Parker, J. Polymer Sci., Vol.21, 589 (1983).
26. S. Hettiarachchi, Y.W. Chan and R.B. Wilson, Jr., "Corrosion Inhibitors for Metals in a Naval Environment", SRI International Project 1178, Naval Air Development Center Contract No N62269-85-C-0290, February 1988.
27. F.R. Longo, "Porphyrins as Corrosion Inhibitors", Naval Air Development Center Report No. NADC-84167-60, July 1984.
28. B. Hoskins, S. Mason, and J. White, Japan Chem. Soc., Chem. Comm., 554-595 (1969).
29. T. Kobayashi, F. Kurokawa, T. Ashida, N. Uyeda, and E. Suito, Japan Chem. Soc., Chem. Comm., 1631-1632 (1971).
30. B. Wheeler, G. Nagasubramanian, A. Bard, L. Schechtman, D. Dinninny, and M. Kenney, J. Am. Chem. Soc., Vol.106, 7404 (1984).
31. K. Wynne, Inorg. Chem., Vol.24, 1339-1343 (1985).
32. T. Marks, Science, Vol.227, 881-889 (1985).
33. Standard Reference Method for Making Potentiostatic and Potentiodynamic Anodic Polarization Measurements, G 5-82, Annual Book of ASTM Standards, Vol 03.02, 1984.
34. W.J. Lorenz and F. Mansfeld, Corrosion Science, Vol.21, 647 (1981).
35. D.J. Quimby and F.R. Longo, J. Am. Chem Soc., Vol.97, 5111 (1975).

TABLE 1

MASS LOSS RESULTS USING TMPyP AND VARIOUS COUNTER ANIONS IN 1.0% NaCl, pH 6 (CONC.: 0.05 mM)

Inhibitor Counter Ion	Corrosion Rate, mdd 12h	48h	% Inhibition Efficiency*
Control	380	370	0
Iodide	53	74	80
Chloride	174	182	50
Benzoate	84	106	70
Sulfate	114	160	59
Toluenesulfonate	96	87	76

All entries are averages of 5 observations.
* Based on 48h data.

TABLE 2

MASS LOSS RESULTS IN THE PRESENCE OF METALLO-DERIVATIVES OF TMPyP-TS IN 1.0% NaCl, pH 6 (CONC.: 0.3 mM).

Incorporated Metal Ion	Corrosion Rate, mdd 12h	48h	% Inhibition Efficiency*
None	380	370	0
VO(II)	71	46	87
Co(II)	53	68	81
Cu(II)	62	49	87
Fe(III)	27	15	96
Ni(II)	59	45	87
Mn(III)	32	28	92
Rh(II)	48	27	93

* Based on 48h data.

TABLE 3

THE EFFECT OF pH AND PORPHYRIN CONCENTRATION ON THE CORROSSION RATE OF IRON.

Inhibitor TMPyP Iodide	<------ Corrosion Rate, mdd ------> Distilled Water	1% NaCl	0.1 mM HCl
0.001 mM	79	97	91
0.01 mM	39	97	80
0.1 mM	21	97	80
1.0 mM	18	103	80

* All measurements were made after 48 hours of immersion.

TABLE 4

RESULTS OF MASS-LOSS STUDIES ON IRON SPECIMENS PREPARED BY VAPOR DEPOSITION OF PORPHYRIN IN 1% NaCl SOLUTION.

Porphyrins	*Corrosion Rate, mdd	% Inhibition Efficiency	Number of Tests
None**	382 ± 37	0	3
TPhP	28 ± 10	93	15
TPyP	36 ± 20	91	6
T(o-ChloroPh)P	38 ± 8	90	4
5-Nitroporphin	62 ± 5	84	4
NiTPhP	202 ± 31	47	3
CoTPhP	182 ± 21	52	3
ZnTPhP	89 ± 17	77	3
VOTPhP	173 ± 40	55	3
Fe(III)TPhPCl	312 ± 37	18	3
Mn(III)TPhPCl	283 ± 18	26	3
RhTPhP	271 ± 26	29	3
ZnTPyP	103 ± 13	73	3
Fe(III)TPyPCl	327 ± 27	14	3
CoTPyP	120 ± 18	68	3

* Average corrosion rate determined by total immersion of specimens for 7 days.
** Specimens heated in vacuum in the absence of porphyrin.

TABLE 5

RESULTS OF ELECTROCHEMICAL POLARIZATION MEASUREMENTS ON MILD STEEL TREATED EITH PHTHALOCYANINES IN 1% NaCl (pH 2).

Inhibitor System	Ecorr mV(SCE)	mV/Decade βa	βc	Icorr mA/cm^2	% Inhibition Efficiency
None	-500	45	-370	1.05	--
*VO-TSPC	-488	43	-350	1.0	5
*Co(II)-TSPC	-498	38	-300	0.95	10
*Fe(III)-TSPC	-490	39	-475	0.93	7
Co(II)-TAPC	-505	45	-325	0.95	10
Co(II)-TAPC (on etched steel)	-493	43	-370	0.82	22
Fe(III)-TAPC	-505	45	-340	0.65	37
Fe(III)-TAPC (on etched steel)	-500	44	-372	0.88	16

* 1 mM concentration in test solution (water soluble).

TABLE 6

RESULTS OF ELECTROCHEMICAL POLARIZATION MEASUREMENTS ON MILD STEEL TREATED WITH POLYPHTHALOCYANINES IN 1% NaCl (pH 2).

Inhibitor System	Ecorr mV(SCE)	mV/Decade βa	βc	Icorr mA/cm^2	% Inhibition Efficiency
None	-538	247	-193	0.48	--
Co(II)-TCPC (3 coats)	-525	260	-205	0.20	55
Fe(III)-TCPC	-495	225	--	0.08	83
Fe(III)-TCPC (on etched steel)	-512	228	--	0.16	66

TABLE 7

RESULTS OF THE AC IMPEDANCE MEASUREMENTS ON MILD STEEL TREATED WITH MONOMER AND POLYMER PHTHALOCYANINES IN 1% NaCl SOLUTION (pH 2).

Inhibitor System	R_p in $Ohm.cm^2$	Wmax, rad./s	C_p in $\mu F/cm^2$	% Inhibition Efficiency
None	42	63	378	--
Poly Co(II)-TCPC (3 coats)	137	10	750	68
Poly Fe(III)-TCPC	240	13	318	83
Poly Fe(III)-TCPC (on etched steel)	159	16	400	74
Poly Fe(III)-TCPC ** (low void fraction)	174	2	3640	77
*Fe(III)-TCAUPC	323	16	196	88
*Co(II)-TCAUPC	243	4	1038	83
*Fe(III)-TCACPC	255	25	157	84
*Co(II)-TCACPC	114	40	222	65

* Phthalocyanine containing long chain hydrocarbon groups:
[TCAUPC] - tetrakis (N-carboxy-12-aminoundecanoic acid)
[TCACPC] - tetrakis(N-carboxy-6-aminocaproic acid).
** Containing p-hydroxy pyridine groups in the voids.

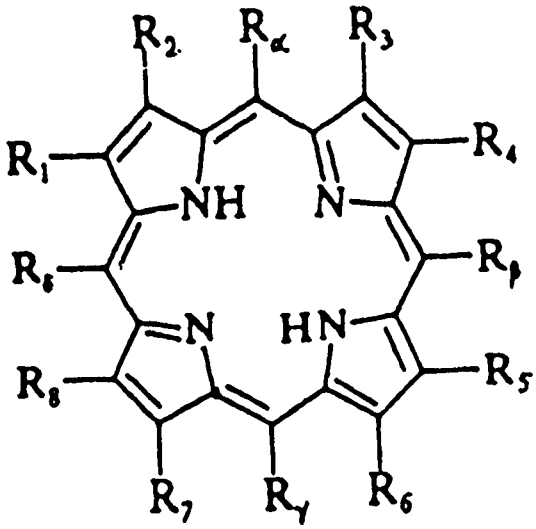

A

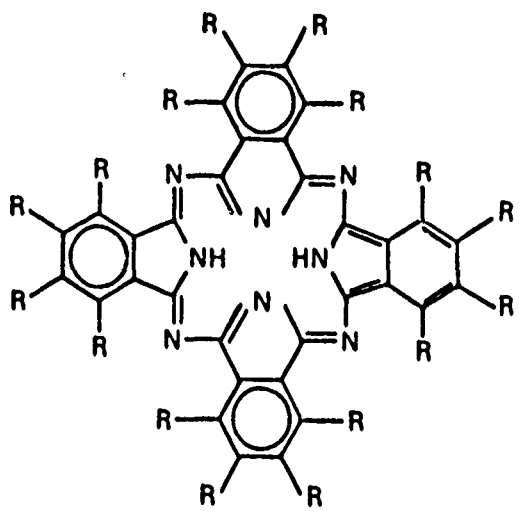

B

Figure 1 - General structures of (A) porphyrin, and (B) phthalocyanine molecules with conjugated double bonds. Metal ions may be chelated at the center of the ring by bonding to the four inner nitrogen atoms.

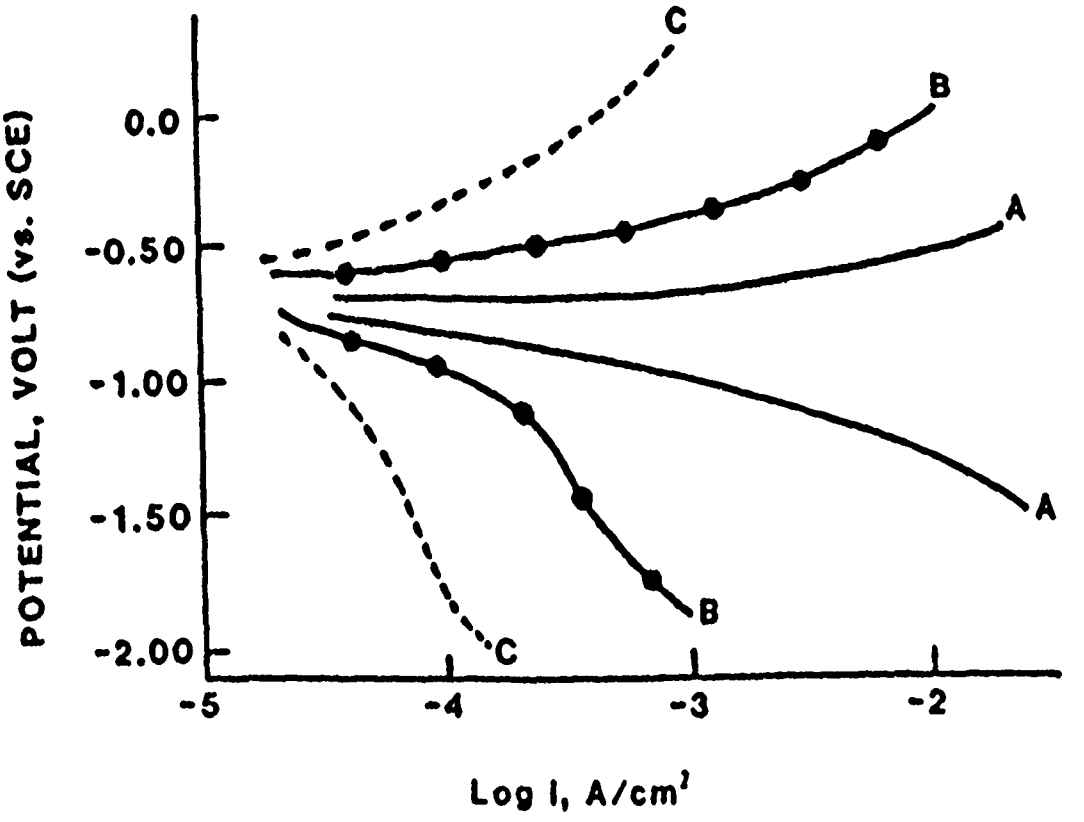

Figure 2 - The effect of porphyrins on the potentiostatic polarization behavior of Armco iron in 1.0% NaCl (pH 2); Curves A: Control (without inhibitor), Curves B: with TMPyP.TS (1.0 mM), Curves C: Vapor deposited TMPyP.

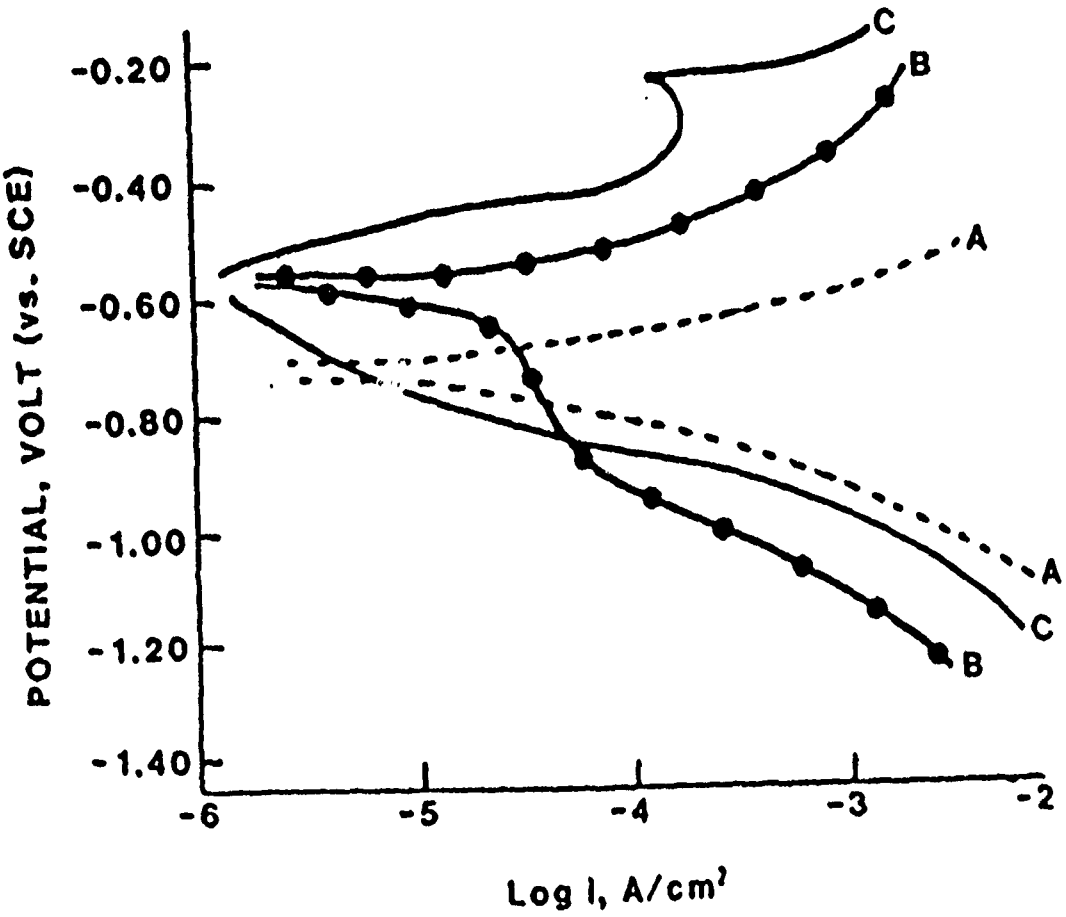

Figure 3 - The effect of water soluble metalloporphyrins on polarization behavior of Armco iron in 1% NaCl (pH 2); Curves A: Control (without inhibitor), Curves B: with Cu(II)-TMpyP.TS, and Curves C: with Fe(III)-TMPyP.TS at 1.0 mM concentration.

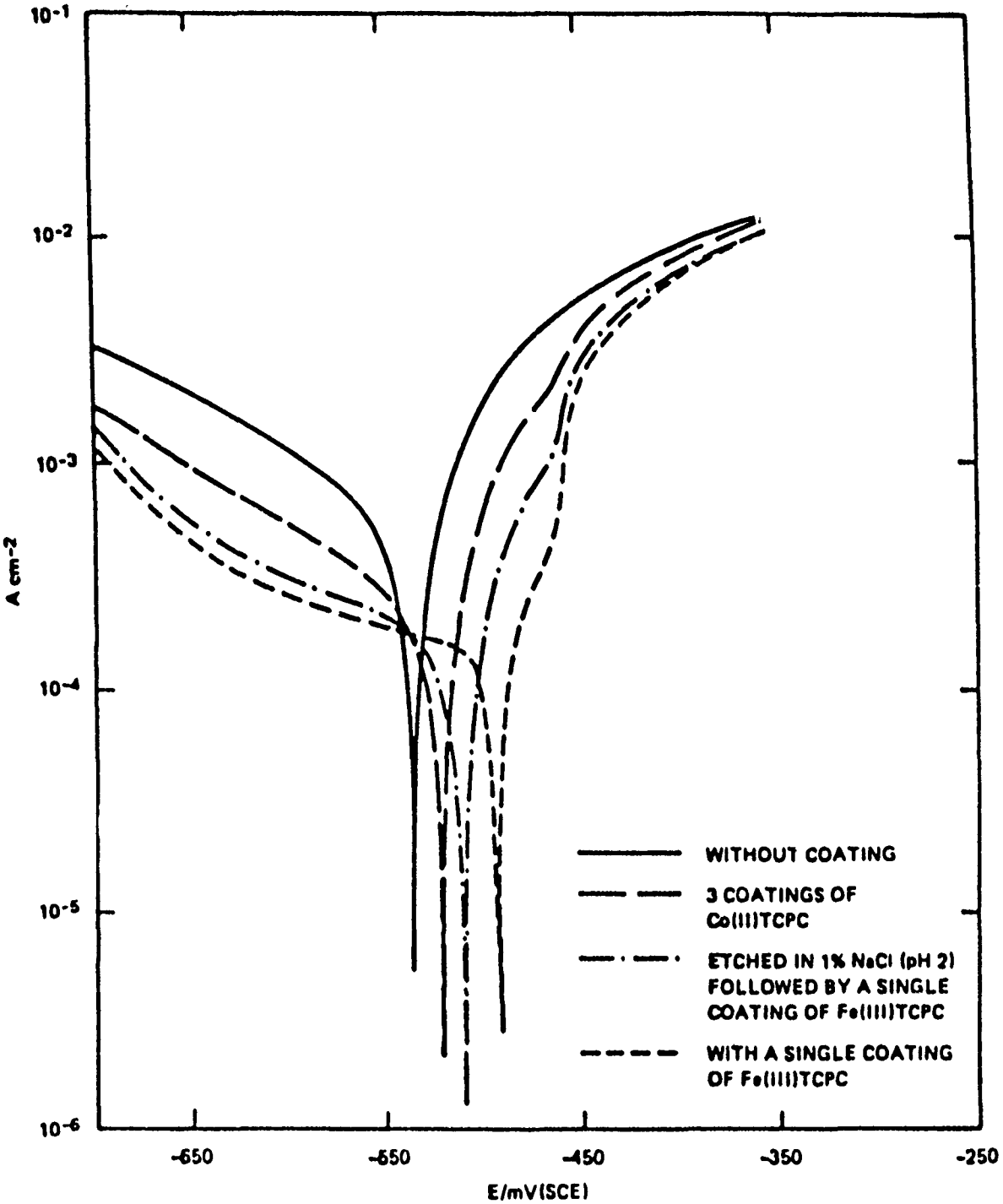

Figure 4 - The effect of polyphthalocyanines on the polarization behavior of mild steel in 1% NaCl solution of pH 2 : (a) without coating, (b) three coatings of Co(II)-TCPC, (c) after etching in 1% NaCl (pH 2) followed by a single coating of Fe(III)-TCPC, and (d) single coating of Fe(III)-TCPC. (dE/dt = 0.1 mV/s)

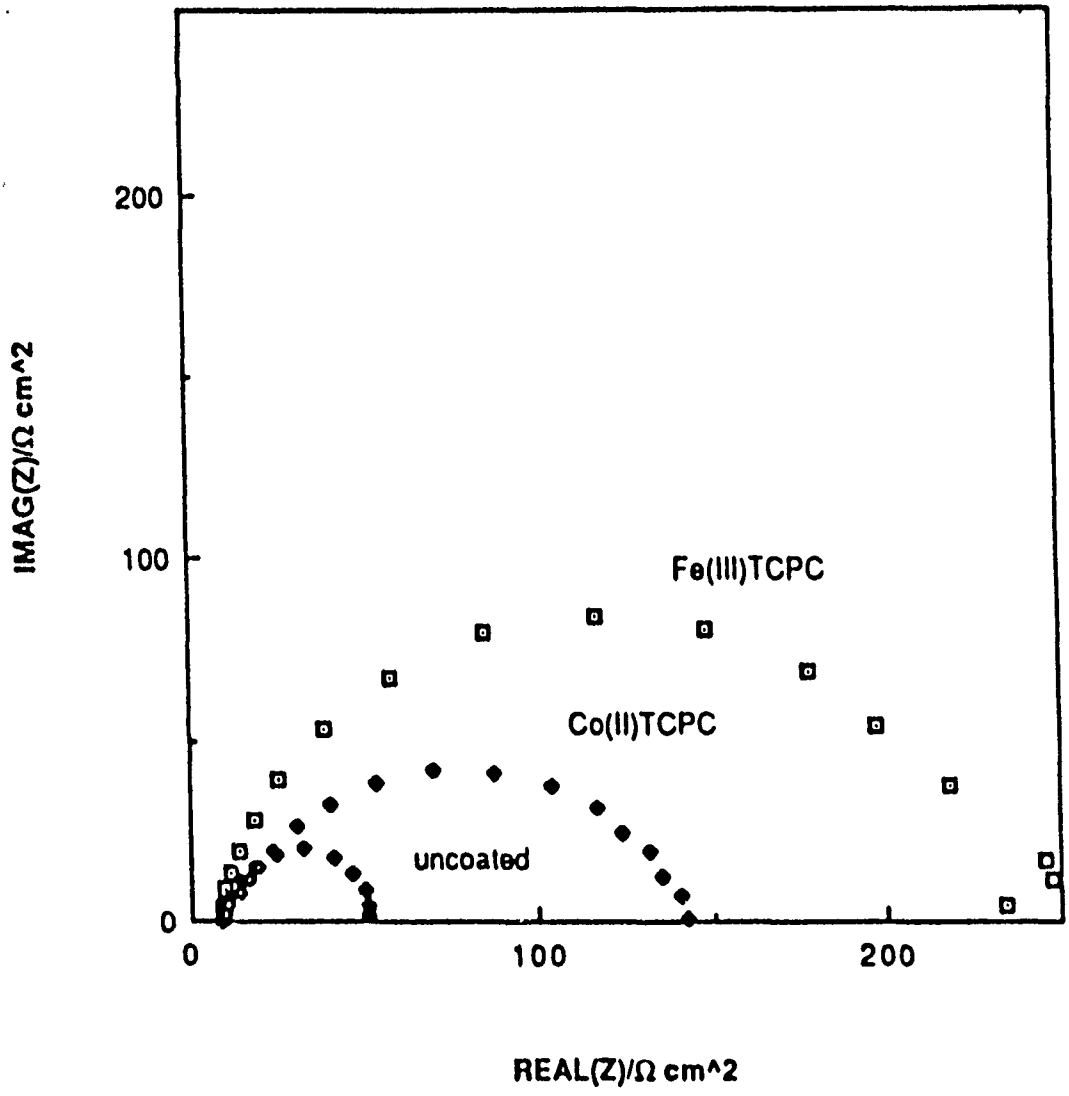

Figure 5 - Nyquist plots [Re(Z) vs. Imag.(Z)] for mild steel in 1% NaCl solution (pH 2) with: (a) uncoated steel, (b) three coatings of Co(II)-TCPC and (c) single coating of Fe(III)-TCPC polymers.

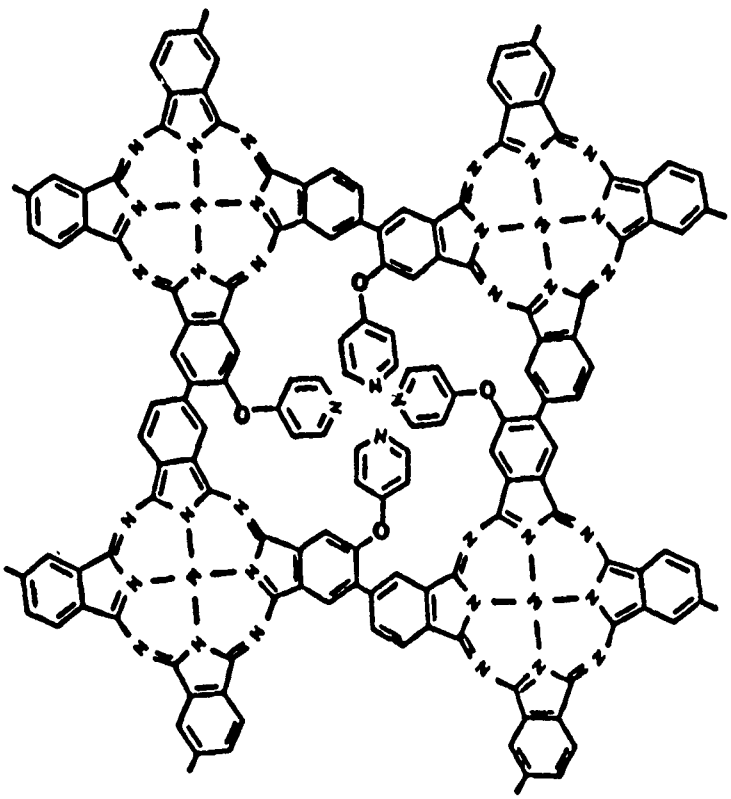

Figure 6 - The structure of void filled polyphthalocyanine with p-hydroxy pyridine groups, and containing central metal ions in the phthalocyanine rings.

ANALYSIS OF PRIMERLESS FINISHING SYSTEMS FOR ALUMINUM PHASE I - ELECTROCHEMICAL IMPEDANCE TESTING

Stephen J. Spadafora, Charles R. Hegedus, Donald J. Hirst and Anthony T. Eng

Air Vehicle and Crew Systems Technology Department
Naval Air Development Center
Warminster, PA 18974-5000

ABSTRACT

A recent trend in the corrosion protection of aluminum alloys used in military equipment is the development of primerless finishing systems, where the topcoat can be applied directly to surface treated aluminum. Currently, two approaches are available to obtain a primerless system: (1) a urethane sealed, sulfuric acid anodized pretreatment which can be directly topcoated and (2) a primerless or self-priming topcoat which can be directly applied to a standard Al surface pretreatment. A two phase study was performed to investigate the properties of these two systems. The first phase investigated the electrochemical properties of both coating-pretreatment systems on aluminum and compared their performance to conventional Navy finishing systems. The second phase compared the physical properties of both conventional Navy finishing systems and the two coating-pretreatment systems on several aluminum substrates. This paper discusses the Electrochemical Impedance Spectroscopy analysis of these systems performed in Phase I. These test results indicate that primerless systems show promise as viable alternatives for the conventional system and should be fully characterized by extensive physical performance testing.

INTRODUCTION

Military airframe and aerospace equipment are primarily constructed with aluminum alloys due to their high specific strength compared to other structural materials. If left unprotected during deployment, these alloys would rapidly corrode, causing the aircraft to be grounded. With the high cost and importance of these systems, protective materials and processing methods which maximize component service lifetime while minimizing failure must be utilized. Therefore, to minimize the threat of environmental deterioration, inorganic

surface treatments and organic coatings are specified for virtually all military aerospace systems. These precautions are particularly important for alloys on Navy aircraft which are normally stationed in highly corrosive marine locations.

Generally, Navy aircraft finishing systems consist of an inorganic surface treatment followed by a series of organic coatings. MIL-S-5002C describes cleaning requirements and surface treatments for aluminum alloys. Surface treatments enhance the adhesion and corrosion inhibition of subsequent organic coatings. These treatments can be either an anodized film produced in accordance with MIL-A-8625 or a chromate conversion coating achieved by applying materials conforming to MIL-C-81706 to produce a conversion coating meeting MIL-C-5541. MIL-F-7179 provides the requirements for paint systems used on U.S. military aircraft. The Navy's standard organic coating system consists of an epoxy primer (MIL-P-23377 or MIL-P-85582) and a polyurethane topcoat (MIL-C-83286 or MIL-C 85285). The primers are adherent, and inhibit substrate corrosion due to a high concentration of strontium chromate (3). The polyurethane topcoats are flexible, chemical and weather resistant, while providing the required optical properties. Some aircraft also require a coat of spray sealant (MIL-S-8802, MIL-S-81733, or MIL-P-87112) between the primer and topcoat around fasteners and areas of excessive flexing. The sealant coat enhances the flexibility of the coating system and prevents cracking of the paint system. This finishing system was specifically designed to protect aluminum aircraft structures from the harsh Navy operational environment. References (1-3) provide more detailed descriptions of corrosion control documents and finishing systems for military equipment.

Although the above finishing system has been the premier aircraft finishing system for 20 years, it has several deficiencies. The primer is brittle, particularly at low operating temperatures (-51oC), resulting in cracking of the paint system on highly flexed areas. Sealants are soft and easily deformed, and are difficult to apply and remove. In addition, increased awareness for environmental preservation has caused state and local governments to begin limiting the volatile organic compound (VOC) emissions during painting operations. These new regulations have impacted both equipment manufacturers and rework depots by limiting the amount and types of paints which they can apply. Finally, increased concern for the effects of carcinogenic chromates on worker safety has caused environmental agencies to issue regulations limiting or eliminating the use of chromates used in the conversion coatings and primers in the current finishing system. These deficiencies have prompted a recent trend to develop finishing systems consisting of a surface pretreatment and only one organic coating (4-7). This has been accomplished by using either conventional topcoats on a modified pretreatment

(4), or a self-priming topcoat on conventional pretreatments (5-6). Either method eliminates the use of a primer, saving application time, manhours, and materials. This effort investigated the effectiveness of these systems to protect aluminum substrates.

DESCRIPTION OF PRIMERLESS FINISHING SYSTEMS

The two currently available approaches to eliminate the primer from a finishing system are: (1) Modify the inorganic pretreatment or (2) Modify the topcoat. Reference (4) discloses a coating composition and application process for a modified anodized surface treatment which precludes the use of a subsequent primer prior to topcoating. This process follows the standard anodizing procedure (8) except for the final sealing step. The conventional process increases the natural oxide surface film thickness, which is normally 1 to 5 nanometers, to an oxide thickness of 0.5 to 100 microns. The resultant anodized film consists of a non-porous underlying layer with a porous oxide structure on the surface. To increase the corrosion resistance of the film, the porous layer is normally sealed with steam, hot water or dichromate solutions. In contrast, the modified procedure utilizes a colloidal suspension of polyurethane resin, typically 7% solids in an alkaline solvent water bath, to seal the porous oxide surface. The particle size of the colloidal suspension is designed to fit within the anodized surface structure. Upon contact with the aluminum surface, normally at 180oC, the solution induces film hydration and also impregnates the porous structure. After sealing, the specimen is exposed to air which allows curing and crosslinking of the polyurethane resin. This results in a hard, water and solvent resistant, flexible and corrosion resistant film. A standard topcoat, MIL-C-83286 or equivalent, can be applied to this substrate one hour after removal from the sealing tank. Adhesion of the polyurethane topcoat to the pretreatment is expected to be good due to the obvious chemical compatibility. Specific formulations and procedures are provided in ref. (4).

The alternative method for eliminating the need for a primer is to use a topcoat which is self-priming. Reference (5) describes the development and properties of one such coating (UNICOAT). This coating can be applied directly to deoxidized, anodized or chromate conversion coated aluminum surfaces, and provides the properties of the conventional primer and topcoat system used on military aircraft. Unicoat consists of titanium dioxide, zinc molybdate, zinc phosphate, an organo-zinc salt, vesiculated polymer bead pigments dispersed in a two component, aliphatic polyurethane binder. While all of the pigments contribute to the film's opacity, the zinc molybdate, zinc phosphate, and organo-zinc salt are responsible for corrosion inhibition. The polyurethane binder provides good adhesion, flexibility, chemical

resistance and weather resistance. The volatile organic compounds (VOC) content of the original formulation has been optimized to give a VOC of 415 grams per liter of paint. The viscosity of this admixed material is sufficient for application by conventional air spray at slightly higher inline pressures. In addition, this formulation is suitable for airless spray application techniques. If a lower viscosity material is desired, the coating can be thinned with either 1,1,1 trichloroethane, which is currently exempt from emission regulations, or with standard urethane thinners.

EXPERIMENTAL

In order to characterize the electrochemical nature of both primerless finishing systems, they were evaluated against the performance of standard paint systems used on Navy and Air Force aircraft. To accomplish this task, nine pretreatment and coating combinations were investigated on a bare 7075T-6 aluminum substrate, which is a widely used alloy on Navy aircraft. The three pretreatments used in this study were: the standard sulfuric acid anodized (SAA) treatment with a dichromate seal (prepared at our laboratories), the urethane sealed-SAA treatment (prepared by Lockheed Georgia) and the standard chromate conversion coating (obtained from Q Panel, Cleveland, OH). The chromic acid and conversion coated specimens represent the common substrates found on military aircraft prior to painting. The three paint systems used in the investigation were: 1) The standard epoxy primer (MIL-P-23377D, Type 1 "Primer Coatings, Epoxy Polyamide, Chemical and Solvent Resistant") and the standard polyurethane topcoat (MIL-C-83286, "Coating Urethane, Aliphatic Isocyanate, for Aerospace Application"); 2) The standard polyurethane topcoat (MIL-C-83286) alone; and 3) UNICOAT, a self-priming topcoat (SPTC). All of the coating systems were applied by conventional air spray and were allowed to cure for seven days prior to testing. Dry film thickness for the primer was 15.2 to 22.9 microns (0.006 to 0.009 inches). The MIL-C-83286 topcoat and Unicoat were both applied to a dry film thickness of 50.8 to 55.9 microns (0.020 to 0.022 inches).

Electrochemical Impedance Spectroscopy was used to evaluate the electrochemical properties of these systems. An EG&G Princeton Applied Research Corp. (PARC) Model M368-4 AC Impedance System with a Model 5208EC Lock-in Analyzer was used to obtain the EIS measurements. The test cell used for this investigation consisted of a glass o-ring joint clamped onto a coated metal specimen as described in reference (9). The electrolyte used for specimen exposure was a 3.5% NaCl solution with a pH of 6. The specimens were exposed to the electrolyte solution for 1200 hours at room temperature and periodic impedance measurements were made over the test exposure time. The first series of tests were

performed after 24 hours of exposure in order to allow the electrochemical system to reach equilibrium.

RESULTS AND DISCUSSION

Electrochemical impedance spectroscopy (EIS) provides qualitative and quantitative information about the corrosion resistance properties of both the coating and the substrate in addition to providing insight on the nature of their interfacial adhesion. Reference (10) provides a detailed description of EIS and its application for analyzing organic coating/metal substrate systems. Figures 1-4 contain Bode magnitude and phase diagrams of the EIS test results obtained at various exposure intervals for several of the coating/pretreatment systems. These specific spectra represent the significant EIS trends that were identified during this investigation.

After 24 hours immersion, all of the self-priming topcoat (SPTC) specimens had an impedance of 1.2x109 ohms in the low frequency range (10-2 Hz) which was the highest impedance of the three coatings as displayed in Figure 1. High impedance values correlate to low conductivity coatings that provide good barrier protection to the substrates to which they are applied. This impedance value is far above 107 ohms which is widely accepted as the lower limit below which no barrier protection is provided by the coating (10). In addition, the shape of the impedance curve is virtually straight over most of the frequency range with a negative slope, again indicating capacitance behavior (i.e. good barrier properties). Unicoat's high frequency phase angles were between -80o and -90o, again indicating good barrier properties, where -90o would be a perfect capacitor/barrier. The results for the SPTC remained the same throughout the 1200 hour test duration as illustrated in Figure 2. On all pretreatments, the low frequency Unicoat impedance remained above 109 ohms, while the high frequency phase angles continued to exhibit capacitive behavior, remaining between -75o and -90o.

The only change in the self-priming topcoat results occurred in low frequency phase angle curve for the SAA-urethane/SPTC system. During the test, the transition from capacitive to resistive behavior had shifted to a slightly lower frequency, indicating an improvement in the barrier properties. This change could have resulted from an increase in coating adhesion enhanced or catalyzed by the presence of some electrolyte at the interface. This increased degree of interfacial bonding with time, was also noted in references (11-12). Finally, during the 1200 hour test period, the chemical corrosion resistance properties of the inhibitors in this coating did not come into play and will not be addressed here.

All of the primer and topcoat (EP-UR) systems had impedance values of 6.3x107 ohms after 24 hours immersion. The EP-UR magnitude curve, although similar to the SPTC curve, was evident at a lower impedance range and leveled off at a higher frequency value. The low frequency impedance magnitude remained between 107 and 108 ohms and the shape of the curve was virtually unchanged over most of the exposure time. Again, these results indicate barrier type properties, however, not as good as Unicoat. The EP-UR system's phase angles were between -60o and -80o, which also shows less capacitive/barrier behavior. Unicoat provided better barrier protection because it was specifically designed to have a smoother less porous surface than the standard epoxy-urethane coating system. Although the EP-UR coating is a poorer barrier coating than the SPTC, it does provide excellent corrosion protection due to the large concentration of strontium chromate (Reference (3)).

At 1200 hours, the chromate conversion coating/EP-UR impedance curve began to show an upward turn after leveling off in the low frequency range as shown in Figure 3. Also, the phase angle curve was beginning to develop a peak in the high frequency range. These two trends indicate the presence of electrolyte at the interface resulting from some adhesion loss. In addition, some type of electrochemical reactions were occurring at the interface, probably corresponding to chemical inhibition of the corrosion process by the inhibitors within the primer.

The performance of the unprimed polyurethane topcoat (UR) varied with the different pretreatments. The topcoated SAA-urethane seal system performed closer to the other two coatings in the impedance diagram with an initial low frequency impedance of 3x108 ohms and a virtually straight magnitude curve. This curve did not significantly change over the test duration. The phase angle curve for this system behaved like the SPTC and standard EP-UR systems in the low frequency range. However, in the high frequency area there was a resistance peak similar to the one described for the conversion coating-EP-UR system at 1200 hours. This peak gradually became more resistive, which relates to interface degradation.

After one day, the UR topcoat on the SAA/dichromate seal and conversion coated pretreatments had low impedance values (1.3x107 and 2.5x106 ohms, respectively) and provided little or no barrier protection to the substrate. Furthermore, unlike the shape of the other impedance curves, the UR impedance curve leveled off in the mid-frequency range and curved upward in the low frequency range. This behavior corresponds to a porous coating with poor adhesion, where electrolyte is allowed to penetrate the film and accumulate at the coating-metal interface. The phase angle behavior for these pretreatments was significantly different than the other two materials (see Figure 4). At 105 Hz the phase

angle was -80, however as the frequency decreased, the phase angle reached a maximum of approximately -5o at about 1 Hz. This gradual change from capacitance to resistance then sharply reversed back to capacitance again in the low frequency area. This was due to a double layer capacitance at the metal surface resulting from the presence of electrolyte at the interface. As exposure continued, the inflections in the impedance curves began to shift to higher frequencies with impedance values below 107 showing no real barrier protection. Also, the peak maximum in the phase angle diagram for the conversion coated specimens shifted from 1Hz at 24 hours to 10 Hz at 504 hours and finally reached 50 Hz at 1200 hours. In addition to shifting, the peak broadened from spanning five decades to six decades and finally spanning seven decades, respectively. These changes indicate that electrochemical reactions were occurring at the interface and possibly represented the onset and propagation of the corrosion process.

While the chemical protection provided by the SPTC 's corrosion inhibitors did not come into play during the EIS testing, Unicoat was by far the best barrier coating. The standard coating system offered barrier protection to the substrates only to a lesser degree than the SPTC. Also, the chemical corrosion inhibition of the EP-UR coating was not specifically demonstrated in the EIS tests, except possibly in the 1200 hour conversion coating results. The UR system offered no chemical protection against corrosion and it provided poor barrier protection, except with the urethane sealed SAA pretreatment. Finally, as exposure time increased the results for the EP-UR and UR coatings changed for the different pretreatments, while all of the SPTC spectra remained virtually the same over the entire 1200 hour test duration.

SUMMARY

Comparison of all the EIS data showed some interesting general trends for the organic coatings and the inorganic pretreatments. Unicoat appeared to have the best overall adhesion and provided the best barrier protection. The standard system was not as effective a barrier as the SPTC, however, it still was a good protective system. Finally, according to the test results, the unprimed polyurethane topcoat provided the worst protection of the three coating systems. In summarizing the performance of the inorganic pretreatments, the SAA-urethane showed promising electrochemical impedance characteristics when coated with the standard urethane topcoat. The SAA-dichromate performed well with the SPTC system and fair with the epoxy-urethane system, however, its performance with the urethane topcoat was poor. Finally, the EIS data indicated that the chromate conversion coating appeared to be the best pretreatment for short term

durations, however, its long term durability was significantly inferior to the SAA treatments.

The objective of this study was to investigate the electrochemical characteristics of two primerless finishing systems obtained by: (1) A modified surface treatment and (2) a modified organic coating. The sulfuric acid anodized-urethane seal method showed promising results in the electrochemical impedance analysis. A pretreatment that forms strong chemical bonds with an applied organic coating is a viable concept and should be further studied. The self-priming topcoat performed well on all pretreatments used in this evaluation. The performance of both systems, in comparison to the standard primer and topcoat system used on military aircraft, was promising and should be fully investigated by extensive physical testing.

REFERENCES

1. J. J. De Luccia, R. D. Gergar, and E. J. Jankowsky, "AGARD Corrosion Handbook, Volume 2, Aircraft Corrosion Control Documents: A Descriptive Catalogue," AGARDograph No. 278, North Atlantic Treaty Organization (NATO), March 1987.

2. S. J. Ketcham, "A Handbook of Protective Coatings For Military and Aerospace Equipment," TPC Publication 10, National Association of Corrosion Engineers (NACE), 1983.

3. S. J. Spadafora, C. R. Hegedus, and D. F. Pulley, "Corrosion Preventive Primers For Military Equipment," National Association of Corrosion Engineers Corrosion'85 Conference, Boston, MA, April 1985, Paper No. 194.

4. U. S. Patent 4,515,919, "Protective Coating Composition and Process For Aluminum and Aluminum Alloys," Inventors: R. E. Bradley and W. R. Keithier, Assignee: Lockheed Corp., May 1985.

5. C. R. Hegedus, "A Combination Primer/Topcoat For Aluminum," Society of Manufacturing Engineers, Finishing '87 Conference Paper FC87-625, Sept. 1987.

6. Statewide Aerospace Coatings Rules Group Seminar, "Low VOC Primers and Topcoats," Ron Savin, Premium Finishes Inc. Oct 1987.

7. Industrial Finishing, page 42, July 1988.

8. W. C. Cochran, "Sulfuric and Chromic Acid Anodizing of Aluminum," ELECTROPLATING ENGINEERING HANDBOOK, L. J. Durney - Ed., Van Nostrand Reinhold Co., 1984.

9. Princeton Applied Research Corp.'s Electrochemical Instruments Group, Application Note: AC-2, "Evaluation of Organic Coatings By Electrochemical Impedance Measurements," not dated.

10. J. R. Scully, "Electrochemical Impedance Spectroscopy For Evaluation of Organic Coating Deterioration and Underfilm Corrosion - A State of the Art Technical Review," David W. Taylor Naval Ship Research and Development Center, Report No. DTNSRDC/SME-86/006, Sept., 1986.

11. S. J. Spadafora and H. Leidheiser Jr., "Water Disbondment Characterization of Polymer Coating/Metal Substrate Systems," Journal of Oil and Colour Chemists Association, Vol. 71. No. 9, Sept. 1988, pp 276-285.

12. V. V. Arslanov and W. Funke, Progress in Organic Coatings, Vol. 15, No. 4, 355 (1988).

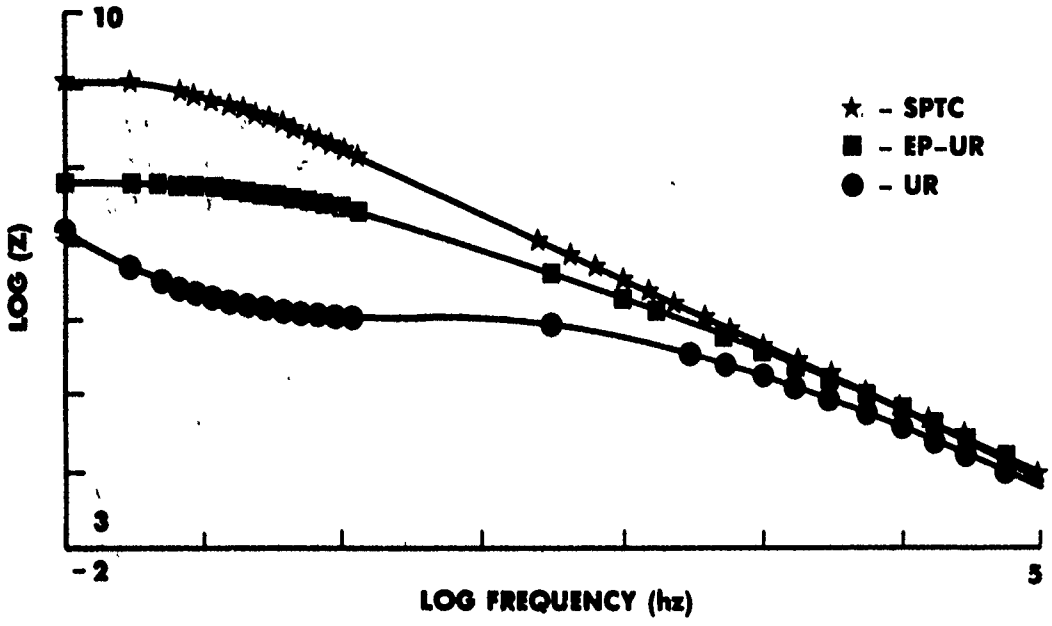

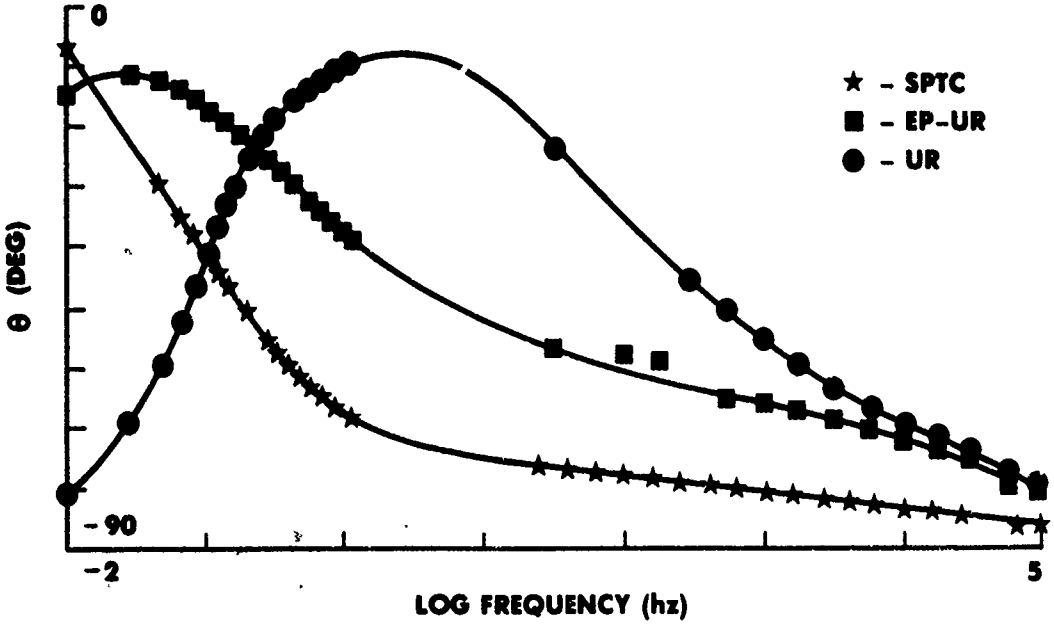

Figure 1. Bode plot of the three coating systems on the bare 7075-T6 aluminum alloy with the SAA/dichromate seal pretreatment after 24 hours.

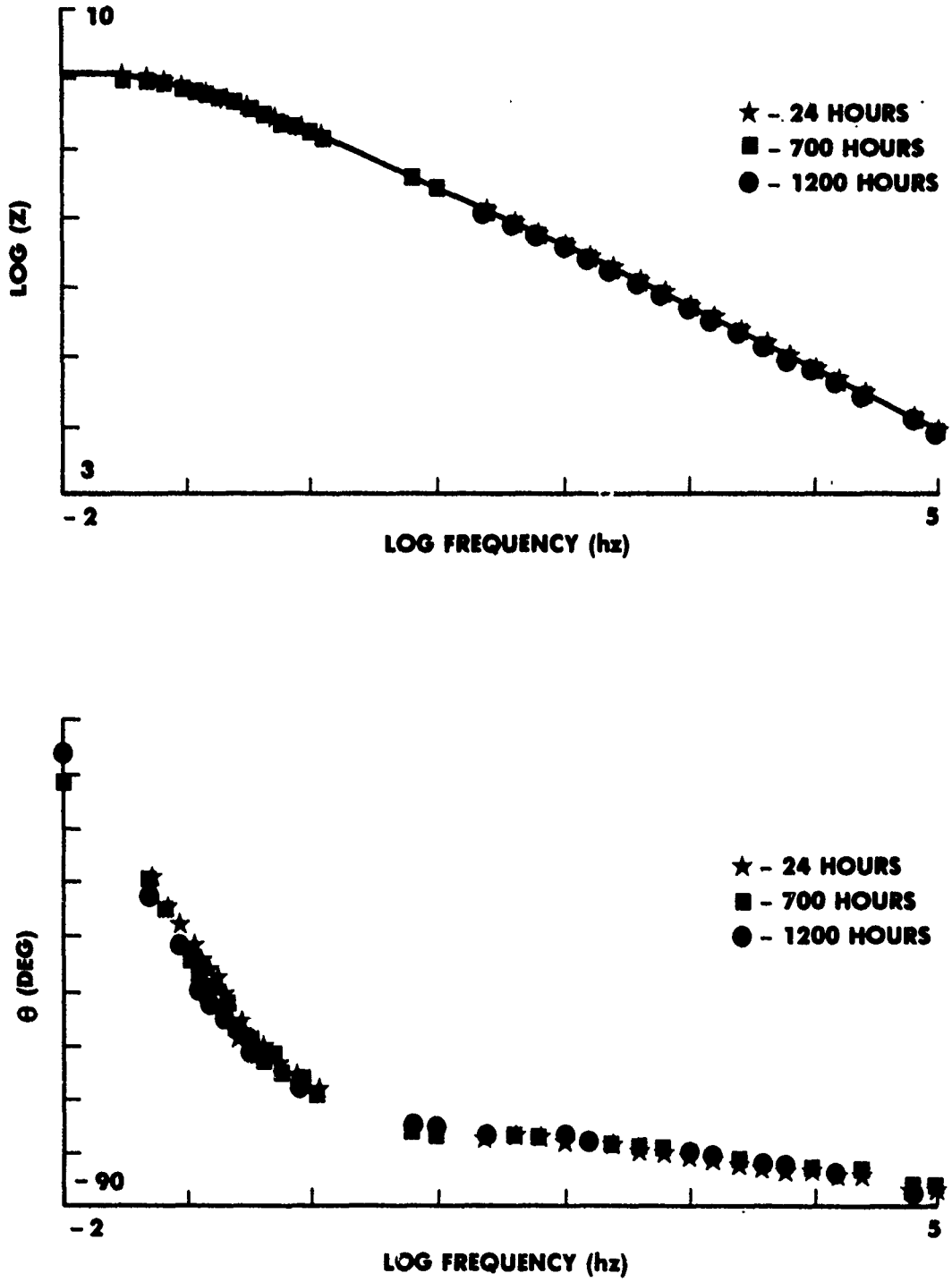

Figure 2. Bode plots for the SPTC system on the bare 7075-T6 aluminum alloy with the SAA/dichromate seal pretreatment at 24, 700 and 1200 hours.

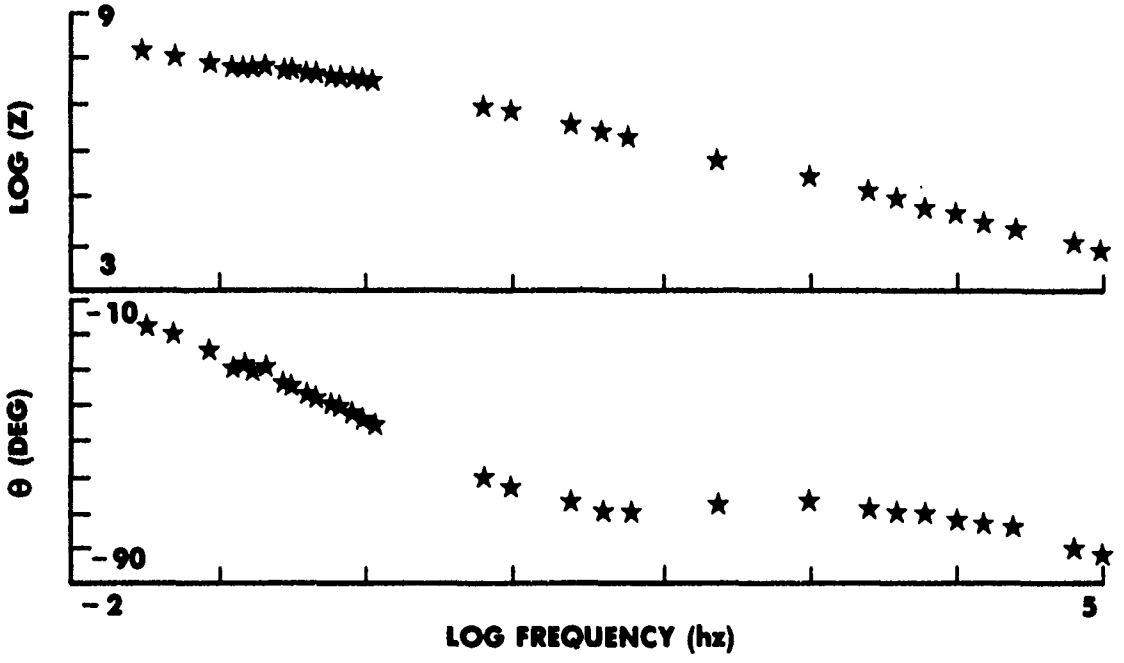

Figure 3. Bode plot of the EP-UR coating system on bare 7075-T6 aluminum with the chromate conversion coating pretreatment at 1200 hours.

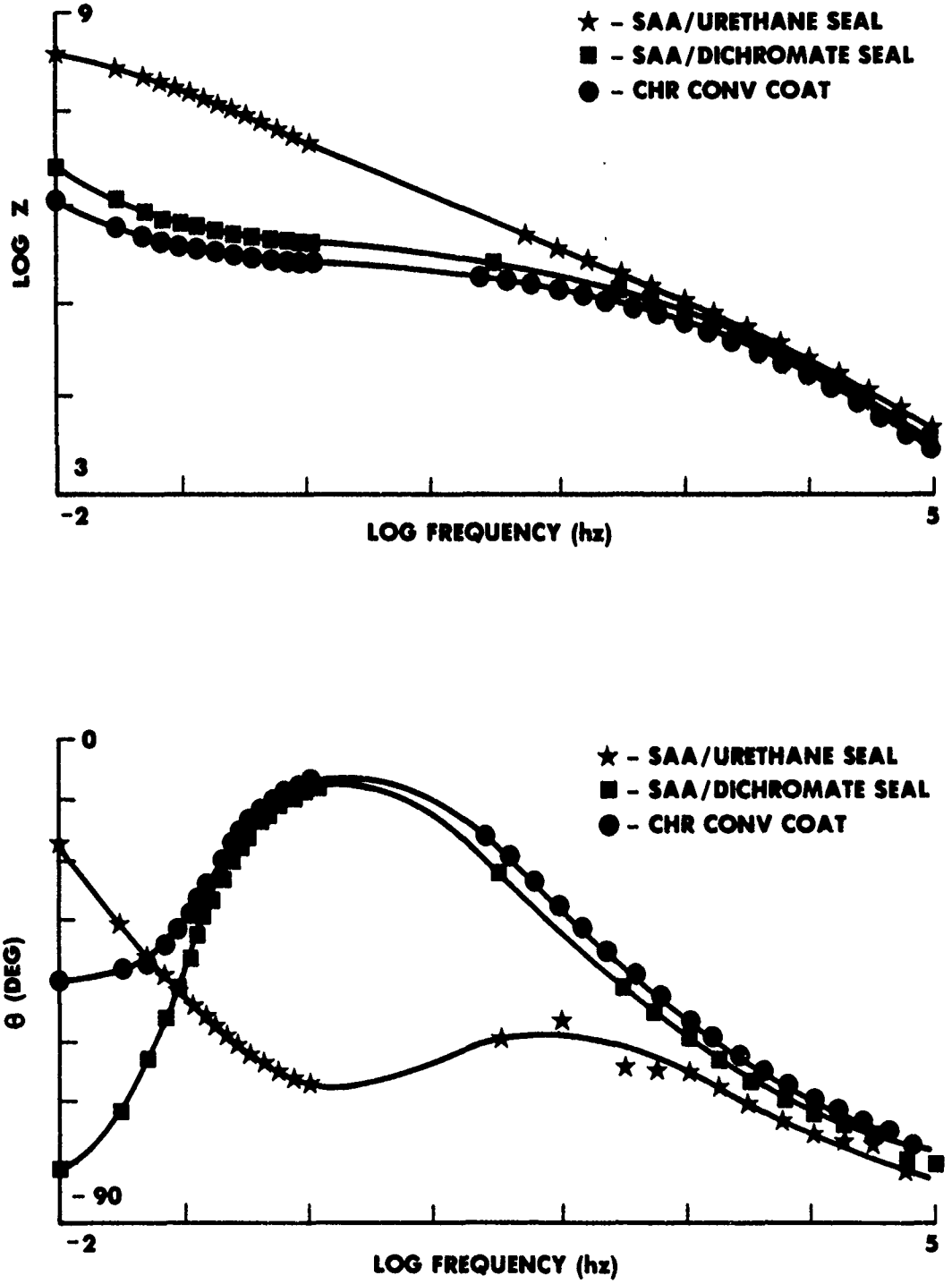

Figure 4. Bode plot of the UR coating on the three pretreatment systems after 24 hours.

ANALYSIS OF PRIMERLESS FINISHING SYSTEMS FOR ALUMINUM PHASE II - PHYSICAL PERFORMANCE TESTS

Charles R. Hegedus, Stephen J. Spadafora, Donald J. Hirst and Anthony T. Eng

Air Vehicle and Crew Systems Technology Department
Naval Air Development Center
Warminster, PA 18974-5000

ABSTRACT

A recent trend in the corrosion protection of aluminum alloys used in military equipment is the development of primerless finishing systems, where the topcoat can be directly applied to surface treated aluminum. A previous investigation evaluated the electrochemical characteristics of two currently available primerless finishing systems: (1) a polyurethane sealed, sulfuric acid anodized pretreatment that can be directly topcoated and (2) a primerless or self-priming topcoat which can be applied directly to a standard aluminum surface pretreatment. This phase of the study evaluates the physical properties of both pretreatment-coating systems on several aluminum substrates and compares their performance to conventional Navy finishing systems. Adhesion, flexibility, chemical and corrosion resistance tests are used to determine the properties of these systems. These results are correlate with the Phase I Electrochemical Impedance Spectroscopy data. Analysis of all of the test results indicate that primerless systems show promise as viable alternatives for the conventional system and should be considered for specific finishing applications.

INTRODUCTION

A recent trend in the corrosion protection of aluminum alloys used in military equipment is the development of primerless finishing systems, where a topcoat can be directly applied to surface treated aluminum. References (1-6) provide more detailed descriptions of corrosion control documents, finishing systems for military equipment and information on the primerless finishing approaches. Phase I of this investigation described the properties and deficiencies of the standard Navy finishing system. In addition, the phase I report discusses the two currently available primerless finishing systems. An evaluation of the electrochemical characteristics of these systems is also

described in this paper. Analysis of the EIS results indicated that primerless systems showed promise as viable alternatives for the conventional system and their properties should be fully defined using conventional physical coatings tests.

The two approaches to eliminate the primer from a finishing system are: (1) Modify the inorganic pretreatment or (2) Modify the organic coating system. Reference (4) discloses a coating composition and application process for a modified sulfuric acid anodized surface treatment which is sealed with a polyurethane colloidal suspension. The resultant film is hard, water and solvent resistant, flexible and corrosion resistant and can be directly topcoated with the standard MIL-C-83286 topcoat or equivalent. Reference (5) describe the development and properties of a topcoat (UNICOAT) which can be applied directly to deoxidized, anodized or chromate conversion coated aluminum surfaces without the use of a primer. This coating provides the properties of the conventional primer and topcoat system used on military aircraft. Either method eliminates the use of a primer, saving application time, manhours, and materials. This effort investigated the effectiveness of these systems to protect aluminum substrates.

EXPERIMENTAL

The performance of the two primerless finishing systems on various aluminum substrates was evaluated against the performance of standard paint systems used on Navy and Air Force aircraft. To accomplish this task, three coating systems were evaluated on twelve substrate-pretreatment combinations for their adhesion, chemical (fluid) resistance, flexibility and corrosion protection properties. The three paint systems used in the investigation were: 1) The standard Navy system (MIL-P-23377D, Type 1 epoxy primer and MIL-C-83286 polyurethane topcoat); 2) The standard MIL-C-83286 topcoat alone; and 3) UNICOAT (a self-priming topcoat). All coating systems were applied by conventional air spray and allowed to cure for seven days prior to testing. Dry film thickness for the primer was 15.2 to 22.9 microns (0.006 to 0.009 inches). The MIL-C-83286 topcoat and Unicoat were both applied to a dry film thickness of 50.8 to 55.9 microns (0.020 to 0.022 inches). The twelve substrate-pretreatment combinations were based on four substrates (Bare and Clad, 2024 T-3 and 7075 T-6 aluminum alloys) and three pretreatments (a dichromate sealed, sulfuric acid anodized (SAA) treatment (NADC), a urethane sealed-SAA treatment (Lockheed Georgia) and the standard chromate conversion coating (Q Panel, Cleveland, OH)). With the exception of the flexibility tests, all of the test procedures were conducted on these substrates. The flexibility tests were conducted on anodized 2024-O (annealed) aluminum specimens sealed with either the urethane colloidal suspension or hot water. The physical properties of each system were determined in accordance

with test methods from the American Society for Testing and Materials (ASTM) and Federal Test Method Standard (FTMS) No. 141B. The following is a description of the experimental procedures use in this investigation.

Adhesion of the finishing systems was evaluated using two methods: wet tape adhesion (ASTM D 3359, method A) and scrape adhesion (ASTM D 2197, method A). The wet tape test was performed on specimens after 24 hours immersion in distilled water. Upon removal, an "X" was scribed through the coating and into the substrate between two parallel lines, 1 inch apart. A strip of 3M 250 masking tape was firmly applied to the scribed surface and immediately removed with one quick motion. The specimens were subsequently examined and the percentage of coating remaining on the surface was recorded. The scrape test was performed using a SG-1605 Scrape Adhesion Tester (Gardner Laboratory) on specimens with a section of the substrate surface exposed. A weighted stylus was guided along the exposed substrate at a 45o angle into the coating system. The scrape adhesion was recorded as the heaviest weight used without shearing the coating from the substrate.

Impact flexibility of the coating systems was evaluated at 23oC (74oF) using FTMS Method 6226 (G.E. Impact). The test apparatus consisted of a steel cylinder with protruding spherical knobs at the end. When the steel cylinder strikes the reverse side of the specimen, the coating system is subjected to elongations of 0.5, 1, 2, 5, 10, 20, 40, and 60%. The imprints formed from the knobs were examined and the impact elongation was recorded as the highest deformation without cracking of the coating. The coating systems were also tested for flexibility at -51oC. The test method, described in ASTM D 1737, is performed by bending the specimen 180o around 1/8, 1/4, 1/2, and 1 inch diameter mandrels. After returning to room temperature, the coatings were examined and the smallest diameter mandrel bend which the coating withstood without cracking was recorded.

The ability of the finishing systems to resist common fluids used in aircraft was evaluated by immersing each test system in different liquids under various exposure conditions. Specimens from each system were immersed for twenty four hours in lubricating oil at 121oC (250oF), hydraulic fluid at 65oC (150oF), and a hydrocarbon solvent at 25oC (77oF). Upon removal, the coatings were examined for softening, uplifting, blistering, and other defects which may have resulted from the exposure. Coated samples were also immersed in water at 49oC (120oF) for 96 hours and again examined after removal.

Four aluminum specimens of each finishing system were scribed with a 5.1 cm (2.0") figure "X" through the coating into the substrate. For each system, two specimens were exposed in 5%

salt spray (ASTM B 117) for 2000 hours and two were exposed to SO2/salt spray (ASTM G 85) for 500 hours. The panels were inspected for corrosion in the scribe area and blistering of the coating. Subsequently, one panel per pair was chemically treated to remove the organic coating without disturbing the substrate and then re-examined for corrosion.

RESULTS AND DISCUSSION

Since a primer is normally applied to a surface to enhance the adhesion of a subsequent topcoat and also to provide the primary source of corrosion inhibition, the suspected weakest point in a primerless system would be the substrate-topcoat interface. Therefore, the finishing systems were analyzed with special emphasis placed on surface interaction phenomena at this interface, primarily adhesion and corrosion. Figure 1 is a series of scanning electron micrographs taken at 10,000X of the three different pretreatments on both bare and clad 2024 aluminum. These photographs illustrate the micro-topography of the pretreatments, which will ultimately effect the interfacial properties between the organic and inorganic coatings.

The results of the adhesion tests are provided in Table 1. All of the scrape adhesion results are significantly higher than the standard 3 kg requirement for this property, indicating adequate adhesion under ambient laboratory conditions. In general, Unicoat exhibited the best overall coating performance in the wet tape test. Systems with a conversion coating treatment also performed well, as expected, since one objective of conversion coatings is to enhance adhesion of subsequent organic coatings. However, many of the finishing systems on the urethane and dichromate sealed anodized specimens exhibited coating removal in the wet tape adhesion test, indicating a susceptibility to coating-substrate water disbondment. This poor wet adhesion is not unusual, since the sealing process minimizes the porosity of the anodized film leaving a smoother surface topography (Figure 1). Although this improves corrosion protection, it also minimizing the potential for mechanical interlocking between the paint and the substrate. Adhesion of the organic coating is then mainly dependent upon chemical bonds which are susceptible to deterioration if water penetrates to the interface (7).

Standard low gloss coating specification criteria for the flexibility tests used in this investigation are 20% elongation and a 2 inch mandrel bend. Most of the systems tested met or exceeded these test requirements. In addition, all of the coatings performed a little better on the water sealed anodized substrates than on the urethane sealed SAA, indicating a slight deficiency at the SAA-urethane seal/coating interface. Furthermore, the urethane topcoat had better impact elongation (40%) than the other two coating systems (20%). Poor flexibility

is expected with the system containing the brittle epoxy primer, especially at the low temperatures common for military aircraft cruising at high altitudes. However, the self-priming topcoat (SPTC) has a polymer system which should provide as much flexibility as the standard topcoat. This is illustrated in the results for the mandrel bend test performed at -51oC where the SPTC is much more flexible (1/4 inch mandrel) than the other two coatings (1 inch mandrels). Although the lowest mandrel used was 1/4 inch, previous results (5) indicate that Unicoat can withstand a 1/8 inch bend at this temperature without cracking.

Good performance in the chemical resistance tests not only indicates good binder integrity, but it can also indicate good coating/substrate interfacial stability. Most of the systems in this investigation exhibited excellent resistance to lubricating oil, hydraulic fluid, hydrocarbons and water. Unicoat, which has resisted these exposures on numerous substrates, peeled from the urethane sealed SAA pretreatment after immersion in lubricating oil. This failure was unexpected, especially since Unicoat has a similar polyurethane binder to MIL-C-83286 which showed no signs of failure. Another coating deficiency was observed in the water resistance test. After 4 days immersion at 49oC, the MIL-C-83286 polyurethane topcoat had tiny blisters over the entire surface of the urethane sealed, anodized panels. Since no other urethane pretreatment system failed the water immersion test, this indicates a slight adhesion weakness at the coating-pretreatment interface. This adhesion weakness, however, could improve with aging of the finishing system.

Corrosion resistance is one of the primary concerns in most high performance Navy coating systems. This is especially true for primerless systems, since a primer normally provides the main source of corrosion inhibition for the substrate. The corrosion resistance properties of the finishing systems were analyzed using both 5% NaCl salt spray and SO2/salt spray exposures. These two types of corrosion promoting conditions were selected because they emphasize the severe nature of Navy operational environments.

Scribed specimens, exposed to 5% salt spray for 2000 hours, were examined for corrosion in the scribe area and for blistering of the coating. Subsequently, the coatings were chemically removed from the surface without disturbing the underlying substrate and the panels were re-evaluated. A summary of the test results is provided in Table 2 and photographs of the specimens with the coatings removed are provided in Figures 2-4. The standard epoxy primer and polyurethane topcoat system performed well on all substrates. There were no significant corrosion products in the scribe or blistering of the coating. The conversion coated 7075 clad specimen with the standard system exhibited several pits along the scribe. In addition, there was some slight surface

corrosion and coating uplifting along the scribe of the 7075 Clad, urethane sealed/SAA specimens with the standard system. Since these deficiencies were minor relative to the other results, they were considered insignificant.

The self-priming topcoat also provided good corrosion protection on all of the substrates. There was no uplifting or blistering of the coating on any section of the specimens. The scribe areas had slight to moderate deposits of aluminum oxide with no pitting, however, examination of these specimens after removing the coating indicated these products were minimal and confined to the scribe area. A previous report (5) indicated that these deposits are formed early during salt spray exposure, but no further corrosion occurs for up to one year. This suggests that these deposits assist in the corrosion inhibition process.

The MIL-C-83286 polyurethane topcoat performed well on the dichromate sealed SAA with no blistering or uplifting of the coating and only slight corrosion in the scribe area of the 7075 specimens. (Corrosion on the corner of the 2024 T-3 specimen in Figure 3 was the result of an edge effect and was discounted.) The good performance of the urethane on this substrate was unexpected because, aside from the dichromate seal which is damaged in the scribe area, there are no other corrosion inhibitors in the system. The polyurethane topcoated substrates with the sulfuric acid anodized-urethane seal showed some corrosion products and pitting in the scribe of all four panels. Poor performance was exhibited by the urethane coated, chromate conversion coating substrates, which had corrosion and pitting along the scribe and underfilm corrosion on every specimen. Superficial corrosion products in the scribe was considered acceptable, however, any pitting in the scribe, corrosion extending from the scribe, or damage to the coating was unacceptable.

Scribed SO2/salt spray specimens were exposed for 500 hours and examined for corrosion in and away from the scribe and damage to the coating system. Again, the organic coatings were chemically stripped and the specimens were re-evaluated. These results are summarized in Table 3. SO2/salt spray exposure is an extremely aggressive environment and simulates industrial stack gases such as those found on diesel powered carriers. The 500 hour exposure period was selected because differences in finishing system performance were observed after this duration. The specimens coated with the standard primer and topcoat system as well as those with the urethane topcoat had severe surface corrosion and/or pitting on all twelve substrates. In addition, the topcoat blistered on the conversion coating pretreatment and on the clad specimens with the SAA-dichromate seal. The extent of the corrosion with the topcoat was expected because of the lack of a corrosion inhibiting pigment. The results with the standard

system were slightly unexpected since this system is considered one of the premier protective systems for aluminum due to the strontium chromate contained within the primer. Unicoat outperformed the other two coating systems on all of the substrates. Although there were some slight spots of surface corrosion and small pits, these areas were considered insignificant relative to the extensive corrosion observed on the other specimens. Figures 5-7 provide vivid illustrations of the performance of all of the systems after sulfur dioxide/salt spray exposure.

SUMMARY

Comparison of all the performance data for the organic coatings indicated some correlation between the test results. Adhesion, SO2-salt spray and water resistance test data show a general trend in adhesion performance from Unicoat as the best system, to the unprimed polyurethane topcoat as the worst. Furthermore, the EIS data from the Phase I effort correlated well with this performance trend for the coating systems. The only exception to this trend was in the 5% NaCl salt spray test results, where the standard primer/topcoat (EP-UR) system properties proved to be just slightly better than those of the self-priming topcoat.

In summarizing the performance of the inorganic pretreatments, the SAA-urethane resulted in poor adhesion and flexibility for nearly all of the alloy/organic coatings analyzed. However, it did assist in providing fair corrosion protection in both salt spray tests, and when coated with the standard urethane topcoat, its electrochemical impedance characteristics were promising. The SAA-dichromate provided fair adhesion for the urethane coatings but poor adhesion for the epoxy-urethane system. Its performance with all of the organic coatings was good in salt spray and fair in SO2-salt spray. The chromate conversion coating provided excellent adhesion for all of the coatings and good corrosion protection when coated with either the standard system or the self-priming topcoat. Performance in the SO2-salt spray was only good when coated with Unicoat. The EIS data indicated that the chromate conversion coating appeared to be the best pretreatment for short term durations, however, its long term durability was significantly inferior to the SAA treatments. There was some disagreement between the EIS results and the wet tape adhesion tests, however, these discrepancies were attributed to differences in the thermodynamic activity of the water used in the wet tape and EIS test solutions (7).

The objective of this study was to investigate the applicability of primerless finishing systems in lieu of the standard primer and topcoat system used on military aircraft. The sulfuric acid anodized-urethane seal method showed promising results in the electrochemical impedance analysis, although it did not perform

as well as the standard system. This approach is a viable concept, however, incorporating corrosion inhibitors in the subsequent coating may be essential to improve the overall corrosion protection. The self-priming topcoat performed well throughout the evaluation and could be used on a variety of substrates. While either primerless finishing system approach would offer numerous advantages for specific applications, three advantages would be prevalent with both approaches: 1) Reduced volatile organic emissions; 2) Reduced chromate emissions; and 3) Reduced finishing system application time.

REFERENCES

1. /S. J. Ketcham, "A Handbook of Protective Coatings For Military and Aerospace Equipment," TPC Publication 10, Nat'l Assoc. of Corr. Eng'rs, 1983.

2. S. J. Spadafora, C. R. Hegedus, and D. F. Pulley, "Corrosion Preventive Primers For Military Equipment," NACE Corrosion '85 Conference Paper No. 194, April 1985.

3. Industrial Finishing, page 42, July 1988.

4. U. S. Patent 4,515,919, "Protective Coating Composition and Process For Aluminum and Aluminum Alloys," Inventors - R. E. Bradley and W. R. Keithier, Assignee - Lockheed Corporation, May 7, 1985.

5. C. R. Hegedus, "A Combination Primer/Topcoat For Aluminum," Society of Manufacturing Engineers, Finishing '87 Conference Paper FC87-625, Sept. 1987.

6. Statewide Aerospace Coatings Rules Group Seminar, "Low VOC Primers and Topcoats," Ron Savin, Premium Finishes Inc., October 1987.

7. S. J. Spadafora and H. Leidheiser Jr., "Water Disbondment Characterization of Polymer Coating/Metal Substrate Systems," JOCCA, Vol 71, No. 9 Sept 1988.

TABLE 1. ADHESION TEST RESULTS

SUBSTRATE / PRETREATMENT / COATING	WET TAPE (% REMAINING)	SCRAPE (Kg)
2024 BARE / SAA-URETHANE / EP & UR	97	9
2024 CLAD / SAA-URETHANE / EP & UR	10	7
7075 BARE / SAA-URETHANE / EP & UR	25	8
7075 CLAD / SAA-URETHANE / EP & UR	100	10
2024 BARE / SAA-URETHANE / URETHANE	0	7
2024 CLAD / SAA-URETHANE / URETHANE	0	4
7075 BARE / SAA-URETHANE / URETHANE	0	6
7075 CLAD / SAA-URETHANE / URETHANE	90	9
2024 BARE / SAA-URETHANE / UNICOAT	100	10
2024 CLAD / SAA-URETHANE / UNICOAT	0	9
7075 BARE / SAA-URETHANE / UNICOAT	75	10
7075 CLAD / SAA-URETHANE / UNICOAT	100	9
2024 BARE / SAA-DICHROMATE / EP & UR	80	9
2024 CLAD / SAA-DICHROMATE / EP & UR	0	5
7075 BARE / SAA-DICHROMATE / EP & UR	75	8
7075 CLAD / SAA-DICHROMATE / EP & UR	0	7
2024 BARE / SAA-DICHROMATE / URETHANE	100	10
2024 CLAD / SAA-DICHROMATE / URETHANE	0	7
7075 BARE / SAA-DICHROMATE / URETHANE	100	10
7075 CLAD / SAA-DICHROMATE / URETHANE	100	10
2024 BARE / SAA-DICHROMATE / UNICOAT	100	10
2024 CLAD / SAA-DICHROMATE / UNICOAT	100	10
7075 BARE / SAA-DICHROMATE / UNICOAT	100	10
7075 CLAD / SAA-DICHROMATE / UNICOAT	100	9
2024 BARE / CHR CONV COAT / EP & UR	100	10
2024 CLAD / CHR CONV COAT / EP & UR	100	10
7075 BARE / CHR CONV COAT / EP & UR	100	10
7075 CLAD / CHR CONV COAT / EP & UR	100	10
2024 BARE / CHR CONV COAT / URETHANE	100	10
2024 CLAD / CHR CONV COAT / URETHANE	100	10
7075 BARE / CHR CONV COAT / URETHANE	70	10
7075 CLAD / CHR CONV COAT / URETHANE	100	10
2024 BARE / CHR CONV COAT / UNICOAT	100	10
2024 CLAD / CHR CONV COAT / UNICOAT	100	10
7075 BARE / CHR CONV COAT / UNICOAT	100	10
7075 CLAD / CHR CONV COAT / UNICOAT	100	10

EP & UR: MIL-P-23377 EPOXY PRIMER AND MIL-C-83286 TOPCOAT
URETHANE: MIL-C-83286 TOPCOAT
UNICOAT: SELF-PRIMING TOPCOAT

TABLE 2. 5% NaCl SALT SPRAY TEST RESULTS

FINISHING SYSTEM	SCRIBE COMMENTS
2B / SAA-UR / EP+UR	No Corrosion Products (Corr. Prod.)
2C / SAA-UR / EP+UR	No Corrosion
7B / SAA-UR / EP+UR	No Corrosion
7C / SAA-UR / EP+UR	Slight Surface Corr. Prod. 100% Of Scribe
2B / SAA-UR / UR	Many Pits & Corr. 1/8" Out From Scribe
2C / SAA-UR / UR	Surface Corr. 100% Of Scribe & A Few Pits
7B / SAA-UR / UR	Extensive Pitting (Pit.) In Entire Scribe
7C / SAA-UR / UR	Surface Corr. In 100% Scribe & A Few Pits
2B / SAA-UR / SPTC	Surface Corr. Prod. In 50% of Scribe
2C / SAA-UR / SPTC	Slight Surface Corr. Prod. 100% Of Scribe
7B / SAA-UR / SPTC	Surface Corrosion Products 100% Of Scribe
7C / SAA-UR / SPTC	Surface Corrosion Products 100% Of Scribe
2B / SAA-DC / EP+UR	No Corrosion
2C / SAA-DC / EP+UR	No Corrosion
7B / SAA-DC / EP+UR	No Corrosion
7C / SAA-DC / EP+UR	No Corrosion
2B / SAA-DC / UR	No Corrosion
2C / SAA-DC / UR	No Corrosion
7B / SAA-DC / UR	Slight Surface Corr. Prod. 100% Of Scribe
7C / SAA-DC / UR	Slight Surface Corr. Prod. 100% Of Scribe
2B / SAA-DC / SPTC	No Corrosion
2C / SAA-DC / SPTC	Slight Surface Corr. Prod. 50% Of Scribe
7B / SAA-DC / SPTC	Slight Surface Corr. Prod. 25% Of Scribe
7C / SAA-DC / SPTC	Slight Surface Corr. Prod. 75% Of Scribe
2B / C.C.C. / EP+UR	No Corrosion
2C / C.C.C. / EP+UR	No Corrosion
7B / C.C.C. / EP+UR	No Corrosion
7C / C.C.C. / EP+UR	Slight Corr. 100% of Scribe & A Few Pits
2B / C.C.C. / UR	Large Pits Along Scribe & Over Surface
2C / C.C.C. / UR	Surface Corr. In Scribe & 2 Severe Areas
7B / C.C.C. / UR	Corr./Pit. Along Scribe & Over Surface
7C / C.C.C. / UR	Corr./Pit. Along Scribe & Under Coating
2B / C.C.C. / SPTC	Slight Scribe Corr. & 2 Areas From Scribe
2C / C.C.C. / SPTC	Slight Scribe Corr. & 1 Area From Scribe
7B / C.C.C. / SPTC	Slight Scribe Corr. & 2 Areas Along Scribe
7C / C.C.C. / SPTC	Slight Surface Corrosion In Scribe

EP+UR:MIL-P-23377 & MIL-C-83286; UR:MIL-C-83286 and SPTC:UNICOAT

2 = 2024-T3 Al. Alloy; 7 = 7075-T6 Al. Alloy; B = BARE & C = CLAD

SAA-UR = Sulfuric Acid Anodized with the Urethane Seal
SAA-DC = Sulfuric Acid Anodized with the Dichromate Seal
C.C.C. = Chromate Conversion Coating

TABLE 3. SO2/SALT SPRAY TEST RESULTS

FINISHING SYSTEM	COMMENTS
2B / SAA-UR / EP+UR	Pit. In 100% of Scribe
2C / SAA-UR / EP+UR	Pit. In & Severe Corr. 1/2" From Scribe
7B / SAA-UR / EP+UR	Pit. In & Extending From The Scribe
7C / SAA-UR / EP+UR	Severe Corr. In & 1/4" From Scribe
2B / SAA-UR / UR	Pitting In 100% of Scribe
2C / SAA-UR / UR	Pit. In & Severe Corr. 1/2" From Scribe
7B / SAA-UR / UR	Pitting In & Extending From The Scribe
7C / SAA-UR / UR	Severe Corr. In & 1/4" From Scribe
2B / SAA-UR / SPTC	No Corrosion
2C / SAA-UR / SPTC	Corrosion Along 10% of The Scribe
7B / SAA-UR / SPTC	No Corrosion
7C / SAA-UR / SPTC	Several Slight Corr. Spots Along Scribe
2B / SAA-DC / EP+UR	Pitting In 100% of Scribe
2C / SAA-DC / EP+UR	Pitting In & Extending 1/8" From Scribe
7B / SAA-DC / EP+UR	Pitting In & Extending From The Scribe
7C / SAA-DC / EP+UR	Surf. Corr./Pitting In & 3/4" From Scribe
2B / SAA-DC / UR	Pitting In 100% of Scribe
2C / SAA-DC / UR	Pit. In & 1/8" From Scribe;Paint Blistered
7B / SAA-DC / UR	Pitting In 100% of Scribe
7C / SAA-DC / UR	Corr./Pit. 3/4" From Scribe;Paint Blistered
2B / SAA-DC / SPTC	No Corrosion
2C / SAA-DC / SPTC	2 Small Pits Along The Scribe
7B / SAA-DC / SPTC	No Corrosion
7C / SAA-DC / SPTC	Several Small Pits Along The Scribe
2B / C.C.C. / EP+UR	Pitting In 100% of Scribe
2C / C.C.C. / EP+UR	Pitting In & Extending From Scribe
7B / C.C.C. / EP+UR	Pitting In & Extending 1/4" From Scribe
7C / C.C.C. / EP+UR	Surf. Corr./Pitting In & 1/2" From Scribe
2B / C.C.C. / UR	Corr./Pitting Over Surf.; Paint Blistered
2C / C.C.C. / UR	Corr./Pitting Over Surf.; Paint Blistered
7B / C.C.C. / UR	Corr./Pitting Over Surf.; Paint Blistered
7C / C.C.C. / UR	Corr./Pitting Over Surf.; Paint Blistered
2B / C.C.C. / SPTC	3 Small Pits Along The Scribe
2C / C.C.C. / SPTC	Several Small Pits Along The Scribe
7B / C.C.C. / SPTC	5 Small Pits Along The Scribe
7C / C.C.C. / SPTC	2 Small Pits Along The Scribe

EP+UR:MIL-P-23377 & MIL-C-83286; UR:MIL-C-83286 and SPTC:UNICOAT

2 = 2024-T3 Al. Alloy; 7 = 7075-T6 Al. Alloy; B = BARE & C = CLAD

SAA-UR = Sulfuric Acid Anodized with the Urethane Seal
SAA-DC = Sulfuric Acid Anodized with the Dichromate Seal
C.C.C. = Chromate Conversion Coating

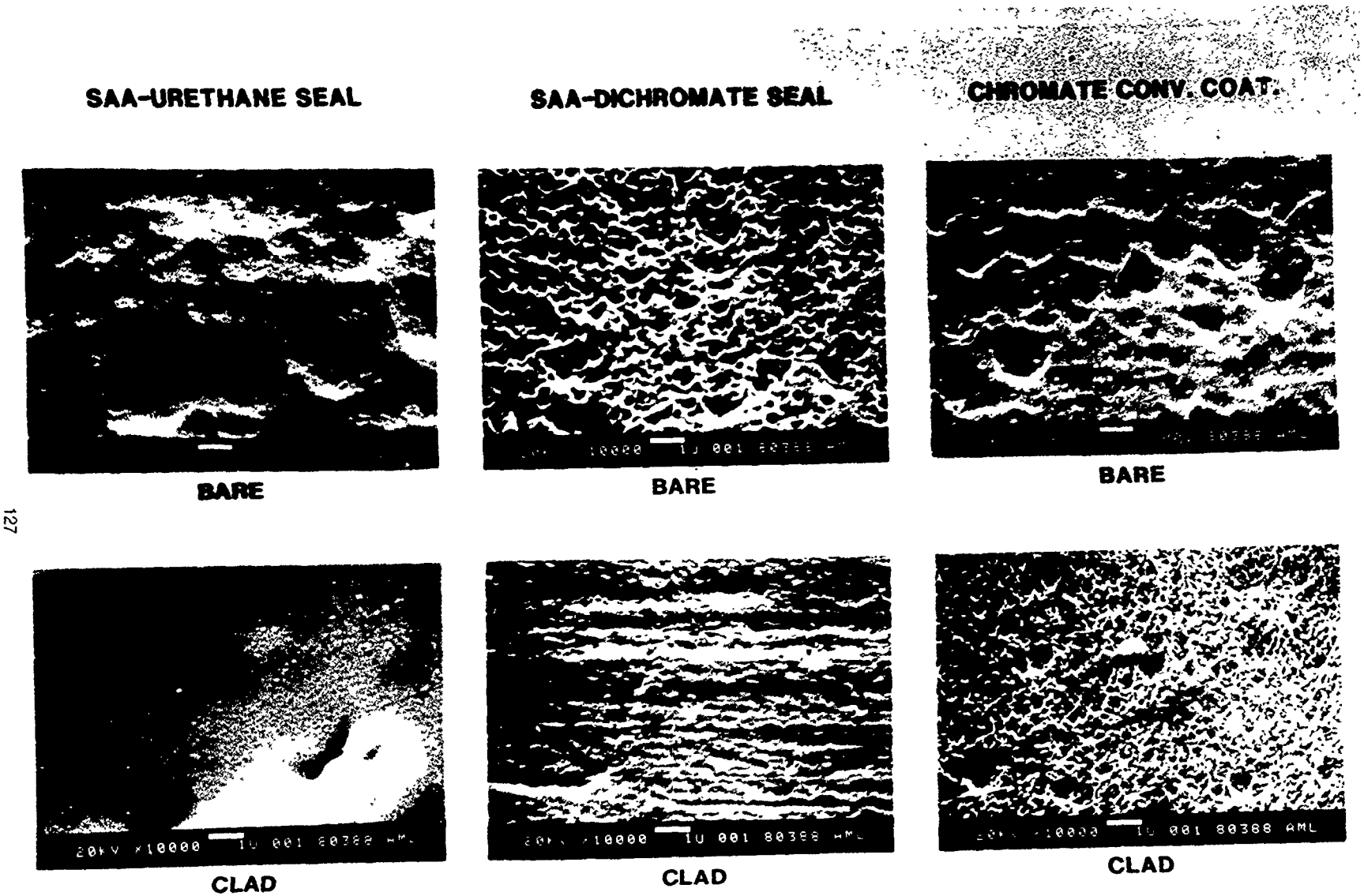

FIGURE 1: SURFACE TOPOGRAPHY OF PRETREATMENTS (10000X).

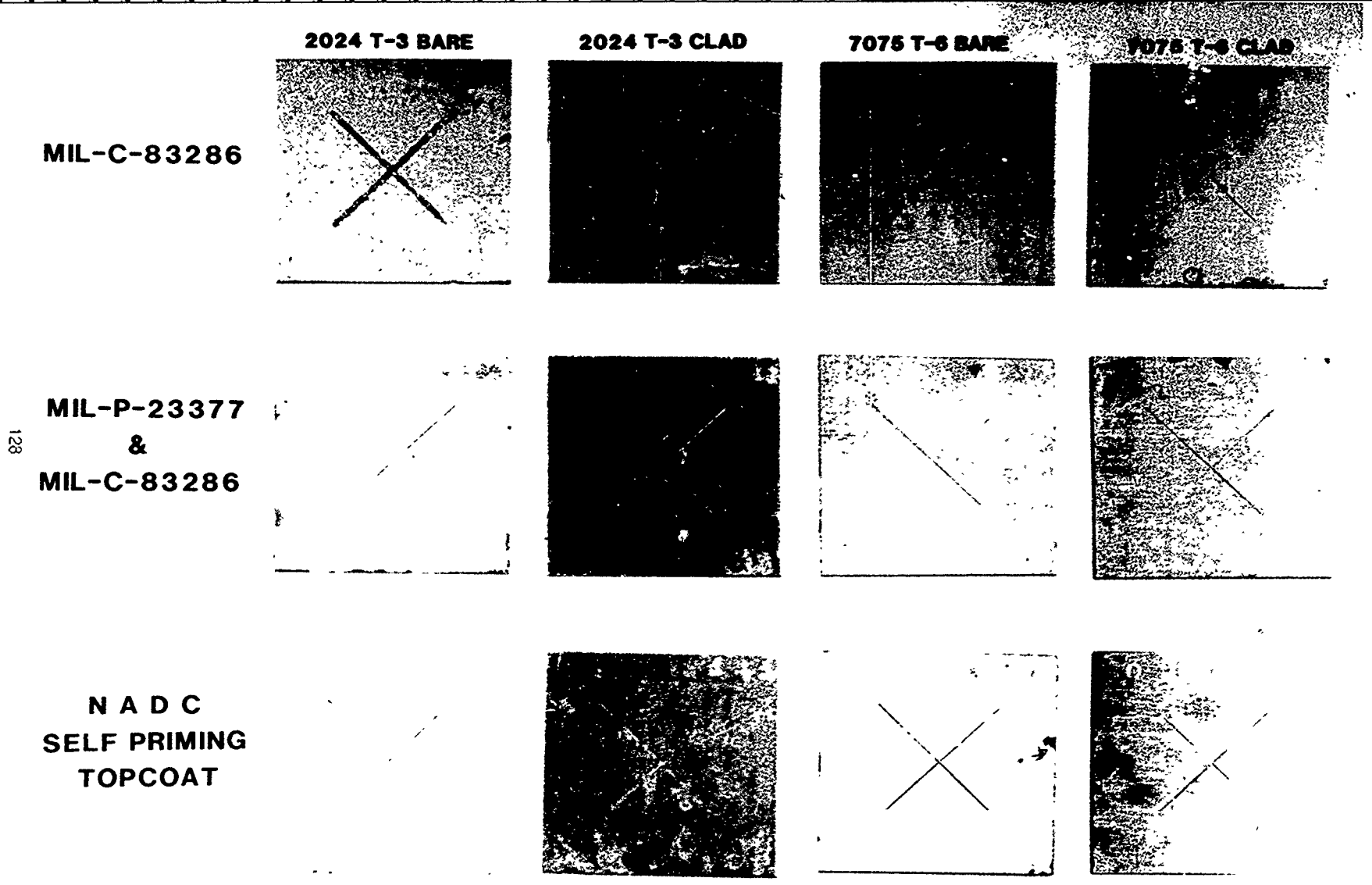

FIGURE 2: SULFURIC ACID ANODIZED-URETHANE SEALED SPECIMENS EXPOSED TO 5% SALT SPRAY FOR 2000 HOURS.

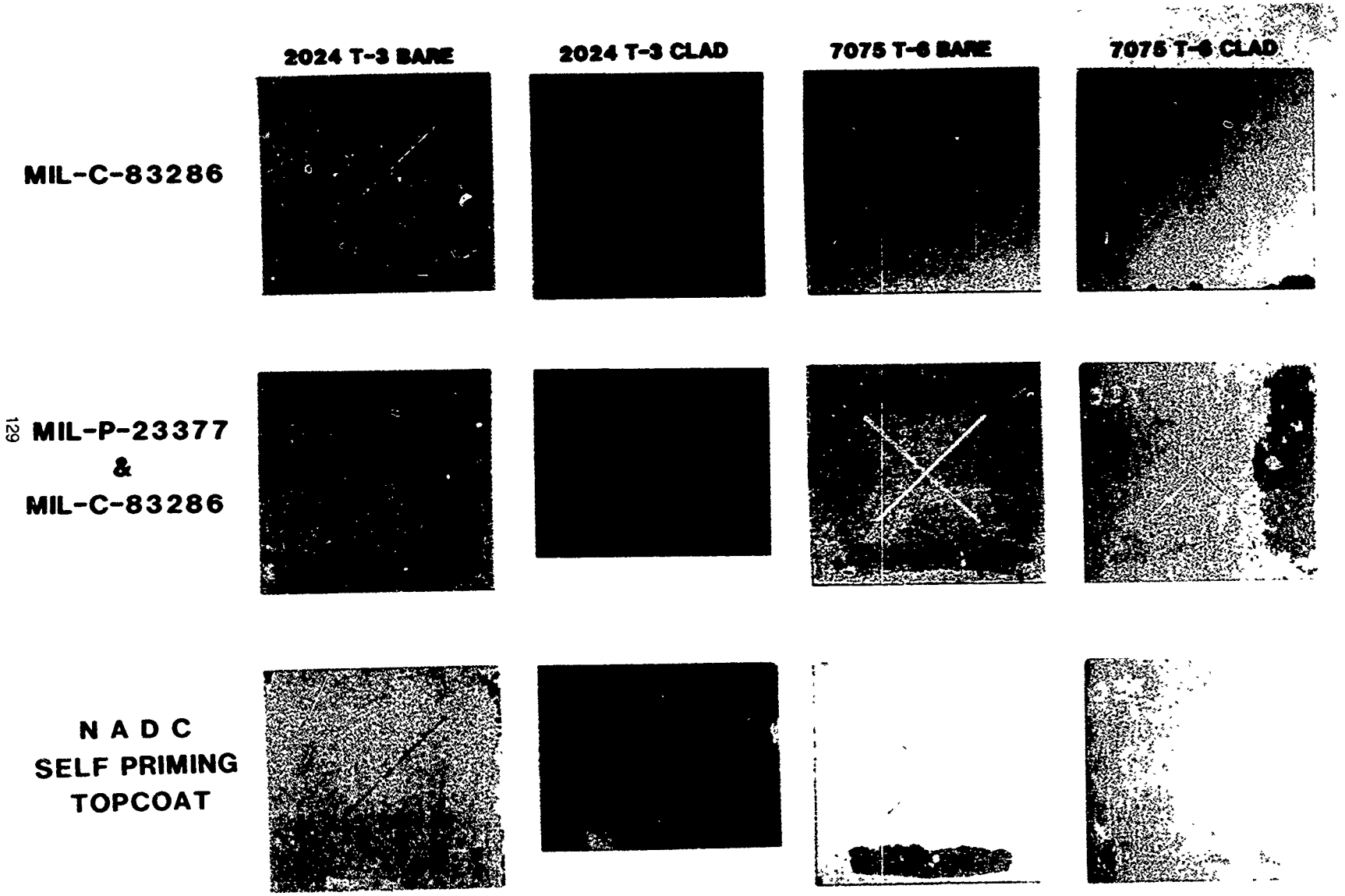

FIGURE 3: SULFURIC ACID ANODIZED-DICHROMATE SEALED SPECIMENS EXPOSED TO 5% SALT SPRAY FOR 2000 HOURS.

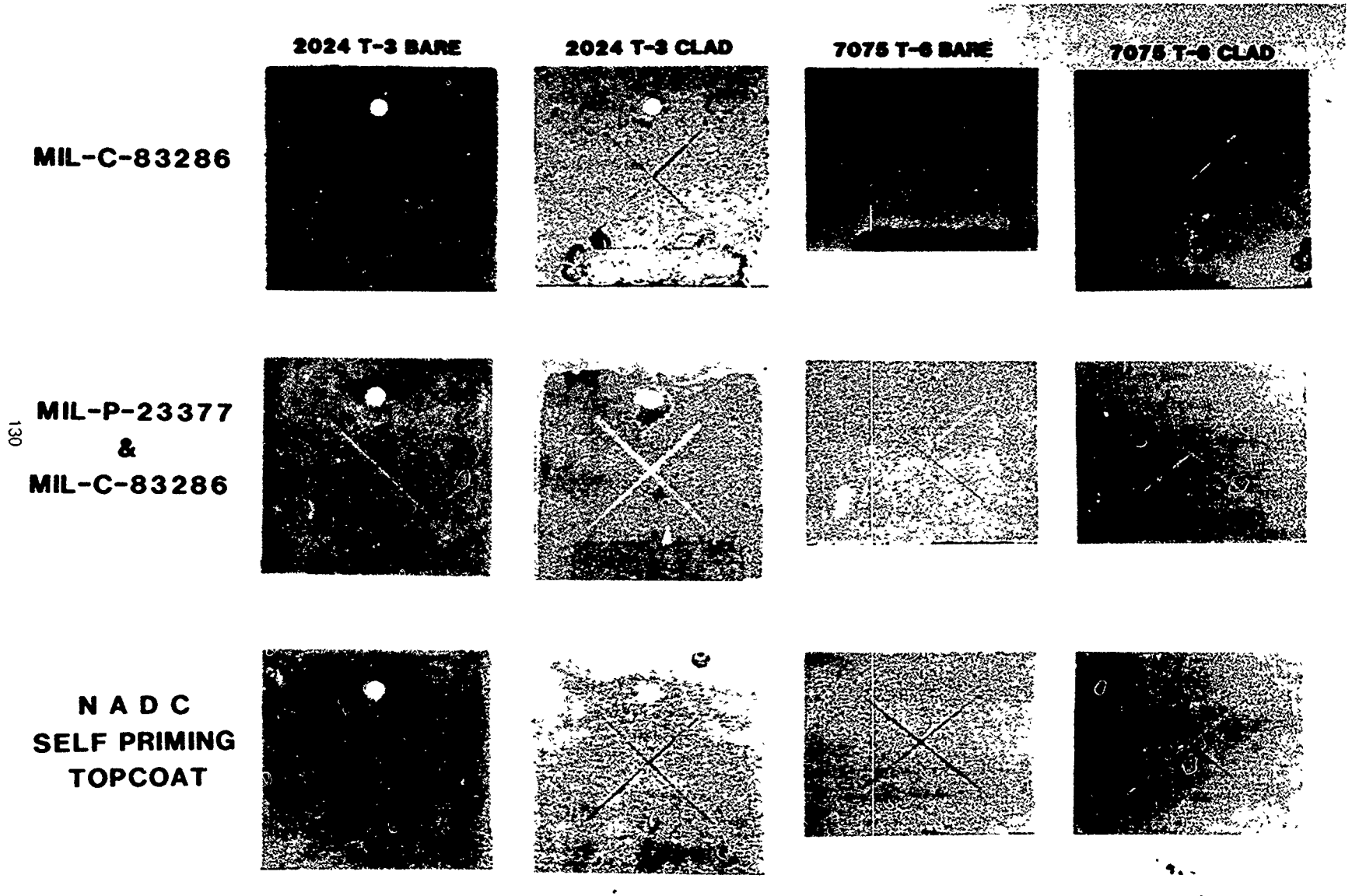

FIGURE 4: CHROMATE CONVERSION COATED SPECIMENS EXPOSED TO 5% SALT SPRAY FOR 2000 HOURS.

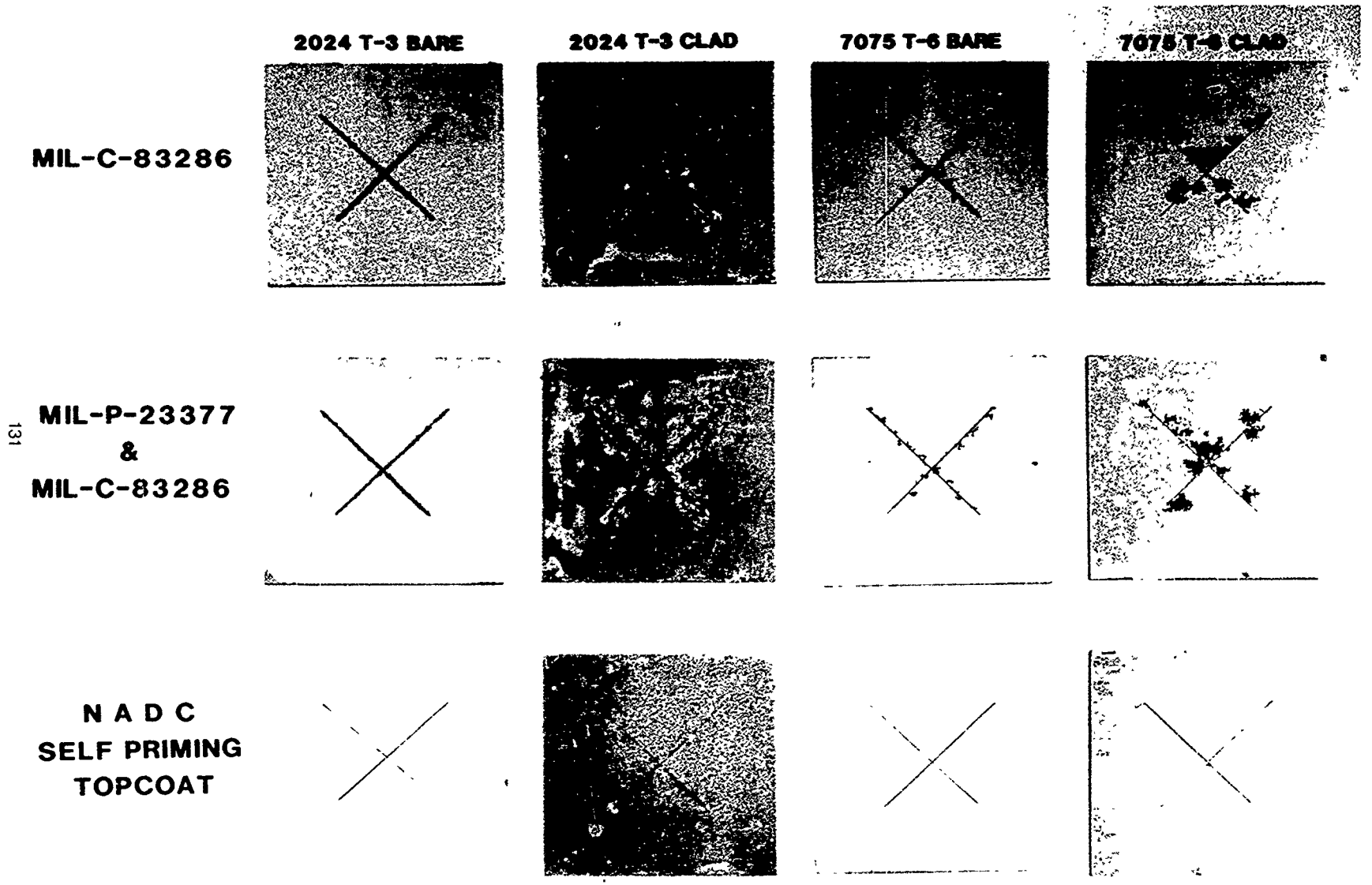

FIGURE 5: SULFURIC ACID ANODIZED-URETHANE SEALED SPECIMENS EXPOSED TO SULFUR DIOXIDE-SALT SPRAY FOR 500 HOURS.

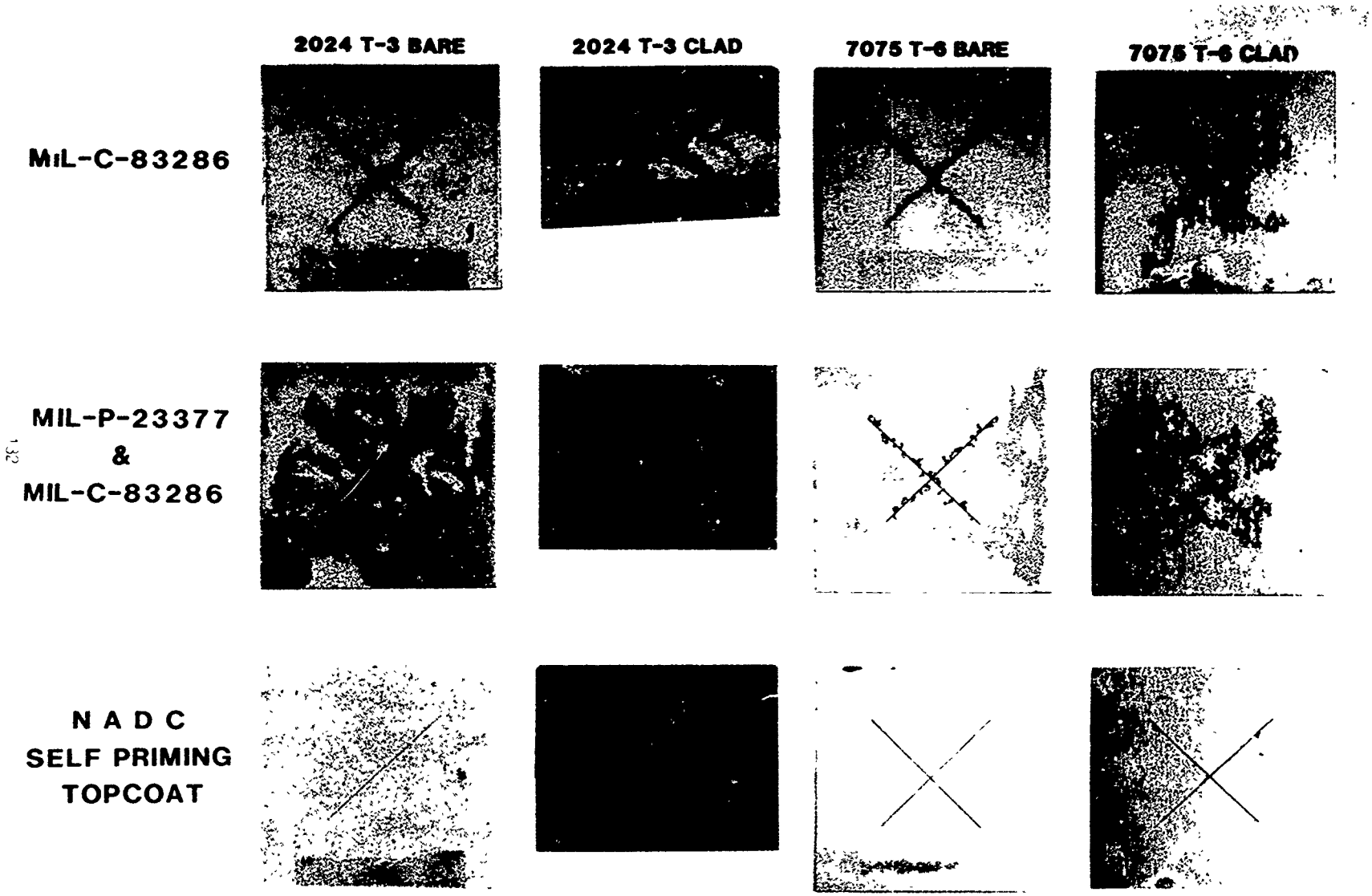

FIGURE 6: SULFURIC ACID ANODIZED-DICHROMATE SEALED SPECIMENS EXPOSED TO SULFUR DIOXIDE-SALT SPRAY FOR 500 HOURS.

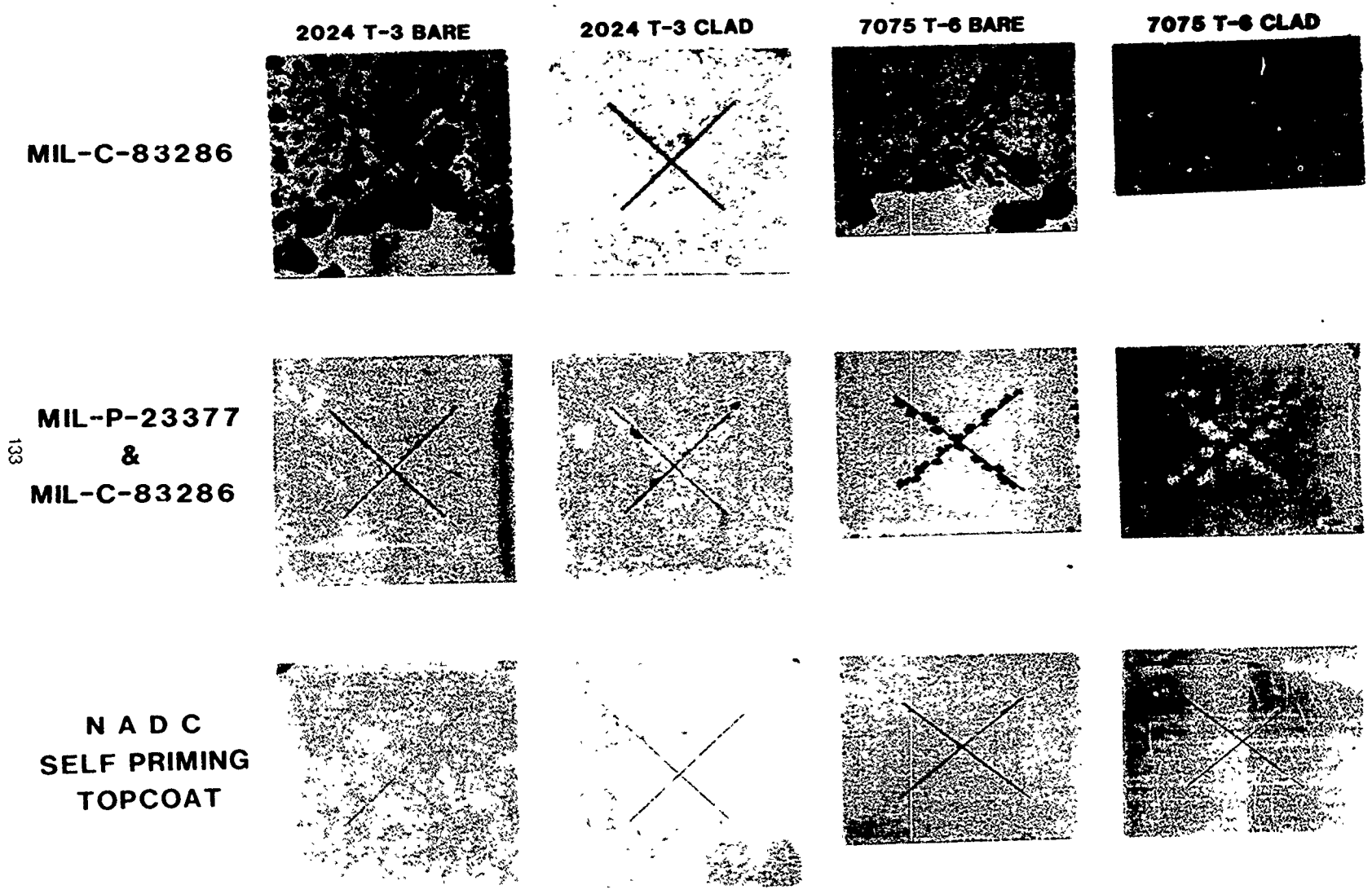

FIGURE 7: CHROMATE CONVERSION COATED SPECIMENS EXPOSED TO SULFUR DIOXIDE-SALT SPRAY FOR 500 HOURS.

PROTECTION OF MAGNESIUM COMPONENTS FOR THE MILITARY ENVIRONMENT

David S. Tawil

Magnesium Elektron Ltd.,
Swinton, Manchester,
England. M27 2LS.

ABSTRACT

The military requirement for optimum performance in portability, payload, range and speed can be aided by the use of lightweight magnesium. However, improved performance has sometimes been offset by corrosion problems resulting in increased maintenance and reduced readiness. One answer to combat this problem is to ensure the best possible corrosion protection at initial build and to educate military personnel in the corrosion maintenance of this "minority" metal. This is particularly important as peace time military equipment life cycles are continually being extended.

The change from simple chromate conversion coatings on magnesium to the more "effective" anodic conversion coatings, as now specified in many military standards, has not generally resulted in the expected improvement in corrosion performance. This has been partly due to the misconception that anodic films are by themselves protective and the recommendation that chromated primer systems be directly applied onto the anodic film. This paper highlights the benefits of resin sealing the anodic film prior to conventional painting and presents recently generated supporting data. Protection against galvanic corrosion and the development of a high temperature (550^{o}F) protection scheme for magnesium is also covered.

INTRODUCTION

Magnesium alloys are currently used in many military applications in order to "lighten the load". Aircraft applications include many examples of aeroengine gearboxes and intermediate casings, constant speed drives and generator sets, ancillary power units, transmission casings, wheels as well as flight controls. Applications on the ground are more limited because of the reduced requirement for weight savings but examples here include manpack radios, lightweight ground to air missiles, launcher

systems and tent frames. In Europe more use of magnesium is made for vehicle applications such as in the French AMX 30 and 40 battle tanks.

Magnesium is invariably compared to its nearest competitor, aluminium, in terms of specific mechanical properties and corrosion performance. With some very new exceptions, magnesium alloys have a much greater corrosion susceptibility not only in terms of general corrosion but more importantly by galvanic action at dissimilar metal contact. Military experience with magnesium has been mixed. Some applications have given long trouble free service whereas others have been beset by corrosion problems resulting in costly refurbishment or replacement programmes. Undoubtedly the operational environment is a major factor - not only in terms of the general environment i.e. temperate/tropical, land based/marine, but more specifically the local environment i.e. warm sheltered engine component or cold exposed component. With today's well travelled military equipment, assumptions about a benign service environment cannot be made and the worst case situation must always be catered for.

GALVANIC CORROSION PROTECTION

Before even considering the options available for general corrosion protection the priority must be for protection against galvanic corrosion. Magnesium's position in the electrochemical series coupled with its inability to polarise or form protective films in salt solution renders it particularly susceptible to galvanic attack. Accelerated salt spray testing (ASTM B117) of unprotected magnesium panels fitted with stainless steel bolts will cause deep ($\leq$ 0.08") pitting corrosion extending up to 1/4" away in 3 1/2 days (Figure 1). Whilst this is an extreme example it aptly demonstrates the relative importance of protection against galvanic corrosion.

Many exposed galvanic couples can and should be eliminated by good design practices. Examples include the use of studs located in blind holes rather than the use of through bolts or the avoidance of metallic identification plates riveted to magnesium assemblies. Dissimilar metals should be plated to improve their compatibility with magnesium. In particular steel or stainless steel inserts, fasteners, washers, spacers etc. should be cadmium plated and chromated passivated (1). Better still would be the use of 5000 or 6000 series aluminium washers or spacers in place of their steel counterparts. Again these should be chromate passivated to improve their polarisation resistance and should be of suitable size to lengthen any electrolytic path (1).

Of real practical benefit is the use of wet assembly procedures when installing dissimilar metals into and onto magnesium. Correct wet assembly involves the application of sealing compounds onto mating faces immediately before assembly and

should not be confused with the daubing of sealants to cover the dissimilar metal after assembly. For permanent or semipermanent joints, corrosion inhibited polymerising assembly compounds should be used (MIL-S-81733) which will remain elastic in service and will not crack. For fasteners which are removed for regular access the non-setting corrosion inhibited pastes or putty type compounds should be used and reapplied as necessary. The use of chromated epoxy primers, i.e. MIL-P-23377, for wet assembly is not recommended as these systems will dry out and rapidly crack in service.

The benefits of wet assembly are illustrated in Figure 2 where galvanic corrosion has occurred on the magnesium flange assembly which was not wet assembled. Both flanges had identical paint schemes and were subjected to the same weathering and accelerated corrosion test.

Final protection at dissimilar metal junctions is the overpainting of the joint area and in particular the cathodic (more noble) metal. This will effectively eliminate electrolyte contact between the metals. Primer and topcoat systems should be applied.

Galvanic corrosion caused by dissimilar metal contact is easily recognised but there are other forms of galvanic corrosion that can occur with magnesium. Cathodic contamination of magnesium surfaces arising from blasting, peening, brushing, tumbling, lapping and other abrasive operations are particularly damaging. A contaminated surface i.e. from wire brushing, will have a greatly increased corrosion rate which cannot be effectively protected by paint coatings. Any abrasive operation with incompatible or contaminated (Fe, Ni, Cu, C etc.) materials should either be avoided or steps taken to thoroughly clean the magnesium surface afterwards. This can be achieved by a range of acid pickling techniques (MIL-M-3171) providing dimensional losses of 0.002" per surface can be tolerated. Recent work (2) has also highlighted the desirability of clean, strong acid baths to obtain the best results. For machine finished components, Fluoride Anodising (3) is an effective cleaning treatment that will not cause significant dimensional loss.

MAGNESIUM CORROSION

Typical corrosion rates for unprotected magnesium alloys as determined in accelerated tests (Table 1) show that magnesium is adversely affected in salt laden environments. In recent years there have been significant advances which have dramatically improved the salt spray resistance of some magnesium alloys to levels comparable with those of aluminium alloys (Figure 3).

TABLE 1 - TYPICAL MAGNESIUM ALLOY CORROSION RATE DATA

ENVIRONMENT	CORROSION RATE ($mg/cm^2/day$)
ASTM B117 Salt Fog	2 - 10
3% NaCl Immersion	2 - 5
Intermittent Seawater Spray*	0.1 - 0.2
Industrial Atmospheric	0.01 - 0.02
Rural Atmospheric	0.005 - 0.01
*Specimens in a sheltered outdoor environment, sprayed 3 times/working day with natural seawater. Test duration 6 months.	

For the magnesium-aluminium series alloys (i.e AZ91, AZ61, AZ31)the corrosion performance benefits of maintaining a high purity (low levels of Fe, Ni and Cu impurities) melt have been demonstrated (2,4).

For the speciality magnesium-zirconium series alloys where superior mechanical properties over a wider range of temperatures is of major importance there has until recently been a necessary compromise of corrosion resistance. All Zr grain refined alloys are "high purity" in that Fe and to a lesser extent Ni impurities are naturally controlled to very low levels by precipitation with Zr. Corrosion performance of these alloys is largely governed by the major strengthening alloy additions such as zinc (i.e. ZE41 alloy) or silver (i.e. QE22 alloy). Recent research (5), using yttrium as the strengthening addition has produced a series of Mg-Y-RE-Zr alloys with good elevated temperature (500^{o}F) mechanical properties and excellent salt spray corrosion resistance as well.

Corrosion resistant sand casting alloys like WE54 (Mg-5%Y,4%RE-Zr) and WE43 (Mg-4%Y, 3%RE-Zr) are expected to enter service in the next few years but the corrosion resistant high purity AZ91E alloy is immediately available for replacement in existing AZ91C applications. This considerable improvement in corrosion resistance does not however protect against galvanic corrosion or surface contamination effects and the advantages of using these alloys can be inadvertently lost by uneducated use.

GENERAL CORROSION PROTECTION

Magnesium corrosion protection is in principle no different to that for any other metal but magnesium is less forgiving if mistakes are made. Protection schemes are usually selected on the basis of expected operational environment, design life, allowable corrosion and cost. For magnesium components in the military environment, quite simply, only the very best protection

schemes should be used. Quality and money spent at initial build will pay off in the long run. This life cycle cost approach is particularly important for peace time military hardware.

Protection of magnesium components is specified by various Military Standards (i.e. MIL-Std-1568) usually with reference to specifications MIL-M-3171 and MIL-M-45202 which detail the various pre-treatments prior to painting. The tendency in recent years has been to move away from the simple chromate conversion coatings to the more abrasion and damage resistant anodic coatings in the expectation that improved corrosion protection would result. This has not unfortunately been the case. To understand why it is necessary to study the nature of conversion coatings on magnesium.

Chromate (Dow 7, Cr/Mn (6)) or anodic (HAE, Dow 17) conversion coatings will passivate magnesium surfaces and provide an effective "key" for painting but they are porous (Figures 4, 5,6) and by themselves offer no corrosion protection. This has three basic implications. The first is that conversion coatings, particularly chromate and thin anodic types, will degrade with time and environmental conditions and should be "painted" as soon as possible after application. Secondly, no component should be put into service with just a conversion coating as protection - a condition that in practice frequently occurs, particularly at mating faces. Finally, to obtain optimum corrosion protection the porosity of the conversion coating should first be sealed before conventional painting.

A process known as Surface Sealing (7) was developed which effectively seals conversion coating porosity. This process is also covered in MIL-M-3171C. In the process a freshly chromated or anodised component is pre-baked at 380-400^{o}F to drive off all surface moisture and after cooling to approximately 140^{o}F is sprayed with, or preferably dipped into, a "water" thin solution of a high temperature curing resin. An epoxy (Araldite HZ/PZ 985) or an epoxy-phenolic (Araldite PT 961) resin is preferred although the technique can be used to good effect with other unpigmented resin systems. The first coat of resin is then partially cured at temperature and the process repeated to obtain three thin coats before final cure at 380-400^{o}F for 45 minutes.

The full three coat system applied onto a chromate film produces a build up of only 0.001" and is intended for use on all component surfaces including mating faces. On anodised surfaces the resin build up is less, due to the higher levels of film porosity. For fine tolerance areas the number of coats can be limited to two or even one coat in extreme circumstances but this will of course reduce the effectiveness of the system. Not only is Surface Sealing an excellent water resistant barrier coating but having sealed the conversion coating porosity, corrosion spread from a damage point is significantly restricted.

Only when the gross porosity of anodic coatings has been effectively sealed can their superior protection abilities, compared to chromate coatings, be realised. This is not achieved by overpainting with conventional primer systems (Figure 7), as recommended by MIL-Std-1568 for example, and goes some way to explain why the switch to anodic coatings has not resulted in improved magnesium corrosion protection.

A.C Impedance data (8) for AZ31 specimens immersed in 0.5 M NaCl at room temperature demonstrates the improvement in protection with the number of coats of Surface Sealing applied (Figures 8, 9 and 10). The data also re-emphasises that chromate and anodic conversion coatings are not protective in saline environments.

Recent work (9) by the Army (MTL, Watertown) has also assessed the effectiveness of the Surface Sealing procedure incorporated into full protection schemes on ZE41 alloy. General corrosion and corrosion spread from scribed damage was significantly less for protection schemes with the Sealer as determined in conventional ASTM B117 salt fog tests (Figures 11, 12). AC Impedance data is also presented.

TABLE 2 ADHESION OF EPOXY POLYAMIDE PRIMERS TO SURFACE SEALING

SUBSTRATE	COATING	POST TREATMENT	ADHESION* VALUE (psi)
Cr/Mn chromated magnesium	Araldite 985 Surface Seal	None	>4,000
Cr/Mn chromated magnesium	MIL-P-23377 primer	None	1,830
Araldite 985 Surface Seal	MIL-P-23377 primer	None	145
Araldite 961 Surface Seal	MIL-P-23377 primer	None	1,170
Araldite 985 Surface Seal	MIL-P-23377 primer	30 mins @ 250°F	1,100
Araldite 985 Surface Seal	Improved adhesion primer	None	485
*approx. 700 psi required to completely pass crosshatch and tape pull test.			

However Levy (9) reported poor adhesion between the sealer (Araldite 985) and the subsequently applied MIL-P-23377 chromated epoxy-polyamide primer. Poor adhesion was also reported in work by Robinson (10). Recent work (11) using a pull off adhesion tester (ASTM D4541) has determined that epoxy-polyamide primer adhesion to Araldite 985 sealer is poor but can be significantly

improved by a post bake at 250°F. Alternatively, improved adhesion primers, incorporating silane additions can be used which do not require post bake treatment. No problems with epoxy-polyamide primer adhesion to Araldite 961 sealer were noted. Results are given in Table 2.

Epoxy and epoxy-phenolic sealers are effective up to temperatures of approximately 400°F. For higher temperature applications, up to 500°F, epoxy-silicone and silicone resins can be used but it is known that these systems are not very resistant to aeroengine lubricants. However considerable military use of magnesium is for oil system casings operating at temperatures up to 350°F and future trends are for hotter applications. These components will require conventional exterior protection but increasingly internal protection is also required. Hot oil systems, particularly when contaminated with water, can produce acid radicals which will corrode magnesium. It has been demonstrated (12) that protection schemes based on Dow 17 anodic coatings are more suited in resisting hot acidic oil attack. Sealing the Dow 17 film with epoxy or phenolic resins provided protection up to 400°F in hot oil environments. Protection up to 500°F was obtained by using a polyimide resin as the sealer. This is beyond the temperature limit for the MIL-L-23699 specification ester lubricants currently in use. A full Dow 17/polyimide protection scheme also afforded good conventional corrosion protection against salt fog/elevated temperature cycling at temperatures up to 575°F.

In conclusion, there is existing technology that will effectively protect magnesium components operating in the aggressive military environment. There are also protection schemes for future applications. The problem has not been for lack of technology but rather the application of known technology. The question to be asked is - why?

REFERENCES

1. Galvanic Corrosion of Magnesium - D. Hawke; 14th International Die Casting Congress and Exposition, Toronto, May 1987.

2. AZ91E Magnesium Sand Casting Alloy. The Standard for Excellent Corrosion Performance - K. Clark; Proc. I.M.A. Conference, Los Angeles, June 1986.

3. MIL-M-3171C - Type VII treatment.

4. Controlling the Salt Water Corrosion Performance of Magnesium AZ91 Alloy - K. Reichek, K. Clark, J. Hillis; SAE Paper 85-0417.

5. WE Alloys - High Performance Corrosion Resistant Casting Alloys for the 1990's - J. King, M. Dudley; 25th Joint Propulsion Conference, Monterey, July 1989.

6. Chrome Manganese chromate pre-treatment - British Military Specification DTD 911C, Bath V.

7. British Military Specification DTD 935.

8. Evaluation of Corrosion Protection Methods for Magnesium - F. Mansfield, S. Kim; Corrosion Research Symposium, NACE, St. Louis, March 1988.

9. Assessment of some Corrosion Protection Schemes for Magnesium Alloy ZE41A-T5 - M. Levy, R. Bombard, R. Hill, K. Lei; World Materials Congress, Chicago, September 1988.

10. Evaluation of Various Magnesium Finishing Systems - A. Robinson, Proc. I.M.A Conference, New York, May 1985.

11. Improving Primer Adhesion to Surface Sealed Magnesium Components - M. Taylor, D. Tawil; Report MR10/Data/199 April 1988, Magnesium Elektron Publication.

12. Improved Protection of Magnesium Alloys Against Synthetic Aviation Lubricants at Elevated Temperatures - M. Rendu, D. Tawil; SAE Paper 88-0869.

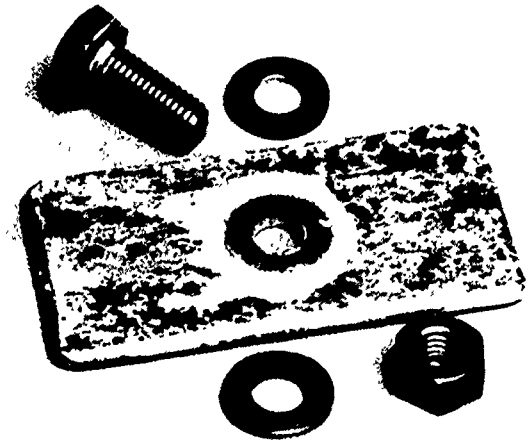

Figure 1 Galvanic corrosion of unprotected magnesium to stainless steel couple after 3 1/2 days ASTM B117 Salt Fog.

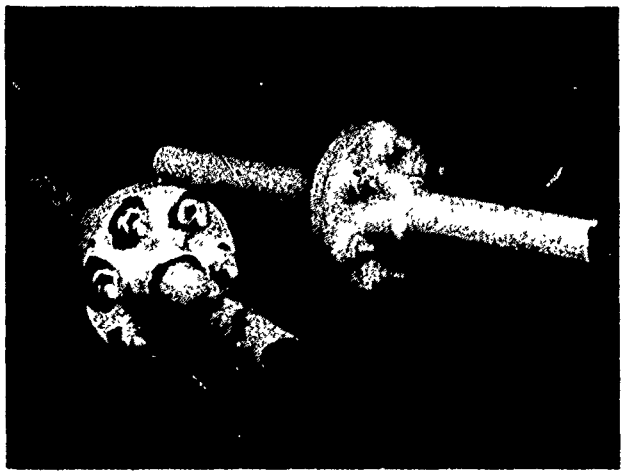

Figure 2 Magnesium alloy flange assemblies with identical paint schemes and subjected to the same corrosion test illustrate the advantages of "wet assembly."

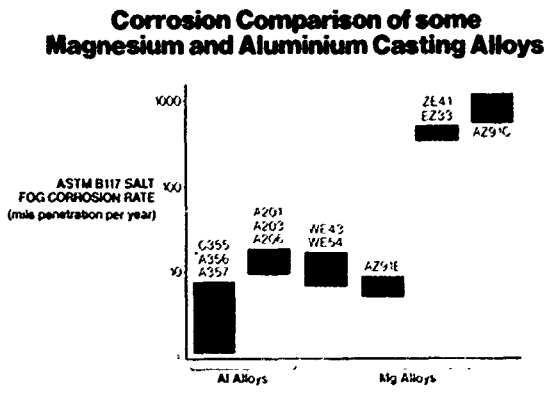

Figure 3 ASTM B117 Salt Fog corrosion rate comparison.

Figure 4 SEM photomicrograph of surface of chromate film on wrought magnesium alloy.

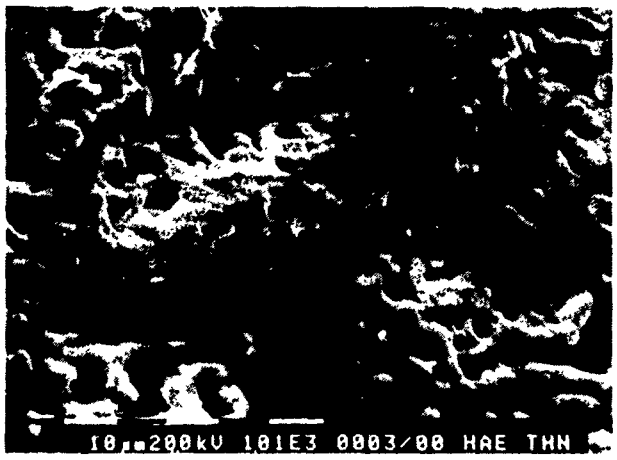

Figure 5 SEM photomicrograph of surface of thin HAE anodic coating on magnesium alloy.

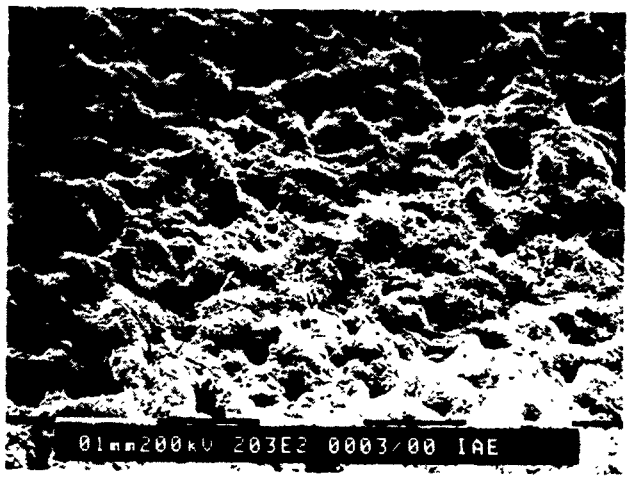

Figure 6 SEM photomicrograph of surface of thick HAE anodic coating on magnesium alloy.

Figure 7 SEM photo-micrograph of cross section through Dow 17 film which has been coated with MIL-P-23377 primer.

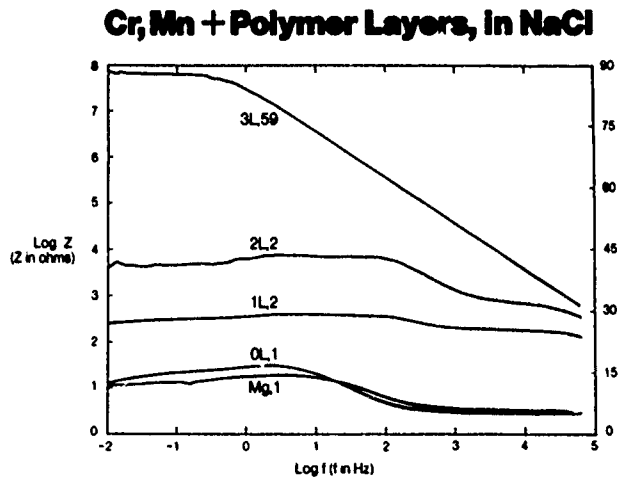

Figure 8 Bode plot of AZ31 magnesium, CrMn chromated with 1, 2 and 3 coats of Surface Sealing resin.

N.B final numbers of plot identification denote number of days under immersion.

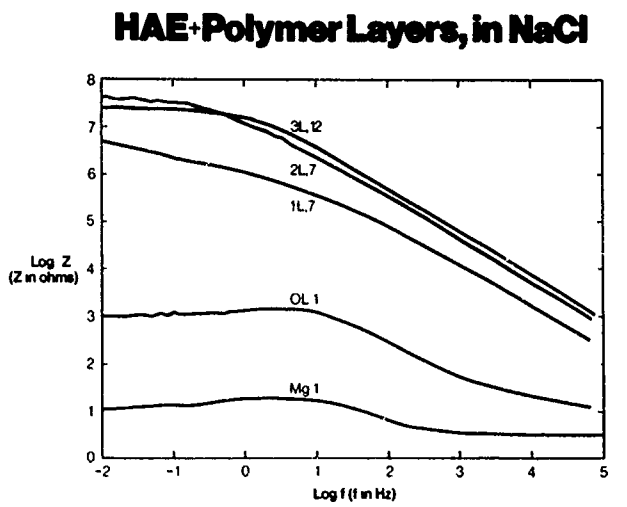

Figure 9 Bode plot of AZ31 magnesium, thick HAE anodised with 1, 2 and 3 coats of Surface Sealing resin.

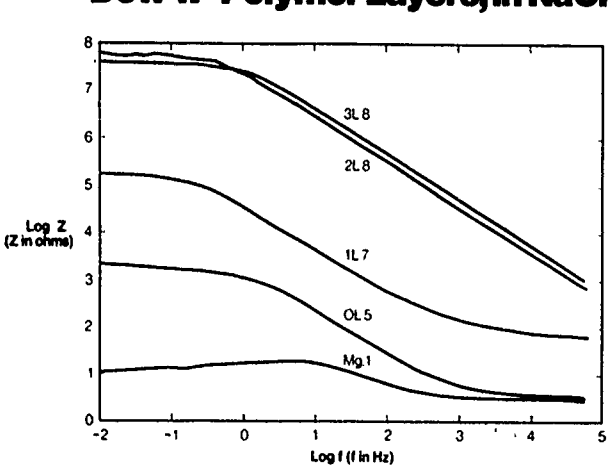

Figure 10 Bode plot of AZ31 magnesium, thick Dow 17 anodised with 1, 2 and 3 coats of Surface Sealing resin.

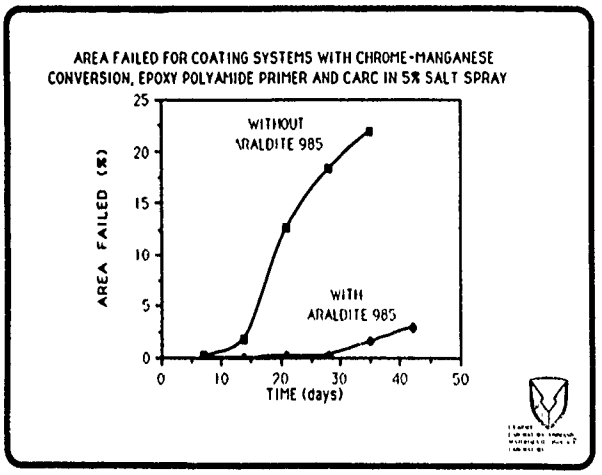

Figure 11 Performance comparison of sealed and non-sealed protection schemes on chromated ZE41 alloy under ASTM B117 Salt Fog.

Data from Levy - ref. 9.

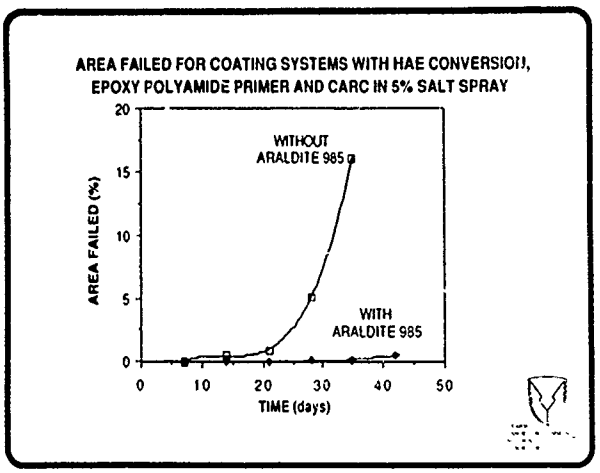

Figure 12 Performance comparison of sealed and non-sealed protection schemes on HAE anodised ZE41 alloy under ASTM B117 Salt Fog.

Ref. 9

VOC COMPLIANT COATINGS FOR AEROSPACE APPLICATIONS

David F. Pulley
Naval Air Development Center
Warminster, PA 18974

ABSTRACT

The Department of Defense has agreed to cooperate with the Environmental Protection Agency with respect to compliance with environmental regulations at government-owned or operated facilities. As part of this effort, the Navy is committed to revising all of the specifications for coatings applied to aircraft and ground support equipment and including limits for volatile organic compounds (VOC) content. This has already been accomplished for most of the epoxy and polyurethane paints using water-borne, high-solids, or exempt-solvent technologies. The new materials are generally equivalent in performance to the existing solvent-borne coatings, but do require special handling by the military and contractor personnel that apply them in production and in the field. They, in turn, are looking at various types of spray equipment (airless, electrostatic, plural-component, etc.) for the efficient application of these materials. This paper will discuss the available compliant paints and how their chemistry affects different properties that are critical to the aerospace industry. Their impact on both the applicator and end-user will also be presented.

INTRODUCTION

The organic coatings specified by the Navy for aerospace applications are unique in that they must function in a corrosive, salt-water environment with a minimum of maintenance. In general, they must adhere to several different metallic and composite substrates, remain flexible at temperatures approaching -60° F, and resist exposure to weathering, corrosion, and harsh chemicals. They must often provide specific properties including resistance to heat, rain-erosion, etc. while minimizing aircraft detection by visual, infrared, and radar techniques.

STANDARD PAINT SYSTEM

The standard paint system for the exterior and interior surfaces of aircraft, weapons, and ground support equipment includes a solvent-borne, epoxy primer and polyurethane topcoat. The primer, which meets specification MIL-P-23377, has a VOC content of 630-670 grams/liter. It possesses good adhesion to aluminum, steel, titanium, and other alloys as well as graphite-epoxy composites and contains a high concentration of strontium chromate as the primary corrosion inhibitor. The topcoat, which meets specification MIL-C-83286, has a VOC content of 560-650 grams/liter. It provides a highly-flexible barrier to moisture with excellent weatherability and chemical resistance. It is furnished in colors ranging from gloss whites, reds, and yellows to flat (camouflage) grays and greens.

ENVIRONMENTAL REGULATIONS

Because of severe air-quality problems, the state of California has implemented the most stringent regulations in the United States. The Navy has rework facilities and contractor plants throughout California. They are located primarily in three local districts: the Bay Area Air Quality Management District, the San Diego Air-Pollution Control District, and the South Coast Air Quality Management District. The Environmental Protection Agency, by enforcing the Clean Air Act, has tried to standardize regulations within the aerospace industry. By definition, aircraft and the weapons attached to them fall under the aerospace rules; while ground support equipment falls under the metal parts rules. These rules are listed as follows:

District	Aerospace Rule	Metal Parts Rule
Bay Area	Regulation 8, Rule 29	Regulation 8, Rule 19
San Diego	Rule 67.3	Rule 67.9
South Coast	Rule 1124	Rule 1107

The current maximum limits for primers are 350 grams/liter (aerospace) and 340 grams/liter (metal parts). For topcoats, the limits are 420 grams/liter (aerospace) and 340 grams/liter (metal parts). Measurements of volatile organic compounds must include not only solvents but any volatile chemicals in the resin, pigment, or additive components of each paint. Exempt solvents such as water or 1,1,1-trichloroethane are not included in the total paint volume. The most common test method is ASTM D 3960.

WATER-BORNE TECHNOLOGY

Water can be used to dilute organic resins with chemical structures that are hydrophilic. Unfortunately, this affinity for water usually results in paint films with poor resistance to moisture. Generally, the most durable finishes employ a combination of water and organic co-solvents.

About ten years ago, Deft used this technology to develop a water-borne, epoxy primer. It was packaged as a high-solids, solvent-borne material with all of the water added at the point of application. This eliminated any problems with freeze-thaw stability. In the laboratory, the Deft primer met all of the performance requirements of specification MIL-P-23377. The primary difference was in the use of barium chromate, rather than the accepted strontium chromate, as the corrosion-inhibiting pigment. This was done because of the incompatibility of the curing agent with the strontium ion, resulting in a short pot life. Concern about filiform corrosion with the less-soluble barium chromate was never confirmed in the field. Extensive service testing and production application on hundreds of fleet aircraft have demonstrated the quality of this new primer.

The major adjustment on the part of the applicator comes from the slower drying time, particularly when the humidity is high. This can be alleviated by increasing the air-flow across the wet primer. It will be dry-hard in six hours at an air velocity of 88 feet/minute. The low volatility of water also results in a smoother surface finish that is evident even after topcoating. The higher density of water (compared to organic solvents) yields significantly less overspray and, therefore, improves the transfer efficiency. Organic contaminants, such as hydraulic fluid, are exposed by the primer due to its high surface tension. Equipment clean-up can be accomplished in many cases with just soap and water.

In 1984, specification MIL-P-85582 was established for the procurement of water-borne, epoxy primers with a maximum VOC content of 340 grams/liter. Deft later resolved the compatibility problem with strontium chromate; and a separate class for that inhibitor was added. Recently, DeSoto was qualified as a second source. Efforts to develop a water-borne topcoat have been unsuccessful, due to the limited weatherability of these resins.

HIGH-SOLIDS TECHNOLOGY

The development of high-solids coatings has been a slow, deliberate process. Reduced solvent concentrations generally yield a higher viscosity, shorter pot life, and rougher surface finish. The use of low molecular-weight resins to lower the viscosity will further shorten the pot life and reduce the flexibility of the applied film. The pot life can be increased by incorporating blocked polymers that inhibit the crosslinking reaction until "unblocked" by moisture in the air. Naturally, the inhibited reaction also extends the drying time. The use of high-boiling solvents to improve the surface finish will further increase the drying time. These solvents can sometimes cause a new phenomenon, where sharp edges are exposed as the paint flows out.

Recently, a number of advances have occurred. An evaluation of seven proprietary, high-solids, epoxy primers showed that the technology is feasible. As expected, they exhibited a higher viscosity and a shorter pot life. In addition, they had a longer drying time and reduced flexibility. However, one of the primers (made by Pratt & Lambert) met all of the performance requirements in specification MIL-P-23377. Despite the high viscosity, it could be sprayed to a dry-film thickness of 0.6-0.9 mil as required for aircraft application. The test results were used to write a new revision to the specification (with a separate high-solids class) that will be issued shortly. The maximum VOC content will be 340 grams/liter.

The Army Belvoir Research and Development Center approved high-solids, epoxy topcoats from the Everseal Manufacturing Company and the Sherwin-Williams Company for use under Army contracts. They each meet the 340 grams/liter VOC content established for metal parts application. We have evaluated both materials and revised specification MIL-C-22750 to include provisions for their use. This revision will be issued in the near future.

Most of the work in this area has been devoted toward polyurethane topcoats, since they represent the optimum performance attainable with regard to flexibility, durability, and weatherability. Specification MIL-C-85285 was revised last year to accomodate high-solids materials at a maximum VOC content of 420 grams/liter (for aircraft application). Since then, we have qualified products from Akzo Coatings, Deft, and DeSoto. For metal parts application, we reduced our flexibility requirements in order to use lower molecular-weight resins and meet the lower VOC content of 340 grams/liter. The latest revision of the specification now includes a separate type for this purpose. No one has qualified a topcoat at this time.

EXEMPT-SOLVENT TECHNOLOGY

1,1,1-trichloroethane (TCA) is listed as an exempt solvent in VOC regulations issued by 45 of the 50 states. This is due to the fact that it is not photochemically reactive and does not contribute to the generation of "smog" in industrial areas. However, it has been linked with other chlorinated compounds in the degradation of the ozone layer in the upper atmosphere. For this reason, TCA may be only a stop-gap solution to existing environmental regulations.

TCA is compatible with most organic resins when used in combination with other strong solvents. It has a number of advantages including no appreciable odor or flammability and low overspray (due to its high density). Contractors often prefer this option, since it requires no modifications to existing contracts or process specifications. Coating performance is virtually unchanged from the original non-compliant paints. In addition, more suppliers can furnish materials at lower cost in comparison to the new water-borne and high-solids coatings.

However, there are many reasons to restrict the use of TCA in paints. In addition to the ozone problem, chlorinated solvents are treated as a hazardous waste and require expensive methods of disposal. They react with aluminum, particularly at high temperatures or pressures. Therefore, airless spray equipment must have all wetted parts composed of stainless steel or other resistant materials.

A special concern for the Navy is the tendency of aggressive ions such as chlorine to cause stress-corrosion cracking within high-strength, structural alloys. Extensive testing by Grumman Aircraft Systems, the McDonnell Aircraft Company, and our laboratory revealed that TCA could be used with certain restrictions. First, the solvent must be an inhibited grade such as Dow Chemical's CHLOROTHENE SM. Then, each paint specification utilizing TCA must limit the maximum solvent retention to 1 percent by weight after seven days air-dry in accordance with test method ASTM F 151. Finally, paints containing TCA must not be used in high-temperature applications such as engine components or where the solvent could become entrapped such as fasteners (wet installation) or faying surfaces.

In 1984, specification MIL-P-23377 was the first to include a separate exempt-solvent class. Since then, epoxy primers from Advanced Coatings & Chemicals, Akzo Coatings, Con-Lux Coatings, Crown Metro, Deft, DeSoto, Kop-Coat, and Seagrave Coatings Corporation have been qualified. Another development by DeSoto, with the tradename KOROFLEX, is an elastomeric polyurethane primer designed for aircraft subject to structural flexing at low temperatures. The only compliant version of this primer ulilizes

TCA. Specification MIL-P-85853 was written for the procurement of KOROFLEX; and it should be issued in the near future. Epoxy topcoats will also be available as a separate, exempt-solvent type under specification MIL-C-22750. Qualification testing will begin when the next revision of the specification is issued.

SPECIALTY COATINGS

A number of specialty coatings are considered to be compliant without any reformulation needed. Rain-erosion coatings are high-solids, elastomeric, polyurethane coatings applied as thick (12 mil) films to provide protection to aircraft radomes from rain impingement at high speeds.

Temporary, camouflage paints are water-borne, acrylic paints applied in the field over a conventional paint system in order to change the camouflage scheme of aircraft scheduled for rapid deployment. They can be easily removed by an alkaline solution after a few weeks without damaging the underlying paints.

Thermal-insulating coatings are high-solids, polyester or epoxy-polysulfide coatings containing reactive fillers that insulate weapons from accidental fuel-fires until the fires can be extinguished. They function by ablative or intumescent mechanisms.

Walkway coatings are high-solids topcoats filled with an abrasive grit that allows workers to walk over horizontal surfaces without slipping.

Passive countermeasures include coatings that prevent the detection of our aircraft by visual, infrared, radar, and other techniques. These materials are generally high-solids; although, in many cases, the exact formulations are classified.

FUTURE WORK

There are other, non-compliant coatings that have not been addressed because of funding limitations and higher priorities. Wash primers are dilute solutions of a polyvinyl butyral resin reacted with phosphoric acid to produce an adherent pretreatment for metals. They are applied as a very thin film (0.3-0.5 mil).

Zinc-rich primers use epoxy or alkyl silicate binders filled with powdered zinc to protect steel substrates from corrosion. The high concentration of zinc requires an equally high solvent content.

Lacquer topcoats are one-component alkyd or acrylic paints that dry by solvent evaporation. These topcoats are useful where ease of application is more important than performance (such as spraying with aerosol cans).

High-temperature paints are those that operate at temperatures from 400oF to 1200oF. They often utilize silicone resins, alone, or in combination with other resins.

METHODS OF SPRAY APPLICATION

Conventional, air-atomized spray equipment is rapidly being replaced by more sophisticated types, because of the trends toward high-solids coatings and improved transfer efficiency. Airless spray equipment atomizes paint by forcing it through an orifice at high pressures (at least 2000 pounds/square inch). This allows the applicator to spray viscous materials easily. However, he must learn to work quickly; since the higher flow rate and solids-content increases the rate of film-build. With airless spray, the surface finish tends to be rougher; although "air-assisted" airless equipment is available to alleviate this.

The transfer efficiency of both types of spray equipment can be greatly improved using electrostatic attraction. With this technique, a high-voltage charge is applied to the paint so that it is drawn toward the surface to be coated (which has been electrically grounded). All new and revised specifications will require every qualified product to be compatible with electrostatic spray application. Paint manufacturers must assure that their materials have the proper resistivity. This can be accomplished with the use of polar solvents.

Airless spray equipment is often combined with plural-component mixing. This is an automated process where the two components in a catalyzed paint are mixed at a precise volume ratio just before flowing to the paint-gun. It eliminates any concern about the short pot life of high-solids coatings; since the paint is mixed seconds before application. When stopping production, only the paint-gun and the hose between the gun and the mixing equipment need to be flushed with thinners and cleaned. Waste disposal, therefore, is also minimized. This technology has raised questions about the need for an "induction time" in most specifications. This is a period of 30-60 minutes during which admixed paints are supposed to prereact before application (theoretically improving the drying time and film properties). Polymer chemists disagree on whether the induction time has any real benefit.

SUMMARY

The impact of VOC regulations has been profound. There are fewer paint suppliers able to keep up with the current state-of-the-art. With less competition, prices have increased substantially. The painting contractor finds that the application of compliant paints is much more complex. Mixing ratios may range anywhere from 1:1 to 4:1 by volume. The short pot life limits his working time to 4 hours or less. Higher viscosities make it difficult to apply a thin film. Longer drying times reduce his productivity. The finished product may exhibit "orange-peel" or other surface imperfections. He will probably have to buy new spray equipment to better handle these materials.

For the end-user, the situation is quite different. The performance of these compliant paints is generally equivalent to the non-compliant paints used in the past. Hopefully, the current VOC limits will remain in effect for a while so that the paint industry can improve the application properties of their products and the aerospace industry can evaluate the durability of these materials over a period of several years. Obviously, the trend for VOC limits will be downward. We just hope that future regulations can be based on proven technology and implemented in a spirit of cooperation.

ASSESSMENT OF SOME CORROSION PROTECTION SCHEMES FOR MAGNESIUM ALLOY ZE41A-T5

Milton Levy, Robert Bombard, and Robert Huie
U.S. Army Materials Technology Laboratory, Watertown, MA 02172-0001

Kuan Lei
Geo-Centers, Inc., Newton Upper Falls, MA 02164

ABSTRACT

The U.S. Army has experienced a continuing corrosion problem with magnesium components of aircraft requiring increased maintenance and impacting both cost and readiness. A recent modernization program has replaced a number of magnesium parts with aluminum to reduce the corrosion problem but with a concomitant weight penalty. In order to fully utilize the advantages of magnesium, more corrosion resistant alloys with improved protective schemes are needed. This paper assesses the corrosion resistance of several protective schemes for magnesium alloy ZE41A incorporating a conversion coating or HAE anodize, with or without a sealer, several primers, and a polyurethane topcoat. The tests employed include 5% salt spray, 100% RH at 100°F followed by tape adhesion, and AC impedance to develop Nyquist and Bode plots. It was concluded that the application of the sealer significantly improved the corrosion resistance of the paint scheme. Best results were obtained when the HAE anodize was used as the initial treatment.

INTRODUCTION

U.S. Army experience with magnesium alloys as components in aircraft has shown a significant corrosion problem requiring increased maintenance, and impacting both cost and readiness. During the Vietnam era there was widespread use of magnesium in Army aircraft to reduce weight and increase performance. In a recent modernization program, however, a number of magnesium parts have been replaced with aluminum to reduce the corrosion problem. It is clear that more corrosion-resistant magnesium alloys with improved protective schemes are needed before their advantages can be fully utilized.

The best current practice for protecting magnesium in Army aircraft employs an anodize or chromate conversion treatment, an epoxy primer, and a polyurethane top coat. This paper assesses a protective scheme for MG alloy ZE41A which has been modified by the British approach of interposing a baked epoxy resin (sealer) between the conversion coating and primer application. For comparison purposes, the current practice described above is also assessed.

MATERIALS

Magnesium alloy ZE41A-T5 was selected because it is presently being used in our newest aircraft. Table 1 contains the nominal composition of this alloy, the heat treatment, and mechanical properties. The corrosion resistance in mpy obtained by both immersion in 3% NaCl solution and electrochemical polarization in both 100 ppm Cl and 3.5% NaCl solutions is also included. Note, that the immersion and polarization data in 3.5% NaCl solution are in good agreement; 120 mpy and 115 mpy, respectively.

The protective schemes evaluated are described schematically in Figure 1. The variables include the initial conversion coating, the presence of the sealer, and the primers. The chemical agent resistant polyurethane topcoat was standard for all systems evaluated. The thickness of each coating layer is shown schematically in Figure 2. The procedure for applying the sealer is contained in Table 2. The application of the conversion coatings, primers, and topcoat was carried out in accordance with the specifications and standards shown in Figure 1.

TABLE 1

Mg ZE41A-T5 PROPERTIES

NOMINAL COMPOSITION	Zinc	3.5-5.0 %
	Rare Earths (Ce)	1.2 %
	Zirconium	0.4-1.0 %
	Magnesium	balance
HEAT TREATMENT	625°F (2 hrs.), AIR COOL	
	340°F (10-16 hrs.), AIR COOL	
MECHANICAL PROPERTIES	TENSILE STRENGTH	28.0 Ksi
	Y.S. (0.2% offset)	19.5 Ksi
	ELONGATION	2.5%
CORROSION RESISTANCE	IMMERSION for 28 days in 3% NaCl	120 mpy
	SALT SPRAY	600 mpy
	POLARIZATION.	
	100 ppm Cl NaCl	7 mpy
	3.5% NaCl	115 mpy

TABLE 2

ARALDITE 985 APPLICATION (D.T.D. 935)

- PRE-HEAT TO 180-200°C
- COOLED TO 60° C
- DIPPED IN RESIN SOLUTION
- DRAINED 15-30 MINUTES
- CURED AT 180° C FOR 15 MINUTES
- COOLED TO 60° C
- REPEAT TWICE
- FINAL CURE AT 180° C FOR 45 MINUTES

EXPERIMENTAL

The testing program included exposure to both salt spray (fog) and 100% humidity. Tape adhesion tests were performed after exposure to 100% humidity. The test panel dimensions and preparation are listed in Table 3. The standard test methods for procedures and evaluation are contained in Table 4. In addition to the above, electrochemical AC impedance measurements were carried out to evaluate the performance of the coating/metal systems. The test cell is shown in Figure 3. AC impedance was performed with a PARC273 potentiostat in conjunction with a PARC 5208 Lock-In Amplifier, Apple II computer, and the PARC Softcorr 368 program. Measurements were obtained at the corrosion potential over the frequency range 100K Hz to 0.01 Hz for up to 42 days in 100 ppm Cl solution. The corrosion potential was monitored before each experiment.

TABLE 3

TEST PANELS

- DIMENSIONS: 6"(l) X 4" (w) X 1/8 " (t)
- Panels were coated on one side and remaining sides were conversion coated, masked with paraffin wax
- One-half of the panels tested were scribed with an "X"
- Tests in duplicate

TABLE 4

STANDARD TEST METHODS FOR PROCEDURES AND EVALUATION

- Salt Spray (Fog) Testing ASTM B117
  - 5% NaCl, 95° F
- Evaluation of Painted or Coated Specimens subjected to Corrosive Environments ASTM D165H
- Transparent Plastic Grids used to estimate area failed for unscribed panels
- Mean creepage from scribe for scribed panels
- Coated Metal Specimens at 100% RH, 100°F, ASTM F2247 prior to
- Measuring Adhesion By Tape Test ASTM D3359, Method 13
  - Rating on scale 0B to 5B
  - 5B best, 0B worst
  - Based on % of coated area removed from substrate

RESULTS AND DISCUSSION

Salt Spray (Fog) Test

Conversion Coatings, Sealer, and Primers

Results of salt spray testing of the three different primers in conjunction with either the HAE anodize or chrome manganese conversion coating are expressed as % area failed as a function of exposure time in Table 5 and Figure 4. The data represent an average of two measurements on duplicate panels. It should be noted that the sealer Araldite 985 was applied to only those schemes employing the epoxy polyamide primer (MIL-P-23377). This primer is currently used in Army aircraft in conjunction with the CARC polyurethane topcoat (MIL-C-46186C). The efficacy of the primers applied over the CrMn conversion coating may be ranked in decreasing order of salt spray resistance as MIL-P-52192 > MIL-P-85582 > MIL-P-23377. The application of the sealer Araldite 985 significantly improves the performance of MIL-P-23377 to a level comparable to MIL-P-52192, as also shown in Figure 5. Similar data for the HAE anodize as an alternate to the Cr Mn treatment shows the same ranking of primers, but the magnitude of the failed area is diminished in each case.

TABLE 5

SALT SPRAY PERFORMANCE OF CONVERSION TREATED AND PRIMED PANELS

		%AREA FAILED	
PANEL ID	COAT SYSTEM	DAY 6	DAY 13
A(HAE)	23377	15 38	36 72
B(HAE)	52192	0 00	0 16
C(HAE)	85582	2 73	14 10
D(HAE)	985, 23377	0 12	0 45
M(Cr Mn)	23377	31 37	63 03
N(Cr Mn)	52192	0 50	1 30
O(Cr Mn)	85582	4 05	17 48
P(Cr Mn)	985 23377	0 96	3 00

Conversion Coatings and Sealer and Primers and Topcoat

The salt spray performance of the protective schemes, which included the polyurethane topcoat is shown in Table 6 and Figures 6 through 9. Again, the % area failed represents an average of measurements on duplicate panels. The variables were HAE anodize or CrMn conversion treatment and the three primers. Considering the CrMn treated systems after 42 hours of salt spray exposure, the best performance was exhibited by the scheme employing the sealer, Araldite 985, and the MIL-P-23377 primer. The marked improvement in performance achieved by interposing Araldite 985 between the conversion coating and the primer is shown in Figure 6, and the photographs of exposed scribed panels are shown in Figure 7. Similar results were obtained with the HAE anodized panels as shown in Figures 8 and 9. However, the HAE treated systems performed better than the comparably treated CrMn systems. Robinson[1] has also reported the beneficial effect of several sealers in reducing salt spray corrosion when used with chromate conversion coating, primed and finish coated.

TABLE 6

SALT SPRAY PERFORMANCE OF CONVERSION TREATED, PRIMED, AND TOPCOATED PANELS

			% AREA FAILED				
PANEL ID	COAT SYSTEM	DAY 7	DAY 14	DAY 21	DAY 28	DAY 35	DAY 42
E(HAE)	23377,46168	0 00	0 46	0 91	5 15	10 44	15 68
F(HAE)	52192,46168	0 00	0 39	1 72	15 01	20 82	26 44
G(HAE)	85582,46168	0 30	0 39	0 42	0 51	0 68	0 89
H(HAE)	985,23377,46168	0 00	0 00	0 00	0 15	0 15	0 48
O(Cr Mn)	23377,46168	0 12	1 84	12 62	15 15	20 45	26 20
R(Cr-Mn)	52192,46168	0 12	0 36	0 48	C 69	0 93	5 75
S(Cr-Mn)	85582,46168	0 21	15 06	20 30	25 30	30 90	37 14
T(Cr Mn)	985,23377,46168	0 01	0 01	0 17	0 24	2 59	3 24

TAPE ADHESION TEST

Conversion Coatings and Sealer and Primers

The cross-cut tape adhesion test was performed after the coated test panels were exposed to 100% relative humidity at 100°F with condensation on the specimens at all times during the 5-week exposure. The coating adhesion of the primers that were applied to either CrMn or HAE-treated panels was rated on a scale of 0B to 5B, as shown in Table 7. These ratings are based on the removal of the coating from the substrate after application, rapid removal of the tape, and inspection of the cross-cut grid area. A rating of 0B represents an affected area of greater than 65%. The best rating, 5B, represents no flaking and detachment of the coating. All of the primers show very good adhesion except for the case where the sealer, Araldite 985, had been applied between the CrMn or HAE conversion coating and the MIL-P-23377 primer. Failure occurred at the sealant/primer interface since only the primer was removed. Despite the poor adhesion of primer to sealant, this coating scheme performed as well as the other primers during the salt spray test. It should be noted that the duration of the 100% humidity exposure was 3 times as long as the exposure to the 3.5% salt spray.

TABLE 7

RESULTS OF THE TAPE ADHESION TEST

PANEL #	COATING SCHEME	RATING
A	HAE, MIL-P-23377	5B
B	HAE, MIL-P-52192	5B
C	HAE, MIL-P-85582	5B
D	HAE, 985, MIL-P-23377	0B
M	Cr-Mn, MIL-P-23377	4.5B
N	Cr-Mn, MIL-P-52192	5B
O	Cr-Mn, MIL-P-85582	4.5P
P	Cr-Mn, 985, MIL-P-23377	0B

AC Impedance Measurements

Electrochemical impedance techniques are finding increased application in both corrosion research and the evaluation of the performance of organic coating/metal systems. Since corrosion processes occurring on metal substrates under organic coatings are electrochemical in nature, assessment of the corrosion resistance of organic coatings has been made employing electrochemical measurements and much data has been reported showing that various electrical parameters can be important in selecting a corrosion--resistant organic coating. Leidheiser[2] has reviewed a number of electrochemical and electrical measurement techniques for predicting corrosion at the metal/organic coating interface. He reported that a coating system resistance measured by both AC and DC resistance techniques degraded with time and a lower limit of about 10^6 ohms/cm^2 existed, below which corrosion occurred underneath the coating. He associated this temporal degradation with ion and water penetration into the coating, transport of ions through the coating, and follow-on electrochemical reactions at the coating/metal interface. Mikhailovskii[3] has reported that in many cases the DC resistance may not be a true measure of the corrosion resistance of paints. Mansfeld[4] has reviewed the current status of polarization resistance measurement and points out the advantages of the AC impedance technique in obtaining the polarization resistance especially for measurements in low conductivity media and for systems with low corrosion rates.[5,6] Mansfeld has also reviewed methods of analyses of AC impedance data.[5,6] The value of polarization resistance Rp has been obtained from both Nyquist and Bode plots. Scantlebury, et al.,[7] have applied analysis of Nyquist plots (also known as Cole-Cole) to provide an estimate of the film integrity and protective capacity of chlorinated rubber and coal tar epoxy coatings.

Figure 10 contains complex impedance plots of the real impedance Z' versus the imaginary impedance Z" for each excitation frequency. These plots compare the behavior of the MIL-P-23377 primer which was applied over an HAE-treated panel (A) and exposed to a solution containing 100 ppm Cl for 1, 7, 14, and 21 days.

Although the behavior after 1 day appears to indicate that the response of the system is solely capacitive over the range shown, the response curve beyond the range of the plot is a large semicircle. The impedance behavior after 7, 14 and 21 days shows that the high frequency intercept of the curves with the Z'-axis is the same, but the reponse curves are smaller semicircles with the center of the semicircle lying along the Z'-axis. An estimate of the polarization resistance may be made from the intersection of the low frequency semicircle with the Z'-axis. Similar impedance behavior for a chlorinated rubber coating has been reported by Scantlebury, et al.[7] After 7 and 14 days of exposure the polarization resistance became increasingly smaller as existing pores were permeated or pathways developed, with electrolyte increasing the ionic conductivity in the coating. After 14 days, a second semicircle appeared at low frequencies and at the same time a small area of corrosion was observed under the coating. It appears that Cl ions and water had penetrated into the coating, followed by transport of ions through the coating and substrate ionic/electronic charge transfer reactions at the coating/metal interface. Similar Nyquist plot behavior was observed for the MIL-P-23377 primer which had been applied over the chrome manganese conversion coating (M). Nyquist plots which show the effect of interposing the sealer between the HAE anodize and MIL-P-23377 primer (D) are contained in Figure 11. There is very little effect of exposure time on the response curves even after 42 days of immersion in 100 ppm Cl solution. Thus, plots for 7, 14, 21, and 28 days are not shown. Corrosion of the underlying Mg alloy was not observed. This behavior attests to the beneficial effect of the sealer, and correlates well with the data obtained from salt spray tests.

The Bode plot, log ¶Z¶ vs. log F (frequency) is an alternative to the Nyquist plot and is more useful because it allows a more effective extrapolation of data from higher frequencies. It provides a better estimate of polarization resistance when data scatter precludes adequate fitting of the Nyquist semicircle.[8] Polarization resistance determinations were made by extrapolation from the linear region of the Bode plot at low frequencies to the log (Z) axis. Figure 12 contains Bode plots for the panel which has been HAE anodized and primed with MIL-P-23377 after immersion in 100 ppm Cl solution for 1, 7, 14, and 21 days. Polarization resistance values extrapolated from these plots are contained in Table 8 and show that polarization resistance decreases with time of exposure as existing pores in the coating are permeated. After 14 days of exposure, the coating system resistance degraded to below 10^6 ohms/cm^2 where corrosion of MgZE41A occurred.

TABLE 8

POLARIZATION RESISTANCE OF PROTECTIVE SCHEMES

DAYS OF IMMERSION	A	D	M	P
1	2 5 X10^7	7 1X10^9	3 0X10^9	2 0X10^7
7	1 6X10^5	2 3X10^9	8 2X10^8	3 0X10^7
14	1 4X10^5	1 7X10^9	4 6X10^6	1 6X10^6
21	1 1X10^5	1 3X10^9	1 1X10^5	3 2X10^4
28		2 0X10^9	7 1X10^4	
35		2 0X10^9	9 1X10^4	
42		6 3X10^8		

The effect of applying the sealer Araldite between the anodize and primer is shown in the Bode plots of Figure 13 and also the polarization resistance values in Table 8. Very little change is apparent even after 42 days of immersion, and the lower limit of Rp is well above the critical value of 10^6 ohms/cm^2. The plots for exposure times between 7 and 35 days are not shown because they fall in the very narrow region between the 1-day and 42-day curves. Again, these data support the results of the salt spray tests.

Table 8 also contains Rp values for the same coating systems except for the replacement of the HAE anodize with the CrMn conversion coating. Without the sealer, the CrMn-treated system performed better than the HAE-treated system over a period of 14 days. The application of the sealer provided no beneficial effect with CrMn-treated-and-primed-system. The HAE anodize, Araldite 985 sealed, and MIL-P-23377-primed system performed the best with no failure after 42 days of exposure. The change in polarization resistance of all of the above described schemes plotted as a function of exposure time is more dramatically shown in Figure 14.

CONCLUSIONS

1. The salt spray resistance of the MIL-P-23377 primer was not as good as either the MIL-P-52192 or MIL-P-85582 primers regardless of the initial treatment (CrMn or HAE anodize).

2. The application of the Araldite 985 sealer significantly improved the performance of the MIL-P-23377 primer particularly when the HAE anodize was used.

3. The AC impedance data also demonstrated the beneficial effect of the sealer in conjunction with the HAE anodize.

4. The Araldite sealer also contributed significantly to improving the salt spray resistance of the polyurethane CARC MIL-C-46186 topcoat regardless of the primer used and the initial treatment.

5. Despite the beneficial effect of the sealer in salt spray resistance of the primers, tape adhesion tests showed that the adhesion of the primer to the sealer was poor after 5 weeks of exposure to 100% relative humidity. As a consequence, efforts are now underway to improve the adhesion of sealer to primer by employing a post-baking treatment in accordance with a recommendation by Taylor and Tawil.[9] Also, other sealers are being investigated.

6. The AC impedance data appeared to provide an estimate of the film integrity and protective capability of the primers which correlated with the salt spray test results. Values of polarization resistance below 10^6 ohm/cm^2 indicated significant degradation.

REFERENCES

1. Robinson, A.I., Evaluation of Various Magnesium Finishing Systems, Proceedings of International Magnesium Association, 42nd World Conference, May 1985, N.Y., N.Y.

2. Leidheiser, H., Jr., Review of Electrochemical and Electrical Measurement Methods for Predicting Corrosion at the Metal-Organic Coating Interface, Corrosion, 38, No. 7, pp 374-383, 1982.

3. Mikhailovskii, Y.N., Leonov, V.V., and Tomashov, N.D., in Corrosion of Metals and Alloys, Israel Program for Scientific Translation, Jerusalem, 1966, pp 202-209.

4. Mansfeld, F., Polarization Measurements Resistance-Today's Status, Electrochemical Techniques, NACE, pp 67-71.

5. Mansfeld, F., Recording and Analysis of AC Impedance Data for Corrosion Studies, Corrosion, Vol. 36, No. 5, May 1981, pp 301-307.

6. Mansfeld, F., Kendig, M.W., and Tsai, S., Recording and Analysis of AC Impedance Data for Corrosion Studies, Corrosion, Vol. 38, No. 11, November, 1982, pp 570-580.

7. Scantlebury, J.D., Ho, K.N., and Eden, D.A., Impedance Measurements on Organic Coatings on Mild Steel in Sodium Chloride Solutions, Electrochemical Corrosion Testing, ASTM STP 727, pp 187-197.

8. EG and G Princeton Applied Research, Electrochemical Instruments Group, Application Note: AC-1, AC-2, Basics of AC Impedance Measurements, Evaluation of Organic Coatings by Electrochemical Impedance Measurements.

9. Taylor, M.R., and Tawil, D.S., Improving Primer Adhesion to Surface Sealed Magnesium Components, Magnesium Electron Limited Report MR10/Data/199, April, 1988.

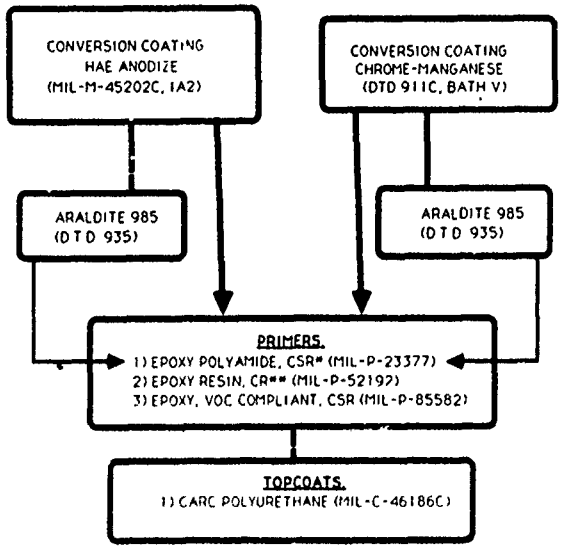

* CHEMICAL AND SOLVENT RESISTANT
** CHEMICAL RESISTANT

Figure 1. Coating schemes for Mg alloy ZE41A-T5.

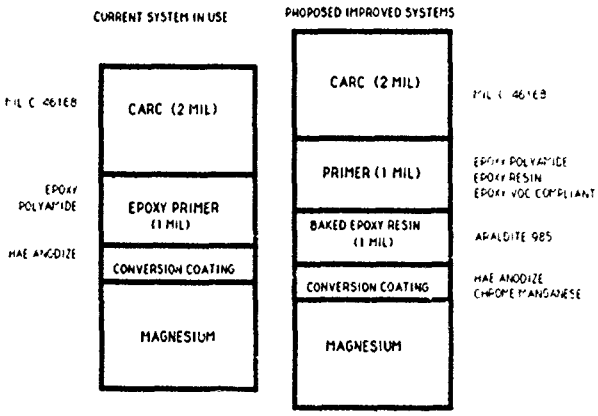

Figure 2. Schematic diagram of current and improved coatings systems.

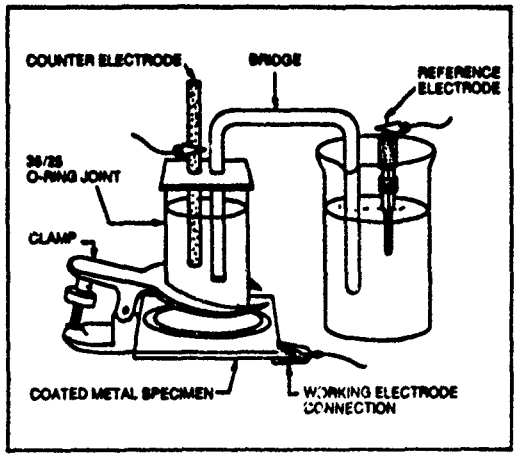

Figure 3. Test cell for AC impedance measurements.

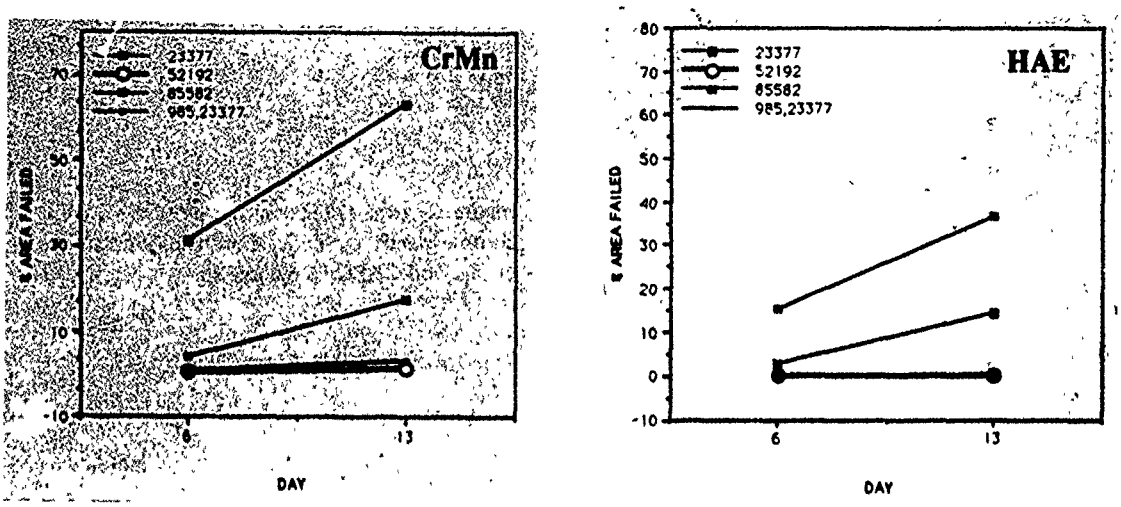

Figure 4. Comparison of salt spray resistance of primers on CrMn coated and HAE anodized Mg.

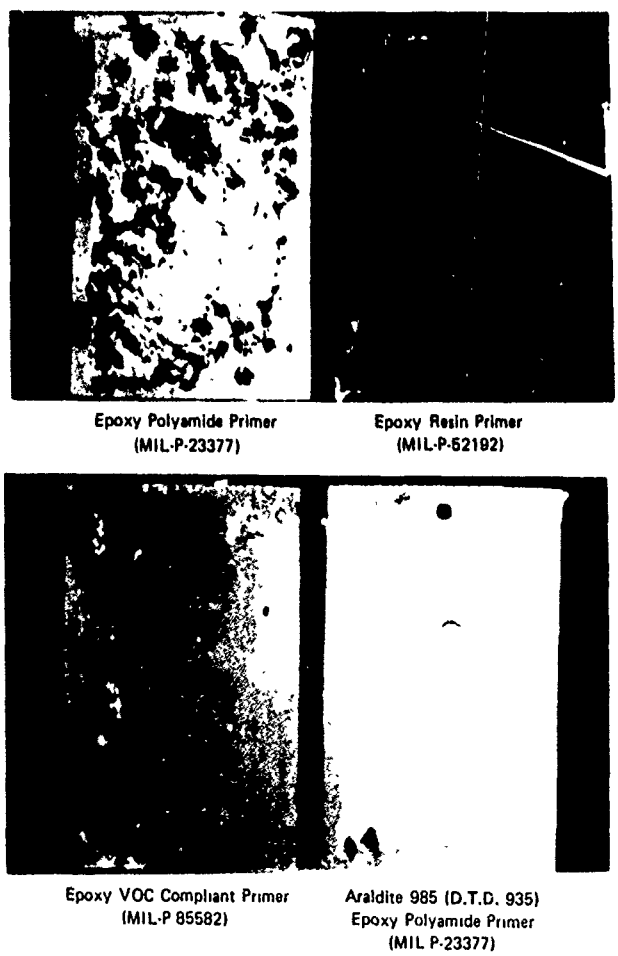

Figure 5. Comparison of primers with chrome manganese conversion coating exposed to 5% salt spray for 14 days.

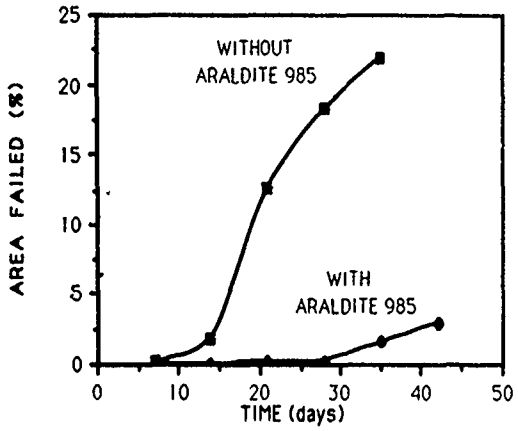

Figure 6. Area failed for coating systems with chrome-manganese conversion, epoxy polamide primer and CARC in 5% salt spray.

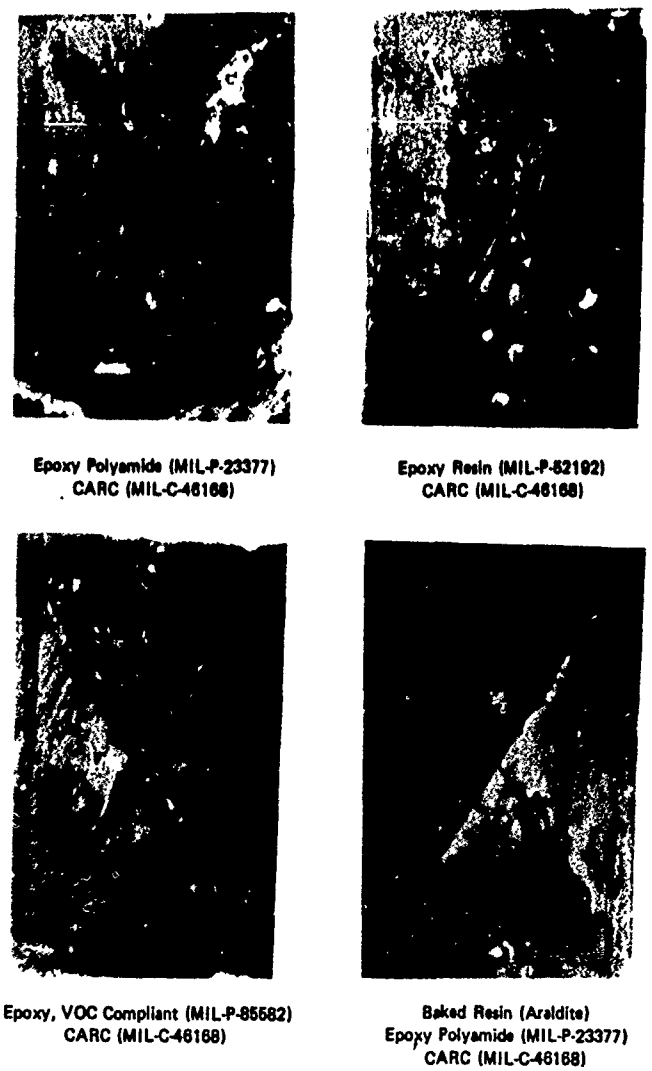

Epoxy Polyamide (MIL-P-23377)
CARC (MIL-C-46168)

Epoxy Resin (MIL-P-82192)
CARC (MIL-C-46168)

Epoxy, VOC Compliant (MIL-P-85582)
CARC (MIL-C-46168)

Baked Resin (Araldite)
Epoxy Polyamide (MIL-P-23377)
CARC (MIL-C-46168)

Figure 7. Comparison of coating systems with chrome manganese conversion coating exposed to 5% salt fog for 14 days.

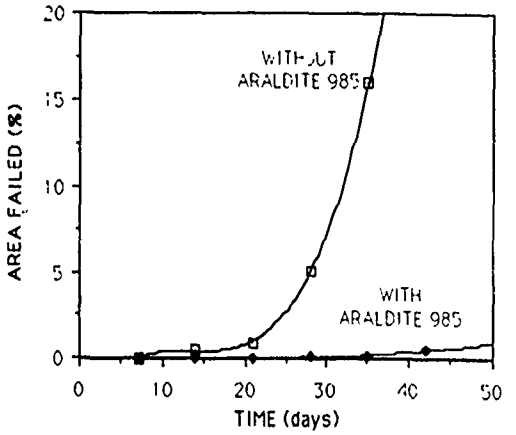

Figure 8. Area failed for coating systems with HAE conversion, epoxy polyamide primer and CARC in 5% salt spray.

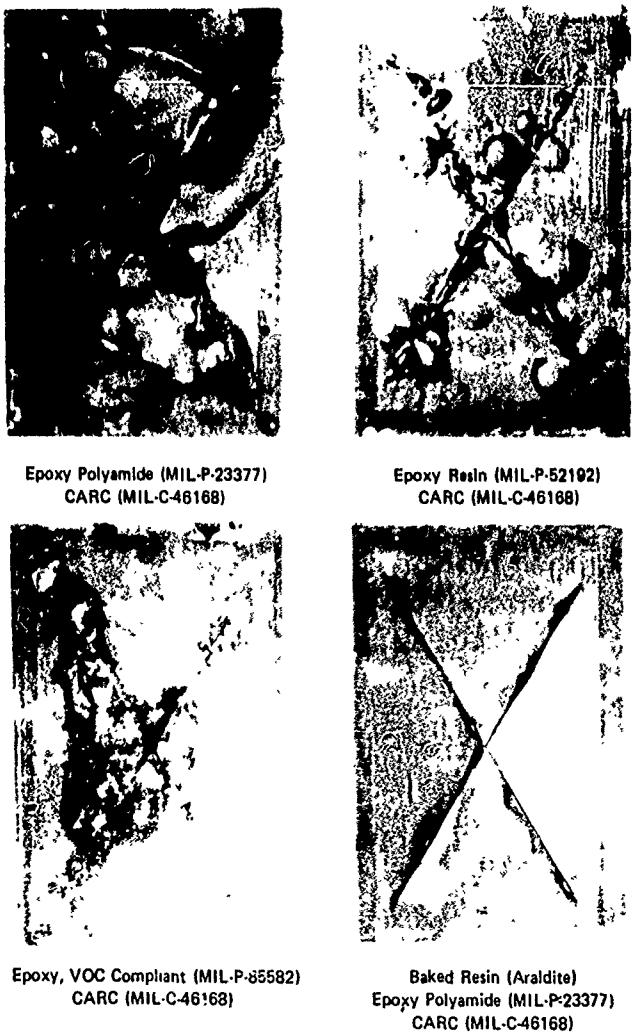

Figure 9. Comparison of coating systems with HAE conversion coating exposed to 5% salt fog for 14 days.

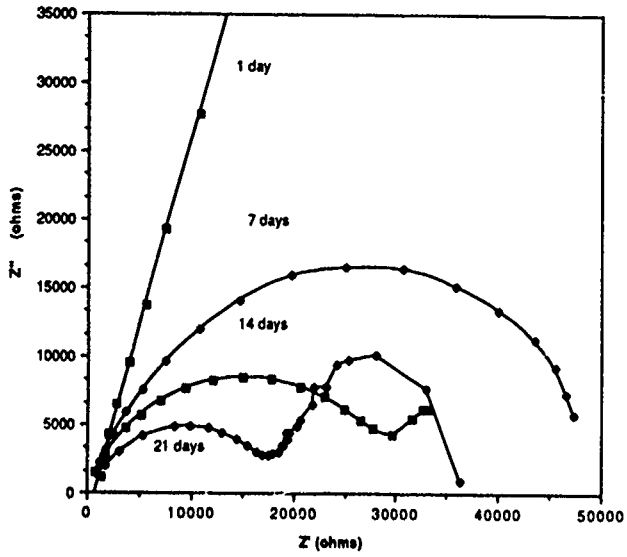

Figure 10. Nyquist plot for system A (HAE, MIL-P-23377) om 100 ppm Cl solution.

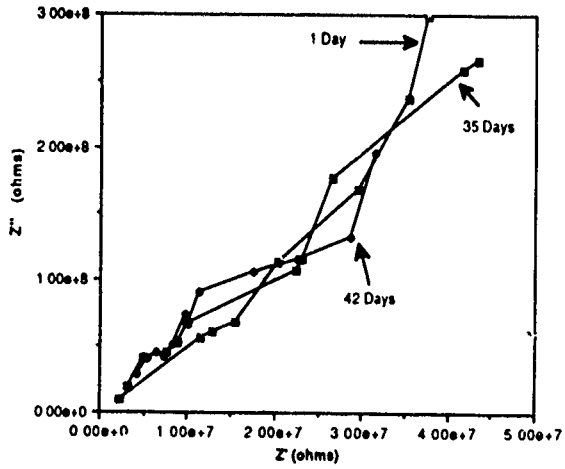

Figure 11. Nyquist plot for system D, (HAE, Araldite 985, MIL-P-23377) in 100 ppm C1 solution.

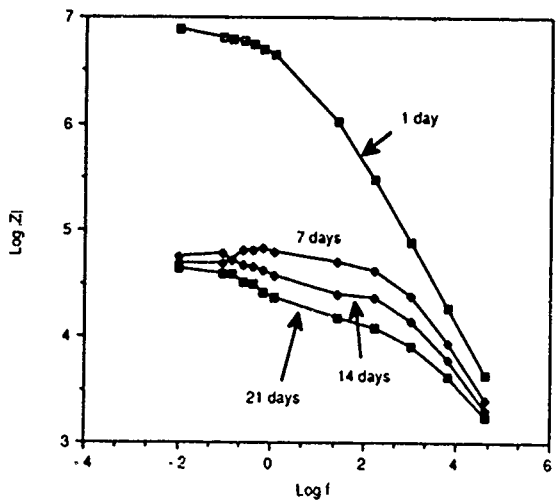

Figure 12. Bode plot of system A (HAE, MIL-P-2337) in 100 ppm Cl solution.

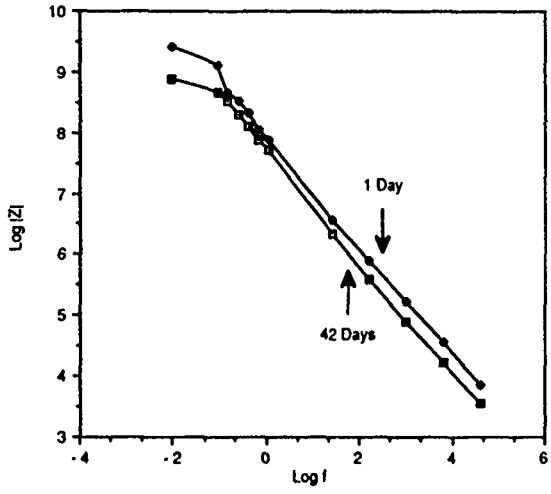

Figure 13. Bode plot of system D(HAE, Araldite 985, MIL-P-23377) in 100 ppm Cl solution.

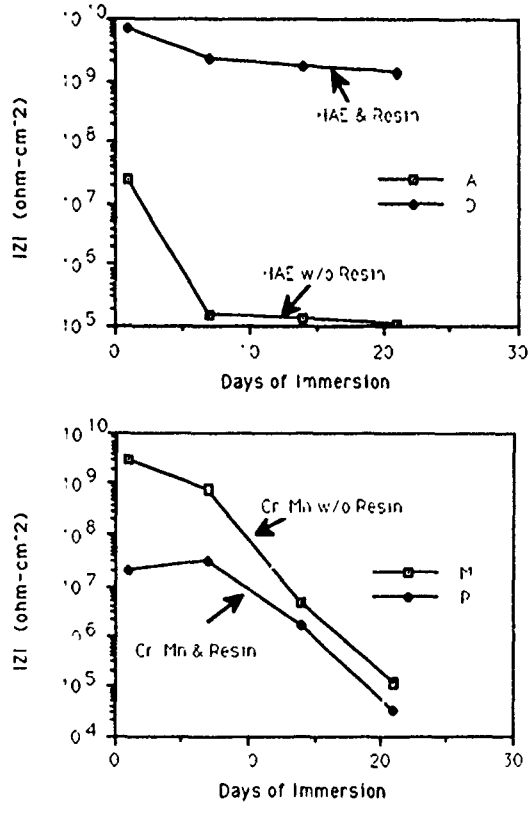

Figure 14. Effect of sealer on the polarization resistance of HAE or or CrMn treated and primed system.

THE LIFE-CYCLE APPROACH TO CORROSION PREVENTION AND CONTROL (CPC) IN SUPPORT OF ARMY AIRCRAFT

Thaddeus Baranowski
U.S. Army Aviation Systems Command
4300 Goodfellow Boulevard
St. Louis, Missouri 63120-1798

John Weisz and Kelly Blades
ARINC Research Corporation
2551 Riva Road
Annapolis, Maryland 21401

ABSTRACT

In a 1986 study, the U.S. Army estimated the cost of corrosion to its worldwide aircraft and vehicle fleets at $2.8 billion annually. More important than the cost to treat and repair components is the impact of corrosion on safety and on the operational readiness of military units.

To most effectively combat the adverse affects of corrosion in aircraft, the U.S. Army Aviation Systems Command (AVSCOM) plans to apply a life-cycle management philosophy to develop a comprehensive Corrosion Prevention and Control (CPC) Program. This initiative is designed to ensure CPC issues are thoroughly addressed and resolved in the material development, deployment, operation, and support phases of the system acquisition life. Furthermore, CPC is an active influence in the design, testing, management, supply, maintenance, and training activities associated with system development.

This life-cycle approach to CPC has been implemented to limited and varying degrees on the UH-60, AH-64, OH-58D and CH-47 helicopter programs, and benefits are being realized This paper will significantly address how AVSCOM and the Army aviation community apply this philosophy to combat corrosion, "the silent enemy."

CORROSION PREVENTION AND CONTROL (CPC) AND ARMY AVIATION

The best way to manage corrosion is through prevention and control. Corrosion can be minimized by proper coating of exposed metal, avoidance of dissimilar metal contact, use of corrosion-resistant alloys, use of proper sealants and water-displacing compounds, avoidance of poor design features, and most important, awareness of corrosion and implementation of an effective CPC Program.

CPC is like many other system design constraints or criteria. The key to implementing an effective CPC Program is to take a life-cycle approach to the problem. That is exactly what the U.S. Army Aviation Systems Command (AVSCOM) Product Assurance Directorate and Quality Engineering Division have done.

Although the life-cycle management philosophy has only recently been formalized as described in this paper, CPC is being practiced throughout the Army aviation community as part of a total AVSCOM life-cycle plan. It is envisioned that the LHX helicopter will be the first system to fully realize a "cradle-to-grave" life-cycle CPC program.

A draft AVSCOM pamphlet has been completed and distributed through the U.S. Army combat development, material development, and user commands for evaluation. This published guide to the proper means of implementing CPC at all levels, all commands, and in all phases of the acquisition life cycle was developed to encourage commitment to and excite the imagination of leaders and staffs throughout the U.S. Army in searching out new technologies, applications, and techniques to implement CPC.

ARINC Research Corporation has provided research, data collection, and analysis support to assist AVSCOM in implementing the initiatives envisioned by its Quality Engineering Division, and in doing so, has extracted, organized, and presented information from many regulations, directives, standards, and policy and procedures documents in a concise "how to" document for new decision makers and managers involved in the acquisition and support of U.S. Army aircraft.

CPC IMPLEMENTING DIRECTIVES

CPC directives are the primary means of establishing the overall CPC Program and identifying specific responsibilities throughout the Army. These CPC-associated directives include the following:

Army Regulation (AR) 750-59, including the Army Materiel Command (AMC) Supplement 1, establishes Army policy and procedures for implementing and managing an effective CPC Program for all Army systems, equipment, and components. AR 750-59 requires that CPC be addressed in design, testing, management, maintenance, and training.

AVSCOM Regulation 702-5 establishes a command-wide CPC Program and delineates the policy, responsibilities, and procedures to be followed to minimize corrosion of Army aviation equipment.

CPC STANDARD

The major CPC-related standard is Aeronautical Design Standard, Air Vehicle Materials and Processes (ADS-13D), which describes the general requirements of AVSCOM for the materials and processes used in the design and construction of Army aircraft. For corrosion resistance to be incorporated into a system, this CPC-related standard is incorporated into all system specifications, requests for proposals (RFPs), statements of work (SOWs), and contracts.

CPC MAINTENANCE MANUALS

CPC Maintenance Manuals are the primary means of implementing CPC policy and procedures in the field. CPC-related maintenance manuals include the following:

Aeronautical Equipment Maintenance Management Policies and Procedures (TM55-1500-328-25) provides all maintenance management policies and procedures for the aviation maintenance organization and is the primary policy manual used by maintenance personnel.

Corrosion Control for Army Aircraft (TM43-0105) provides information on materials and procedures for the general control and prevention of corrosion of aircraft and aircraft equipment.

Aircraft-Specific Technical Manual Series provide all of the required information and procedures needed to perform repairs on an aircraft at the aviation unit maintenance (AVUM) and aviation intermediate maintenance (AVIM) levels.

Depot Maintenance Work Requirements (DMWRs) provide inspection and maintenance procedures for the highest level of maintenance performed on an aircraft or system.

THE LIFE-CYCLE APPROACH TO CPC

AVSCOM takes a life-cycle approach to managing the CPC Program for U.S. Army aircraft. This philosophy is significant because it recognizes a commitment to fighting corrosion from conceptualization of a need until the retirement of the system that meets that need; which sometimes occurs as long as 30 or more years later. Only in this manner can the benefits of the program be maximized. Anything less, and a positive initiative in one life-cycle phase will be compromised by an oversight in another part of the system life. For example, during the design phase, Army technology surveys identify a finishing compound to protect the skin of the aircraft. Cost benefits and other analyses indicate that the compound should be applied at production. If the program manager does not ensure that the logistic support system also recognizes this special process, subsequent maintenance actions on the fielded system may result in unprotected portions of the aircraft. Just as quality assurance, reliability, and integrated logistic support are system parameters addressed throughout the life of an aircraft, so must CPC be considered.

OVERVIEW OF THE CPC LIFE CYCLE

To put the AVSCOM CPC life-cycle management approach in perspective, a schematic highlighting the major phases and the activities in each phase is provided in Figure 1. Note that the traditional acquisition process has been simplified to a scheme involving four major phases. Each phase as it relates to CPC is as follows:

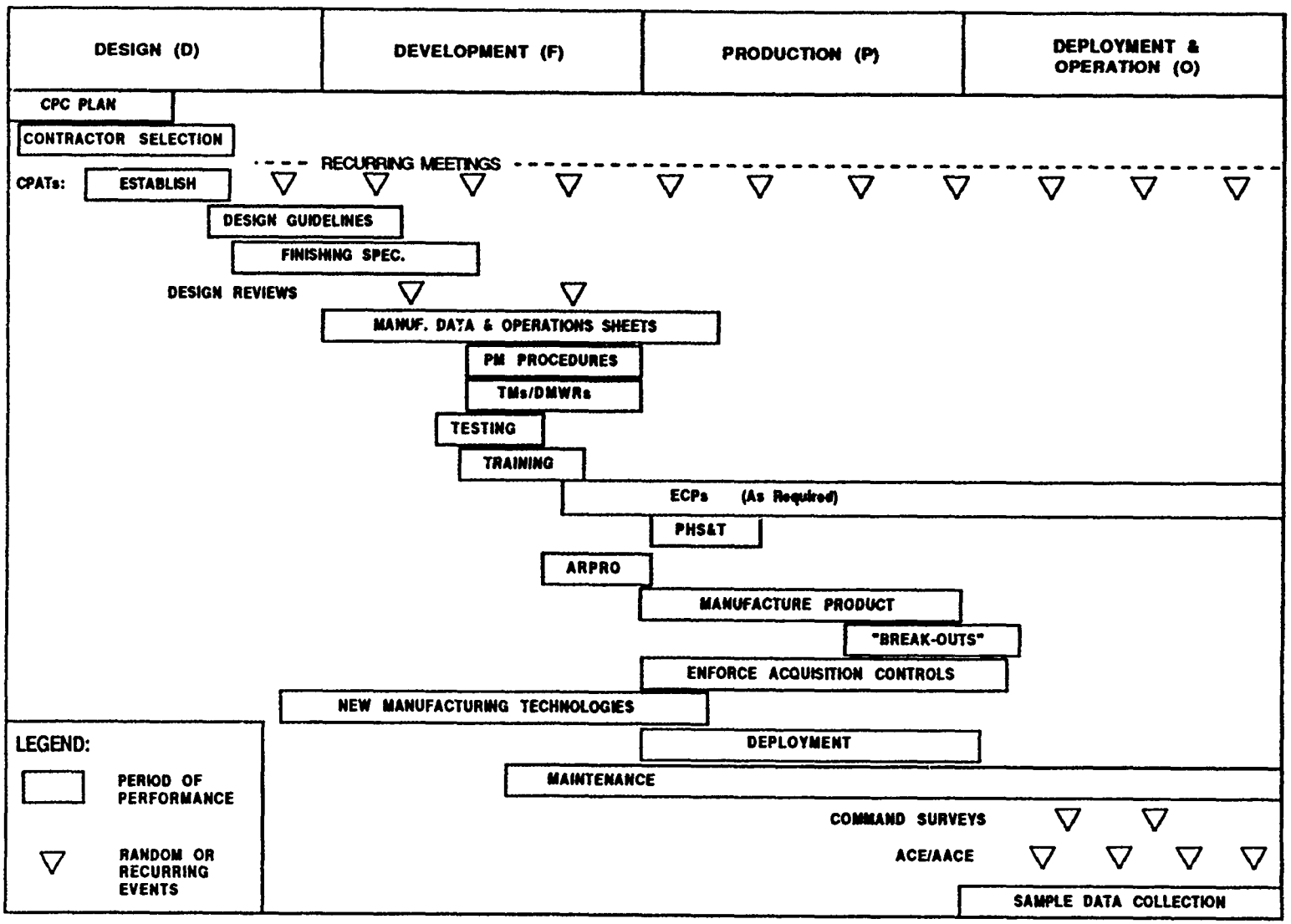

FIGURE 1: CORROSION PREVENTION AND CONTROL (CPC) LIFE CYCLE

1. Design - Corrosion is minimized by using design practices that address selection of materials, coatings, system geometry, environmental extremes, storage and packaging requirements, and repair requirements.

2. Development - Corrosion is prevented by ensuring that the system is properly developed, integrated, and tested.

3. Production - Corrosion is controlled by establishing proper manufacturing processes; establishing and enforcing controls for acquisition, packaging, handling, storage, and transportation; and improving the manufacturing process.

4. Deployment and Operation - Corrosion is controlled by carefully planning and monitoring deployment, maintaining the system (including the integrity of the CPC implementation), and evaluating the system in the field.

DESIGN PHASE

As depicted in Figure 1, five tasks are associated with the design phase of the CPC life cycle. These tasks are (1) preparation of the CPC Plan, (2) selection of the prime contractor, (3) establishment of the Corrosion Prevention Action Team (CPAT), (4) establishment of general design guidelines and material selection criteria, and (5) preparation of the Finishing Specification.

Preparation of the CPC Plan

The CPC-related Standard ADS-13D dictates that a CPC Plan be developed for each aircraft program. The AVSCOM CPC Program is implemented through the CPC Plan. The Army's Program Manager provides system-level CPC specifications or design guidelines in accordance with AMC policy. The initial draft of the CPC Plan is submitted by the prime contractor as part of a proposal package. The plan describes the contractor's approach to meeting the Government requirements for CPC. The final plan is submitted for approval after contract award. Updates to the CPC Plan are accomplished as required.

Selection of the Prime Contractor

The prime contractor is selected in accordance with normal source selection criteria; one of which is the effectiveness of the proposed CPC program, as identified in the CPC Plan. Although the weighting scheme for addressing CPC criteria in the proposal evaluation process will vary for each Request for Proposals, any proposal offering an effective CPC Program Plan that will increase aircraft availability and reduce life-cycle costs will surely enhance the evaluation of the contractor's overall offering. The program, project, or product manager verifies that the prime system contractor possesses the necessary skills and capabilities in CPC and appoints a coordinator to interface with the selected prime contractor on matters involving CPC Plan implementation.

Establishment of the Corrosion Prevention Action Team (CPAT)

The CPAT is established to bring the designer, maintainer, trainer, and user of a system together so they may contribute their unique experiences to problem definition and the formulation of recommendations or solutions. The CPAT meets throughout the life of the program. The CPAT is chaired by an AVSCOM representative and includes engineering representatives from the contractor. The primary function of the CPAT is to ensure that CPC objectives are met.

Establishment of General Design Guidelines and Material Selection Criteria

The primary consideration in the design and construction of aviation systems is the ability of the design to comply with structural and operational requirements. In the selection of suitable materials and appropriate processing methods, consideration must also be given to those materials, processing methods, and protective treatments that reduce service failures resulting from corrosion of parts and assemblies in service.

Preparation of the Finishing Specification

The contractor prepares a finishing specification. The specification describes the specific corrosion protection finish or techniques to be used on the various substrates of all components and assemblies to protect them against corrosion in the environments to which they will be exposed. This document is prepared in accordance with MIL-F-7179. After AVSCOM approval, the requirements contained therein are included in all applicable production drawings. The Finishing Specification is submitted for approval 60 days following contract award or in accordance with DD-1423. Through design reviews, analysis of field reports, and field inspections, data are collected for required revisions to this document.

DEVELOPMENT PHASE

Eight tasks are associated with the development phase of the CPC life-cycle (see Figure 1). These tasks are (1) participation at design reviews, (2) preparation of CPC-related manufacturing data and operations sheets, (3) preparation of system-peculiar corrosion preventive maintenance procedures, (4) development and modification of TMs and DMWRs, (5) testing, (6) development of training, (7) modification and enhancement of the original design, and (8) packaging, handling, storage, and transportation, and care of supplies in storage.

Participation at Design Reviews

In the normal development cycle of a system, preliminary and critical design reviews are conducted. CPC specifications and their impacts on other system specifications are defined at the system design review (design phase). CPC is considered in trade-off analyses at the preliminary design review (PDR). Drawings and process specifications are reviewed for compliance with CPC requirements at the critical design review (CDR).

Preparation of CPC-Related Manufacturing Data and Operations Sheets

Manufacturing engineers face a special challenge when developing manufacturing instructions. In addition to their normal task of converting design drawings to man- or machine-readable data, they must also ensure that CPC requirements are included while minimizing the impact on producibility, quality, and cost goals. For example, operations sheets must address forging or casting machinery and other means of fabricating parts from raw materials. Process specifications must address finishes, coatings, or special metallurgical processes. Assembly drawings must address fasteners and how to avoid trapping moisture or contaminates. Test specifications must ensure that no fabrication process or assembly has adversely affected the functional operation of any subassembly or the total system.

Preparation of System-Peculiar Corrosion Preventive Maintenance (PM) Procedures

The contractor prepares system-peculiar corrosion control procedures that detail the maintenance procedures to be utilized by personnel in the aviation unit maintenance (AVUM), the aviation intermediate maintenance (AVIM), and depot levels of maintenance. Maximum use is made of the Tri-Service Aircraft Weapon Systems Cleaning and Corrosion Control Manual (TM55-1500-344-23) and the Avionic Cleaning and Corrosion Prevention/Control manual (TM55-1500-343-23). Through field inspections and CPAT feedback, this procedure is updated as required.

Development and Modification of TMs and DMWRs

CPC manuals are the primary means of implementing CPC policy and procedures in the field. CPC technical manuals provide (1) policy and procedures, (2) general instructions, and (3) criteria and standards. The AVUM and AVIM manuals contain information on calendar-based corrosion inspections, corrosion prevention and correction techniques, nondeferrable maintenance requirements, and appropriate accept and reject criteria. DMWRs contain CPC measures for depot-level repair and overhaul. DMWRs provide inspection and maintenance procedures for aircraft or systems. They contain corrosion inspection and repair information, as well as requirements for disassembly, cleaning, inspection, repair, reconditioning, rehabilitation, modification, reassembly, servicing, testing, and storage of assemblies or parts. DMWRs are reviewed by a CPAT to ensure adequacy of CPC procedures, data, reporting requirements, and contract requirements.

Testing

Program managers and developers ensure that appropriate issues for testing, related to corrosion, are included in all technical test (TT) and user test (UT) programs so that corrosion problems will be detected and corrected prior to production of the system. Testing includes exposure and performance tests in natural and accelerated environments where corrosion is most likely to occur. The Test and Evaluation Master Plan (TEMP) integrates the tests into the normal agenda of operational, performance, and support testing.

Development of Training

User training is developed for manufacturing engineers, product assurance and test specialists, operators, and maintenance and packaging personnel and is an essential ingredient in the identification and control of corrosion. The Training and Doctrine Command and U.S. Army Materiel Command/Materials Technology Laboratory (MTL) corrosion control training programs ensure that military and civilian personnel are trained in CPC.

Modification and Enhancement of the Original Design

Engineering change proposals (ECPs), prepared by the contractor and identified through a Product Improvement Program (PIP), Multi-Stage Improvement Program (MSIP), or other design change program, help to identify design deficiencies and provide a means of implementing corrective action. They also provide a realistic projection of budget and depot resource requirements to implement design changes. Modification work orders (MWOs) are the vehicle for implementing hardware modifications in the field or at the depot level.

Packaging, Handling, Storage, and Transportation (PHS&T) and Care of Supplies in Storage (COSIS)

AVSCOM Regulation 702-5 requires that CPC be addressed in PHS&T because of the tremendous potential loss of stored material from corrosion. Within AVSCOM, the Director of Materiel Management is responsible for PHS&T. The appropriate Program Management Offices determine the storage environment parameters to minimize corrosion. The Director of MTL at the AMC Center of Excellence in Corrosion reviews all packaging and shipping methods. Special attention is given to the design and finishing of metal shipping and storage containers. Procedures such as coating parts, using weld-through primer or continuous welding, or applying organic sealant are techniques that are considered.

COSIS ensures that the true condition of material is known and properly recorded, and that material is maintained in a ready-for-issue condition to meet supply demands by using units.

PRODUCTION PHASE

The production phase consists of five tasks (see Figure 1). These tasks are (1) assignment and coordination of the ARPRO CPC coordinator, (2) product manufacturing, (3) subcontracting of alternate sources of supply ("Breakouts"), (4) enforcement of CPC acquisition controls, and (5) application of new processes and technologies.

Assignment and Coordination of the ARPRO CPC Coordinator

An Army Plant Representative Office (ARPRO) CPC Coordinator (ACC) is appointed for each system in production and serves on the CPAT. The ACC monitors the contractor's compliance with CPC specifications and with the CPC Product Assurance Plan. The ACC also provides for an exchange of information between the ACC and the AVSCOM CPC point of contact (POC) on all CPC matters.

Product Manufacturing

The Subordinate Commodity Command CPC Action Office (e.g., materiel developers such as AVSCOM, MICOM) ensures compliance to all CPC requirements in manufacturing. Adequate precautions are taken during manufacturing operations to maintain the integrity of corrosion prevention requirements and to prevent the introduction of corrosion or corrosive elements.

Subcontracting of Alternative Sources of Supply ("Breakouts")

The Competition Advocacy Subcontracting Management Office (CASMO) ensures that potential bidders are aware of CPC requirements. The Competition Advocacy Shopping List (CASL) categorizes the types of business that vendors can provide AVSCOM and provides detailed information as to documentation required for qualification as an approved vendor. Qualification testing, first article inspections (FAI), and pre-award surveys are designed to assess a potential vendor's capability and plant capacity to meet AVSCOM manufacturing requirements.

Enforcement of CPC Acquisition Controls

The Deputy Chief of Staff for Development, Engineering, and Acquisition (DCSDEA) provides policy, procedures, and guidance to ensure that CPC is fully considered in all acquisition documents. DCSDEA further ensures that proper emphasis is given to CPC in funding programs. The Deputy Chief of Staff for Product Assurance and Testing (DCSPAT) ensures that all major acquisition programs are subjected to a CPC review. The major subordinate commands (MSCs) incorporate the applicable CPC Program requirements into all acquisition contracts. The CASL provides acquisition controls for AVSCOM suppliers by categorizing the types of business vendors can provide. All suppliers must fall into one of the categories in order to be considered. These categories are enforced to ensure high quality in the supplies procured.

Application of New Manufacturing Processes and Technologies

The Deputy Chief of Staff for Production at Headquarters, AMC ensures that CPC is considered in all Manufacturing Methods and Technology (MMT) and Military Adaptation of Commercial Items (MACI) projects and production reviews; and that CPC objectives are stressed in the Production Engineering and Planning (PEP) and Value Engineering Programs (VEPs) in order to improve the product during the manufacturing process. New MMT projects will be initiated within the Production Engineering Measures (PEM) appropriations and activities. The AVSCOM Production Engineering Division Facilities and Technology Branch (AMSAV-EMC) validates processes and equipment to be utilized and ensures that CPC is considered in all MMT related to Army aircraft.

DEPLOYMENT AND OPERATION PHASE

As depicted in Figure 1, the Deployment and Operation phase consists of five tasks. These tasks are (1) aircraft deployment ("fielding"), (2) maintenance of fielded systems, (3) conduct of command survey, (4) accomplishment of

airframe condition evaluation (ACE) and aircraft analytical corrosion evaluation (AACE), and (5) updating of the sample data collection (SDC) system.

Aircraft Deployment (Fielding)

Fielding refers to all efforts undertaken to introduce a new system to the end user (i.e., operational unit). It includes the delivery of the end item to the user and initialization of user operations and maintenance. During deployment, units receiving new equipment at operational sites prepare the equipment for initial use. These procedures are detailed in the appropriate technical manuals (TMs) for the weapon system and are based on guidelines set down in the CPC Plan for that aircraft. Areas that influence corrosion protection and avoidance most are cleaning and preservation methods, storage and handling, inspection procedures, and repair procedures. These procedures are incorporated into the appropriate TMs for the weapon system. If, during operations, a corrosion problem arises that is not covered by the TMs, the unit prepares a Quality Deficiency Report (QDR) that is forwarded to the AVSCOM Maintenance Directorate for incorporation of changes into the TM or further engineering action. When alternate fielding procedures are found to be necessary, the CPAT is informed and a "lessons learned" report is developed.

Maintenance of Fielded Systems

The contractor or user conducts continuous examinations of the system and component parts to ensure maximum use of CPC coatings and treatments. The contractor or user also monitors and inspects the corrosion prevention measures instituted by all subcontractors, enforces standards, and performs overall preventive maintenance. Three levels of maintenance currently exist: AVUM, AVIM, and depot. The severity of the corrosion, as well as other maintenance factors, determine which level of maintenance is responsible for repair.

Conduct of Command Survey

A survey of all Regular Army, Reserve, and National Guard battalions, as well as depots, is conducted at least once every four years. All equipment, including aircraft, weapons, communications and electronic equipment, and vehicles is surveyed to determine its condition. CPC Program management and maintenance facilities are also evaluated. Surveyed activities provide proposed corrective actions and milestones to AMC Product Assurance and Testing (AMCQA-AE) within 60 days. Status of the action is reported to AMC quarterly. AMC provides feedback of the survey results to the proper agencies.

Accomplishment of Airframe Condition Evaluation (ACE) and Aircraft Analytical Corrosion Evaluation (AACE)

It is the policy of the U.S. Army Aviation Systems Command in accordance with AVSCOM Regulation 750-7 that an ACE/AACE be performed annually on all

first-line/mission-essential Army aircraft worldwide. ACE involves an annual structural evaluation of each aircraft in the operational fleet to identify those in the greatest need of depot maintenance, which is performed in accordance with AVSCOM Pamphlet series 750-1. AACE, a special corrosion evaluation program, was established as a companion to ACE and is performed in accordance with AVSCOM Pamphlet series 750-2. The on-site AVSCOM Senior Maintenance Specialist coordinates all ACE team operations with AMC Logistics Assistance Officers (LAOs).

Updating of the Sample Data Collection (SDC) System

The SDC allows major readiness commands (MACOMs) to collect management data on a select number of end items in the field environment. The SDC system collects unscheduled maintenance and time between overhauls (TBO) data. These data are used to conduct cost-benefit analyses related to implementation of ECPs and MWOs and to support other CPC trade-off studies.

CPC RELATIONSHIP WITH THE FLIGHT SAFETY PARTS PROGRAM

In recent years, the U.S. Army has identified numerous aircraft parts, assemblies, and installation procedures whose failure, malfunction, or absence could cause loss of, or serious damage to, the aircraft, or worse, cause serious injury or death to the occupants. These aircraft parts are referred to as flight safety parts (FSPs).

The FSP Program, developed by AVSCOM, provides for the life-cycle identification and control of all FSPs and their critical characteristics. A critical characteristic is defined as any feature such as dimension, tolerance, finish, material or assembly, manufacturing/inspection process, operation, field maintenance, or depot overhaul requirements that if nonconforming, missing, or degraded would cause failure or malfunction of the FSP.

Failure of an FSP due to corrosion can be extremely costly and detrimental to aircraft and life. For this reason, identification and application of CPC techniques are of great importance. In most cases, CPC life-cycle activities can be directly interfaced with FSP Program tasks.

Applying CPC techniques to FSPs increases (1) safety, (2) readiness, (3) the overall life of the part or component, and (4) FSP reliability and maintainability.

FUTURE CPC ACTIVITIES

A parallel effort under way at AVSCOM Quality Engineering is the development and utilization of a quantitative Corrosion Prevention and Control Decision Support System (CPCDSS). This software gives each program manager, integrated logistic support (ILS) manager, and quality engineer a parametric cost-benefit analysis tool to determine if an individual ECP or MWO is worth implementing on the basis of cost savings over the system life cycle. CPCDSS will also determine the value of additional information and permit sensitivity analyses

to test assumptions about input parameters. Additional versions of the model will go beyond analysis of hardware only and analyze the cost savings attributable to CPATs, special technical manuals (such as the Tri-Service Corrosion manual), and even the infrastructure of staff needed to support CPC at AVSCOM (Government and contractor). Validation of the model and development of a user's guide has recently been completed. Analysis and prioritization of ECP candidates will follow immediately.

SUMMARY

It has been estimated that corrosion costs the U.S. Army billions of dollars yearly for treatment and repair of aircraft and components, and results in reduced troop safety and in lowered readiness of combat units. To lessen the costs and hazards associated with corrosion, prevention and control techniques are enforced. The AVSCOM CPC Program is the Army's fundamental method for ensuring that corrosion is minimized to sustain high levels of performance and readiness of aviation systems. CPC has been applied already to a limited extent on current aircraft programs. In future aircraft programs, the CPC Program will be implemented in every phase of the aircraft life cycle, as described herein, in order to provide the greatest payback to Army aviation of the future.

NUCLEAR, BIOLOGICAL, AND CHEMICAL (NBC) CONTAMINATION SURVIVABILITY - AN UPDATE

Joseph J. Feeney
U.S. Army Chemical Research, Development and Engineering Center (CRDEC)
Aberdeen Proving Ground, MD 21010-5423

ABSTRACT

DOD Instruction 4245.13, Design and Acquisition of NBC Contamination-Survivable Systems, establishes DOD policy and procedures for the design and acquisition of systems that must perform mission essential functions in an NBC-contaminated environment. Army Regulation 70-71, Secretary of the Navy Instruction 3400.2, and Air Force Regulation 80-38 establish policy and procedures for the developing and acquisition of materiel to ensure its survivability and sustainability in an NBC-contaminated environment.

NBC contamination survivability is the capability of a system and its crew to withstand an NBC-contaminated environment, including decontamination, without losing the ability to accomplish its assigned mission. Characteristics of NBC contamination survivability are decontaminability, hardness (against agents and decontaminants), and compatibility of the NBC-protected man with his equipment. Decontaminability is the ability of a system to be decontaminated to reduce the hazard to personnel operating, maintaining, and resupplying it. Hardness is the ability of a system to withstand the damaging effects of NBC contamination and any decontamination agents and procedures required to decontaminate it. Compatibility is the ability of a system to be operated, maintained, and resupplied by personnel wearing the full NBC protective ensemble. These characteristics are based on engineering design criteria which are intended for use only in a developmental setting.

INTRODUCTION

The material damaging effects of contaminants such as chemical agents are often overlooked in comparison to the harmful, and often deadly, effects thay can produce. For example, nerve agents, which act by deactivating acetylcholinesterase, are generally

organophosphorus compounds which can pose considerable problems in storage due to their corrosive hydrolysis products which attack metals. The hydrolyses of such nerve agents as sarin (GB) or soman (GD) vary with pH but hydrofluoric acid (HF) is a primary hydrolysis product for both. Other types of chemical agents, when hydrolyzed, also produce corrosive by-products, e.g., choking (phosgene-hydrochloric acid), blister (mustard-hydrochloric acid), and blood (hydrogen cyanide-ammonia and formic acid) agents. Hydrolysis of methyl phosphonyldifluoride (DF), a binary component of chemical agent munitions, also produces HF. Decontaminants, such as supertropical bleach (STB), are also very corrosive to metals. Additionally, chemical agents, as well as their decontaminants, pose considerable problems, e.g., softening, blistering, etc., for non-metals such as plastics, rubber, etc., even when exposed for short duration.

On 15 June 1987, DOD initiated a formal program for NBC contamination-survivable systems with the publication of DOD Instruction 4245.13. The purpose of this instruction is to provide management and document directions for NBC contamination survivability activities conducted during the development and acquisition of systems that are critical to force-wide survivability in NBC environments. This includes conventional forces, non-strategic nuclear forces, strategic nuclear forces and supporting command, control, communications and intelligence (C^3I) systems.

This paper will outline the requirements in DOD Instruction 4245.13 and the service regulations/instructions, present examples of the effects of chemical contaminants and decontaminants on materials and electronics, and discuss effective methods and techniques available for achieving NBC contamination survivability. The aim of this paper is to provide an overview/update of NBC contamination survivability, not to present a means of implementing DODI 4245.13 or a service specific regulation/instruction.

BACKGROUND

DOD Instruction 4245.13, "Design and Acquisition of Nuclear, Biological and Chemical (NBC) Contamination-Survivable Systems", is the central DOD document providing NBC contamination survivability policy. This instruction, intended for use in conjunction with DOD Directive 4245.5 "Acquisition of Nuclear-Survivable Systems", calls for consideration of the effects of residual radiological contamination and chemical/biological agents and their decontaminants on the design and acquisition of systems. DOD Instruction 4245.13 applies to all programs, systems and subsystems designated as major system acquisition programs as well as any other programs reviewed periodically by the Under Secretary of Defense for Acquisition, USD(A), under exceptional management procedures. Execution of the provisions for nonmajor systems is the responsibility of the military services.

NBC contamination results from the deposition and/or sorption of residual radioactive material, or biological, or chemical agents on or by structures, areas, personnel, or objects. Nuclear (N) refers to residual radioactive material resulting from fallout, rainout, or irradiation produced by a nuclear explosion and persisting longer than one minute after burst. Biological (B) refers to all the general classes of micro-organisms and toxins that cause disease in man, plants, or animals or cause the deterioration of materiel. Chemical (C) refers to all known chemical substances intended for military operations to kill, seriously injure, incapacitate, or temporarily irritate or disable man through their physiological effects.

NBC contamination survivability is defined as the capability of a system and its crew to withstand an NBC-contaminated environment, including decontamination, without losing the ability to accomplish the assigned mission. Characteristics of NBC contamination survivability include decontaminability, hardness (to both agents and decontaminants), and compatibility for personnel wearing the full NBC protective ensemble.

CHARACTERISTICS of NBC CONTAMINATION SURVIVABILITY

Quantitative criteria, or characteristics, are designed to ensure that all materiel systems developed to perform mission essential functions can be used by personnel who are wearing protective clothing and equipment, and that such systems survive the effects of contamination by chemical and biological agents, radioactive contaminants and decontamination processes. These criteria are based upon engineering design criteria, intended for use only in a developmental setting. They do not define doctrinal or operational criteria for decontamination of systems or specify how to achieve the required survivability.

Decontaminability

Decontaminability is the ability of a system to be decontaminated to reduce the hazard to personnel operating, maintaining, and resupplying the system during its normal mission profile, which shall not exceed 12 hours. Decontaminability is enhanced by maximum use of materials that do not sorb NBC contaminants and facilitate their rapid removal with decontaminants, by incorporating designs that reduce or prevent accumulation of NBC contamination and provide ready accessibility for decontamination, by incorporating contamination control devices and techniques to reduce the amount of contamination, and by providing space on equipment for such NBC equipment as detectors, alarms, etc.

Hardness

Hardness is the ability of a system to withstand the damaging effects of NBC contamination and any decontaminants and

procedures required to decontaminate it. Hardness refers to the condition of equipment, including critical operational and functional performance characteristics, after it has been subjected to contamination and decontamination cycles.

Compatibility

Compatibility is the ability of a system to be operated, maintained, and resupplied by personnel wearing the full NBC protective ensemble. Compatibility requires consideration of the NBC-protected man and machine interface.

DEPARTMENT OF DEFENSE INSTRUCTION 4245.13

For those military services and DOD agencies designing and acquiring systems to be NBC contamination survivable, DOD Instruction 4245.13 requires each DOD component to:

- Assess NBC-contamination survivability and identify vulnerabilities and associated risks for systems with NBC contamination survivability requirements.
- Present cost and operational trade-offs to the Defense Acquisition Board (DAB) at Milestone I. For the Army Streamlined Acquisition Process (ASAP), this will occur at the Milestone I/II Program Decision.
- Ensure that nonmajor mission-essential systems are scrutinized closely for potential impacts on mission-essential functions.
- Develop and employ procedures similar to those contained in DOD Instruction 4245.13 to ensure that these nonmajor mission-essential systems exhibit appropriate NBC contamination survivability.
- Advise the Under Secretary of Defense for Acquisition, USD(A), at each milestone review if another major or nonmajor system has become a critical survivability limitation in the operation of the major system under development.
- Develop NBC contamination survivability criteria and standards and submit them to USD(A) for review.

Each DOD component can use different procedures to attain NBC contamination survivability, including trade-offs for cost, operational effectiveness, etc.

SUMMARY

DOD Instruction 4245.13 established a formal NBC contamination survivability program throughout the Department of Defense. The instruction provides management and documentation requirements for the survivability of systems designed and acquired to perform mission essential functions in an NBC-contaminated environment.

CANNON TUBE BORE CORROSION CAUSED BY PRESERVATION MATERIALS

BY

Donald M. Winegar and John R. Cammarene
Department of the Army
Benet Laboratories
Watervliet Arsenal
Watervliet, NY 12189-4050

Benet Laboratories Corrosion Control personnel developed a cyclic test to confirm that spontaneous decomposition of 1, 1, 1 - trichloroethane (Methyl Chloroform), a halogenated hydrocarbon cleaning solvent contained in MIL-L-63460, caused corrosion of the bore surface of gun tubes that were sealed for long term storage. It was also found that there was a marked increase in corrosion when impregnated type Volatile Corrosion Inhibitor (VCI) paper was used. This test may also be used for comparing other combinations of preservation oils and VCI papers to determine which will provide better protection from corrosion.

INTRODUCTION

Letterkenny Army Depot reported a reddish discoloration in four 105MM M68 tube bores that had been preserved and packaged for long term storage. The materials utilized comprised of MIL-L-63460 Lubricant, Cleaner, and Preservative Oil (CLP) and MIL-P-3420 Packaging Materials, Volatile Corrosion Inhibited Treated (VCI). A random inspection of 105MM M68 tubes stored at Watervliet Arsenal using a borescope revealed that some tubes had minor etching and pitting of the bore surface caused by corrosion.

ACTION TAKEN

Review and change Packaging Data Sheets as required. Since CLP had been recently implemented and upon consultation with the vendor and other sources, it was determined that CLP was the most plausible cause. CLP was suspended from use as a long term preservative and the Packaging Data Sheets were immediately changed to replace CLP with MIL-L-3150, (P-7), preservative oil. All appropriate depots, arsenals, and agencies were notified of the corrosion problem and of the replacement of CLP with MIL-L-3150 preservative oil.

Inspect and reprocess all cannon tubes stored at Watervliet Arsenal. Each cannon tube stored at Watervliet Arsenal and awaiting shipment was unpacked, cleaned of CLP preservative oil, and its bore surface inspected with a borescope. Upon opening of the bore covering, a pungent, vinegar-like odor was detected in many tubes. The entire bore surface was affected by the

corrosion process. Many tubes had excess liquid laying in the bottom of the bore. No excess corrosion action was present in the surface area covered by this liquid. It was evident that a vapor chemical reaction had occurred.

After inspection, each tube was cleaned in a hot alkaline cleaner to stop the corrosion action. Each tube was then rinsed, borescoped again, and reprocessed back into storage.

Twenty-nine of thirty 155MM M199 tube bores inspected were found to have Stage 1 corrosion, and two 155MM M185 tube bores were found to have Stage 1 corrosion. Table I summarizes the inspection report of 276 105MM M68 tubes.

TABLE 1

105MM M68 Tubes Inspected

Packaged Month	Year		Tubes Examined	Extent of Corrosion None	Stage 1	Stage 2	Stage 3
May	83		60	7	22	23	8
Jun	83		54	8	18	15	13
Jul	83		70	18	35	15	2
Aug	83		55	42	13		
Sep	83		37	29	8		
		Total	276	104	96	53	23

The stages of corrosion and their definitions are tabulated in Table 2. No stage 4 corrosion was found.

TABLE 2

Corrosion Stages
(Adopted from MIL-STD-624)

Stage	Description
1	Discoloration, staining. No direct visual evidence of pitting, etching, or other surface damage.
2	Loose rust, black, or white corrosion accompanied by minor etching and pitting of surface. No scale or tight rust.
3	Rust, black, or white corrosion accompanied singly or in combination with etching, pitting or more extensive surface damage. Loose or granular condition.
4	Rust, black, or white corrosion progressed to the point where fit, wear, function, or life of the item has been affected. Powdered or scaly condition, with pits or irregular areas of material removed from surface of item.

Review shop procedures for processing tubes. The Packaging Data Sheet required that the bore and chamber and all unpainted tube surfaces, except surfaces protected by dry film lubricant, be preserved with MIL-L-63460 CLP oil. Application of the oil was by fogging. All excess oil was thoroughly drained before further processing. The muzzle end of the tube was to be elevated approximately 10 degrees to allow for continuous drainage of cleaning solvents and preservative oil during processing. The ends were then sealed after insertion of VCI paper and the tube wrapped and containerized.

As designed, the fogging device was not operating properly because teflon particles in the CLP were clogging the holes. The holes were enlarged to provide a continuous flow of CLP. As modified, the device was delivering a plurality of small streams of CLP. As the fogging device was pulled through the tube, the VCI paper was attached to the rear of the device and pulled through at the same time. When the device was removed, the ends were sealed and the tube further packaged.

Review CLP specification and determine its composition. The MIL-L-63460 material (CLP) used had been manufactured by the Break-Free Division of San/Bar Corporation and were all of the same batch. Revision B, Amendment 1, of the military specification was in effect at the time of manufacture, August 1982. San/Bar Corporation was approved for listing on QPL 63460, dated 4 February 1982, and the reference test or qualification was MD-9427 for Break-Free CLP®.

The qualifying agency for Break-Free CLP provided a copy of a chemical analysis of "CLP" material as determined by the Naval Weapons Center, China Lake, California and published April 1981.[1] The General Electric Company, Schenectady, NY was contracted to perform a chemical analysis of the suspect CLP material. San/Bar Corporation provided a chemical analysis by telephone and through a personal representative. Table 3 tabulates a general analysis derived from these sources.

TABLE 3

Analysis of CLP

% by weight	Ingredient
12%	1-1-1 Trichloroethane (Methyl Chloroform)
7%	Freon TF
5%	Butyl Carbitol Acetate Ester
4%	N-Butyl Acetate Ester
2%	Isopropyl Alcohol
1%	Isobutyl Acetate
0.5%	Methyl Ethyl Ketone (MEK)
0.5%	Heptane
32%	Total Solvents
67.7% to 67.8%	Total Fats
0.2%-0.3%	Water

The cleaning portion of CLP is Freon TF and methylchloroform. The water content of CLP is approximately 0.17% by weight, but may be as great as 0.3%.

All the requirements of specification MIL-L-63460 were met when a sample of the suspect CLP material was tested by the qualifying agency.

Review the requirements of specifications MIL-P-3420 and MIL-I-8574 and retest the papers used in packaging the corroded tubes.

(1) Packaging Materials, Volatile Corrosion Inhibited Treated - MIL-P-3420

MIL-P-3420 is strictly a performance specification. No specific Volatile Corrosion Inhibitor (VCI) material composition is specified. The VCI material is applied by coating or impregnating the carrier paper. The base specification required a pH of 6.0 to 8.0 with 7.0, preferred for the carrier paper and Amendment 1, specified an upper limit of pH 8.5. Revision B, and all other revisions to MIL-P-3420 did not specify any pH value for the carrier paper. Additionally no water content is specified for the finished product. The treated carrier paper is to be used in accordance with the requirements of MIL-I-8574.

All of the MIL-P-3420 packaging material of the same manufacturer and lot number employed in packaging the affected cannon tubes were collected from the packaging area and the storeroom and stored separately from the remaining stock of material. Revision E of the specification, was in effect at the time paper was manufactured. Two different manufactures of Class 2, Style A and B materials were involved. They were Ludlow's Laminating and Coating Division, Holyoke, MA and Daubert Coated Products of Cullman, AL. The product and plant of each manufacturer was on the specification's Qualified Products List.

The General Electric Company (GE) also analyzed and determined the qualitative chemical composition of the Ludlow and Daubert VCI papers. GE also chemically reacted samples of each of the VCI papers with CLP to see if there was any evidence of one, or the other, paper being more reactive with the CLP. From the test results, GE concluded that:

- The main ingredients in the coating on the Ludlow VCI paper are dicyclohexylammonium nitrite and a phosphate. In addition, there are smaller amounts of another nitrite, nitride, sulfate, and chloride anions, as well as a number of other elements in trace amounts in this paper.

- The main ingredients in the impregnant of the Daubert VCI paper are sodium nitrite and sodium nitrate. In this paper, there are also smaller amounts of another nitrite, sulfate, and chloride anions, but no phosphate. In this paper also, there are a number of other elements in trace amounts.

- No significant reaction occurred between either of the two papers and the CLP fluid under room temperature conditions.

- The major surprise in the results of this work is the finding of large amounts of sodium nitrate present in the Daubert VCI paper.

Samples of each manufacturer's packaging material were submitted to the responsible qualifying agency for testing and evaluation. All samples passed the qualification test for QPL listing. Some samples were deliberately soaked in water and excess water removed by squeezing before testing to evaluate the affect of excess moisture content in the impregnated VCI paper.

(2) Inhibitors, Corrosion, Volatile, Utilization of - MIL-I-8574

This specification covers procedures for the use of volatile corrosion inhibitors in the packaging of parts and assemblies. Revision E of the specification, was in effect at the time of the corrosion problem. Engineering requirements state that VCI material must be protected from acids and their vapors. Hydrochloric acid type metal cleaners should not be used for cleaning items to be protected by VCI material. VCI material should not be exposed to industrial fumes containing hydrogen chloride, hydrogen sulfide, sulfur dioxide or other acidic vapors. A representative unit pack is to be submitted for a compatibility test of the materials to be employed in packaging the item to be preserved. The testing is performed in a chamber at 90% humidity for 72 hours at 140°F.

Perform jug tests to obtain possible corrosion conditions. Samples of cannon steel were obtained from excess metal cut from finished machined tubes. Each sample was cleaned, preserved, and packaged in one of a variety of packaging arrangements utilizing the packaging procedures practiced prior to using CLP (P-9 oil conforming to VV-L-800), during the use of CLP, and during the newly adopted MIL-L-3150 (P-7) oil period. The samples were placed in mason jar-like glass containers, tightly sealed to keep out the surrounding ambient, and placed on a window ledge in direct sunlight. No corrosion occurred during a test period of 16 weeks. Because of these negative results, further investigations were necessary.

Investigate and evaluate the storage environment of the tubes at the Arsenal.

The gun tubes are sealed at both the breech and the muzzle ends, and the gas ports are either covered and sealed by packaging material or enclosed by the bore evacuator attached to the tube. The tube is enclosed in a wooden container which is open to the ambient on the bottom - spaced boards - and closed on the remaining four sides and top. The packaged cannon is stored in the open, on a concrete pad, and stacked at least three high.

The exposure to the weather during late spring, summer, and early fall causes cyclic vaporization and condensation of any liquid in the cannon bore. The degree of vaporization and condensation is dependent on temperature and the vapor pressure of the material involved.

Interview corrosion personnel and perform a literature survey. Discussions of possible corrosion processes were held with various fellow corrosion prevention specialists, consultants, seminar instructors, etc. Always, the corrosion theory proffered was that water vapor present caused a portion of the methyl chloroform to form hydrochloric acid (HCl).[2] The HCl then attacked the VCI material of the carrier paper forming nitrates, nitrides, acetates, and the like, which form a corrosion media of mixed acids which then attacked the steel of the bore. Packaging handbooks, corrosion prevention information, and government publications caution one to be aware that methyl chloroform will hydrolize to HCl in the presence of moisture.

Fortunately, a chance inquiry one day elicited information that a government worker had accidently discovered that a selected group of halogenated hydrocarbon materials could undergo metal halide catalyzed hydrolysis. In particular, the investigator produced phosgene from carbon tetrachloride. Other metal halide catalyzed reactions were also studied. Some of the chemical reactions took place at room temperature and pressure conditions.

A literature search discovered an article titled "Metal Halide Catalyzed Hydrolysis of Trichloromethyl Compounds" authored by Marion E. Hill of the U.S. Naval Ordnance Laboratory Chemical Research Department.[3] Hill reports "1,1,1 - trichloroethane reacted very vigorously at room temperature with hydrated ferric chloride, giving acetic acid as the hydrolysis product". A 70% yield of acetic acid was obtained in an experiment. This appeared to be a possible chemical reaction that produced the odor noted upon opening the packaged tubes at the Arsenal!

THE MECHANISM FOR THE CORROSION OF THE BORES OF THE GUN TUBES

Freon TF and 1,1,1-trichloroethane (methyl chloroform) are the principal ingredients of the cleaning portion of CLP. The cleaning portion comprises approximately 30 percent, by weight, of CLP. Freon TF comprises 8 to 12 percent by weight. 1,1,1-trichloroethane comprises approximately 12 percent by weight. Water comprises about 0.17 percent, by weight, of CLP.

It is well known that vapors of chlorinated hydrocarbons will undergo hydrolysis to form hydrochloric acid (HCl) when continuously exposed to a humid atmosphere. The HCl attacks the clean surfaces of the bore producing ferric chloride as a reaction product. The ferric chloride absorbs moisture present in the tube bore to produce hydrated ferric chloride. A portion of the remaining 1,1,1-trichloroethane undergoes a catalyzed (ferric chloride) hydrolysis to produce mainly acetic acid (70% yield) as well as vinyl chloride and a product having the formula $C_6H_5O_2Cl$.[2]

The aforementioned chemicals can react with the VCI treated papers. Coated carrier papers such, for example, as Ludlow VCI material bonded to one side of the carrier paper will undergo little, if any, chemical action with the available reaction products. The carrier paper has little or no porosity and the VCI material is not readily soluble in water. However, impregnated carrier paper has a porous structure and contains water soluble VCI materials.

These water soluble VCI materials can be readily ionized thereby enabling further chemical actions to occur involving the acids and solvents present with material such as the nitrites and nitrates present in the Daubert paper. Such chemical reactions when they occur will enhance the corrosion of the bore tube surface.

CYCLIC TEST PROCEDURE TO DEMONSTRATE CORROSION MECHANISM

A cyclic test procedure was developed to prove the theory of corrosion reaction. Rifled sections of 105MM M68 finished tubes, when cut to size, approximately 8-10 inches in length, were packaged in a manner which duplicated the process employed for the corroded tubes except the plywood muzzle cover was replaced with a plexiglas cover for viewing. Other tube samples were prepared to evaluate various packaging material and preservation process means. Application of CLP was done without the use of an exhaust hood to minimize evaporation of the cleaning portion of CLP and to simulate actual shop procedures. The samples were prepared as follows:

(1) Cleaning process and agents prescribed by MIL-P-116 (Preservations, Method of), C-3, solvent cleaning utilizing P-D-680 dry cleaning solvent and MIL-L-15074, corrosion preventative, finger print remover.

(2) Drying procedure prescribed by MIL-P-116, D-4, wiping using clean white dry cloths.

(3) The preservative oil was applied to the rifled bore area utilizing clean cloths.

(4) A VCI strip was cut to form a tube and inserted into the gun tube section.

(5) One end was sealed using a wooden disc sealed in protective wrap. The other end was sealed with a 1/4" PLEXIGLAS® disc which allowed visual monitoring of the rifled bore area.

The CLP and VCI papers were from the same lots of materials employed in packaging the cannon which experienced the corroded tube bores.

Initially, the prepared samples were to be tested in an environmental chamber wherein a 24 hour cycle would simulate the hourly average temperature each corroded tube experienced during storage at the Watervliet Arsenal. However, the chamber was not available because of needed repair work. A second environmental chamber was available, but the test temperature could only be changed every 24 hours because of personnel availability and the elapsed time required to bring the chamber to a desired equilibrium temperature. Cyclic exposure conditions consisted of 24 hour periods at each temperature of 35F, 75F, 110F and all of them at 70% humidity. Each test specimen was examined at each change of temperature. The results are tabulated in Table 4, from Benet Weapons Laboratory Internal Technical Report[4].

TABLE 4

Cyclic Testing Data

Sample Number	Preservative Oil	VCI Paper	Number of Days Until Corrosion Observed
1-1	CLP	Daubert Style B	8
1-2	CLP	Daubert Style B	8
1-3	CLP	Daubert Style B	12
2-1	None	None	6
2-2	CLP	None	8
3-1	CLP	Ludlow Style B	14
3-2	CLP	Ludlow Style B	116+
3-3	None	Ludlow Style B	116+
4-1	CLP	Daubert Style A	6
4-2	CLP	Daubert Style A	7
4-3	None	Daubert Style A	8
A-1	P-7	None	16
A-2	P-7	None	7
A-3	P-7	Daubert Style A	55
A-6	P-7	Daubert Style A	64
A-7	P-9	None	11
A-9	P-7	Ludlow Style B	46
A-10	P-7	Ludlow Style B	64
A-12	P-9	None	29
A-13	P-9	Daubert Style A	116+
A-14	P-9	Daubert Style A	69
A-15	P-9	Ludlow Style B	116+
A-16	P-9	Ludlow Style B	116+

+ Testing terminated - no corrosion

VV-L-800 (P-9) was used prior to using P-7. We had no problems with it. However, Rock Island Arsenal had found that P-9 caused corrosion in gasoline tanks of armored vehicles and told Watervliet Arsenal not to use it anymore for long term storage of Arsenal products.

Examination of the test samples indicate that corrosion of the tube bore surface occurred more quickly when only CLP and CLP with VCI impregnated carrier paper were employed as the preservation means.

CONCLUSIONS

a. Corrosion of the bore tubes occurred as a result of a vapor phase chemical reaction which resulted in the chemical attack of the entire bore surface of the cannon. The effect of chemical concentration is noted by the fact that although 155MM cannons experienced corrosion, the degree of corrosion was less than that experienced by the 105MM cannon.

b. The corrosion was initiated by the catalyzed hydrolysis of the 1,1,1-trichloroethane present in CLP. It is believed that the "1,1,1" material was of the uninhibited variety, rather than inhibited. However, it was an improper utilization of the CLP since halogenated hydrocarbons should never be used in a closed system.

c. The corrosion process, in this instance, was enhanced by the presence of impregnated VCI packaging material. However, the same paper if used with MIL-L-3150 preservation oil will not present a corrosion problem regardless of its water content.

d. A compatability test of a sample pack in accordance with the requirement 4.3.1 of MIL-I-8574 probably would not have detected a corrosion problem because of the method of testing specified therein.

e. All users of CLP material were not made aware of the presence of halogenated hydrocarbon material therein, the requirement that the article to be preserved had to remain open until all "1,1,1" material had been evaporated, and that CLP was hazardous to people exposed to its use in poorly ventilated areas.

f. Personnel aware of the China Lake CLP report failed to communicate its contents to the packaging personnel involved in processing the cannon tubes.

RECOMMENDATIONS

a. Amend MIL-P-3420.

(1) Reinstate the pH requirement of 6.5 to 7.5 for carrier paper.

(2) List coated paper and impregnated paper separately.

(3) Provide a maximum acceptable water content for all VCI treated carrier paper.

Note: (1) and (2) have been adopted.

b. The agency responsible for qualifying a product for a QPL must know and understand all the materials, including proprietary material, present in a QPL product. A knowledgable person should be designated that can be contacted to evalute the use of the QPL product and alert the user of any possible toxicity and/or corrosion problems.

Note: ARDEC has designated a person to perform this task.

c. A better means of supplying corrosion/corrosion prevention reports and information should be initiated.

Note: Corrosion Prevention Action Team (CPAT) now performs this function.

d. A re-examination and a more detailed investigation of Hill's experiment should be conducted. Such an investigation should include other closed systems such as hydro-pneumatic systems, hydraulic systems, fuel lines, and the like, for all military applications.

REFERENCES

1. Heller, Cordes, Lowe-Ma and Moore, "Break-Free CLP®": A Partial Chemical Analysis of This Cleaner/Lubricant/Preservative, NWC TM4526, 1981, Naval Weapons Center, China Lake, California.

2. Packaging of Material Preservation (Volume 1), Defense Logistics Agency, Departments of the Army, the Navy, and the Air Force, August 1982, Pages 1-18.

3. Hill, Metal Halide Catalyzed Hydrolysis of Trichloromethyl Compounds, J. Organic Chem, 25, 1115-1118, (1961).

4. Cyclic Testing of VCI Papers and Preservative Oils for Corrosion Protection of Gun Tubes, J. Cammarene, D. Winegar, and G. Spencer, 1985.

ACKNOWLEDGEMENTS

We wish to thank all the individuals for their technical assistance during the testing and writing of this report.

Mr. Gerald L. Spencer, Chief, Specifications and Packaging, Benet Laboratories

Mr. Anthony Alfano, Chemist, Material Development and Readiness Command, Packaging, Storage and Containerization Center, Tobyhanna, PA

Mr. Edward Slussar, Physical Science Technician, Material Development and Readiness Command, Packaging, Storage and Containerization Center, Tobyhanna, PA

Mr. Donald Yoder, Technical Director, San/Bar Corp., Irvine, CA

Mr. Niko V. Gjaja, Chemist, General Electric Analytical Chemistry Turbine Technology Laboratory, Schenectady, NY

Mr. Donald Harms, Chemist, General Electric Analytical Chemistry Turbine Technology Laboratory, Schenectady, NY

CORROSION BEHAVIOR OF AA-7175-T74 EXPOSED TO ARTIFICIAL SEAWATER AND OTTO FUEL

J. F. McIntyre
Naval Surface Warfare Center
Materials Division
Electrochemistry Branch
10901 New Hampshire Avenue
Silver Spring, MD 20903-5000

T. S. Dow
Naval Surface Warfare Center
Energetic Materials Division
Synthesis & Formulation Branch
10901 New Hampshire Avenue
Silver Spring, MD 20903-5000

ABSTRACT

It is well known that 7XXX series aluminum alloys are susceptible to corrosion in seawater environments; however, in the presence of Otto fuel and seawater, a synergistic reaction occurs which greatly accelerates the corrosion rate of these alloys. Because of this synergism, a large number of anodized AA-7175-T74 torpedo fuel tanks have suffered rapid localized attack after as few as six exercises. Otto fuel is a liquid dinitrate ester monopropellent containing dibutylsebacate as a desensitizer and 2-nitrodiphenylamine as a stabilizer. This research was initiated to study the interactions between Otto fuel and seawater to better understand the mechanisms by which premature failure occurred. Weight-loss measurements were conducted in ASTM seawater, Otto fuel, and a mixture of Otto fuel and seawater. The solution chemistries of the Otto fuel-seawater mixture were analyzed using ion chromatography. Additional testing was performed using electrochemical techniques to study the pitting and cathodic polarization behavior of this alloy. A mechanism for premature failure of exercise torpedo fuel tanks is proposed herewith.

INTRODUCTION

The navy is currently using anodized AA-7175-T74 exercise torpedo fuel tanks. Many of these torpedos are powered by Otto fuel. Otto fuel is a liquid dinitrate ester monopropellent containing dibutylsebacate as a desensitizer and 2-nitrodiphenylamine as a stabilizer. During torpedo operation, Otto fuel comes in contact with seawater, seawater entering

the fuel tank in amounts equal to spent Otto fuel. At the conclusion of a test run, the torpedo fuel tank contains seawater, i.e., Otto fuel is completely displaced. After recovery of the torpedo, the seawater is flushed from the tank with potable water, and several more rinses are performed before the tank is refilled with Otto fuel. Unfortunately, a large percentage of the exercise fuel tanks undergo rapid localized attack and must be refurbished in as little as six runs - worse yet, the fuel tank must often be discarded because of near penetration of the fuel tank wall. One such fuel tank was acquired by this lab for analysis. Representative photographs of localized attack in several locations can be seen in Figure 1. The large pit in Figure 1a is nearly 60% of the way through the hull thickness. In Figure 1b the rib-stiffener is severely attacked. This particular torpedo was removed from active service after nine exercises. Research was initiated to study the possible interaction between Otto fuel and seawater to better understand the mechanisms by which rapid failure occurred.

EXPERIMENTAL

The corrosion behavior of AA-7175-T74 was determined by weight-loss (WL) measurements and electrochemical techniques. All specimens were obtained from an actual forged fuel tank. The chemical composition of AA-7175-T74 is given in Table 1. WL samples were cut into 1"x2" coupons and the surfaces were machined smooth. No further surfacing of the coupons was performed, except the edges were rounded with a file. All samples were

TABLE 1. CHEMICAL COMPOSITION OF AA-7175-T74

Si	Fe	Cu	Mn	Mg	Cr	Zn	Ni
.10	.12	1.5	.01	2.24	.17	5.5	.01

washed with a detergent, rinsed with distilled water, rinsed with acetone, followed by a rinse in ethanol, and air dried. Prior to exposure testing each sample was weighed to the nearest 0.1 mg. Samples were exposed to ASTM seawater (ASTM D1141), Otto fuel, and a mixture of Otto fuel and ASTM seawater in triplicate at room temperature and one sample at 60°C. Exposure testing was completed in 30 days. Samples were removed from their respective test environment and immediately rinsed with distilled water and dried in an air stream; samples were then weighed and photographed. After the initial examination, the corrosion product layers were removed by exposure to concentrated HNO_3 for 1-2 minutes. The corrosion product-free samples were then rinsed with distilled water, dried in an air stream, and reweighed; this procedure was repeated until no weight changed was recorded. Corrosion rates are reported in mils per year (mpy).

The pH of seawater from both the one- and two-phase test solutions was recorded at the end of the test. In addition, the seawater solutions were analyzed using ion chromatography. Ion chromatography was performed using a Dionex® 2021 Ion Chromatograph interfaced with two detectors: a conductivity detector and a variable ultraviolet absorbance detector, set at 206 nm. Three separation columns were used to detect for the presence of Cl^-, NO_2^-, NO_3^-, SO_4^{2-} and Br^- in the ppm range. Ion chromatographic analyses are still in progress and only qualitative results will be reported herewith. Samples similar to those used in the WL studies were used for all electrochemical tests. AA-7175 fuel tank samples were cut into ½"x½" coupons, lead wires were attached with Ag contact paint, and cold-mounted in an acrylic polymer. Sample surfaces were wet-ground through successive size SiC papers to a final 600 grit finish; this was followed by rinsing with liberal amounts of distilled water, the surface was cleaned with a moist cotton swab, first in the direction of the abrasion lines, rinsed, then swabbed transverse to the abrasion lines, rinsed again in distilled water, and dried in a hot air-stream. Samples were immediately immersed in the appropriate solution for electrochemical testing. Potentiodynamic cyclic pitting scans were performed in deaerated synthetic seawater. All solutions were deaerated for a minimum of two hours before sample introduction. Samples were pre-immersed for ½ hour, scans were started at open circuit potential (Eocp), scanned in the noble direction at a rate of 0.2 mV/sec, and reversed at 250 $\mu A/cm^2$. Pitting behavior as a function of pH was studied by adjusting the pH of the seawater with NaOH or HCl to the desired value. The effect of NO_3^- and NO_2^- additions to seawater on the pitting potential (Ep) were also investigated. Potentiodynamic cathodic polarization scans were conducted in neat 3.5% NaCl and in 3.5% NaCl solutions with various additions of NO_3^- and NO_2^-.

RESULTS

Corrosion rate data obtained from WL studies are summarized in Table 2.

TABLE 2. CORROSION RATE DATA OBTAINED FROM WEIGHT-LOSS TESTS

Solution	°C	WL (mg)	mpy
ASTM Seawater	24	5.0	0.89
	60	6.0	1.10
½Otto Fuel-½Seawater	24	31.0	5.60
	60	358.0	64.20

All samples exposed to neat Otto fuel at 24°C and 60°C showed no change in weight over the duration of the test. Only moderate rates of corrosion were obtained in neat seawater at both temperatures, but samples exposed to the two-phase seawater-Otto fuel mixture exhibited higher

rates of corrosion. The corrosion rate was about five times greater at 24°C and two orders of magnitude higher at 60°C compared to samples exposed to only seawater at 24°C and 60°C. The severity of attack on the samples exposed to the two-phase environment is highlighted in Figure 2. The attack on the sample exposed to the two-phase seawater-Otto fuel mixture at 60°C was so severe at the interface that localized attack penetrated about 80% of the way through the sample; a cross-section micrograph of the largest and deepest pit can be seen in Figure 3.

Analysis of seawater after sample exposure to the one- and two-phase environments was performed to determine if the presence of Otto fuel changed the solution chemistry. A transformation of the synthetic seawater to a more aggressive environment would explain the rapid rate of attack on samples exposed to the two-phase environment The pH of all seawater solutions was adjusted to 8.2 prior to sample introduction. A summary of the recorded pH at the conclusion of the test is given in Table 3. Ion chromatography analyses revealed that both NO_3^- and NO_2^- were present in the seawater layer of the two-phase environment. Qualitative and quantitative results indicated that higher concentrations of both anions were present in the seawater of the two-phase environment at 60°C. Neither anion was present in the seawater from the one-phase environment. This result indicated that a reaction had occurred between the Otto fuel layer and the seawater.

TABLE 3. SUMMARY OF pH VALUES RECORDED AFTER SAMPLE EXPOSURE TO ASTM SEAWATER AND ASTM SEAWATER-OTTO FUEL MIXTURE FOR 30 DAYS AT 60°C & 24°C

Condition	°C	pH
ASTM Seawater	24	8.06
	60	7.06
½Otto Fuel-½Seawater	24	7.06
	60	7.72

Electrochemical testing was initiated to better understand the influence of NO_3^- and NO_2^- on the corrosion behavior of AA-7175-T74. Results from preliminary tests will be used in the discussion section to help provide some insight into the mechanism of rapid attack of exercise torpedo fuel tanks.

DISCUSSIONS

Analysis of the test environments indicated that the only striking difference between the one- and two-phase environments is the presence of NO_3^- and NO_2^- in the seawater of the two-phase system. It is proposed that

the seawater hydrolyzes the dinitrate ester, which constitutes 76% of Otto fuel, to release NO_3^-. Similar reactions are documented in the literature[1], and the proposed mechanism is:

$$CH_3[CHONO_2]_2 + 2H_2O \longrightarrow CH_3(CHOH)_2 + 2H^+ + 2NO_3^-.$$

As indicated, highly soluble NO_3^- is liberated and simultaneously promotes a lowering of the pH. Although the pH is not much different in the two seawater environments at the end of the test (see Table 3), it is possible that the local pH is acidic near the interface between seawater and Otto fuel. Ep values were observed to decrease with decreasing pH as determined by potentiodynamic cyclic pitting scans (see Figure 4). However, if a near neutral pH occurs at the interface as indicated by measured values at the conclusion of the test, pitting susceptibility would actually decrease as shown in Figure 4. In addition, in the presence of NO_3^- at several concentrations it was observed that Ep increased, which suggested that NO_3^- had an inhibiting effect (see Table 4). Studies on the effect of NO_3^- concentration and pH was only recently started, but preliminary results indicated that in the presence of NO_3^- the Ep is independent of pH. Similar behavior was observed for NO_2^-.

TABLE 4. SUMMARY OF PITTING POTENTIALS FOR AA-7175-T74 EXPOSED TO DEAERATED ASTM SEAWATER WITH ADDED NITRATE AND NITRITE ANIONS

Concentration (moles/liter) NO_3^-	NO_2^-	pH	Ep(mV)
.005@	-	8.2	-742±7
.01@	-	8.2	-739±3
.05*	-	8.2	-709
.05*	-	6.5	-742
-	.005@	8.2	-743±3
-	.05@	8.2	-768±2
-	.10*	8.2	-712
-	-	8.2	-768±17#

@ average of three experiments
* only one experiment
# average of six experiments

It is well known that the nitrate anion is an effective inhibitor for the protection of aluminum alloys.[2-3] The results from this study show that corrosion is accelerated when seawater comes in contact with Otto

fuel. This observation suggests that NO_3^- behaves in a synergistic way to exacerbate the rate of attack. Research by Foley et al. has shown that for certain NO_3^-/Cl^- ratios the corrosion rate of AA-7075-T6 is increased by 5-10 fold.[4-5] One of their early theories attributed increased attack to the reduction of NO_3^- to NO_2^- and it was shown that the corrosion rate of AA-7075-T6 was increased by an order of magnitude for exposure to a 0.01N NO_2^-/0.01N Cl^- solution. It was later proposed by Foley et al. that perhaps the continued reduction of NO_2^- to NH_3 was responsible for accelerated attack; they found in certain ammonium salt solutions that the corrosion of aluminum reaches a catastrophic rate, specifically for certain mixtures of NH_4NO_3 and NH_4Cl.[5] This observed effect was attributed to the ability of NH_3 to form soluble complexes with $MgZn_2$ intermetallics found in AA-7075 alloys.[5] The seawater solutions in this test were not analyzed for NH_3 but analyses will be conducted in the future. Electrochemical studies will also be conducted to study the effect of NH_4^+ additions to seawater on Ep.

The failure of fuel tanks probably occurs because small amounts of seawater remain behind after repeated flushes prior to reintroduction of Otto fuel. This small volume of seawater is envisioned to be surrounded by a large volume of Otto fuel. The time before the next exercise is not known, but with sufficient time the aggressive nature of the seawater combined with the presence of NO_3^- and an initially low pH favors rapid attack of the anodized coating. Compromise of the anodized coating exposes bare aluminum which continues to corrode on subsequent exposures to both seawater and Otto fuel-seawater mixtures. A fundamental aspect of all corrosion reactions is the need for readily reducible species; in seawater the reduction of oxygen is the most common cathodic process. A small volume of seawater would presumably contain a relatively small concentration of dissolved oxygen, and once the oxygen is consumed the corrosion reaction should cease. This is obviously not the case because of the documented evidence of severe corrosion. The presence of a moderate supply of NO_3^- provides an alternative cathodic reaction so corrosion can take place in the absence of oxygen. In fact, potentiodynamic polarization curves conducted in 3.5% NaCl with and without the presence of NO_3^- or NO_2^- revealed that these anions were effective cathodic depolarizers (see Figure 5). In addition, the cathodic activity remains high even in deaerated solution as shown in Figure 6. Although the specific synergisms between seawater and NO_3^-, NO_2^-, and perhaps NH_3 is known not conclusively, it is obvious from these preliminary results that the corrosion rate of AA-7175-T74 is increased catastrophically.

CONCLUSION

The proposed mechanism for accelerated failure of exercise torpedo fuel tanks is:

- small volumes of seawater remain after repeated flushes with potable water

- seawater hydrolyzes the Otto fuel to release NO_3^- and, at least temporarily, lowers the pH

- NO_3^- acts as a cathodic depolarizer, which sustains the corrosion process

- NO_2^- is formed from the cathodic reduction of NO_3^- and also acts as a cathodic depolarizer

- NO_2^- may be further reduced to NH_3, which, according to the literature, results in rapid corrosion of AA-7075 because of the ease of formation of soluble NH_4^+ complexes with intermetallic species.

REFERENCES

1. T. Urbanski, "Chemistry and Technology of Explosives," Vol. II, Pergammon Press, New York (1965), pp. 7-10.

2. H. Böhni and H.H. Uhlig, J. Electrochem. Soc. 116(7), 906 (1969).

3. M. Koudelkova and J. Augustynski, J Electrochem. Soc. 126(10), 1659 (1979).

4. A.M. McKissick, A.A. Adams, and R.T. Foley, J. Electrochem. Soc. 117(11), 1459 (1970).

5. A.A. Adams, K.E. Eagle, and R.T. Foley, J. Electrochem. Soc. 119(12), 1692 (1972).

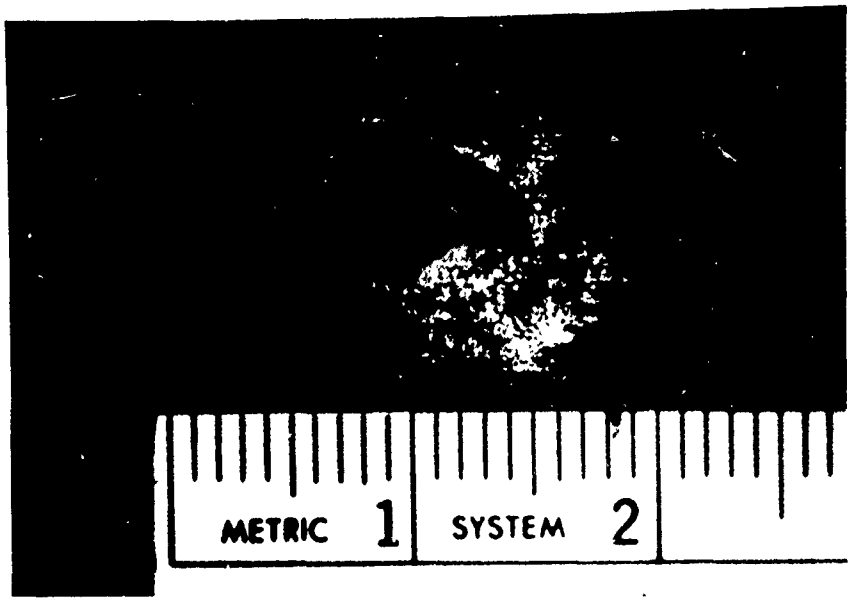

FIGURE 1A. LARGE PIT ON AA-7175-T74 FUEL TANK AFTER NINE EXERCISES OF TORPEDO

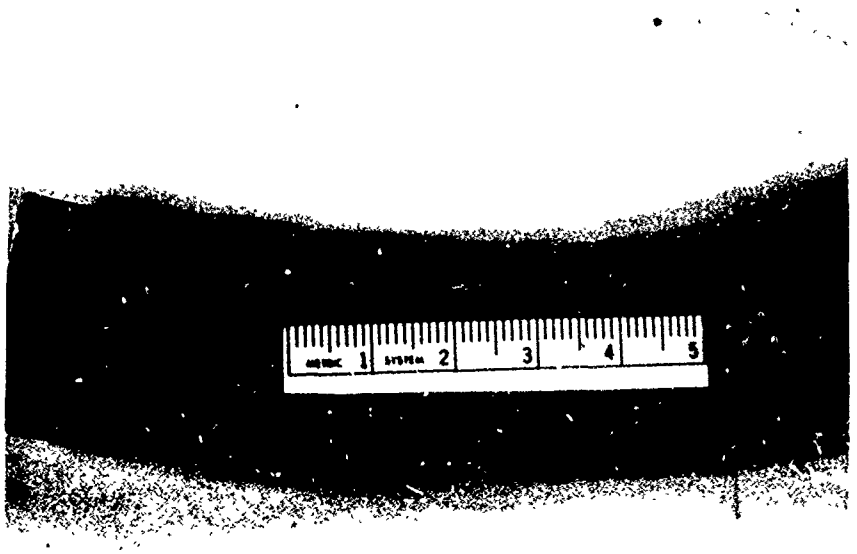

FIGURE 1B. SEVERE ATTACK OF FUEL TANK RIB-STIFFENER

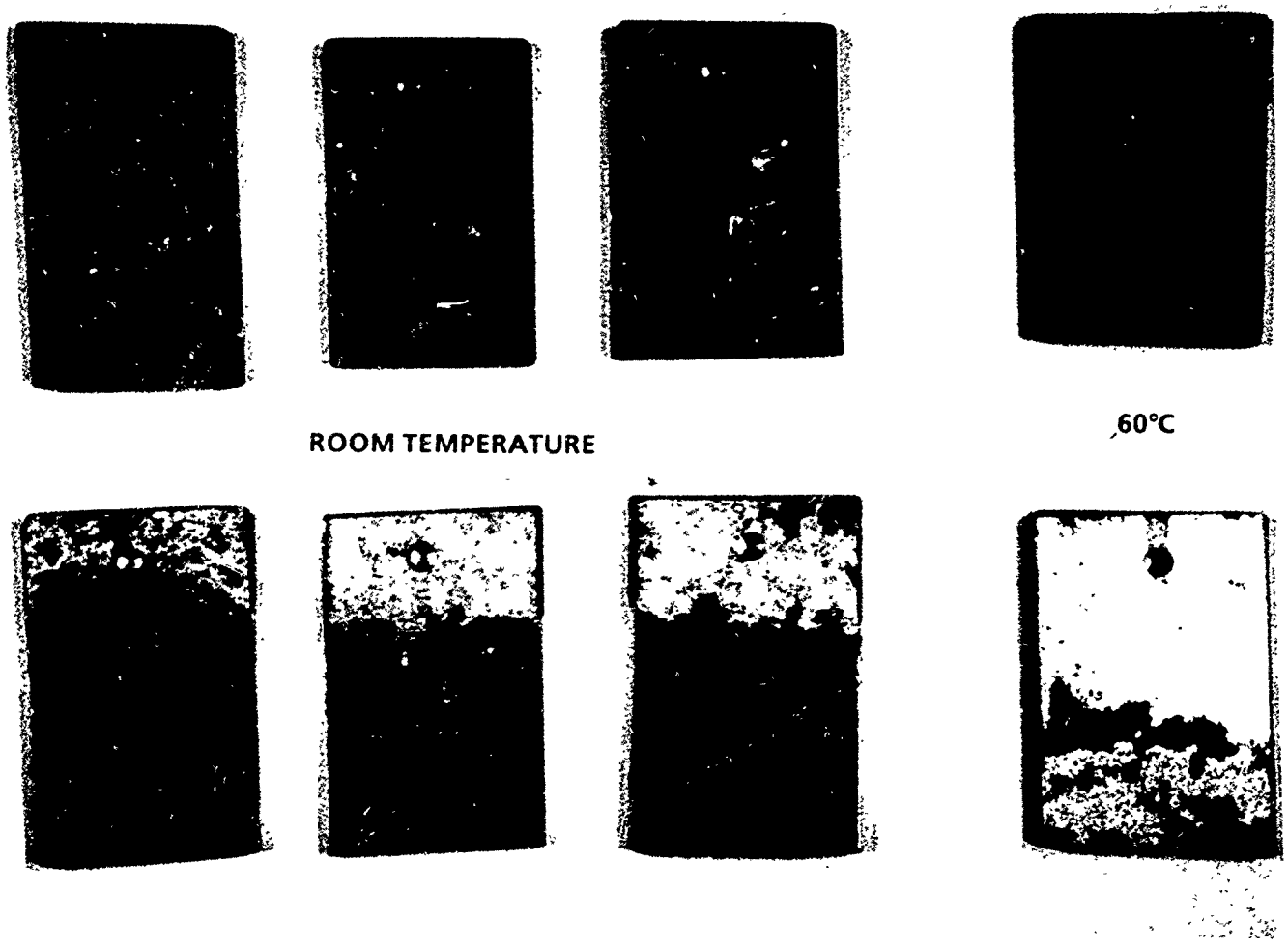

FIGURE 2. TOP ROW: AA-7175-T74 SAMPLES EXPOSED TO ASTM SEAWATER FOR 30 DAYS
BOTTOM ROW: AA-7175-T74 SAMPLES EXPOSED TO SEAWATER-OTTO FUEL MIXTURE FOR 30 DAYS

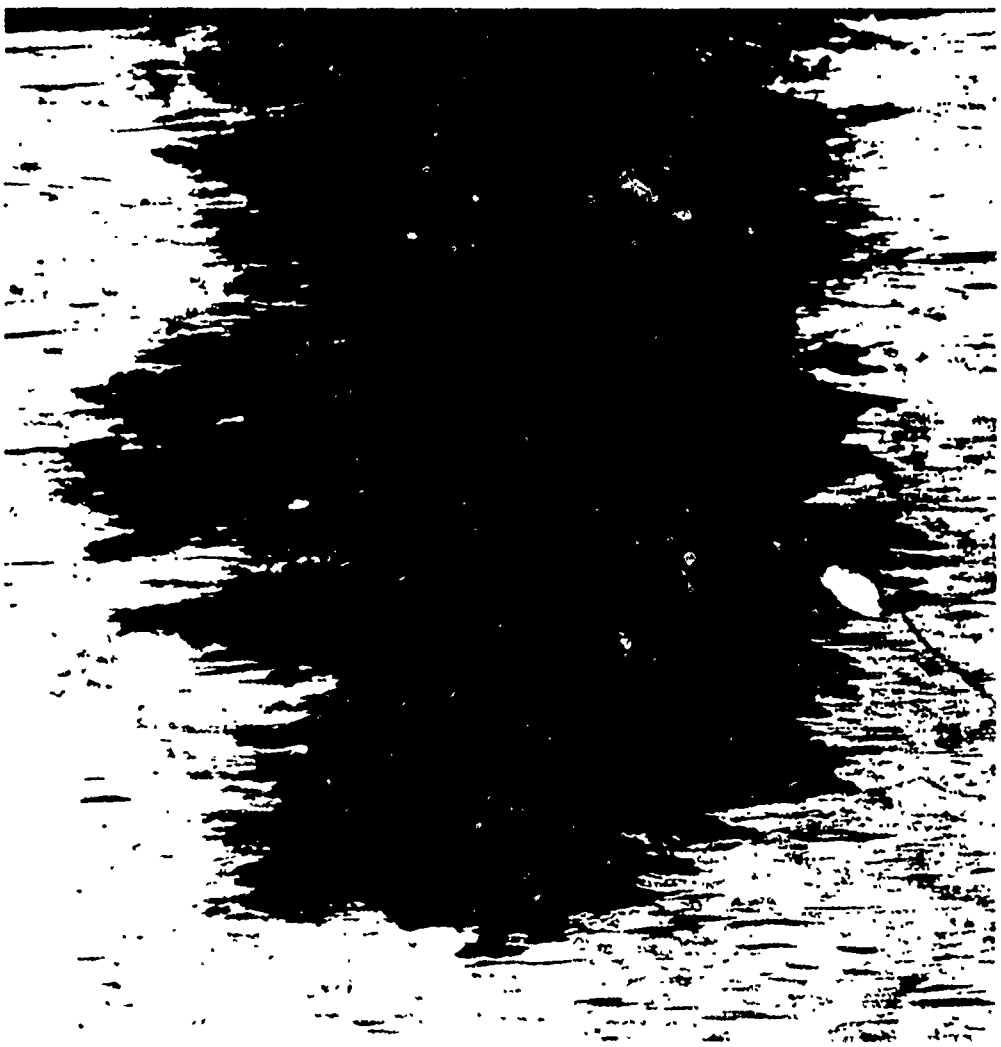

FIGURE 3. MICROGRAPH OF LOCALIZED ATTACK ON AA-7175-T74 AFTER 30 DAYS EXPOSURE TO ASTM SEAWATER-OTTO FUEL MIXTURE @ 60° C (46.5X)

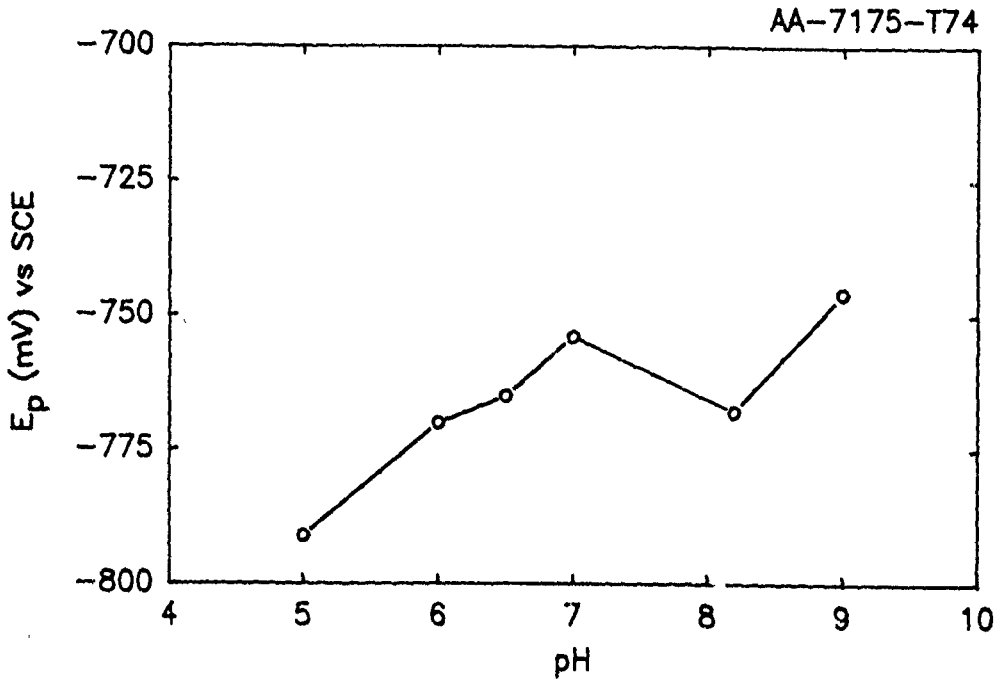

FIGURE 4. Effect of pH on Pitting Potential

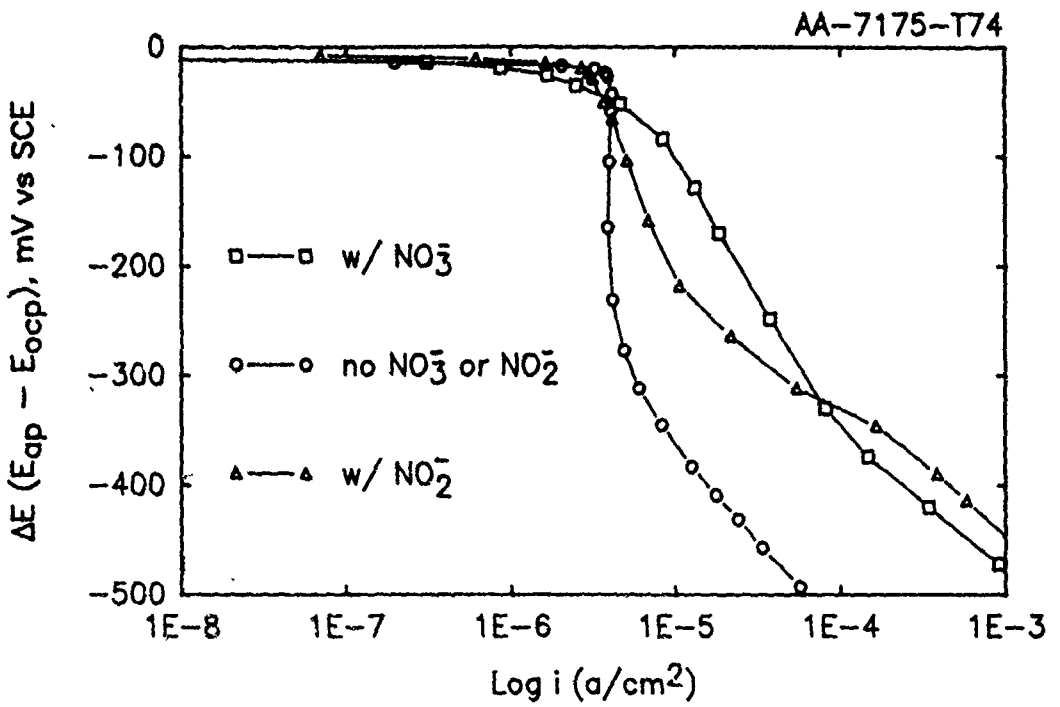

FIGURE 5. Cathodic Polarization Curves in 3.5% NaCl with and without NO_3^- or NO_2^-

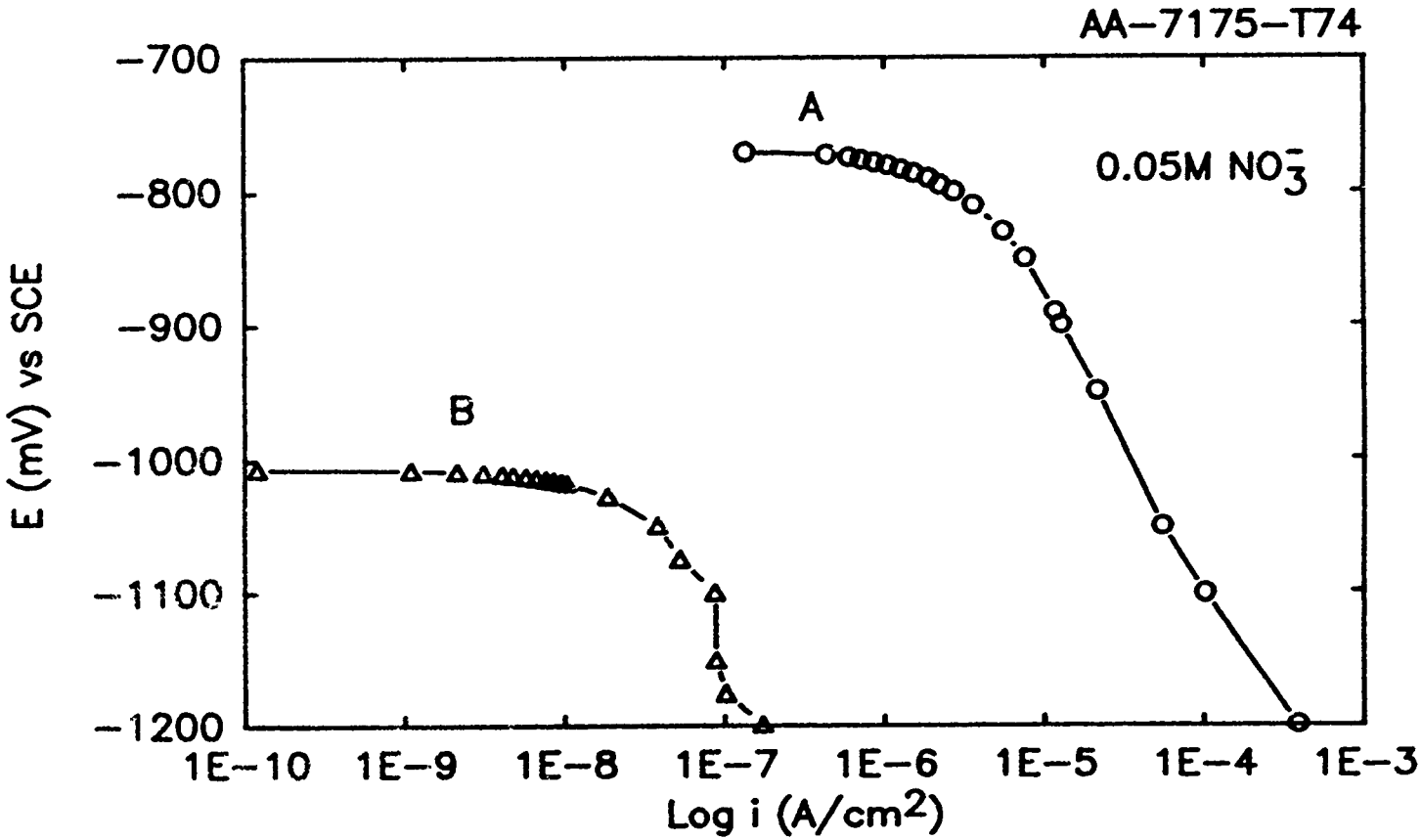

FIGURE 6. Cathodic Polarization Curves in Deaerated 3.5% NaCl: A – NO_3^- Added; B – No NO_3^-

EVALUATION OF THE CORROSION PROTECTION OF VARIOUS METHODS OF REPAIR OF ION VAPOR DEPOSITED ALUMINUM (IVDA) COATINGS

Christine L. Martuch
Cleveland Pneumatic Company
3781 East 77 Street
Cleveland, OH 44105

ABSTRACT

The chipping of Ion Vapor Deposited Aluminum (IVDA) coatings in service has become a common problem in the aircraft industry in recent years. An investigation was conducted into the effects of various repair methods for IVDA coatings specifically as a function of corrosion resistance of the repaired area. Several materials were tested by utilizing their respective recommended methods of repair:

(1) Alseal 518, an aluminum refractory coating;
(2) Sermetel 249, a high-temperature resistant aluminum refractory coating;
(3) Dow Corning's 1-2577 silicone resin conformal coating; and
(4) Brush cadmium plating using the Dalic 2023 solution.

In addition, the application of primer, sealant, and paint was also investigated as a means of repair. The treated panels were subjected to salt spray testing per ASTM B117 for a period of four weeks. Of the four repair methods which were tested, the catalyzed Sermetel 249 was found to offer the greatest advantages as a method of repairing IVDA in that it is relatively easy to apply, requires few tools or materials, cures at room temperature, and offers excellent salt spray corrosion resistance. Moreover, it was determined that for Sermetel 249 to be a feasible repair coating, the interfaces between the Sermetel and the IVDA must be blended in smoothly to prevent the formation of bubbles in the paint.

INTRODUCTION

Flaking and chipping have been common problems for IVDA coatings in the past. Recently, a subcontractor of the Cleveland Pneumatic Company (CPC) had reported problems of flaking and chipping of IVDA coatings on parts while they were being handled between various processing steps and had requested information as to a possible method of repair.

Presently, CPC Customer's specification for IVDA coating requires that bare areas shall not exceed four (4) spots 0.10 inch in diameter or equivalent. Parts having bare areas larger than this must be either stripped and recoated per the Engineering Drawing or subjected to the Materials Review Board MRB disposition. It was decided that an investigation to determine suitable repair procedures that would not require any embrittlement relief would be very useful. The other critical feature to be considered for such repair is that the IVDA coated landing gear axles are often exposed to appreciable temperatures in service. The possible high temperature service environment excludes any repair procedure that utilizes cadmium alloy coatings.

EXPERIMENTAL METHODS

The test program outlined at CPC was discussed with the Technical personnel currently involved in the IVDA Group at McDonnell Douglas Aircraft Corporation (McAir - St. Louis) (1). It may be noted that the McAir Technical Group was responsible for developing the IVDA process. The Alseal 518 aluminum refractory coating was strongly recommended by McAir as they had experienced considerable success using the Alseal as a repair coating. However, the Alseal requires a minimum of 400^{o}F cure. Since elevated temperature bakes have on occasion caused blistering of IVDA coatings, it was decided that this product would be evaluated without such a bake. Sermetel 249, another aluminum refractory coating, was known to fully cure at room temperature, so it was tested as a possible repair method. Dow Corning's conformal coating, 1-2577, which is a silicone resin, was considered as a possible repair method as it was also known to cure at room temperature. A fourth procedure for effective protection consisting of epoxy primer, polysulfide sealant, and polyurethane enamel paint was also tested. Brush (stylus) cadmium plating using SIFCO's Dalic 2023 solution was included for comparison purposes.

Twenty (20) 4130 grade steel salt spray panels, 4 inches X 6 inches in size, were IVDA coated to a thickness of 0.0015 inches per side; one-inch diameter spots were deliberately masked before IVDA coating to create sizes for repair. The spots to be repaired were cleaned by grit blasting with 80-120 mesh SiO_2 and air sprayed to remove residual grit. Scotchbrite (3M Company) was used to scuff a 1/2 inch wide section around the periphery of the repair areas in order to blend in the steel with the IVDA. Using the five different repair methods, namely Alseal 518, Sermetel 249, Dow Corning 1-2577, the primer/sealant/paint application, and brush cadmium plating, the samples were repaired to the thickness levels shown in Table I.

TABLE 1

RESULTS OF SALT SPRAY TESTS
PERFORMED ON REPAIRED IVDA COATED PANELS

NO.	METHOD OF REPAIR	AVERAGE THICKNESS OF REPAIR COATING IN MILS	EFFECT OF SALT SPRAY
A1	Alseal 518	Did not cure	Not applicable
A2	Alseal 518	Did not cure	Not applicable
A3	Alseal 518	Did not cure	
S1	Sermetel 249	6.0	Black interfacial stains after 240 hours
S2	Sermetel 249	9.0	Black interfacial stains after 240 hours
S3	Sermetel 249	1.8	Black interfacial stains after 216 hours
S4	Sermetel 249	0.8	Black interfacial stains after 240 hours
S5	Sermetel 249, Primer, Sealant, Paint	2.3*	Paint bubbled at interface, 288 hours
S6	Sermetel 249, Primer, Sealant, Paint	0.8*	No effect
S7	Sermetel 249	2.7	Black interfacial stains after 288 hours
S8	Sermetel 249	2.7	Black interfacial stains after 288 hours
S9	Sermetel 249	2.7	Black interfacial stains after 288 hours
BC1	Clean with MEK, Dalic Brush Cad	0.6	Black interfacial stains after 240 hours
BC2	Scotchbrite, Dalic Brush Cad	0.6	Black Interfacial stainless after 96 hours
BC3	Scotchbrite, Dalic Brush Cad	0.6	Black interfacial stains after 96 hours
BC4	Etch, Desmut, Dalic Brush Cad, Primer, Sealant, Pain	0.6*	No effect
P1	Primer, Sealant, Paint	N/A	No effect
P2	Primer, Sealant, Paint	N/A	No effect
P3	Primer, Sealant, Paint	N/A	Small rust spots visible through paint away from scratch after 288 hours
P4	Primer, Sealant, Paint	N/A	No effect

* Repair thickness before paint application.

TABLE 1 (Con't.)

RESULTS OF SALT SPRAY TESTS
PERFORMED ON REPAIRED IVDA COATED PANELS

NO.	METHOD OF REPAIR	AVERAGE THICKNESS OF REPAIR COATING IN MILS	EFFECT OF SALT SPRAY
CP1	Sermetel 249 & 273 Catalyst; Scotchbrite applied to interface; Primer and paint applied	1.0*	Slight paint bubbling at interface after 280 hours
CP2	Sermetel 249 & 273 Catalyst; Scotchbrite applied to interface; Primer and paint applied	1.0*	Slight paint bubbling at interface after 280 hours
CP3	Sermetel 249 & 273 Catalyst; Scotchbrite applied to interface; Primer and paint applied	0.8*	Slight paint bubbling at interface after 280 hours
CP4	Sermetel 249 & 273 Catalyst; Scotchbrite applied to interface; Primer and paint applied	0.9*	Five very small paint bubbles on repaired surface after 256 hours
CP5	Sermetel 249 & 273 Catalyst; Scotchbrite applied to interface; Primer and paint applied	0.9*	Slight paint bubbling at interface after 280 hour
CP6	Sermetel 249 & 273 Catalyst; Scotchbrite applied to interface; Primer and paint applied	1.1*	Slight paint bubbling at interface after 256 hours
CP7	Sermetel 249 & 273 Catalyst; Scotchbrite applied to interface; Primer and paint applied	1.0*	Small amount of bubbling in paint at interface and away from repaired area after 280 hours
CP8	Sermetel 249 & 273 Catalyst; Scotchbrite applied to interface; Primer and paint applied	0.9*	No bubbling occurred in 672 hours
CP9	Sermetel 249 & 273 Catalyst; Scotchbrite applied to interface; Primer and paint applied	1.0*	Slight paint bubbling at interface after 280 hours
CP10	Sermetel 249 & 273 Catalyst; Scotchbrite applied to interface; Primer and paint applied	0.8*	Slight paint bubbling at interface after 280 hours

* Repair thickness before paint application.

Originally the Sermetel was applied to panels S1-S9 without the use of the Sermetel 273 catalyst. The technical personnel from Sermatech, which is the manufacturer of Sermetel, informed CPC that although corrosion problems may not be experienced with the panels on which Sermetel was used in the uncatalyzed form, Sermatech would not guarantee the performance of the Sermetel without the proper use of its catalyst. For the study of the catalyzed Sermetel 249, ten (10) salt spray panels, CP1-CP10, were then IVDA coated to a thickness between 0.0015-0.0020 inches per side; the same method of surface preparation was followed for these panels. The thickness levels of the catalyzed Sermetel coatings are also presented in Table I. Scotchbrite was used to smooth out the rough interfaces between the Sermetel and the IVDA.

The repair areas of panels A1-A3 were painted with Alseal 518 aluminum paint. Panels S1-S9 were repaired by painting with Sermetel 249. The panels repaired with Sermetel 249 and Alseal 518 were left to cure to room temperature for 24 hours. Brush alodine was then applied to the areas of panels repaired with Alseal 518 and Sermetel 249, and the panels were allowed to dry for a minimum of one hour.

Panels BC1-BC4 were brush cadmium plated using certified Dalic 2023 cadmium solution. Before brush cadmium plating any repair areas, various cleaning methods were tested, including wiping with methyl ethyl ketone, scuffing with Scotchbrite, and reverse etching with Dalic's etching and desmutting solution.

In addition, panels S5, S6, BC4, and P1-P4 were primed with one coat of MMS 425 primer, then coated with one layer of Products Research and Chemical Corporation's PR 1436-G sealant (approved per MIL-S-81733), then given two coats of MMS 420 polyurethane enamel (MMS 420).

For panels CP1-CP10, Sermetel 249 was used as a repair method along with the Sermetel 273 catalyst. On the areas to be repaired, the Sermetel 249 was first painted and left to dry for one-half hour. The Sermetel 273 catalyst was then painted directly over the Sermetel 249; this catalyst was allowed to set for one hour, and then was rinsed off the panel using deionized water. To these panels, one coat of primer (MMS 425) and two coats of polyurethane enamel (MMS 420) was applied.

Panels D1, D2, and D3 were repaired using Dow Corning's 1-2577 silicone resin conformal coating. This coating was simply brushed over the repair area allowed to cure at room temperature for five days. An attempt was made to apply primer (MMS 425) to panels D2 and D3, but this primer would not adhere to silicon coating. On all painted panels, a diagonal line was scribed down to the base metal by using a X-Acto knife.

All panels were subjected to salt spray testing at CPC's plating facility for a period of four weeks (672 hours). The results were recorded and the appearances reported in Table I.

Adhesion testing was performed on panels painted with Sermetel 249 by bending the panels over a 90° radius mandrel. The results are shown in Table II.

TABLE 2

RESULTS OF ADHESION TESTS

NO.	METHOD OF TREATMENT	AVERAGE THICKNESS OF COATING IN MILS	BEND TEST RESULTS
ST1	Sermetel 249	1.7	Passed
ST2	Sermetel 249	0.9	Passed

DISCUSSION

Alseal 518 (room temperature cured)

Twenty-four (24) hours after the Alseal 518 had been applied to the IVDA coated panels, it was noted that the surface of this coating appeared to be dry. However, when an attempt was made to brush alodine the repair areas, the Alseal coating flowed freely. Thus, room temperature is not sufficiently high for curing the Alseal coating. No further testing could be performed on these panels as the Alseal did not cure. Obviously, uncured Alseal 518 could not be employed to repair IVDA coated surfaces.

Sermetel 249

The Sermetel 249 was the easiest repair coating to apply. Also, this coating did fully cure after 24 hours. After four (4) weeks in the salt spray chamber, no evidence of any red or white corrosion product was noted on the surfaces of the IVDA coated panels which were repaired with Sermetel. Some dark stains and discoloration was noted at the interface between the Sermetel and the IVDA. These stains were visible in the salt spray chamber as early as 216 hours. Figures 1 and 2 illustrate this staining characteristic. The stains appear more severe in panel S9 (Figure 2) which was coated with 2.7 mils of Sermetel, compared to those on the surface of S1 which was coated with 6.0 mils of Sermetel. The cause of the staining could not be exactly determined. However, no evidence of corrosion was present in any of the stained areas. Specimen S4 which had 0.8 mils of Sermetel 249 exhibited no evidence of corrosion. As a result, a minimum coating thickness of 0.8 mils is recommended for repair.

In the areas in which the Sermetel came in contact with the IVDA, the Sermetel flaked off. On panel S5 which had been repaired with Sermetel and on which primer, sealant, and paint had been applied, bubbling occurred in the paint in areas where there was a rough interface between the Sermetel and the IVDA. This paint bubbling is clearly illustrated in Figure 3. In certain areas in which bubbles had formed in the paint on panel S6, the paint was removed by using either an X-Acto knife locally or swabbing areas with Turco paint stripper. The removal of paint from the bubbled areas did not reveal the presence of any red corrosion product on the surface of the steel, as illustrated in Figure 6. Panel S6 was also repaired using Sermetel and coated with primer, sealant, and paint. No signs of bubbling were noted at the interface between the repaired area and the IVDA. (See Figure 4.) It appeared that the bubbling in the paint formed most often when the transition area between the Sermetel and the IVDA was rough. However, in order for the Sermetel to be effectively utilized as repair method, the interfacial areas must be blended in smoothly using an abrasive, such as Scotchbrite.

Panels ST1 and ST2, which had been painted with Sermetel 249, and were subjected to bend testing, exhibited no evidence of flaking or chipping of the Sermetel as reported in Table II. The coating remained completely intact upon bending 90^{o} over a mandrel.

On those panels on which catalyzed Sermetel had been applied, namely CP1-CP10, no evidence of any red rust had been found after four weeks of salt spray testing. A small amount of bubbling had been noted in the paint in areas where the Sermetel - IVDA interface was rough. The majority of the panels displayed that the smoothing of the Sermetel - IVDA interface by using Scotchbrite greatly minimized the formation of paint bubbles. Figure 7 illustrates the changes in the painted surface of panel CP9 after four weeks of salt spray testing. In this figure it can be seen that at the edges, some bubbling had occurred in the paint. For panel CP8, shown in Figure 8, no bubbling had been noted in the paint. Again, the occurrence of the bubbling in the paint appears to be related to the surface texture of the Sermetel - IVDA interface.

Although it appears that rough surface textures is a possible cause of the paint bubbling on the panels repaired with Sermetel, it has not been firmly established as the <u>only</u> source of the bubbling. The questions of the bubbling in the paint is being further addressed through additional testing of panels which were coated with IVDA and repaired with Sermetel. The prevention is critical because the majority of parts which would be repaired with Sermetel would then be coated with primer and paint. CPC is directing future investigative efforts toward determining the primary cause(s) of the bubbling which occurs in the paint on panels which had been repaired with Sermetel.

Dow Corning 1-2577 Conformal Coating

When applied by itself with no additional coatings such as primer or paint, Dow Corning's 1-2577 conformal coating served as a satisfactory means of corrosion protection, as evidenced by the performance of panel D1 in the salt spray test (ref. Table I). After four weeks of salt spray testing, no corrosion had been noted on this panel. However, when an attempt was made to apply primer to this coating on panels D2 and D3, it was found that the primer would not adhere to the silicon coating. When the question of improving paint adhesion was referred to the Product Information Center of Dow Corning, it was indicated by Dow Corning that there was probably no practical means of promoting adhesion of the primer to the silicon coating (2). The 1-2577 was originally intended for use as an insulating compound for coating printed circuit board assemblies.

Brush Cadmium

Brush cadmium plating using the Dalic solution proved to be a feasible alternate repair method, but was not the easiest in terms of application. During plating it was noted that if the stylus came in contact with the IVDA coating just past the steel - IVDA interface, the brush cadmium plating solution would not transfer to the steel area to be repaired. In such cases it was necessary to repeat the cleaning procedure, change the stylus cover and begin brush plating again, taking caution not to allow the stylus to come in contact with the IVDA. The presence of dark stains was also noted at the interfaces between the brush cadmium plate and IVDA surfaces as seen in Figure 5 for sample BC3. Again, no evidence of any corrosion product was visible on the surface of the brush cadmium plated panels, regardless of the cleaning method applied.

Primer/Sealant/Paint

Panels P1-P4, on which only primer, sealant, and paint were applied as a means of repair, did not display any significant corrosion problems. On panel P3 some small pinpoints of corrosion product were noted through the paint in areas away from the repaired areas and the scratch, but these were minimal.

CONCLUSIONS

The following conclusions may be drawn from this study:

1) The Alseal 518 did not cure at room temperature; thus it cannot be used as a method of repairing IVDA coating surfaces.

2) The Dow Corning 1-2577 silicone coating cannot be used as a repair method as primer and paint would not adhere to this coating.

3) The other three (3) repair methods which were tested, namely, Sermetel 249, brush cadmium plating using the Dalic 2023 solution, and the application of primer, sealant, and paint, offered satisfactory corrosion resistance as displayed by repaired panels which were subjected to four (4) weeks of salt spray testing.

4) Of the three (3) possible repair methods, the Sermetel 249 used with the Sermetel 273 catalyst displayed the greatest advantages in that it is relatively easy to apply, requires few tools or materials, cures at room temperature, and offers excellent salt spray corrosion resistance.

5) For Sermetel 249 to be a feasible repair coating the interfaces between the Sermetel and IVDA must be blended in carefully to prevent the formation of bubbles in the paint.

FOOTNOTES

1) Telecon Between C. L. Martuch (Cleveland Pneumatic Company and J. Reilly (McAir), 6/9/87.

2) Telecon between C. L. Martuch (Cleveland Pneumatic Company) and G. Congdon (Dow Corning), 11/4/87.

FIGURE 1, SAMPLE S1

REPAIRED WITH 6.0 MILS
OF SERMETEL 249
DISPLAYS BLACK INTERFACIAL STAINS
AFTER 240 HOURS OF SALT SPRAY
TESTING.
NO CORROSION PRODUCT IS VISIBLE
(1X)

FIGURE 2, SAMPLE S9

REPAIRED WITH 2.7 MILS
OF SERMETEL 249
DISPLAYS HEAVY BLACK INTERFACIAL
STAINS WHICH WERE FIRST PRESENT
AFTER 288 HOURS OF SALT SPRAY
TESTING.
NO CORROSION PRODUCT IS VISIBLE
(1X)

FIGURE 3, SAMPLE S5

RPAIRED WITH 2.3 MILS
OF SERMETEL 249, AND COATED WITH
PRIMER, SEALANT, AND PAINT,
DISPLAYS BUBBLING IN PAINT
AFTER 288 HOURS OF SALT SPRAY
TESTING DUE TO ROUGH SERMETEL -
IVDA INTERFACE
(1X)

FIGURE 4, SAMPLE S6

REPAIRED WITH 0.8 MILS
OF SERMETEL 249, AND COATED WITH
PRIMER, SEALANT, AND PAINT,
DISPLAYS LESS BUBBLING IN THE
PAINT AS THE IVDA - SERMETEL
INTERFACE WAS SMOOTH
(1X)

FIGURE 5, SAMPLE BC3

REPAIRED WITH 0.6 MILS
OF DALIC BRUSH CADMIUM PLATING
DISPLAYS STAINS AT THE IVDA -
BRUSH CAD INTERFACE. NO CORROSION
PRODUCT IS VISIBLE
(1X)

FIGURE 6

REMOVAL OF PAINT FROM AREAS IN
WHICH BUBBLES HAD FORMED IN PAINT
ON SAMPLE S5 WHICH HAD BEEN
REPAIRED WITH SERMETEL,
PRIMER, AND PAINT.
NO EVIDENCE OF ANY CORROSION
PRODUCT HAD BEEN NOTED UNDER
THE PAINT BUBBLES
(5X)

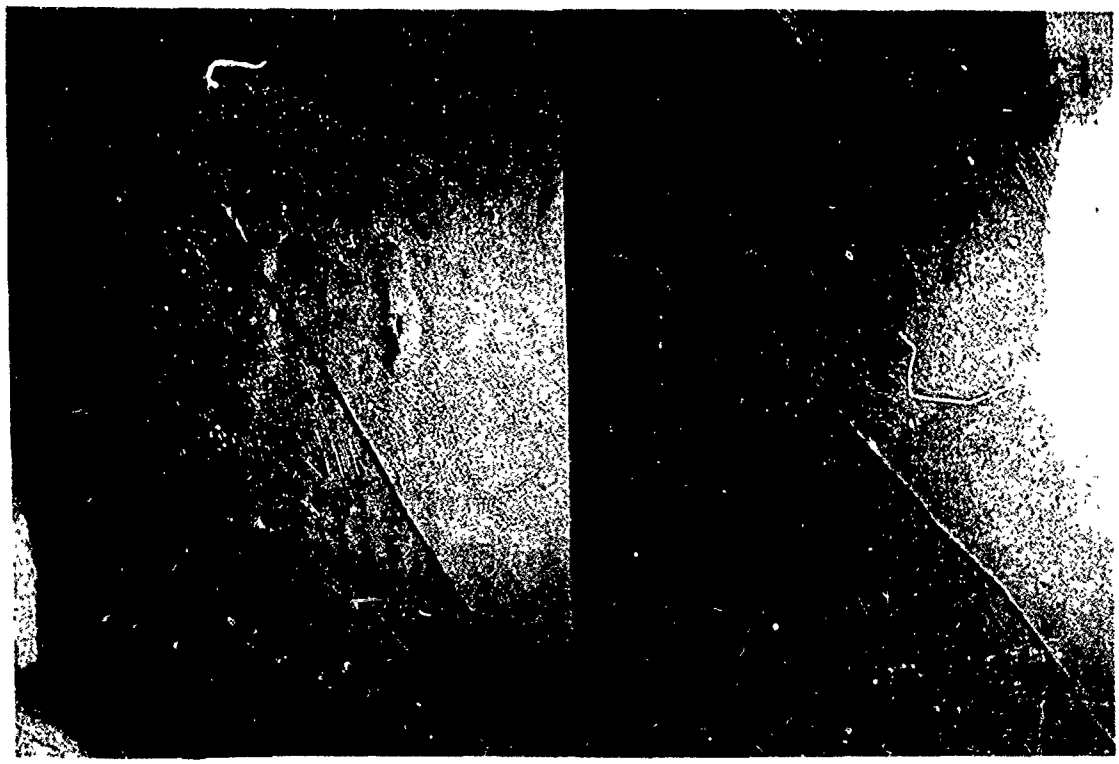

FIGURE 7, SAMPLE CP5

REQUIRED WITH 1.0 MILS OF SERMETEL 249 & 273 CATALYST; INTERFACIAL EDGES SMOOTHED OUT WITH SCOTCHBRITE SMALL AMOUNT OF BUBBLING NOTED AT INTERFACE AFTER 280 HOURS IN SALT SPRAY CABINET (1X)

FIGURE 8, SAMPLE CP8

REPAIRED WITH 0.9 MILS OF SERMETEL 249 & 273 CATALYST; INTERFACIAL EDGES SMOOTHED OUT WITH SCOTCHBRITE NO BUBBLING NOTED IN PAINT AFTER 672 HOURS IN SALT SPRAY CABINET (1X)

POLYACRYLIC ACID-MODIFIED ZINC PHOSPHATE CONVERSION COATINGS FOR CORROSION PROTECTION OF STEEL

T. Sugama, L. E. Kukacka, and N. Carciello
Department of Applied Science
Process Sciences Division
Brookhaven National Laboratory
Upton, New York 11793

Polyacrylic acid, p(AA), electrolyte macromolecules diffused into crystalline zinc phosphate (Zn•Ph) conversion coatings that are precipitated onto cold-rolled steel by dissolution-recrystallization processes, enhance the corrosion protection of steel. One of the specific subserviences was that, when the NaOH-dissolution of Zn•Ph is considered, the Zn-OOC electrostatic bonds at p(AA)-Zn•Ph interfaces are transformed into $Na^{+-}OOC$ ionic bonds which associate with the salt complexed macromolecules. Another is the intermolecular chemical reactions between p(AA) and polymeric topcoats. These contributions relate directly to a lower cathodic delamination rate.

INTRODUCTION

Insoluble crystalline zinc phosphate (Zn•Ph) conversion coatings can be produced on steel surfaces by immersing the surface-cleaned steel substrate into a phosphating solution containing three components, zinc orthophosphate dihydrate [$Zn_3(PO_4)_2 \cdot 2H_2O$], H_3PO_4, and water. The major phase in the conversion coating derived from this simple phosphating solution is the same zinc phosphate dihydrate as that used in the converting solution. This suggests that the conversion to the Zn•Ph occurs through a dissolution-recrystallization process of the original $Zn_3(PO_4)_2 \cdot 2H_2O$ powders. As a result, all of the conversion coatings which are discussed in this paper were prepared using the above process.

When cold-rolled steel surfaces are treated with zinc phosphating solutions containing polyelectrolyte macromolecules having proton-donating type pendant groups such as carboxylic acid or sulfonic acid, several corrosion protective benefits are accrued. The positive surface sites of phosphate crystal embryos at the beginning of the precipitation of Zn•Ph conversion coatings on the steel surface are strongly chemisorbed by the anionically charged segments of the polyelectrolytes.[1-3] This segmental chemisorption of polyanions either on newly precipitated nuclei or on growth sites during the primary crystallization processes, not only acts to array a uniformly packed fine crystal morphology brought about by the suppression and delay of the crystal growth, but also

significantly improves the stiffness and ductility characteristics of the normally brittle Zn•Ph layer. Enhancement of adhesion with subsequent polymeric finishers is also obtained. The latter relates directly with the chemical bonds formed at the interface between the functional organic species such as ionic carboxylate and carboxylic acid groups existing at the outer-most surface sites of the conversion coating and the polymeric topcoats.

On the other hand, Leidheiser, et al.[4] have reported that cathodic delamination of polymeric coatings from zinc phosphated steel surfaces is due mainly to alkaline dissolution of the phosphate coating. This is caused by the hydroxyl ions generated by oxygen reduction reactions, $H_2O + 1/2\ O_2 + 2\ e^- = 2\ OH^-$, and the migration of alkali metal cations through the topcoat to the reaction zone for charge balance. Thus, it has been demonstrated that the sodium hydroxide solution dissociates a larger amount of zinc and phosphate ions from the Zn•Ph coating surfaces. Since the OH^- ions which cause delamination at paint/Zn•Ph interfaces form at pores and defects in the Zn•Ph layers, the formation of highly dense, thick, and low porosity conversion coatings should yield inherently slow oxygen reduction kinetics.

Therefore, studies were conducted to explore the effects of polyacrylic acid [p(AA)] polyelectrolyte macromolecules when they are internally diffused throughout the crystalline Zn•Ph, and on the degree of the alkaline dissolution of coatings. Cathodic delamination studies for polyester-modified polyurethane (PU)-coated Zn•Ph specimens were also performed to determine the role of the intermolecular chemical reaction at PU modified Zn•Ph interfaces in reducing the delamination rates of the PU topcoat from the Zn•Ph.

RESULTS AND DISCUSSION

In order to investigate the ability of p(AA)-chemisorbed conversion coatings to provide corrosion protection to steel, p(AA) macromolecules at concentrations of up to 5 wt% were incorporated into a convertible solution consisting of 1.3 wt% $Zn_3(PO_4)_2 \cdot 2H_2O$, 2.7 wt% H_3PO_4 and 96.0 wt% water. Figure 1 shows SEM microtexture views and associated EDX data for the unmodified, and 1 and 2% p(AA)-modified conversion coatings. It is evident from comparisons of the topographical features of the crystals precipitated on the steel surfaces, that the addition of p(AA) serves to decrease the crystal size. This is due primarily to the chemisorption of p(AA) on the precipitated crystal nuclei faces at the beginning of recrystallization processes, thereby suppressing the crystal growth.[3] The accompanying EDX data indicate that the Fe/Zn ratios for the conversion coatings increase with increased p(AA) concentration. Since the only source of Fe is the steel, the extent of suppression of crystal growth by the p(AA) relates directly to the precipitation rate of iron-rich phosphate compounds. At a 5% p(AA) concentration, a further increase in the Fe/Zn ratio was obtained (not shown in figure). The surface morphological image shows two discriminable crystal phases: one is that of a reticular crystal network and the other is the plate-like crystal network. From the EDX quantitative evaluation, the former is associated with the Fe-rich phosphate crystalline coatings and the latter is from the Zn-rich phosphate compounds. The identification of these different phosphate phases was made using x-ray powder diffraction (XRD) with CuKα radiation at 50 KV and 16 mA.

As a result, for the 2% p(AA) samples, all of prominent spacing lines in the XRD pattern ascribe to zinc phosphate dihydrate [$Zn_3(PO_4)_2 \cdot 2H_2O$], which is representative of the recrystallization of the starting material dissolved in the phosphating solution.[5] In contrast, the XRD pattern for the 5.0% p(AA) sample has two new spacings at 0.311 and 0.437 nm. These spacings reveal the presence of strengite ($FePO_4 \cdot 2H_2O$).[6] Therefore, the Fe-rich reticular and Zn-rich plate-like crystals which were observed by SEM-EDX analyses, are associated with the formation of $FePO_4 \cdot 2H_2O$ and $Zn_3(PO_4)_2 \cdot 2H_2O$ phases, respectively.

This results in the production of thinner conversion coatings containing a high proportion of ferric phosphate compounds. Thus, the coating thickness and iron content appears to depend on the amount of p(AA). Experimentally, the measured thicknesses for coatings containing 0, 1, 2 and 5% p(AA) were approximately 30, 28, 25 and 20 μm, respectively.

Efforts were made to determine how the proportions of Fe existing in the conversion layers participate in the corrosion protection process. To obtain this information, the polarization behavior of p(AA)-modified conversion specimens in an aerated 0.5M NaCl solution was determined, and the resultant polarization curves were correlated as a function of EDX Fe/Zn ratios for various p(AA) concentrations. These results are given in Figure 2. A comparison of the cathodic polarization areas from the unmodified Zn•Ph and p(AA)-modified Zn•Ph specimens indicates two noteworthy features: (1) the short-term steady-state current value for the modified specimens is lower than that for the unmodified one in the potential region between -1.0 and -1.1 v, and (2) the incorporation of 5% p(AA) resulted in a shift in corrosion potential to a more negative site and an increase in current density at the potential axis. The lower current density for the modified specimens (result No.1 above) compared to that of the specimen without p(AA), is attributed to a low hydrogen reduction as well as to a less active surface. This confirms that the oxygen reduction reaction is inhibited by the p(AA) macromolecule chemisorbed on the crystal faces. With regards to the second observation, the introduction of 5% p(AA) into the conversion layer seemed to reduce the corrosion-resistive effectiveness. From this observation and the previously discussed SEM-EDX data, it can be concluded that the presence of agglomerated strengite in the $Zn_3(PO_4)_2 \cdot 2H_2O$ layer results in an increase in intrinsic phosphate porosity, thereby giving poor corrosion protection.

Another important goal of our work was to obtain knowledge regarding possible interactions between p(AA) and the crystal conversion coating, and then to understand how the interfacial reaction products act to increase the corrosion resistance of Zn•Ph-coated steel. The former was investigated by means of XPS, and it was observed that even when a high concentration of 5% p(AA) was used, the p(AA) film deposited at the outermost surface sites was thin enough to see the photoemission signal from the underlying Zn- and Fe- phosphate compounds. The binding energy (BE) scale in the XPS spectra was calibrated with the C_{1s} of the principal hydrocarbon, "CH_n", peak fixed at 285.0 eV as an internal reference standard.

The C_{1s} core level photoemission spectra for bulk p(AA), and 1% p(AA)- and 5% p(AA)- modified conversion coating surfaces are shown in Figure 3. The C_{1s} region of the bulk p(AA) (Figure 3-a) has two main peaks; 285.0 eV corresponds

to the hydrocarbons in the main chain and 288.9 eV ascribes to the carbon originating from the carboxylic acid, COOH, in the p(AA). The spectrum for the 5% p(AA)-modified coating (Figure 3-b) shows a shift in the peak to a lower BE site and the appearance of a new peak at 287.2 eV, as compared to that of the bulk p(AA). The new peak emerging at about 1.7 eV lower BE from the COOH peak, is located between a carbonyl carbon, C=O, at approximately 288.0 eV and a carbon-oxygen single bond at approximately 286.5 eV.[7] For samples containing 1% p(AA) (Figure 3-c), a further shift in the COOH peak toward lower BE was observed.

Figure 4 shows typical 2p doublet separation spectra for the Zn2p3/2 and 2p1/2 lines from unmodified and modified conversion coatings. The distance separating the 2p3/2 and the 2p1/2 energies for both the unmodified and modified coatings is in the range of 23.7 to 23.5 eV. This means that the presence of p(AA) in the conversion coatings does not change the separation distance. Therefore, these peaks appear to be assigned to zinc originating from the zinc phosphate dihydrate crystal. The main difference between these spectra is the shift of the 2p3/2 and 2p1/2 peaks to higher energy sites when the p(AA) content is reduced. For 5% and 1% p(AA) concentrations, the values of 1022.5 eV (Figure 4-e) and 1022.9 eV (Figure 4-f) for the 2p3/2 core level correspond to increases of 0.1 and 0.5 eV, respectively, compared to unmodified coatings. The reason for the increased Zn2p peak energy, the decrease in BE of the COOH carbon, and the new peak at 287.2 eV for the C_{1s} region, may be charge transfer from the Zn in the crystal coating to the electron accepting oxygen portion in the functional pendent group of p(AA). In fact, the O_{1s} core level (not shown) at the p(AA)/Zn•Ph interfaces indicated the presence of a strong peak at 531.4 eV which ascribes to the formation of COO-metal complexes. Two possible Zn-O bond formations for carboxylate-linked Zn complexes yielded through a mechanism involving charge transfer reactions at p(AA)-Zn•Ph interfaces are discussed below.

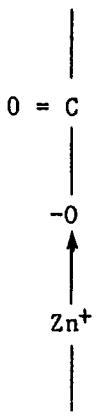

(I)

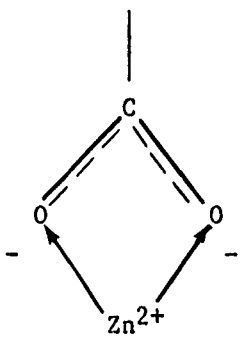

(II)

One of the complex formations is a zinc-oxygen-carbon (Zn-O-C) bond structure (I) which is produced by the reaction of an oxygen atom in the carboxylic anion with a Zn atom. The other (II) may be formed by a charge transferring interaction between both oxygens in the carboxylate group and the Zn atom. The latter

formation relates to the assignment of the new line at 287.2 eV which is situated between the C=O and the C-O bond peaks. It was found that the interfacial reaction products at the p(AA) - Zn•Ph interfaces are Zn-O-C complexes containing an electrostatic bond yielded through the charge transferring reaction.

The studies were extended further to investigate the influence of these interfacial complex products upon the alkali-dissolution of the conversion coatings. Table 1 indicates the changes in the EDX intensity ratios of P/Zn and Fe/Zn, and E_{corr}, as a function of p(AA) for phosphated steel specimens after exposure to a 0.1M NaOH solution for 1 hr at 25°C. As seen in the table, the P/Zn ratios for all exposed specimens are significantly lower than those for the unexposed specimens. All of the Fe/Zn ratios increased. The former suggests the dissociation of a greater amount of phosphate brought about by the alkaline dissolution of Zn•Ph. Thus, this seems to imply that interfacial reaction products composed of Zn-O-C complexes do not significantly inhibit the alkali-dissolution of conversion coatings. However, the differences in Fe/Zn ratios compared with those from the unexposed samples decreased significantly with increased p(AA) concentrations, thereby suggesting that p(AA) macromolecules diffused electrostatically onto Zn•Ph crystal faces act to decrease the rate of ferrous ion dissociation from the steel.

The E_{corr} values for specimens after exposure to NaOH were determined from the polarization curves in aerated 0.5M NaCl solutions. To investigate the variation in Na atom percentages as a function of p(AA), the surfaces of the exposed specimens were also examined using XPS. As noted in Table 1, the E_{corr} values for all the exposed specimens containing p(AA) shifted to less negative positions, as compared to those for the unexposed ones. The largest shift was observed for specimens modified with 5% p(AA). Figure 5 gives comparisons between the C_{1s} spectrum features of 1% p(AA)-modified Zn•Ph before (Figure 5-j) and after (Figure 5-k) exposure to NaOH solutions. The most striking features in the spectrum of the exposed samples were the shift in

$$-\underset{\underset{\|}{O}}{C}-O-$$

the carboxyl carbon, peak to a higher BE site, and a decrease in intensity of the peak at 287.2 eV, while maintaining the same position of hydrocarbons at 285.0 eV. In conjunction with the increase of 0.3 eV in the BE of carboxyl carbon, there was a corresponding decrease in the BE in the Zn2p3/2 region for the sample subjected to NaOH exposure (see Figure 6-m), as compared with that of the unexposed sample (Figure 6-l). The excitation of the new line at 1020.4 eV for the exposed samples is assigned to the formation of new Zn-based compounds brought about by the alkali-dissolution of the conversion coating. This seems to suggest that during the exposure to the NaOH solution, Na ions act to promote the breakage of the Zn-OOC electrostatic bonds. The breakage may be related to an elemental substitution of Zn for Na. However, the corresponding Na_{1s} core level spectra have not yet been clearly resolved because of a very noisy exciting peak feature.

On the basis of the above information, the following statements can be made regarding the function of p(AA) in reducing the dissociation of Fe and improving the protection of the conversion coatings when subjected to NaOH. When the p(AA)-modified conversion coatings come in contact with a NaOH solution, the reactive Na^+ ion will break the Zn-OOC electrostatic bonds in the interfacial

reaction products to form a $-COO^- Na^+$ salt complex which contains an ionic bond. This transformation from a Zn-O electrostatic bond to a Na-O ionic bond can be expressed as follows:

$$-COO-Zn- + 2NaOH \longrightarrow -COO^- Na^+ + NaO-Zn- + H_2O$$

It can therefore be assumed that the precipitation of a salt complexed macromolecule formed by an ionic reaction between the carboxylic anion and the Na^+ cation during the progression of the alkaline dissolution of the conversion layers can serve as a barrier to the ferrous ion dissociation from the steel. This reflects on the corrosion resistance of the steel.

The effect of p(AA) macromolecules existing at the outermost surface sites of the modified Zn•Ph coatings on the resistance to the cathodic delamination of the polymeric topcoat from the Zn•Ph, was also investigated. In these studies, a polyester-modified polyurethane (PU) topcoat was applied to modified Zn•Ph specimens. The cathodic delamination tests for the PU-coated Zn•Ph specimens were conducted in an air covered 0.5M NaCl solution using an applied potential of -1.5 volts vs SCE for up to 6 days. A defect was made using a drill bit with a diameter of approximately 1 mm. After exposure, the specimens were removed from the cell and allowed to dry. The PU coating was removed by cutting, and a delaminated region which appeared as a light gray area adjacent to the defect, was detected. These test results are reported in Table 2. The PU to-blank steel joint systems exhibited considerable delamination of the PU after exposure for only one day. In contrast, the presence of a conversion coating as an intermediate layer in the PU/steel joint system significantly reduced the rate of cathodic delamination. Further improvement was obtained using the p(AA)-modified conversion coating systems. As seen in table, the delamination rates for the 6 day-exposed specimens decrease with increased p(AA) concentrations ranging from 1 to 5%.

In the PU/p(AA)-modified coating joint systems, the major reason for reducing the rate of delamination is the intermolecular chemical reactions between the carboxylic acid groups of p(AA) existing at the outermost surface sites of the conversion coating and the isocyanate groups of PU. The interfacial reaction product formed through the interaction mechanism given below could result in a lower susceptibility to hydrolysis of the particular isocyanate which is essentially hyrolyzed to substitute the primary amine in the presence of NaOH.[8,9]

$$-R-NCO + HOOC-R- \longrightarrow -R-NH-CO-O-CO-R- \longrightarrow -R-NH-CO-R- + CO_2$$

The above statements suggest that the initial failure in this joint system occurs at the conversion coating/steel interface, in contrast with the PU/conversion coating interfacial regions for the PU-unmodified coating joint systems.

CONCLUSIONS

The following generalizations can be drawn from our results.

1. The precipitation of a dense crystalline conversion coating on cold-rolled steel by a dissolution-recrystallization process using zinc orthophosphate dihydrate as a starting material, considerably reduced the corrosion rate of steel in an aerated NaCl solution.

2. When modified with p(AA) electrolyte macromolecules, the conversion coatings yield low hydrogen evolution as well as a less active surface.

3. The precipitation of a large amount of strengite, $FePO_4 \cdot 2H_2O$, formed by adding an excessive amount of p(AA), seems to result in a less effective protective coating.

4. The interfacial reaction products at the p(AA)-zinc phosphate interfaces, were identified to be Zn-OOC complexes yielded by a charge transfer reaction between Zn atoms in the crystalline conversion coating and the electron accepting oxygen portions of the p(AA).

5. The resultant Zn-O electrostatic interfacial bond had no significant effect on the rate of alkaline dissolution of conversion coatings subjected to NaOH exposure, because of the breakage of the Zn-O bond by the attack of reactive Na^+.

6. The formation of $-COO^- Na^+$ salt complexed macromolecules precipitated by transformation of Zn-O electrostatic bonds into Na-O ionic bonds are subservient to the corrosion resistance of steel.

7. The intermolecular chemical reaction between the carboxylic groups of the p(AA) existing at the outermost surface sites of the conversion coating and the isocyanate groups in polyurethane topcoats led to a lower rate of cathodic delamination of the polyurethane film from the substrate. Thus, the beginning of the delamination failure occurs through the conversion coating/steel interface, as compared to that at the polyurethane/conversion coating interface in the polyurethane unmodified coating joint system.

REFERENCES

1. Sugama, T., Kukacka, L.E., Carciello, N., and Warren, B., "Polyacrylic Acid Macromolecule - Complexed Zinc Phosphate Crystal Conversion Coatings," J. Appl. Polymer Sci., 30, 4357 (1985).

2. Sugama, T., Kukacka, L.E., Carciello, N., and Warren, B., "Factors Affecting Improvement in the Flexural Modulus of Polyacrylic Acid-Modified Crystalline Films," J. Appl. Polymer Sci., 32, 3469 (1986).

3. Sugama, T., Kukacka, L.E., Carciello, N., and Warren, B., "Chemisorption Mechanism and Effect of Polyacrylic Acid on the Improvement in Bond Durability of Zinc Phosphate-to-Polymer Adhesive Joints," J. Mater. Sci., 22, 722 (1987).

4. Sommer, A. J. and Leidheiser, H. Jr., "Effect of Alkali Metal Hydroxides on the Dissolution Behavior of a Zinc Phosphate Conversion Coating on Steel and Pertinence to Cathodic Delamination," Corrosion, 43, 661 (1987).

5. Joint Committee on Powder Diffraction Standards, Card 30-1491.

6. Joint Committee on Powder Diffraction Standards, Card 33-667.

7. Bartha, J.W., Hahn, P.O., LeGoues, F., and Ho, P.S., "Photoemission Spectroscopy Study of Aluminum - Polyimide Interface," J. Vac. Sci. Technol., 3, 1390 (1985).

8. Sugama, T., Kukacka, L.E., Clayton, C.R., and Hua, H.C., "Effects of Polyacrylic Acid Primers on Adhesion and Durability of FPL-Etched Aluminum/Polyurethane Systems," J. Adhesion Sci. Tech. 1, 265 (1987).

9. Arnold, R.G., Nelson, J.A., and Verbanc, J.J., "Chemistry of Organic Isocyanates," p. 13. E.I. duPont de Nemours, Wilmington, DE (1956).

Table 1. Variations in P/Zn and Fe/Zn Intensity Count Ratios and Corrosion Potential Values, E_{corr}, as a Function of p(AA) Concentration for Phosphated Steel Specimens After Exposure to 0.1M NaOH Solution.

PAA,	Before Exposure			After Exposure		
%	P/Zn	Fe/Zn	E_{corr}, Volt	P/Zn (Difference*)	Fe/Zn (Difference)	E_{corr}, Volt
0	0.55	0.49	-0.592	0.26 (-52.7%)	0.72 (+46.9%)	-0.620
1	0.54	0.56	-0.595	0.24 (-55.6%)	0.75 (+33.9%)	-0.540
2	0.57	0.60	-0.610	0.23 (-59.7%)	0.79 (+31.7%)	-0.521
5	0.55	0.74	-0.651	0.25 (-54.6%)	0.89 (+20.3%)	-0.480

*Difference compared with that of unexposed specimen; difference, % = [(ratio of exposed specimen - ratio of unexposed specimen)/ratio of unexposed one] x 100.

Table 2. Comparison Between the Delaminated Areas of Polyurethane-Coated Steel, Unmodified Zn•Ph, and p(AA)-Modified Zn•Ph Panels Exposed to 0.5M NaCl Solution.

p(AA), %	Delaminated Area, mm^2		
	1 Day	3 Day	6 Day
PU/Steel Joint	113	1256	---
0	0.8	4.9	19.6
1	0.2	2.5	10.8
2	0.2	0.9	7.1
5	0.2	0.9	4.9

P(AA): 0%

Element	Intensity Counts/100 sec.	Intensity ratio/Zn
Fe	18134	0.49
Zn	36843	1.00
P	20107	0.55

a

P(AA): 1.0%

Element	Intensity Counts/100 sec.	Intensity ratio/Zn
Fe	19068	0.56
Zn	34050	1.00
P	18387	0.54

b

P(AA): 2.0%

Element	Intensity Counts/100 sec.	Intensity ratio/Zn
Fe	18368	0.60
Zn	30611	1.00
P	17295	0.57

c

Figure 1. SEM photographs and associated EDX data for unmodified and p(AA)-modified conversion coatings.

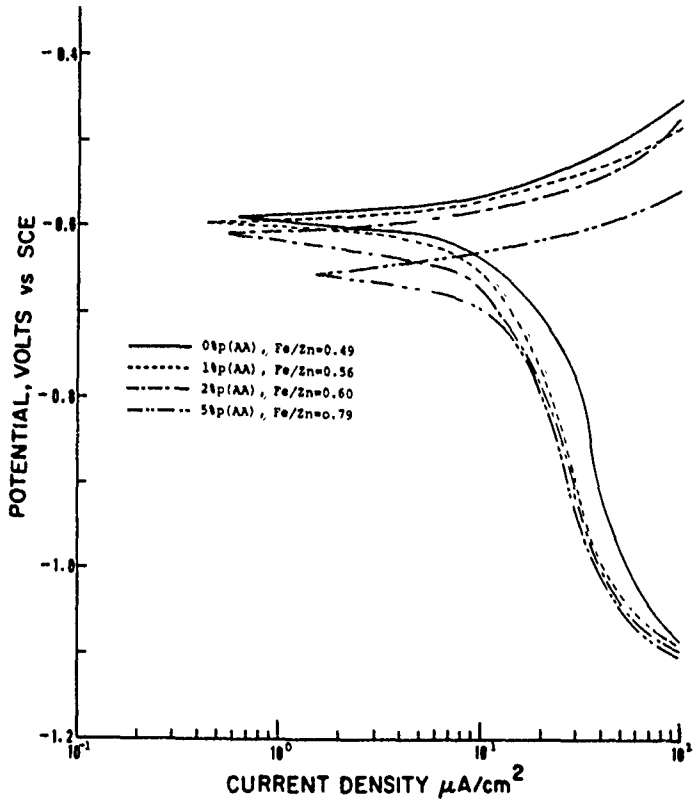

Figure 2. Polarization curves for zinc phosphated steel specimens containing p(AA) concentrations of up to 5% in aerated 0.5M NaCl solutions.

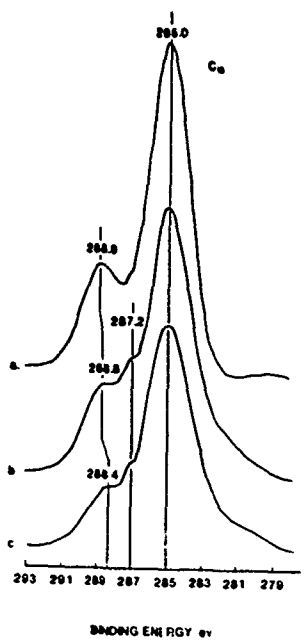

Figure 3. C_{1s} spectra for bulk p(AA) (a), 5% p(AA)-Zn·Ph interface, (b) and 1% p(AA)-Zn·Ph interface (c).

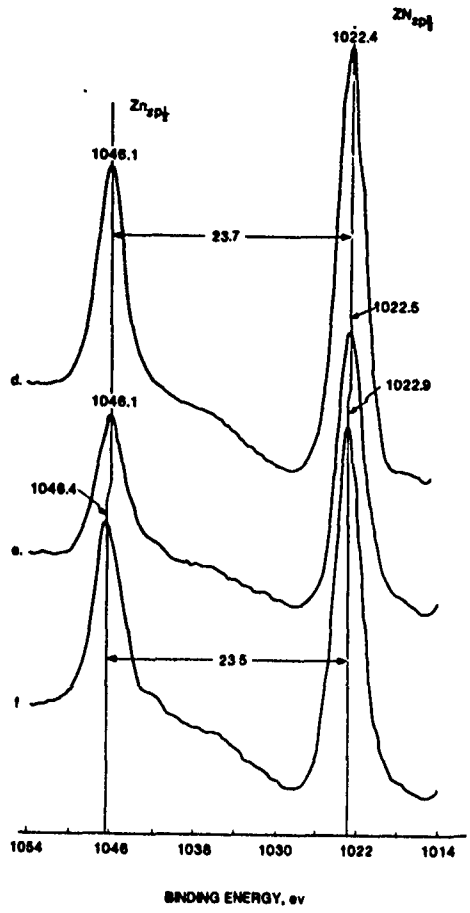

Figure 4. Zn2p separation spectra for unmodified Zn•Ph (d), 5% p(AA)-modified (e) and 1% p(AA)-modified Zn•Ph (f).

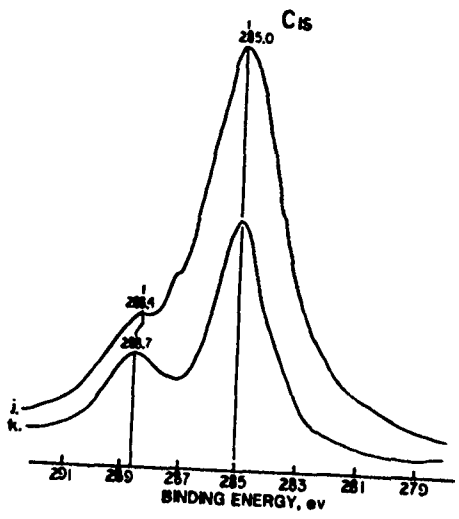

Figure 5. C_{1s} spectra for 1% p(AA)-modified Zn•Ph before (j) and after (k) exposure in 0.1M NaOH solution.

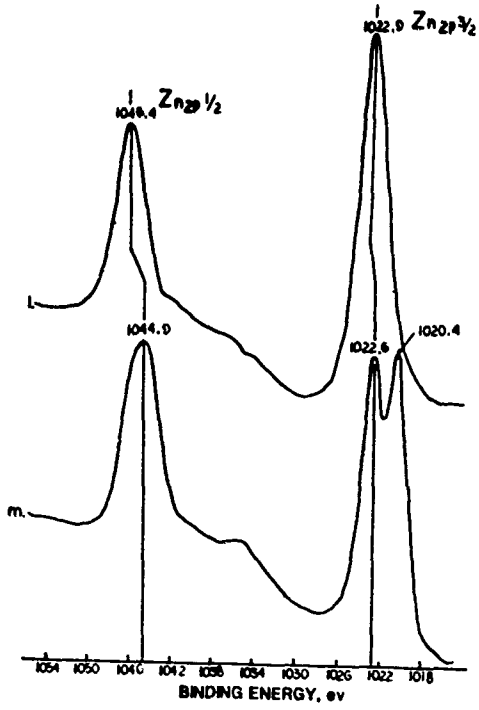

Figure 6. Zn2p regions for unexposed (l) and NaOH - exposed p(AA)-Zn•Ph (m).

A METHOD FOR LOW HYDROGEN EMBRITTLEMENT CADMIUM PLATING

R. Varma
SRI International
Menlo Park, CA
and
V. S. Agarwala
Naval Air Development Center
Warminster, PA

ABSTRACT

The conventional (direct current) electroplating introduces a high dose of hydrogen in the plated parts such as a high strength steel, which may cause embrittlement. Thus, a reverse pulse plating method was investigated using a fast cathodic pulse which was separated from the subsequent anodic and/or cathodic pulses with long rest periods. A fluoborate bath was used to produce silvery cadmium coating. In combination with laminar electrolyte flow system, the pulse method produced almost hydrogen-free, fine grain deposit of cadmium.

INTRODUCTION

In aerospace applications, high-strength steel components (such as landing gears, fasteners) may fail mechanically prematurely (1,2) during service from the conjoint action of stress and hydrogen-embrittlement. Corrosion of steel is concomitant with production of hydrogen which may diffuse into the bulk of steel and cause embrittlement. Electrodepositing of cadmium onto steel components as a sacrificial coating is a conventional practice for corrosion protection in naval/marine environments. However, hydrogen is also codeposited with Cd during conventional electroplating and, therefore, is a cause for concern. Usually cadmium is electroplated from a cyanide bath [an aqueous solution prepared from $CdCO_3$, CdO, $Cd(CN)_2$, NaCN, and NaOH] in the industry (3).

Generally, electroplating is conducted with direct current, DC, at low current densities (e.g., 30 mA/cm^2) and for a long time. Most significantly, the cyanide plating invariably is accompanied by hydrogen codeposition which may be responsible for hydrogen embrittlement related failures of cadmium coated high strength steel components.

Cadmium plating from fluoborate electrolyte has been claimed to be less prone (4) to result in hydrogen codeposition. In a recent study Varma and Vargas (5) have emphasized a need to control the electrodeposition overpotential during the initial stage of film growth to avoid hydrogen codeposition. Study on high-rate electrodeposition of cadmium from cadmium fluoborate solution, using pulse currents and forced electrolyte-convection, provided preliminary indications that less hydrogen was deposited. This paper reports the investigations, for the first time, of almost hydrogen-free electrodeposition of fine-grained cadmium on 300 M steel substrate from fluoborate electrolyte.

The important factors that control the rate of cadmium deposition and the quality of electrodeposits in plating are: (i) the overpotential (4) or the current density, (ii) mass-transport limitation for the cadmium ions in the electrolyte, (iii) the pH of the electrolyte and, (iv) the nature of the substrate surface. The electrochemical deposition of cadmium from aqueous fluoborate electrolyte is a diffusion controlled process, and the maximum rate for deposition is given by the limiting current density, i_{Dl}. In the DC mode it is given by the equation,

$$i_{Dl} = ZF [C_o / d] \quad (1)$$

where,
- z = number of electrons involved in the electroreduction step
- F = Faraday's Constant
- C_o = bulk concentration of cadmium ions

and
- d = diffusion layer thickness.

Here, the magnitude of i_{Dl} is limited by d or the limitation of Cd ions that are able to reach the cathode surface. However, in the pulse method, the use of high cathodic peak current pulses (- 0.5 to 1 A/cm^2) of short duration (< 0.5 ms) followed by sufficiently-long rest periods and/or anodic pulses provides a number of advantages. Cathodic peak pulse current (< pulse limiting current, iPl defined as the maximum pulse current density at which the surface concentration of the cadmium electroactive species reaches zero at the end of pulse) can be increased many fold in comparison to i_{Dl} with proper (short) choice of pulse durations to assure high deposition rates which result in finer grains.

For a short total pulse cycle period, T << 1 s, and simple cathodic-rest-cathodic pulse (Pulse A, see Figure 1) sequence the ratio i_{Pl} / i_{Dl} approaches the reciprocal of the duty cycle, 0, as given below:

$$[i_{Pl} / i_{Dl}] \xrightarrow[T << 1]{} [1/0] \quad (2)$$

where $T = t_{on} + t_{off}$ (3)

and $0 = [t_{on} / T]$ (4)

where t_{on}, and t_{off} are durations of cathodic pulse and rest periods. Use of cathodic pulse current at high-limiting values can become mass-transport limited. Forced convection of electrolyte has been utilized in this work to reduce the thickness of diffusion boundary layer, d. This is achieved by use of laminar/turbulent electrolyte flow past the steel coupon surface to result in high Reynold's number, Re, helpful in mass transport according to the relationship

$$d = [\ 1 / (Re)^{0.2}\ ] \qquad (5)$$

Recently Vargas and Varma (5) investigated the codeposition of hydrogen during the nucleation stage of cadmium electrodeposition. It was observed that the use of cathodic overpotentials (vs. SCE) of 200 mV or higher resulted in hydrogen deposition. The cathodic peak pulse currents of 0.7 A/cm^2 or lower may indeed give rise to overpotentials which do not exceed hydrogen deposition overvoltage, during the cadmium deposition.

EXPERIMENTAL

The electroplating set-up used for depositing thin coatings ($\sim$15 μm) of cadmium on 50 x 50 x 0.25 mm 300 M steel coupons is shown in Figure 1. The electrode assembly consists of a cadmium-plated copper plate cathode on which the steel coupon is held by a magnet and an anode disc, 18 cm-diameter, of cadmium foil (1 mm thick of 3N purity from Good Fellow Metals). The cadmium foil-disc is wrapped around and is fastened to a rotating 18 cm-diameter, steel plate disc, which is attached to the rotor shaft of a Pine Instrument Model DPR-70-100-400 Rotating Electrode System. The cadmium anode is placed $\sim$ 25 mm above the steel cathode and can be rotated to provide forced electrolyte convection at the cathode surface boundary. The electrolyte was prepared in triple distilled water and had the following composition: 22.5 g NH_4BF_4 (99.9% Cerac/Pure chemicals); 60 g/L H_3BO_3 (99.9% Fisher Sci.); 242.3 g/L $Cd(BF_4)_2$; rest water, pH adusted to 2.2 - 2.3 by adding ammonia. The electrolyte conductivity and pH were measured and arranged to be kept near 0.1/ Ohm.cm and 2.24, respectively.

To ensure tight adhesion of the cadmium deposits to the 300 M steel substrate, the machine-finished coupons were mechanically polished to 600 grit SiC paper. This was followed by degreasing and anodic cleaning. The anodization with a commercial alkaline cleaner (Kemtex 195 PG from Bristol, Inc.) was conducted for 2 minutes at 80^{o}C with 60 mA/cm^2 current density. The thoroughly washed and dried steel coupon was now mounted on a cadmium-plated copper platform and held close to the anode, and rotated at 300 RPM, using a magnet on the opposite side as shown in Figure 1. The platings were produced, utilizing the pulse profiles shown in Figures 2(i) and 2(ii). The pulse profiles used in the experiments were: (i) Pulse A, the cathodic-rest-cathodic, and (ii) Pulse B, a Periodic Reverse Pulse consisting of cathodic-rest-anodic-cathodic sequence. The pulses were generated by Dynatronix Model 70-100-400 pulse generator. After plating one

side of the steel coupon, it was turned over and the unplated side now plated under the same conditions. The thickness of cadmium films on steel obtained in a large number of experiments were found to be in the range 10-15 μm. The relative amounts of hydrogen diffused into the 300 M steel during cadmium plating of the coupons were measured using Barnacle Electrode cell system (6). The cell system is based on the couples Ni/NiOOH, NaOH, H/H^+. The technique is described in detail elsewhere (6). The cadmium plate of the steel coupon was removed with a swab impregnated with saturated aqueous solution of ammonium nitrate and then wiped with a Scotch Brite pad. The steel coupon is made with the anode against a reference Ni/NiOOH cathode in 0.2 M NaOH solution. The cell is short circuited through a zero resistance ammeter and Coloumbs during 30 minutes of cell discharge measured; the current in the steady state is then directly related to the diffusible hydrogen in the steel.

Table 1a

Summary of Cadmium Plating Parameters and Hydrogen Measurement Values

Plate No.	Pulse A			Peak Current		Total Coulombs A.min	[H] μA/cm²	Thickness, mil
	i_c A/cm²	t_c ms	t_o ms	cathodic A/cm²	anodic A/cm²			
00	0.7	0.4	4.6	--	--	12	--	--
01	0.8	0.5	9.5	0.8	0.0	10	--	--
02	0.8	0.5	9.5	0.8	0.0	10	--	--
03	0.8	0.4	4.6	0.8	0.0	12	0.40	0.60
04	0.7	0.4	4.6	0.7	0.0	12	--	--
05	0.7	0.4	4.6	0.7	0.0	12	0.46	0.63
06	0.7	0.4	4.6	0.7	0.0	12	0.44	0.63
07	0.5	0.4	4.6	0.5	0.0	14	0.51	--
08	0.5	0.4	4.6	0.5	0.0	14	0.49	0.38
09	0.5	0.4	4.6	0.5	0.0	14	0.42	0.62
10	0.5	0.4	4.6	0.5	0.0	16	0.40	0.46
11	0.5	0.4	4.6	0.5	0.0	16	0.46	0.59

Table 1b

Summary of Cadmium Plating Parameters and Hydrogen Measurement values

Plate No.	Pulse B						Peak Current		Total Coul- ombs, A.cm^2	[H] μA/ cm^2	Plate Thick- ness, mil
	i_c A/cm^2	i_a	t_c ms	t_o ms	t_a ms	t_1 ms	Cathodic A/cm^2	anodic A/cm^2			
12	0.5	0.25	0.4	4.6	0.2	1.8	0.5	0.25	16	0.45	0.4
13	0.5	0.25	0.4	4.6	0.2	1.8	0.5	0.25	16	0.55	0.4
15	0.5	0.25	0.4	4.6	0.2	1.8	0.5	0.25	16	--	--
16	0.6	0.25	0.4	4.6	0.2	1.8	0.5	0.25	20	--	0.6
17	0.5	0.25	0.4	4.6	0.2	1.8	0.5	0.25	20	--	0.6
B1	Unplated Specimen (Control)									0.40	0.0
B2	Unplated Specimen (Control)									0.40	0.0

The morphology of cadmium electrodeposits on the coupon surfaces as well as the steel-cadmium interface were examined by scanning electron and optical microscopy.

RESULTS AND DISCUSSION

The electrochemical operating conditions used in the plating of 300 M steel coupon and the results obtained with use of Pulse A and Pulse B plating along with the measured values of diffusible hydrogen in steel are included in Table 1a and 1b.

The results on hydrogen measurements on steel coupons plated, under Pulse A or Pulse B with forced convection of electrolyte, show that mobile or diffusible hydrogen in cadmium-plated steel coupons are $\sim$0.40 - 0.50 μA.cm^{-2} where as the measured value for bare coupons is approximately 0.4 μA.cm^{-2}. The conventional DC plated coupons with - 0.5 mil thick plate will show $\sim$0.8 μA.cm^{-2} hydrogen.

Certainly, the experimental results shows that codeposition of hydrogen during cadmium plating has been reduced significantly. The risk of hydrogen embrittlement by use of fast pulses in conjunction with forced electrolyte convection is minimized. Use of modest cathodic peak pulse current of $\sim$ 0.5 - 0.7 A.cm^{-2}, a short duration ($\sim$0.4 ms), and a long rest period ($\sim$5 ms)

followed by cathodic or anodic quick pulses provides plating with almost 100% Faradaic efficiency, when plated under laminar electrolyte flow conditions. It appears the hydrogen overvoltage of approximately - 200 mV vs SCE reference is never attained by the cathode under these conditions, and hence, hydrogen codeposition is significantly minimized. Laminar flow conditions at the cathode are created by the anode rotating at 300 RPM. The Reynolds Numbers, Re, of fluid flow near the cathode flat surface can be calculated by the equation,

$$Re = \frac{\chi \Omega p S^2}{\mu (R - r_o)} \qquad (6)$$

where,

χ = the distances from the center of rotating shaft
Ω = angular velocity in radians per second
μ = viscosity, 0.1 gm/cm
p = 1 gm/cm^3
$R-r_o$ = 5.08 cm
S = Separation of electrodes, 2.54 cm

The calculated Reynolds numbers are given in Table 2.

Table 2
Reynolds Number of Aqueous Electrolyte
with Electrode Separation of 2.54 cm.

RPM(m)	Re(Inside)	Re(Outside)	Re(Average)
300	15,193	35,451	25,322
350	17,724	41,355	29,540

The thickness of diffusion on boundary layer S is related to the Reynolds number by relation,

$$d = \frac{1}{(Re)^{0.2}} \qquad (5)$$

A crude estimate reveals that a 300 RPM rotation of anodic disc across the steel coupon cathode results in at least a tenfold reduction of d. This enhances the mass transport of electroactive species across the diffusion boundary layer; a coupling of this with pulse parameters produces smooth deposits both in case of Pulse A and Pulse B depositions.

The examination of surface morphology [see Figures 3 to 4(i)] of electrodeposits as well as the steel-cadmium cross section [see Figure 4(ii)] interfaces provided the following results: (a) the cadmium coating shows strong adhesion, see Figures 4(ii), to the steel substrates without any voids or inclusions, (b) the micrographs suggest that uniform fine-grain electrodeposits of cadmium can be obtained with Pulse A and Pulse B in conjuction with forced electrolyte convection, and (c) the use of periodic reverse pulse or Pulse B provided finer grains of cadmium in the electrodeposits (see Figures 4) in comparison to coatings obtained with Pulse A (see Figure 3), other conditions remained unchanged.

CONCLUSIONS

The Periodic Reverse Pulse plating method, incorporating a fast cathodic pulse which is separated from the subsequent anodic/ cathodic pulses by a long rest period, has been highly successful in producing silvery cadmium coatings on steel from an aqueous fluoborate electrolyte. Also, the deposition obtained by combination of pulse currents and laminar electrolyte flow system (forced convection of electrolyte at Re ~ 20,000 - 25,000) result in a near hydrogen-free electrodeposition of fine-grained cadmium. This is confirmed by the determination of diffusible hydrogen by the electrochemical (Barnacle Electrode) method.

ACKNOWLEDGMENT

Financial support from the Naval Air Development Center is greatly appreciated. Technical assistance of Lee Biggs of Naval Air Development Center is thankfully acknowledged.

REFERENCES

1. C. G. Interante,"Basic Aspects of the Problems of Hydrogen in Steels," Proc. First Conf. on Current Solutions to Hydrogen Permeation in Steels, pp. 3-17 (1982), Am. Soc. of Metals, Washington, DC.
2. H. H. Lee and H. H. Uhlig, "Corrosion Fatigue of High Strength Steels", Met. Trans., Vol. 3, 2949 (1972).
3. S. J. Ketchum,"A Handbook of Protective Coatings for Military and Aerospace Equipment", NACE Publication, No.TPC-10, pp. 43-48 (1983).
4. T. E. Such, Electroplating and Metal Finishing, Vol. 14, 115 (1961).
5. T. Vergas and R. Varma, "Nucleation Phenomenon in Electro-deposition of Cadmium from Cadmium Fluoborate Solutions", J. Electrochem. Soc. (Submitted for Publication)
6. J. J. DeLuccia and D. A. Berman, "Electrochemical Techniques to Measure Diffusible Hydrogen in Metals" in Electrochemical Corrosion Testing, ASTM STP-727, p. 256 (1981).
7. D. A. Berman and V. S. Agarwala, "The Barnacle Electrode Method to Determine Diffusible Hydrogen in Steels" in Hydrogen Embrittlement Prevention and Control, ASTM STP-962, pp. 98-104 (1988).

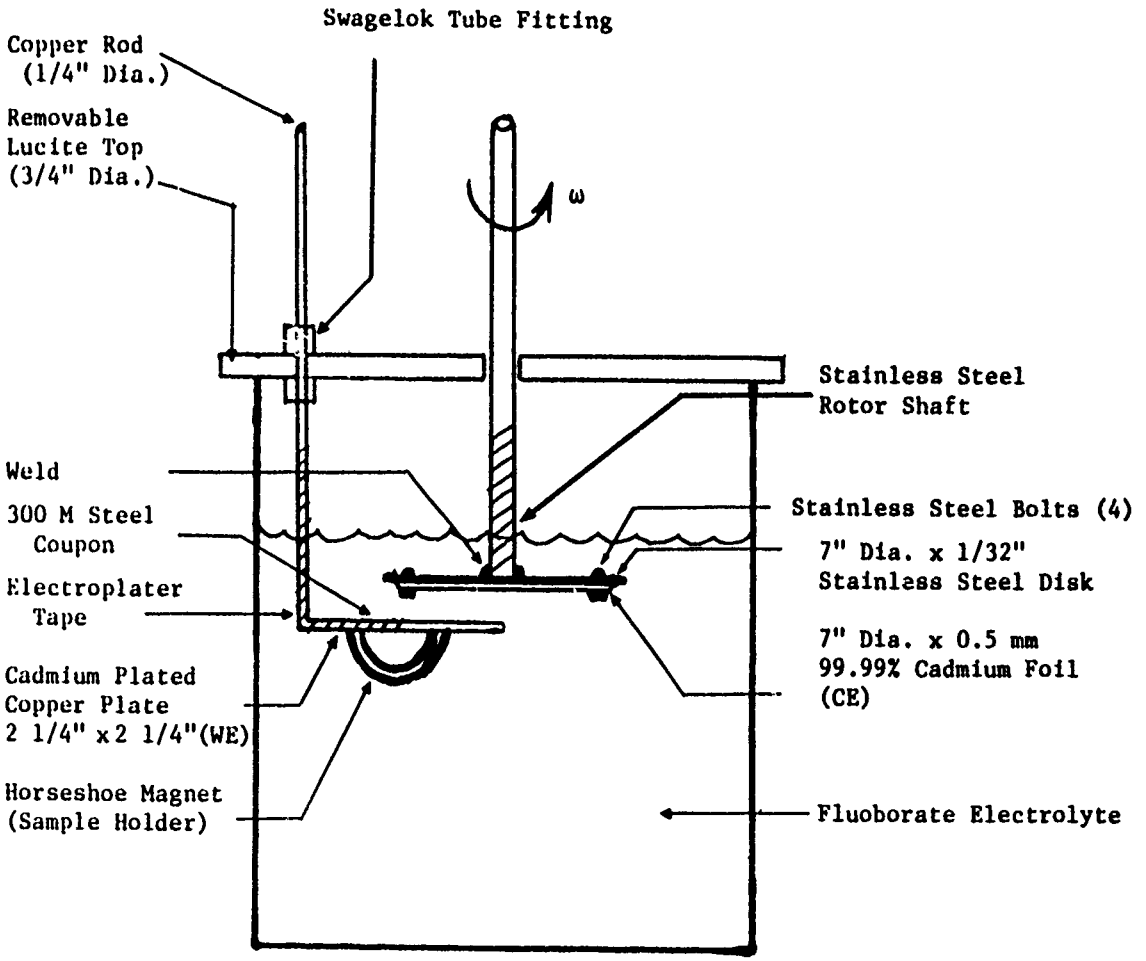

Figure 1 - Electrochemical cell set-up for pulse plating of cadmium under forced electrolyte convection.

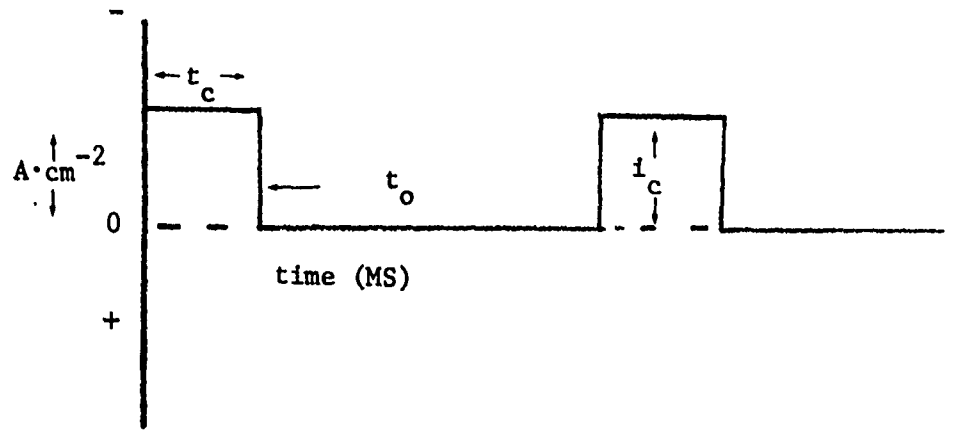

Pulse A

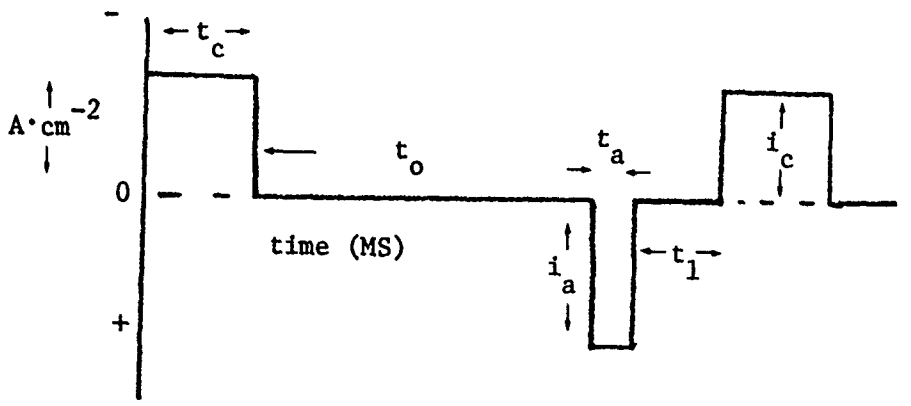

Pulse B

Figure 2 - Pulse current wave-forms used in cadmium electrodepositon: (i) pulse A, (ii) pulse B.

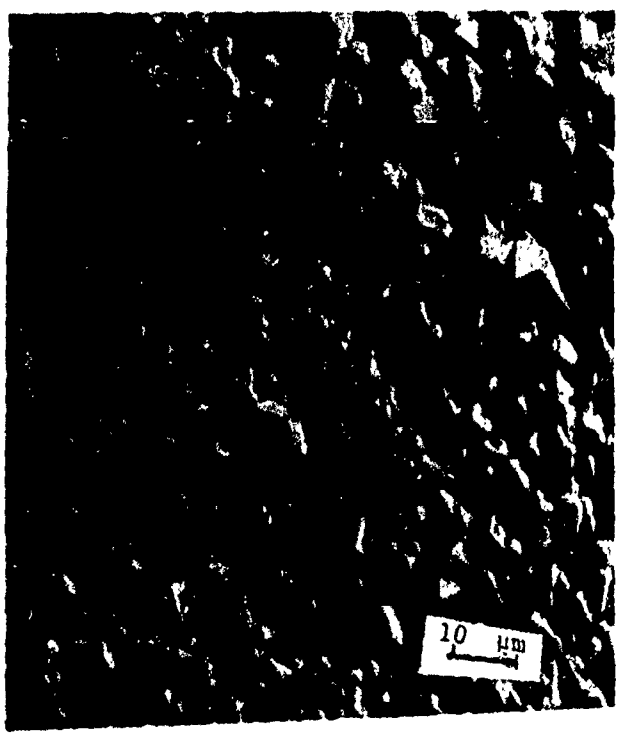

Figure 3 - Scanning electron micrograph of cadmium electrodeposit on 300 M steel from aqueous fluoborate electrolyte under pulse currents (pulse A; i_c = 0.7 A/cm^2 , t_c = 0.4 ms, and t_o = 4.6 ms), and forced electrolyte convection (ω = 300 rpm).

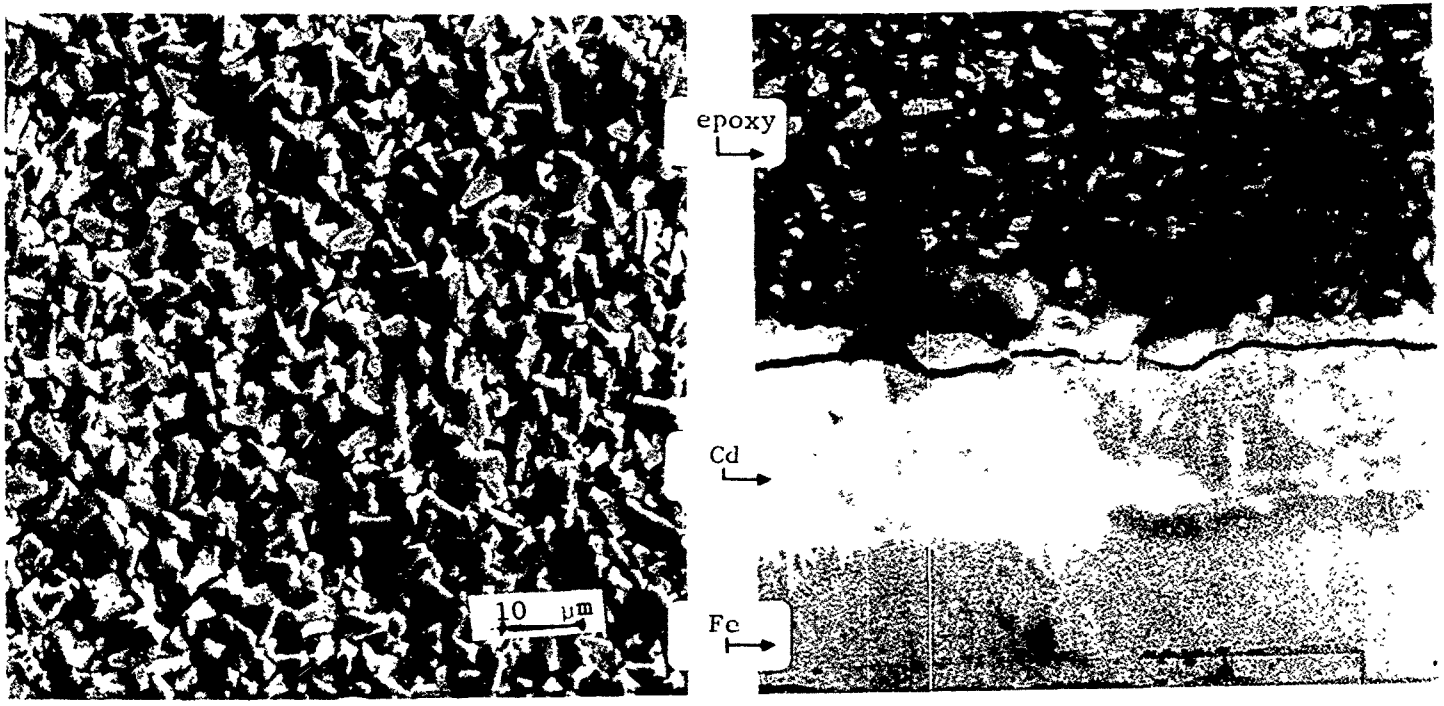

(i) (ii)

Figure 4 - Scanning electron micrographs of cadmium electrodeposited on 300 M steel from aqueous fluoborate electrolyte under pulse currents (pulse B; i_c = 0.6 A/cm^2, t_c = 0.4 ms, t_o = 4.6 ms, i_a = 0.25 A/cm^2, t_a = 0.2 ms, and t_1 = 1.8 ms), and forced electrolyte convection (w = 300 rpm): (i) surface and (ii) cross section.

RED PLAGUE IN COATED COPPER WIRE

Saul Isserow
Army Materials Technology Laboratory
Watertown, MA

ABSTRACT

The moisture-induced oxidation of silver-plated copper wire serves as a textbood example of galvanic corrosion. The generation of red cupric oxide accounts for the team Red Plague. The resulting destruction of copper conductors can have serious consequences in critical electrical circuits. Red Plague was the subject of several investigations in the 60's. In recent years the subject seems to have lain dormant in apparent attempts at benign neglect. Yet its manifestation is reported sporadically and it cannot be disregarded. This presentation will re-assess the occurrence of Red Plague, the causes, inspection procedures and changes in materials and/or processing to minimize Red Plague or eliminate it completely.

[Manuscript Not Available at the Time of Printing]

SHAFT SEAL CORROSION

Richard E. Rebis and Edward B. Bieberich
David Taylor Research Center
Bethesda, MD 20084

ABSTRACT

Corrosion in metal to metal crevices and on O-ring sealing surfaces on shaft sleeve and seal components has contributed to leakage through the shaft seals on ships. Three corrosion mechanisms that occur in the seals area are stray current, galvanic, and crevice corrosion. Since the contribution of each of these three mechanisms, which may act singly or in concert, to overall shaft seal corrosion has not been determined, a program was developed to identify the operative modes of corrosion attack.

The shaft seal materials studied in this investigation were 70/30 copper-nickel, Inconel 625*, and Monel 400*. To study the contribution of the three corrosion mechanisms, corrosion tests of various mechanical and material configurations were performed. Testing consisted of plate specimens of the shaft seal materials that were immersed in 30°C quiescent natural seawater for one year.

Test results indicate that the galvanic driving force is enough alone to cause excessive corrosion in copper-nickel/Monel crevices and appears to be the dominant mode of attack, while stray current does not appear to contribute significantly to the attack in these crevices. However, the copper-nickel specimens had an increase in weight loss due to the stray current. Inconel did not suffer corrosion attack on boldly exposed surfaces or in metal to metal crevices.

INTRODUCTION

Corrosion attack in metal to metal crevices and on O-ring sealing surfaces on shaft sleeve and seal components, Figure 1, is an important factor related to service performance of shaft seals on

* Inconel 625 and Monel 400 are registered trademarks of Huntington Alloys Products Division, The International Nickel Company, Huntington, West Virginia

ships. The areas in the seals system that corrode and potentially contribute to leakage are the lock ring groove (LRG) and O-ring grooves on the sleeve and on the outside diameter of the seal ring. Since minor corrosion attack may lead to leakage, corrosion attack in the 0.25 mm to 0.50 mm (0.010 to 0.020 inch) range is considered significant for this investigation of shaft seal materials.

To improve corrosion performance of the shaft sleeve and under O-ring grooves of seal parts, alternate materials for shaft seal construction were studied. The materials investigated were 70/30 CuNi, Monel 400, and Inconel 625. The success of these materials in terms of improved corrosion performance depends on how well they withstand the corrosion mechanisms that occur in the seal area. These mechanisms, which act singly or in concert, are stray current, galvanic, and crevice corrosion. Since the contribution of each of these three mechanisms has not been determined, tests were conducted to identify the operative modes of corrosion attack. The objective of the corrosion tests was to study the overall material compatibility in the shaft seals area and the effect of galvanic, crevice, and stray current corrosion mechanisms on the bimetallic crevices in the seals area.

CORROSION TEST PROCEDURES

70/30 CuNi, Monel 400, and Inconel 625 were used in the corrosion tests. The 70/30 CuNi specimens were cut from a centrifugally cast shaft sleeve, while the Monel 400 and Inconel 625 specimens were machined from 6.35 mm (0.25 inch) thick plate that was hot rolled and annealed. Alloy compositions are in Table 1.

All the corrosion tests were performed at the LaQue Center for Corrosion Technology (LCCT), Wrightsville Beach, NC. Static immersion tests of various material combinations were conducted in filtered 30°C natural seawater for a one year period. A small flow rate through the tank replaced the water approximately 4 to 5 times a day. Triplicates of each material configuration were tested. Specifics of these immersion tests (Tests 1-4) follow.

Test 1. To study the LRG galvanic crevice corrosion problem, the following plate test was implemented. A metal to metal crevice was made by bolting two dissimilar metal plates together with titanium fasteners and tightening to 75 in.lbs. The fasteners were coated after assembly with an enamel based paint to prevent galvanic interactions. To simulate the shaft sleeve, a 66 mm (2.6 inch) square plate with an O-ring groove machined in it was made from 70/30 CuNi or Inconel 625, while a 127 mm (5.0 inch) square plate of Monel 400 or Inconel 625 was chosen to simulate the mating and lock rings' contribution to the crevice, Figure 2. The remote specimen in Figure 2 was used only for tests 3 and 4. Although an O-ring groove was machined into the sleeve specimen, O-rings were not inserted and thus the name "plates without O-rings" was

designated for this test. The metal to metal crevice gap was approximately 40 microns. The material test matrix is presented in Table 2.

Test 2. A second configuration of the plate set-up was exposed using the same parameters and material matrix as for the first test, except that O-rings were inserted. They were inserted to study crevice corrosion under O-rings which occurs in the shaft seals area. The test was designated "plates with O-rings". The metal to metal crevice opening was approximately 100 microns.

To discuss and document surfaces for tests 1 and 2, both the sleeve and mating specimen surfaces were designated as a crevice side and a backside. The crevice side was defined as the surface that formed the metal-to-metal crevice with the other plate, while the backside was defined as the surface not in direct contact with the other plate. The crevice side of the sleeve was subdivided into three areas: the crevice, the O-ring groove, and the area inside the O-ring groove. For this test, the crevice was defined as the area between the metal surface outside of the O-ring groove and the outer edge of the sleeve plate.

Test 3. A third test configuration was devised to study the effect of improved grounding on corrosion in the seals area. Improved grounding of the shaft sleeve to the housing occurs when the ship is stopped, the shaft is at rest and a direct electric path exists through the reduction gears. The sleeve is also grounded to the housing through the shaft grounding strap.

As a result of the improved grounding in the current configuration, the 70/30 shaft sleeve is coupled to a greater area of Monel material, which is cathodic to 70/30 CuNi.[1] Increasing the cathode:anode ratio causes the corrosion rate of the anodic material to increase.[2] To determine the effect of increasing the cathodic area on the corrosion of the galvanic lock ring/LRG crevice, the following setup was employed. A 127 mm (5 inch) square piece of remote material of Monel or Inconel was electrically connected to the sleeve/mating couple. The connection was made by bolting an insulated copper wire to the corners of the remote and mating specimens and then sealing the exposed ends of the wire with epoxy to prevent galvanic interactions. The test configuration is shown in Figure 2 and the material matrix for the "plates with remotes" is given in Table 3.

Test 4. The fourth configuration permitted evaluation of the effect of low levels of stray-current. To investigate the increase in attack of both general and galvanic crevice corrosion due to imposition of stray current, the test configuration and material matrix used in test 3 was repeated except that a potentiostat was connected to maintain a voltage difference between the sleeve/mating couple and the remote specimen.

For these "plate tests with overvoltages", the remote specimen was held 0.2 volts (V) cathodic to the sleeve/mating couple. The 0.2 V difference was chosen by assuming that the voltage would in general be the result of incomplete, inadequate or poor shaft grounding practices which would result in a partial voltage reduction between the shaft and the hull.

To document the corrosion attack on all plate specimens evaluated, the following procedure was used. Corrosion attack was measured on the back and crevice sides of the sleeve and mating materials with a micrometer. In addition, depth of attack measurements were taken on the remote specimens with a micrometer.

Weight loss of the sleeve, mating, and remote specimens after the one-year exposure were calculated by subtracting the final weight of the specimen from the weight of its unexposed condition. Potential measurements were taken weekly. Current measurements between the remote and the sleeve/mating couple were measured with a zero resistance ammeter. Readings were taken at the same frequency as the potential measurements.

To discuss the corrosion data, the following abbreviations are used to describe various material combinations. For the plate tests with and without O-rings, a sleeve/mating material combination will be designated by the sleeve material first followed by the mating material. For example, CuNi/Monel (C/M) indicates the sleeve material is 70/30 CuNi and Monel is the mating material which is bolted to the sleeve material. For the plates with remotes and overvoltage tests, the three specimens of the couple are indicated by the following code: sleeve/mating/remote. So CuNi/In625/Monel (C/I/M) indicates a CuNi sleeve material, an Inconel mating specimen, and a Monel remote which is electrically coupled to the sleeve/mating couple, Figure 2.

RESULTS AND DISCUSSION

Crevice Attack of the 70/30 CuNi Sleeve Material

The maximum depth of crevice attack on the 70/30 CuNi and Inconel 625 sleeve materials under the four test conditions is presented in Figures 3-6. For each material configuration, the Figures 3-6 show three data points to illustrate the maximum depth of crevice attack on each sleeve specimen of the triplicate exposures. Under all test conditions, the Inconel 625 sleeve material suffered no attack in metal to metal crevices.

Comparable to the Inconel sleeve materials' crevice corrosion resistance, the CuNi/CuNi couple had no attack in two of the three crevices and a maximum of only 0.05 mm (0.002 inches) attack in the crevice on one of triplicate specimens for the plate without O-ring

configuration, Figure 3. This test indicates that 70/30 CuNi would provide very adequate service if it were the sole material of construction or if it could be electrically isolated from more noble materials in the seals system.

The CuNi/Monel couple of the plate without O-ring configuration, which represents the present shaft sleeve and lock ring materials, had a maximum of 0.43 mm (0.017 inches) attack on the CuNi sleeve crevice face. For the CuNi/Inconel couple without O-rings, a maximum of 0.32 mm (0.012 inches) attack occurred on the sleeve crevice. Monel or Inconel in direct bimetallic crevices with CuNi causes increased attack in CuNi crevices. Compared to the performance of the CuNi/CuNi couple, it can be seen that the relatively poor performance of 70/30 CuNi shaft sleeves in the fleet are more related to the dissimilar metals (Monel or Inconel) used in contact with them, than on any particularly intrinsically poor performance of the material itself. Thus, the galvanic influences on the performance of shaft seal materials has been demonstrated to be of major importance.

For the plates with O-rings, Figure 4, the Inconel sleeve crevices suffered no attack and the crevices on the sleeve material of the CuNi/CuNi combinations had virtually no attack. However, attack on the 70/30 CuNi sleeve crevice when coupled to Monel or Inconel increased by an order of magnitude over the same combinations without O-rings. For the CuNi/Inconel and CuNi/Monel combinations, the maximum attack on the sleeve crevice was 2.87 mm and 3.51 mm (0.113 inches and 0.138 inches), respectively. The only explanation to be proffered at this point for the increase in attack compared to plates without O-rings is that insertion of the O-ring increases the gap between the two plates by roughly a factor of two, permitting refreshment of the electrolyte in the gap, and an increased rate of galvanic corrosion. This provides an interesting insight into the interplay of mechanisms operative in bimetallic crevices. Under typical single-metal crevices, the tightness of the crevice is usually related to the time of initiation for attack, as a tighter crevice tends to increase concentration differences (metal ion or oxygen) from inside to outside the crevice and thus reduce the initiation time to reach a critical crevice solution.[3] With the bimetallic crevices tested here, it appears that the main driving force for attack in the crevice is galvanic, and those conditions which favor the cathodic reactions inside the crevice stimulate faster rates of attack.

For the plates with remotes, Figure 5, the maximum depth of crevice attack on the CuNi sleeves for the all couples was between 0.28 mm (0.011 inches) and 0.38 mm (0.015 inches). Since the plates with remotes test is the plate without O-rings test, Figure 3, plus additional remote material electrically coupled, the effect of remote material on the crevice corrosion of the sleeve material can be studied. The addition of cathodic material to the couple did

not significantly increase the depth of crevice attack on the CuNi sleeve material coupled to Monel or Inconel mating specimens. Electrically coupling a Monel remote to the CuNi/CuNi sleeve/mating couple increases the attack in the CuNi/CuNi crevice up into the range of the direct bimetallic crevices. In terms of the shaft seals area, if a CuNi lock ring was employed to create a CuNi/CuNi crevice with the LRG, the Monel seal ring should be electrically isolated to reduce its galvanic influence on the CuNi/CuNi crevice. The data suggests that, from a galvanic standpoint, crevice corrosion of the 70/30 copper nickel sleeve is equally affected by either direct metal crevice contact or electrical contact to either Inconel or Monel. As expected, the addition of the increased area of cathodic material accelerated the weight loss of the CuNi sleeve material two to ten fold compared to the plates without O-ring specimens.

The depths of crevice attack of the sleeve material for stray current tests, or plates with 0.2 V overvoltage tests, are illustrated in Figure 6. The maximum depth of crevice attack on the CuNi sleeve material for the C/C/M 0.2 V overvoltage (ov), C/M/M ov, C/I/I ov, and C/I/M ov couples was between 0.20 mm (0.008 inches) and 0.36 mm (0.014 inches). The sleeve specimen for one of the triplicates of the C/M/M ov combination was machined thinner than the other two and suffered penetration through the back of the specimen to the bottom of the O-ring groove. As a result, the crevice was exposed to seawater from both sides and attack was accelerated to achieve a maximum depth of attack of 0.90 mm (0.035 inches). However, this data point was not considered due to the penetration of the thinner sleeve specimen.

The effect of stray current on crevice corrosion of the sleeve material can be examined by comparing the plates with remotes tests, Figure 5, to the plates with 0.2 V overvoltage tests, Figure 6. The effect of the stray current (ie. holding the remote specimen 0.2 volts cathodic to the sleeve/mating couple) caused little or no increase in the crevice corrosion of the CuNi sleeve specimens. While there was essentially no increased corrosion on the copper nickel crevice due to stray current, all copper nickel sleeve samples did have an increase in the overall weight loss.

The plate tests (Tests 1-4) indicate that the main corrosion mechanism driving the attack in the simulated lock ring/LRG crevice is galvanic. Stray current and extra cathodic remote material have little or no effect on increasing the depth of attack in bimetallic crevices of CuNi and Monel or Inconel and thus do not appear to be the dominant corrosion mechanisms.

Corrosion Performance of Monel

The deepest attack on the Monel mating specimens occurred on the face of the material which formed a crevice with the sleeve

specimen. The depth of attack on the Monel mating specimen is depicted in Figure 7. When the Monel mating specimen is coupled to a CuNi sleeve material, the maximum depth of attack is 0.52 mm (0.020 inches). For the I/M plate tests with and without O-rings and I/M/M plate test, the maximum depth of attack is similar to the same configurations with CuNi as the sleeve material. In the I/M/M ov combinations, the attack is increased compared to the same couples with a CuNi sleeve. In the I/M/M ov test, the maximum depth of attack on the Monel mating specimen was 2.81 mm (0.110 inches) versus 0.57 mm (0.022 inches) with a CuNi sleeve.

As these were static tests, the Monel in direct contact with CuNi probably performed somewhat worse than one might expect under flow conditions. Since the plates were exposed vertically and crevice corrosion occurred at the sleeve/mating interface, corrosion products accumulated on the mating material below the crevice. These corrosion products created additional crevices on the mating surface and thus more attack. Exposure to flow conditions would reduce the amount of accumulated corrosion product and attack of the Monel would probably be less.

The depth of attack on the Monel remote specimens is plotted in Figure 8. The attack on the Monel remote dramatically increased when it was coupled to Inconel compared to CuNi. When coupled to CuNi, the deepest attack on a Monel remote was 0.05 mm (0.002 inches). However, in the I/I/M couple the deepest attack on the Monel remote was 1.18 mm (0.046 inches) and even with a 12:1 area ratio of Monel to Inconel in the I/M/M couple, the maximum attack on the remote was over 1.02 mm (0.040 inches). The deepest attack usually occurred in crevices formed between the remote specimen and the bolt washers. Bolt washers were made of the same material as the plate specimen, in this example a Monel washer on the Monel remote. Therefore, a small area of Inconel can cause significant attack of Monel compared to the tolerances of the shaft seals area. From this limited amount of data, one might expect that the seal housing will have accelerated attack, particularly in crevices, when Inconel sleeves and seal parts are used.

Corrosion Performance of Inconel 625

Under all conditions tested, Inconel did not suffer corrosion attack in the metal to metal crevices or on the boldly exposed surfaces of the sleeve, mating, and remote specimens. Stray current, at the 0.2 V overvoltage level, did not affect the corrosion resistance of Inconel. However, two cases of attack on Inconel occurred in a metal to non-metal crevice formed between the Inconel and epoxy used to seal the electrical connection. In the plates with O-rings test, slight crevice attack of 0.15 mm (0.006 inches) occurred on the Inconel under the epoxy. Since no attack was noted on the Inconel under 0.2 V overvoltage condition, a decision was made to increase the stray current to 0.5 volts on

one of the triplicates of I/I/I and I/I/M. On these two specimens, crevice attack perforated the 6.35 mm (0.25 inch) thick plate under the epoxy crevice.

CONCLUSIONS

The plate tests (Tests 1-4) indicate that the main corrosion mechanism driving the attack in the simulated lock ring/LRG crevice is galvanic.

Of all metal to metal crevice tests, single metal crevices of either 70/30 CuNi or Inconel 625 performed well. Mixed metal crevices of 70/30 CuNi with Monel or Inconel 625 had higher rates of crevice corrosion. Even the remote galvanic coupling of Monel to an all CuNi crevice produced adverse crevice performance rivaling the mixed metal crevice performance.

Stray current and extra cathodic remote material have little or no effect on increasing the depth of attack in bimetallic crevices of CuNi and Monel or Inconel and thus do not appear to be the dominant corrosion mechanisms.

Although stray current driven by a 0.2 V overvoltage caused increased weight losses of anodic (CuNi or Monel) sleeve and mating specimens, crevice attack was not significantly increased.

The introduction of O-rings into bimetallic crevices between plates of CuNi and Monel or Inconel caused increased attack of the CuNi at the outer edge of the crevice.

Inconel 625 performed well in all metal to metal crevices, however, crevice attack under epoxy indicates a possible problem for all-Inconel designs. 0.5 volts induced heavy stray current attack under epoxy.

Monel suffered increased rates of attack when coupled to Inconel, particularly in crevices.

REFERENCES

1. Ferrara, R. J., Taschenberg, L. E., Moran, P. J., "The Effects of Chlorinated Seawater on Galvanic Corrosion Behavior of Alloys Used in Seawater Piping Systems", paper number 211 of Corrosion 85, March 25-29, 1985.

2. Fontana, M. G., Corrosion Engineering, Mc-Graw-Hill Book Company, New York, pg. 46-47, 1986.

3. Oldfield, J. M. and Sutton, W. H., Br Corros. J., 1980 15(1), pg 31.

Table 1: Chemical compositions of materials used in the plate tests.

	Fe	Cu	Al	Ni	Cr	Nb	Pb	C	Mn	P	S	Si	Co	Mo	Ti
70/30 CuNi	0.52	65.9	-	30.2	-	1.29	0.003	0.006	1.04	-	-	0.25	-	-	-
Monel 400	2.12	32.0	-	64.3	-	-	-	0.090	1.17	-	0.005	0.26	-	-	-
Inconel 625	3.64	-	0.25	60.5	21.8	3.45	-	0.039	0.082	0.007	<.001	0.095	0.060	9.00	0.21

Table 2: Material matrix for the "plates without O-rings" and "plates with O-rings" tests (Tests 1 and 2).

Sleeve	Mating
1) 70/30 CuNi	70/30 CuNi
2) 70/30 CuNi	Monel
3) 70/30 CuNi	Inconel 625
4) Inconel 625	Inconel 625
5) Inconel 625	Monel

Table 3: Material matrix for the "plates with remotes" and "plates with 0.2 V overvoltage" tests (Tests 3 and 4).

Sleeve	Mating	Remote
1) 70/30 CuNi	70/30 CuNi	Monel
2) 70/30 CuNi	Monel	Monel
3) 70/30 CuNi	Inconel 625	Monel
4) 70/30 CuNi	Inconel 625	Inconel 625
5) Inconel 625	Inconel 625	Inconel 625
6) Inconel 625	Inconel 625	Monel
7) Inconel 625	Monel	Monel

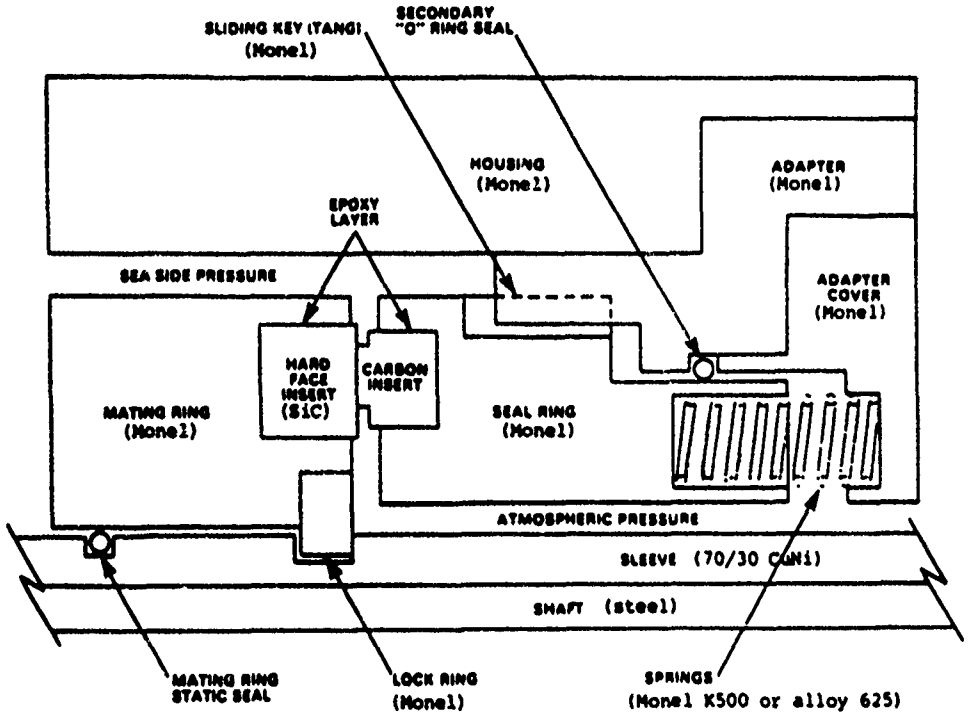

Figure 1: Schematic diagram of shaft seal assembly.

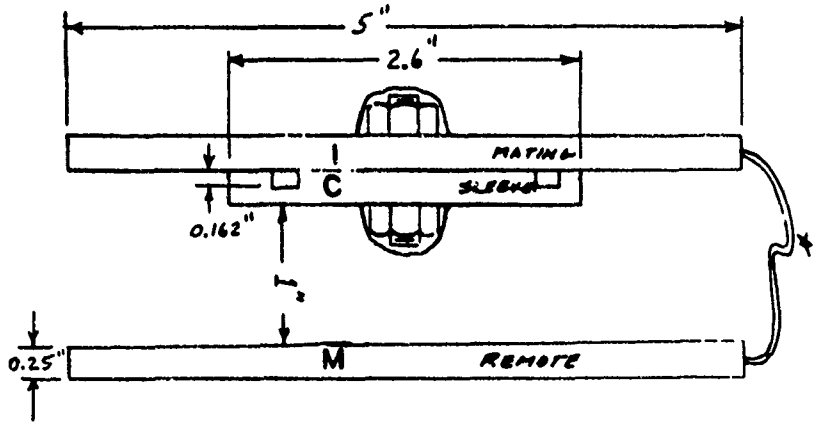

EXAMPLE C/I/M

70/30 CuNi Sleeve/Inconel 625 Mating/Monel Remote

Figure 2: Schematic diagram of the test assembly for the plates with and without O-rings (disregard the remote specimen for these two tests) and for the "plates with remotes" and "plates with 0.2 V overvoltage" configurations.

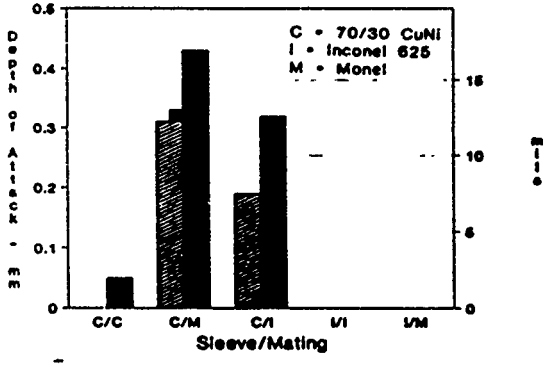

Figure 3: Maximum depth of crevice attack on each of three sleeve specimens from triplicate exposures of the "plates without O-rings" test.

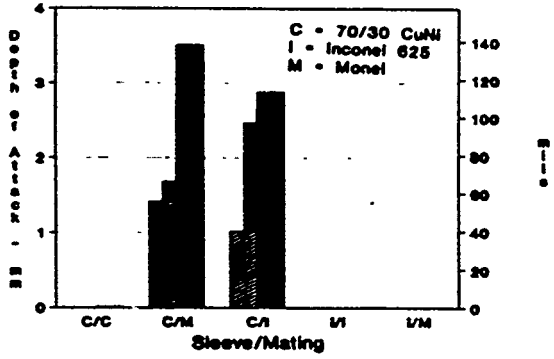

Figure 4: Maximum depth of crevice attack on each of three sleeve specimens from triplicate exposures of the "plates with O-rings" test.

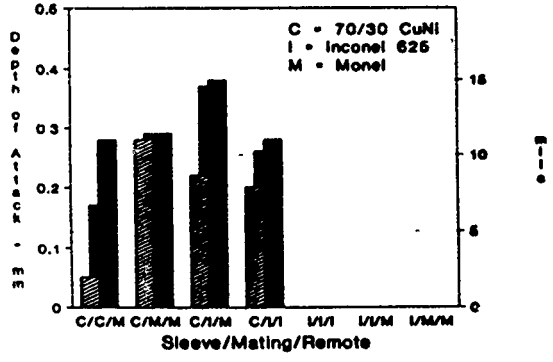

Figure 5: Maximum depth of crevice attack on each of three sleeve specimens from triplicate exposure of the "plates with remotes" test.

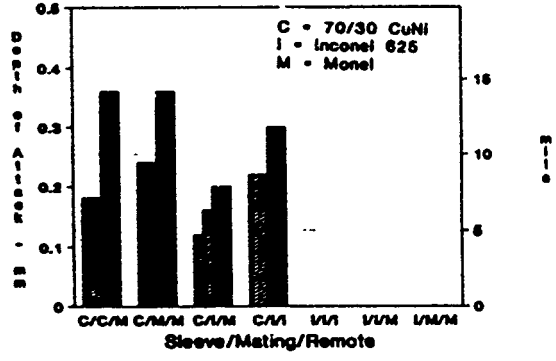

Figure 6: Maximum depth of crevice attack on each of three sleeve specimens from triplicate exposure of the "plates with 0.2 V overvoltage" test.

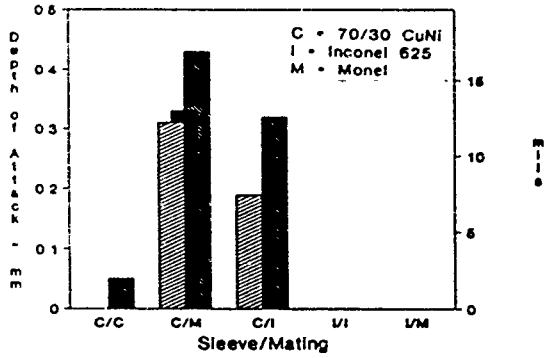

Figure 3: Maximum depth of crevice attack on each of three sleeve specimens from triplicate exposures of the "plates without O-rings" test.

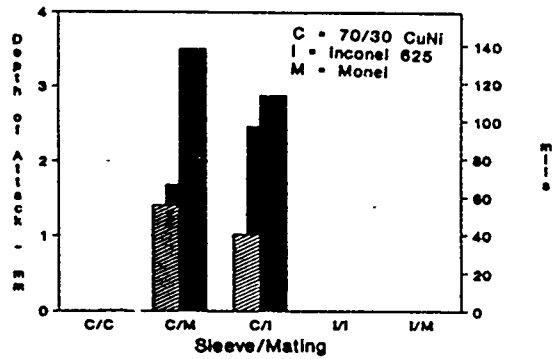

Figure 4: Maximum depth of crevice attack on each of three sleeve specimens from triplicate exposures of the "plates with O-rings" test.

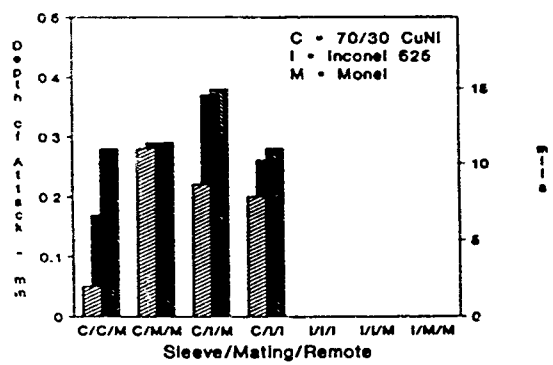

Figure 5: Maximum depth of crevice attack on each of three sleeve specimens from triplicate exposure of the "plates with remotes" test.

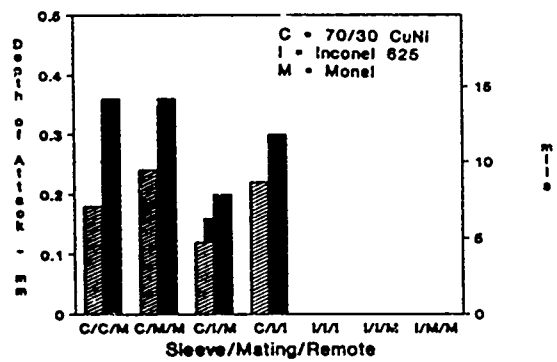

Figure 6: Maximum depth of crevice attack on each of three sleeve specimens from triplicate exposure of the "plates with 0.2 V overvoltage" test.

NEW STAINLESS STEELS FOR THE MARINE ENVIRONMENT

A. J. SEDRIKS
Materials Division
Office of Naval Research
Arlington, Virginia

ABSTRACT

A review is presented of the research and development effort which has been aimed at providing new stainless steels for use in seawater and seawater cooled systems. Three new categories of highly corrosion resistant stainless steels are described, namely the superaustenitics (i.e. austenitic nitrogen-containing 6% molybdenum grades), the titanium-stabilized superferritics, and the duplex grades containing molybdenum and nitrogen. The key microstructural and alloy composition effects which improve resistance to localized corrosion (which is the main mode of failure of stainless steels in seawater) are discussed. The joint effect of molybdenum and nitrogen is found to be exceptionally beneficial for the localized corrosion resistance of the austenitic and duplex grades, whereas inclusions and second phases are generally detrimental for all grades. Problems encountered with thick sections, such as sigma and chi phase precipitation in the superaustenitics and high ductile-to-brittle transition temperatures in the superferritics are identified and areas for research are noted.

INTRODUCTION

It has been recognized for some time that it is mainly the lack of resistance to localized corrosion (i.e. crevice corrosion and pitting) which limits the suitability of stainless steels for seawater service (1). This recognition has provided the stimulus for developing new stainless steels with high resistance to crevice corrosion and pitting for long term service in seawater.

The chemical mechanisms for crevice corrosion and pitting are similar, although these forms of attack manifest themselves in different ways. Crevice corrosion occurs within the crevices formed by rivets, nuts, bolts, gaskets, valve seats, surface deposits and barnacles, as the stagnant solution within the crevices becomes depleted of oxygen and acidifies due to the hydrolysis of metal ions. On the other hand, pitting occurs on an open surface and does not require the presence of a crevice. In terms of electrochemical descriptors, pitting initiates when the corrosion potential equals, or in noble to, the pitting potential, Figure 1 (2). This condition can result from the displacement of the pitting potential in the active direction and/or the displacement of the corrosion potential in the noble direction. The former can be caused by increasing the temperature of the seawater while the latter can be caused by contamination of the seawater with strong oxidizers such as chlorine or the facilitation of the cathodic reactions by biofilms.

For stainless steels the same metallurgical variables which improve crevice corrosion resistance also improve pitting resistance (2), and this improvement is seen in both seawater tests and in ferric chloride tests (3). This has enabled extensive alloy development work to be carried out employing accelerated laboratory tests with only occasional long-term seawater tests being necessary for confirmation purposes.

As a result of this effort over the past decade or so, three new generic groups of stainless steels have been identified as strong candidates for long-term seawater service, namely the superaustenitics, the superferritics and the duplexes containing molybdenum and nitrogen (i.e. superduplexes).

It is the purpose of this review paper to describe and define the effects of alloy composition and microstructure on the localized corrosion resistance of these new stainless steels, identifying benefits, possible problem areas and needed additional research.

SUPERAUSTENITICS

Historically the superaustenitics derive from an alloy originally identified as IN-748, containing 27%Ni,20%Cr and 8.5%Mo. This alloy, covered by U.S. Patent 3,547,625, was developed in the 1960's by the research laboratories of the International Nickel Company with the original objective of providing a stainless steel for marine wire rope which would not be susceptible to crevice corrosion in seawater. Subsequent modifications involving lowering the molybdenum content and adding nitrogen have led to the presently available superaustenitics described in Table 1. Their localized corrosion resistance derives primarily from the combination of 20%Cr, 6%Mo and 0.2%N. Also, currently being evaluated (4) are modifications containing higher chromium and lower molybdenum (i.e. 25%Cr, 5%Mo and 0.2%N).

The importance of nitrogen in raising the pitting potential in the noble direction is shown in Figure 2 (5) and in increasing the crevice corrosion temperature in ferric chloride is shown in Table 2 (6,7).

To maintain the high resistance to localized corrosion the alloying elements must be in solid solution. Precipitation of carbides and nitrides can lead to chromium depletion in the vicinity of the precipitate and the precipitation of intermetallics such as sigma, chi and Laves phases can cause similar depletion of chromium and molybdenum in surrounding regions. These depleted regions can present areas of low corrosion resistance and serve as sites for the initiation of pitting, crevice corrosion, and in some cases also intergranular corrosion. In the case of superaustenitics, experience has shown that it is the precipitation of sigma that can cause a loss in localized corrosion resistance (8). The appearance of sigma is shown in Figure 3 (1).

In the Fe-Cr-Ni-Mo alloy system, high nickel contents minimize and high chromium plus molybdenum contents enhance the precipitation of sigma and chi at elevated temperatures. High nitrogen contents retard the precipitation of these intermetallics (9), as do additions of mischmetal to the melt to alter their precipitation characteristics at grain boundaries, rapid cooling or heat treatment. A combination of these procedures prevents the formation of sigma and chi in commercial sheet material. In thicker plate material these phases may be present at the center of the material (10) where cooling rates have been slower. Unless these phases are present at the surface, corrosion resistance is not likely to be affected.

Reheating at temperatures in the range 540-1040°C can lead to the precipitation of sigma and chi at the surface grain boundaries with the possible impairment of corrosion resistance if molybdenum and/or chromium depletion occurs, Figure 4 (11). Post-weld or homogenizing heat treatments, if necessary, should be carried out in the temperature range 1120-1180°C to dissolve the sigma and chi phases, followed by rapid cooling to prevent their re-precipitation in the range 540-1040°C. In welding superaustenitic alloy plate overmatched fillers (e.g. Inconel alloy 625) are used to ensure that the high localized corrosion resistance is maintained by the weld.

As a general point regarding these alloys, the question should be asked whether the traditional fear of the presence of any and all sigma and chi in the microstructure is fully warranted. Obviously the presence of continuous or semicontinuous networks of brittle phases at grain boundaries is not tolerable. However, dispersed phases of this type, not surrounded by envelopes of material depleted in the alloying elements needed for corrosion resistance may be less detrimental with regard to corrosion resistance. Further metallurgical and corrosion research in this area could be both informative and useful, particularly for sea water applications. Also needed for these alloys are well characterized time-temperature-precipitation diagrams defining the regimes for the formation of sigma, chi, Laves phases, carbides and nitrides. Such diagrams are particularly useful in identifying cooling rates needed to avoid precipitation.

Further studies are also needed to establish whether there is any role of manganese sulfide inclusions in initiating localized corrosion in superaustenitics. Manganese sulfides are the preferred sites for pit initiation in type 304 and 316 stainless steels (2) which contain between 5 and 10 times more sulfur (e.g. 0.01%) than the superaustenitics (e.g. 0.001-0.002%).

SUPERFERRITICS

Historically the superferritics derive from a high purity 29%Cr-4%Mo alloy developed and patented by M.A. Streicher at the DuPont Experimental

Station in the 1960's (12). The criteria evaluated by Streicher in the identification of the 29%Cr-4%Mo composition are shown in Figure 5 (12). In the subsequent commercial development it became evident that the carbon plus nitrogen contents of these high chromium superferritics had to be kept at 0.025% maximum. Exceeding this level resulted in susceptibility to intergranular corrosion due to chromium depletion adjacent to precipitated chromium carbides and nitrides at grain boundaries. Accordingly, the earlier superferritic variants such as 29-4 were made from low carbon materials by vacuum induction melting (13), since the C+N=0.025% max. requirement could not be attained by the less costly argon-oxygen decarburization (AOD) process. However, subsequent development led to the adoption of AOD as the preferred production technique in conjunction with titanium stabilization to tie up the carbon and nitrogen. Most superferritics produced to-day contain up to 0.04% carbon plus nitrogen and are stabilized with about 0.5%Ti, Table 3. The one exception is 29-4-2 which is still produced by vacuum melting with a low carbon plus nitrogen level and without titanium, Table 3. The titanium in the stabilized grades causes the carbon and nitrogen to precipitate as titanium carbide and nitride at high temperatures so that little of these two elements is left to precipitate as chromium carbide and nitride on cooling.

As in the case of the superaustenitics, the superferritics can also precipitate intermetallics such as sigma, chi and Laves phases on heating to elevated temperatures. The time-temperature-precipitation diagram defining the regimes for the precipitation of these phases is shown in Figure 6 (14). A heat treatment (1 hour at 871°C) selected to produce sigma precipitation has been shown to be detrimental to the crevice corrosion resistance of the 29-4-2 grade (15). Heating at 1050°C will dissolve these intermetallics.

No studies appear to have been carried out to determine the effect of the alpha prime phase on the localized corrosion resistance of the superferritics. This phase, which is responsible for the phenomenon known as "475°C embrittlement" in lower chromium ferritics (2), has been shown to reduce the pitting resistance of a 19%Cr-2%Mo ferritic stainless steel (16).

Also, no studies appear to have been carried out to determine whether sulfide inclusions play any role in the initiation of localized corrosion in superferritics, or which sulfides are present.

The main drawback to greater utilization of the superferritics remains their low ductile-to-brittle transition temperatures (DBTT's) in thicker sections. The variation of the DBTT with thickness for the 29-4-2 grade is shown in Figure 7 (17). This figure shows that the transition temperature for 29-4-2 is below room temperature for thicknesses up to 12.7mm (0.5in), which enables the alloy to be manufactured and sold as plate. The ductility enforced maximum thicknesses for Monit and for 29-4C are much less than for 29-4-2, partly reflecting the fact that carbon, nitrogen and titanium raise the DBTT for a given thickness. Nickel is one alloying element that lowers the DBTT for a given thickness, Figure 8 (18), and further research could possibly identify other even more effective alloying elements. Considering the technological significance of this effect, there has been surprisingly little research devoted to this topic. Nor is there much fundamental insight into the brittle transition which is generally thought to be associated with constraints in thicker materials that prevent deformation through the thickness.

The addition of nickel, in addition to lowering the DBTT, also increases corrosion resistance of high chromium superferritics in reducing acids (12). However, it also makes the alloys susceptible to stress-corrosion cracking in

the magnesium chloride test (12,18) and promotes the formation of sigma and chi phases.

To-date the DBTT problem of superferritics has been largely circumvented by using these materials in applications such as thin-walled condenser tubing for seawater cooled power plants, Table 4. As noted in Table 4, superferritics have been in condenser service since about 1980 so that service experience is now available. Two service problems have been encountered. This first is hydrogen-induced cracking, which is encountered with the 29-4C and SEA-CURE alloys when these materials are cathodically polarized to potentials in the range -0.9 to - 1.4 volts (S.C.E.), Figure 9 (19). Cathodic protection at about - 0.8 volts (S.C.E.) is often necessary to protect the condenser tubesheets or waterboxes from corrosive attack. Accordingly, the data of Figure 9 demonstrate that overprotection at potentials more negative than -0.8 volts (S.C.E.) must be carefully avoided. Since hydrogen can also be picked up from annealing in hydrogen atmospheres or acid pickling, these processes should be avoided for superferritic stainless steels. The second problem which has been encountered, and is also related to tubesheets, is crevice corrosion. The use of type 316 tubesheets with superferritic tubing produces a metal-to-metal crevice in which one of the metals (type 316) is much less resistant to crevice corrosion. The attack which initiates on the type 316 member of the crevice generates significant acidity which ultimately destroys the passive film on the superferritic (20). These sort of problems can be prevented by using alloys more resistant to crevice corrosion for the tubesheet (e.g. AL-6XN), seal-welding, or cathodic protection (20).

DUPLEX STAINLESS STEELS WITH MOLYBDENUM AND NITROGEN (SUPERDUPLEXES)

These stainless steels contain both austenite and ferrite, often in the ratio 50:50, and are hence referred to as duplex. The duplexes containing molybdenum and nitrogen, sometimes known as superduplexes by analogy with the superaustenitics and the superferritics, historically derive from the American Castings Institute alloy CD-4MCu which was formulated in the 1950's by Ohio State University to contain 2% molybdenum (21). The nitrogen addition came later as a result of research and development by Langley Alloys Ltd., England, initially resulting in an alloy designated as LANGALLOY 40V, and finally as FERRALIUM alloy 255. To-day the latter alloy is available as both cast material and wrought material. Some of the modern commercially available wrought superduplexes are shown in Table 5.

The phase diagram for a duplex stainless steel is shown in Figure 10 (22). This figure is a pseudo-binary diagram at 65% Fe and is an interpolation of the 60%Fe and 70%Fe pseudo-binary diagrams of Pugh and Nisbet (23). The phase diagram shows that at 25% chromium the alloy will solidify as ferrite. Austenite precipitation will start at the $\alpha / \alpha + \gamma$ boundary and the amount of austenite precipitated will be dependent on the cooling rate. Low cooling rates will enable more austenite to form. Commercial practice is to process or heat treat the alloy at temperatures in the range 1050 to 1150°C and to water quench to maintain a structure of about 50% ferrite and 50% austenite.

Slow cooling or re-heating to high temperatures can give rise to a wide variety of precipitates shown in Figure 11 (24). In addition to the phases shown in Figure 11, the nitrogen containing superduplexes also precipitate chromium nitride approximately within the same temperature-time regime in which $M_{23}C_6$ is precipitated (25).

Of the phases identified, only chromium nitride and sigma have been shown to have a deleterious effect on the localized corrosion resistance of duplexes. The precipitation of chromium nitride, which can lead to chromium depletion in the vicinity of the nitride, has been shown (26) to provide sites for crevice corrosion initiation in cast and annealed duplex stainless steels.

The presence of sigma in duplexes will reduce pitting resistance, as shown in Figure 12 (27), and crevice corrosion resistance (15). Annealing in the alpha prime precipitation region for 4 hours did not have an adverse effect on pitting resistance, possibly because of insufficient precipitation of alpha prime (Figure 12).

Manganese sulfide would be expected to be present in the duplex stainless steels at the manganese levels shown in Table 5. The possibility exists, therefore, that the pitting resistance of the duplex stainless steels could be improved further by reducing the manganese content to levels at which chromium sulfides are formed. This approach has been explored, for example, in the development of a new duplex stainless steel in England (28).

The high localized corrosion resistance of the superduplexes derives primarily from their high chromium, molybdenum and nitrogen contents, with the beneficial effect of nitrogen having been re-confirmed by recent studies (29). A comparison of the pitting potentials in synthetic seawater as a function of temperature for the superduplex grade DP-3 and AISI type 316 austenitic stainless steel is shown in Figure 13 (30), with more noble values being exhibited by the superduplex grade at all temperatures.

Regarding other alloying elements it should be noted that some duplex stainless steels contain tungsten additions in the range 0.5-1.0% (28,30). Tungsten additions in this range have been shown to improve the crevice corrosion resistance of duplex stainless steels (31). Copper additions of the order of 1 to 2% are used to extend the application of duplex stainless steels to include sulfuric acid service.

The nitrogen content of weld metal can be maintained by adding 5 vol.% nitrogen gas to the argon shielding gas during TIG-welding both for the superduplexes (32) and austenitics (33,34).

COMPARISONS AND EMERGING USES

The mechanical properties and crevice corrosion temperatures determined in 10% $FeCl_3$ solution according to ASTM Procedure G-48 are shown in Table 6 (3,5, 7,17,18,35). The superduplexes provide the highest mechanical strength whereas the super-ferritics exhibit the highest crevice corrosion resistance in the ferric chloride test.

Results from crevice corrosion tests in seawater are shown in Figure 14 (36,37) for a large number of alloys, with the superferritics 29-4C and MONIT exhibiting complete resistance to attack under all the test conditions selected. SEA-CURE is shown here as susceptible. However, this result pertains to an earlier alloy containing only 25%Cr and 3%Mo. SEA-CURE is now produced with 27.5% Cr and 3.5%Mo and would, therefore, be expected to be more resistant. No seawater data is available for Al-6XN, but it would be expected to be comparable with 254-SMO in view of its similar Cr, Mo and N content. Similarly, the duplex alloy 2205 was not included in the seawater evaluation shown in Figure 14.

Further seawater crevice corrosion tests should be carried out to document the behavior of these newer alloys.

In conclusion it should be noted that many alloys in the superaustenitic, superferritic and superduplex stainless steel families are now past the development stage and are seeing application in seawater service. The substantial utilization of the superferritics as thin-walled condenser tubing was noted earlier in Table 4. The superaustenitics have been seen more diverse use in seawater applications such as cooling water tubing, plate heat exchangers and seawater piping for offshore platforms (38). The superduplexes have seen specialized Navy uses such as submarine shaft seals, pumps, retractable bow plane systems and missile launcher components, carrier catapult trough covers, patrol boat propellers and propeller shafts and hovercraft propellers and rudders (39,40).

ACKNOWLEDGEMENTS

Many of the figures are used in this review by permission of copyright owners. The author acknowledges permissions granted by INCO Ltd., Metallgesellschaft AG, Haynes International, The Metals Society, Carpenter Technology Corporation, American Society for Metals, American Society for Testing and Materials and National Association of Corrosion Engineers.

REFERENCES

1. A.J. Sedriks, International Metals Reviews, Vol 27, p.321, 1982.

2. A.J. Sedriks, Corrosion of Stainless Steels, Wiley-Interscience, New York, N.Y., 1979.

3. N.S. Nagaswami and M.A. Streicher, "Accelerated Laboratory Test for Crevice Corrosion of Stainless Alloys", Corrosion/83, Paper No: 71, National Association of Corrosion Engineers, Houston, Texas, 1983.

4. J. Charles, P. Soulignac, J.P. Audouard and D. Catelin, "Superaustenitic Stainless Steel for Marine Applications", Stainless Steels/87, Paper No: 31, The Institute of Metals, London, England, 1987.

5. Anon., "Cronifer 1925hMo - alloy 904hMo, an Advanced High-Alloy Austenitic Stainless Steel for Offshore Seawater Applications", VDM Report No. 10, July, 1985, Vereinigte Deutsche Metallwerke AG, Duisburg, West Germany.

6. A. Garner "Crevice Corrosion of Stainless Steels in Seawater: Correlation of Field and Laboratory Tests", Corrosion/80, Paper No: 35, National Association of Corrosion Engineers, Houston, Texas, 1980.

7. Anon. "Allegheny Ludlum AL-6XN Alloy", Allegheny Ludlum Steel Corporation, Pittsburgh, PA, 1984.

8. F.L. LaQue, "Qualification of Stainless Steel for OTEC Heat Exchanger Tubes", Ocean Thermal Energy Conversion (UC-64), ANL/OTEC-001, Argonne National Laboratory, Illinois, January 1979.

9. R.F.A. Jargelius, "The Effect of Nitrogen Alloying on the Sensitization Behavior of Two Highly Alloyed Austenitic Stainless Steels", Stainless Steels/87, Paper No: 32, The Institute of Metals, London, England, 1987.

10. Anon., "Avesta Stainless Steels", Information Brochure No. 7945, Avesta Jernverks, Avesta, Sweden, 1979.

11. R.B. Leonard and R.W. Kirchner, "Effect of Heat Treatment on Corrosion of Nickel-Base Alloys", Report 7520, Haynes International (formerly Cabot Corp.), Kokomo, Indiana, 1968.

12. M.A. Streicher, "Stainless Steels: Past, Present and Future", Stainless Steel/77, Paper No: 1, Climax Molybdenum Company, London, England, 1977.

13. R.A. Lula, Metal Progress, p.24, July, 1976.

14. H. Cao, S. Hertzman and B. Hutchinson, "Formation of Intermetallic Phases and their Influence on Mechanical Properties and Corrosion Behavior in 25Cr-4Ni-4Mo Ferritic Stainless Steel (Monit)", Stainless Steels/'87, Poster Paper E, The Institute of Metals, London, England, 1987.

15. P.B. Lindsay, Materials Performance, Vol.25, No.12, p.23, 1986.

16. E.A. Lizlovs and A.P. Bond, J. Electrochem. Soc., Vol.122, p.589, 1975.

17. Anon., "Allegheny Ludlum AL 29-4-2", Allegheny Ludlum Steel Corporation, Pittsburgh, PA, 1982.

18. Anon., "Monit Stainless", Carpenter Technology Corporation, Reading, PA, 1984.

19. J.F. Grubb and J.R. Maurer, "Use of Cathodic Protection with Superferritic Stainless Steels", Corrosion/84, Paper No: 28, National Association of Corrosion Engineers, Houston, Texas, 1984.

20. J.R. Kearns, M.J. Johnson and J.F. Grubb, "Accelerated Corrosion in Dissimilar Metal Crevices", Corrosion/86, Paper No: 228, National Association of Corrosion Engineers, Houston, Texas, 1986.

21. M.G. Fontana, Corrosion: A Compilation, p.133, The Ohio State University, Columbus, Ohio, 1957.

22. H.D. Solomon, "Age Hardening in a Duplex Stainless Steel", Paper No. 8201-003, ASM Metals Congress, St. Louis, Mo., October, 1982, American Society for Metals, Metals Park, Ohio.

23. J.W. Pugh and J.O. Nisbet, Trans. AIME, Vol. 188, p.268, 1950.

24. H.D. Solomon and T.M. Devine, in American Society for Testing and Materials STP 672, p.430, 1979.

25. E. Herbsleb and P. Schwaab, "Precipitation of Intermetallic Compounds, Nitrides and Carbides in AF22 Duplex Steel and Their Influence on Corrosion Behavior in Acids", Paper No: 8201-002, ASM Metals Congress, St. Louis, Mo., October, 1982, American Society for Metals, Metals Park, Ohio.

26. H.J. Dundas and A.P. Bond, "Corrosion Resistance of Stainless Steels in Seawater", Corrosion/85, Paper No: 206, National Association of Corrosion Engineers, Houston, Texas, 1985.

27. J.E. Truman and K.R. Pirt, "Properties of a Duplex (Austenitic-Ferritic) Stainless Steel and Effects of Thermal History", Paper No: 8201-006, ASM Metals Congress, St. Louis, Mo., October, 1982, American Society for Metals, Metals Park, Ohio.

28. C.V. Roscoe, "Steels for the Salt Solution", Iron and Steel International, p.9, February, 1985.

29. A.P. Bond and H.J. Dundas, "Resistance of Stainless Steels to Crevice Corrosion in Seawater", Corrosion/84, Paper No: 26, National Association of Corrosion Engineers, Houston, Texas, 1984.

30. H. Miyuki et.al., "25%Cr Containing Duplex Phase Stainless Steel for Hot Sea Water Application", Paper No: 8201-005, ASM Metals Congress, St. Louis, Mo., October, 1982, American Society for Metals, Metals Park, Ohio.

31. H. Nagano et.al., "Highly Corrosion Resistant Duplex Stainless Steel", paper presented at the 19th Journees des Aciers Speciaux, St. Etienne, France, May, 1980.

32. K-J. Blom, "Improving the Properties of Weld Joints in Duplex Stainless Steel by Welding with Shielding Gas Containing Nitrogen", Stainless Steels/'87, Paper No: 14, The Institute of Metals, London, England, 1987.

33. J.R. Kearns, in New Developments in Stainless Steel Technology, American Society for Metals, Metals Park, Ohio, 1985.

34. T. Ogawa et. al., Welding Research Supplement, p. 139s, May, 1982.

35. Anon., "Trentweld Alloy UNS S31803 Pipe and Tube; Alloy 2205", Trent Tube Division, Colt Industries, East Troy, WI, 1983.

36. T.S. Lee and R.M. Kain in Final Report of Sea Grant Program on Marine Corrosion, Vol.1 p.59, University of Delaware, Lewes, Delaware, August, 1984.

37. T.S. Lee and R.M. Kain, "Factors Influencing the Crevice Corrosion Behavior of Stainless Steels in Seawater", Corrosion/83, Paper No: 69, National Association of Corrosion Engineers, Houston, Texas, 1983.

38. Anon., "Avesta 254-SMO/References and Applications", Avesta Jernverks, Avesta, Sweden, 1981.

39. Anon., "Ferralium Alloy 255 - Success Against Sea Water", Langley Alloys Limited, Slough, England, 1980.

40. Anon., "Industrial and Marine Applications Continue Growing Rapidly for FERRALIUM Alloy 255 - A "Super" Duplex Stainless Steel", Cabot Digest, Vol.36, No.5, September, 1985, Cabot Corporation, Kokomo, Indiana.

TABLE 1. Typical Compositions of Some New Austenitic 6% Mo Stainless Steels Containing Nitrogen.

Alloy	UNS Number	Composition (wt%)* Cr	Ni	Mo	Mn	Si	C	N	P	S	Other
Al-6XN[1]	N08367	20.75	25.0	6.5	0.50	0.4	0.02	0.2	0.025	0.002	-
254 SMO[2]	S31254	20.0	18.0	6.1	0.50	0.4	0.02	0.2	0.025	0.001	0.7Cu
1925hMo[3]	N08925	20.0	25.0	6.5	1.0	0.4	0.02	0.2	0.025	0.002	0.8Cu

*Balance Fe

(1) Allegheny Ludlum Steel Corporation, Pittsburgh, Pennsylvania.
(2) Avesta Jernverks AB, Avesta, Sweden.
(3) Vereinigte Deutsche Metallwerke AG, Duisburg, West Germany.

TABLE 2. Effect of Alloy Composition on Crevice Corrosion Temperature.

Alloy	%Cr	%Mo	%N	CCT,°C
Type 316L	16.3	2.80	0.06	-2.5
Al-6X	20.3	6.57	0.03	32.5
7V-2	19.4	6.00	0.22	37.5
AL-6XN	20.7	6.50	0.20	45.0
7V-4	19.3	6.68	0.21	50.0

CCT - Crevice Corrosion Temperature in 10% $FeCl_3$
(ASTM Procedure G-48)

TABLE 3. Nominal Compositions of Several Superferritic Stainless Steels.

Alloy	UNS Number	Composition (wt %)* Cr	Mo	Ni	Mn	S	C	N	Si	P	Other
29-4C[1]	S44735	29.00	4.00	0.30	0.50	0.01	0.02	0.02	0.35	0.03	0.50Ti
Sea-Cure[2]	S44660	27.50	3.50	1.20	0.50	0.01	0.02	0.02	0.30	0.02	0.50Ti
Monit[3]	S44635	25.50	4.00	4.00	0.50	0.01	0.02	0.02	0.35	0.03	0.50Ti
29-4-2[1]	S44800	29.00	4.00	2.10	0.05	0.01	0.003	0.015	0.10	0.02	-

*Balance Fe

(1) Allegheny Ludlum Steel Corporation, Pittsburgh, Pennsylvania.
(2) Trent Tube Division, Colt Industries, East Troy, Wisconsin.
(3) Nyby Uddeholm AB, Karlstad, Sweden, and Carpenter Technology Corp., Reading, Pennsylvania.

TABLE 4. High Chromium Superferritic Stainless Steel Installations in U.S. Power Plant Condensers.

Power Plant	Installation (year)	Grade	Tube Length (meters)
New Orleans Public Service	1980	29-4C[1]	55,000
Southern California Edison	1980-81	29-4C	50,263
Freeport Power	1980	Sea-Cure[2]	57,000
Houston Lighting & Power	1980-84	Sea-Cure	1,335,799
New Orleans Public Service	1980	29-4C	146,300
Florida Power & Light	1980-81	Sea-Cure	417,600
Florida Power & Light	1981	29-4C	246,000
Northeast Utilities	1981-84	Sea-Cure	309,372
Southern California Edison	1983	Sea-Cure	243,840
Virginia Electric Power	1982	29-4C	518,160
Central Hudson	1981	29-4C	12,265
Central & Southwest Services	1984	29-4C	510,668
Duquesne Light	1984	Sea-Cure	1,127,760
Gulf States Utilities	1982	29-4C	396,240
Niagara Mohawk	1984	Sea-Cure	57,323
Orlando Utilities	1982	Sea-Cure	106,680
Public Service Gas & Elec. of N.J.	1982	Sea-Cure	213,360
San Diego Gas & Electric	1983	Sea-Cure	653,273
San Diego Gas & Electric	1983	29-4C	487,630

Source: Climax Molybdenum Company
(1) 29-4C, Fe-29Cr-4Mo-0.5Ti, Supplier: Allegheny Ludlum Steel Corporation
(2) Sea-Cure, Fe-27.5Cr-3.5Mo-2.0Ni-0.5Ti, Supplier: Trent Tube Division, Colt Industries

TABLE 5. Typical Compositions of Some New Duplex Stainless Steels and of an AOD[1] Melted Austenitic AISI 316 Stainless Steel.

Alloy	UNS Number	Composition (wt%)*										
		Cr	Ni	Mo	Mn	Si	C	N	P	S	Cu	W
Ferralium[2] 225	S32550	26.0	5.5	3.0	0.8	0.45	0.04	0.17	0.04	0.03	1.70	-
Alloy 2205[3]	S31803	22.0	5.5	3.0	1.7	0.80	0.03	0.14	0.03	0.02	-	-
DP 3[4]	-	25.4	6.2	3.3	0.9	0.61	0.02	0.14	0.01	0.01	0.44	0.5
AISI 316	S31600	18.0	11.3	2.1	1.8	0.60	0.04	0.06	0.045	0.01	-	-

*Balance Fe

(1) AOD = argon-oxygen decarburization.
(2) Bonar Langley Alloys, Ltd. Slough, England, and Haynes International, Inc., Kokomo, Indiana
(3) AB Sandvik Steel, Sandviken, Sweden, and Eastern Stainless Steel, Baltimore, Maryland.
(4) Sumitomo Metal Industries, Ltd., Osaka, Japan.

TABLE 6. Mechanical Properties and Crevice Corrosion Temperatures of Various Alloys

Alloy	UNS Number	0.2% Offset Yield Stress (ksi)	Ultimate Tensile Strength (ksi)	Elongation (%)	Hardness, Rockwell B.	CCT* (°C)
AL-6XN	N08367	55	110	50	90	45
254-SMO	S31254	43	94	35	97	46
1925hMo	N08925	44	101	35	-	41
29-4C	S44735	75	90	25	95	55
SEA-CURE	S44660	75	90	30	95	45
MONIT	S44635	93	104	25	100	47
29-4-2	S44800	80	100	25	95	50
FERRALIUM 225	S32550	98	126	30	103	37
2205	S31803	82	120	30	98	20

*Crevice corrosion temperature in 10% $FeCl_3$ (ASTM Procedure G-48).
1 ksi = 6.8948 MPa.

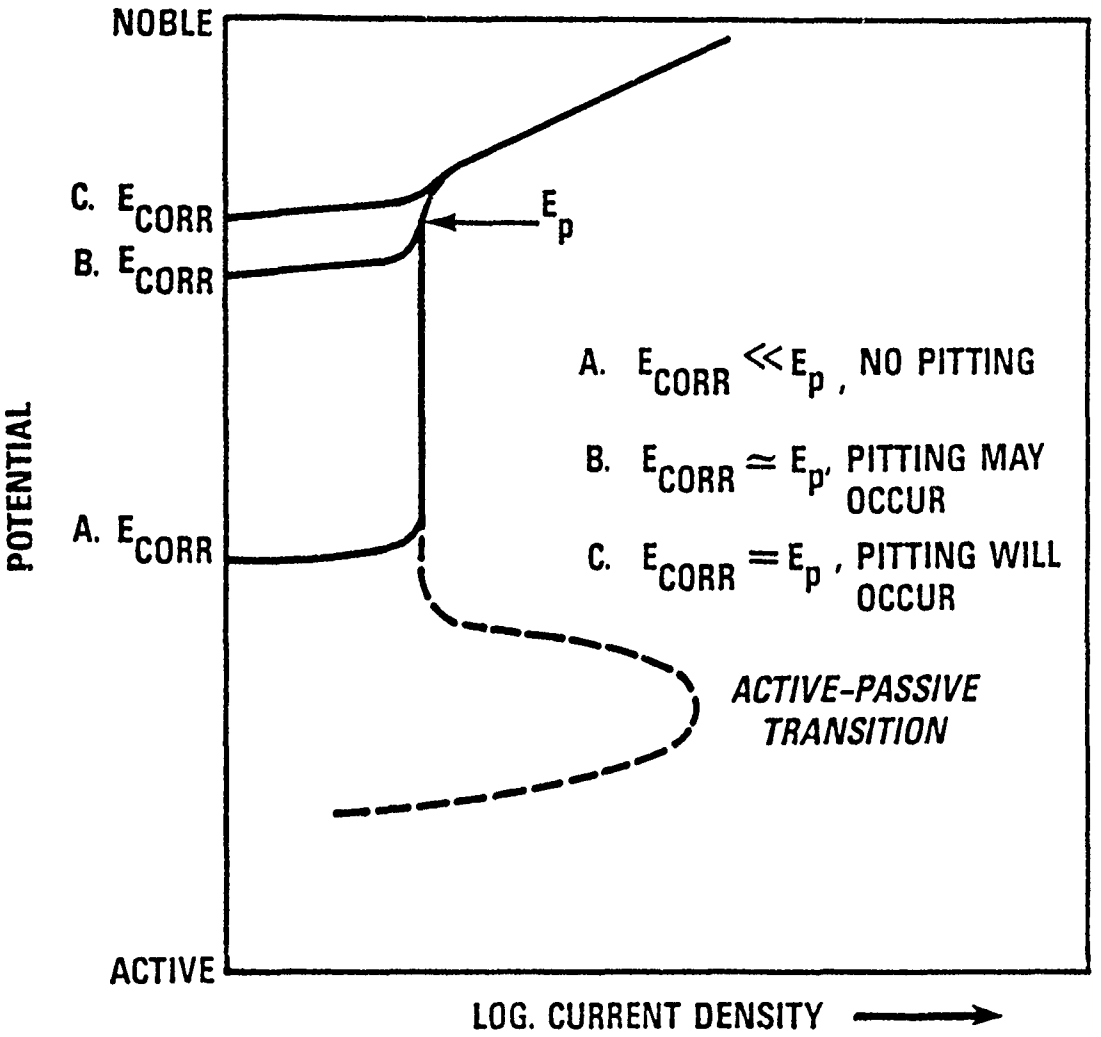

Figure 1. Schematic polarization curve illustrating conditions under which pitting may or may not occur.

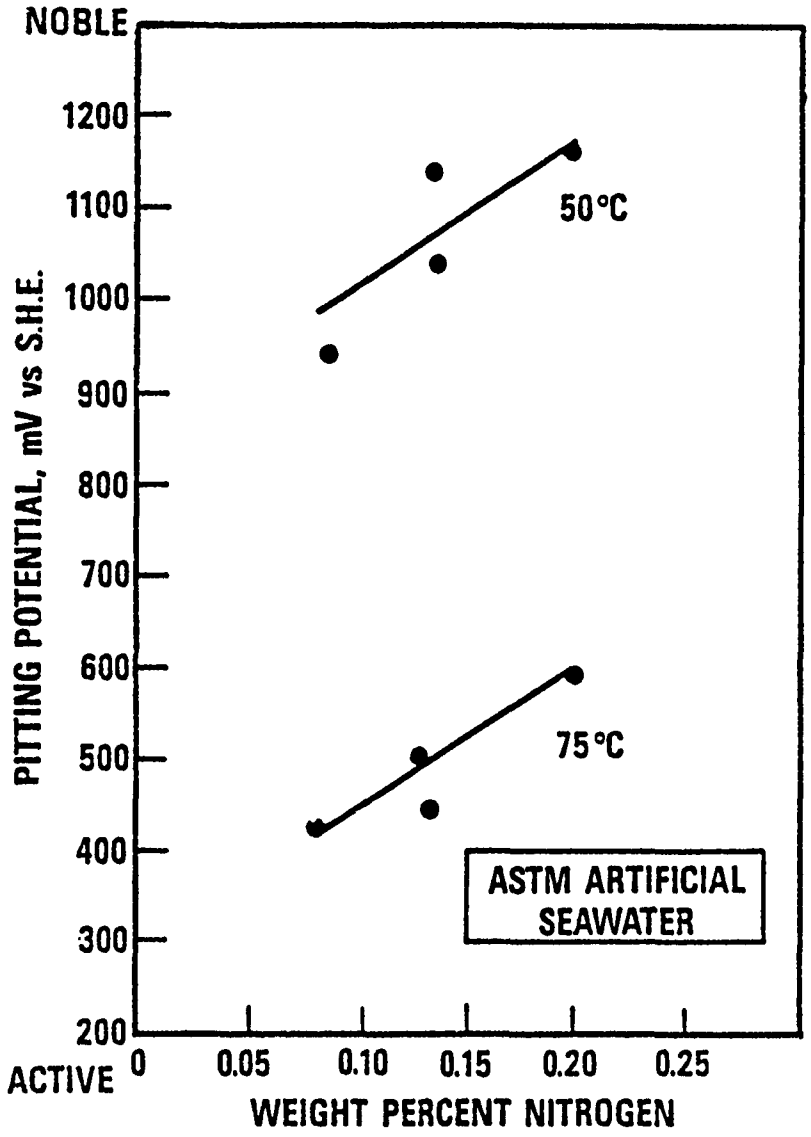

Figure 2. Variation of pitting potential with nitrogen content of CRONIFER 1925hMo in aerated ASTM artificial seawater.

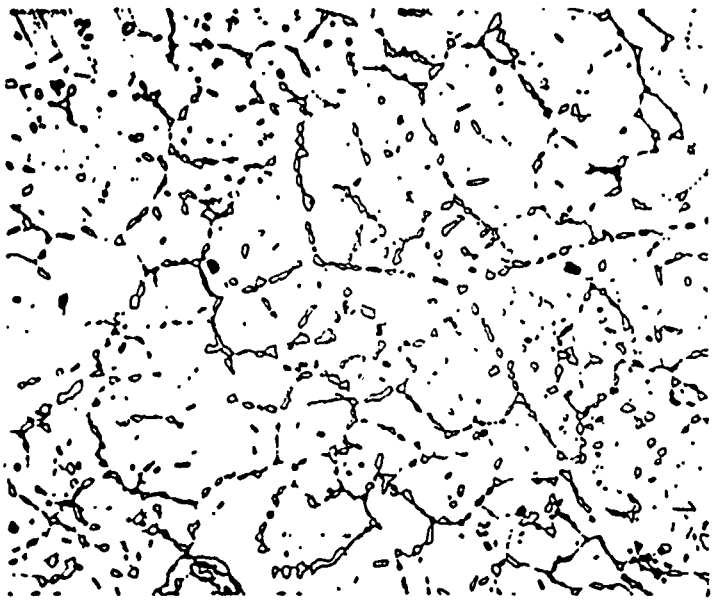

Figure 3. Sigma phase produced in an Fe-20.8%Cr-24.8%Ni-7.2%Mo alloy heated for 1 hour at 1093°C and air cooled. Etched in 3% sulfuric acid electrolytically. Magnification = 500X.

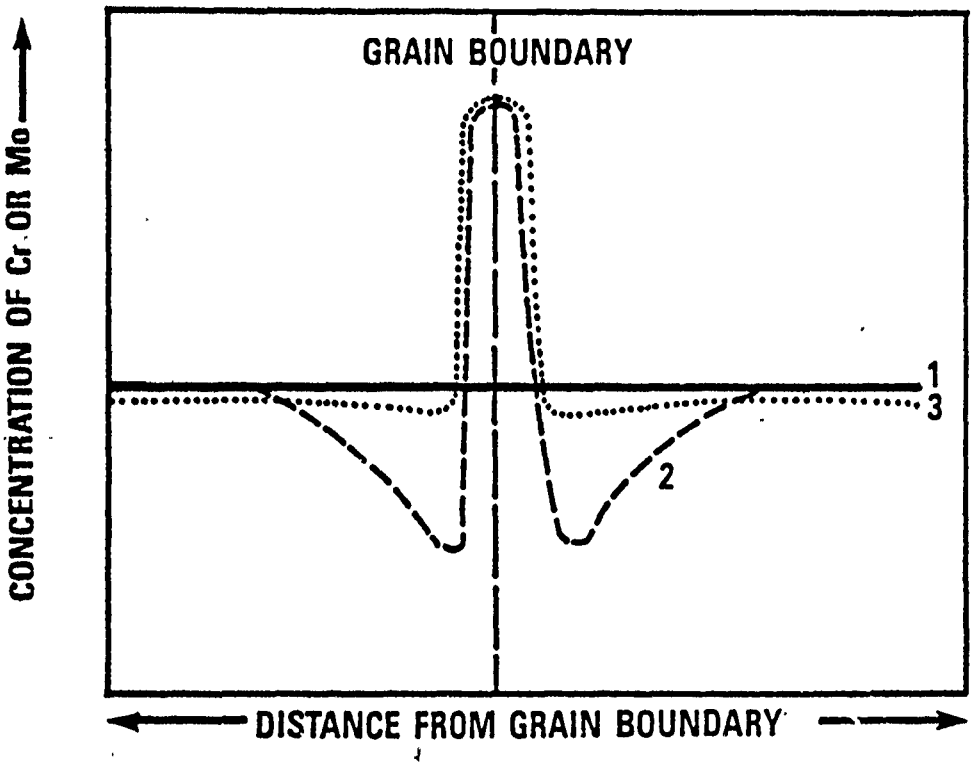

1. HOMOGENEOUS STRUCTURE
2. PRECIPITATION OF SIGMA ALONG GRAIN BOUNDARIES WITH LOW DIFFUSION OF Cr OR Mo
3. PRECIPITATION OF SIGMA ALONG GRAIN BOUNDARIES WITH SUFFICIENT DIFFUSION

Figure 4. Schematic of concentration of chromium and molybdenum at a grain boundary.

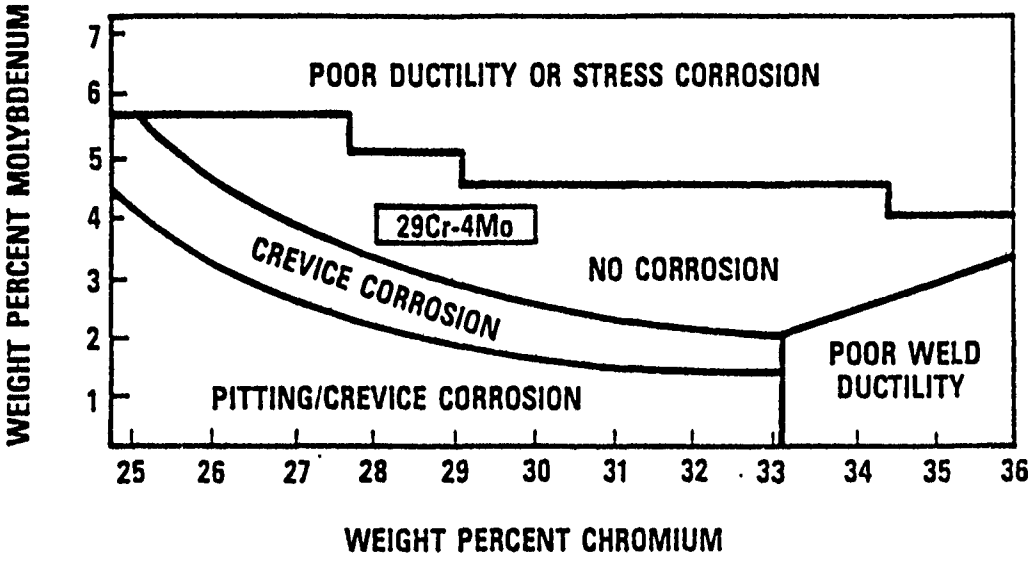

Figure 5. Effect of chromium and molybdenum on the properties of Fe-Cr-Mo alloys.

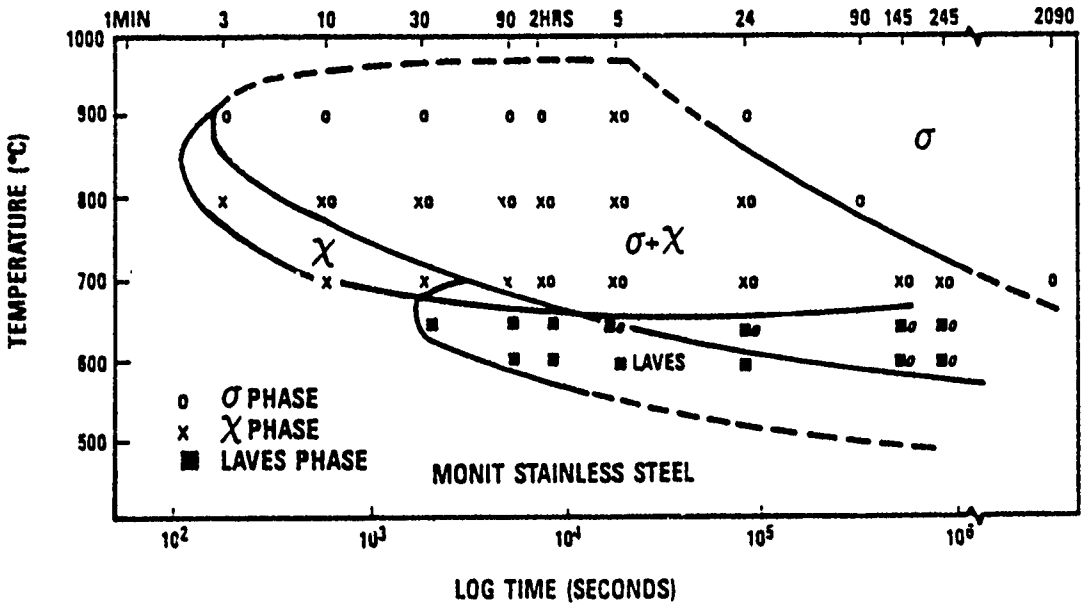

Figure 6. Time-temperature-precipitation diagram for MONIT stainless steel. Aged after solution treatment at 1000°C for ten minutes and water quenching.

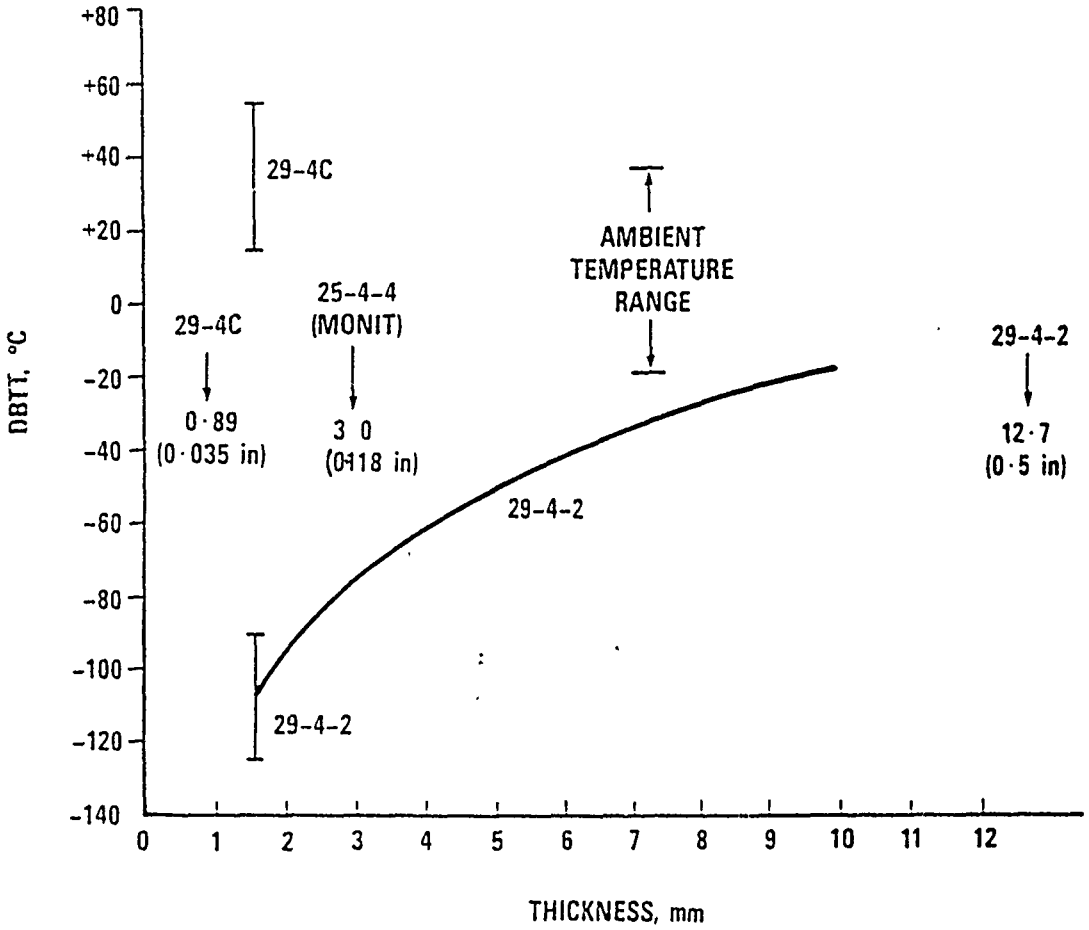

Figure 7. Variation of the ductile-to-brittle transition temperature as a function of thickness for various superferritic stainless steels.

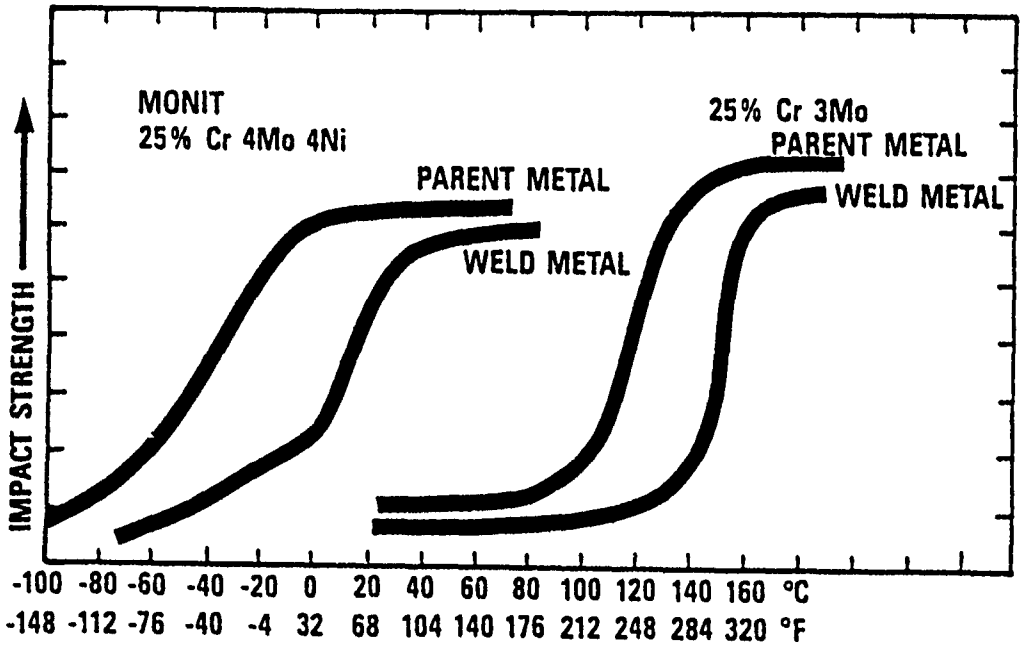

Figure 8. Comparison of the ductile-to-brittle transition temperatures for two superferritic stainless steels with and without nickel.

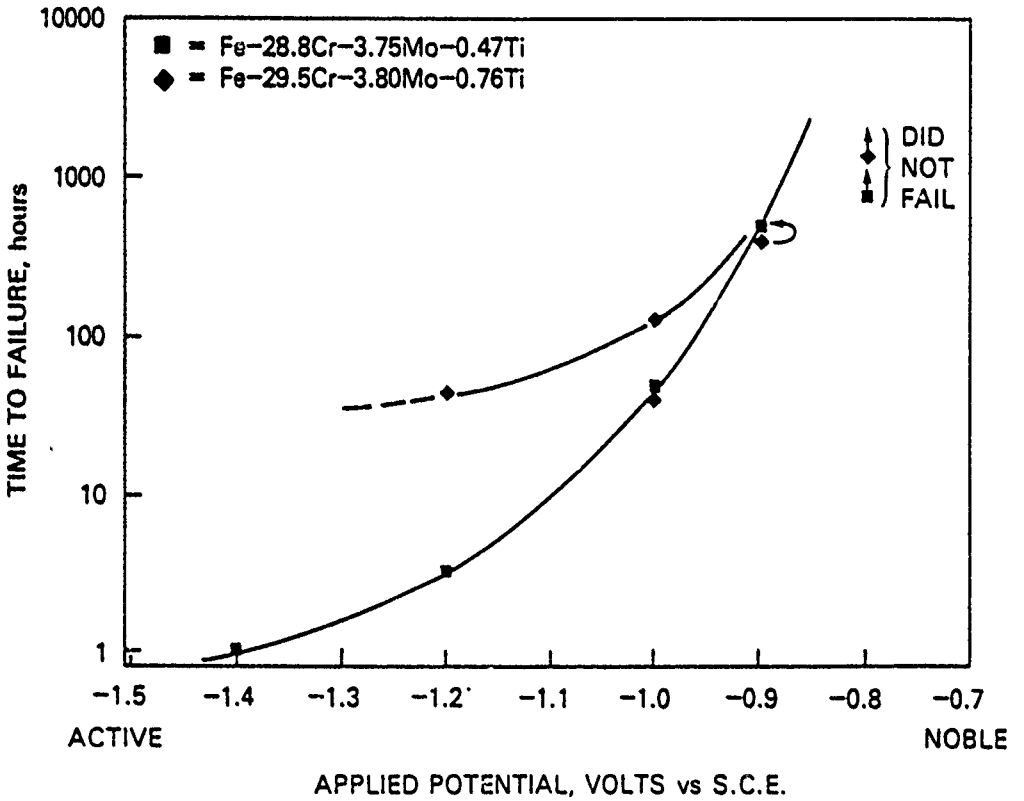

Figure 9. Time to failure by hydrogen embrittlement of two heats of as-welded AL 29-4C stainless steel in ambient temperature synthetic seawater as a function of applied potential.

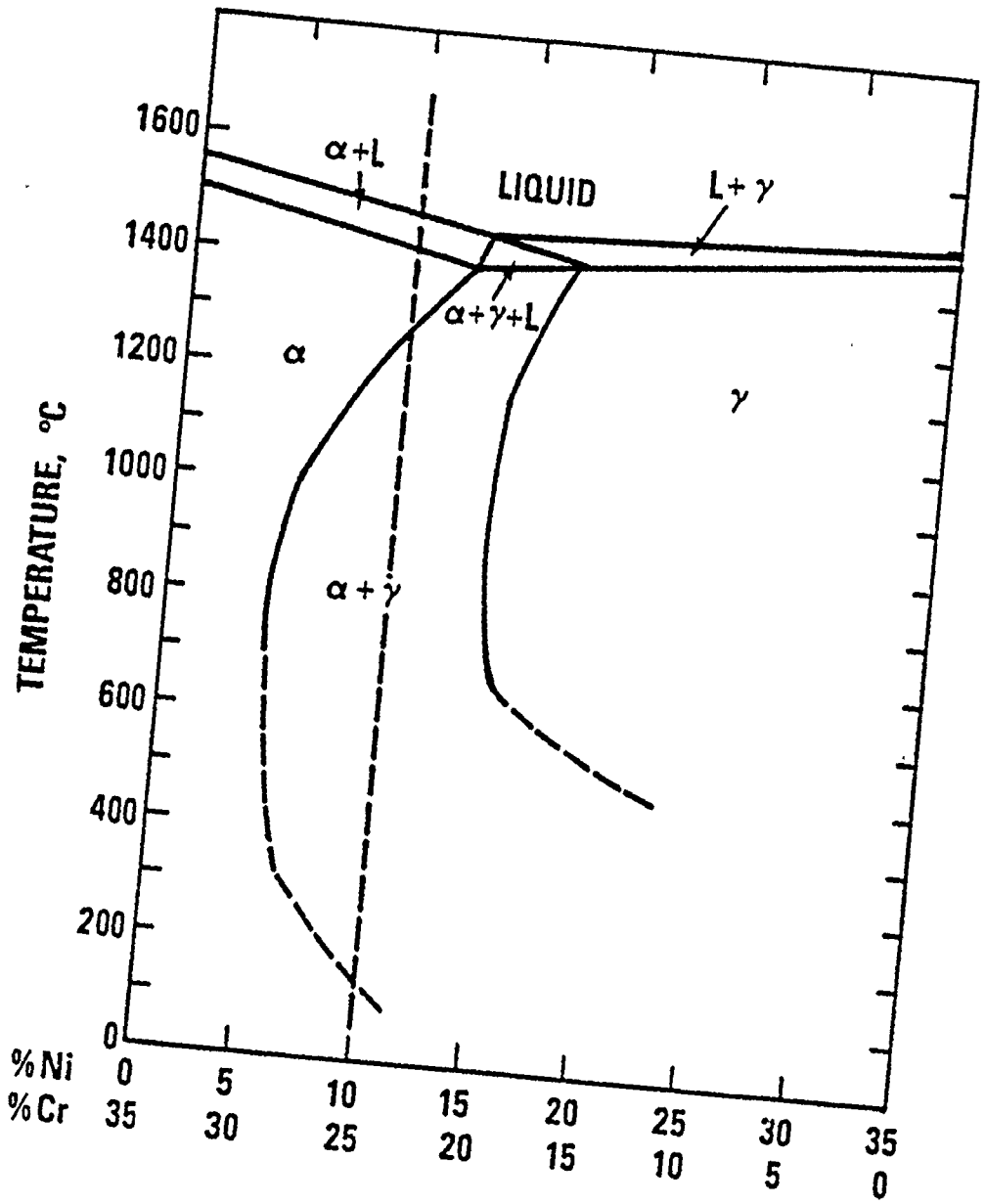

Figure 10. Pseudo-binary phase diagram for 65%Fe-Cr-Ni.

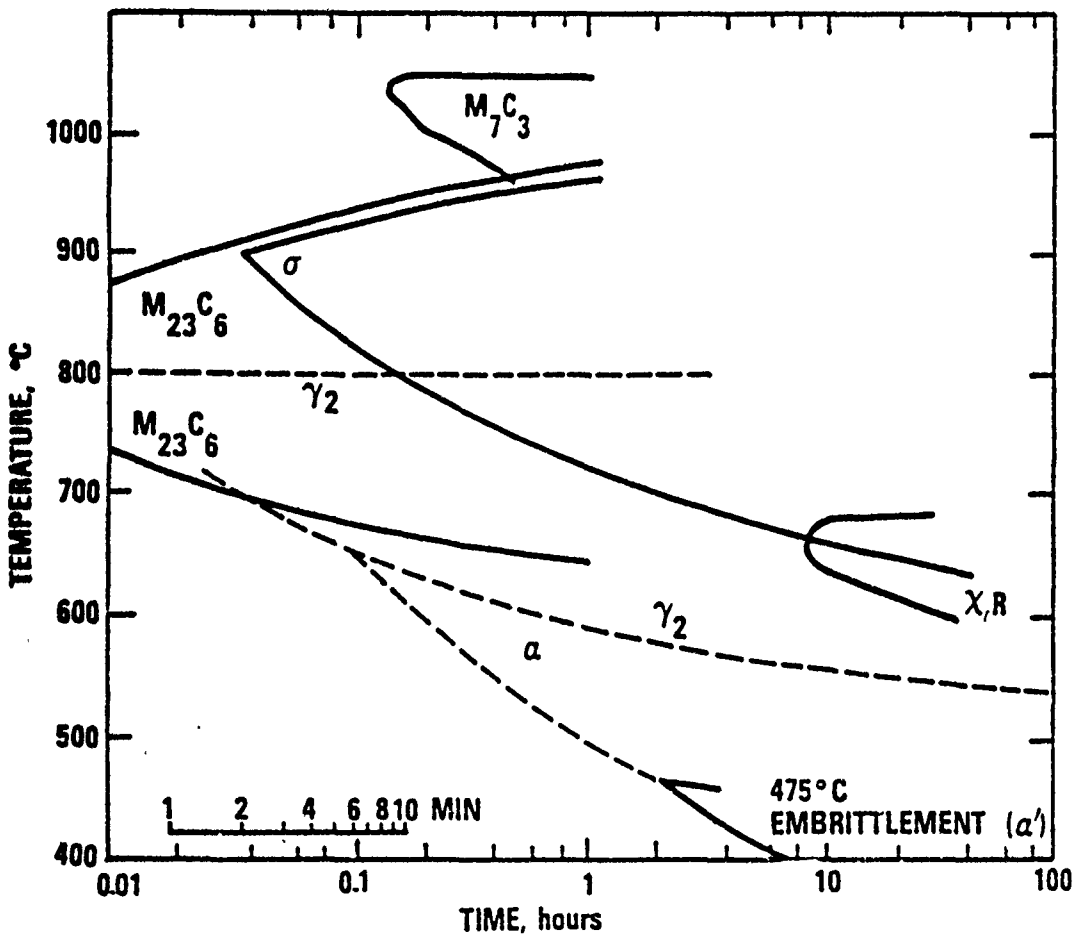

Figure 11. Time-temperature-precipitation diagram for the duplex stainless steel URANUS 50.

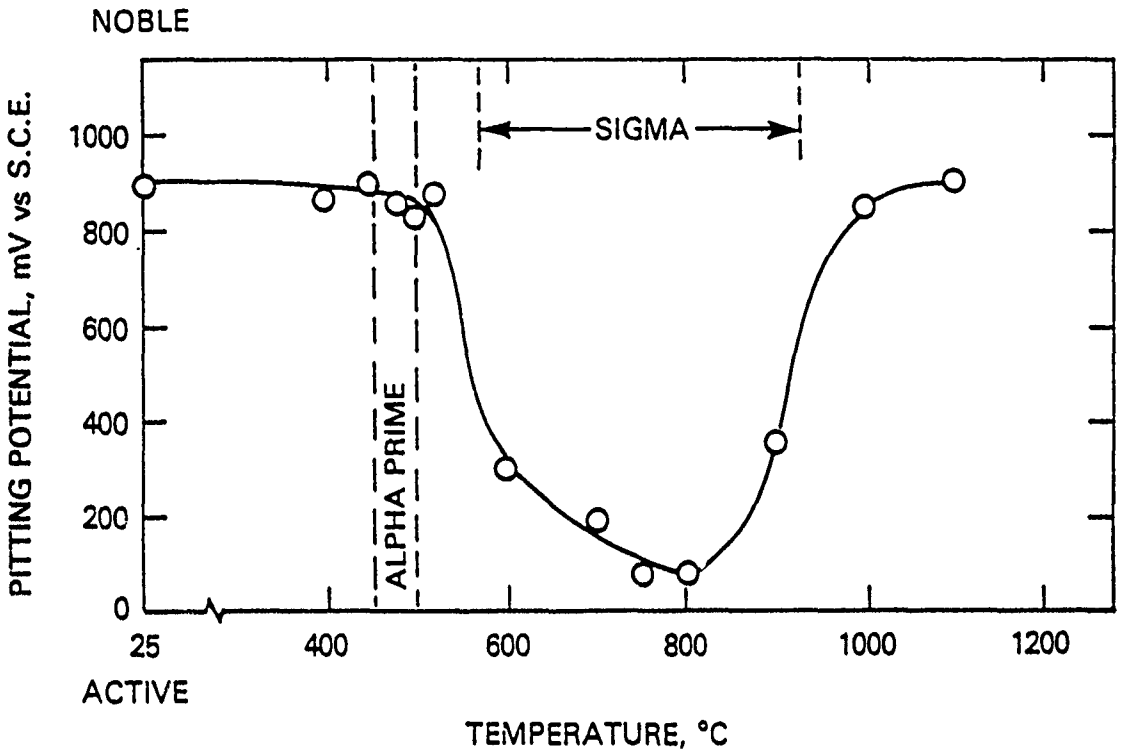

Figure 12. Effect of isothermal heat treatment temperature (4 hours) on the pitting potential of a duplex stainless steel (Fe-26%Cr-5.5%Ni-1.5%Mo-0.2%N) in an aerated 0.6M NaCl + 0.1M $NaHCO_3$ solution at 25°C.

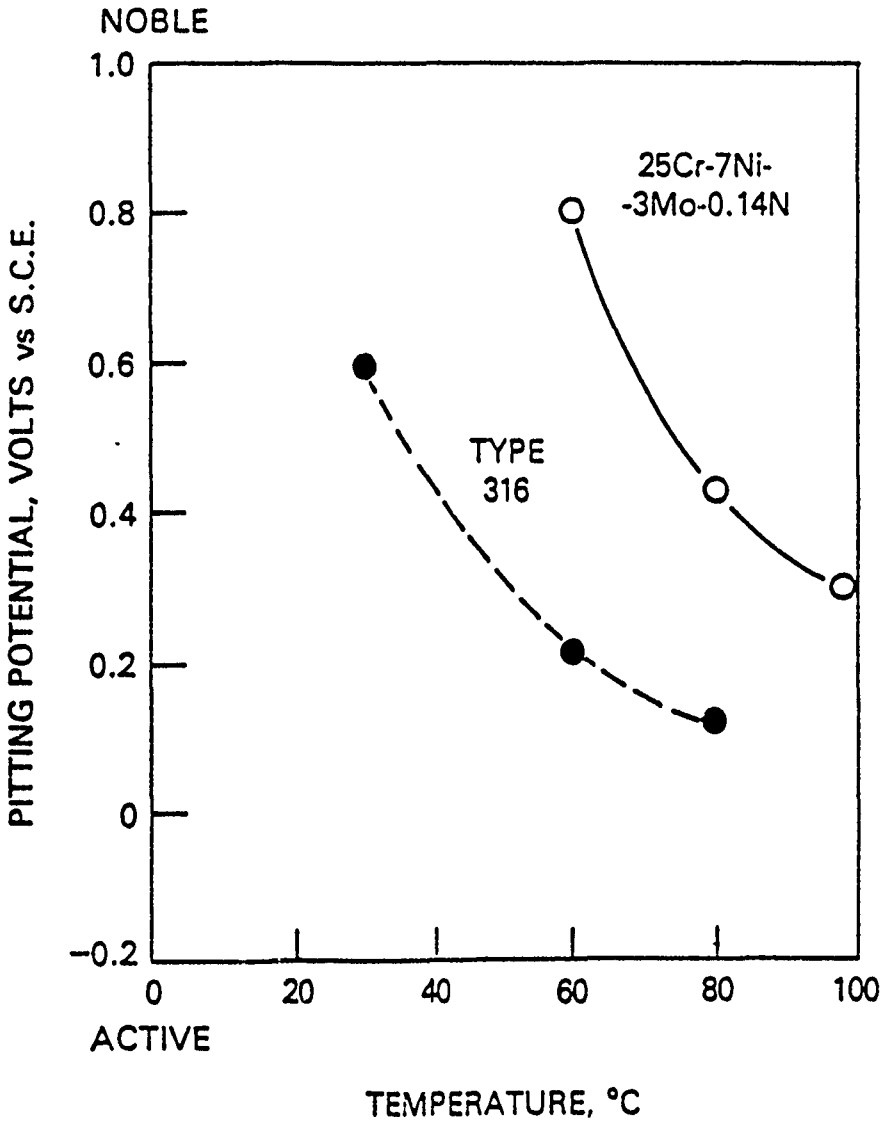

Figure 13. Pitting potentials of type 316 and of a duplex stainless steel containing 25%Cr-7%Ni-3%Mo-0.14%N in deaerated synthetic seawater as a function of temperature.

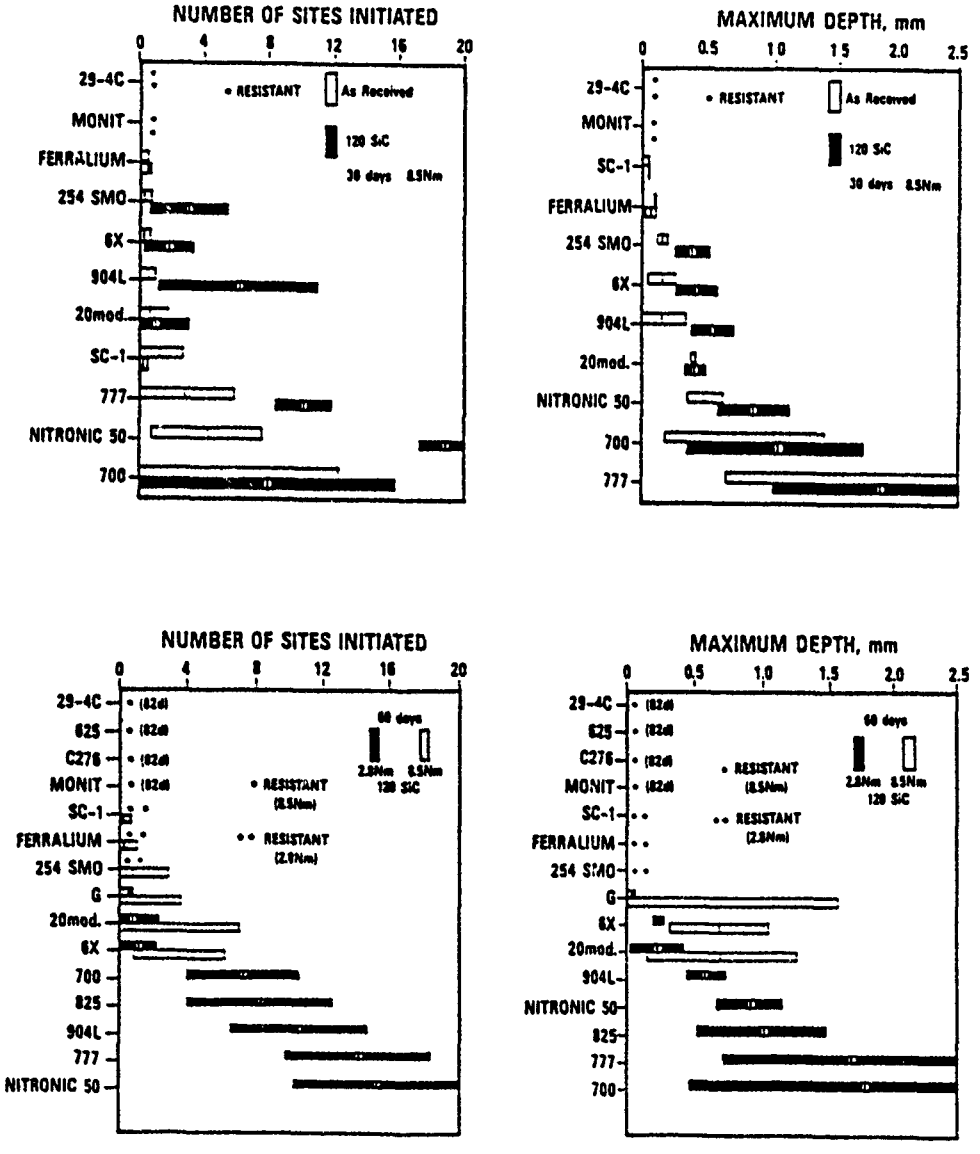

Figure 14. Analysis of multiple crevice assembly test data describing the effects of surface finish (top) and initial assembly torque level (bottom) on initiation and penetration resistance. Bar graphs represent the mean values (plus and minus one standard deviation) for replicate tests at 30 days and 60 or 82 days, respectively.

A COMPARATIVE CORROSION STUDY OF TITANIUM AND COPPER-NICKEL ALLOYS

Anh H. Le and Mark W. Dust

Naval Surface Warfare Center
Materials Division
Electrochemistry Branch
10901 New Hampshire Avenue
Silver Spring, MD 20903-5000

ABSTRACT

Copper-nickel (Cu-Ni) alloys are very susceptible to erosion corrosion and crevice corrosion when used in marine applications for seawater piping systems and heat exchangers. Titanium has been suggested as an alternative material for this application. The corrosion behavior of titanium (grades 2 and 5) was investigated in sodium chloride solutions by electrochemical techniques. The corrosion data of titanium were compared to those of Cu-Ni alloys 70/30 and 90/10 in terms of localized corrosion and erosion corrosion tendencies.

I. INTRODUCTION

The selection of a suitable material for seawater piping and heat exchangers in naval applications presents many difficulties. Traditionally, 70/30 or 90/10 Cu-Ni alloys have been the materials of choice. These alloys exhibit the following favorable characteristics: corrosion resistance; ductility; joining by soldering, brazing, or welding; castability; and low cost (1).

Unfortunately, Cu-Ni alloys have problems in use. In certain portions of piping systems, particularly at bends and elbows, Cu-Ni alloys are susceptible to failure caused by erosion corrosion and crevice corrosion (2). Small amounts of iron, typically 0.3 to 2.0%, have been added to Cu-Ni alloys to improve their resistance to erosion corrosion (3), however, the failures continue to occur.

In similar applications for petroleum refinery heat exchangers, titanium is increasingly used as a replacement material for Cu-Ni alloys (4,5). The properties that make titanium attractive to petroleum engineers also make titanium attractive for marine applications. Titanium has higher yield and tensile strengths, lower density resulting in overall weight reduction, and greater resistance to erosion corrosion than Cu-Ni alloys (2).

The purpose of this study is to compare the corrosion behavior of Cu-Ni alloys (70/30 and 90/10) and titanium alloys (grades 2 and 5). Electrochemical testing was conducted to investigate the effect of the following variables: sodium chloride concentration, pH, deaeration (dissolved oxygen) effect, simulated flow rate and temperature.

II. EXPERIMENTAL

1. Samples

Materials used in this study were titanium alloys, grades 2 and 5 and Cu-Ni alloys, 70/30 and 90/10. Titanium alloys were obtained from Titanium Metals Corporation of America. The elemental compositions of these alloys are:

Titanium Alloys

Per Cent	O	Fe	H	C	N	Al	V	Ti
Grade 2	0.25	0.20	0.015	0.10	0.03	--	--	Bal.
Grade 5	0.20	0.40	0.015	0.10	0.05	5.5-6.7	3.5-4.5	Bal.

Copper-Nickel Alloys

Per Cent	Cu	Ni	Fe	Mn	Zn	Pb	P
90/10	88.15	9.51	1.53	0.6	0.098	0.005	0.003
70/30	68.81	30.0	0.53	0.51	0.02	0.003	0.003

Samples were prepared by abrading with sandpaper (240, 400 and 600 grit) and then ultrasonically cleaned in distilled water.

2. Equipment setup

An EG&G Corrosion Measurement Console Model 350A, EG&G Potentiostat/Galvanostat Model 273, SoftCorr Corrosion 342 software and a corrosion cell consisting of two graphite electrodes, a working electrode and a saturated calomel reference electrode were used to obtain the anodic polarization and potentiostatic pitting curves. Potentials were reported in volts versus saturated calomel electrode reference unless otherwise noted. Open-circuit potentials were determined when the potential shifted less than 10 mV in 10 minutes. Corrosion rates are reported in mils per year (mpy).

Sodium chloride solutions with a normality ranging from 0.001 to 3.0 were used to study the concentration effect. The solutions were prepared with analytical grade sodium chloride and distilled water. Nitrogen was purged into solutions for at least 3 hours for deaerated tests. Hydrochloric acid (HCl) and sodium hydroxide (NaOH) were added as necessary to 3.5 wt.% (0.6 N) sodium chloride solution to obtain the desired pH in the range from pH 2 to pH 10. A rotating electrode setup was used to simulate the effect of the flow of seawater. Different rotating speeds were chosen from 1000 rpm up to the maximum speed of 10,000 rpm. A temperature-controlled water bath was used to study the effect of temperature at room temperature (25°C), 50°C, 75°C and 100°C.

III. RESULTS AND DISCUSSION

1. Effect of chloride concentration

In general, the protection of a metal from hostile environments is achieved by forming a self-healing oxide film on the metal surface. Tomashov et al (6) reported that for titanium the composition of the oxide film varies across its thickness. The film contained TiO next to the base metal, TiO_2 at the outer surface, and an interior consisting mainly of Ti_2O_3. The chloride solution retards the repassivation process by attacking the titanium oxide to form a soluble titanium complex. Increasing the chloride concentration will accelerate the corrosion process.

As shown in Figure 1, corrosion rates of titanium, grades 2 and 5, in sodium chloride solutions are more than two orders of magnitude smaller compared to those Cu-Ni alloys. For all four alloys, the corrosion rate increased as concentration of sodium chloride increased up to 0.1 N and leveled off at 0.6N (3.5 wt.%). The corrosion rates of Cu-Ni 70/30 in general are less

than those of Cu-Ni 90/10. Similarly, corrosion rates of titanium grade 5 are less than those of titanium grade 2.

2. Effect of oxygen

Copper alloys are subject to increased attack in the presence of oxygen. To eliminate the dissolved oxygen, nitrogen gas was purged into 3.5 wt.% NaCl solution for at least three hours before the test. The effect of deaeration on Cu-Ni alloys and titanium alloys is shown in Figure 2. A general behavior was observed for the four alloys in that the corrosion rates are reduced in deaerated 3.5 wt.% solution.

3. Effect of pH

Corrosion rates of Cu-Ni and titanium alloys were determined from the anodic polarization technique at various pH values ranging from pH 2 to pH 11.5. The maximum corrosion rate of Cu-Ni alloys was in the range of pH 6 and pH 8 while the corrosion rate of titanium alloys was independent of pH. It is shown in Figure 3 that titanium grade 5 corroded less than titanium grade 2 in either acidic or basic solutions.

4. Effect of stirring rate

Titanium is normally resistant to localized corrosion (pitting and crevice corrosion) in seawater. Only very slight uniform weight loss occurs under stagnant flow conditions (0.03 mpy for 4.5 years) or under high velocity (>138 ft/sec) conditions (0.2 mpy for 4.5 years)(7). To simulate the effect of the flow rate of the liquid medium on the corrosion rate of the metal, a rotating electrode setup was employed. Cylindrical samples of Cu-Ni, 70/30 and 90/10, and titanium grade 2 were used. The top and bottom surfaces were covered by an insulator coating so only the lateral surface was exposed to the 3.5 wt.% NaCl solution. The corrosion rates of Cu-Ni alloys increased as the stirring rate increased. Cu-Ni 70/30 is less susceptible to the stirring rate effect than Cu-Ni 90/10. The corrosion rate of titanium alloy grade 2 remained constant even at the maximum stirring rate of 10,000 rpm (see Figure 4).

5. Effect of temperature

Pure titanium (99.9%) is highly resistant to pitting corrosion, (with a pitting potential of 9.0-10.5 volts in 0.5N NaCl), but it is impractical to use because it has a low tensile strength. The addition of relatively small amounts of oxygen (0.1-0.4%) and nitrogen (0.01-0.025%), as well as small amounts of iron, carbon, and hydrogen improves the strength of titanium at the cost of

reduced pitting resistance (8). Posey and Bohlmann (9) showed that the pitting potential of titanium-aluminum alloys shifted to more negative potentials as the temperature increased. Also, they observed that as the aluminum content increased, the pitting potential decreased. It is assumed that the development of pits on titanium occurs through the formation of titanium complexes in chloride solution ($TiCl_4$). Therefore, the formation of the titanium salts at the base of the pit is much more important than a low pH for propagating pits (10). The solubility of the titanium complex increases as the temperature increases, resulting in greater pitting corrosion.

It has been reported that in 3.5 wt.% NaCl, titanium grade 2 is considered to be immune to corrosion, especially pitting corrosion up to 150°C (11). In Figure 5, the corrosion rates of Cu-Ni and titanium alloys increased as the temperature increased. Pitting corrosion of titanium alloy grade 5 shifted to a more negative potential as the temperature increased. Pitting corrosion of titanium grade 2 was not observed visually, however, pitting on the titanium grade 5 became very distinct, even at the temperature of 35 °C. At room temperature (25°C) pitting potential of titanium grade 5 is 6.350 V, but the value drastically decreases to a potential of 2.6 V at 45°C (see Figure 6). Pitting corrosion of titanium alloy grade 5 occurs at low temperature, perhaps due to the selective dissolution of aluminum or iron from the titanium alloy surface, forming aluminum or iron ionic complexes. In addition, aluminum and iron may interact with the titanium to form a local galvanic cell. As a result, the total corrosion reaction of titanium grade 5 is accelerated.

IV. CONCLUSION

Titanium shows great promise as a replacement material for Cu-Ni alloys in seawater piping and heat exchanger applications because of its improved corrosion behavior in marine environments. In this study, titanium grades 2 and 5 were compared with Cu-Ni, 70/30 and 90/10, in terms of corrosion resistance under a variety of environments. The effects of chloride concentration, deaeration, pH, solution velocity, and temperature were examined. The following conclusions were made:

1. The corrosion rates for Cu-Ni 70/30 were marginally lower than those for Cu-Ni 90/10 under the conditions listed below:

- NaCl concentrations from 0.001N to 2N
- Deaerated or aerated 3.5 wt.% NaCl solutions
- Stirring rates from 0 to 6000 rpm
- Temperatures from 25°C to 100°C

2. The corrosion rates for Cu-Ni 70/30 were not significantly different from those of Cu-Ni 90/10 at various pH levels from 2 to 12.

3. The corrosion rates for titanium grade 5 were marginally lower than those for titanium grade 2 under the conditions listed below:

- NaCl concentrations from 0.01N to 2N
- Deaerated or aerated 3.5 wt.% NaCl solutions
- pH levels from pH 2 to pH 10
- Temperatures from 25°C to 100°C

4. Titanium grade 5 is more susceptible to pitting corrosion than titanium grade 2.

5. Both grades of titanium demonstrated greater corrosion resistance than either Cu-Ni alloy for all of the tested conditions.

V. REFERENCES

1. "Special Navy Ship Material Characteristics", Engineering Duty Qualification Program Study Paper T-025, Rev 0, Engineering Duty Officer School, Mare Island, California, p. 23-25, March 1978.

2. R. W. Schutz and M. R. Scaturro, "Titanium Outperforms Rivals for Improving Seawater Systems", Sea Technology, p. 49-51, June 1988.

3. H. S. Campbell, "A Review: Pitting Corrosion of Copper and Its Alloys", Localized Corrosion NACE-3, Ed. by R. W. Staehle et al, National Association of Corrosion Engineers, Houston, Texas, 1974.

4. R. L. Jacobs and J. A. McMaster, "Titanium Tubing: Economical Solution to Heat Exchanger Corrosion", Materials Protection and Performance, Vol. 11, p. 33, No. 7, July 1972.

5. J. A. McMaster, "Selection of Titanium for Petroleum Refinery Components", Materials Performance, Vol. 18, No. 4, p. 28-31, April 1979.

6. N. D. Tomashov, R. M. Altovskii and M. Takushnerev, Dokl. Akad Nauk (USSR), No. 4 , p. 2, Table 1, 1961.

7. H. H. Uhlig, "Corrosion and Corrosion Control", p. 323, John Wiley & Sons Inc., New York, London, 1963.

8. H. P. Godard, W. B. Jepson, M. R. Bothwell and R. L. Kane, "The Corrosion of Light Metals", p. 316, John Wiley & Sons Inc., New York, 1967.

9. F. A. Posey and E. G. Bohlmann, "Desalination", Vol. 3, p. 269, 1967.

10. H. J. Raetzer-Scheibe, Corrosion, Vol. 34, p. 437, 1978.

11. R. Baboian, W. D. France, Jr., L. C. Rowe, and J. F. Rynewicz, Editors, 'Galvanic and Pitting Corrosion - Field and Laboratory Studies", American Society for Testing and Materials, p. 150, 1976.

VI. ACKNOWLEDGEMENT

The authors wish to acknowledge R. W. Schutz of the Titanium Metals Corporation of America for providing the titanium samples used in this study and Christine Yoon, a summer SEAP student, for her laboratory work with the Cu-Ni alloys.

Figure 1 : Chloride Concentration Effect

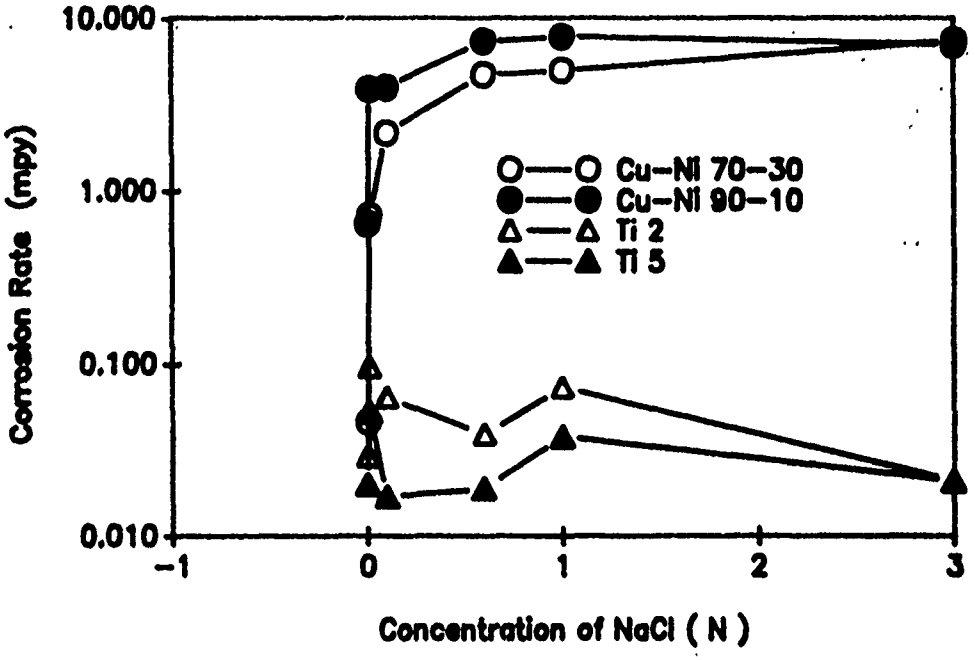

Figure 2 : Oxygen Effect

3.5 wt% NaCl

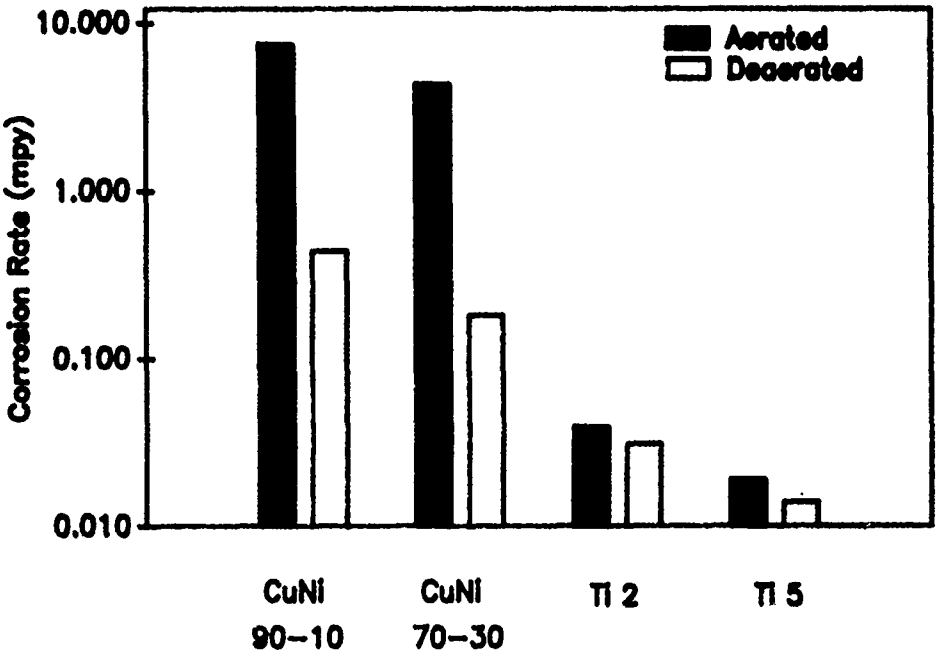

Figure 3 : Effect of pH
3.5 wt% NaCl (+ HCl or NaOH)

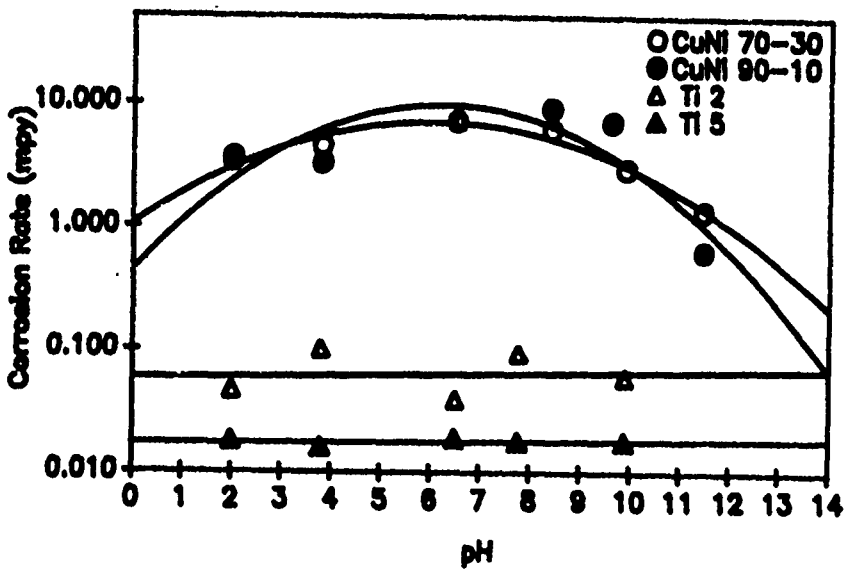

Figure 4 : Effect of Stirring Rate
3.5 wt% NaCl

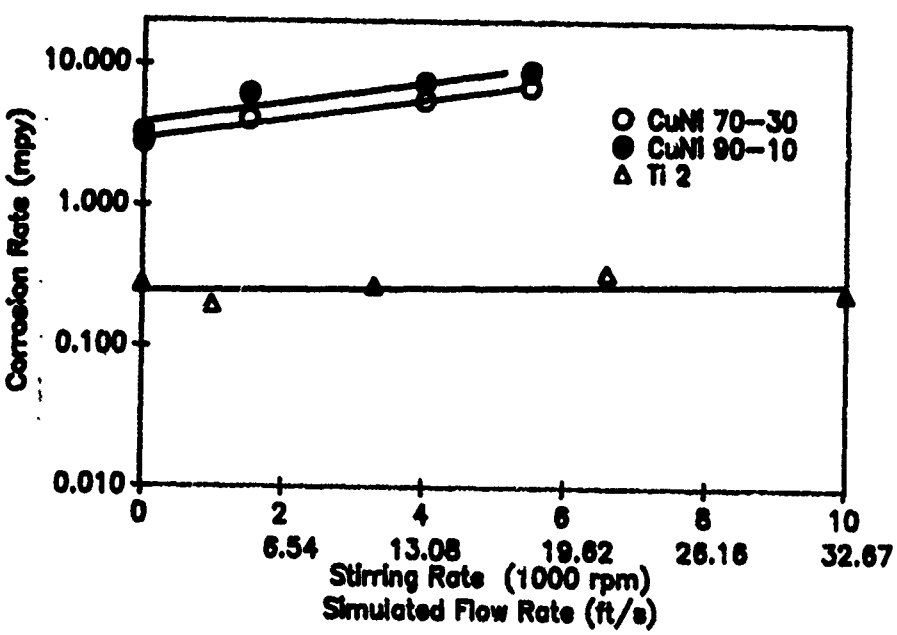

Figure 5 : Effect of Temperature
3.5 wt% NaCl

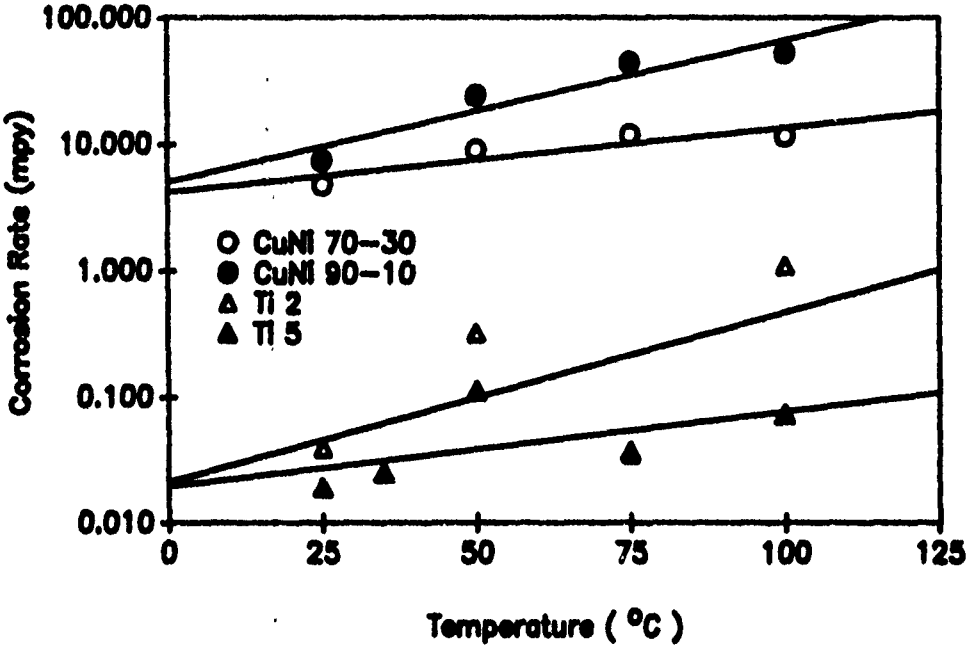

Figure 6 : Effect of Temperature on Pitting Potential
Titanium 5 in 3.5 wt% NaCl

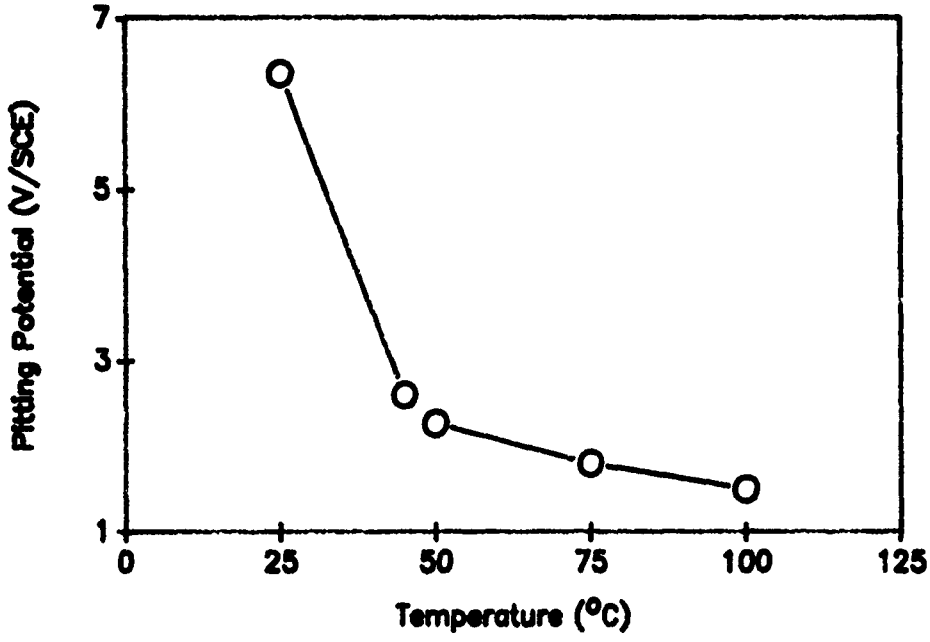

OXIDATION AND HOT CORROSION OF SOME ADVANCED SUPERALLOYS AT 1300°-2000°F (704°-1093°C)

M. Levy and R. Huie
U.S. Army Materials Technology Laboratory, Watertown, MA 02172-0001

F. Pettit
University of Pittsburgh, Pittsburgh, Pennsylvania 15261

ABSTRACT

The cyclic oxidation resistance and the hot corrosion resistance of three single crystal nickel-base superalloys and DS MAR M 200 are compared. The comparison is made by using burner rig oxidation tests at 2000°F (1093°C), and tube furnace oxidation and hot corrosion tests at 2000°F (1093°C), 1650°F (900°C), and 1300°F (704°C). The rig tests and the tube furnace tests produce similar results with the single crystal alloys being more oxidation resistant than DS MAR M 200. A significant difference between the hot corrosion resistance of these alloys was not observed. All four alloys were extremely susceptible to hot corrosion induced by a liquid deposit.

INTRODUCTION

Superalloy solidification procedures are now available whereby single crystal gas turbine blades can be fabricated. Superalloys with such structures have certain mechanical properties that are superior to conventionally cast and directionally solidified alloys.[1] Since the single crystal alloys do not require alloying elements to provide grain boundary strengthening, their compositions are different and somewhat less complicated than their polycrystalline counterparts. In a previous paper,[2] the oxidation resistances of several single crystal superalloys in air at 2000°F (1093°C) were compared to a polycrystalline alloy, DS MAR M 200,* under both isothermal and cyclic conditions. The oxidation resistances of all the single crystal alloys were superior to the polycrystalline alloy. A significant difference between the oxidation of the different single crystal alloys was not observed.

In this previous investigation, the cyclic oxidation tests were performed by using a tube furnace in which the specimens were cycled to room temperature once every one-half hour of exposure at 2000°F (1093°C). Another method of oxidation testing is to use a dynamic burner rig.[3,4] Burner rig testing often utilizes high gas velocities (200-300 m/s) and, while not reproducing the exact conditions in a gas turbine, it does simulate more closely such conditions than the tube furnace oxidation test. One of the objectives of the present paper is to compare the oxidation behavior of the single crystal alloys and DS MAR M 200 by using dynamic burner rig testing at 2000°F (1093°C), as well as tube furnace cyclic oxidation testing at 2000°F (1093°C) and 1650°F (900°C).

For some gas turbine operating conditions, deposits may accumulate upon the surfaces of turbine hardware. The compositions of such deposits depend upon the operating conditions (e.g., fuel impurities, air

* Registered trade name.

1. GELL, M., DUHL, D. N., and GIAMEI, A. F. *Superalloys 1980.* TIEN, J. K., WLODEK, S. T., MORROW, III, H., GELL, M., MAURER, G., ed., American Society for Metals, Metals Park, Ohio, 1980, p. 205.
2. LEVY, M., FARRELL P., and PETTIT, F. *Oxidation of Some Advanced Single-Crystal Nickel-Base Superalloys in Air at 2000°F (1093°C).* Corrosion, v. 42, no. 12, 1986, p. 708.
3. DOERING, H. V., and BERGMAN, P. A.. *Mat. Res. Stand,* v. 9, 1969, p. 35.
4. DILS, R. R., and FOLLENSBEE, P. S. Corrosion, v. 33, 1977, p. 385.

contaminants, and temperatures). Very often, the deposits are sulfates containing sodium and calcium. Such deposits can significantly affect the degradation of superalloys at temperatures of 1300°F (704°C) and above. Another objective of this paper is to compare the Na_2SO_4-induced hot corrosion of the single crystal superalloys to DS MAR M 200 by using tube furnace tests at 1650°F (900°C) and 1300°F (704°C).

EXPERIMENTAL

Table 1 presents the nominal compositions of the alloys used in this study. To protect the proprietary rights of the various alloy manufacturers that supplied material, the compositions are simply identified by a letter rather than by their commercial name. A state-of-the-art directionally solidified alloy (DS MAR M 200 with hafnium) has been included for comparison purposes.

Table 1. NOMINAL COMPOSITIONS OF ALLOYS (WEIGHT PERCENT)

Designation	Ni	Cr	Co	Mo	W	Ta	Ti	Al	Cb	Hf
Alloy A	bal	10	5		4	12	1.5	5		
Alloy B	bal	7.5	4	0.5	7.5	6	0.9	5.5		0.1
Alloy C	bal	8	5	0.5	8	6	1	5.5		
DS MAR M 200	bal	8.75	10		12		2	5	1	3

All of the alloys were received as 1.3 to 1.6 cm (0.5 to 0.63 in.) diameter rods. From these rods, specimen discs 1.3 cm (0.5 in.) in diameter and 3 mm (0.118 in.) thick were fabricated. These discs were polished through 600 grit SiC paper, scrubbed with hot soapy water, and rinsed with acetone before using in the cyclic oxidation and hot corrosion tests. The burner rig specimens were also machined from these rods. Their bases were cylindrically shaped, 1.3 cm (0.5 in.) in diameter, and 2.4 cm (0.95 in.) long. The remainder of these specimens were 8 cm (3.15 in.) long and wedge shaped. The leading edge of the wedge had the curvature of the original cylinder, and an average length of 3 cm (1.2 in.). The trailing edge had an average length 0.3 cm (0.12 in.) and the center was about 1.3 cm (0.5 in.) from the center of the leading edge. The surfaces of the burner rig specimens were not polished after final machining to a 90 RMS finish.

The laboratory tube furnace apparatus that was used for the cyclic oxidation and cyclic hot corrosion tests has been described previously.[2] It consists of an electrically heated vertical tube furnace with the bottom sealed to inhibit convective flow. A suspension chain and an electrically motorized arm are used to move the specimens cyclically into and out of the hot zone of the furnace through the top end. The specimens remain in the hot zone for 30 minutes and then in the cool zone (just outside the furnace) for 5 minutes, where they cool to 212°F (100°C). The cyclic oxidation tests were performed at 2000°F (1093°C) and 1650°F (900°C) in air. The cyclic hot corrosion tests employed temperatures of 1650°F (900°C) and 1300°F (704°C) in air. The specimens usually were examined after every 20 hours of exposure; however, when the attack was not substantial, exposure and observation intervals of 150 hours were used. The specimens were examined using a low power microscope and weighed. In the case of the hot corrosion tests, the specimens were coated with about 1 mg/cm^2 of Na_2SO_4. This deposit was applied by heating specimens to 250°F (121°C) and spraying them with an aqueous mist saturated with Na_2SO_4. The specimens were coated with the deposit at the beginning of the test. They were washed in hot water at each observation period prior to weighing. A new deposit was applied just prior to the next exposure.

The burner rig was used only to assess the oxidation behavior of the alloys at 2000°F (1093°C). This type of rig has been described in the literature.[3,4] It consists of a combustor with the specimens placed on a rotating platform in front of the nozzle from which the hot gases emerged. The specimens were exposed at test temperature for 12 minutes and then exposed to forced air cooling for 4 minutes. The fuel was JP5. The specimen platform held eight erosion bars and it was rotated at 120 rpm. The specimen temperature was measured by using a two color pyrometer (Ircon Modline).

All of the alloys subjected to oxidation or hot corrosion conditions in each of the test methods were sectioned and mounted using standard metallographic techniques. When etching was required, AG21 (50 cm^3 lactic acid, 30 cm^3 HNO_3, and 2 cm^3 HF) was used. All specimens were examined by optical metallography and scanning electron microscopy (SEM).

RESULTS AND DISCUSSION

Characterization of the as received specimens

The four cast alloys identified in Table 1 were solution heat treated at 2350°F to 2400°F (1288°C to 1315°C) for two to four hours and then air cooled. The resulting microstructures have been described in previous papers.[1,2,5] All of the single crystal alloys contained a fine (0.2-0.5μ) dispersion of γ' particles in a γ matrix. In addition, these alloys contained a much larger globular shaped γ' (enriched in Ta and W). The former γ' was formed upon cooling below the solvus of the γ-phase, whereas the latter evidently developed during freezing of the liquid, and is often referred to a eutectic γ'. The MAR M 200 alloy contained fine γ', eutectic γ' at grain boundaries, and carbides, all in a matrix of γ-phase.

Cyclic oxidation

The cyclic oxidation was performed at 2000°F and 1650°F (1093°C and 900°C). In the case of the testing at 2000°F (1093°C), weight change data are presented in Figure 1 for both burner rig and tube furnace tests. If weight loss is used as a means of comparing the alloys in these tests, both tests give the same ranking of the alloys. In particular, MAR M 200 has undergone more degradation than any of the single crystal alloys. For both tests, all of the single crystal alloys require at least twice the exposure time as MAR M 200 to have the same weight loss. In the case of the tube furnace test, there is not a significant difference in weight loss between any of the single crystal alloys. The burner rig data show smaller losses for Alloy A than for Alloys B or C. The ranking of the oxidation resistances of the single crystal alloys must be done with care since the differences in weight losses are not large, and all the oxidation products may not spall from the specimen surfaces. Optical metallographic and scanning electron microscope observations of the exposed specimens also must be considered in making these comparisons.

In Figures 2, 3, 4, and 5, photographs are presented to compare the microstructural features that developed during the degradation of MAR M 200 and the single crystal alloys in the tube furnace test and in the burner rig. Photographs to show the degradation of MAR M 200 after 250 hours in the cyclic oxidation furnace are presented in Figure 2. A thick external scale has been formed and internal oxidation of the aluminum to form a discontinuous subscale is evident. The etched specimen in this figure exhibits an aluminum depleted zone below a thick external oxide scale and a subscale zone. The degradation microstructure of MAR M 200 after 80 hours in the burner rig test at 2000°F (1093°C) is presented in Figure 3. The microstructural features developed in this alloy are considered to be identical in both tests. The microstructural features that developed in the single crystal alloys during exposure in the cyclic tube furnace and in the burner rig are presented in Figures 4 and 5, respectively. Zones depleted of γ' have been developed in both tests with localized regions having thick scales of oxide. In the zones depleted of γ', a phase having a platelet shape has been formed. This phase does not develop in MAR M 200. It has been determined to contain nickel, tungsten, tantalum, and molybdenum, and to be susceptible to preferential oxidation. With the exception of the platelet phase, the microstructural features of the MAR M 200 are very similar to those of the single crystal alloys. As shown in a previous paper,[3] both MAR M 200 and all of the single crystal alloys are Al_2O_3 - formers when oxidized isothermally with different amounts of transient oxidation occurring before these Al_2O_3 scales develop continuity. Hence, in cyclic oxidation tests such as those used in the present investigation, the similarity between the degraded microstructures is to be expected.

5. OBLAK, J. M., and OUCZARSKI, W. A. *Cellular Recrystallization in a Nickel-Base Superalloy.* Trans. Met. Soc. of AIME. v. 242, 1968, p. 1563.

The weight change data for the cyclic oxidation of the alloys at 1650°F (900°C) are presented in Figure 6. The weight change data are weight gains rather than the weight losses obtained at 2000°F (1093°C). Moreover, the weight gains of the single crystal alloys are significantly less than those for MAR M 200. Finally, the data for the single crystal alloys appear to follow a parabolic rate law. This may be the case for MAR M 200 also, but only up to about 1000 hours of testing. In Figure 7, the weight change versus time data for two of the single crystal alloys (Alloys A and C) are plotted to show conformance with the parabolic rate law. Some scatter in the data show that a small amount of cracking and spalling of the oxide scale has occurred. Nevertheless, it is apparent that these data can be approximated by a parabolic relationship. Similar results were obtained for the other single crystal alloy in the cyclic oxidation test at 1650°F (900°C). If the scatter in the measurements is not considered, the three single crystal alloys have parabolic rate constants of 1.5×10^{-15}, 0.9×10^{-14}, and 1.3×10^{-14} (g^2/cm^4-S) for Alloys A, B, and C respectively. MAR M 200 conforms to the parabolic relationship for about 1000 hours and has a parabolic rate constant of 4.7×10^{-13} (g^2/cm^4-S). If data in the literature [6] for the growth of Al_2O_3 scales on Ni-Cr-Al alloys are used to obtain the parabolic rate constant for the growth of Al_2O_3 scales, a value of 1.10×10^{-14} (g^2/cm^4-S) is obtained. The results show that the oxidation kinetics for Alloys A, B, and C are controlled by the growth of Al_2O_3 scales. Parabolic growth may also be approached for the oxidation of MAR M 200 for exposure times of 1000 hours and less. These conclusions must be substantiated by metallographic observations since it is apparent that some cracking of the alumina scales is occurring during the thermal excursions, and is responsible for the very small parabolic rate constant of Alloy A.

Figures 8 and 9 are typical degradation microstructures of MAR M 200 and one of the single crystal alloys after 3150 hours of exposure in the cyclic oxidation at 1650°F (900°C). The MAR M 200 specimen has a relatively thick external scale above the subscale Al_2O_3 as shown in Figure 8. Evidence of nitride formation is visible below this subscale zone in the zone which is denuded of γ'. Such microstructural features clearly show that this alloy is no longer an Al_2O_3 - former. The microstructure typical of the single crystal alloys after exposure in the cyclic oxidation test at 1650°F (900°C) is presented in Figure 9. Zones of γ-phase adjacent to the surfaces of these alloys which are denuded of γ' have been formed. Moreover, zones of coarsened γ' are also evident beneath these γ zones. The coarsening of the γ' is being examined in more detail. Results available in the literature [5] indicate that this coarsening of γ' is due to recrystallization. Specimens of Alloy B were grit-blasted to create a surface totally covered with coarsened γ' upon recrystallization. The weight changes of such specimens during isothermal oxidation at 2000°F (1093°C) and 1650°F (900°C) were not different from those of specimens given the surface preparation described in the experimental section. The microstructure in Figure 9 is clearly consistent with external protective scales of Al_2O_3 having been present on the surfaces of these alloys during cyclic oxidation at 1650°F (900°C), since no internal oxidation is evident. The cyclic oxidation data obtained at 2000°F (1093°C) and 1650°F (900°C) show that the single crystal alloys have better oxidation resistance than MAR M 200. This is the same conclusion that was obtained from the tube furnace cyclic oxidation tests at 2000°F (1093°C) in a previous paper,[2] however, these data have now been corroborated by the burner rig tests at 2000°F (1093°C) and tube furnace cyclic oxidation testing at 1650°F (900°C). As discussed in a previous paper,[2] the better oxidation resistance of the single crystal alloys results from the different compositions of these alloys compared to MAR M 200, Table 1, rather than microstructural effects. The cyclic oxidation data obtained for the single crystal alloys at 1650°F (900°C) show that these alloys may not need coatings for applications at temperatures below about 1600°F (871°C).

The results from the burner rig tests and the tube furnace cyclic oxidation tests are essentially the same. The burner rig test is more severe and permits the differences in performance among the alloys to be discerned more quickly. It should be noted that the cycle used in the burner rig was such that more thermal cycling occurred in this test. On the other hand, the tube furnace is a much cheaper test and much more amenable to the controlled variation of critical parameters than the burner rig. The data obtained in the current investigation show that tube furnace cyclic oxidation can be used in place of burner rig oxidation tests. Longer times will be required to produce the degradation, but the temperature and gas composition can be maintained at controlled and defined levels throughout the test. Both of these tests must always be accompanied by detailed metallographic examination of the exposed specimens upon the conclusion of the test.

6. GIGGINS, C. S., and PETIT, F. S. J. Electrochem. Soc. v. 118, 1971, p. 1782.

Cyclic hot corrosion

Weight change data for the Na_2SO_4 - induced hot corrosion of the alloys at 1650°F (900°C) in air are presented in Figure 10. After about 100 hours, all of the alloys show large weight losses indicative of very severe hot corrosion attack. Typical degradation microstructures for MAR M 200 and one of the single crystal superalloys are presented in Figures 11 and 12. The microstructural features formed as a result of the hot corrosion of MAR M 200 and the single crystal alloys are the same. All of the alloys had thick corrosion products composed predominantly of oxides near the gas interface and of sulfides adjacent to the unaffected substrate. The hot corrosion behavior of all of the alloys in this test is comparable. The hot corrosion degradation microstructures are typical of those that are observed on structural alloys for high temperature Na_2SO_4-induced attack.[7,8]

When hot corrosion testing is performed at 1300°F (704°C), the gas composition is a more critical parameter than at 1650°F (900°C).[9] Furthermore, the composition of the salt deposit that is used is also important since some deposits may be solid. The initial hot corrosion tests at 1300°F (704°C) were performed using Na_2SO_4 deposits in air. After 100 hours of testing, all the alloys exhibited a few milligrams/cm^2 of weight loss, which shows that the deposit was affecting the hot corrosion process. Based on the cyclic oxidation data obtained at 1650° F (900°C) for these alloys, very small weight gains would be expected for oxidation at 1300°F (704°C). A micrograph of a specimen exposed for 120 hours in this test is presented in Figure 13. The attack is small; nevertheless, there are some areas of localized degradation that show the deposit has affected the oxidation of all the alloys. In this test, it was not possible to determine if one of the alloys had been attacked less than the others.

In order to attempt to accelerate the hot corrosion attack at 1300°F (704°C), the tests were performed in air but using a Na_2SO_4-45 mole percent $MgSO_4$ deposit which is a liquid at 1300°F (704°C). The liquid deposit of Na_2SO_4-45 mole percent $MgSO_4$ caused much more severe attack of the alloys at 1300°F (704°C) than Na_2SO_4. Weight change versus time data for this test is presented in Figure 14. The specimens were washed and brushed to remove loose corrosion products before weighing. Very substantial weight gains or losses for exposure at 1300°F (704°C) have been obtained (Figure 14). Even though some specimens gained weight and others lost weight, the magnitude of the weight changes are very large compared to those produced d. ' oxidation. All of the alloys have undergone very severe hot corrosion degradation. In Figure 15, the micros..cture of Alloy C is presented after 120 hours in the hot corrosion test using the Na_2SO_4 45 mole percent $MgSO_4$ composition. Some of the corrosion products have spalled from the surface of this specimen. Comparison of this microstructure to that presented in Figure 13 shows much more attack has occurred with the Na_2SO_4-45 mole percent $MgSO_4$ deposit. In Figures 16 and 17, the microstructures of MAR M 200 and one of the single crystal alloys are presented upon termination of the cyclic hot corrosion tests using deposits of Na_2SO_4-45 mole percent $MgSO_4$ after 750 hours. The amount of attack is extremely severe for all of the alloys, but a ranking is not possible. Tungsten and tantalum were detected in the corrosion products by energy dispersive analysis. It is not the purpose of this paper to attempt to develop models for the hot corrosion of these alloys. A liquid deposit produces more attack of these alloys. Based upon data available in the literature,[8] the hot corrosion of these alloys should be affected by their refractory metal content. It, therefore, is proposed that the rapid hot corrosion is caused by the liquid deposit reacting with oxides of the refractory elements in these alloys.

At 1300°F (704°C), the hot corrosion of many alloys becomes more severe as SO_3 is added to gas mixtures containing oxygen. Such a test is not really critical to the hot corrosion of the alloys studied in this program because very severe attack of all of the alloys occurred in air. Nevertheless, in order to provide a comparison, one of the single crystal alloys was coated with deposits of Na_2SO_4-45 mole percent $MgSO_4$ and exposed isothermally at 1300°F (704°C) to oxygen containing SO_3 at 3×10^{-5} atm. The weight change as a function of time for one of these specimens is presented in Figure 18. The weight change data show that very significant attack is occurring since virtually no weight change would be observed for this alloy in the absence of the deposit at this

7. BORNSTEIN, N. S., and DECRESCENTE, M. A Trans. Met. Soc. AIME, v. 245, 1969, p. 1947.
8. SEYBOLT, A. U. Trans. TMS-AIME, v.242, 1968, p. 1955.
9. BARKALOW, R. H., and PETTI, F. S. *Proc. of the 4th Conference on Gas Turbine Materials in a Marine Environment*. Naval Sea Systems Command, Annapolis, MD, R. v. 493, 1979.

temperature. A photomicrograph of the specimen exposed to the conditions described in Figure 18 is presented in Figure 19. Very substantial attack is evident after an exposure time of 24 hours. A specimen of the alloy that was used in the experiment with Na_2SO_4-45 mole percent $MgSO_4$ deposit and exposed at 700°F in oxygen with SO_3 was also exposed under the same conditions but with no deposit on its surface. The resulting weight change after 20 hours is indicated in Figure 18. This weight change is very small. The absence of attack was also confirmed by visual examination of the specimen upon conclusion of this test. These results shown that the liquid deposit is the most important parameter in causing the hot corrosion attack of the alloys rather than the composition of the gas. The attack may be more severe when SO_3 is present in the gas, but also occurs at an unacceptably high rate in air. In the case of hot corrosion resistant coatings, the composition of the gas is critical, and SO_3 is required for attack to occur. In the case of nickel-base superalloys, however, the presence of refractory metal oxides must be a sufficient condition to cause severe hot corrosion attack even in the absence of SO_3.

CONCLUSIONS

Nickel-base alloys have been tested at 2000°F (1093°C) in cyclic oxidation tests using a tube furnace and a burner rig. The same ranking of the alloys was obtained in both tests with the single crystal superalloys having better oxidation resistance than the directionally-solidified alloy MAR M 200. These results show that tube furnace tests can be used in place of burner rig tests to rank alloys providing that the tests are accompanied with detailed metallographic examination of the exposed specimens. This ensures that the conditions produce degradational microstructures similar to those of the burner rig or the service application of interest.

Oxidation tests at 1650°F (900°C) using the tube furnace produced a ranking of the alloys consistent with the 2000°F (1093°C) results and showed that the nickel-base single crystal alloys had protective scales of Al_2O_3 that did not extensively crack or spall after 3000 hours of cyclic oxidation. The single crystal alloys probably can be used uncoated for applications involving oxidizing conditions and temperatures below 1650°F (900°C).

All of the alloys were severely degraded when a liquid sulfate deposit was placed upon their surfaces at 1650°F (900°C) and 1300°F (704°C). There is no significant difference between the hot corrosion resistance of these alloys when tested in air or in oxygen with SO_3, provided a liquid deposit was present in both cases. All of the alloys would require a coating if they were to be exposed to any type of hot corrosion conditions at temperatures of 1300°F (704°C) or higher.

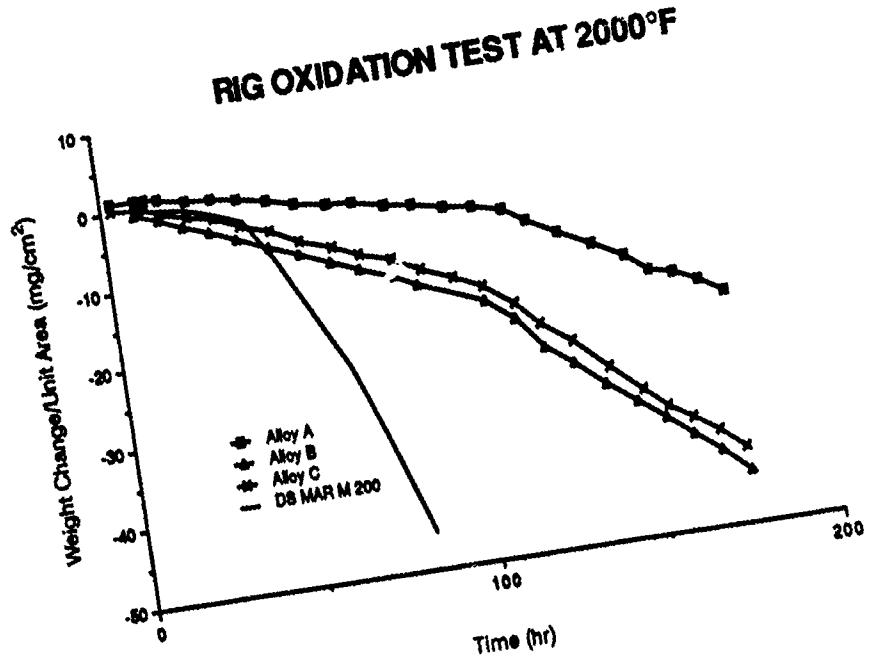

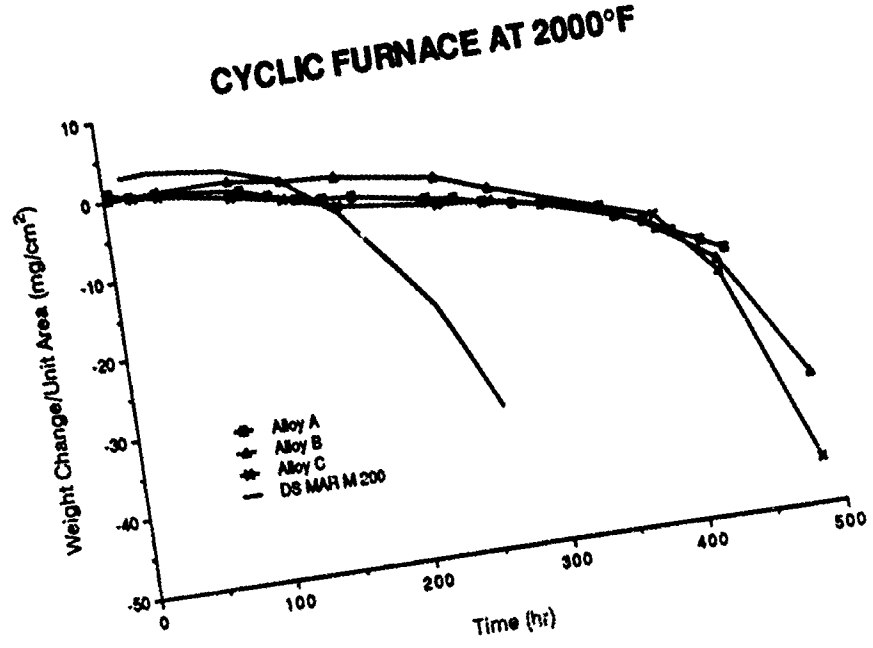

Figure 1. Weight change data for both burner rig and cyclic furnace tests.

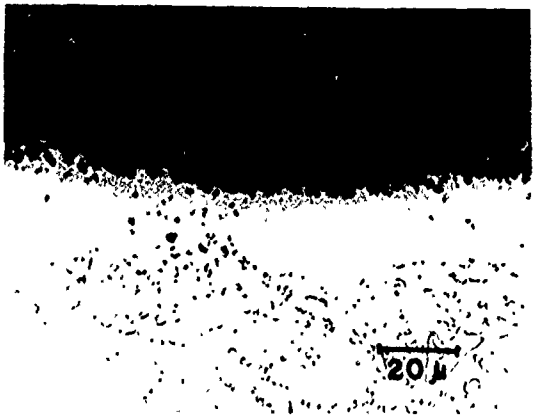

Figure 2. Typical microstructure that developed during cyclic oxidation of MAR M 200 in the tube furnace test at 2000°F (1093°C).

Figure 3. Typical microstructure that developed during cyclic oxidation of MAR M 200 in the burner rig at 2000°F (1093°C).

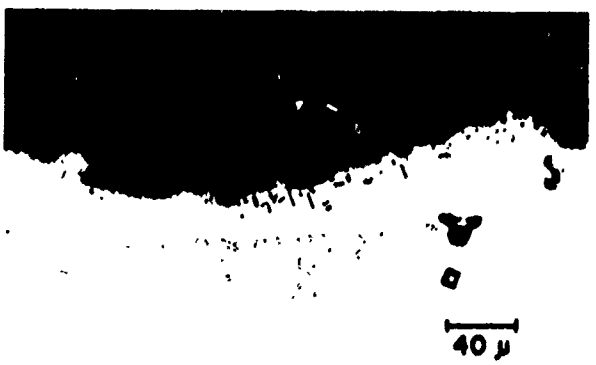

Figure 4. Typical microstructure that developed during cyclic oxidation of single crystal superalloys in the tube furnace at 2000°F (1093°C), (Alloy B).

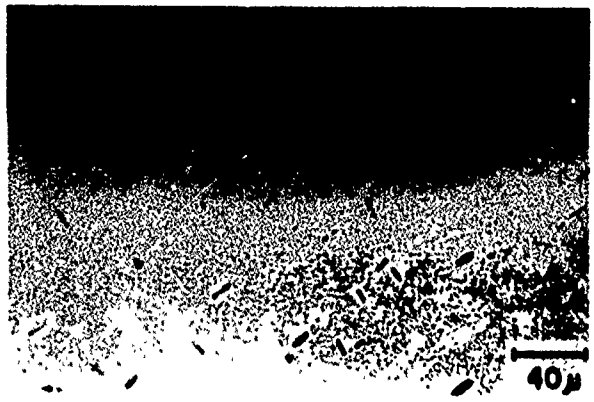

Figure 5. Typical microstructure that developed during cyclic oxidation of single crystal superalloys at 1650°F (900°C).

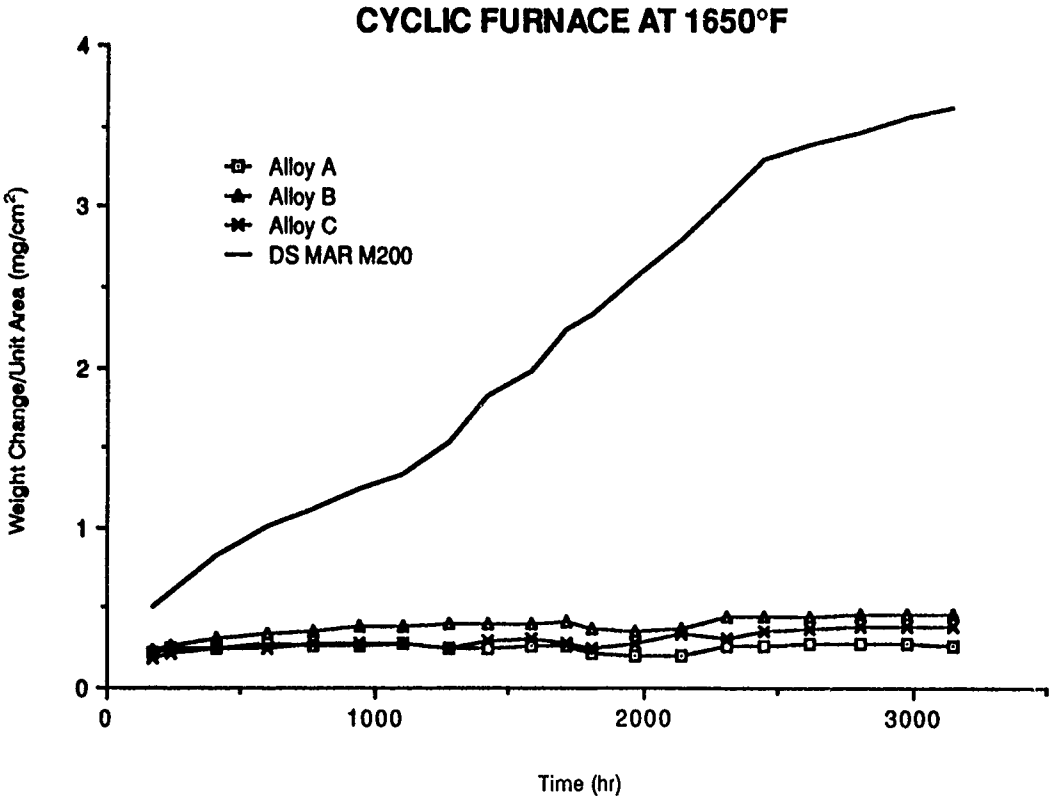

Figure 6. Weight change data for the cyclic oxidation of the alloys at 1650°F (900°C).

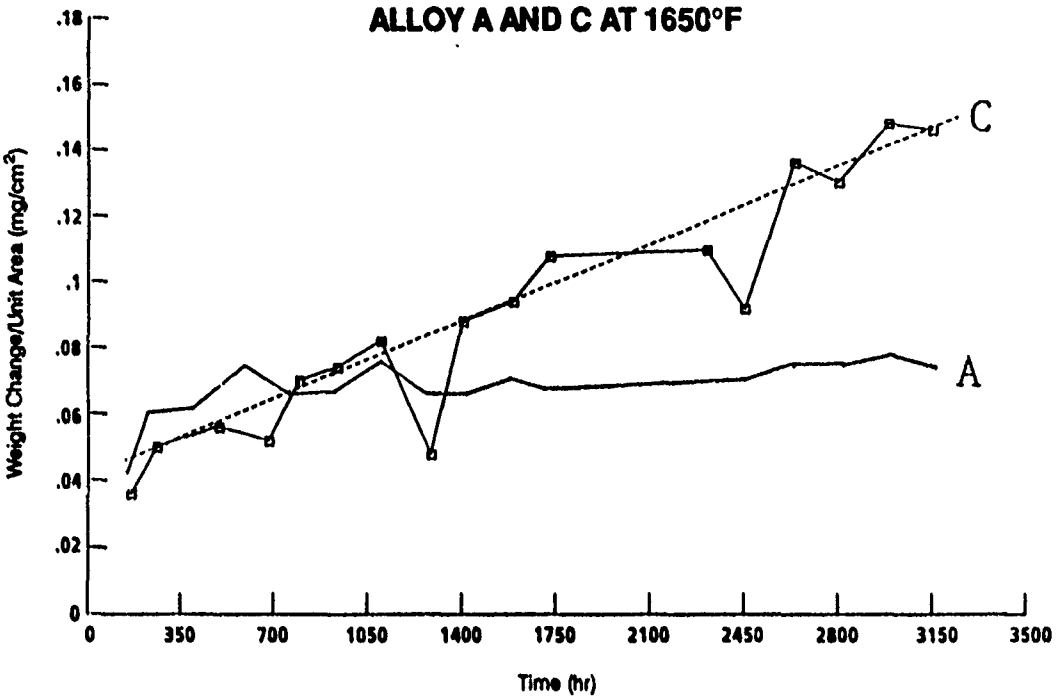

Figure 7. Weight change squared versus time data for Alloy A and C.

Figure 8. Typical microstructural features developed on MAR M 200 after 3150 hours of cyclic oxidation at 1650°F (900°C).

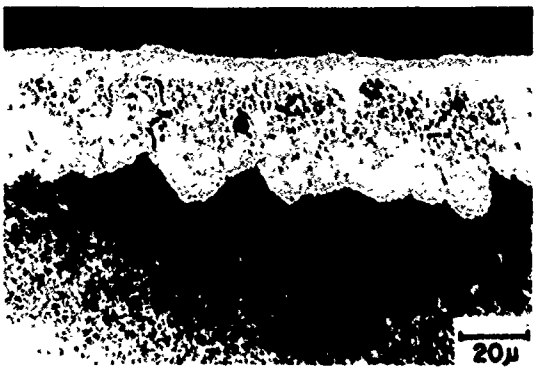

Figure 9. Typical microstructural features developed on all of the single crystal superalloys after 3150 hours of cyclic oxidation at 1650°F (900°C).

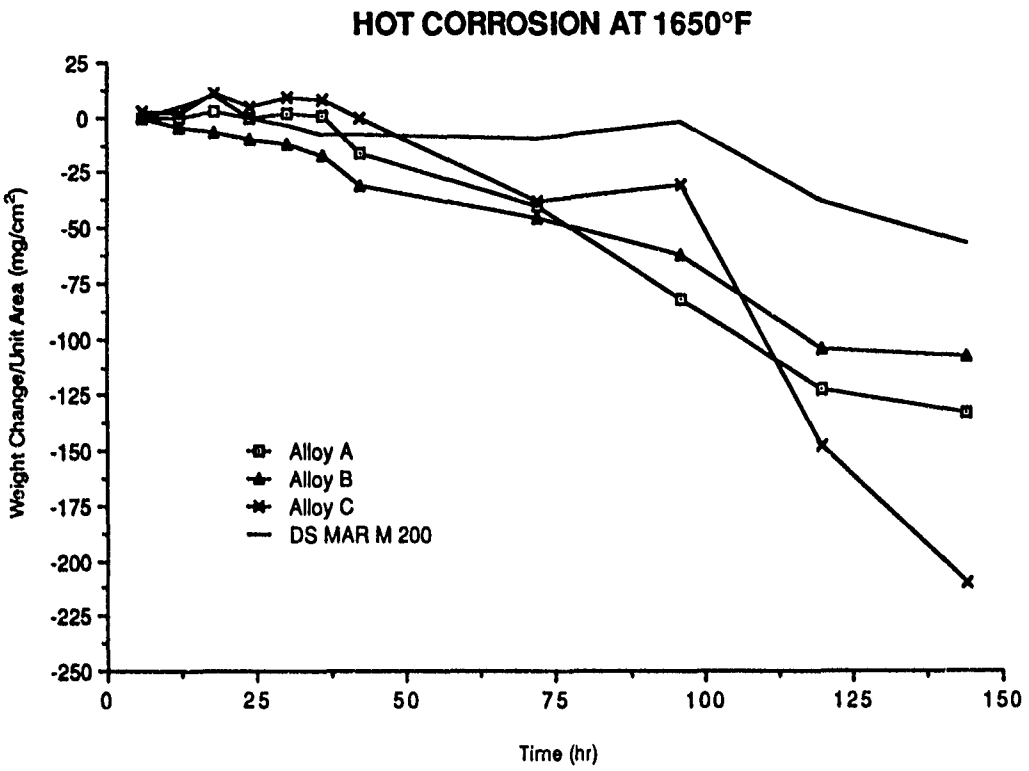

Figure 10. Weight change data for the Na_2SO_4-induced hot corrosion of the alloys at 1650°F (900°C) in air.

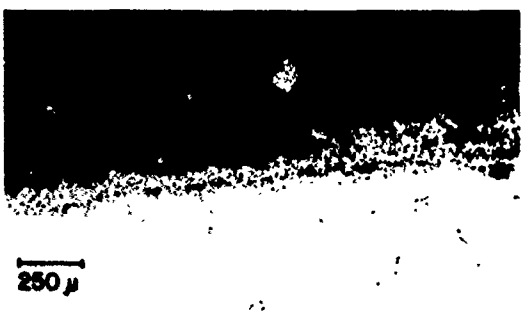

Figure 11. Typical features observed after exposure of MAR M 200 in the cyclic hot corrosion test at 1650°F (1093°C).

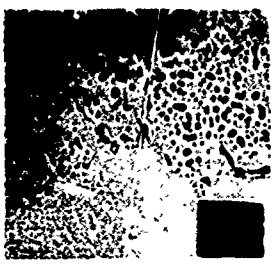

Figure 12. Typical features observed after exposure of the single crystal alloys in the cyclic hot corrosion test at 1650°F (1093°C), a) corrosion products, b) sulfides at corrosion products - alloy interface.

Figure 13. Typical microstructural features that developed on MAR M 200 and on the single crystal alloys after 120 hours of cyclic hot corrosion at 1300°F (704°C) using deposits of Na_2SO_4 (Alloy B).

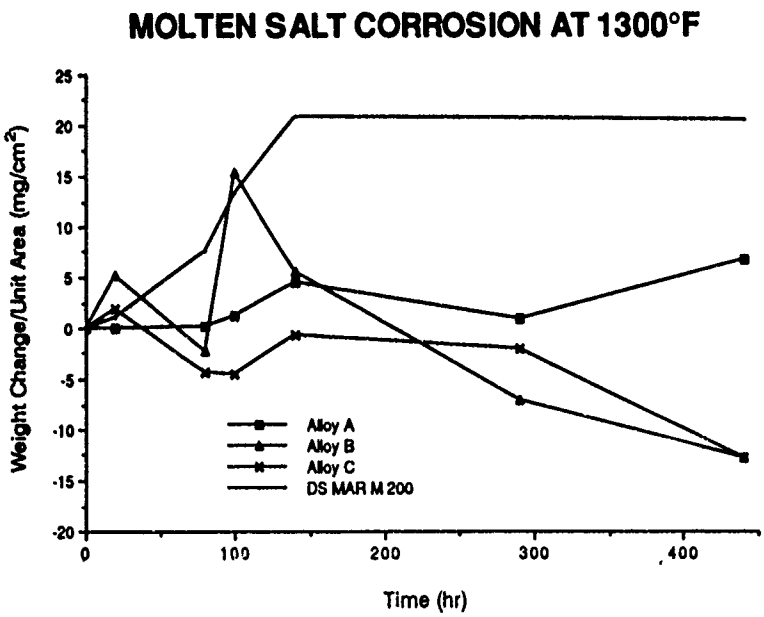

Figure 14. Weight change data versus time data for the cyclic hot corrosion of all the alloys at 1300°F (704°C) in air using deposits of Na_2SO_4-45 mole percent Mg SO_4.

Figure 15. Photomicrograph of Alloy C after 120 hours in the cyclic hot corrosion test at 1300°F (704°C) using Na_2SO_4-45 mole percent Mg SO_4 deposit.

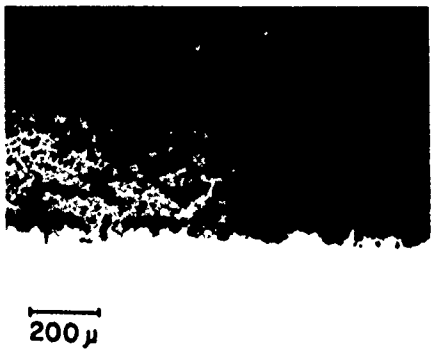

Figure 16. Photomicrograph showing microstructures of MAR M 200 upon conclusion of the cyclic hot corrosion test (750 hours) at 1300°F (704°C) using deposits of Na_2SO_4-45 mole percent Mg SO_4.

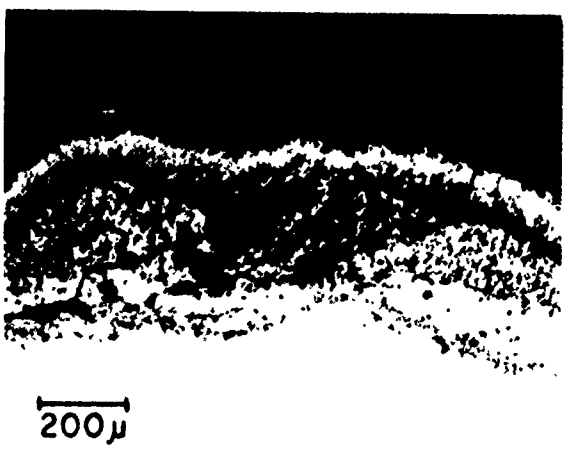

Figure 17. Photomicrograph showing microstructures of Alloy A upon conclusion of the cyclic hot corrosion test (750 hours) at 1300°F (704°C) using deposits of Na_2SO_4-45 mole percent Mg SO_4.

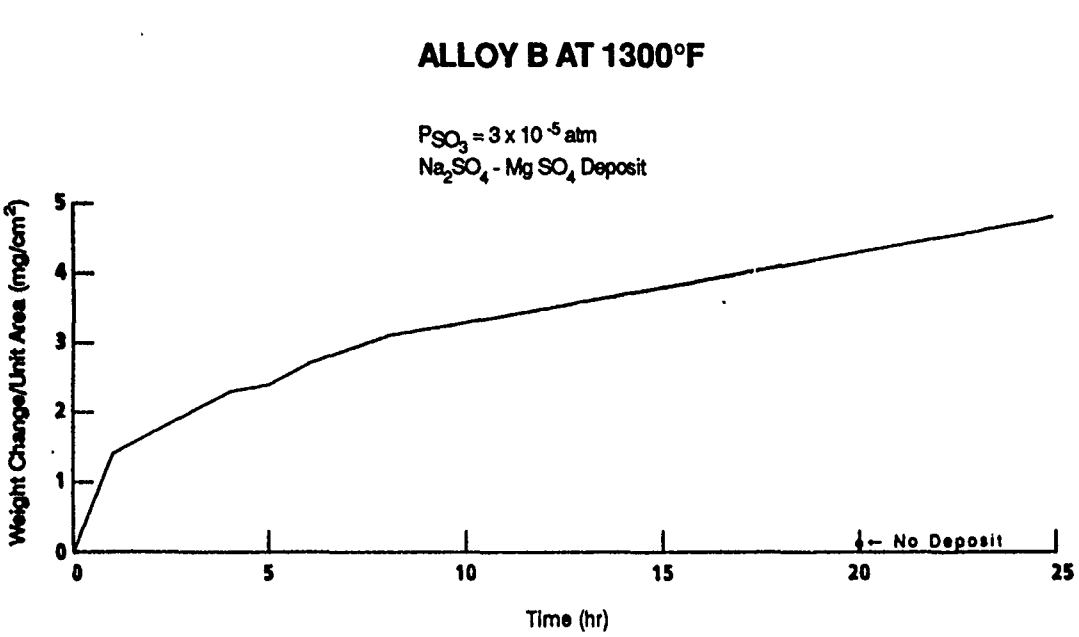

Figure 18. Weight change versus time data for the isothermal hot corrosion (Na_2SO_4-45 mole percent Mg SO_4 deposit) of a single crystal alloy (Alloy B) at 1300°F (704°C) in oxygen with an SO_3 pressure of 3×10^{-5} atm. Data are also presented for the alloy exposed to the same conditions but with no deposits on its surface.

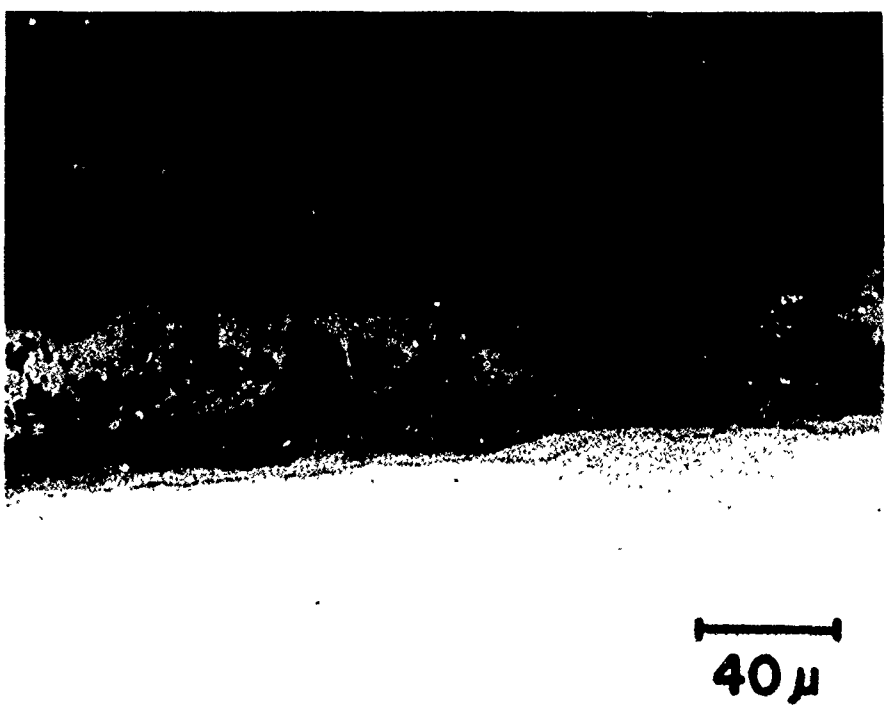

Figure 19. Typical photomicrograph of single crystal alloy after exposure to hot corrosion conditions at 1300°F (704°C) with oxygen containing SO_3 at a pressure of 3×10^{-5} atm.

EFFECTS OF HIGH TEMPERATURE EXPOSURE ON THE PERFORMANCE OF ELECTROLESS NICKEL AS A CORROSION RESISTANT COATING ON STEEL

R. D. Daniels and H. B. Harpalani
University of Oklahoma
Norman, Oklahoma 73019

Corrosion induced failures of steel aircraft components plated with electroless nickel indicate that embrittlement and cracking of the coating caused by heating can aggravate the corrosion problem on the steel. Studies were made of the changes in structure and hardness of electroless nickel after heating to temperatures that are encountered in service. Electroless nickel-phosphorus coatings in three phosphorus composition ranges were studied, 1-3 wt% P, 6.5-8 wt% P, and 10.5-11 wt% P. The coatings as deposited are microcrystalline or amorphous. Recrystallization and grain growth (often with preferred orientation) and precipitation of nickel-phosphide, Ni_3P, occur with increasing temperature. Peak hardness is produced by heating to about 350°C. Maximum hardness is independent of phosphorus composition. Heating above 400°C softens the material; the lower the phosphorus content the greater the softening. Ni_3P becomes the matrix phase for the two higher phosphorus compositions. The results suggest that the low phosphorus coating may be successfully employed in the 300-400°C temperature range if it is preconditioned by heating to an overaged condition.

INTRODUCTION

Aircraft jet engine cartridge starter assemblies made of steel are plated with electroless nickel to protect them from atmospheric corrosion. In analyzing service failures of the starter breech chambers, it has been observed that structural changes, hardness changes, and cracking have occurred in electroless nickel coatings exposed repeatedly to temperatures above 300°C [1,2,3]. Such temperatures are routinely encountered on the chamber dome surface each time a solid fuel cartridge is burned in the chamber. The structural changes embrittle the coating. Cracking of the coating appears to occur by a process of thermal fatigue.

Electroless nickel is a barrier type coating, providing protection from corrosion for the substrate by sealing it off from the environment. It provides excellent corrosion resistance in the atmosphere and in many other environments so long as the barrier remains intact. However, a cracked coating can promote localized corrosion on a steel substrate through galvanic action since the coating is more noble than the substrate, Figure 1.

Electroless nickel plating is produced by reduction of nickel from aqueous solution with a suitable reducing agent [4]. The usual source of nickel is nickel sulfate and the reducing agent is sodium hypophosphite. The deposit is an alloy of nickel and phosphorus. Phosphorus content can range from 1 to 12 wt% and is determined by the solution temperature and pH. The electroless nickel coating on the steel breech chambers contains 9-10 wt% P.

The mechanical properties of an electroless nickel coating are sensitive to its phosphorus content and to exposure at elevated temperatures [5]. The phosphorus content also influences the resistance of the coating to corrosion in chemical environments [6]. Experience with the aircraft starter breech chambers suggested a need to reexamine the effects phosphorus content and elevated temperature exposure on the structure and properties of electroless nickel to determine if coatings more tolerant of thermal cycling could be produced.

EXPERIMENTAL PROCEDURES

Electroless nickel coatings in three phosphorus composition ranges were studied, 1-3 wt% P, 6.5-8 wt% P, and 10.5-11 wt% P. The samples were prepared by Enthone, Inc., West Haven, Connecticut. The plating process has been described by Tracy et al. [6]. The coatings were plated on 0.15 cm thick coupons of 1010 steel to a thickness of 25 μm. The coupons were cut into 1.5 cm x 2.5 cm x 0.15 cm specimens for heat treatment. Specimens were heated in an air furnace at ten temperatures over the range from 235°C to 800°C, with closer temperature intervals in the region of significant hardness changes. Specimens were heated for one hour and then cooled in ambient air.

Specimens for hardness and metallographic examination were mounted in cross section and wet ground and polished. Specimens for x-ray diffraction analysis were lightly ground and polished on the coating surface to remove tarnish. For microstructural examination the cross-sections were chemically etched. Nital (2% nitric acid in methanol) was suitable for specimens heated above 400°C, but it was necessary to use a special etchant (5g NaCN and 5g $(NH_4)_2SO_4$ in 100ml water) for as-plated specimens and those given the lower temperature heat treatments.

Hardness was determined on the coating cross section using a Wilson "Tukon" microhardness tester with a Knoop indentor. The

load obtained with a 200 g mass was used to measure the hardness of the coatings with 1-3 wt% and 6.5-8 wt% phosphorus. This load caused cracking in the 10.5-11 wt% coating heated at 350°C, so a mass of 100 g was used with specimens of this composition. There was reasonable agreement between hardness values obtained with 100 g and 200 g masses below 350°C. Hardness measurements are reported in units of KHN_{200}.

A recording x-ray diffractometer with copper Kα radiation was used to obtain x-ray diffraction patterns of the as-plated and the plated and heated specimens for each phosphorus composition. Specimens were scanned over the diffraction angle 2θ from 30 degrees to 100 degrees at intervals of 0.05 degrees 2θ for a period of one second. Pole figures to determine preferred crystallographic orientations in the coatings were obtained for selected specimens [7].

RESULTS AND DISCUSSION

The hardness of the electroless nickel coatings following exposure to elevated temperatures is presented in Figure 2. Hardness is plotted versus temperature for each of the three coating compositions. The coating with 1-3 wt% phosphorus has a higher hardness in the as-plated condition than the 6.5-8 wt% P and 10.5-11 wt% P alloys, 850 KHN_{200} compared to about 650 KHN_{200}. All three coating compositions showed increasing hardness when heated and achieved maximum hardness at about 350°C. The maximum hardness of about 1000 KHN_{200} was independent of composition. Above 400°C the hardness decreased. The hardening can be attributed to a precipitation hardening reaction.

X-ray diffraction patterns obtained on the as-plated coatings are presented in Figure 3. The diffraction pattern for 1-3 wt% P coating, Figure 3(a), exhibits two major diffraction peaks which index as the (111) and (200) reflections of the nickel phase. The diffraction patterns for the 6.5-8 and 10.5-11 wt% P coatings, Figures 3(b) and 3(c), exhibit one broad diffraction peak characteristic of an amorphous material.

The x-ray diffraction patterns obtained after heating the coatings for one hour at 385°C are presented in Figure 4. The diffraction pattern for nickel is now more well defined in the 1-3 wt% P coating, Figure 4(a), making it possible to index the (220), (311), and (222) reflections. No second phase is in evidence. In the 6.5-8 and 10.5-11 wt% P coatings, Figures 4(b) and 4(c), the nickel phase is now well defined but a second phase is also present. This second phase was indexed as body-centered tetragonal, with lattice constants a_o = 8.9739 angstrom and c_o = 4.3974 angstrom. This is nickel phosphide, Ni_3P [8].

The diffraction patterns obtained after heating the coatings for one hour at 800°C are presented in Figure 5. Evidence of a small amount of the second phase is present in the 1-3 wt% P alloy, Figure 5(a). This is expected since the maximum solubiltiy of phosphorus in nickel is reported to be 0.17 wt% [9]. Increasing amounts of the Ni_3P phase are present with increasing phosphorus content in the coating. The diffraction peaks for the Ni_3P phase are indexed on the patterns in Figures 5(b) and 5(c).

There is evidence for development of preferred orientation or texture in these coatings, i.e., a non-random clustering of crystallographic orientations of grains about some particular orientation. This is evident from a consideration of the relative intensities of the (111) and (200) lines in the 1-3 wt% P coating. The relative intensities shift with annealing temperature as can be seen by comparing Figures 3(a), 4(a), and 5(a). Results of a detailed study of the as-plated textures and the textures produced by annealing the coatings are reported elsewhere [7].

Metallographic examination of as-plated coatings in cross-section revealed a laminated structure with the laminations parallel to the substrate surface. This structure was obtained regardless of phosphorus content, Figure 6. The laminations are probably the result of periodic variations of phosphorus composition as the coating is deposited on the substrate. After heating to 400°C, remnants of the laminated structure persist, but evidence of a two phase mixture of nickel (containing very little phosphorus in solution) and the intermetallic compound nickel phosphide is present. After heating at 800°C, an equilibrium distribution of the two phases is produced. In the low phosphorus coating, nickel is the matrix phase. In the high phosphorus coating, nickel phosphide becomes the matrix phase, Figure 7. In the 6.5-8 wt% P coating neither phase is continuous across the entire thickness of the plating, but nickel phosphide appears to be the matrix phase at the coating/substrate interface. This may be a consequence of some diffusion of nickel into the iron substrate.

Most studies of the mechanical properties and corrosion resistance of electroless nickel have been concerned with the as-plated coatings. This has lead to the conclusion that high phosphorus coatings have greater ductility than low phosphorus coatings and that their corrosion resistance is superior [4]. This may be the case when the coating is amorphous or microcrystalline as are the two higher phosphorus coatings studied here. (Note the lower hardness of these compositions in the as-plated condition, Figure 2). However, when nickel phosphide is formed the situation is changed. Nickel phosphide is a brittle phase and produces a brittle coating even in the overaged condition where the hardness is determined by the

relative amounts of the two phases in the microstructure [5]. This can be seen in Figure 2 for specimens heated to 800°C.

For materials which will be subjected to elevated temperatures in service sufficient to produce a microstructure with a brittle nickel phosphide matrix, the advantages of the phosphorus content will be lost if the coating cracks through a process of thermal fatique. A lower phosphorus coating may be more appropriate under such circumstances. Its corrosion resistance is still good, generally superior to that of pure nickel [4], and the microstructure produced by heating to the overaged condition will produce a more ductile, crack resistant coating.

CONCLUSIONS

Cracking of high phosphorus electroless nickel coatings in applications where the coatings are subjected to elevated temperatures indicated the need to consider coating compositions more resistant to thermal fatigue. Evaluation of low, medium and high phosphorus content coatings for structural changes produced by heating indicated that the low phosphorus coating, 1-3 wt% P, may be the most suitable for this application. A matrix of nickel can be produced by heating the coating into an overaged condition, i.e., above 400°C. In this softened condition the low phosphorus coating should be more resistant to cracking during thermal cycling than the higher phosphorus coatings.

ACKNOWLEDGEMENTS

This work was supported in part under Air Force Contract F34601-87-C-1906.

REFERENCES

1. Coleman, W. R., Block, R. J., and Daniels, R. D., "Corrosion Problems in Aircraft Components -- Case Studies of Failures," in Proceeding of the 1980 Tri-Service Corrosion Conference, AFWAL-TR-81-4019, Vol. II, 1981, p. 241-170.

2. Bauccio, M. L., "Corrosion of Powerplants," in Metals Handbook, Nineth Edition, Volume 13, Corrosion, ASM International, Metals Park, OH, 1987, p. 1037-1045.

3. Perkins, P. C., Daniels, R. D., and Gillies, A. B., in Analyzing Failures: The Problems and the Solutions, V. S. Goel Editor, ASM International, Metals Park, OH, 1986, p. 143-149.

4. Fields, W. D., Duncan, R. N., and Zickgraf, J. R., "Electroless Nickel Plating," in Metals Handbook, Ninth Edition, Volume 5, Surface Cleaning, Finishing, and Coating, ASM International, Metals Park, OH, 1982, p. 219-243.

5. Graham, A. H., Lindsay, R. W., and Read, H. J., "The Structure and Mechanical Properties of Electroless Nickel," Journal Electochemical Society, Vol. 12, 1965, p.401-414.

6. Tracy, R. P., Colaroutolo, J., Misercola, A., and Chuba, B. R., "Corrosion and Economics of Electroless Nickel Coatings in Chemical Process Environments," Materials Performance, Vol. 25, No. 3, 1986, p. 21-29.

7. Mai, Q. X., and Daniels, R. D., "Structural Changes Induced by Heating in Electroless Nickel-Phosphorus Alloys," Thin Solid Films, Vol. 166, 1988, p. 235-247.

8. Perkins, P. C., Structure and Property Changes of Electroless Nickel at Elevated Temperatures, Masters Thesis, University of Oklahoma, Norman, OK, 1985.

9. Elliot, R. P., Constitution of Binary Alloys, First Supplement, McGraw-Hill, New York, 1965, p. 661-662.

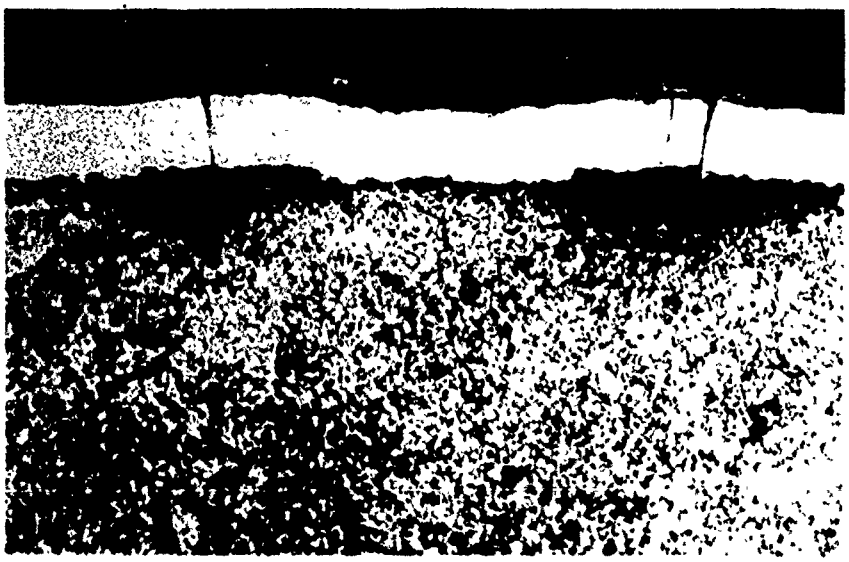

Fig. 1. Localized corrosion of steel under cracks in electroless nickel coating.

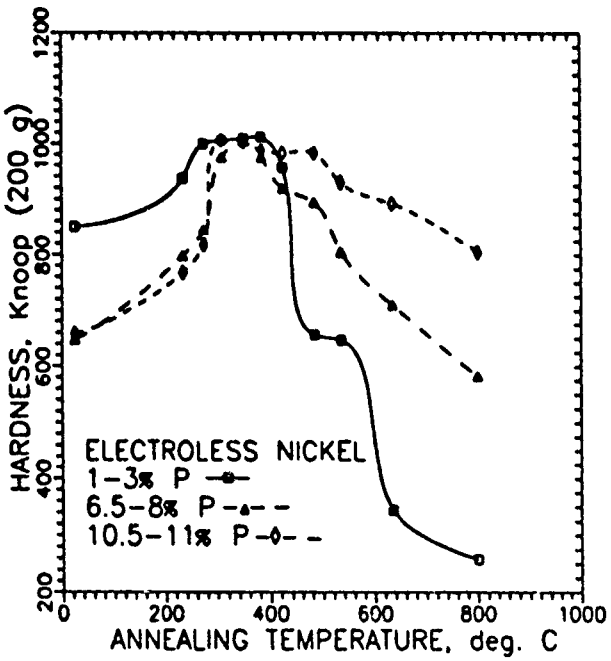

Fig. 2. Hardness of electroless nickel coatings after annealing at the temperatures indicated.

(a)

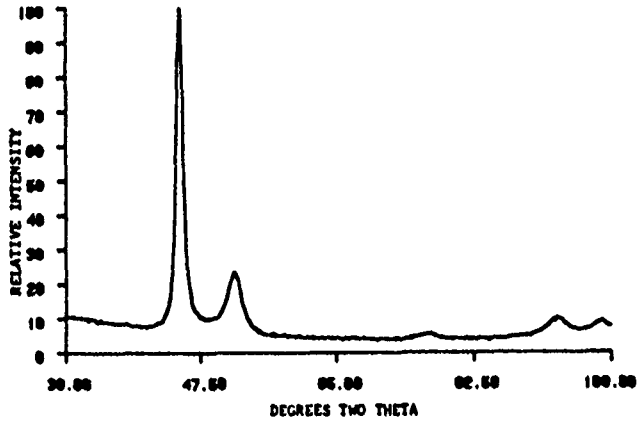

(b)

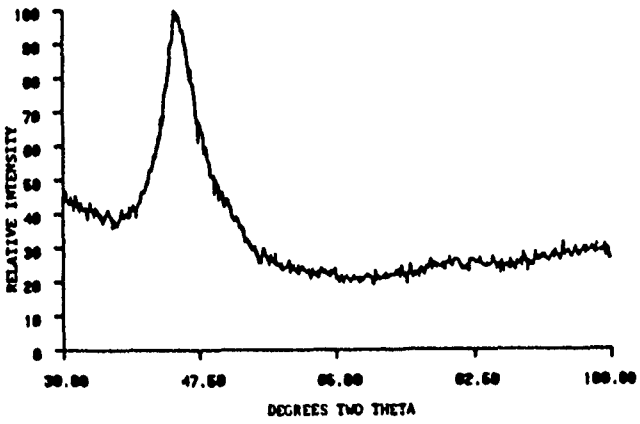

(c)

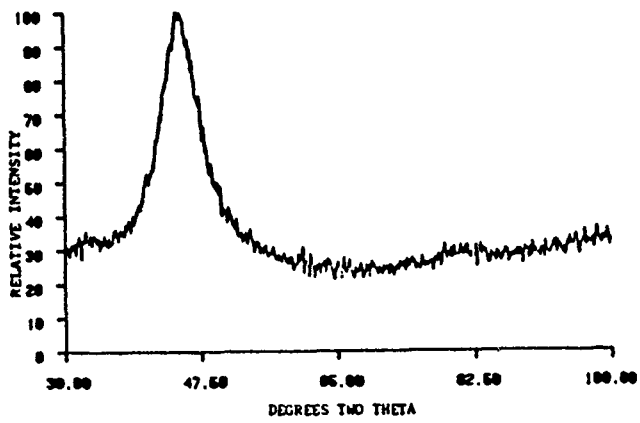

Fig. 3. X-ray diffraction patterns obtained on as-plated electroless nickel coatings. Phosphorus compositions: (a) 1-3 wt%, (b) 6.5-8 wt%, and (c) 10.5-11 wt%.

(a)

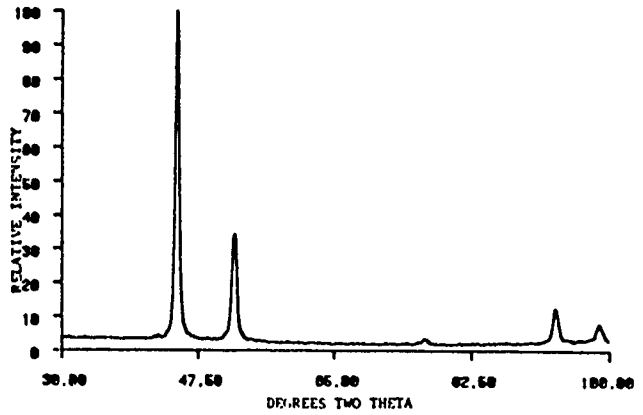

(b)

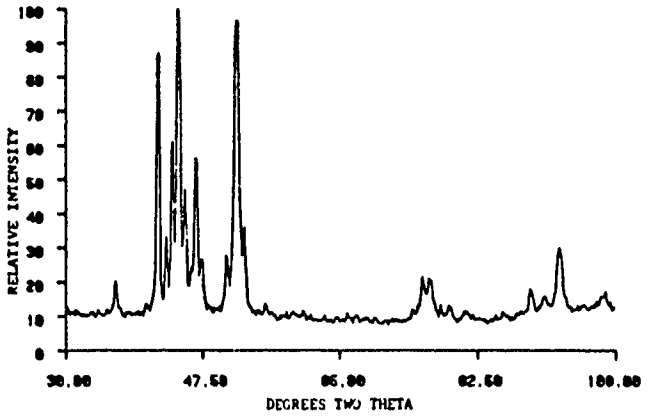

(c)

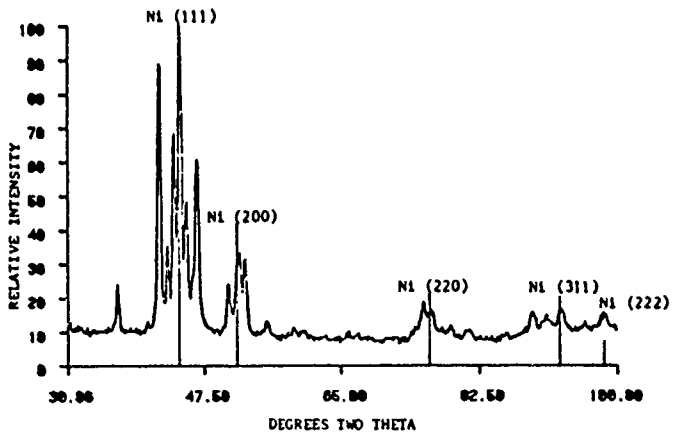

Fig. 4. X-ray diffraction patterns obtained on electroless nickel coatings annealed at 385°C. Phosphorus compositions: (a) 1-3 wt%, (b) 6.5-8 wt%, and (c) 10.5-11 wt%.

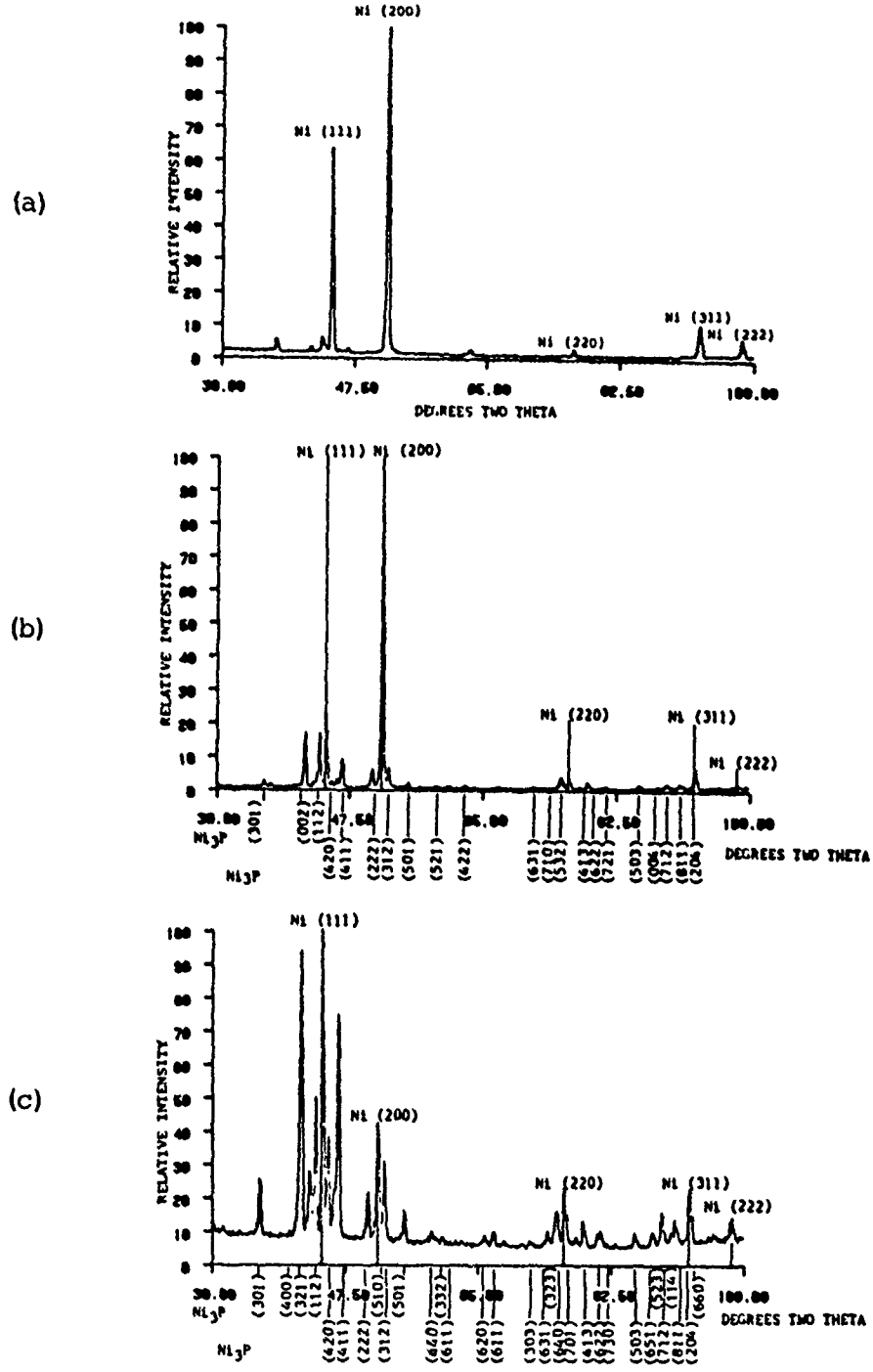

Fig. 5. X-ray diffraction patterns obtained on electroless nickel coatings annealed at 800°C. Phosphorus compositions: (a) 1-3 wt%, (b) 6.5-8 wt%, (c) 10.5-11 wt%.

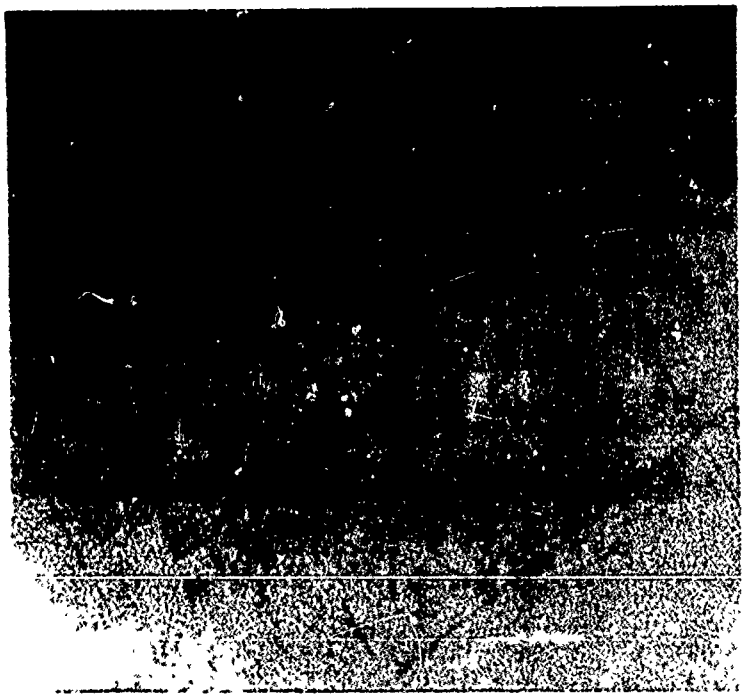

Fig. 6. Cross-section through as-plated electroless nickel coating with 9 wt% phosphorus (from Reference 8). $NaCN-(NH_4)_2SO_4$ etch. Magnification 400X.

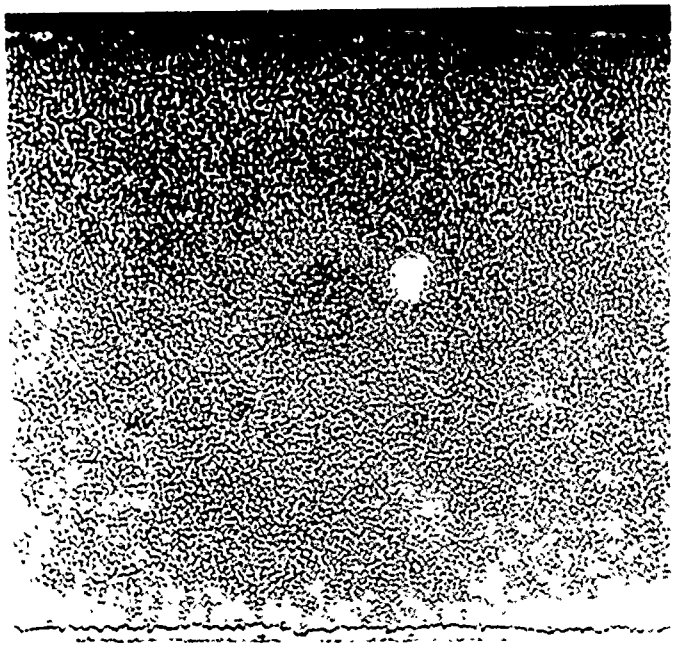

Fig. 7. Cross-section through electroless nickel coating of same composition as Fig. 6, after annealing at 800°C for 1 hour. In this two-phase structure the lighter etching is nickel. The darker phase is Ni_3P. 2% nital etch. Magnification 400X.

PROTECTIVE COATINGS FOR OPTICAL FIBERS

J. COVINO
RESEARCH DEPARTMENT
NAVAL WEAPONS CENTER
CHINA LAKE CA. 93555-6001

Optical fibers are being used in varied environments for communication links. Among the harsh environments seen by fibers today are: salt water, cold/hot temperatures, high speeds and dynamic high shock environments. In order for a data link to be effective in these environments the fiber and the coating must be well designed. This paper addresses fiber properties and coatings designed for these environments. Among some of the desirable properties are: moderate to high strength, small bend radius, and small dB losses while the fiber is in use. The coating on the other hand must be very effective in protecting the fiber from the environment. Coatings should be "hermetic", very light weight, shock resistant, and stable at both low and high temperatures.

INTRODUCTION

Communication in today's societies is not only essential but also technologically quite complex. Many forms of communication systems have appeared over the years. The principal motivations behind each new system was either to improve the transmission fidelity, to increase the data rate so that more information could be sent, or to increase the transmission distance between relay stations. Communication today can be made at a multitude of frequencies ranging from radio, millimeter wave, infrared, visible trough ultraviolet.[1-2] Communication using an optical carrier wave guide along a glass fiber has become extremely attractive. Among some advantages of such a data link are:[3]

1. Enormous potential band width
2. Small size and weight
3. Electrical isolation
4. Immunity to interference and cross talk
5. Signal security
6. Low transmission loss
7. Ruggedness and flexibility
8. System reliability and ease of maintenance
9. Potential low cost

Due to the attractiveness of optical fiber data links for military applications, much emphasis has been placed on the evaluation of their assets and limitations. Optical fibers are being investigated for use in a variety of environments. These environments range from salt water, cold/hot temperatures, high speeds to dynamic high shock. However, in order for a data link to be effective in these environments, the fiber and its coating must be well designed. This paper addresses some fiber properties and coating designs for these environments.

The paper is divided into two areas. The first area discusses the use of a single mode fiber for "Pay-out" environments. These environments are at high speeds and involve extreme temperature fluctuations. The data presented addresses the basic mechanical properties of these fibers and properties of a few protective coatings which are being considered for such environments. The second area will address the use of the Sol-Gel method for the development of a protective coating which is impermeable to water and can also withstand large temperature gradients.

FIBER MECHANICAL CHARACTERIZATION

Conventional tensile tests were made on three different fibers. · Details on the measurement techniques and background for these measurements are found elsewere.[4-8] The fiber lengths used for these measurements were 25 inches long. The data from these measurements is tabulated in Table I. All fibers had a cladding size of 125 μm. Fiber A and Fiber B had a ultraviolet (UV) cured acrylate coating of 125 μm making the total diameter of the fiber 250 μm. Fiber C was a hermetic coated fiber with cladding size of 125 μm.

Table I shows the UV cured acrylate coated fibers are about 100 kpsi stronger than the "hermetically" coated fiber. This implies that the process used to apply the "hermetic coating is possibly degrading the quality of the SiO_2 fiber.

TABLE I. Ultimate Tensile Strength for the Three Different Fibers.

FIBER TYPE	ULTIMATE TENSILE STRENGTH (kpsi)
A	687-718
B	640
C	563

Bend measurements were also performed on the three different fibers. As a fiber unspools during a "pay-out" test it would be expected to experience a bending radius where it leaves the spool. In order to simulate this, tensile tests were performed on the fibers about a bend. Fibers were pulled with a 90 degrees bend around pins of varying diameter. The fiber lengths used in these experiments were 25 inches. Frictional effects were neglected. Figure 1 illustrates the ultimate tensile strength versus fiber bend radius about a pin for the three different fibers. As can be seen from these measurements, the "hermetically" sealed fiber is also less bend resistant when compared to the UV cured acrylate coated fibers. Note that the fracture stress measured by this method at the larger diameters (above 0.65 inch) is essentially the same as the measured ultimate tensile strength for these fibers (see Table I).

Measurements were also made of the fibers to evaluate the number of revolutions required for a given fiber under a fixed load to fail. These measurements were made in order to simulate the twisting that a fiber undergoes during unspooling off of a bobbin. The data is tabulated in table II.

TABLE II. Twisting Measurements Under a Given Load for the Three Different Fibers.

Fiber Type	Load (lbs)	Number of Revolutions to Break	Ultimate Tensile Strength
A	5	238	255
	10	130	510
B	5	191	....
	10	121	....
C	5	127	255
	10	54	510

The data in table II illustrates that Fiber C is less resistive to twisting under a given load when compared to Fibers A and B. However, when looking at the ultimate tensile strength of Fiber A verses Fiber C at failure for either a 5 lbs or a 10 lbs load the values are identical. This indicates that if a fiber fails in a torsional mode it is the SiO_2 core that fails and the buffer coating does not appear to enter into the failure mechanism.

The data from all three mechanical measurements presented show that the "hermetic " fiber (Fiber C) is weaker than the other two fibers (Fiber A and B) under all types of load conditions. The UV cured acrylate coating appears to be more shock and stress resistive. However, Fiber C, because of its hermeticity, can withstand temperatures well above 500°C and still maintain its optical integrity while Fibers A and B start to degrade at temperatures ranging from 300 to 500°C. Furthermore, Fiber C is expected to have better aging properties due to the nature of the protective coating.

Fibers of the same class as Type A and Type B were first wound on a bobbin and than subject to unspooling ("Pay-out") at high speed. Scanning Electron Microscopy (SEM) photographs were taken of the fibers at points at which failure took place. Representative SEM photographs are included in this paper for Fiber B only. However similar observations have been made for Fiber A. Figure 2a and b are SEM images of Fiber B after it has been damaged. Figure 2a shows the glass (g) and buffer (e) regions along with the probable region of fracture initiation (arrow). Figure 2b is a high magnification view of the fracture initiation site (arrow). What appear to be diametrically opposed projections of the buffer coating in figure 2a are actually regions of adhesive.

Figure 3 is an SEM of the fiber taken at 45 degrees from the fiber axis, showing the extensive damage in the buffer region and the initiation site (arrow). Figure 4 a and b are also SEM images of the buffer coating showing extensive damage in a region away from the fracture site. Such damage could have taken place from possible chemical reactions of the buffer with the adhesive used to hold the fiber on the bobbin or from high temperatures reached during "pay-out" of the fiber. The damage could have also been caused by mechanical means. Either by a scoring of the fiber during spool manufacture or by hitting a sharp object during "pay-out".

Most of the fracture surfaces seen in micrographs of damaged fibers of both Type A and Type B fibers exhibited brittle cleavage patterns. Inclusions or regions of high porosity were not observed in the core material. In most cases, some debris was present on both the glass fracture surface and the buffer material. By energy dispersive X-ray (EDX) capability of the SEM, the debris was analyzed as being mostly silicon (from the fracture of the SiO_2 fibers). Most of the fracture surfaces exhibited extensive damage and the fracture initiation site could not be determined. However, a few fiber breaks showed the mirror (k), mist (l) and hackle (m) regions indicative of a glass fracture surface as illustrated in figure 5. It has been demonstrated by Mecholsky et. al.[6] and Jonhson et. al.[7] that a linear relationship exists between flaw size and mirror radius. Flaw size relates to the fracture stress of a material in the following relationship: [6-7]

$$\text{Constant} = \text{Fracture Stress} \times (\text{Mirror Radius})^{1/2}$$

$$\text{Constant used for } SiO_2 \text{ glass} = 270 \text{ kpsi } (m)^{1/2}$$

For the fracture in Figure 5 a mirror radius of 8 microns was measured and a fracture stress of approximately 96 kpsi was calculated using the above equation. An average stress of 50-100 kpsi was calculated for both Fiber A and B. Other fracture morphology observation of similar fibers in high speed/dynamic environments are indicative of a high stress failure (see fig 6a. and 6b.). In Figure 6a cracks in the buffer are indicated with arrows. Figure 6b is a higher magnification of Figure 6a showing the core (glass) of the fiber. The fracture initiation site could not be located although the general direction of the crack movement is probably as indicated by the arrow (Figure 6b.). The fracture surface in this break appears most likely what one would expect for a high stress fracture.

Such fracture probably originated on the site of the fiber where cracks in the buffer were observed. What is significant in this data is that during actual use of the fiber two things happen. These are: a) the strength of the fiber drops an order of magnitude and b) the UV acrylate protective buffer does not offer much protection to the fiber. In the case of acrelate coated fibers, the damage of the coating is manifested by deformation while in the case of the "hermetic" coated fiber damage of such coating would most likely propagate throught the fiber causing the fiber to shatter. At times the buffer becomes damaged, or separates from the fiber thus introducing stresses or damage sites for the fiber to fail. Similar data for the "Hermetic" coated fiber is not presently available due to the lack of availability of such material. However, since the coating material is brittle and hard the failure processes might be totally different.

SOL-GEL DEPOSITED PROTECTIVE COATINGS FOR SiO_2 FIBERS

The "Sol-Gel" process [9] is one in which the final product is obtained from reactive precursor materials (such as metal organics or metal alkoxides) by chemical or thermal means. This process involves the formation of a solution or colloidal suspension (SOL) followed by a gelling stage (GEL) prior to the conversion to the final product. The Sol-Gel process offers the means to coat these fibers by simple dipping techniques during production as well as to "fine tune" the chemical bonding of these coatings onto the fibers for strength and durability in harsh environments. There are many fiber optical communication applications which can only be made possible if truly "hermetic" sealed coatings for SiO_2 fibers which are durable, nonpermeable to moisture, do not degrade the optical quality of the original fiber, are cost effective and available. Materials of choice for the SiO_2 fiber coatings are lithium aluminum silicate (LAS) glass ceramics having the stuffed b-quartz structure. These materials have crystalline phases which range from 60 to 100% and show low helium permeability. They have low thermal expansion coefficient with a varying from $\pm 10^{-8}$ to 10^{-6} in the 0 to 600K temperature range.[10]

Figure 7 shows SEM pnotograph of the uncoated and coated SiO_2 fibers. The coated fiber was coated with the LAS-like gel after dipping in 49% hydrofloric acid (HF) solution. Details on the synthesis and coating application have been reported

elsewhere.[11] Figure 8a and 8b are SEM photographs taken at larger magnifications of the coated fiber. As it can be seen from the SEM photographs, the coating is well dispersed on the fiber (Fig 8 (a and b)) making virtually total covering. Figure 8b shows that the surface of the fiber is undamaged from the acid treatment, even when 49% HF is used.

Basic observation during the coating process suggested that the more viscous gels gave thicker coatings which were more likely to crack and unbound during drying, while the less viscous gels gave thinner coatings which dried more uniformally and were less likely to crack.

It was determined that the coating adhesion and/or quality depends on:

1. Type and viscosity of the gel
2. Pretreatment of the SiO_2 fiber
3. Drying/annealing profile of the coated fibers (slower heating rates showed better coating adhesion).
4. Coating thickness

X-ray diffraction data on the coated fiber showed that the coating remained non-crystalline up to 800°C . Above 800°C, the coating appears to crystallize and separate from the fiber.

CONCLUSIONS

In the first section of this paper, an overview of critical properties necessary for a fiber optic data link used in military environments has been presented. It has been shown that a variety of thermal and mechanical properties both of the fiber and of the coating are very important. The data presented shows that what appear to be improvements on the coating (for example "hermetic" coating) might ultimately degrade the mechanical properties of the fibers.

In the second section of the paper, a synthetic method for coating applications has been addressed. The data presented illustrates that the Sol-Gel offers the means to coat fibers by simple dipping techniques during production and to "fine tune" the chemical bonding of the coating to the fiber for strength and durability. It also offers a cost-effective and mass-production method to coat fibers during the drawing stages.

AKNOWLEDGEMENTS

The author would like to thank R. Scheri and L. Sawyer of the Material Characterization Group at the Naval Weapons Center for providing both ultimate tensile strength data and SEM photographs used in this paper.

REFERENCES

1. A.B. Carlson, ***Communication Systems***, Mc Graw-Hill, New York 1975.

2. G. Keiser, ***Optical Fiber Communications***, Mc Graw-Hill, New York. 1983.

3. J.M. Senior, ***Optical Fiber Communications Principles and Practice,*** Prentice-Hall International, Inc., 1985.

4. EIA Standard No. 455-28A, ***Method for Measuring Tensile Failure Point of Optical Waveguide Fibers.***

5. S.T. Gulati, C.B. King and F. Quan, "Some Recent Results of Fracture Stress and Mirror Size for Optical Fibers," ***Proceedings of the 27th International Wire and Cable Symposium***, pp. 342-344, 1978.

6. J.J. Mecholsky, R.W. Rice and S.W. Freiman, "Prediction of Fracture Energy and Flaw Size in Glass from Measurements of Mirror Size," ***J. Amer. Ceramic Soc.***, 57(10), pp.440-443, 1974.

7. J.W. Johnson and D.G. Holloway, "Size and Shape of Fracture Zones on Glass Fracture Surfaces," ***Phil. Mag.***, 14(130), pp.731-743, 1966.

8. E.B. Shand, "Breaking Stresses of Glass Determined from Dimensions of Fracture Mirrors," ***J. Amer. Ceramic Soc.***, 42(10), pp.474-477, 1959.

9. V. Gottardi, Ed.***Glasses and Glass-Ceramics from Gels***, Proc. Int. Workshop of Glasses and Glass Ceramics from Gels, North-Holland, Amsterdam 1982.

10. J. Covino and J.M. Bennett, ***Laser-Gyro Materials Studies*** Naval Weapons Center, China Lake, CA., NWC (NWC TP6705) March 1986. (Publication Unclassified).

11. J. Covino and K. Wilson "Sol-Gel Methods for SiO_2 Optical Fiber Coatings," ***Third International Conference on Ultrastructure Processing of Ceramics, Glasses and Composites***, San Diego, California, Feburary 23-27, 1987. John Wiley and Sons, (in press) New York.

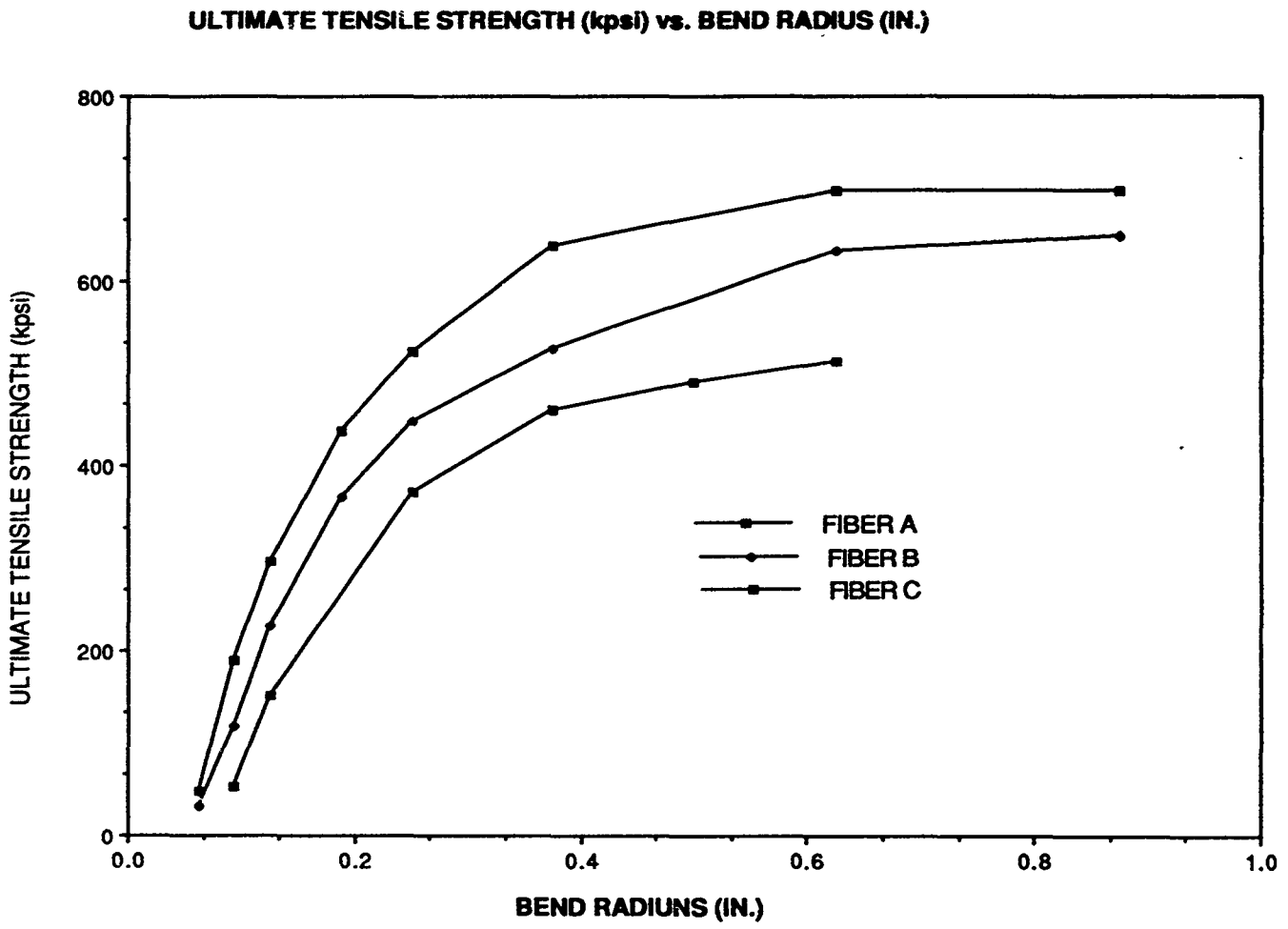

Figure 1. Bending radius data. for Fiber A, B and C.

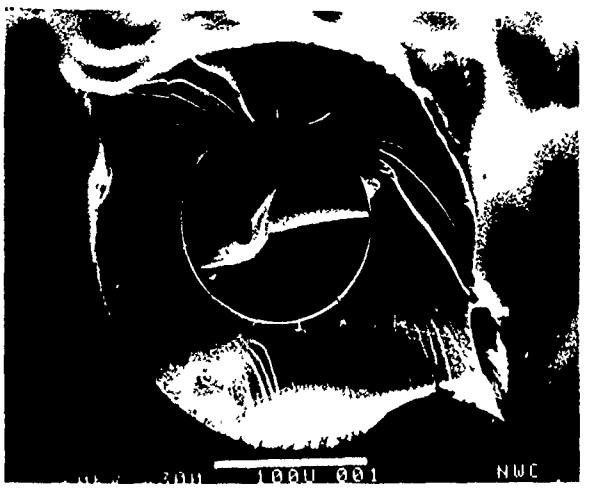

a)

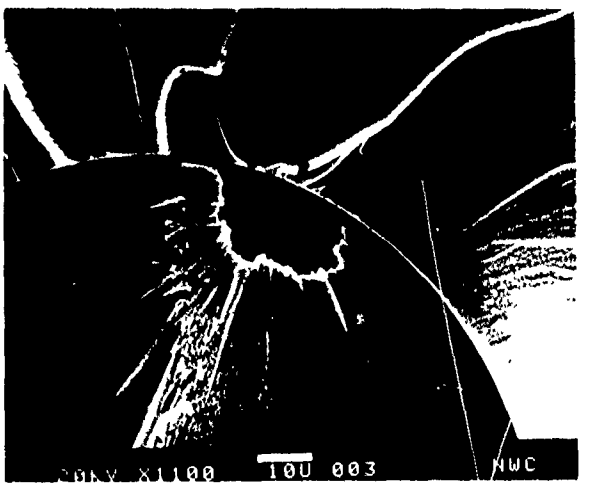

b)

Figure 2. SEM images of Fiber B after it has been damaged from "pay-out" experiments. a) Shows the glass (g) and buffer (e) regions, along with the fracture initiation site (arrow). b) Shows a high magnification view of a with the fracture initiation site indicated with an arrow.

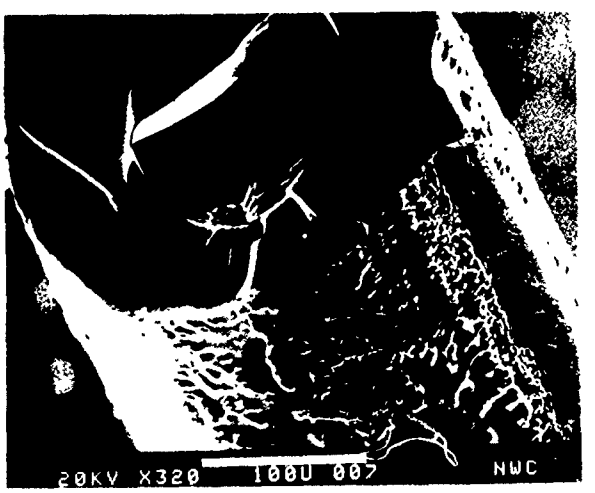

Figure 3. SEM photograph of Fiber B taken 45 degrees from the fiber axis showing the fracture initiation site (arrow) and extensive buffer damage.

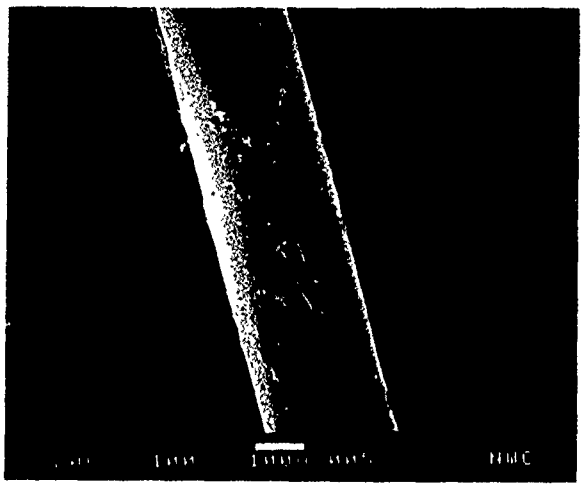

a)

Figure 4. SEM images of fiber B taken 45 degrees from the fiber axis showing an extensively damaged buffer in a region away from the fracture site. b) shows a higher magnification view of a).

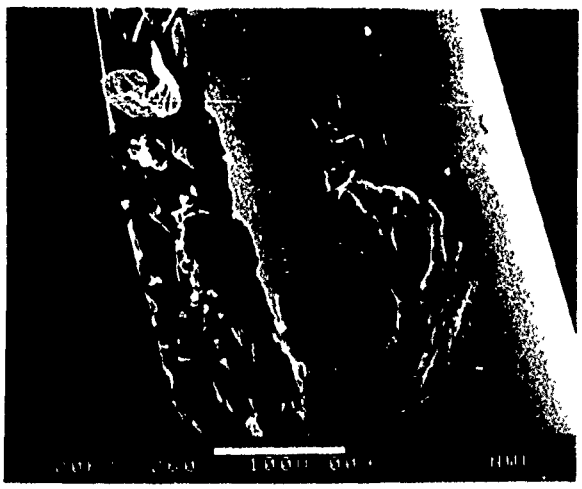

b)

Figure 5. High magnification SEM photograph of Figure 2 showing the mirror (k), mist (l) and hackle (m) region of the fracture surface.

a) Shows the glass (A) and buffer (B) regions of the biber. Cracks in the buffer are indicated with arrows.

b) Higher magnification view of a showing the glass portion of the fibe The arrow indicates direction of crac growth.

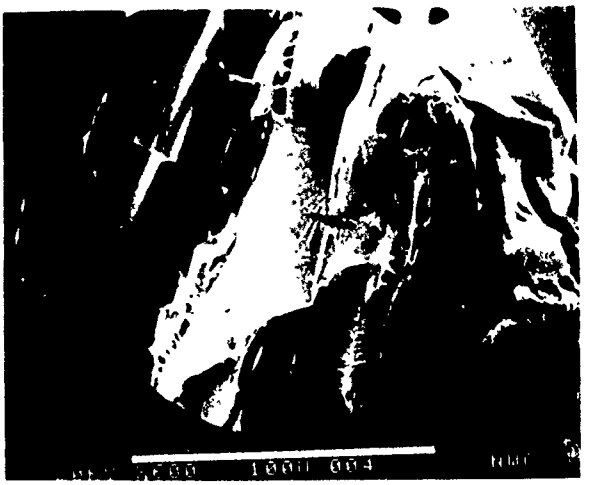

Figure 6. Representative SEM photographs of a high stress failure in Fiber B.

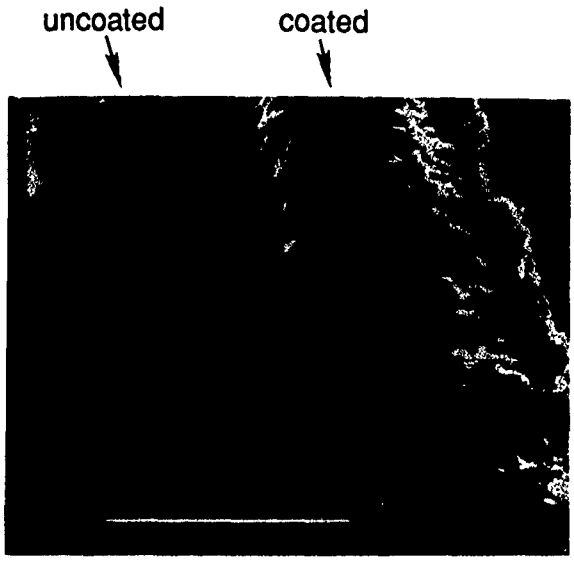

Figure 7. SEM Photograph of the SiO_2 fiber uncoated and coated with an "LAS-like" coating using the Sol-Gel Method.

a)

Figure 8. Higher magnification SEM photographs of the SiO_2 "LAS-like " coated fiber. a) Shows the coating surface. b) Shows the smooth interface between the fiber and the coating

CORROSION RESISTANCE OF MULTILAYER ELECTRODEPOSITED COATINGS

R. Weil and C. Sheu

Stevens Institute of Technology,
Hoboken, NJ 07030

ABSTRACT

The corrosion properties of multilayer Cr-Mo and Ni/NiSn/Ni and Sn/NiSn/Sn sandwich electrodeposits were determined by voltammetry and compared to those of single-layer coatings. When the thickness did not exceed a value where cracks developed, single-layer Cr-Mo deposits had smaller critical current densities for the onset of passivity and in the passive region than pure chromium. In multilayer deposits these current densities were even smaller. Sandwiching a NiSn layer between tin or nickel improved the strength without detrimentally affecting the ductility. The NiSn layer prevented pits from penetrating through nickel, but increased the corrosion rate of tin.

INTRODUCTION

Multilayer, electrodeposited coatings have exhibited improved corrosion resistance. Duplex nickel deposits under chromium are the best known examples. In these coatings, a bright nickel layer acts as a sacrificial anode to a semi-bright one preventing pits from penetrating to a steel substrate. Many electrodeposits exhibit the so-called banded structure in which alternate darker and lighter layers are observed on metallographically prepared cross sections. In alloy electrodeposits the banded structure is generally due to compositional variations (1). The banded structure has been reported (2) to improve corrosion resistance. Multilayer deposits can be intentionally produced in several ways. It has been shown (3,4) to be possible to vary the composition of electrodeposited alloys only by changing pulse-plating parameters. By alternately changing the peak current density or other pulse-plating parameters, layers of different composition can be deposited in the same plating solution. It is, of course also possible to produce layers of different composition by plating each layer in a different solution. A study of the corrosion resistance of two types of multilayer coatings produced by varying the plating parameters in the same solution

and by deposition in different baths is reported here.

One type were chromium-molybdenum electrodeposits in which the layers were produced by only varying the plating conditions. Composites in which a layer of an intermetallic phase, NiSn was sandwiched between tin or nickel, constituted the second type. In these deposits the NiSn layer was plated in a different solution than the pure metals. The corrosion resistance of single-layer deposits of the same thickness as the multilayer ones was determined for comparison purposes. The mechanical properties of some single and multilayer deposits were also measured.

EXPERIMENTAL PROCEDURE

The Cr-Mo deposits were electroplated in a solution containing 300 g/l chromic acid and 75 g/l ammonium molybdate. The substrates were sheets of low-carbon steel. The thicknesses of the single-layer deposits were 1µm, 2µm and 5 µm. The compositions were about 0.1, 0.3, 0.8 and 1.4% Mo. The different compositions were obtained by varying the current density between 0.2 and 1 A/cm^2 at 60C. The multilayer deposits consisted of 250 nm thick layers of 0.1% Mo and 250 nm thick ones of 1.4 % Mo for total thicknesses of 2 µm and 5 µm. The layers of different composition were obtained again by varying the current density. Chromium of the same thickness as the single-layer Cr-Mo deposits was also plated on steel for comparison. The 5 µm thick single and multilayer deposits were also annealed at 70C for 10 hours and at 120C for 2 hours.

Corrosion testing consisted of varying the potential between -0.5 and 1.5 V and measuring the current at a scanning rate of 1mV/sec in a 5 % sulfuric-acid solution. The surface structures of all deposits and those of the cross section of the multilayer ones were observed by scanning electon microscopy. The chemical compositions were determined with energy-dispersive X-rays in the same instrument.

The Sn/NiSn/Sn and Ni/NiSn/Ni composites were plated on low-carbon steel and on electropolished copper substrates. Tin was pulse plated in a solution composed of 200cc/l stannous fluoborate, 15 cc/l fluoboric acid, 6 g/l gelatin and 1 g/l beta-naphthol at 50C and a pH of 2.5-3.5. The square-wave, peak current density was 0.4A/cm^2, the frequency was 5 Hz and the duty cycle 0.5. After tin was plated to a thickness of 20 µm, the samples were transferred to a solution composed of 192 g/l potassium pyrophosphate, 71 g/l nickel chloride and 20 g/l glycine in which the NiSn layer was deposited. Layers of NiSn varying in thickness from 50 to 250 nm were pulse plated with a peak current density of 60 mA/cm^2. The other pulse variables

were the same as those used for tin plating. The samples were then returned to the tin-plating solution to plate an additional 20 µm thick layer of tin. Tin without NiSn was also deposited to a thickness of 40 µm. The Ni/NiSn/Ni sandwiches were produced by first plating a 20 µm thick nickel deposit in a standard Watts solution containing 300 g/l $NiSO_4 x7H_2O$, 60 g/l $NiCl_2 x6H_2O$ and 37.5 g/l boric acid at 50C and a pH was 3. The peak current density was 0.1mA/cm^2; the pulse frequency and duty cycle were again the same as those used for plating tin. After transferring the samples to the solution for NiSn plating in which layers varying in thickness from 50 to 400 nm were deposited, they were returned to the Watts solution. Here an additional 20 µm of nickel was deposited. Forty µm thick nickel deposits were also plated in the Watts solution. Deposits of only NiSn of various thicknesses were also plated on steel and copper substrates.

The deposits on steel substrates were corrosion tested. Testing consisted of varying the potential between -0.5 and 2 V vs a standard calomel electrode at a scanning rate of 1 mV/sec and recording the current. The Ni/NiSn/Ni sandwiches were tested in 3% sulfuric acid; the Sn/NiSn/Sn deposits in a solution containing 1% sulfuric acid and 0.4% sodium nitrate. The deposits plated on copper substrates were used to determine the mechanical properties. The substrates were dissolved in a chromic-sulfuric acid solution after the shape of the tensile specimen had been imprinted on the deposit using photolithography. The preparation and size of the tensile specimens and the device to test them have been previously described (4) in detail.

RESULTS AND DISCUSSION

Chromium-Molybdenum Deposits

The effect of the deposition current density on the composition of the Cr-Mo alloys is shown in Figure 1. It is seen that the molybdenum content can be varied from about 0.1 to 1.4% by only changing the current density. At current densities below 0.2 A/cm^2 the deposits were dull. Above 1 A/cm^2 rough deposits were obtained. Therefore only the range of 0.1 to 1.4% Mo was investigated.

A typical voltammetric curve for a 2 µm deposit containing 1.4% Mo is shown in Figure 2. The current densities for the onset of passivity, i.e., the critical current density and the ones in the passive region for single-layered deposits with several molybdenum contents and for the multilayer one are listed in Table 1.

Table 1
Corrosion Data for Two Micrometer Thick Deposits

Deposit	Critical Current Density (mA/cm^2)	Passive Region C. D. (mA/cm^2)
Chromium	0.3	0.2
Cr-0.1% Mo	1.1	0.1
Cr-0.3% Mo	0.5	0.1
Cr-0.4% Mo	0.2	0.1
Cr-0.8% Mo	0.2	0.1
Cr-1.4% Mo	0.2	0.1
Multilayer	0.07	0.03

It can be seen from Table 1 that the deposits containing 0.1 and 0.3% Mo have higher critical current densities than chromium. Deposits containing more than 0.4% Mo have smaller critical current densities than chromium. The current density in the passive region of the single-layer Cr-Mo deposits is also lower than than of chromium and even smaller for the multilayer one. The results for the single-layer deposits are in agreement with previous ones. Multilayer Cr-Mo deposits have not been previously investigated. Malinin and Falicheva (5) reported a decrease in the passivation current by a factor of 2.4 when 7 g/l K_2MoO_4 was added to a chrome-plating solution. A lowering of the critical current with increasing molybdenum content in chromium-base alloys was also reported by Shluger, et.al. (6).

The reason for the corrosion behaviour of the 2 μm thick deposits may be deduced from their structures. As observed by scanning electron microscopy, all deposits exhibited a nodular structure as illustrated in Figure 3. This structure is characteristic of many fine-grained deposits. It consists of grooves surrounding groups of many small grains. The grooves may be caused by compositional variations resulting locally in a slower deposition rate. It appears that corrosion started in the grooves as they were observed to become deeper. After raising the potential into the transpassive region, more grooves were observed to have formed as shown in Figure 4. The decrease in the measured critical current density with increasing molybdenum content was due to the nodules being larger, i.e., fewer grooves. If the corrosion current is concentrated in the grooves, the fewer there are, the higher is the current density. Therefore if there are few grooves, the critical current density will be reached at a lower overall value. The deposition of multiple layers resulted in fewer and shallower grooves and thus in the lowest observed critical current density.

Deposits thinner than 2 μm did not exhibit a passive region. Pits, which had penetrated to the steel substrates were

observed. Apparently, the deposit in grooves was either very thin or non-existant. Thus before reaching the critical current density, the steel substrate became exposed. Before corrosion testing, some 5 µm thick deposits exhibited a few fine cracks which followed the grooves surrounding the nodules. These cracks, one of which is indicated by an arrow in Figure 5, undoubted resulted from the high stresses which are characteristic of chromium electrodeposits. The critical current densities for the onset of passivity and the current density in the passive region are listed in Table 2 for some 5 µm thick deposits.

Table 2
Corrosion Data for Five Micrometer Thick Deposits

Deposit and Heat Treatment	Critical Current Density (mA/cm^2)	Passive Region C. D. (mA/cm^2)
Cr-0.3% Mo As Plated	1.1	0.08
Cr-1.4% Mo As Plated	1.7	0.07
Multilayer As Plated	2.7	0.08
Cr-0.3% Mo 10 Hr at 70C	0.4	0.03
Cr-1.4% Mo 10 Hr at 70C	1.4	0.04
Multilayer 10 Hr at 70C	1.2	0.05
Cr-0.3% Mo 2 Hr at 120C	0.1	0.03
Cr-1.4% Mo 2 Hr at 120C	0.4	0.03
Multilayer 2 Hr at 120C	0.2	0.04

The higher critical current densities of the 5 µm thick, as-plated samples were probably due to the fine cracks. The 5 µm thick deposits also cracked in the transpassive region. However, these cracks, which are the more prominent ones seen in Figure 5, are much wider than the ones present before corrosion testing. The 2 µm thick ones did not show any cracks before or after corrosion testing. Apparently the stresses had not reached the magnitudes to cause cracking in the thinner deposits. It is probable that stress corrosion cracking occurred in the thicker deposits. High internal stresses in chromium deposits have been attributed primarily to hydrogen (7). To assess the effect of hydrogen on the corrosion behaviour, the 5 µm thick samples were annealed in vacuum. The results are also recorded in Table 2. Annealing reduced the critical current densities for the onset of passivity and in the passive region. It is possible that the grooves around the nodules may also have become more corrosion receptive because of stress or higher hydrogen contents. The annealed deposits still cracked after the potential was raised into the transpassive region. Possibly

there were causes of stress other than hydrogen.

Sn/NiSn/Sn and Ni/NiSn/Ni Deposits

The main reason for plating tin and nickel with a NiSn layer sandwiched in them was to determine the effect on the mechanical properties. However, the effect of the intermetallic-phase layer on the corrosion resistance was also of interest. The mechanical properties of tin and nickel deposits containing NiSn layers of various thicknesses are listed in Table 3.

Table 3
Mechanical Properties

NiSn Thickness (nm)	Yield Strength (MPa)	Tensile Stength (MPa)	Elongation (%)
Ni/NiSn/Ni Composites			
0	283	445	3
50	369	600	3
100	369	616	3
150	374	617	3
200	356	590	3
250	396	646	3
300	364	618	3
350	371	625	3
400	377	618	3
Sn/NiSn/Sn Composites			
0	17	18	23
50	20	24	6
100	21	25	6
150	23	26	5
200	24	27	5
250	27	31	3

As seen from Table 3, the presence of a NiSn layer substantially increased the strengths of the deposits. The NiSn layer apparently did not affect the ductility of the nickel deposits, but caused the tin deposits to become considerably more brittle. Attempts to determine the mechanical properties of the intermetallic phase by itself were not successful as it was to brittle to handle for testing. NiSn is a metastable phase having a hexagonal nickel arsenide structure and therefore would be expected to be brittle.

It would have been desirable to plate the entire deposits in one solution. By adjusting the plating variables it was possible to deposit almost pure nickel or pure tin in the solution used to plate NiSn. However the nickel deposits were so highly stressed that they exhibited cracks on their surfaces. The tin deposits did not crack but were considerably less ductile than the one listed in Table 3. It was therefore necessary to plate the matrix and the intermetallic-phase layer in different solutions.

The voltammetry graphs of nickel from the Watts solution showed a critical current density of about 1 mA/cm^2. This current density also prevailed in the passive region. When a layer of NiSn was sandwiched between nickel, the critical current density was 5 mA/cm^2. The current density in the passive region was again 1 mA/cm^2. A deposit consisting only of NiSn also exhibited essentially the same critical and passive-region current densities as the single-layer nickel deposit. It was also observed that fewer pits had formed in the Ni/NiSn/Ni composite after bringing the potential into the transpassive region than in nickel by itself. The pits which were observed in the nickel deposit when a NiSn layer was present were wider, had flat bases and did not penetrate to the steel substrate . A posssible explanation for the effect of the NiSn layer is that is was the cathode for a few pits in the nickel which reached it. This effect would result in a higher critical current in the nickel and consequently the wider pits. The deposition of a NiSn layer probably resulted in fewer pits in the top nickel deposit because the plating interruption resulted in nucleation rather than continued growth. Being the cathode, the NiSn layer prevented pits from penetrating into the bottom nickel layer and reaching the steel substrate.

Tin with and without a NiSn layer did not passivate in the 1% H_2SO_4 solution. When a pit in the top tin layer reached the NiSn, corrosion was accelerated. The top tin layer then disappeared rapidly.

CONCLUSIONS

It has been shown that Cr-Mo multilayer deposits can have better corrosion resistance provided they are not so thick that the internal stresses reach values at which cracking occurs. Sandwiching a layer of an intermetallic phase, NiSn between tin or nickel increases the strength without a detrimental decrease in ductility. One aspect of the corrosion resistance of nickel is improved by the NiSn layer in that pits do not penetrate to steel substrates. The corrosion rate of tin was accelerated by the presence of the NiSn layer.

REFERENCES

1. C.C. Nee and R. Weil, Surface Tech., v.25 (1985) 7.
2. M. Rasker, D.S. Lashmore, K.W. Pratt, Plating and Surf. Finish., v.73, No.9 (1986) 74.
3. C.C. Nee, W. Kim, R. Weil, J. Electrochem. Soc., v.135 (1988) 1100.
4. I. Kim, R. Weil, Testing of Metallic and Inorganic Coatings, ASTM STP 947, W.B. Harding, G.A. DiBari, eds., Am. Soc. Testing & Materials, Philadelphia, PA (1987) 11.
5. V.F. Malinin, A.I. Falicheva, Zashchita Metallov, v.18 (1982) 954.
6. M.A. Shluger, N.V. Shorikova, ibid., v.9 (1973) 105.
7. B.U. Adzhiev, Z.A. Solov'eva, ibid., v.15 (1979) 481.

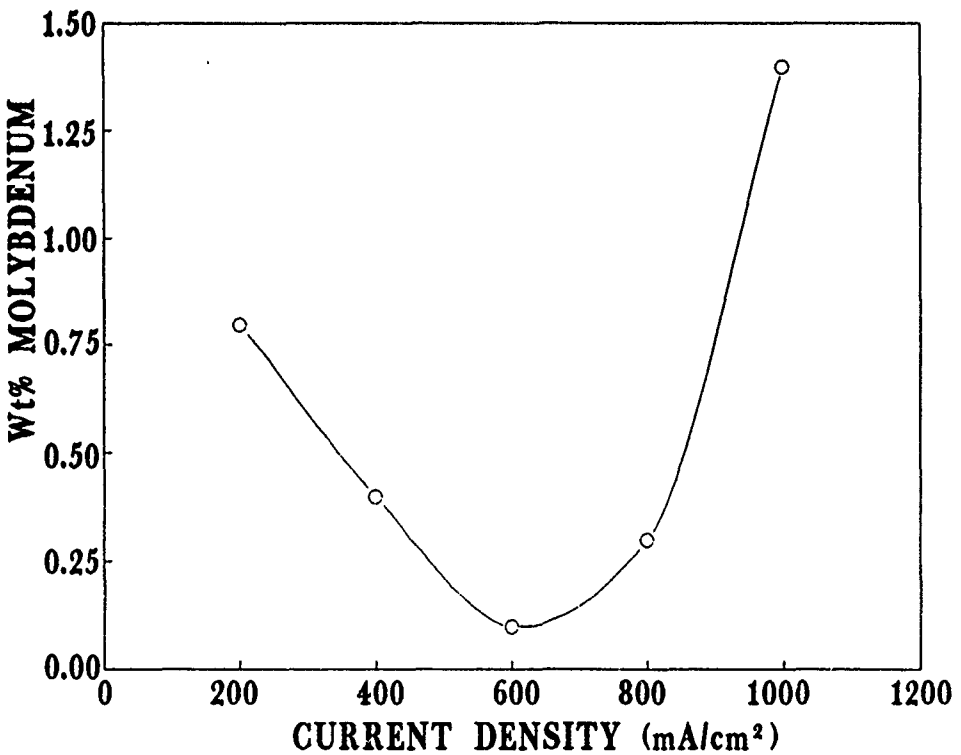

Fig.1 MOLYBDENUM CONTENT VS. CURRENT DENSITY.

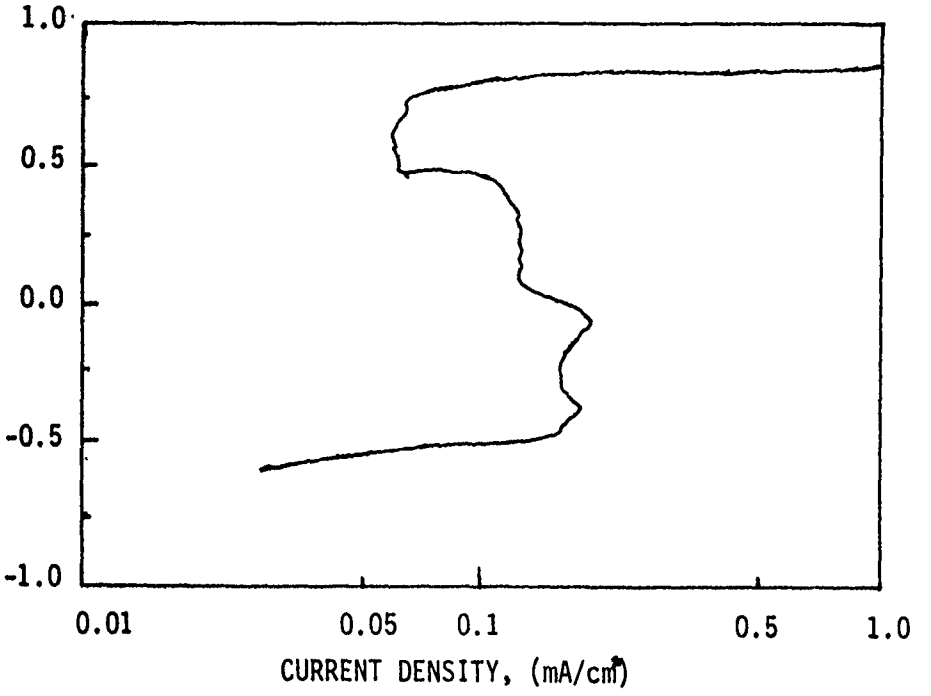

Fig.2 VOLTAMMETRIC PLOT OF 2 μm THICK DEPOSIT CONTAINING 1.4% Mo.

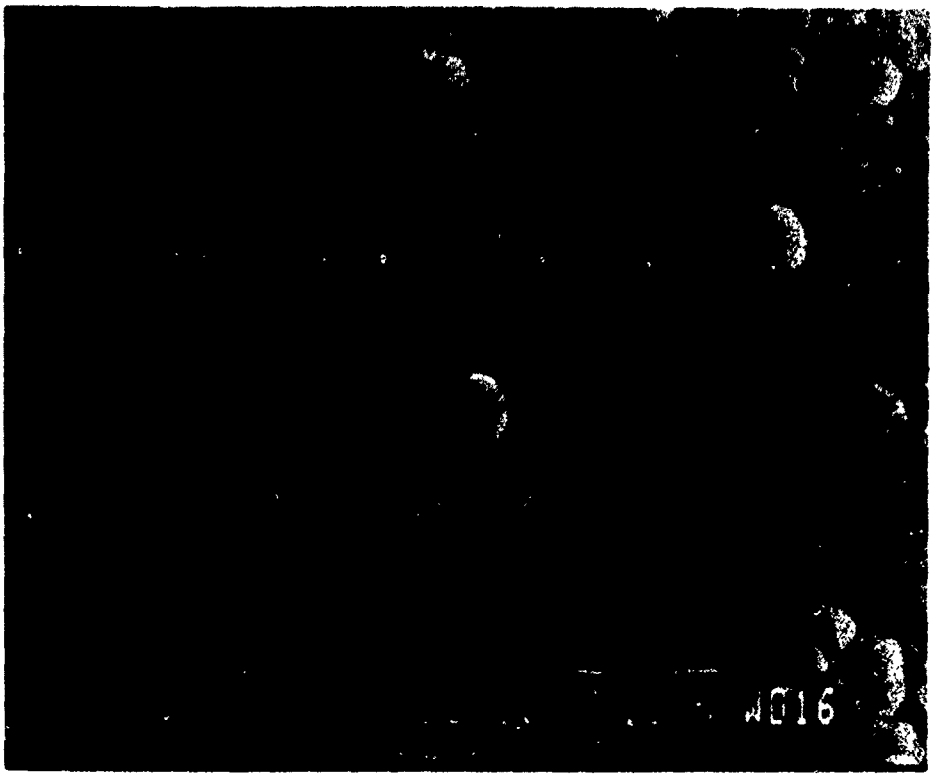

Fig.3 SCANNING ELECTRON MICROGRAPH OF 2 μm THICK MULTILAYER DEPOSIT SHOWING NODULAR STRUCTURE.

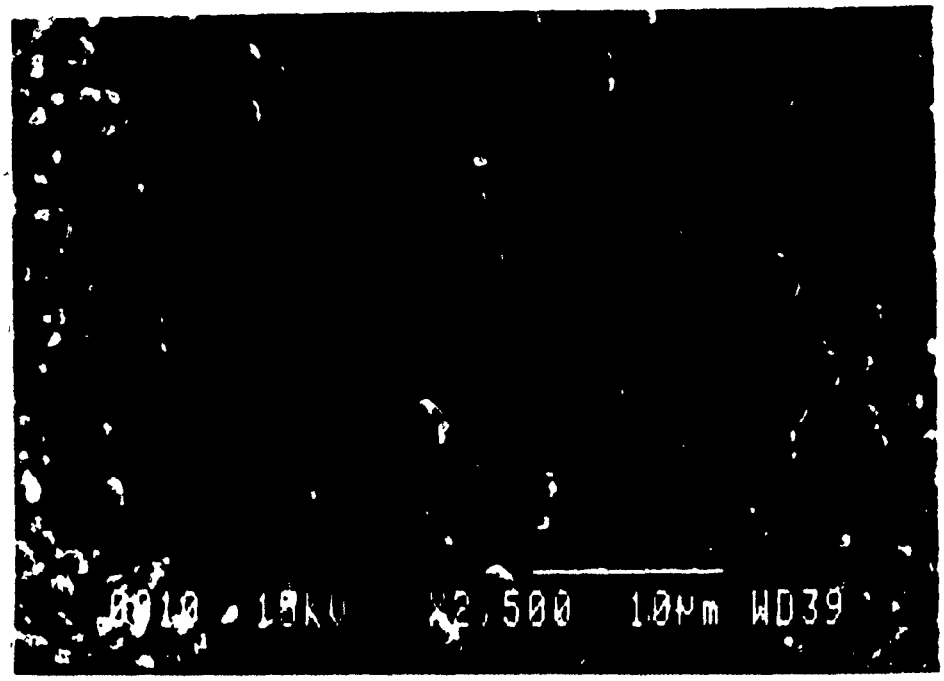

Fig. 4 SCANNING ELECTRON MICROGRAPH OF 2 μm THICK MULTILAYER DEPOSIT AFTER CORROSION TEST.

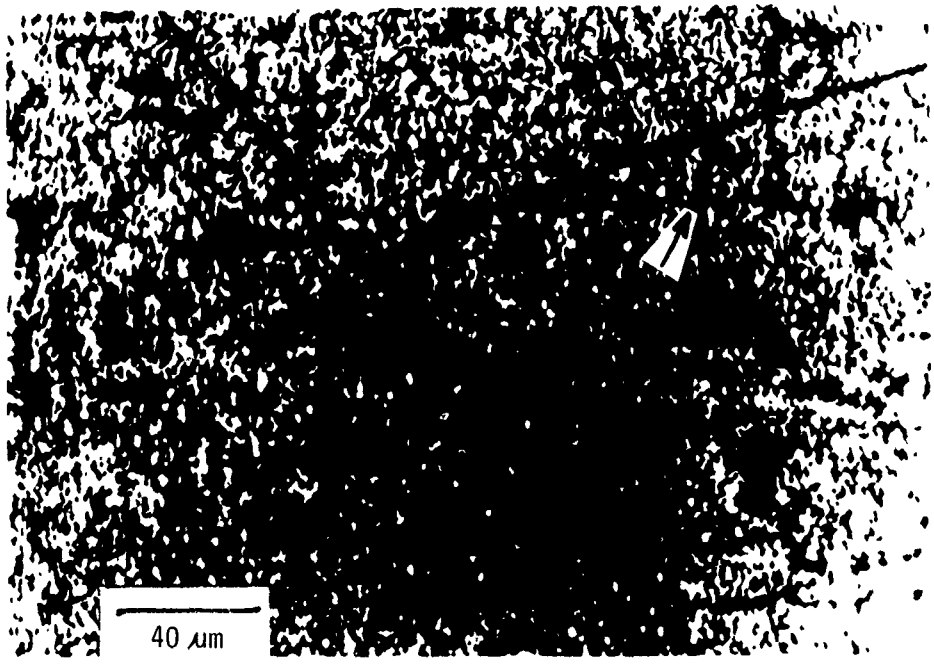

Fig. 5 OPTICAL MICROGRAPH OF 5 μm THICK DEPOSIT SHOWING FINE CRACKS (INDICATED BY ARROW) AND COARSE ONES DUE TO STRESS CORROSION

COST-EFFECTIVENESS OF TOPSIDE SHIP COMPONENTS PRESERVED WITH METAL-SPRAYED COATINGS (MSC) TOPPED WITH ORGANIC POWDER COATINGS (OPC)

by Paul D. Schlunt / Robert A. Sulit
Integrated Systems Analysts, Inc.
740 Bay Boulevard
Chula Vista, CA 92010-5254
(619)-422-7100

and

Fred West
Shore Intermediate Maintenance Activity
Naval Station, Box 106
San Diego, CA 92136
(619)-235-1195

ABSTRACT

Shore Intermediate Maintenance Activity, San Diego, (SIMA(SD)), lead SIMA for the evaluation and introduction of corrosion-control technologies evaluates the applicability and cost-effectiveness of metal-spray coating (MSC) and organic powder-coating (OPC) systems for topside shipboard components as applied by Navy enlisted personnel. This paper compares the technical characteristics of aluminum flame-wire and flame-powder MSCs; the application equipments, processes and quality-control checkpoints; the application times for coating shipboard components; and the 3 months performance evaluation of topside shipboard components preserved with MSC topped with OPC.

1. INTRODUCTION

Metal-spray coatings (MSC) and organic powder coatings (OPC) have been applied to naval ship components at the Shore Intermediate Maintenance Activity, San Diego (SIMA (SD)) Corrosion Control Shop for over four years. As the technologies advance, new forms of materials and methods of application are evaluated. Those which prove to be the most cost effective are implemented to improve product thoughput and service life.

2. BACKGROUND

The Corrosion Control Shop, SIMA (SD), was established in September 1984 to provide MSC to topside ship components, as well as high pressure steam valves, and provide materials or guidance on the remaining 15 NAVSEA designated Corrosion Control Systems, as they are described in reference (1). At the shops inception, the primary service provided on site at the shop was MSC in the form of wire sprayed aluminum, with the required sealer, barrier and topcoat paint systems as specified in DOD-STD-2138 (Ref. 2). OPC services were initially coordinated by the shop and provided by local coating service vendors. On-site OPC services became available in November 1985 at SIMA (SD), in the form of epoxy powder coatings. References (3) and (4) describe the standard time development, shop services, and service life evaluation of coatings applied during the Pilot Corrosion Control Shop Service Test.

The Corrosion Control Shop is fully manned and operated by Navy enlisted personnel. Turnover of personnel is rapid due to shore duty, rate training and deployment schedules; therefore, new technicians are continously being trained.

The product processed by the Corrosion Control Shop has typically been topside ship components from surface ships, which have been in service for 0-20 years. They include water tight doors and latches, vent screens, fire fighting equipment, light fixtures, stanchions, steam riser valves, etc. The aluminum MSC is applied to thick steel items to provide galvanic and barrier protection against corrosion. The epoxy powder coatings are applied to aluminum and thin gage or geometrically complicated steel components, providing barrier protection. The majority of components are in a service environment of salt spray and sunlight exposure, as well as mechanical abuse from members of Ship's Force.

During the first three years that the shop was operating, MSC was applied as wire-sprayed aluminum (WSA). The WSA process consists of gun fed with aluminum wire, which is melted by an oxygen-acetylene flame and sprayed with a continuous stream of pressurized clean dry air.

Over the past six months the shop has begun using a powdered alunimum spray gun. This system is similar in that it uses an oxygen-acetylene flame to melt the aluminum, and compressed air to deliver the melted aluminum to the steel product, but the aluminum is fed as a fine powder, conveyed by air or an inert gas to the gun.

The organic powder coatings have been applied utilizing electrostatic spray equipment and epoxy powder coatings. The component being coated is electrically grounded, and the powder is charged up to 100 kV static electricity. The static charge and having the component preheated above 300°F facilitates providing a 8-12 mil thick coat.

Within the past year, a planned evaluation of applying OPC over MSC and surveying its performance has been carried out. The OPC serving as a sealer, barrier and topcoat in lieu of the standard five coat paint system reduces the shop time from 5-6 days to 1-2 days. This is due to the OPC being fully cured upon removal from the curing oven, where as the standard paint system required drying periods between coats.

3. EQUIPMENT, PROCESSES AND QUALITY CONTROL

3.1 Metal Spray Coatings (MSC)

Both MSC processes utilized by the Corrosion Control Shop have the same work station functions and quality control checkpoints. The primary difference lies in the application equipment and their specific operation procedures. Table I lists the work stations function and quality checkpoints.

TABLE I
WORK STATION FUNCTION AND QUALITY CONTROL CHECKPOINTS FOR ALUMINUM METAL SPRAY COATINGS

WORKSTATION	FUNCTIONS	
	PRODUCTION	QC CHECK
1. Surface Preparation	• Solvent clean • Trisodium phosphate wash • Abrasive cleaning • Heat cleaning • Caustic bath	• Clean substrate
2. Masking	• Mask fit/function surfaces	• Properly masked
3. Anchor-Tooth Blasting	• 50-75 μm (2-3 mil) anchor tooth • White-metal finish	• Al_2O_3 grit quality/size • Clean, dry air • SSPC-5 finish
4. Thermal Spraying	• Preheat substrate to 120°C • Spray 90-45° to substrate and 13-20 cm standoff - 75-100 μm (3-4 mils) per crossing pass - 175-250 μm for ≤ 80°C service; 250-375 um for > 80°C service	• Substrate > 5°C dew point • Pounds per hour determination (for powdered Al) • Proper time between anchor-tooth blasting and start/completion of spraying • Coupon bend test (equipment system check) • Thickness measurement • Visual examination
5. Sealing/Painting	• ≤ 80°C service: 5-coat paint schedule; 250 μm total thickness • > 80°C service: 2-coat paint schedule; 75 μm total thickness	• Wet film thickness • Minimum/maximum drying times between paint coats • Dry film thickness

3.1.1 Wire Sprayed Aluminim (WSA)

WSA was the initial metalizing process implemented by the SIMA Corrosion Control Shop. Specific spray guns utilized at SIMA Corrosion Control Shops include Metco 10E, 11E and 12E, and the Mogal TJ-5. Training programs were developed for each type of application system. Reference 3 describes the process, as implemented at SIMA San Diego, meeting the requirements of DOD-STD-2138. Continued feed of aluminum is very sensitive to exact wire size and the lack of nicks or bends in the wire. A wire spray gun has numerous moving parts, due to the wire feed mechanism being driven by the compressed air stream. These parts include an air turbine, reduction gears, controlling clutches and feed rollers. It is the weight and maintenance (or lack of maintenance) of these parts that make the gun difficult to use.

3.1.2 Powder Sprayed Aluminum

The powder sprayed aluminum process began its implementation in October 1988. The Corrosion Control Shop retains the same requirements as specified in DOD-STD-2138 for the powdered aluminum, as for the wire aluminum. Those requirements include:

- o Surface profile of 2-3 mil accomplished with aluminum oxide.
- o 7-10 mil thick aluminum coating.
- o Certification requirements for operators and facility.

In the past, powder sprayed aluminum coatings were considered to have lower tensile strength than WSA coatings (Ref. 5). This has not been the case at SIMA (SD) with the current equipment, tensile pulls of the powder sprayed coatings have been around 4000-6000 psi (3000-4000 psi is typical for tensile pulls of WSA at SIMA SD). The coatings surface is also smoother than for WSA. WSA typically has small globules (2 mm diameter) occuring on the coating surface which are susceptible to being chipped off, even when topcoated with paint or OPC. These chips can lead to premature breakdown of the coating system at these areas. The smoother powder spray coating has a better visual appearance as well, but ample roughness to accept paint or OPC.

Initially, when the Corrosion Control Shop began implementing the powdered aluminum MSC process, only one brand of equipment had been procured by the U.S. Navy. The equipment manufacturer recommended that only their aluminum powders be utilized. SIMA (SD) worked with other manufacturers to get additional sources of compatible powder. At this date SIMA (SD) is able to procure aluminum from three sources (Miller Thermal, Metco and Wear Control Technology). The price per pound of aluminum powder verses wire are essentially the same.

Overall, the process is proving to be more efficient for Corrosion Control Shop use. The powder sprayed aluminum process requires only one operator, but the WSA process often required an additional person to straighten the wire feeding into the gun. The process has proven to be faster, from 30 to 50% faster than the WSA process. For example, a 50 cal. Machine Gun Tripod, which normally took 33 man-minutes to apply WSA, where as only 23 man-minutes are required for powder sprayed aluminum. The numbers include a 2.55 shop allowance factor (Ref. 6), but only view the aluminum spray application. Of the total man-hours required to process an item (from its receipt by the shop, through surface preparation, MSC application and painting) the MSC application makes up one fifth of the man-hours. Therefore, any impacts on the man-hours for applying MSC must be multiplied by a factor of 0.2 to determine the total effect on SIMA labor hours (eg. a 50 % change in MSC application time changes the total process time by 10%).

A potential problem with the rapid spray rate is the chance that the operator can get ahead of the preheated region. In the slower WSA process, the heat transfer from the area being coated to the surrounding area occurs easily. A lack of proper preheat diminishes the adhesion of a MSC. This would not be detectable on the tensile pull coupons, nor the bend test coupons. Their small size is rapidly preheated. A tensile test such as ASTM D4541 needs to be accomplished on pieces of product which have been coated at high speeds.

The powder spray aluminum process does require an additional quality control step, concerning the pounds per hour spray rate of the gun. The rate is determined by spraying the gun into a tared, noncombustible container, over a measured period of time. The container is then weighed again to yield the sprayed aluminum weight. A step by step procedure has been developed and is in use at SIMA (SD). This test is accomplished at the beginning of each shift. Adjusting the gun to specific pounds per hour (15 lbs/hr typical) is more critical for the powdered aluminum process because of the additional gas controls (carrier gas) and the potential speed of this type of application process.

3.2 Organic Powder Coatings (OPC)

The electrostatic spray powder coating process is being utilized by SIMA Corrosion Control Shops as an alternative to the standard paint systems. OPC's provide a tough pore free finish that cures quickly and releases almost no volitiles (0-5%). The low organic volitile compound (VOC) output adapts well to the increasingly stringent air pollution regulations. Originally, NAVSEA required 8-12 mil of epoxy to be applied, but thick coatings are more likely to chip, and some of the stock epoxy powders available to SIMA's were not formulated for that thick of film. SIMA (SD) has recently requested permission to use only 6-10 mils of epoxy powder instead.

Having a fast curing organic coating which fulfills the sealer, barrier and topcoat requirements for MSC's is advantageous to shop operations. The entire powder coating process and product cool down is accomplished within a day, and several items can often be coated at once. Approximate process time will be two hours, including suspension, preheat, application, curing and cool down. The five coat paint system will require five days for the required drying time between coats. Ovens could be used to more quickly cure the paint systems, but the time limits and temperatures would be extremely critical with minute variations capable of causing extreme porosity, wrinkling or cracking of the paint films.

The reduced coating and curing time allows for more product to be processed because of more floor space being immediately available. However, the initial SIMA man-hours are not impacted as significantly as the products residence time in the shop, because it is the cure time that is reduced, not the application time.

A two-coat application of OPC is employed. Powders can be formulated and ground to provide the proper thickness (6-10 mils) in one coat. However, good protective coating practice requires mulitple coats to ensure no holidays. Dry powder's physical appearance prior to baking makes bare or thinly coated areas difficult to see.

The process for applying OPC's over MSC requires the same concerns as for coating over porous castings. A MSC has a porous region at its surface. If a preheated part cools down before or during application of the OPC, air in the pores will expand when the item is placed in the oven for final curing. The gas then bubbles through the coating while the coating is setting up, leaving holes, or pores, in the film. This can be avoided by preheating the component 50-70° above the cure temperature, and then applying the two coats and curing at a normal cure temperature. For example, preheat at 390-400°F then gel and cure at 340-350°F (the gel step is an intermediate partial cure in the oven performed between the application of the first and second coats). The procedure was developed and refined during the trial application on the USS Elliot (DD 967) and USS

Barbey (FF 1088). The step by step procedure has been forwarded to NAVSEA for official dissemination to other SIMA's. The MSC applied to both of these ships was WSA.

Currently the Navy only approves the use of epoxy OPC for corrosion control. A performance specification has been drafted, but not finalized. SIMA shops are permitted to purchase standard stock powders from commercial vendors, so long as the color is similar to the Navy requirements, and the powder meets some basic physical requirements on hardness, salt spray resistance, impact strength and thickness capability. Most manufacturers will not produce custom colored powders until an official specification is finalized. However, two manufacturers have produced color materials for the Navy standards in haze gray, white, black, yellow, red and a few other colors. Due to the exact color match requirements not in effect until the specification is finalized, the current color matched powders are often overlooked for cheaper approximate matches.

3.3 Other Coating Process Evaluation

Another organic powder coating process is that for flame sprayed epoxy. Flame sprayed thermoplastics, such as nylon, have been utilized in specialized applications, but flame sprayed thermosetting resins are part of a new technology.. One of the driving forces for NAVSEA to look more seriously at powder fed flame spray systems for corrosion control was the idea of using the same spray unit to apply both aluminum and the organic topcoat. NAVSEA requested the powder gun manufacturers (METCO, EUTECTIC and UTP) to provide a system which could apply both the aluminum and epoxy resin, without changing guns or nozzels. A simple one-step control for changing from the aluminum to the epoxy hopper was desired.

The project has required modification of the spray systems, and research on the epoxy resin materials. At this point the application process is very slow. For example, to utilize the same gun and nozzle for both coatings required a compromise due to the coating materials having different thermal properties. One system that could do both has to utilize a nozzle that has to operate around 4 lbs/hr. The powder sprayed aluminum process, with a more efficient nozzle can spray at 15 lbs/hr, allowing more surface to be coated. The electrostatic powder spray guns currently in use at SIMA for applying OPC's have output capacities of 28 lbs/hr.

The cost effectiveness of flame sprayed epoxy is questionable at this time. It may have application in new construction for preparing equipment foundations. However, it does not appear as a viable alternative to the electrostatic sprayed OPC with oven curing in a Corrosion Control Shop.

4. EVALUATED SERVICE LIFE OF MSC COATED WITH OPC

Of the two ships chosen for a detailed service test of the MSC coated with OPC, only one, the USS Barbey (FF 1088) has been evaluated. The USS Elliot (DD 967) was still in the shipyard completing its overhaul at the writing of this report. The USS Barbey underwent a six month review on 24 August 1988. The scheduled 12 month review could not be accomplished due to the ship being deployed.

Components were evaluated according to the following condition definitions:

EXCELLENT	No failures, or failures are negligible.
GOOD	Failures in isolated spots, slight failures thinly distributed.
FAIR	Failures concentrated in definite patches (over one square foot): Slight failure distributed.
POOR	Failures covering most of area.

These conditions are based on "failures" that lead to Ship's Force having to perform maintenance. In many cases, very negligible degradation may have occurred to the actual substrate, but the coating has problems that will make its visual appearance unacceptable.

Twenty-five components, coated with OPC over MSC, were surveyed on the USS Barbey on 24 August 1988. Three of those items (stanchions) were already painted over by Ships Force because of the bad color match. Twelve items were considered in excellent condition with no discoloration. These twelve items were typically stowed inside, or had sides that faced interior areas. Six of those same components had surfaces which faced the exterior, and these were rated as good, with discoloration. The remaining five components were considered in fair condition, primarily due to pinholing.

Yellowing was the primary type of discoloration observed on components receiving exposure to the sun. This is a common problem with epoxies. It is anticipated that chalking will be present on the next survey.

Protection of the MSC from corrosion was accomplished by the OPC. No problems with blistering or peeling of properly applied coating were noted.

SIMA (SD) is in the process of requesting authorization from NAVSEA to perform a service test with a more sun resistant OPC. The most common type recommended by powder manufacturers for the Navy's exterior applications is a Triglycedial Isocyanurate (TGIC) polyester. The service test would be performed on a ship, with half of its doors being coated with epoxy and the other half with TGIC polyester, after application of the MSC. Periodic six month surveys will then be accomplished to monitor the coating's relative performance.

5. SUMMARY

The SIMA (SD) Corrosion Control shop has initiated the implementation of powdered aluminum MSC and the utilization of OPC as a sealer, barrier and topcoat over the MSC for naval corrosion control purposes. The adhesion of flame-powder MSC on large components needs to be investigated, to assure that coating quality is not being sacrificed in lieu of the more rapid application speed. The flame-powder MSC gun has been easier to maintain, and the aluminum powder of similar cost to the wire. Early results from the service test of MSC coated with OPC indicate that corrosion protection is being satisfactorly provided. Additional tests are under development to further reduce Ship's Force maintenance manhours with sunlight resistant OPC's.

REFERENCES

1. NAVSEA S9630-AM-MAN-010/LST1179, Corrosion-Control Manual for LST-1179 Class, Jan 1985.

2. DOD-STD-2138(SH), Metal Sprayed Coating Systems for Corrosion Protection Aboard Naval Ships, 23 Nov 1981.

3. Kullerd, S., P. Schlunt and R. Sulit, "SHORE INTERMEDIATE MAINTENANCE ACTIVITY CORROSION CONTROL SHOP", NACE Conferance Paper 603, 1989.

4. Sulit, R., S. Kullerd and F. West, "Wire-Sprayed Aluminum Coating Services in a SIMA Corrosion Control Shop, Proceedings of the National Thermal Spray Conference, Orlando, FL, 14-17 September 1987.

5. "Thermal Spraying: Practice, Theory, and Application", American Welding Society, 1985.

6. Adkins, W., S. Kullerd, C. McPherson, M. Miller, O. O'Brien, M. Robinson, P. Schlunt, and R. Sulit, "Corrosion-Control Program: SIMA Pilot CC-Shop Service Test and Technical Support," ISA (WC)-ITR-107, 30 Nov 85. Contract N66001-85-C-0350 (1985).

DETERIORATION CONTROL/LIFE PREDICTION OF POLYMERIC MATERIALS

Dr. Robert E. Sacher
Material Durability Branch (SLCMT-TMM)
US Army Material Technology Laboratories
Watertown, MA 02172-0001

ABSTRACT

Polymeric materials must be exposed in natural environmental and realistic accelerated aging conditions to simulate field conditions. The materials also must be well characterized before and after exposure to provide the Army with a database for the design and appropriate implementation in current and next generation systems. Lack of materials durability knowledge and polymeric materials, especially structural composites, in Army systems and has had a significant impact on materials costs, design, and perceived reliability. Studies involving long term exposure at environmental test sites (up to 16 years) and accelerated testing will be presented for composite materials and coatings. Test sites include Panama Everglade test site in Florida, Desert Sunshine (hot/dry), Maynard, MA (temperature), Alaska and various accelerated atmoshpere such as EMMAQUA, EMMA and the Weatherometer. Chemical, physical and mechanical data will be used to illustrate the various correlations between the natural and exposed environmental test sites. In fact a life prediction strategy using an acceleration factor of 10 will be discussed and recommended for the deterioration control/life prediction of composite materials used in Army systems.

[Manuscript Not Available at the Time of Printing]

EVALUATION of COMPOSITE AVIONIC CONNECTORS

M. Marchese, B. Dobbs, E. White and G. Slenski
Materials Integrity Branch
Systems Support Division
Wright Aeronautical Laboratories
Wright-Patterson Air Force Base, Ohio

ABSTRACT

Composite connectors were placed in a salt spray test according to ASTM-B117. This was done to determine if these special metallized plastic connectors are resistant to corrosion. Surface and insulation resistance measurements were periodically made during the 500 hour test. All the connectors functioned within specification with no evidence of corrosion. The composite connector should provide adequate corrosion resistance in most field applications.

INTRODUCTION

Electrical connectors are an inportant part of the packaging when used in avionic application. This results from the multiple requirements placed upon the connector; lightweight, corrosion resistant, tough, and reliable. The composite connector (metallized plastic in the simplest case) fulfills these requirements very well. The requirement that the connector be corrosion resistant results from the moisture condensation that collects on the connectors when aircraft descend from the cold high altitudes into moist, warm, tropical environments. A test of corrosion resistance was given to three metallized plastic Deutsch connectors. A description of the test and the results are provided in the following article.

CORROSION TESTING

Three Deutsch connectors were placed in a panel. Two of the connectors were opened to show the interiors. The connector sizes were 12, 16, and 20 gauge wire, respectively. The connector shells were a metallized plastic. The characteristic X-Ray analysis of the metal in the scanning electron microscope (SEM) showed that tin was a principle constituent.

Three wires were connected to each side of the connectors so that electrical continuity through the pins could be measured. One

was connected to the middle pin, and one wire was connected to the lower middle pin. The resistance of each of these three circuits through the connector and out the opposited side of the connector was measured. The resistance from each of the three pins to the connector shell was measured and the resistance from the front to the back of the connector shell was also measured. For each connector, seven resistance measurements were made. The test procedure used was MIL-STD--1344A, Method 3004.1.

A salt spray chamber was adjusted to meet ASTM-B117 and the connectors were placed in it for 500 hours. During the test, the connectors and wires were laid out horizontally and resistance measurements were made at 24, 48, 120, 192, 384 and 500 hours. The insulation resistance measurements from the connector pins to the connector shell were made at the 100 volt bias. The pin-to-pin measurements were made at a constant voltage of 20 millivolts.

TEST RESULTS

The three deutsch connectors before testing are shown in Figure 1. Figure 2 shows two of the connectors thath were opened before testing. Figures 3 and 4 show the opened connectors after salt spray testing.

The initial and final reisistance measurements are given in Table I. The reisistance measurements at the other times did not deviate substantially from these values.

All connectors functioned within specifications after the 500 hours salt spray test and no corrosion was evident on either the connector shells or the connector pins.

CONCLUSIONS

The metallized plastic Deutsch connectors successfully passed the corosion resistance salt spray test. We believe thath these connectors will function well in field application of avionic equipment.

TABLE 1: DEUTSCH CONNECTORS 500 HOUR SALT SPRAY TEST RESULTS

	Initial Resistance (ohm)	Final Resistance (ohm)
12 Gauge Wire Connector		
Outer Tip Pin	1.2×10^{-3}	1.2×10^{-3}
Center Pin	1.3×10^{-3}	1.1×10^{-3}
Lower Middle Pin	1.2×10^{-3}	1.0×10^{-3}
Outer TopPin to Shell	1×10^{13}	1×10^{7}
Center Pin to Shell	8×10^{12}	1×10^{7}
Lower Middle Pin to Shell	1.5×10^{13}	1.5×10^{7}
Connector Shell-to-Shell	9.8×10^{-3}	20.8×10^{-3}
16 Gauge Wire Connector		
Outer Tip Pin	2.6×10^{-3}	2.9×10^{-3}
Center Pin	2.5×10^{-3}	2.4×10^{-3}
Lower Middle Pin	2.5×10^{-3}	2.4×10^{-3}
Outer Top Pin to Shell	2×10^{12}	8×10^{6}
Center Pin to Shell	4×10^{12}	8×10^{6}
Lower Middle Pin to Shell	3×10^{12}	8×10^{6}
Connector Shell-to-Shell	9.4×10^{-3}	8.7×10^{-3}
20 Gauge Wire Connector		
Outer Top Pin	4.8×10^{-3}	7.9×10^{-3}
Center Pin	5.1×10^{-3}	5.0×10^{-3}
Lower Middle Pin	4.9×10^{-3}	4.7×10^{-3}
Outer Top Pin to Shell	5×10^{12}	1×10^{8}
Center Pin to Shell	2×10^{12}	1×10^{8}
Lower Middle Pin to Shell	3×10^{12}	1.5×10^{8}
Connector Shell-to-Shell	8.6×10^{-3}	19.6×10^{-3}

FIGURE 1 - 12, 16 and 20 gauge wire Deutsch connectors, as received, installed in a panel before the 500 hour salt spray test.

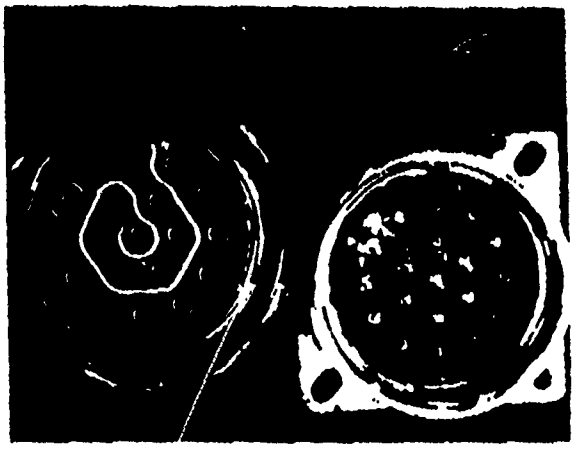

FIGURE 3 - Open connector after salt spray test.

FIGURE 2 - Open connector before salt spray test.

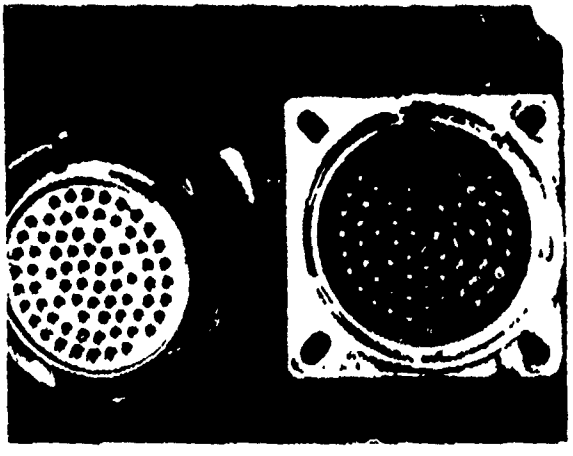

FIGURE 4 - Open connector after salt spray test.

CORROSION PROPERTIES OF HIGH STRENGTH LOW ALLOY STEELS FOR SHIP STRUCTURAL APPLICATIONS

Denise M. Aylor
David Taylor Research Center
Bethesda, MD 20084

ABSTRACT

Corrosion properties of HSLA-80 and HSLA-100 were compared to high tensile steel (HTS) and HY80. Overall, the test results indicated similar corrosion behavior for all steels. The steels exhibited uniform corrosion in seawater immersion, tidal zone, and marine atmospheric environments. The crevice corrosion resistance of these steels was excellent after 9-12 months' seawater exposure. High velocity corrosion testing (parallel flow and cavitation) identified a similar degree of corrosion attack on HSLA-80, HSLA-100, and HY80 at seawater velocities up to and including 80 ft/s. HSLA-80 exhibited a slightly higher corrosion rate than the other steels at 100 ft/s, presumably due to a lower total nickel content for HSLA-80 which limited its ability to form a protective film. Jet impingement resistance was excellent for all steels.

INTRODUCTION

The utilization of higher yield strength (HY) steels for ship construction has always been of interest to the U.S. Navy. HY steels have been extensively used in the Navy due to their high strength and toughness properties (1,2). However, these martensitic steels require strict fabrication controls to guarantee quality welds that are free of cracking. These stringent requirements result in high fabrication costs (2). High strength, low alloy (HSLA) steels were developed with the goal of increased weldability (thus reduced fabrication costs), along with high strength and toughness properties similar or better than the HY steels. The HSLA steels are currently replacing HY steels as well as high tensile steel (HTS), where the higher strength HSLA steels allow significant weight savings due to the reduced cross sections required (3).

Effective utilization of the HSLA steels requires corrosion properties that are at least comparable to the currently used steels. The objective of this paper is to examine the marine corrosion behavior of the HSLA steels (specifically HSLA-80 and -100) and to compare their properties to HY80 and HTS. The corrosion rates quantified by the tests reported in this paper are not directly applicable to seawater

applications since steels are never exposed unprotected. Alloy steels must be protected by coatings and cathodic protection to provide the necessary long life corrosion resistance.

MATERIALS AND METHODS

The chemical compositions of each of the steels evaluated are included in Table 1. Each of the corrosion tests performed is briefly described below. All testing was done at the LaQue Center for Corrosion Technology (LCCT) in Wrightsville Beach, North Carolina.

General Corrosion

General corrosion specimens (24 in^2 (155 cm^2) size) of HTS, HY80, HSLA-80, and HSLA-100 were exposed in the following environments: (1) full immersion in natural seawater flowing at 1.6 ft/s (0.5 m/s), (2) alternate tidal immersion, where specimens are alternately wetted and dried with fluctuations in the tide, and (3) marine atmospheric exposure, 25m from the ocean and angled 30^o from horizontal facing the ocean. Duplicate panels were exposed for 9-12 months.

Crevice Corrosion

Crevice corrosion specimens consisted of a 36 in^2 (232 cm^2) panel with two 1 in^2 (6 cm^2) crevice washers of the same material as the panel. Duplicate specimens of HSLA-80, HSLA-100, HTS, and HY80 were exposed in 1.6 ft/s (0.5 m/s) flowing seawater for 9-12 months. Holes were drilled in the center of each panel and the washers. The steel washers were bolted to opposite sides of each panel with Teflon washers and a metal rod containing a Teflon sleeve.

High Velocity Corrosion

High velocity corrosion testing was performed on HSLA-80, HSLA-100, and HY80 specimens. Parallel flow, cavitation, and jet impingement testing was done to characterize the steels in a variety of high velocity test conditions under varying seawater flow rates.

The parallel flow test utilized a nylon nozzle, into which the specimens (0.75 x 3.5 x 0.125 in. (1.9 x 8.9 x 0.3 cm)) were inserted and oriented parallel to the seawater flow. Nonmetallic spacers were positioned within the nozzle to allow establishment of the seawater flow and to prevent excessive corrosion at the leading and trailing edges of the specimens. Duplicate specimens of each steel were run for 30 days at velocities ranging from 5-100 ft/s (1.5-30 m/s).

Cavitation testing was performed for 30 days on duplicate specimens at seawater flow velocities of 50-100 ft/s (15-30 m/s). The cavitation specimens were identical to the parallel flow specimens except for the hole drilled in one end of each specimen. The hole created a seawater flow disturbance, causing cavitation downstream. The cavitation erosion

damage to the specimen downstream of the hole was the primary measure in the test.

Jet impingement specimens were positioned vertically in a holder located at a fixed distance from a seawater jet nozzle. The holder was completely immersed in seawater and a constant impingement velocity was maintained throughout the test (4). Tests were run on 3-4 specimens/material (each 0.5 x 3.5 x 0.25 in. (1.3 x 8.9 x 0.6 cm)) for 30 and 60 days at seawater velocities of 5-50 ft/s (1.5-15 m/s).

RESULTS AND DISCUSSION

General and Crevice Corrosion

General corrosion results for the steels are included in Table 2. The scatter seen in the corrosion data is common, with a scatter range of approximately 3 mils per year (mpy) typical for low-alloy steels (5). All of the steels generally displayed similar corrosion rates in each environment, with specimens in the 25m atmospheric environment showing significantly less severe corrosion than in the other two environments. All panels exhibited uniform corrosion after the exposure.

Crevice corrosion results are compiled in Table 3. No crevice attack was noted between the washers and the panel for any of the steels evaluated. The corrosion rates reported in Table 3 give an indication of the general corrosion behavior of the panels due to the absence of any crevice corrosion. These rates were calculated based on the boldly exposed surface areas, excluding the unaffected crevice area. The corrosion rates are comparable to the general corrosion rates reported above.

High Velocity Corrosion

The parallel flow, cavitation, and jet impingement data reported here contain a large degree of data scatter. This degree of scatter is common in high velocity testing, predominantly due to flow and cavitation instabilities in the test apparatus as well as specimen vibration during exposure and seawater temperature fluctuations related to moving large volumes of water at high speeds.

The parallel flow and cavitation data are plotted in terms of corrosion rate and maximum depth of attack versus seawater flow velocity in Figures 1-4. The maximum depths of attack reported are due to corrosion on the bold surface of each specimen. The depth of attack measurements represent the deepest pit depth on each specimen and are reflective of local metallurgical defects in the specimens or more likely, local flow-turbulence extremes caused by the test apparatus. Corrosion due to edge attack under the specimen holder also occurred during the parallel flow and cavitation testing. This edge attack is presumably caused by specimen movement within the holder with consequent removal of any protective films/corrosion products formed, and is not an indication of

the erosion resistance of the material. The corrosion due to attack at the edges is not reported separately here but is incorporated into the overall corrosion rates plotted, as they are determined from mass loss measurements.

The parallel flow data is included in Figures 1 and 2. In general, the corrosion rates increased with flow velocity. The extent of data scatter in both the corrosion rate and depth of attack data reported is typical, as stated above. The corrosion rates were similar among the steels at each velocity up to and including 80 ft/s (24 m/s). Slightly higher corrosion rates were exhibited by HSLA-80 at 100 ft/s, but the maximum depth of attack measurements at this velocity (and at 50, 65, and 80 ft/s (15, 20, and 24 m/s)) were similar. The higher corrosion rate reported at 100 ft/s (30 m/s) is likely due to the lower total nickel content of this steel compared to the other steels, which reduces the formation of protective films.

Corrosion rate and maximum depth of attack data for the cavitation tests is plotted in Figures 3 and 4. The type of corrosion attack on these specimens resembled the attack on the parallel flow specimens. No increased corrosion was evident on the cavitation specimens directly downstream of the hole. The cavitation corrosion rates were similar for all of the steels tested except at 100 ft/s (30 m/s). Again, the HSLA-80 exhibited higher corrosion rates at 100 ft/s (30 m/s), and the maximum depths of attack at this velocity (and at 80 ft/s (24 m/s)) were also slightly higher.

Jet impingement results are compiled in Table 4. No measurable depth of attack was reported at the impingement site for any of the three steels, although some staining was observed in the impingement area for HSLA-80 and HY80 in the 15 and 30 ft/s (5 and 9 m/s) tests. Although no depth of attack was measured in the impingement area for any of the specimens, general corrosion did occur outside the area of impingement. The corrosion rates listed in Table 4 document the extent of general corrosion between the three steels at varying flow rates. For the HSLA-80 and HY80 steels, the corrosion rates generally increased with flow velocity. The corrosion rates reported for HSLA-100 were significantly higher than the other steels in the 5-30 ft/s (1.5-9 m/s) range. This difference in corrosion rates can be attributed to variations in the oxygen content of the seawater. The 5-30 ft/s (1.5-9 m/s) impingement tests run on HSLA-100 were all conducted during the winter months when the oxygen content is typically higher (average of 9 ppm in the winter versus 6 ppm in the summer). The higher oxygen content promotes an increased corrosion rate. All other jet impingement tests were run in the spring/summer months when the oxygen content was lower.

In summary, all three steels exhibited excellent impingement corrosion resistance. The increased general corrosion rates found for the

HSLA-100 in comparison to HY80 and HSLA-80 were not a result of reduced impingement resistance, but can be attributed to differences in the oxygen content of the seawater during the test runs.

SUMMARY

The objective of this paper was to compare the marine corrosion properties of HSLA steels with the conventionally used HY and high tensile steels. The results have shown that overall, the corrosion properties of HSLA-80 and HSLA-100 are similar to HY80 and HTS. No adverse corrosion problems are anticipated by replacing the HY steels and HTS with HSLA-80 or -100. However, all alloy steels in seawater applications must be protected by coatings and cathodic protection for adequate corrosion resistance.

Specific test results showed that all of the steels evaluated (HSLA-80, HSLA-100, HY80, and HTS) exhibited uniform, general corrosion, averaging 5-7 mpy in seawater and tidal immersion environments and 1-2 mpy in the marine atmosphere. The crevice corrosion behavior of all of the steels was excellent, with no crevice attack found after 9-12 months' exposure in natural seawater. The high velocity corrosion tests identified increasing corrosion rates with increasing flow velocity for HSLA-80, HSLA-100, and HY80. In particular, the parallel flow and cavitation data showed a similar degree of corrosion attack for all steels up to 80 ft/s (24 m/s) flow velocity. Marginally higher corrosion rates were reported for HSLA-80 at 100 ft/s (30 m/s) in these tests, which was attributed to the lower total nickel content of HSLA-80 that limited its protective film forming capability. Jet impingement resistance was excellent for all three steels evaluated.

REFERENCES

1. Heller, S.R., Fioriti, I., and Vasta, J., "An Evaluation of HY80 Steel as a Structural Material for Submarines," Naval Engineers Journal, pp. 29-44 (1965).

2. Heller, S.R., Fioriti, I., and Vasta, J., "An Evaluation of HY80 Steel as a Structural Material for Submarines," Naval Engineers Journal, pp. 193-200 (1965).

3. Montemarano, T.W., et al., "High Strength Low Alloy Steels in Naval Construction," Journal of Ship Production, Vol. 2, No. 3, pp. 145-162 (1986).

4. Ferrara, R.J. and J.P. Gudas, "Corrosion Behavior of Copper-Base Alloys with Respect to Seawater Velocity," NACE Corrosion '74, Chicago, Illinois (1974).

5. Boyd, W.K. and F.W. Fink, Corrosion of Metals in Marine Environments. Metals and Ceramics Information Center, Columbus, Ohio, pp. 17-23 (1978).

TABLE 1 - CHEMICAL COMPOSITIONS OF MATERIALS

MATERIAL	THICKNESS (INCH)	SPEC. CODE	COMPOSITION (%) C	Mn	P	S	Si	Mo	Cb	V	Ni	Cr	Cu	Al
HSLA-80	0.1875	GAB	0.04	0.58	0.01	0.004	0.28	0.21	0.042	---	---	1.18	---	---
	0.625	FZZ	0.06	0.48	<0.002	0.004	0.36	0.23	---	---	0.94	0.72	1.30	0.03
	1.25	FUQ	0.05	0.59	0.009	---	0.26	0.189	0.048	---	0.88	0.65	1.20	0.030
HSLA-100	0.25	GJY	0.04	0.90	0.006	0.003	0.25	0.60	0.025	---	3.50	0.60	1.60	0.030
HY-80	0.263	FNR	0.15	0.23	0.012	0.02	0.27	0.47	---	<0.001	2.83	1.61	0.046	---
HTS	1.25	GAK	0.16	1.2	---	---	0.2	---	---	0.2	---	---	---	---

Table 2

General Corrosion Results

Material	Code	Exposure Location	Average Corrosion Rate (mpy)
HSLA-80 (12 month exposure)	FZZ	Seawater Immersion	5
		Tidal Zone	6
		25m Atmospheric Lot	2
	FUQ	Seawater Immersion	6
		Tidal Zone	7
		25m Atmospheric Lot	2
HSLA-100 (9 month exposure)	GJY	Seawater Immersion	7
		Tidal Zone	5
		25m Atmospheric Lot	2
HY-80 (12 month exposure)	FNR	Seawater Immersion	5
		Tidal Zone	4
		25m Atmospheric Lot	1
HTS (12 month exposure)	GAK	Seawater Immersion	6
		Tidal Zone	8
		25m Atmospheric Lot	2

Table 3

Results of Crevice Corrosion Testing in 1.6 ft/s (0.5 m/s) Flowing Seawater

Material	Average Corrosion Rate (mpy)	Comments
HSLA-80 Panel	8	No crevice attack
Washer	10	between washer and
(12 month exposure)		panel
HSLA-100 Panel	8	No crevice attack
Washer	9	between washer and
(9 month exposure)		panel
HY80 Panel	6	No crevice attack
Washer	6	between washer and
(12 month exposure)		panel
HTS Panel	7	No crevice attack
Washer	7	between washer and
(12 month exposure)		panel

Table 4

Results of 30- and 60-Day Jet Impingement Tests in Filtered Natural Seawater

Material	Velocity ft/s(m/s)	Corrosion Rate (mpy) 30 Days	60 Days	Maximum Depth of Attack (mils) 30 Days	60 Days
HSLA-80	5(1.5)	7	6	No measurable attack at impingement site	
	8(2)	6	6		
	15(5)	9	10	Staining	Staining
	30(9)	11	11	Staining	Staining
	50(15)	16	--	No measurable attack at impingement site	
HSLA-100	5(1.5)	20	15	No measurable attack at impingement site	
	10(3)	19	15		
	15(5)	20	16		
	30(9)	17	13		
	50(15)	21	--		
HY80	5(1.5)	6	6	No measurable attack at impingement site	
	8(2)	6	6		
	15(5)	10	10	Staining	Staining
	30(9)	12	10	Staining	Staining
	50(15)	18	--	No measurable attack at impingement site	

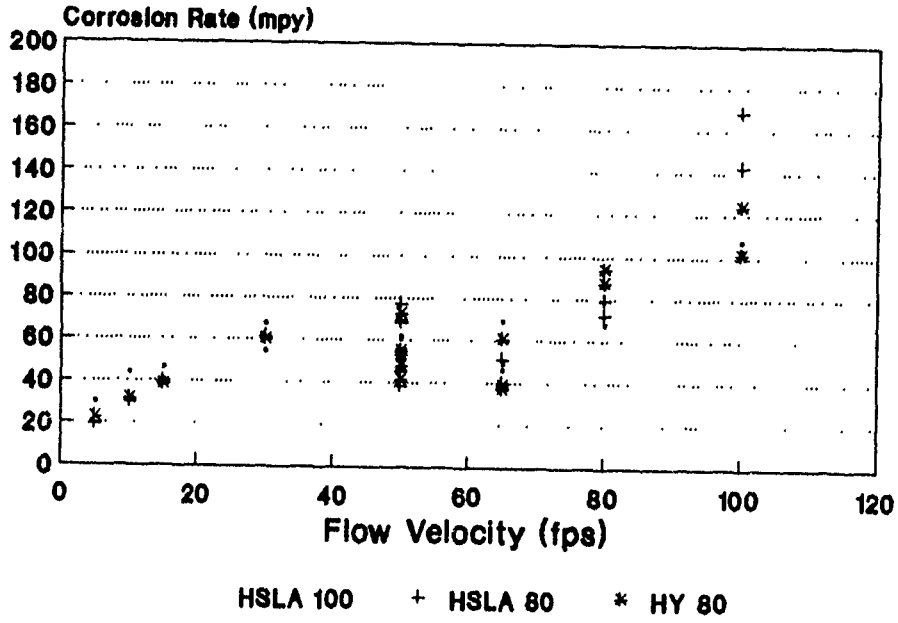

Figure 1 - Parallel Flow Corrosion Rate Test Results

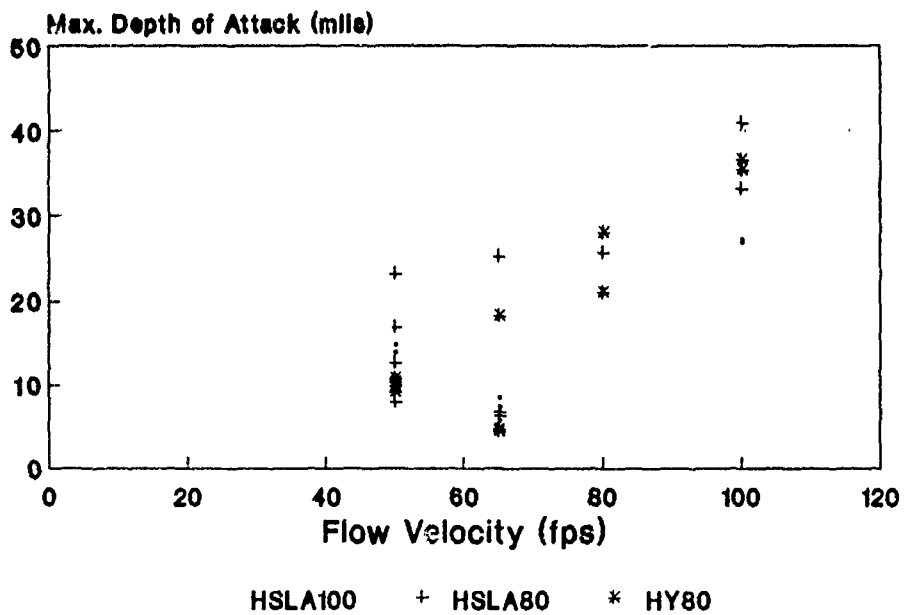

Figure 2 - Parallel Flow Maximum Depth of Attack (Bold Surface Data)

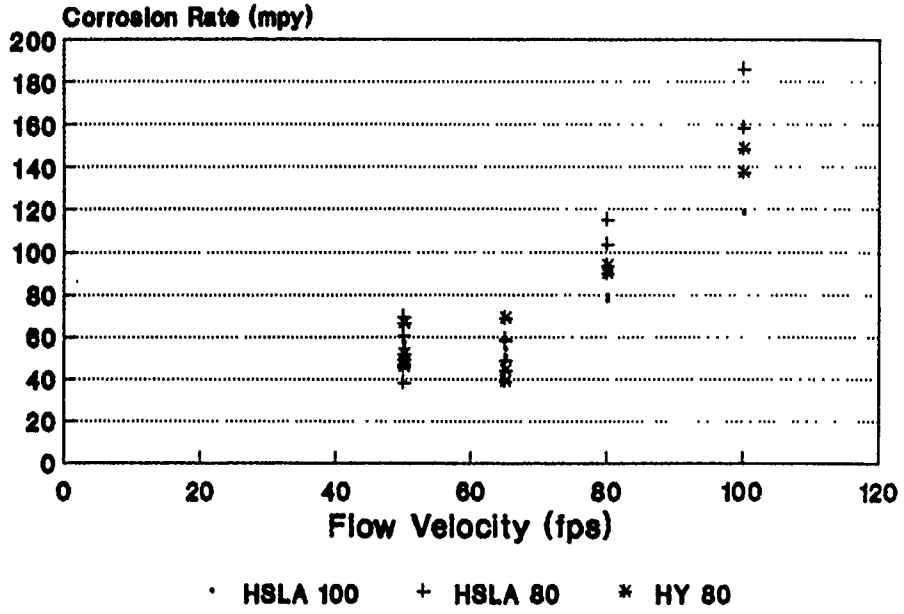

Figure 3 - Cavitation Corrosion Rate Test Results

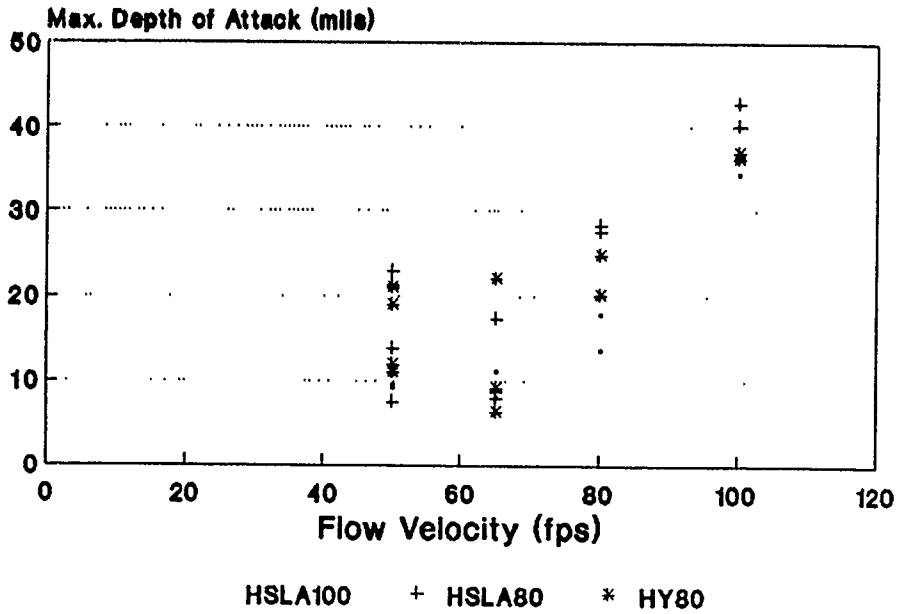

Figure 4 - Cavitation Maximum Depth of Attack (Bold Surface) Data

CORROSION CHARACTERIZATION OF DEPLETED URANIUM-2% MOLYBDENUM PENETRATORS IN SYNTHETIC SEAWATER

K. L. Vasanth and C. M. Dacres

Naval Surface Warfare Center
Materials Division
Electrochemistry Branch
10901 New Hampshire Avenue
Silver Spring, MD 20903-5000

The corrosion behavior of depleted uranium-2% molybdenum alloy penetrators and their assemblies with nylon sabots were studied in synthetic seawater for eight months at 50°, 60° and 70°C. The results indicate that the nylon sabots can prevent corrosion of the bare depleted uranium (DU) alloy in salt water environment provided that the temperature does not exceed 50°C. At higher temperatures, cracking of the nylon sabots and severe corrosion of the depleted uranium-2% molybdenum alloy penetrators were observed. Exposure of the bare DU alloy and their assemblies to 93% relative humidity at room temperature for nearly eight months did not cause any adverse effect.

INTRODUCTION

Depleted uranium and depleted uranium alloys are used for a variety of applications like aircraft counter weights, subatomic particle detectors for accelerators and radioactive waste shielding (1). Defense agencies are interested in depleted uranium alloys because of their high-density, low-cost, availability and their excellent ballistics capability. The tri-services (Army, Navy and Air Force) have at least one program in which a depleted uranium alloy is a candidate material for ballistic applications (2). The Navy currently uses depleted uranium alloy with 2 weight% Mo (DU-2 Mo) for manufacturing kinetic energy penetrators. Depleted uranium alloys are known to be susceptible to general corrosion and stress corrosion cracking (SCC), particularly at high humidity (95%) and high temperature (74°C). Trazaskoma (3) has documented a comparison of the corrosion and stress corrosion cracking resistance of two depleted uranium alloys: DU-0.75 Ti used by the Air Force and DU-2 Mo used by the Navy.

In an attempt to prevent the corrosion of DU alloys, metallic coatings of Ni and Ni-Zn on DU-2 Mo alloy were investigated by Crowe (4). A recent study (1) has shown that galvanizing DU-0.75 Ti and DU-6 Nb alloys with Zn provided corrosion protection which was in turn enhanced by treating coated zinc with chromate conversion coatings. Orman (5) and Orman and Walker (6) have reported that an organic coating of styrene-butadiene copolymer containing powdered aluminum can significantly reduce corrosion in humid air.

BACKGROUND

Unalloyed uranium suffers from poor corrosion resistance of the stable alpha phase, low hardness and yield strength, lack of dimensional stability and inability to be heat treated (7). Addition of Nb, Zr, Mo, or Ti tends to stabilize the body centered cubic (bcc) gamma phase, which permits heat treatment and results in increased corrosion resistance. A detailed investigation has been made of the corrosion behavior of binary alloys U-Mo and U-Ti, and the effects of the other alloying elements by M. Levy et al (7).

The objective of this investigation was to characterize the corrosion behavior of DU-2 Mo alloy penetrators (bare) and their assemblies with nylon sabots in synthetic seawater.

EXPERIMENTAL

The following types of samples were received from suppliers for corrosion studies: 1. DU-2 Mo with Mod.0 nylon jacket (#68-0), 2. DU-2 Mo with Mod.1 nylon jacket (#68-1) and 3. bare DU-2 Mo (#68). The specified chemical composition of the DU-2 Mo alloy is given in Table 1.

Table 1

ALLOWABLE CONCENTRATION RANGE OF ELEMENTS

Depleted Uranium	97.7% min. by weight
Molybdenum	1.8 to 2.2% by weight
Hydrogen	5 ppm max.
Nitrogen	80 ppm max.
Oxygen	75 ppm max.
Iron	50 ppm max.
Carbon	300 ppm max.
Total Impurities[1]	1000 ppm max.

1. Include hydrogen, nitrogen, oxygen, iron, carbon, titanium aluminum, silicon, phosphorus, nickel, copper, calcium, magnesium, sulphur and zirconium.

Laboratory Immersion Tests

The DU-2 Mo alloy samples and their assemblies with nylon sabots were weighed in the as received condition. A test matrix was developed to systematically investigate the corrosion behavior of DU-2 Mo alloy samples and their assemblies immersed in synthetic seawater (see Table 2). Each sample was immersed in a bottle containing 200 ml of synthetic seawater and maintained at 50°, 60°, and 70°C. These samples were monitored carefully and water loss due to evaporation was compensated by periodically adding distilled water. Samples in 70°C bath needed water replenishing every other day. The temperatures of the three baths were controlled thermostatically within ± 0.5°C.

Table 2

TEST MATRIX FOR DU-2 Mo ALLOY PENETRATORS AND THEIR ASSEMBLIES

	Immersion in Synthetic Seawater			93% R. H.*
Sample	50°C	60°C	70°C	
68-0	3	3	3	3
68-1	3	3	3	3
68 (Bare)	3	3	3	3

* R. H.= relative humidity.

The first set of samples were removed from the three temperature baths after 30 days immersion in synthetic seawater. Each sample was carefully rinsed with distilled water and cleaned in an ultrasonic cleaner for five minutes to remove loose corrosion products. These samples were later air dried and weighed. The second and third set of samples were removed and treated in a similar manner after 128 days and 224 days immersion, respectively.

Relative Humidity Test

A saturated aqueous solution in contact with an excess of a definite solid phase at a given temperature will maintain a constant humidity within any enclosed space (8). In the present investigation a saturated aqueous solution of $Na_2SO_4.10\ H_2O$ was used in contact with its solid phase to maintain 93% relative humidity in a closed container. The penetrator samples were kept on a porous plate just above this solution. The container with samples and sodium sulphate solution was main-

tained at ambient temperature. The loss of water due to evaporation was compensated by the addition of distilled water.

Surface Evaluation

Scanning electron micrographic examination (SEM) and energy dispersive X-ray spectrum analysis (EDAX) were performed on unexposed DU-2 Mo alloy. Stereomicroscopic pictures were taken for the unexposed alloy and for the samples removed from immersion test in synthetic seawater at 50°C, 60°C and 70°C. The results are discussed in the following sections.

RESULTS AND DISCUSSION

Weight loss/weight gain data obtained for DU-2 Mo alloy penetrators and their assemblies were used to compute corrosion rates. Figures 1 through 3 show plots of corrosion rate in mils per year (mpy) as a function of time in days for three different temperatures. Figure 4 shows the two types of penetrators, 68-0 and 68-1 with nylon assemblies and 68 bare DU-2 Mo alloy penetrators in the as received condition and before the immersion test. Samples 68-0 and 68-1 contain 68 bare DU-2 Mo alloy penetrators enclosed in a nylon jacket of modification Mod.0 and Mod.1, respectively.

After 30 days immersion in synthetic seawater at 70°C, only the bare DU-2 Mo alloy penetrators showed slight corrosion. A small amount of black corrosion product, possibly UO_2, was found on the bottom of the glass bottle. The penetrator assemblies removed from 50°C, 60°C and 70°C baths after 30 days immersion in synthetic seawater did not show any degradation. But, after 128 days immersion at 60°C and 70°C, the nylon assemblies showed cracks exposing the bare alloy to corrosion. The cracks were wider ($\gtrsim$3 mm) in the assemblies removed from 70°C bath compared to those taken out from 60°C bath. At each temperature, the corrosion rate for bare DU-2 Mo alloy was higher than that obtained for the penetrator with assemblies. In addition, it can be seen from the plots of corrosion rate versus immersion time (see Figures 1-3) that the corrosion rate for the bare alloy increased as a function of immersion time for each test temperature. The downward trend observed in the corrosion rate for the penetrator with assemblies can be attributed to the weight gain recorded as a result of trapping some of the corrosion products and traces of moisture within the cracked nylon assembly. The similar variation of these plots for the two types of assemblies with Mod.0 and Mod.1 sabot, show that these two designs or models of nylon sabots, perform in a similar manner in synthetic seawater environment.

The condition of the penetrator assemblies and the bare DU-2 Mo alloy penetrators after 224 days immersion test in synthetic seawater at 50°C, 60°C and 70°C are shown in Figure 5, respectively. The bare DU-2 Mo alloy penetrators corroded the most at each temperature as compared to the ones with assemblies. The penetrator removed from 70°C temperature bath showed cracks on the main body of the penetrator alloy and severe corrosion. The two types of penetrator assemblies with Mod.0 and Mod.1 sabot, showed increased cracking of the nylon sabots as a function of temperature. It appears that initially crevice corrosion occurred due to the interaction of seawater with bare DU-2 Mo alloy in the assemblies. The buildup of corrosion products between the DU-2 Mo and the nylon sabot created a force which was sufficient to initiate a crack in the sabot assembly. The cracking of the assembly exposed more DU-2 Mo to the environment and combined with the high temperature further increased the corrosion of the alloy. In fact, the assemblies from 70°C bath showed large cracks and significant shape distortion as well. In these cases, a small weight increase was recorded due to trapped corrosion products within the cracked nylon sabots.

The corrosion of uranium by humid air as well as by aqueous media can be represented by the following reactions:

$$U + 2H_2O \text{ -------> } UO_2 + 2H_2$$

$$2U + 3H_2 \text{ -------> } 2UH_3$$

$$2UH_3 + 4H_2O \text{ ----- -> } 2UO_2 + 7H_2$$

If excess moisture is present, UO_2 on the surface of uranium may react with moisture to form greenish-black foliations of the hydrate, $UO_2.2H_2O$. A higher oxide like U_3O_8 when present may react with water to form $U_3O_8.H_2O$ which is yellow (9). In the tests performed here black UO_2 was the predominant corrosion product. However, partial oxidation of this to U_3O_8 was observed in some cases by the yellow color that appeared on the surface of the bare penetrators and on the inner walls of the glass container in which the test was carried out.

The DU-2 Mo alloy penetrators and their assemblies exposed for eight months to 93% relative humidity at room temperature, appeared good. No signs of spalling or other forms of corrosion were observed. It should be noted that DU alloy with 2% Mo has been reported to form voluminous corrosion products after 103 days exposure to 74°C and 95% relative humidity (4).

Surface Evaluation Results

Figure 6 shows a SEM of the surface of the unexposed DU-2 Mo alloy. The surface appeared smooth with some light colored patches similar to the one shown in the center of the picture. These were identified by EDAX to be silicon inclusions. A typical EDAX spectrum of this alloy is given in Figure 7. It can be seen that this alloy contains small quantities of silicon, aluminum and molybdenum along with the major element, uranium.

Stereomicroscopic pictures were taken for the samples removed from immersion test in synthetic seawater maintained at 50°C, and 70°C. Figures 8 and 9 show how the bare alloy suffers from increased corrosion as the immersion time is increased from 128 to 224 days at 50°C. Figures 10 and 11 show the severity of corrosion that occurred at 70°C with increase in immersion time. Cracking of the nylon sabots and corrosion of the inner bare penetrator in the assembly are shown in Figure 10. In some cases, the surface showed circular areas around which corrosion was severe. This may possibly be due to local galvanic interactions between DU and the various inclusions. As observed from SEM photograph and the EDAX spectrum of DU-2 Mo alloy inclusions of Si, Al (see Figures 6 and 7) may be responsible for establishing local galvanic cells with DU.

SUMMARY

1. Bare DU-2 Mo alloy penetrators showed mild corrosion after 30 days immersion in synthetic seawater at 50°C. Even at this temperature, the rate of corrosion increased as a function of immersion time.

2. Temperatures higher than 50°C lead to severe corrosion and shape distortion of the bare alloy penetrator and their assemblies.

3. The penetrator assemblies with nylon sabots did not show any degradation after about six months immersion in synthetic seawater at 50°C. The nylon sabots cracked at higher temperatures exposing the bare alloy to corrosion. The cracking of the sabots resulted in shape distortion as well.

4. Both the bare DU-2 Mo alloy and their assemblies showed no signs of corrosion on exposure to 93% relative humidity at room temperature.

REFERENCES

1. J. L. Briggs., "The Corrosion Resistance of Zinc Coatings on Depleted Uranium and Uranium Alloys," RFP-3651 UC-25 Materials, DOE/TIC-4500 (Rev.73), Jan. 27, 1985.

2. S. G. Fishman and C. R. Crowe., "The Mechanism of Stress Corrosion Cracking in Close-in Weapon System Penetrators Exposed to Moist-air Environments," NSWC/DL TR-3363, Sept. 1975.

3. Patricia P. Trazaskoma., "A Comparison of the Corrosion and Stress Corrosion Resistance of Two Depleted Uranium Alloys: DU-0.75 Ti and DU-2 Mo," NRL Memorandum Report 4518, May 27, 1981.

4. C. R. Crowe, "Coating Evaluation For Atmospheric Corrosion Protection of Phalanx Rounds," NSWC/WOL TR 78-9, May 19, 1978.

5. S. Orman, Atom, No.150, 93, 1969.

6. S. Orman and P. Walter., J. Oil and Color Chemists Assoc., 48, 2336, 1965.

7. Milton Levy, Chester V. Zabielski and Gilbert N. Sklover., "Corrosion Behavior of Depleted Uranium-Ti and DU-Molybdenum Alloys," AMMRC TR 73-11, March 1973.

8. Hugh M. Spencer, "Laboratory Methods for Maintaining Constant Humidity," International Critical Tables of Numerical Data, Vol.I, 67, 1926.

9. W. D. Wilkinson, "Uranium Metallurgy," 815, 830, Interscience N. Y., 1962.

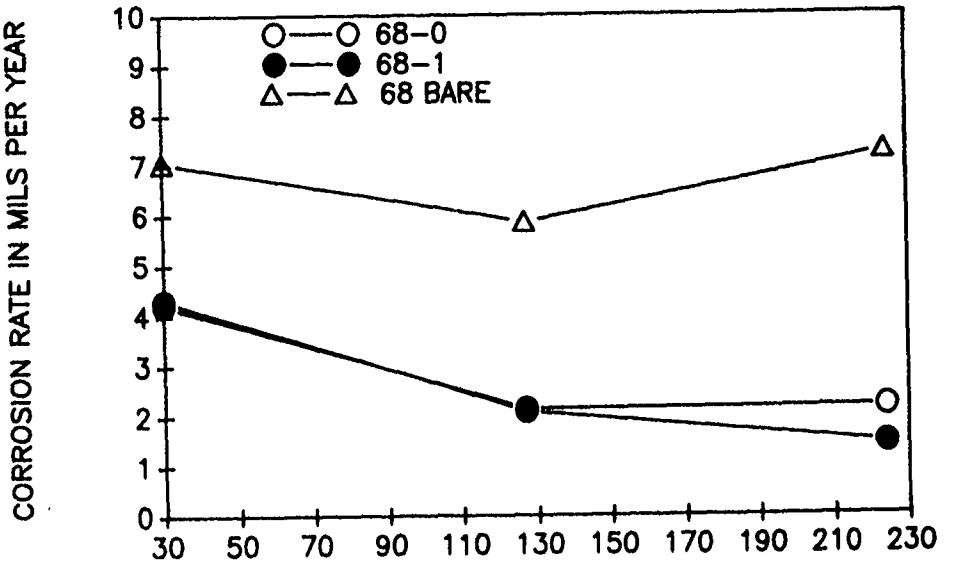

FIGURE 1. CORROSION RATE VS IMMERSION TIME FOR DU PENETRATORS AT 50 C.

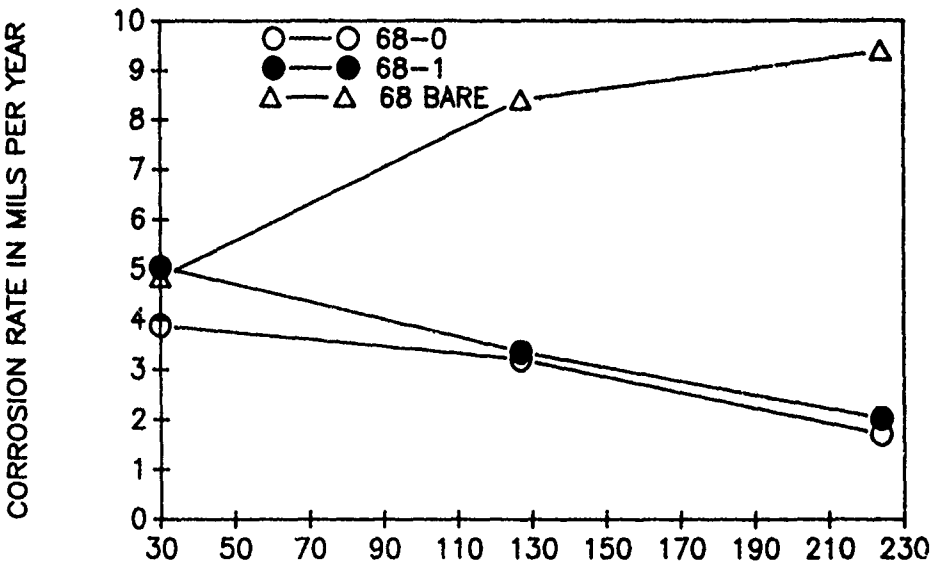

FIGURE 2. CORROSION RATE VS IMMERSION TIME FOR DU PENETRATORS AT 60 C.

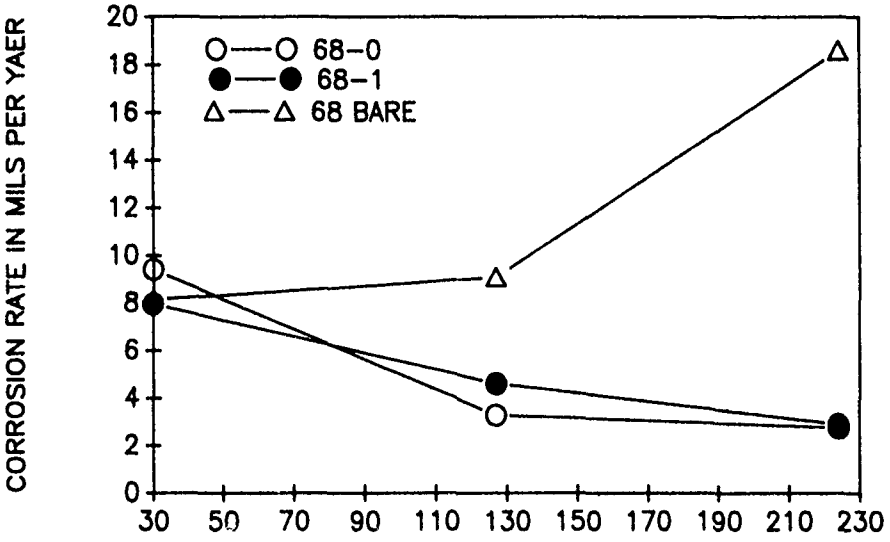

FIGURE 3. CORROSION RATE VS IMMERSION TIME FOR DU PENETRATORS AT 70 C.

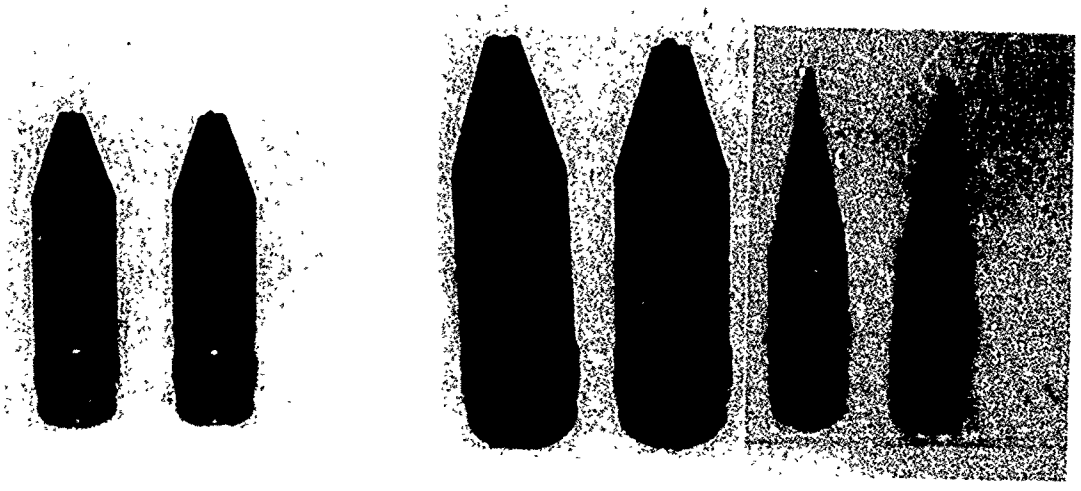

Figure 4. DU Penetrators and Assemblies before Corrosion Test.
a) 68-0 b) 68-1 and c) 68 Bare

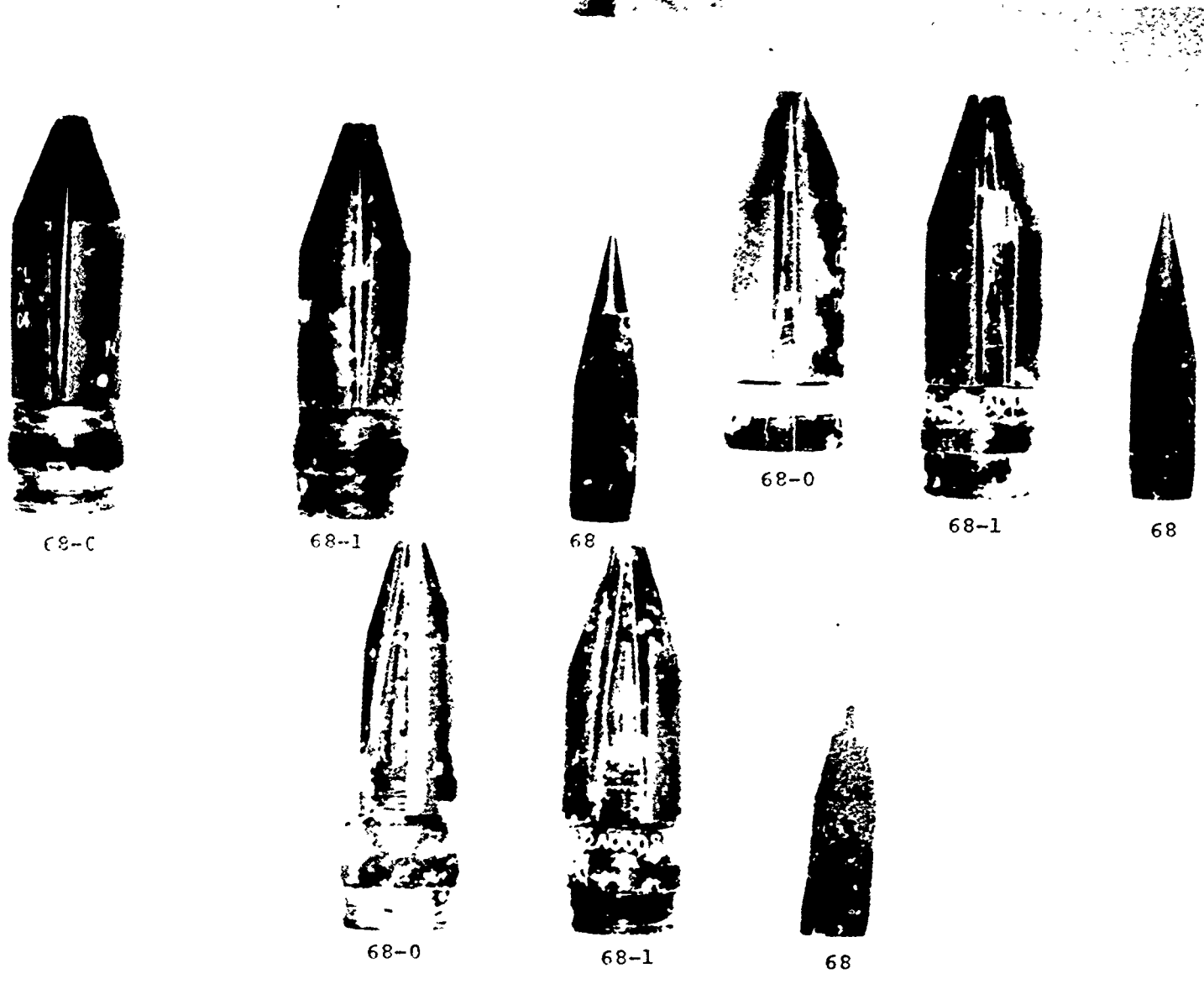

FIGURE 5. DU PENETRATORS AFTER IMMERSION IN SYNTHETIC SEA WATER FOR 224 DAYS AT 50°C, 60°C AND 70°C.

Figure 6. SEM of unexposed DU-2 Mo alloy.

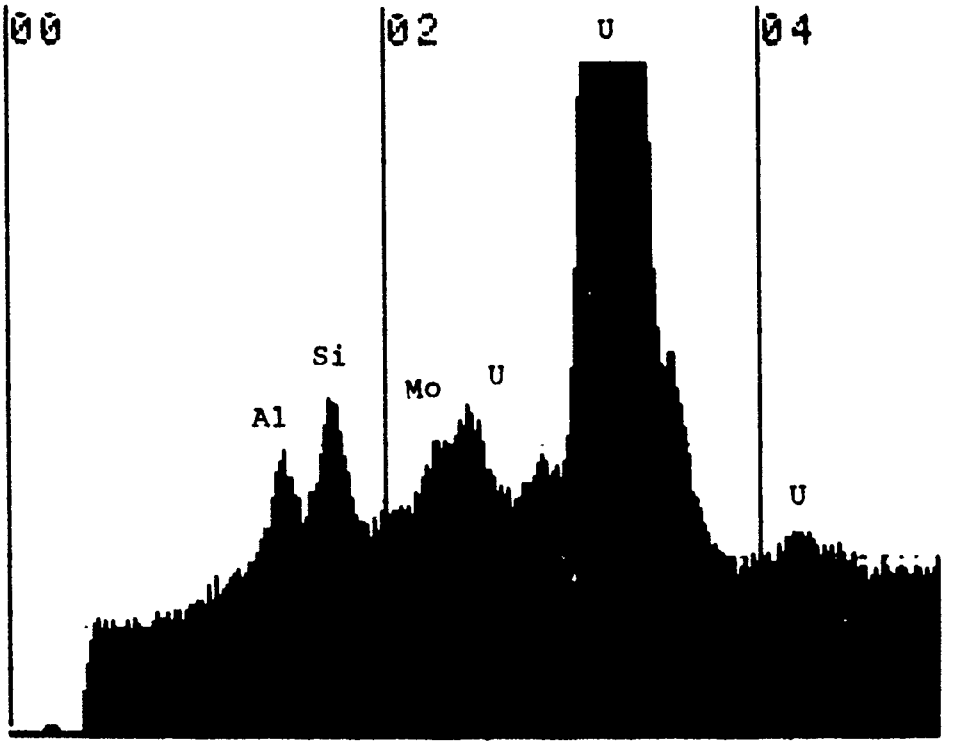

Figure 7. EDAX Spectrum of DU-2 Mo alloy.

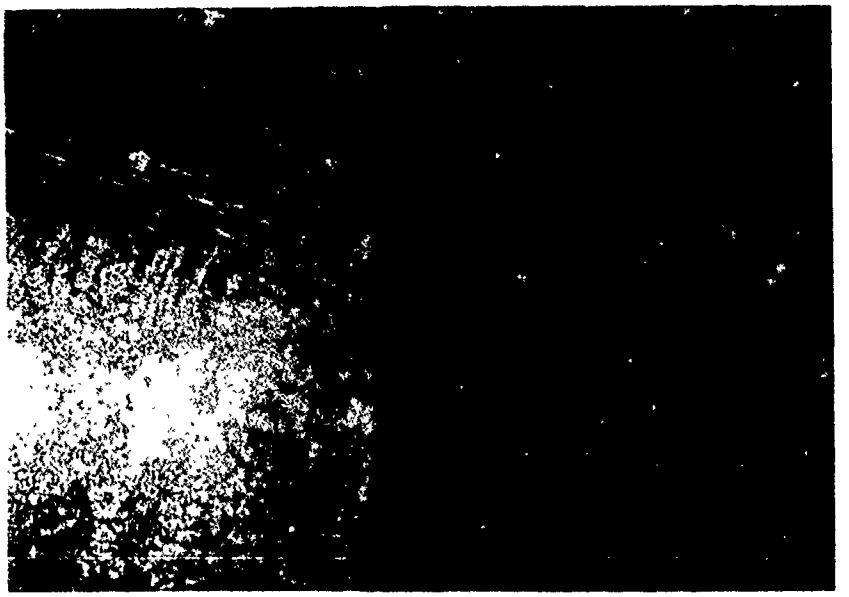

Figure 8. Surface of bare DU-2 Mo alloy after 128 days immersion in synthetic sea water at 50 C.(40X)

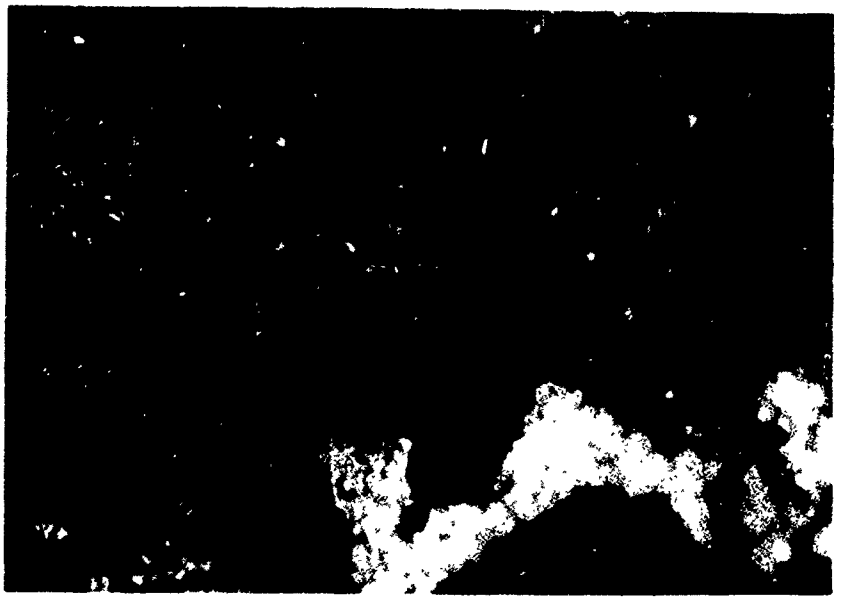

Figure 9. Surface of bare DU-2 Mo alloy after 224 days immersion in synthetic sea water at 50 C. (40X)

Figure 10. Cracking of nylon sabot and corrosion of DU alloy in the assembly after 128 days immersion in synthetic sea water at 70 C. (40X)

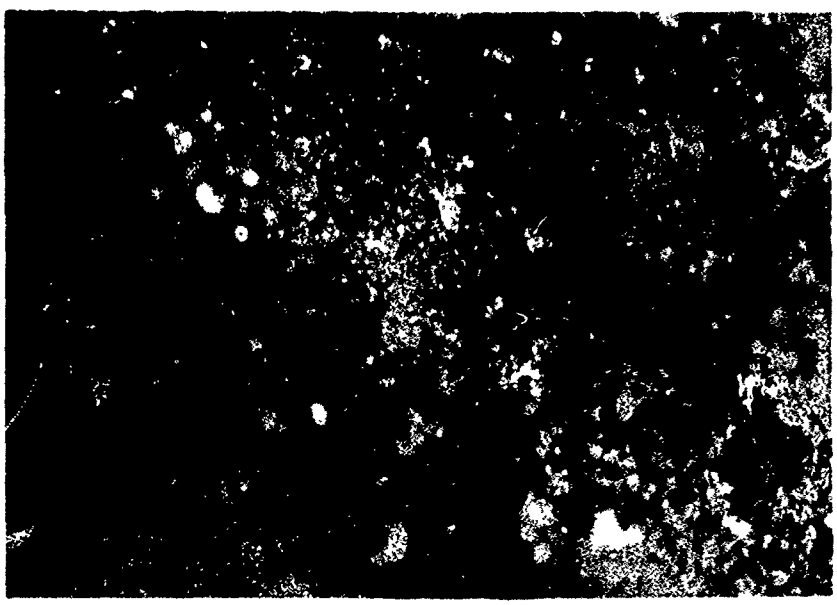

Figure 11. Severe corrosion of bare DU-2 Mo alloy after 224 days immersion in synthetic sea water at 70 C. (40X)

THE USE OF CERAMIC COATINGS FOR INHIBITION TO VANADIUM ATTACK IN GAS TURBINE COMPONENTS

Robert L. Clarke and Joel S. Patton
David Taylor Research Center
Code 2813
Annapolis, MD 21402

ABSTRACT

Zirconia-based ceramic coatings were evaluated for hot-corrosion resistance in standard low-velocity low-pressure burner-rig tests. These tests were conducted at both the low temperature, 704°C (1300°F) and high temperature, 900°C (1650°F) hot-corrosion regime. The coatings were applied by either the electron beam-physical vapor deposition (EB-PVD) process or by vacuum plasma spraying (VPS). The use of zirconia at higher temperatures requires a stabilizer in order to provent undesirable phase transformations which would lead to lower corrosion resistance. The most commonly used stabilizer is yttria, however, other stabilizers are being evaluated such as ceria. Results of several ceramic coating candidates are presented and compared by means of measuring overall depth of attack in the coating.The analysis of the results will also include a comparison of the ceramic coating to present metallic coatings. It is expected that the lives achievable with a successful ceramic coating would be approximately 20X better than current metallic coatings could achieve when used with high impurity fuels.

[Manuscript Not Available at the Time of Printing]

NAVY AIRCRAFT GAS TURBINE ENGINE CORROSION PREVENTION/CONTROL

G. T. Browne, Materials Advisor
COMNAVAIRLANT (Code 528)
Norfolk, VA 23511-5188

K. G. Clark, Materials Engineer
Naval Air Development Center (Code 6062)
Warminster, PA 18974-5000

All Navy aircraft gas turbine engines have experienced significant hot corrosion problems at one time or another. Oxidation, sulfidation, chloride attack, acidic and basic fluxing are predominant corrosion mechanisms. In an attempt to control this problem, solvent emulsion cleaning compounds (qualified to MIL-C-85704) are used to remove sea salt and other contaminants from engine blades and vanes. In addition to reducing corrosion, cleaning removes the sticky organic deposits which trap corrosive agents, dirt and dust and rob the engine of power due to losses in compressor efficiency. A water-base cleaner is under development at NADC which may be used on fired (operating) turbine engines.

BACKGROUND

Gas path corrosion has been observed on all Navy gas turbine engines (GTE). At ambient temperatures, corrosion occurs only in the presence of an electrolyte, but at temperatures above 650 ^{o}C oxidizing gases can cause rapid corrosion of even the more noble metals. The rate at which corrosion occurs depends strongly on the presence of corrosive contaminants. In the cold section (compressor), contaminants ingested into the inlet duct stick to oxidized oil deposits and accumulate. This is often referred to as the "flypaper effect." In the hot section (turbine), contaminants are entrained in the hot combustion gases. To reduce corrosion rates, aircraft engines are periodically washed with a diluted solvent emulsion cleaner and rinsed with fresh water. The cleaner removes oxidized oil films and entrapped debris including corrosive agents such as salt, dirt, dust, and environmental pollutants. This cleaning process has two important benefits. First is the removal of potentially harmful contaminants, thereby minimizing corrosion. This occurs mainly in the compressor section. But since the cleaner flows through the entire engine gas path, some contaminants are also removed from the turbine blades and disks. The second benefit, perhaps even more important than the first, is the restoration of compressor efficiency by removing the "flypaper effect"

debris which interferes with airflow. Table 1 shows some examples of Navy engine wash cycles.

TABLE 1. Examples of Navy Engine Wash Cycles.

Aircraft	Engine	Required wash intervals
H-46	T-58	Each 50 operating hours ashore *
		Each 25 operating hours at sea
H-53	T-64	Each 50 operating hours ashore *
		Each 25 operating hours at sea
F-14	TF-30	Each 180 operating hours
A-6	J-52	Each 200 operating hours
P-3	T-56	Each 300 operating hours

* Fresh water rinses after overwater flight

CORROSION OF GAS TURBINE ENGINES

Aircraft turbine engines corrode both on the ground at ambient conditions and in flight, when temperatures up to 400 ^{o}C are achieved in the high pressure stages of the compressor section and in excess of 850 ^{o}C in the turbine section. On aircraft carriers, salt spray, maintenance fluids, ship stack gases and exhaust from other engines can contaminate non-operating engines. Although aqueous electrochemical corrosion can occur at ambient temperature and the lower temperatures found in an operating compressor, this mechanism is not important in an ambient turbine section due to the highly corrosion resistant alloys which must be used to minimize the effects of hot corrosion. Since hot corrosion reactions cannot occur below about 650 ^{o}F, these mechanisms are not responsible for compressor corrosion damage.

In a turbine engine compressor, corrosive agents are ingested during operation and contaminate and corrode only surfaces on which they adhere. Some particulates are trapped on blade and vane surfaces by sticky thin films derived from leaking engine oil or accumulated airborne organic materials. Hygroscopic particulates may adhere without assistance under the proper humidity and surface temperature conditions. Subsequently, absorption of moisture from humid air forms an electrolyte solution which attacks compressor alloys by uniform, galvanic, pitting and intergranular corrosion. Table 2 shows contamination levels for helicopter and fighter engine compressors operated in Western Europe as reported by Kolkman and Mom [1]. Sulfate, a significant component of sea salt and a reduction product of atmospheric sulfur dioxide, was found to be the predominant ionic contaminant and is present in concentrations which appear to be independent of rinsing frequency. Either sulfate is not removed by rinsing or it

accumulates rapidly and maintains a constant thickness by spalling.

TABLE 2. Contamination Levels in Engine Compressors Operated in Western Europe ($\mu mol/m^2$ of airfoil surface) [1]

Engine Type	Helicopter	Fighter	Fighter
Environment	Land	Land & Sea	Land & Sea
Water Rinse	Daily	Weekly	Never (774 hrs)
Ion species			
F^-	< 50	250	na
Cl^-	1 900	6 900	6 100
SO_4^{-2}	19 000	17 000	16 400
PO_4^{-3}	na	na	< 80
NO_3^-	2 700	1 500	590
H^+	2 000	1	50
NH_4^+	14 000	230	90
Na^+	na	na	29 500
K^+	na	na	1 900
Ca^{+2}	na	na	4 200
Mg^{+2}	na	na	3 800

na = not analyzed

In the turbine section of an operating gas turbine engine, erosion and hot corrosion (occurring above 650 ^oC) damage occurs continually but at a rate which depends on the presence of corrosive agents. Turbine corrodents include those which are ingested by the compressor as well as those derived from fuel and some engine alloys themselves. Table 3, from Jones [2], lists some of the agents responsible for hot corrosion, mechanisms and required temperatures.

TABLE 3. Species Degrading Gas Turbine Blades [2]

Corrodent	Mechanism	Temperature (^oC)
O_2	Oxidation	> 1000
Na_2SO_4	Hot corrosion Sulfidation	850 - 950
SO_2	Sulfidation/ Oxidation	650 - 950
Na_2O	Basic fluxing	850 - 950
MoO_3 (WO_3, V_2O_5)	Acidic fluxing	850 - 950
Eutectic sulfates ($CoSO_4$-Na_2SO_4)	Low temperature hot corrosion	650 - 750
NaCl	Chloride attack	650 - 950

The direct reaction of turbine superalloys with oxygen occurs at temperatures above 1000 °C, but sulfidation/oxidation reactions can occur as low as 650 °C. Dissolution of protective oxide films through basic and acidic fluxing and the catalytic effect of chloride are also significant mechanisms.

In order to minimize the effects of hot corrosion, engine manufacturers have invested their resources in the development of harder, more corrosion resistant alloys. The development of diffusion, metallic overlay, and ceramic protective coatings has resulted in a marked improvement in the service life of turbine components [3]. However, given enough time all protective coatings erode allowing corrosion to resume. Especially rapid blade failures were observed for aircraft deployed in the Middle East following erosion caused by airborne sand.

An additional source of contamination which can lead to premature coating or alloy corrosion due to some of the above mechanisms is unauthorized cleaning compounds. Although heat resistant coatings can reduce corrosion at high temperatures, some are affected by highly alkaline cleaning compounds. For these reasons, strict pH limits (7.5 to 9.5) and limits on the elemental content of cleaners (see Table 4) have been established by engine manufacturers and incorporated into a military specification [4].

TABLE 4. Composition Limits on Turbine Engine Cleaner [4]

Element	Maximum concentration (ppm)
Sulfur (S)	500
Chlorine (Cl)	100
Sodium (Na)	50
Potassium (K)	50
Phosphorus (P)	50
Other metals	10

Examples of typical engine component corrosion problems are shown in Figures 1 through 8.

CLEANING OF GAS TURBINE ENGINES

For more than 20 years, Navy aircraft gas turbine engines have been cleaned to minimize corrosion and to recover lost engine power. When incoming airborne particulates stick to partially oxidized oil deposits in a compressor section, the aerodynamic characteristics of blades and vanes are slightly altered resulting in decreasing engine pressure ratios, increasing temperatures, and subsequent loss of performance. To restore

engine efficiencies, a solvent emulsion cleaner is applied using the Navy GTE corrosion control cart. This towable cart is charged with 3000 psi (21 MPa) compressed air and uses a 1:4 mixture of cleaner concentrate to water. An engine wash begins with a cold engine being motored by the starter and a spray ring or a wand is used to direct the cleaning solution into the inlet duct at 45 to 65 psi (3.1 to 4.1 MPa). The engine is stopped to allow 15 minutes for the cleaner to degrease the compressor. Fresh water is then sprayed into the inlet duct with the engine motoring again until the discharge water runs clear. To prevent corrosion caused by trapped water, the engine is finally dried by running for at least 5 minutes or by "windmilling" using the starter for at least 15 minutes.

DEVELOPMENT OF A NEW GTE CLEANER/METHOD

The above procedure has several drawbacks. First, an engine must be cold to prevent the hydrocarbon solvents in the cleaning solution from vaporizing too quickly or even igniting. Second, the solvent in such cleaners are a source of air and water pollution. For example, each corrosion control cart in the San Diego Air Pollution Control District can only be used with a permit. Third, if the engine is not completely dried by running or windmilling, corrosion is promoted. One solution to these problems is to apply a water-base cleaner to an operating engine. Although not as effective as solvent emulsion cleaners at ambient temperatures, water-base cleaners can be very effective at the temperatures encountered in an operating compressor. If this approach is successful, the time required for engine cooling and drying can be eliminated, corrosion problems which occur with the omission of the drying cycle will disappear and the pollution attributed to engine washing will be minimized. Finally, engine washing at temperatures below 0 ^{o}C will be feasible.

Reference [4], developed by the Naval Air Development Center, makes use of an oxidized engine oil laboratory soil for cleaning efficiency testing. Water-base cleaning products are being evaluated using the same soil and test equipment, but applied using steam to simulate the hot engine conditions of a fired (operating engine) wash. However, currently available proprietary products exhibit cleaning efficiencies of only 30 percent compared to the 90 percent efficiencies of the current solvent emulsion cleaners.

CONCLUSION

Even though the engine wash program does not stop corrosion, documentation indicates that this program extends the useful life of many GTE components. However, more research is needed to develop high performance alloys and coatings which can

survive and function in the high temperature erosive/corrosive GTE environment. With the emphasis on higher temperatures to develop more thrust with less fuel, erosion/corrosion effects must be a major consideration for all engine developers.

REFERENCES

1. Kolkman, H. J. and Mom, A. J. A., "Corrosion and Corrosion Control in Gas Turbines, Part I: The Compressor Section", National Aerospace Laboratory NLR (The Netherlands), NLR MP 83041 U Part I, 5 Jul 83.

2. Jones, R. L., Naval Research Laboratory Memorandum Report 5070, "Hot Corrosion in Gas Turbines," 27 Apr 83.

3. Mom, A. J. A. and Kolkman, H. J., "Corrosion and Corrosion Control in Gas Turbines, Part II: The Turbine Section," National Aerospace Laboratory NLR (The Netherlands), NLR MP 83041 Part II, 5 Aug 83.

4. Military Specification MIL-C-85704 (Cleaning Compounds, Turbine Engine Gas Path) of 7 Apr 86.

Figure 1. Corrosion Cracking of T-56 Turbine Vane

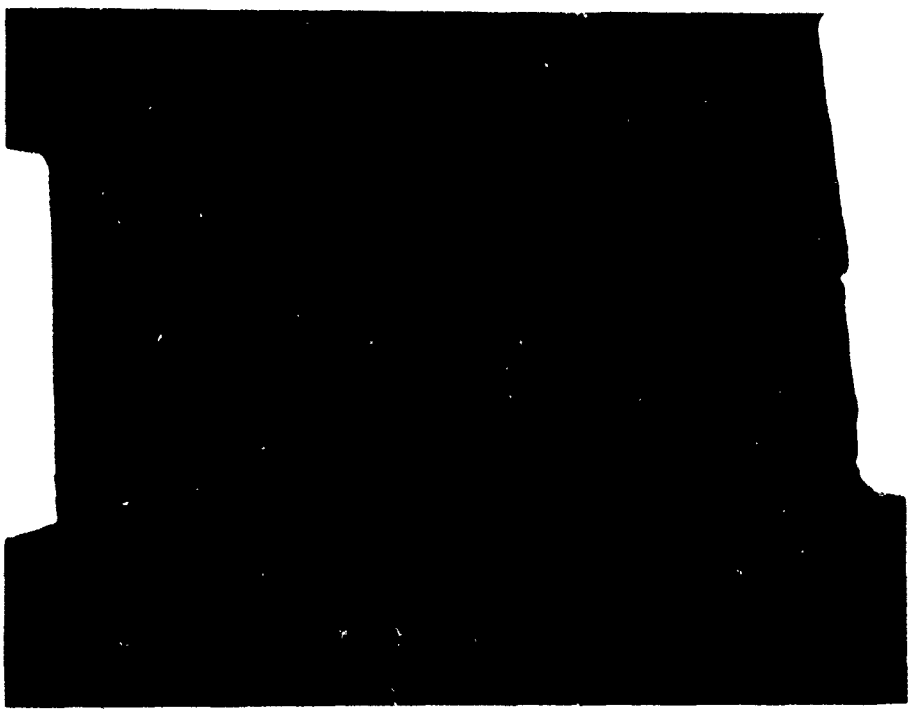

Figure 2. Catastrophic Failure of T-56 Turbine Vane

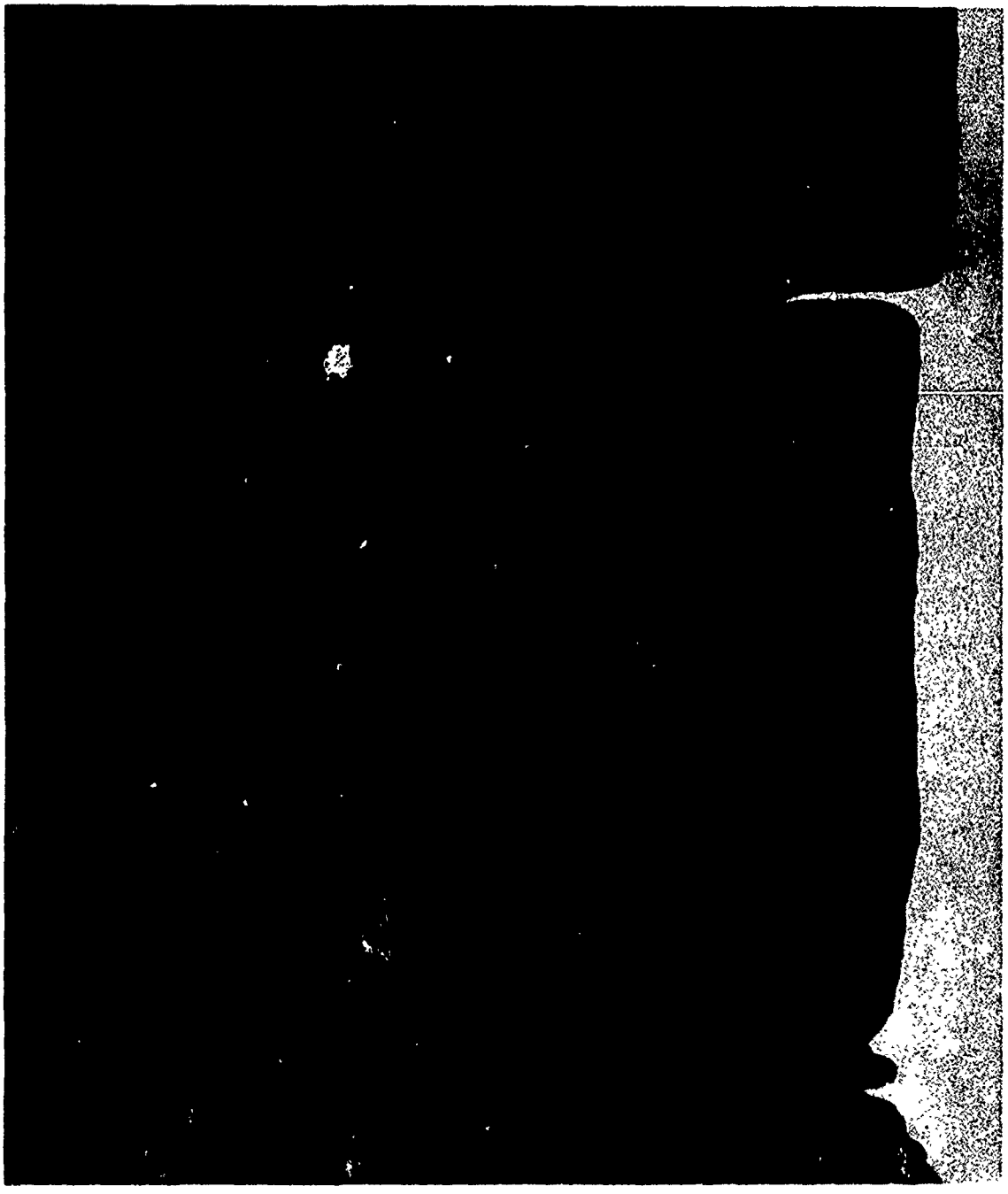

Figure 3. Erosion of Coating and Cracking of T-56 Turbine Vane

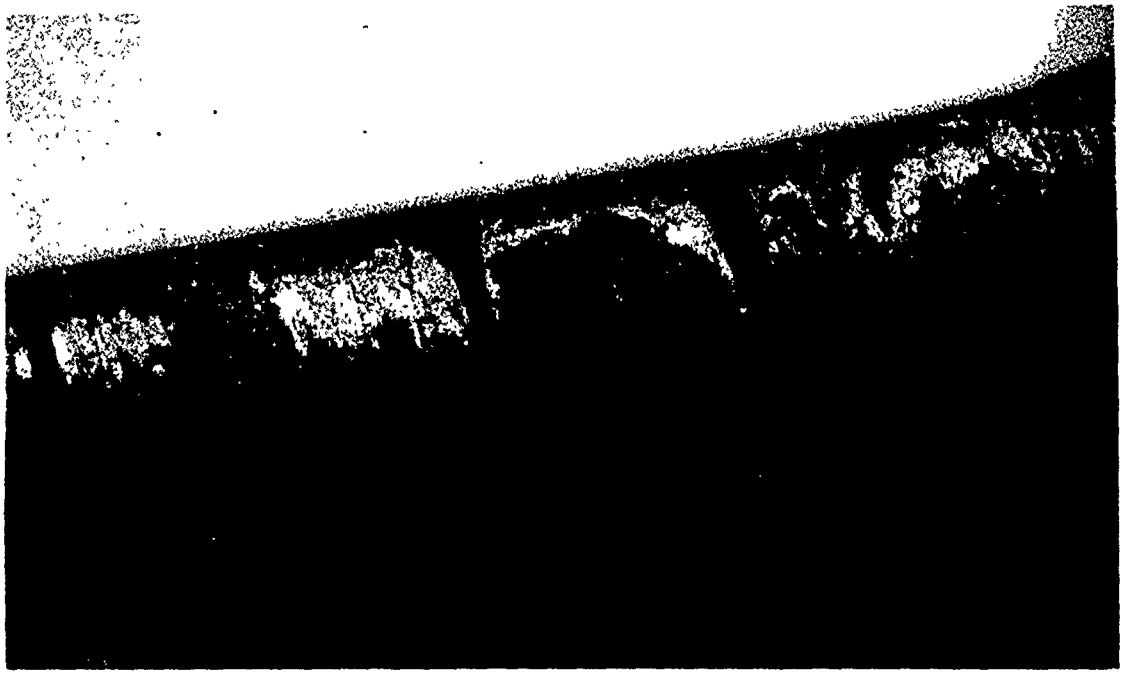

Figure 4. Coating Failure and Cracking of F402 Turbine Vane

Figure 5. Corrosion at Trailing Edge of F402 Turbine Vane

Figure 6. Rust at Disk Attach Point on F402 Turbine Blade

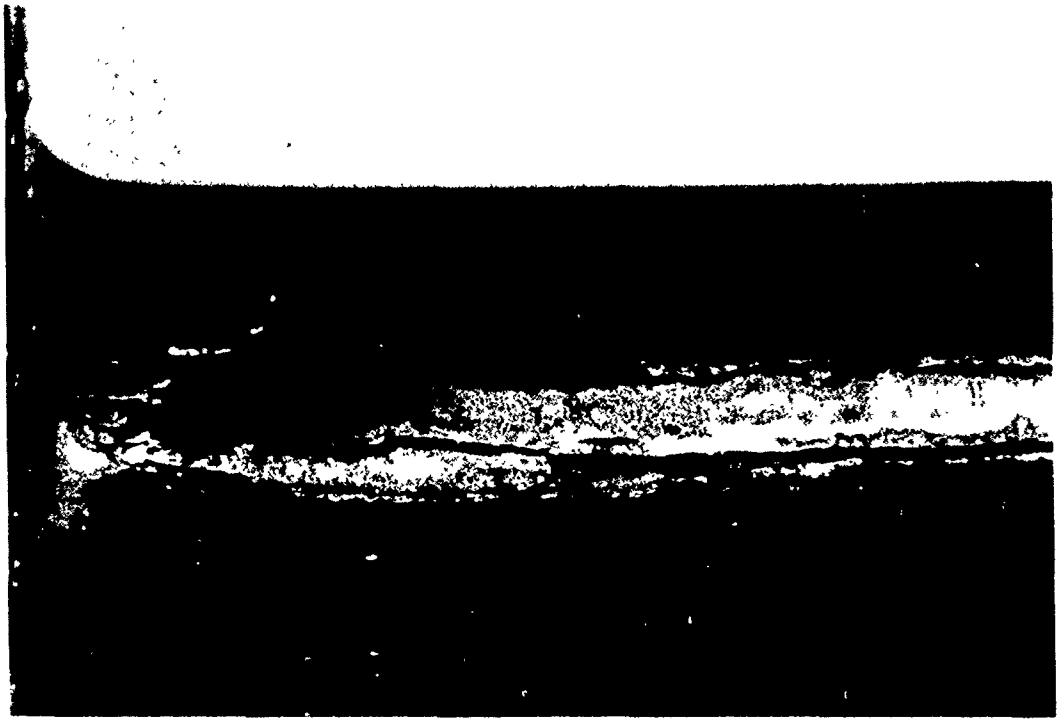

Figure 7. Cracking and Corrosion on J-52 Turbine Vane

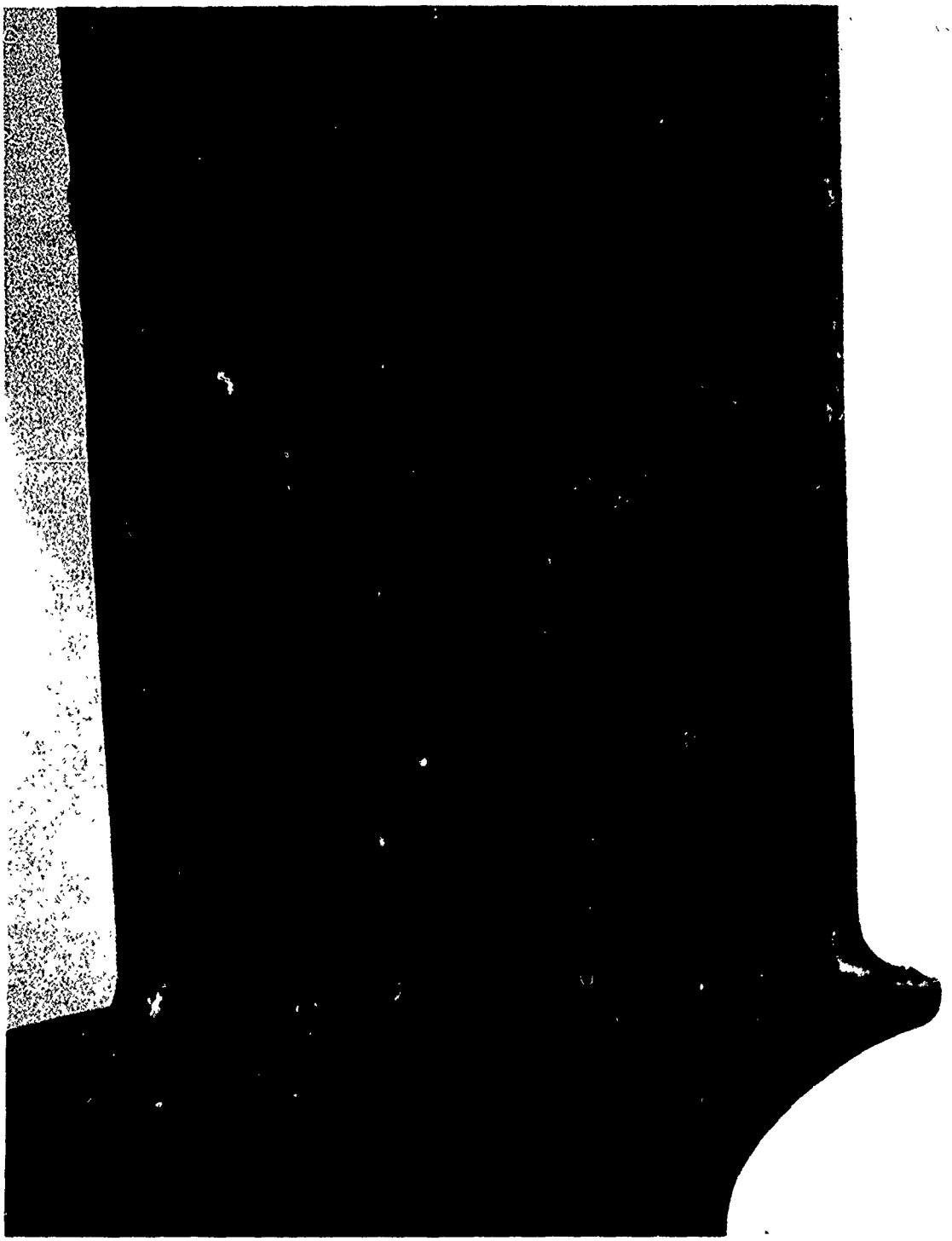

Figure 8. Erosion and Corrosion of TF-34 Turbine Blade

MICROSCOPY OF THE CORROSION OF HIGH-TEMPERATURE COATINGS

G. H. Meier and F. S. Pettit
Department of Materials Science and Engineering
University of Pittsburgh

The results of morphological studies of the oxidation and hot corrosion of diffusion aluminide, CoCrAlY overlay, and zirconia thermal-barrier coatings are presented. The influence of Pt additions on the cyclic oxidation and hot corrosion behavior of diffusion aluminides is described in detail. It is shown that the composition of the substrate has a substantial influence on the corrosion rates and morphologies. The development of the hot corrosion morphologies of CoCrAlY coatings on Ni-base superalloys is described and the use of transmission electron microscopy in characterizing the fine details of these morphologies is discussed. Finally, the development of the hot corrosion morphologies of stabilized zirconia thermal barrier materials is described.

INTRODUCTION

Gas turbine engines are widely used in propulsion systems and in power generating equipment. Materials used in gas turbines may be subjected to a range of environmental conditions depending upon their location in the engine and the operating characteristics of the unit. Materials used for the high pressure turbine are exposed to rather severe conditions in that temperatures are high and salt deposits can accumulate on the surfaces of hardware. The temperature of high pressure hardware depends on operating conditions and the particular application in which the gas turbine is being used. Aircraft gas turbines usually operate hotter than marine or land-based gas turbines. High pressure turbine materials can be exposed to temperatures in the range 600 to 1100°C where the upper limit is encountered only intermittently. The formation of deposits on hardware is determined by the composition of the gas and the temperature of the hardware. Depending on the purity of the fuel and ingested air and temperature, deposits such as Na_2SO_4 can accumulate on hardware surfaces at metal temperatures in the range from 600 to about 1000°C. Some fuels can contain vanadium which can lead to the presence of vanadium compounds, such as $NaVO_3$, in the deposits.

The severe environments encountered in turbines generally require that the superalloy components be protected by coatings. The coatings may be divided into two categories: those applied for corrosion protection and thermal barrier coatings. Coatings applied for corrosion protection consist of diffusion coatings and overlay coatings. The most widely used diffusion coatings are the aluminides while typical overlay coatings are physically vapor deposited(PVD) CoCrAlY coatings. Thermal barrier coatings are typically plasma sprayed coatings of stabilized zirconium dioxide. The purpose of the thermal barrier coatings is to reduce the temperature of the underlying metallic components. These coatings reduce the environmental degradation of the components but are not inert. The aluminide and overlay coatings are subject to several forms of degradation. In high temperature applications(e.g. aircraft engines) the coatings undergo isothermal and cyclic oxidation and interdiffusion with the superalloy substrate. At lower temperatures the coatings are subject to degradation which is accelerated by the presence of surface deposits such as sulfates(hot corrosion). Thermal barrier coatings are susceptible to corrosion associated with sulfate deposits particularly when vanadium is present. The major effect of this form of degradation is preferential removal of the stabilizing oxides such as yttria.

An important aspect of minimizing the effects of the above-mentioned forms of degradation involves understanding the mechanisms of degradation. The development of this understanding involves

the ability to reproduce the corrosion morphologies found in service by conducting well-controlled laboratory experiments. This paper presents the results of experiments used to ascertain the pertinent variables which reproduce the corrosion morphologies observed in service.

RESULTS AND DISCUSSION

Diffusion Aluminide Coatings

Pack cementation is a very common CVD process used to produce diffusion aluminide coatings. In this process a part is immersed in a pack mix and heated in a retort purged with an inert gas. The pack mix includes an aluminum source, an inert filler, and an activator to accelerate Al transfer from the source to the substrate. The final microstructure depends on the temperature of the pack, the pack mix, and any pretreatment of the part to be coated. The coating microstructures that result from the pack process have been divided by Goward and Boone into two types [1,2], those produced by a high Al activity source and those produced by a low activity source. Often these types are referred to as the low temperature and high temperature types, respectively. This coating classification was established using Jannsen and Rieck's work on diffusion in nickel aluminides.[3] Their work showed that only Al atoms are mobile in the aluminum rich aluminides and Ni atoms are the only mobile species in aluminum deficient aluminides. From this work it was concluded that outward growing coatings form mainly by Ni diffusion out to the coating surface. Inward growing coatings were concluded to form predominantly from Al diffusion into the substrate.

Aluminide coatings are degraded via reaction with the environment(corrosion) and by interdiffusion with the substrate. Both processes result in depletion of aluminum from the coating. A significant advance in the technology of diffusion aluminides was made when other elements such as Cr, Ta, Si, and most notably Pt were incorporated into aluminide coatings.[4,5] The platinum modification to straight or normal diffusion aluminides resulted in a much more degradation resistant coating.[5-11] Platinum modified aluminide coatings are used commercially in the hot section of turbine engines.[11]

Various processing schemes have been developed to add platinum to diffusion aluminide coatings each of which produces coatings with different microstructures. In most of these processes platinum is electroplated as a thin layer ($\approx$ 3-10μm) on the surface prior to aluminizing. The platinum aluminides formed using high activity packs involve aluminum diffusion through the platinum layer. If the Pt content of the layer is high enough at the surface a continuous $PtAl_2$ phase will form. Lower Pt contents may cause NiAl(β) precipitates to form in $PtAl_2$ or vice versa. When the Al reaches areas in the Pt layer where the Pt content is lower than that needed to form $PtAl_2$, a hyperstoichiometric NiAl (β) phase forms. Al is mobile in this phase until the Al content decreases to where Ni atoms become the mobile species. The resultant structure is similar to that for a straight aluminide with the exception of the zone containing the $PtAl_2$. Some inclusions of alumina may also be present in this zone as a result of the grit blasting of the substrate prior to Pt electroplating and are excellent markers of the original surface. The platinum aluminide structures formed with a low activity pack evolve in a different manner. The Al still moves through the Pt layer eventually forming a hypostoichiometric NiAl phase in regions where the Pt content is lower. Nickel atoms are the only mobile species in this phase. The continued growth of the coating is mainly by Ni movement outward which results in a two zone structure. The first zone at the surface of the coating contains $PtAl_2$ precipitates in hyperstoichiometric NiAl. The second zone is a Ni-rich NiAl that forms via interdiffusion.

Platinum improves the lives of aluminide coatings. However, coatings can be degraded by different processes such as oxidation, high temperature hot corrosion and low temperature hot corrosion. This section of the paper is concerned with defining the types of degradation for which platinum is an effective means to extend coatings lives. In addition, the mechanisms by which platinum produces such beneficial effects will be described.

Several straight aluminide and platinum aluminide coatings were studied on the superalloy substrates

Table 1 Compositions of Alloy Substrates(wt%)

Sample	Ni	Cr	Al	Ti	Co	Ta	Mo	W	Hf	B	Zr	C	Nb
IN738	Bal.	16	3.4	8.5	1.7	1.7	1.7	2.6	-	.01	-	.17	.9
MAR M200	Bal.	9	5	2	10	-	-	12	-	.015	.05	.15	1
RENE 80	Bal.	14	3	5	9.5	-	4	4	*	.015	.32	.17	-
CMSX-3	Bal.	7.7	5.5	.9	4.9	5.8	.6	7.8	.1	-	-	-	-
PWA 1480	Bal.	9.8	5.1	1.5	4.7	11.9	-	4	-	-	-	-	-

*EDS indicated the presence of Hafnium.

whose compositions are indicated in Table 1. Micrographs showing the microstructures of typical as-processed coatings are presented in Figure 1. The coatings are a straight aluminide(PWA 73) and a Pt-aluminide on IN738. The light discontinuous phase evident at the surface of the Pt-modified coating is $PtAl_2$ which lies in a matrix of (Pt,Ni)Al. Carbides exist in the inner zone. Alumina particles from the grit blasting are also evident in the Pt-aluminide coating. These particles are in the inner zone and appear to be from 1-4 μm in diameter. Alpha-refractory metal precipitates can be observed beneath the $PtAl_2$ layer. The PWA 73 coating has a three zone structure.

Isothermal oxidation tests were performed on a number of the coating systems at 1100°C in air. The platinum modified coatings usually had smaller weight increases than the conventional aluminide coatings, however, some of the conventional aluminides also exhibited very small weight increases. This test was further complicated by the fact that some weight losses may have occurred on the platinum modified samples due to PtO_2 vaporization from the platinum tabs used to support the coupons for electroplating. Cross sections of the scales of both coating types on MAR M200 are presented in Figure 2. The scale upon the straight aluminide coating is about 4 times thicker than that on the Pt-modified coating. These thicknesses were used to calculate parabolic rate constants. Values of 2.8×10^{-12} and 2×10^{-13} g^2/cm^4-sec were obtained for the oxides formed upon the conventional and platinum aluminides, respectively. The value of 2×10^{-13} is in good agreement with alumina growth on platinum-aluminum alloys.[22] The coating microstructures after isothermal oxidation are compared in Figure 3. The difference in the amount of degradation between the coatings is evident. The straight aluminide had formed an appreciable amount of γ' next to the scale. In some areas a lighter imaging γ phase is next to the scale. This view of the coating also shows that the scale formed on the straight aluminide is much thicker than that shown in Figure 2 in some places. The platinum aluminide on the other hand displays a continuous layer of β phase adjacent to the scale with a another phase, γ', appearing at the grain boundaries.

Cyclic oxidation tests were performed at 1100, 1135 and 1200°C and typical weight change versus time measurements from these tests are presented in Figures 4 and 5 for different coating systems. In all of these tests the platinum modified coatings performed better than the conventional aluminides. In particular, protective alumina scales were maintained for longer periods of time on the platinum modified coatings compared to the conventional coatings. Some platinum modified coatings exhibited lives greater than others because substrate elements influenced the coating lives. Figure 6 shows micrographs of the surface of coated IN738 after 322 cycles of testing. The Pt-aluminide coating displays alumina whiskers and outgrowths upon a web or lacy structure. Little variation in the scale morphology is observed. The EDS of the general scale on a Pt-aluminide indicates a scale rich in Al and Cr. The surface of the straight aluminide shows a considerable amount of relief and no one oxide morphology dominates. The EDS analyses of these scales are similar to the Pt modified coating but indicate a higher amount of Ti. Figure 6 indicates substantial spalling of the alumina from both coatings. Therefore, it does not appear that the beneficial effects of Pt are associated with improved scale adherence.

Results obtained from acoustic emission tests with several coating systems are presented in Figure 7 and are consistent with the proposal that the platinum modified coatings do not exhibit substantially better oxide scale adherence than the straight aluminide coatings. Therefore, it is proposed that Pt improves the ability of the coatings to reform alumina scales after spalling.

The various aluminized alloys were exposed to high temperature hot corrosion conditions which consisted of coating with Na_2SO_4 deposits and exposing to air at 1000°C under thermal cycling. Results obtained from these tests are presented in Figure 8. These data show conclusively that the platinum modified coatings are better than coatings that do not contain platinum. Typical microstructures of specimens exposed to cyclic hot corrosion conditions are presented in Figure 9. The amount of degradation is much more extensive in the coating that does not contain any platinum. Examination of the data presented in Figure 8 shows that there also is an effect of substrate composition. Coatings have shorter lives on Rene 80 compared to CMSX-3 which in turn are not as good as coatings on PWA 1480. The significant difference between these substrates is the amount and type of refractory elements. Rene 80 contains both Mo and W. CMSX-3 contains mainly W whereas PWA 1480 contains predominantly Ta. In the hot corrosion literature [12] it is well documented that refractory elements such as Mo and W can have a profound effect upon hot corrosion behavior. The results obtained for the high temperature hot corrosion tests show that platinum extends the lives of diffusion aluminide coatings. Optimum lives, however, depend on the composition of the superalloy substrate. These results are interpreted in terms of the Pt additions excluding refractory metals from the outer regions of the coatings and in improving the ability to reform alumina scales under cyclic conditions as described above.

Low temperature hot corrosion experiments were conducted by coating the aluminized alloys with Na_2SO_4 and exposing them to oxgyen plus SO_3 under isothermal conditions at 700°C. The weight change data for coating systems exposed to low temperature hot corrosion conditions are presented in Figure 10. The weight changes are not as large as those of the high temperature hot corrosion test but still very much larger than would have been observed in the absence of a deposit and without any SO_3 in the gas phase. Examination of these results show that the weight changes for the coatings which contain platinum are usually significantly less than those which do not contain any platinum. This observation is also supported by metallographic examination of the exposed specimens. As can be seen in Figure 11, less attack of the coating on CMSX-3 with platinum has occurred than of the coating with no platinum. No obvious influence of substrate composition was evident in the low temperature hot corrosion tests.

Hot Corrosion of CoCrAlY Overlay Coatings

The exposure of CoCrAlY overlay coatings to the low temperature hot corrosion conditions described above, for example in marine turbines, is known to cause even more severe degradation than is experienced by the aluminide coatings. The typical morphology is a pitting type as illustrated in Figure 12(a). Higher magnification SEM observation of the corrosion front, Figure 12(b), indicates some preferential attack of the Al-rich β-CoAl phase and the precipitation of sulfides ahead of the corrosion front. EDS analysis of these sulfides, Figure 12(c), shows them to be Ti-sulfides. The Ti has diffused up from the IN738 substrate. Combination of SEM, Cross-sectional TEM, and selected area electron diffraction, Figure 13, indicates that the bulk of the pit contains Cr_2O_3 and a mixed spinel of Co, Cr, and Al. Combination of bright-field and dark-field transmission electron microscopy, Figure 14, indicated that the metal islands in the lower part of the pit were virtually pure Co. The combination of the above morphological observations with thermodynamic and kinetic analyses, which have been eliminated for the sake of brevity, have lead to a model for this form of degradation. This model involves the preferential removal and reprecipitation of Al and Cr at the corrosion front, which prevents a protective oxide from forming, followed by the dissolution of Co into the sulfate melt.

Vanadium-Induced Corrosion of Thermal Barrier Coatings

Thermal barrier coatings, such as stabilized zirconia, are now being used to reduce metal surface temperatures. It is well established that deposition of vanadium-containing compounds on these coatings can cause severe corrosive attack. Under some conditions this attack is associated with the removal of the stabilizer from the coating. The experimental procedure to examine the effects of vanadium was similar to that for sulfate hot corrosion except that $Na_2SO_4 + NaVO_3$ deposits were used and, in some experiments, the activity of V_2O_5 was fixed in the gas phase by flowing gases over a crucible of V_2O_5 at a fixed temperature. Polycrystalline zirconia specimens bilized with 6 and 12% Y_2O_3 were examined. A single crystal of ZrO_2-6% Y_2O_3 was also studied. At 900°C it was found that the corrosion attack could be described by measuring the thickness of a porous zone which developed at the surface of the specimens, Figure 15. The thickness of this zone as a function of time is presented in Figure 16 for 6 wt% Y_2O_3 - ZrO_2. The kinetics are linear and the rates become greater as the activity of V_2O_5 in the deposits is increased. Examination of degraded specimens shows that Y_2O_3 is removed from the ZrO_2 and precipitated at the surface of the specimen as YVO_4, Figure 15. Some zirconium is also removed from the samples since a small amount of a phase containing zirconium and vanadium was detected upon the surfaces of specimens, Figure 15. The porosity is concentrated at grain boundaries of the specimens but a porous zone was also observed on the single crystal. The depths of the porous zones formed upon the 12% Y_2O_3 specimens were not as great as those formed upon the 6 % specimens.

The morphological observations have lead to a model for the development of the porous zone and compound formation on the specimen surfaces which is presented in Figure 17. The model involves the dissolution of Y_2O_3 from the ZrO_2 by reactions of the type,

$$Y_2O_3 + 3VO_3^- = 2Y^{3+} + 3VO_4^{3-} \qquad (1)$$

At sufficiently high V_2O_5 activities precipitation of YVO_4 occurs on the specimen surface.

SUMMARY

The above examples have illustrated the use of various forms of microscopy in the evaluation of high temperature corrosion morphologies. They have, hopefully, illustrated the necessity for utilizing this tool in developing mechanisms for high temperature corrosion processes.

ACKNOWLEDGEMENT

The authors gratefully acknowledge the financial support of this work by the Office of Naval Research under Contract No. N00014-81-K-0355/P00007 and the Materials Technology Laboratory(Department of the Army). They also acknowledge the experimental contributions of J. Caola, G. Kim, J. Schaeffer, and B. Warnes.

REFERENCES

1. G.W. Goward and D.H. Boone, Oxid. Metals, 3, 475(1971).

2. G.W. Goward and D.H. Boone, Trans. ASM, 60, 228(1967).

3. M.M.P. Jannsen and G.D. Rieck, Trans. Met. Soc. AIME, 239, 1372(1967).

4. D.A. Josphep, U.S. Patent No. 3,495,748 , 1970.

5. H.H. Todd, U.S. Patent No. 33,494,748.

6. M.J. Fleetwood, Metals Sci., 98, 503(1970).

7. P. Deb and D.H. Boone,"Microstructural Formation and Effects on the Performance of Platinum Modified Aluminide Coatings", Tech. Report, Naval Postgraduate School, 1985.

8. K. Bungardt et al, U.S. Patent No. 33,677,789 , 1972.

9. G.J. Tatlock, T.J. Hurd, and J.S. Punni, Platinum Metals Rev., 31, 26(1987).

10. G.R. Johnston and P.G. Richards, "The Relative Durabilities of Conventional Aluminide and Platinum-Modified Aluminide Coatings in an Operational Gas Turbine Engine" in Corrosion in Fossil Fuel Systems, I.G. Wright ed., The Electrochem. Soc., 1983, p. 456.

11. R. Bauer, K. Schneider and H.W. Grunling, High Temp. Tech., 3, 59(1985).

12. F.S. Pettit and C.S. Giggins, "Hot Corrosion" in Superalloys II, C.T. Sims, N.S. Stoloff, and W.C. Hagel, eds., Wiley, 1987, p. 327.

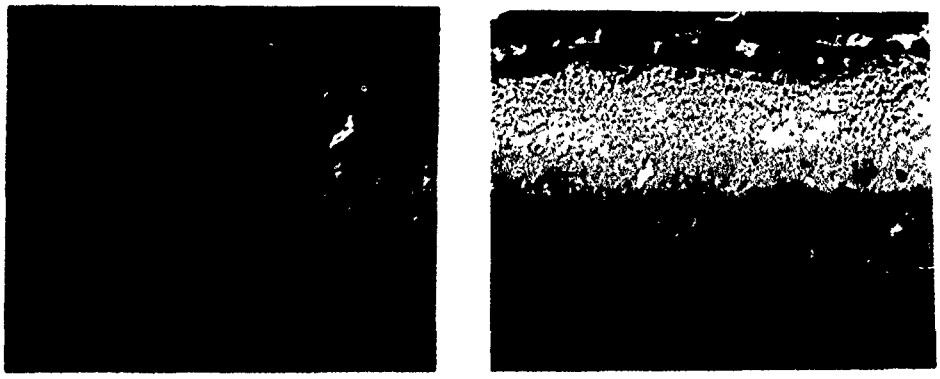

Figure 1 SEM micrographs of typical diffusion aluminide coating microstructures. Left is PWA 73 on IN738. Right is Pt-aluminide on IN738.

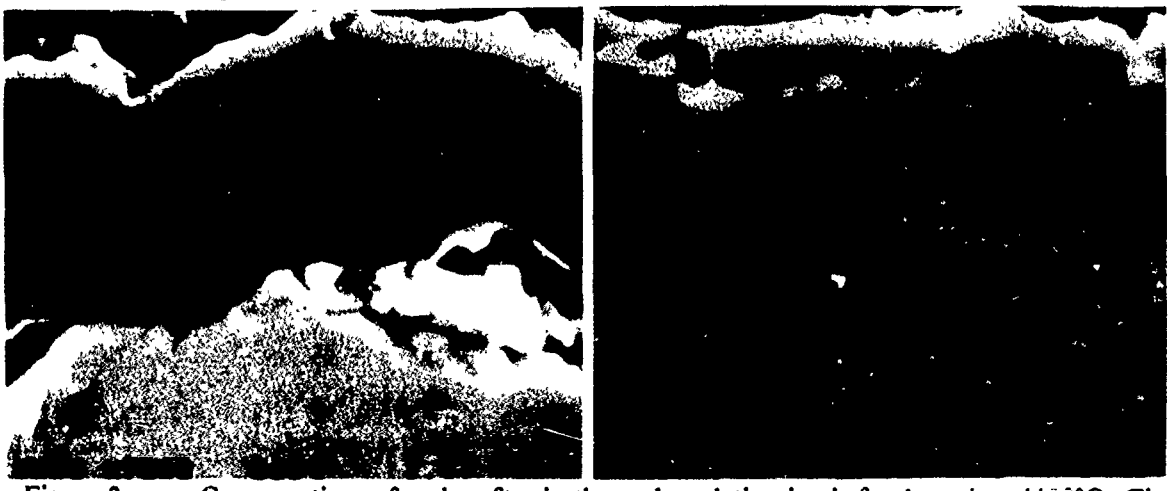

Figure 2 Cross-sections of scales after isothermal oxidation in air for 1 week at 1100°C. The left is PWA 73 on MAR M200 and the right is a Pt-aluminide on MAR M200.

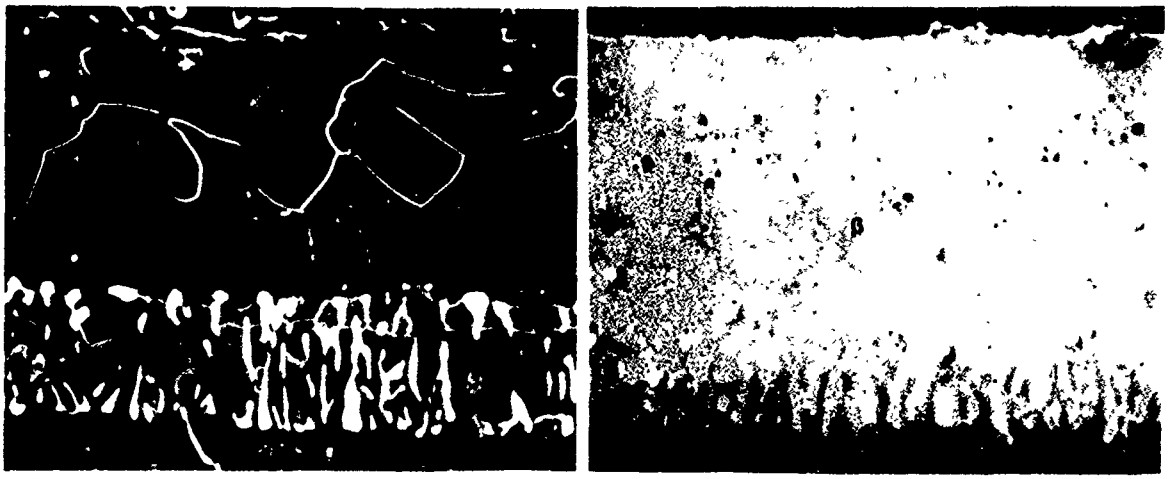

Figure 3 Cross-sections of PWA 73(left) and Pt-aluminide(right) on MAR M200 after isothermal oxidation in air at 1100°C for 1 week.

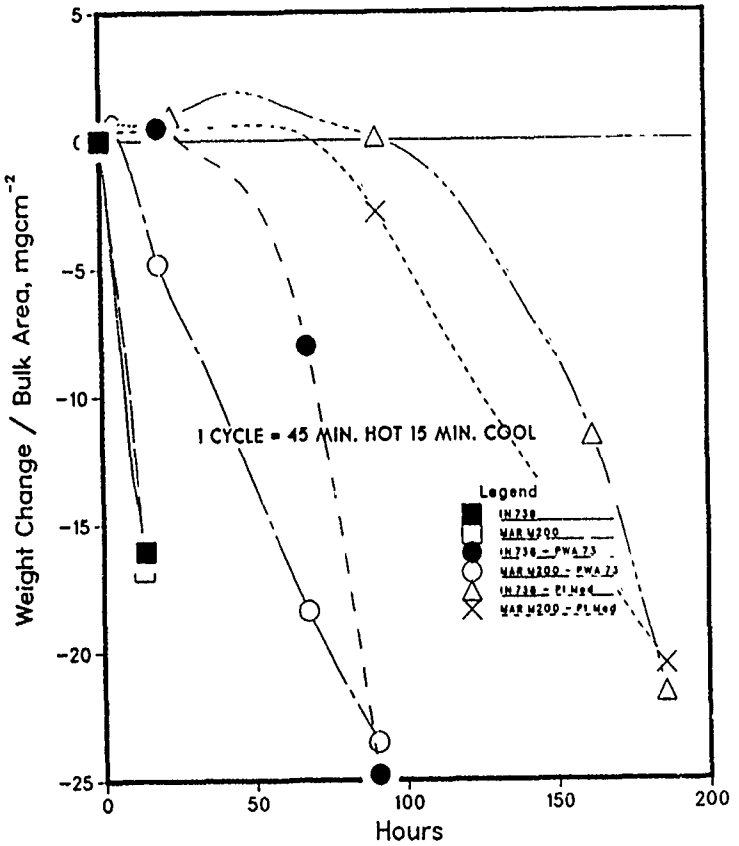

Figure 4 Cyclic oxidation kinetics of various systems at 1200°C in air.

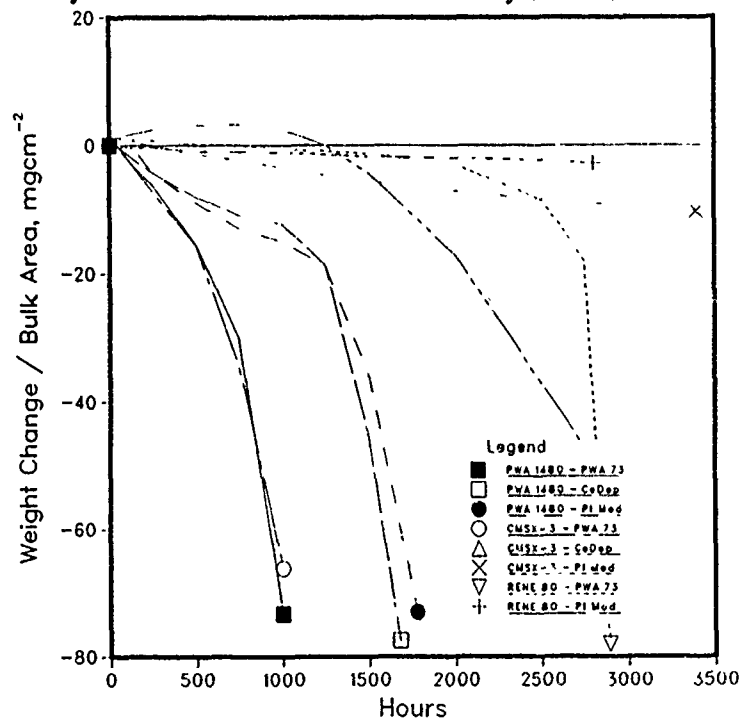

Figure 5 Cyclic oxidation kinetics of various system at 1135°C in air.

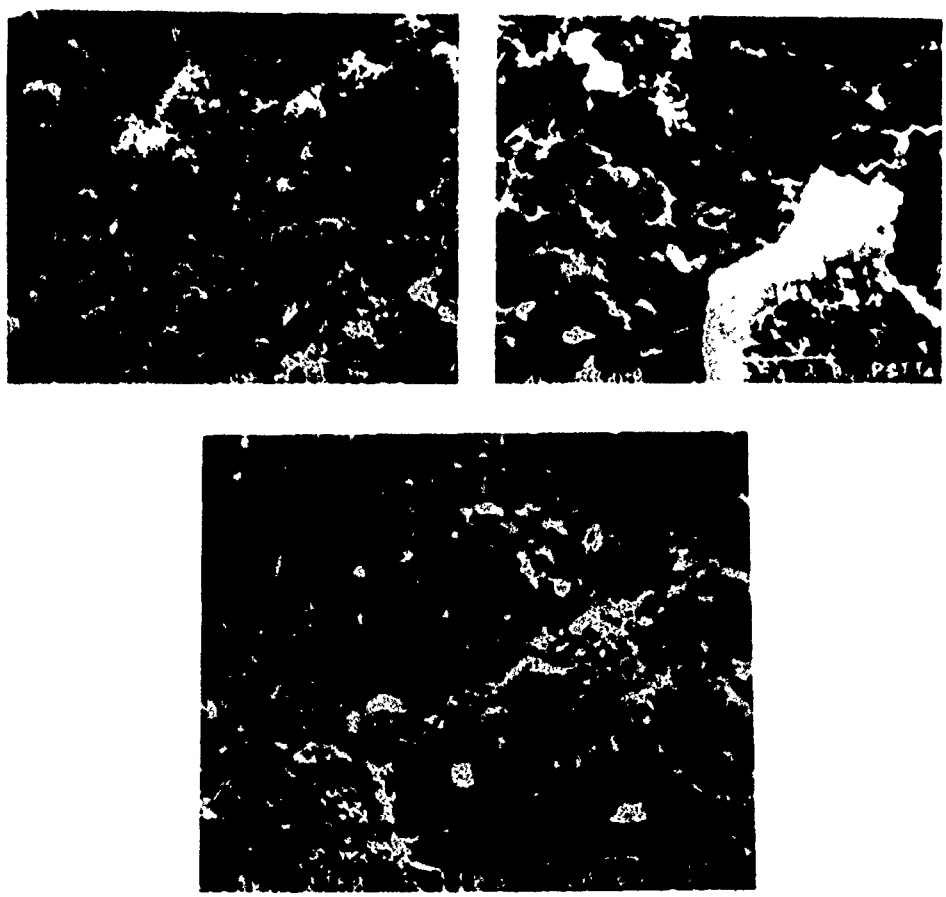

Figure 6 Surface micrographs of PWA 73(top) and Pt-aluminide(bottom) on IN 738 after 322 hours of cyclic oxidation at 1100°C. Note that there is evidence of scale spalling from both coatings.

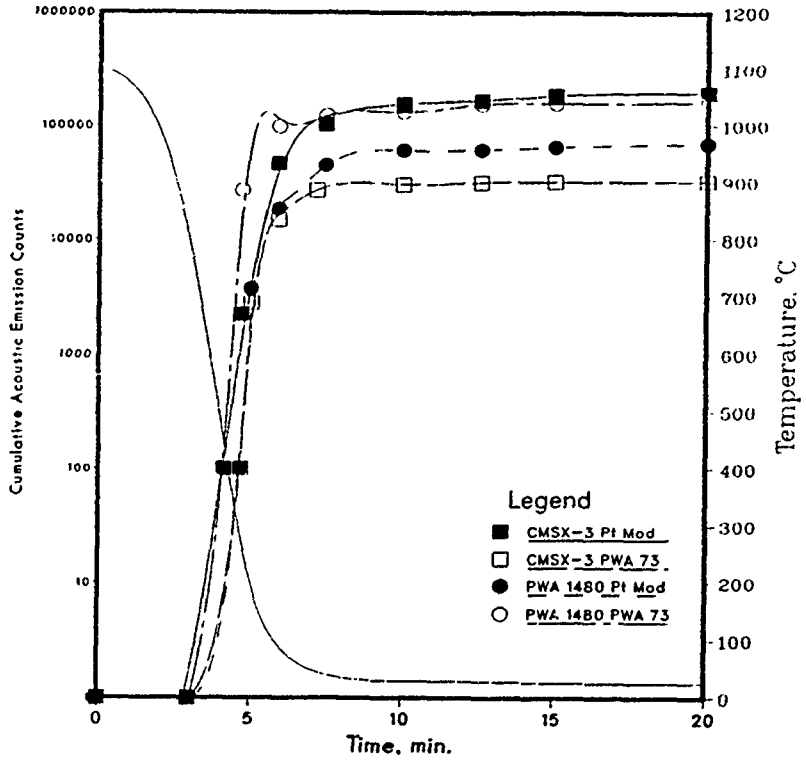

Figure 7 Acoustic emission results for various coating-substrate systems.

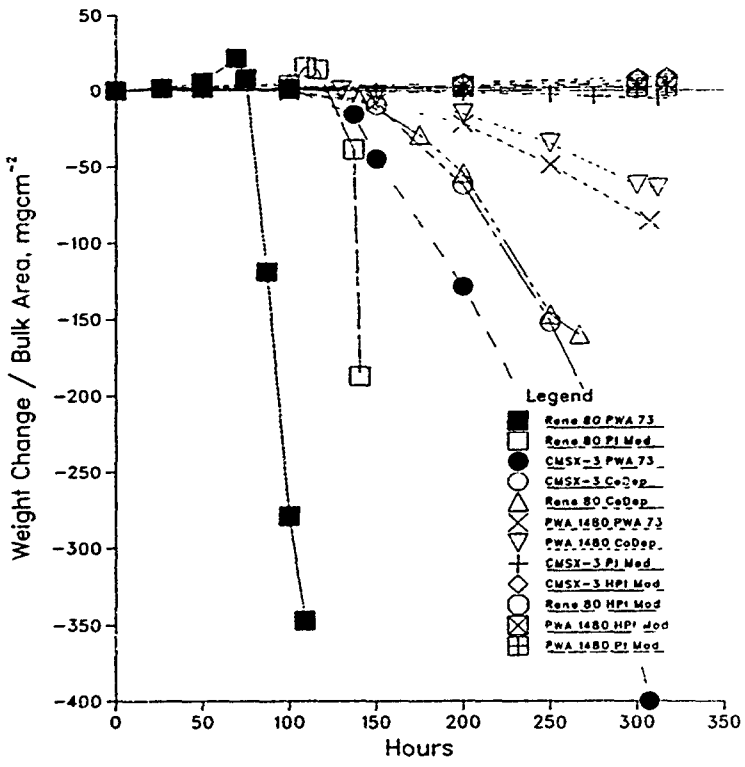

Figure 8 Cyclic high temperature hot corrosion kinetics for various systems at 1000°C with 1 mg/cm^2 Na_2SO_4 deposits.

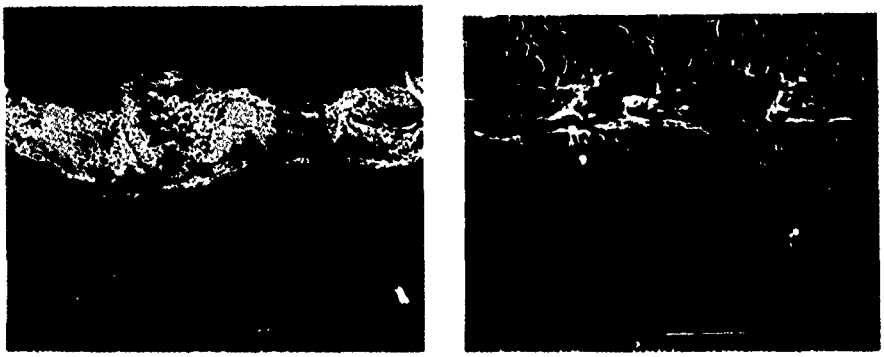

Figure 9 Cross-sections of coated PWA 1480 after 300 hours of cyclic hot corrosion in air at 1000°C. Coating at left is PWA 73 while at right is Pt-aluminide.

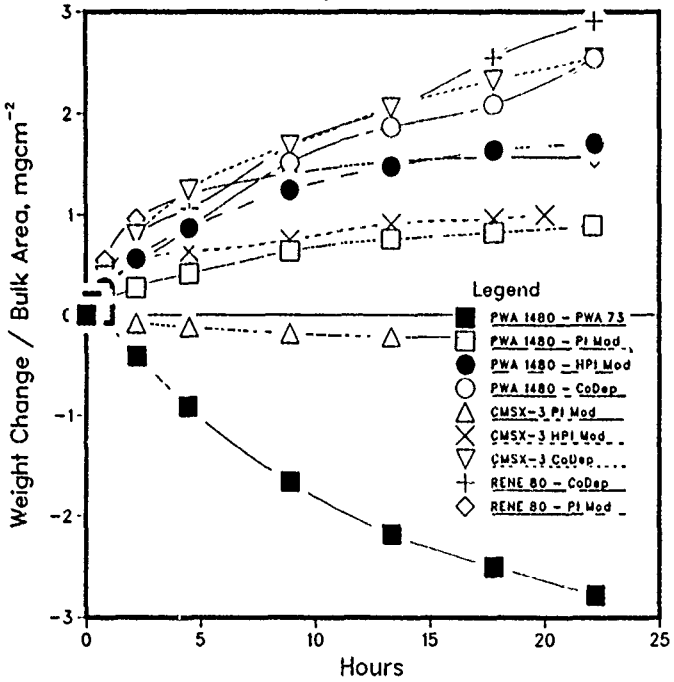

Figure 10 Low temperature hot corrosion kinetics for various systems at 700°C and 10^{-4} atm. SO_3.

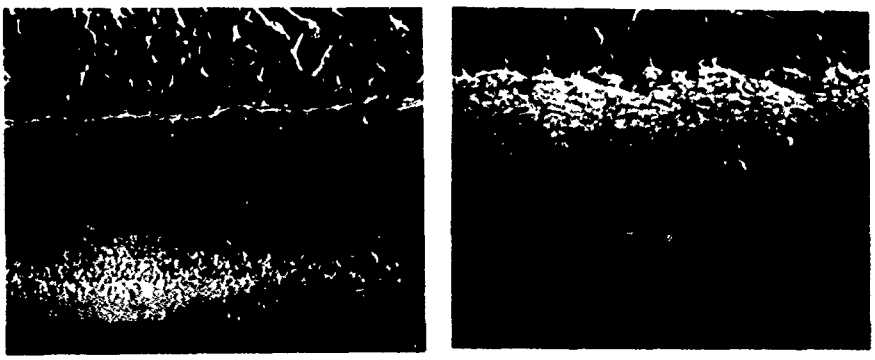

Figure 11 Cross-sections of coated CMSX-3 after 24 hour exposure to low temperature hot corrosion conditions at 700°C. Left is PWA 73 while right is Pt-aluminide

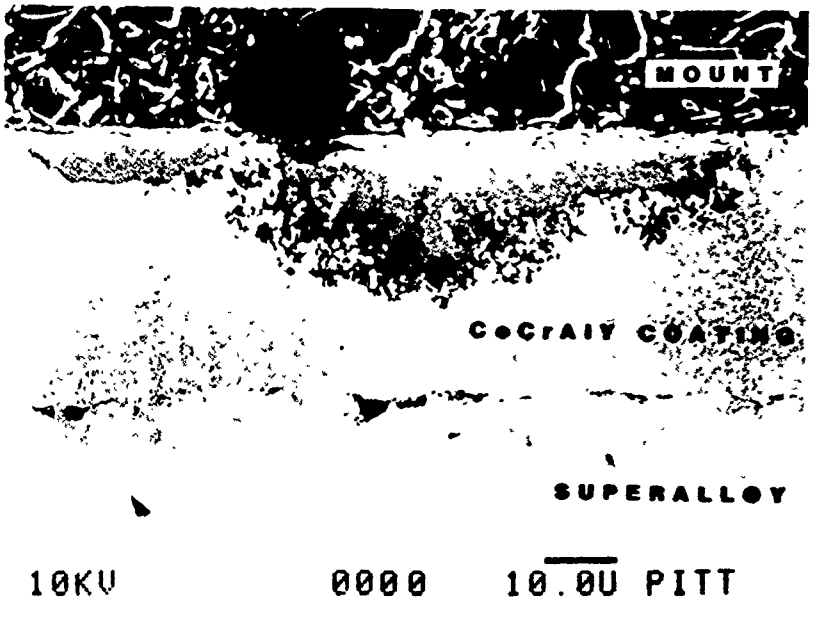

(a)

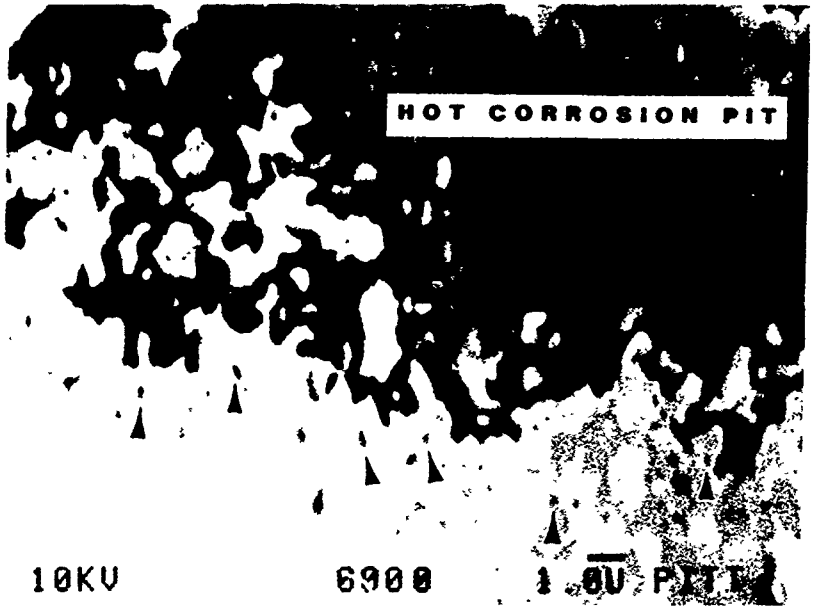

(b)

(c)

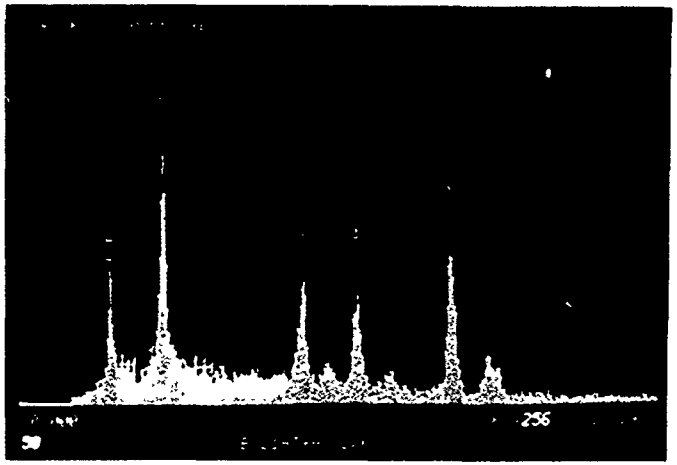

Figure 12 (a) Overall cross-sectional SEM view of a hot corrosion pit in a CoCrAlY overlay coating after 2 weeks at 700°C. (b) High magnification micrograph of the reaction front with arrows showing titanium sulfides in the coating. (c) Typical EDS spectrum from one of the sulfides.

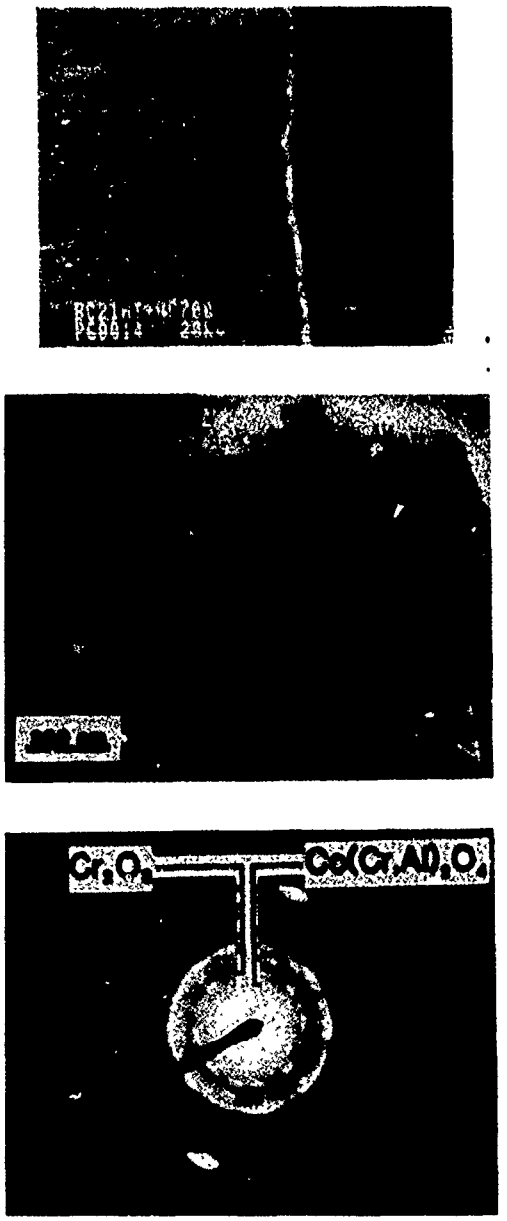

Figure 13 (Top) SEM image of a typical low temperature hot corrosion pit. (Center) TEM image of the corrosion product in the center of the pit. (Bottom) Selected area electron diffraction from the reaction product in the pit.

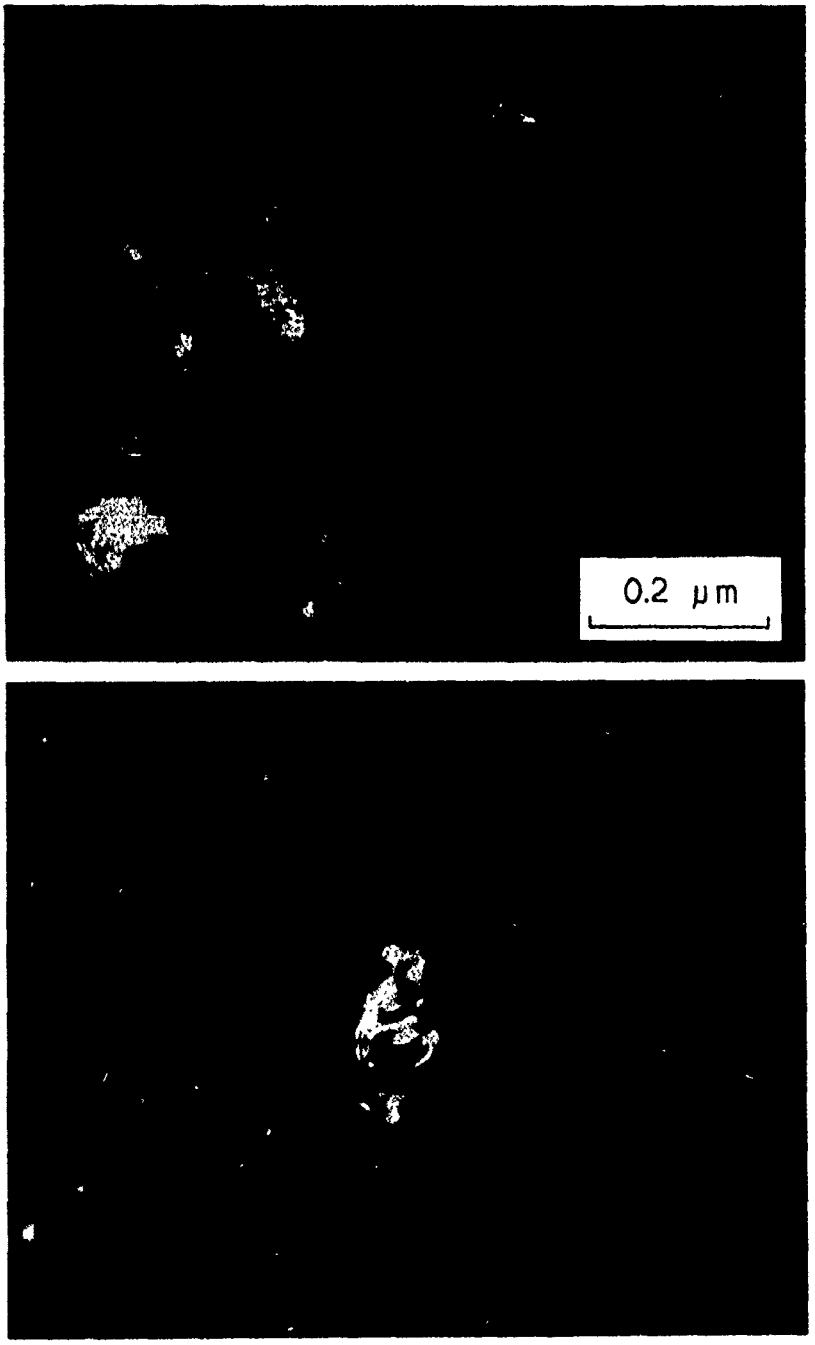

Figure 14 (Top) TEM image of the corrosion product at the base of a low temperature hot corrosion pit showing a metallic particle at arrow. (Bottom) Bright-field image of the particle obtained using an fcc-Co reflection.

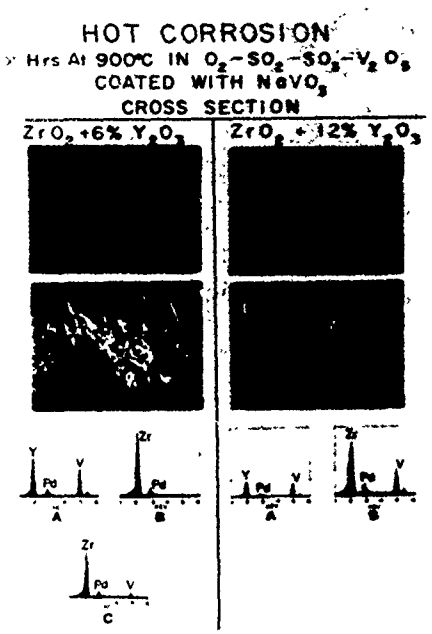

Figure 15 SEM micrographs and EDS spectra from the cross-sections of ZrO_2 + 6wt% Y_2O_3 and 12wt% Y_2O_3 after cyclic hot corrosion at 900°C.

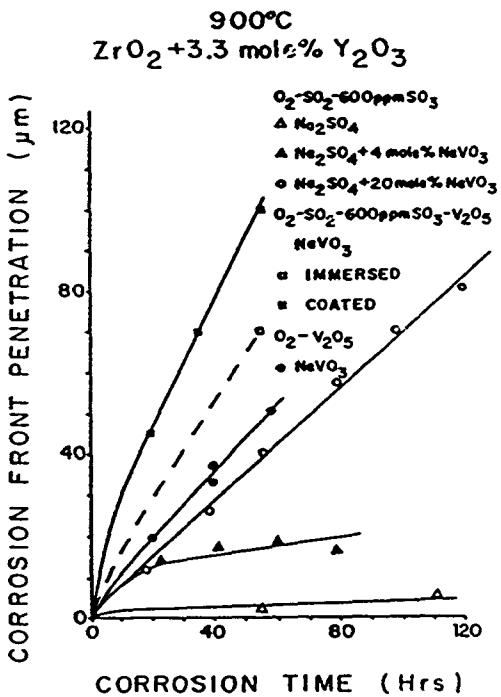

Figure 16 Kinetics of cyclic hot corrosion of ZrO_2 + 6% Y_2O_3 at 900°C in three different deposit-gas combinations.

$$Y_2O_3 + 3NaVO_3 \rightleftharpoons 2YVO_4 + 3Na_3VO_4$$

$$Y_2O_3 + 3Na_2S_2O_7 \rightleftharpoons Y_2(SO_4)_3 + 3Na_2SO_4$$

$$ZrO_2 + 3NaVO_3 \rightleftharpoons ZrV_2O_7 + Na_3VO_4$$

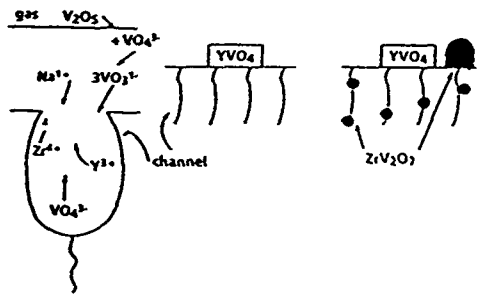

Figure 17 Important chemical reactions and model for hot corrosion of Yttria-stabilized Zirconia.

HOT CORROSION RESISTANT Sc_2O_3-STABILIZED ZrO_2 COATINGS

Robert L. Jones

Naval Research Laboratory
Code 6179
Washington, DC 20375-5000

A Navy/industry effort is underway to develop corrosion-resistant ceramic coatings for gas turbine blades which would allow burning of cheaper, and more abunduant vanadium- and sulfur-containg fuels in Navy ship propulsion gas turbines. Scandia-stabilized zirconia (SSZ) has been identified by NRL as a promising candidate for this purpose. NRL results indicate that SSZ is substantially more resistant to molten vanadate/sulfate hot corrosion than yttria-stabilized zirconia. The acid-base theory of ceramic corrosion which pointed to scandia as a corrosion-resistant stabilizer for zirconia, and the experimental findings that confirmed the idea, will be described.

INTRODUCTION

The Navy currently has about 100 gas turbine powered ships, including guided missile frigates, destroyers, and the Aegis equipped cruisers intended to provide AAW/ASW defense for the carrier battle groups. It is imperative that the engines in these ships operate with maximum power, fuel economy, reliability, and endurance. A major potential problem for gas turbines in ships is hot corrosion; i.e., high temperature corrosion of the gas turbine blades by molten salt deposits produced from contaminants in the engine fuel and/or sea salt in the intake air. In the early development of gas turbines for boat and ship propulsion, it was not unusual for unprotected engines using aircraft alloys to be corroded to uselessness in 300 hrs or so. However, on present day US Navy ships, gas turbine blades normally exceed 10,000 hrs of service before requiring replacement for hot corrosion damage. This huge improvement has been made possible by use of advanced air filtering systems, limits on allowable fuel impurity levels (e.g., below 1% sulfur), and particularly by industry/Navy development of corrosion-resistant blade superalloys and coatings for marine gas turbines.

Among the Navy's fuel limitations is the requirement that the fuel should be vanadium-free. Most crude oils contain trace vanadium but, since this vanadium is combined with heavy organic molecules and tends to remain with the residual in distillation, it has been possible to meet Navy specifications of no vanadium by burning distillate fuel. As petroleum reserves diminish, however, and lower quality crudes having higher levels of vanadium must be used, it will be increasingly difficult to insure vanadium-free fuel for Navy ships, especially for fuel purchases in foreign ports.

Vanadium in the fuel will present a new problem in hot corrosion prevention for the Navy. Burner rig tests at NSRDC, Annapolis (1) have shown, for example, that the hot corrosion rate of CoCrAlY (an alloy of Co, Cr, Al and Y), the current Navy anti-corrosion blade coating, is increased by up to 5X by less than 10 ppm of vanadium in the fuel. The increase in the hot corrosion rate of MCrAlY (where M = Co, Ni or Fe) coatings caused by vanadium has been confirmed by Seiersten and Kofstad (2).

A general approach to improving the hot corrosion resistance of CoCrAlY has been to raise the Cr level while reducing the Al content. However, laboratory studies at NRL (3) indicate that even Co-35w/oCr-6w/oAl-0.5w/oY undergoes accelerated attack by vanadate-containing melts. Using higher levels of Cr results in brittleness of the CoCrAlY coating, lessened corrosion and oxidation resistance at 900°C and above, and the possibility of detrimental sigma phase formation within the substrate superalloy. Therefore, while it might be possible to reformulate CoCrAlY (or some other metallic coating) to include molten vanadate corrosion resistance, it must be borne in mind that the requirements for molten sulfate and vanadate protection, for oxidation resistance, and for appropriate physical properties of the coating are complex, and in some instances conflicting. Another point to recall is that CoCrAlY essentially represents the culmination of more than 40 years of development of metallic coatings for gas turbines, and that the potential for further improvement in metallic coatings may be limited.

For these reasons, a part of the Navy's effort in gas turbine material development is being turned to ceramics as a potential new material for gas turbine coatings. Contracts have been awarded by NAVSEA to the Garrett Auxiliary Power Division of Allied-Signal Aerospace Co. (formerly Garrett Turbines) and to General Electric for the development of vanadate-resistant ceramic coatings for use on blades in Navy shipboard gas turbines. The Navy interest is spurred also by NASA development of stabilized zirconia for use as thermal barrier coatings in aero gas turbines, where many of the problems associated with ceramic blade coatings such as coefficient of thermal expansion mismatch, thermal fatigue and spalling, and bond coat oxidation appear to have been solved. The NRL research reported below, which has identified scandia as a corrosion-resistant stabilizer for zirconia, was conducted in support of the NAVSEA program for development of ceramic coatings for shipboard gas turbines.

SCANDIA AS A CORROSION-RESISTANT STABILIZER FOR ZIRCONIA

It seems paradoxical to propose zirconia as a molten vanadate-resistant gas turbine coating, when yttria-stabilized zirconia (YSZ) is well known to be degraded by vanadium impurities in fuel. But we must note that, while YSZ is attacked by certain molten vanadates, it has not been shown that the rate of attack is greater than that of metallic CoCrAlY under the same conditions. Indeed, preliminary burner rig tests (4) indicate that YSZ is significantly less degraded than CoCrAlY by low concentrations of vanadium in 1% sulfur-containing fuel. Other burner rig tests (5) also show YSZ to be substantially more resistant to combined SO_3/Na_2SO_4 attack at 700°C (i.e., "low temperature hot corrosion") than CoCrAlY.

In addition, closer study reveals that the critical step in YSZ degradation is the reaction between the Y_2O_3 component of YSZ and V_2O_5 from the vanadate melt, which is essentially a Lewis acid-base reaction, viz

$$Y_2O_3 \text{ (base)} + V_2O_5 \text{ (acid)} = 2\ YVO_4 \text{ (salt)} \qquad [1]$$

The acid-base nature of reaction [1] was demonstrated in experiments (6) which examined the reaction of the various vanadates and V_2O_5 with the different ceramic oxides. The results are summarized in Table 1, where the acidity (i.e., V_2O_5 activity) of the vanadium compounds increases from Na_3VO_4 to V_2O_5, and the acidity of the ceramic oxides from Y_2O_3 (most basic) to Ta_2O_5 (most acidic).

Table 1

Reaction Behavior of Ceramic Oxides with Vanadium Compounds of Increasing V_2O_5 Activity, Showing Products Formed

	Na_3VO_4	$NaVO_3$	V_2O_5
Y_2O_3	NR*	YVO_4	YVO_4
CeO_2	NR	NR	$CeVO_4$
ZrO_2	NR	NR	ZrV_2O_7 (but slowly)
GeO_2	$Na_4Ge_9O_{20}$	$Na_4Ge_9O_{20}$**	NR
Ta_2O_5	$NaTaO_3$	$Na_2Ta_4O_{11}$	alpha-$TaVO_5$

* NR = no reaction
** As ppt from H_2O solution

The reactions in Table 1 follow classical acid-base behavior, with acids reacting with bases, and vice versa, but no reaction occurring between compounds of comparable acid-base strength. For example, note that $NaVO_3$ reacts as an acid with basic Y_2O_3 but as a base with acidic GeO_2 and Ta_2O_5. More importantly, Table 1 shows that ZrO_2 itself is resistant to reaction even with pure V_2O_5, and that vanadate-resistant zirconia engine coacings should be possible if a more acidic ceramic oxide than Y_2O_3 could be found for use as a stabilizer for zirconia.

Following this hypothesis, we identified scandia (Sc_2O_3) as a potential corrosion-resistant stabilizer for zirconia. Scandia is the most acidic of the rare earth oxides (7) and is an effective stabilizer for zirconia (8); that is, low percentages of scandia (5-7 mole-percent) added to zirconia stabilize the tetragonal zirconia structure, and prevent the catastrophic tetragonal-to- monoclinic phase transformation that normally occurs when pure zirconia is cycled between high and low temperature. The following experiments were then conducted to confirm that scandia in fact provides a vanadate-resistant stabilized zirconia, and to give some indication of the improvement in corrosion resistance that might be expected for scandia-stabilized zirconia (SSZ) over yttria-stabilized zirconia.

TESTS CONFIRMING VANADATE-RESISTANCE OF SCANDIA-STABILIZED ZIRCONIA

The tests were performed in a progressive manner, looking in order at:

1) the chemical reactions of pure scandia
2) the resistance of laboratory-prepared sintered SSZ pellets vs. sintered YSZ pellets to molten $NaVO_3$ at 700° and 900°C
3) and then (as a preliminary to preparation of plasma sprayed zirconia coatings), the performance of SSZ vs. YSZ plasma spray powders against high temperature mixtures of $NaVO_3/V_2O_5$, and $NaVO_3/Na_2SO_4$ under different SO_3 partial pressures.

Chemical reactions of scandia with vanadium compounds and SO_3/Na_2SO_4

Scandia was tested, in the same manner as in Table 1, for chemical reaction with vanadium compounds at 700° and 900°C. X-ray diffraction showed that $NaVO_3$ produced some $ScVO_4$ formation at 700°, but none at 900°C; with V_2O_5, formation of $ScVO_4$ occurred at both temperatures. Scandia is thus confirmed to be more acidic than Y_2O_3 (which forms YVO_4 readily at both 700° and 900°C at the V_2O_5 activity associated with $NaVO_3$), but still sufficiently basic that some $ScVO_4$ formation occurs with $NaVO_3$ at 700°, although not at 900°C.

Yttria can be leached from YSZ by other reactions than the yttrium vanadate reaction. One such reaction is a mixed sulfate formation, which is also a Lewis acid-base reaction but with SO_3 as the acid, and which can be written as

$$Y_2O_3(\text{in } ZrO_2) + 3\ SO_3 + Na_2SO_4 = Y_2(SO_4)_3\text{-}Na_2SO_4(\text{as mixed sulfate}) \qquad [2]$$

To test the extent that a similar reaction might occur with scandia, 50 mole-percent mixtures of Y_2O_3-Na_2SO_4 and Sc_2O_3-Na_2SO_4 were brought to equilibrium at different temperatures under air containing 13 Pa of equilibrated SO_2-SO_3 (chosen as approximately equivalent to the SO_2-SO_3 partial pressure in gas turbines burning moderately sulfur-contaminated fuel). The degree of sulfate formation was calculated from the weight gain of the mixtures, in accordance with reaction [2]. Complete sulfation of the oxide corresponds to 50 mole-percent sulfate formation. As seen in Fig. 1, Y_2O_3 is essentially completely sulfated even at 800°C (46.3 mole-% sulfate formation, 93% conversion of oxide). Scandia, on the other hand, gives only 9.9 mole-percent sulfate formation (20% oxide conversion) at 700°, and only 0.3 mole-percent sulfate formation (0.6% oxide conversion) at 800°C. These results confirm that Sc_2O_3 acts as a stronger acid than Y_2O_3 in reaction with SO_3, and indicate that SSZ should be significantly more resistant to degradation via a sulfation mechanism than YSZ, especially above 800°C.

Reaction/destabilization behavior of SSZ vs. YSZ ceramic pellets against $NaVO_3$ at 700° and 900°C

Sintered pellets of Sc_2O_3(5wgt-%)-ZrO_2 and Y_2O_3(8wgt-%)-ZrO_2 were subsequently prepared for us by Dr. Jay Wallace (formerly of the Ceramics Branch, NRL, and now at NIST), using identical techniques of preparation. Both sets of pellets were essentially 100% tetragonal as prepared, which verifies the effectiveness of Sc_2O_3 as a stabilizer for ZrO_2. When these pellets were coated with 10 mg/cm^2 of $NaVO_3$ and heated at 700°, the YSZ pellets reacted strongly with the $NaVO_3$, producing large quantities of YVO_4 crystals on the ceramic surface (Fig.

2), and giving extensive destabilization of the YSZ tetragonal structure. Conversely, the $NaVO_3$ film on the SSZ pellets remained effectively unreacted (Fig. 2), with little evidence of SSZ destabilization after long periods at 700°C. No indication of $ScVO_4$ was seen, even though some $ScVO_4$ formation was found above in $NaVO_3$ reaction with pure Sc_2O_3 at 700°C. This is not inconsistent, however, since the activity of Sc_2O_3 in solid solution in ZrO_2 would be lower than with pure Sc_2O_3.

In the 900° experiments, $NaVO_3$ was deposited onto the YSZ and SSZ pellets by a vapor deposition method where the pellets were supported over a boat containing molten $NaVO_3$ during the furnace exposure. At the end of the run, the vanadate films were gently washed from the pellet surfaces, and the pellet surfaces x-rayed. The x-ray diffraction pattern from SSZ (Fig. 3) showed only the tetragonal ZrO_2 peaks (marked T in Fig. 3), and no evidence of $ScVO_4$, establishing that the scandia-stabilized zirconia was not attacked or destabilized. The yttria-stabilized zirconia, in contrast, was strongly attacked and destabilized, with the x-ray diffraction pattern showing large YVO_4 (marked Y) and monoclinic ZrO_2 (marked M) peaks and much diminished tetragonal ZrO_2 peaks.

Resistance of SSZ vs. YSZ plasma spray powders to mixed $NaVO_3$-V_2O_5-Na_2SO_4 salts

While SSZ is thus superior to YSZ in resistance to molten $NaVO_3$, the deposits encountered in engines will not be $NaVO_3$, but rather complex sulfate/vanadate mixes. Fuels containing vanadium will also likely contain sulfur, and depending on the relative amounts of Na, S and V ingested, certain activities of Na_2O, SO_3, and V_2O_5 will be produced in engine gas. The SO_3 and V_2O_5 will then compete for reaction with Na_2O in the deposit formation process. Under marine gas turbine conditions, the equilibrium reaction determining the blade deposit composition, as shown by Luthra and Spacil (9), is expected to be

$$2\ NaVO_3 + SO_3 = V_2O_5 + Na_2SO_4 \qquad [3]$$

For fixed Na/V ratios, an increased SO_3 partial pressure in the engine will tend, e.g., to increase the V_2O_5 activity in the $NaVO_3$-V_2O_5-Na_2SO_4 melt on the blade surface.

Experiments were therefore conducted to evaluate the resistance of plasma spray powders of SSZ and YSZ (obtained preliminary to the production of plasma sprayed zirconia test coatings) to sulfate/vanadate mixes intended to simulate engine deposits. For these tests, the SSZ (7 mole-percent Sc_2O_3, 90% tetragonal as received) and YSZ (8 wgt-percent Y_2O_3, 100% tetragonal) powders were exposed (using 0.6 g ceramic to 0.6 g salt mix) to $NaVO_3$-V_2O_5 mixtures, or $NaVO_3$-Na_2SO_4 mixtures under equilibrated SO_2-SO_3 in air, at 700 and 900°C.

The destabilization rates were monitored during these tests, with the degree of destabilization at the various times being estimated by

$$\%\ \text{destabilization} = \frac{M}{(M + T)} \qquad [4]$$

where M is the monoclinic $(11\bar{1})$ peak height at 28.2° in Fig. 3, and T is the tetragonal (111) peak height at 30.2°. Equation [4] gives nearly quantitative results for simple mixtures of tetragonal and monoclinic zirconia (10). In

the present case, the 50% salt contained in the x-ray specimens causes interferences, so that the individual % destabilization data points can only be considered as qualitative. The behavior trends are highly consistent, however, and provide informative insight concerning the destabilization kinetics.

Table 2 summarizes the results obtained in experiments where the SSZ and YSZ spray powders were mixed with $NaVO_3$ containing progressively increasing mole-fractions of V_2O_5 and heated at 700 and 900°C for up to 300 hrs.

Table 2

Destabilization Behavior and Products Formed for Yttria- and Scandia-Stabilized Zirconia Powders Reacting with Melts of Different $NaVO_3$-V_2O_5 Compositions

Salt Composition	YSZ	SSZ
$NaVO_3$	DS, YVO_4	no DS
10 m/o V_2O_5 in $NaVO_3$	--	no DS
15 m/o V_2O_5 in $NaVO_3$	--	DS starting, $ScVO_4$
20 m/o V_2O_5 in $NaVO_3$	--	DS, $ScVO_4$
NaV_3O_8 (50 m/o V_2O_5-$NaVO_3$)	DS, YVO_4	DS, $ScVO_4$
V_2O_5	DS, YVO_4, ZrV_2O_7 at 700, but not 900°C	DS, $SCVO_4$, ZrV_2O_7 at 700, but not 900°C

DS = destabilization

The data in Table 2 are explainable in terms of acid-base reaction behavior. Yttria is sufficiently basic that it forms YVO_4, with destabilization of the zirconia resulting, at the V_2O_5 activity associated with pure $NaVO_3$. Scandia on the other hand, being more acidic, requires about 15 mole-percent excess V_2O_5 before $ScVO_4$ formation and destabilization commences. And finally zirconia is the most acidic and reacts only with pure V_2O_5, and then not strongly, as evidenced by the instability of the ZrV_2O_7 product at 900°C.

The effect of SO_3 in the corrosion environment was then examined by exposing YSZ and SSZ to combinations of $NaVO_3$ and Na_2SO_4 while having different partial pressures of SO_2-SO_3 in the furnace gas. The results can be described as follows: Neither SSZ or YSZ was destabilized by being mixed with pure Na_2SO_4 and exposed at 800°C under equilibrated SO_x (where $SO_x = SO_2 + SO_3$) partial pressures as high as 150 Pa. This indicates that sulfation or mixed sulfate formation per se is not a controlling reaction in the destabilization process for either SSZ or YSZ (except perhaps for very high SO_3 partial pressures). In tests with 50 mole-percent $NaVO_3$-Na_2SO_4 under air containing no SO_3, SSZ was not attacked, but YSZ was rapidly destabilized at 850°C (cf. Fig. 4). Evidently the V_2O_5 activity at 850°C, even when the salt mixture contains 50 m/o Na_2SO_4, is high enough to react with the Y_2O_3 in YSZ, but not high enough to react with Sc_2O_3 in SSZ.

Experiments to determine the highest SO_3 partial pressures that scandia-stabilized zirconia could tolerate without destabilizing produced these

results: With both pure $NaVO_3$ and 50 m/o $NaVO_3$-Na_2SO_4 at 700 and 800°C, destabilization occurred within 24-48 h at SO_x partial pressures as low as 5 Pa (the lowest partial pressure obtainable in our gas control system as currently configured). However, with 50 m/o $NaVO_3$-Na_2SO_4 at 850°C, SSZ withstood (Fig. 4) up to 25 Pa SO_x for 100 h without any indication of destabilization, although destabilization did commence at about 48 h with 125 Pa SO_x. (Note: the SSZ was 90% tetragonal, or 10% "destabilized", as received, but simply mixing with $NaVO_3$ (in its HT form) perturbs the zirconia peaks so as to indicate about 15% destabilization even at time = 0.)

The SSZ behavior in Fig. 4 can also be explained in oxide acid-base terms. The critical factor in destabilization is the V_2O_5 activity, which is diminished by addition of Na_2SO_4, but increased by the SO_3 overpressure according to reaction [3]. Raising the temperature tends to prevent destabilization in two ways: first, the equilibrium reaction, $SO_3 = SO_2 + 1/2\ O_2$, moves to the right as temperature increases, with the SO_3/SO_2 ratio in air decreasing from 1.09 at 700° to 0.22 at 850°C (11), and second, a higher V_2O_5 activity is required, as the temperature increases, for the $ScVO_4$ formation that leads to destabilization of SSZ (cf. Table 2). Scandia-stabilized zirconia can then be expected to be stable at the higher engine operating temperatures, and with high Na to V contaminant ratios, and not excessive sulfur in the fuel; at lower temperatures, and with high V and S, SSZ may be destabilized, but in either case, SSZ should be substantially more resistant than YSZ to molten vanadate/sulfate corrosion.

CLOSURE

Further furnace and burner rig tests are planned, using plasma sprayed SSZ coatings on coupons and burner rig test pins, to quantitatively define the limits of temperature and Na, S and V contaminant fuel levels that can be tolerated by scandia-stabilized zirconia coatings. The thermal shock resistance and other thermomechanical properties of SSZ will also be studied. If these prove acceptable, engine testing of scandia-stabilized zirconia coatings will be recommended.

Scandia is expensive, and currently costs about the same as platinum ($20/g). However, platinum itself is used in gas turbine blade coatings, as, for example, in the commercially successful, and widely used platinum-augmented aluminide coatings. In these coatings, a platinum underlayer approximately 0.3 mils (7.5 microns) thick is deposited onto the blade prior to aluminization, with the platinum cost being about $0.32/cm^2 of coating. On the other hand, the cost for Sc_2O_3 in a Sc_2O_3(7m/o)-ZrO_2 coating of 10 mils (250 microns) thickness would be $0.20/cm^2, and only $0.10/cm^2 for a 5 mil coating, which is of the order of coating thickness used in many marine gas turbines. Although measures would be required for recovery of the SSZ ceramic in plasma spraying, etc., the additional materials cost for SSZ coatings thus should not be prohibitive, especially considering the potential benefits of a vanadate-resistant blade coating to the Navy in fuel cost savings, increased availability of fuel, and insurance against engine damage by low quality fuel use in emergency situations.

Finally, the Lewis acid-base approach appears to be a powerful technique for understanding the reactions of oxide ceramics. It could well be useful in other ceramic problem areas such as the prediction and prevention of

interaction between ceramic (or metal) fibers and ceramic matrices in composite ceramics for future ultra-high temperature aerospace engines.

ACKNOWLEDGEMENTS

This research was sponsored under the Gas Turbine Component Improvement Task of the NAVSEA Ship Propulsion Technology Program, and the support is gratefully acknowledged. Thanks are also due to Dr. Jay S. Wallace for preparation of the scandia- and yttria-stabilized zirconia test pellets.

REFERENCES

1. L. Aprigliano, in "Proc. of the Workshop on Gas Turbine Materials in a Marine Environment. Vol 1.", Paper 5, Session I, UK-US Navy, Bath, UK (November 1984).
2. M. Seiersten and P. Kofstad, in "Advanced Materials Research and Development for Transport. Ceramic Coatings for Heat Engines," p. 191-199, Les editions de physique, Les Ulis, France (November 1985).
3. R. L. Jones and C. E. Williams, Matls. Sci. and Engr. **87**, 353 (1987).
4. R. L. Clarke, DTNSRDC-Annapolis, personal communication.
5. Unpublished DTNSRDC-Annapolis and industry data.
6. R. L. Jones, C. E. Williams and S. R. Jones, J. Electrochem. Soc. **133**, 227 (1986).
7. M. C. Sneed and R. C. Brasted, in "Comprehensive Inorganic Chemistry. Vol. Four," Van Nostrand, New York, p. 168 (1955).
8. R. Ruh, H. J. Garrett, R. F. Domagala and V. A. Patel, Am. Ceram. Soc. **60**, 399 (1977).
9. K. L. Luthra and H. S. Spacil, J. Electrochem. Soc. **129**, 649 (1982).
10. H. K. Schmid, J. Am. Ceram. Soc. **70**, 367 (1987).
11. K. H. Stern and E. L. Weise, in "High Temperature Properties and Decomposition of Inorganic Salts. Part 1. Sulfates" NSRDS-NBS 7, National Bureau of Standards, Washington, DC p. 4 (1966).

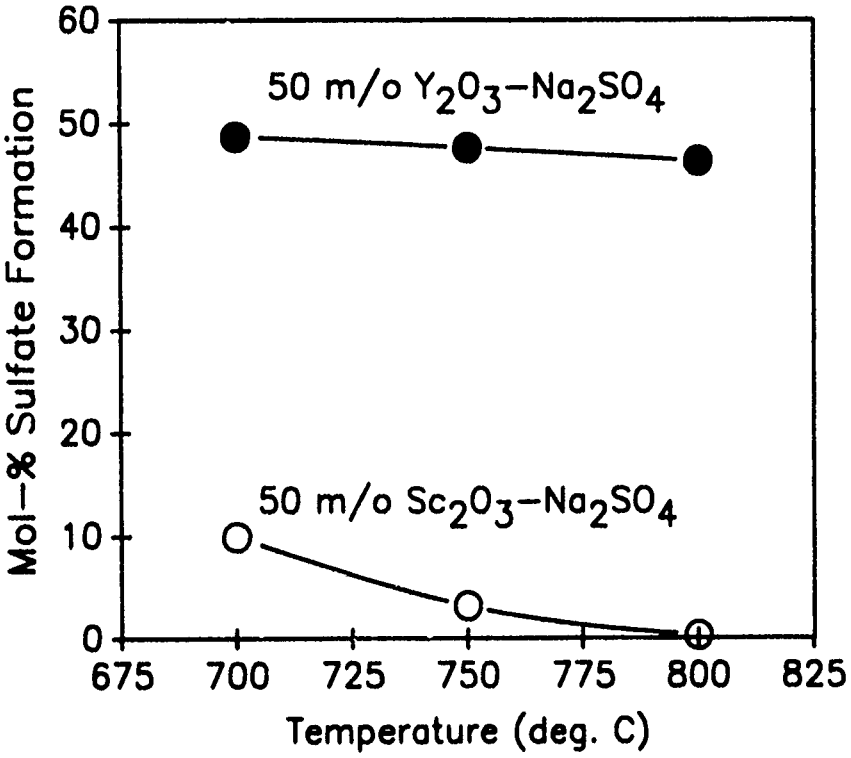

Fig. 1 Sulfation behavior of 50 mole-percent Y_2O_3-Na_2SO_4 vs. 50 mole-percent Sc_2O_3-Na_2SO_4 under 13 Pa of equilibrated SO_2-SO_3 in air at 700°C.

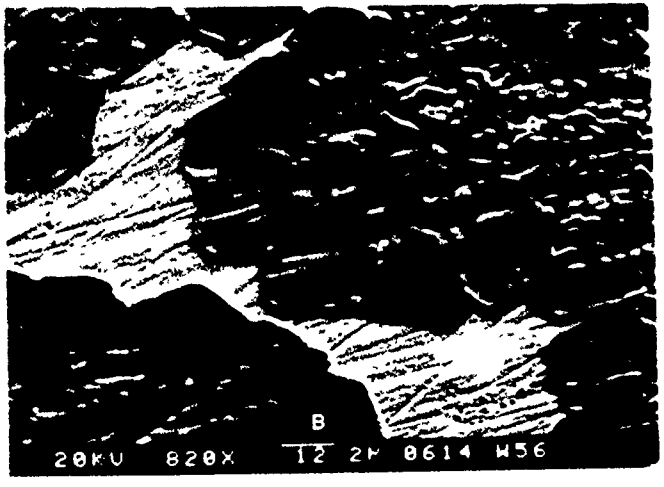

5 w/o Sc_2O_3-ZrO_2

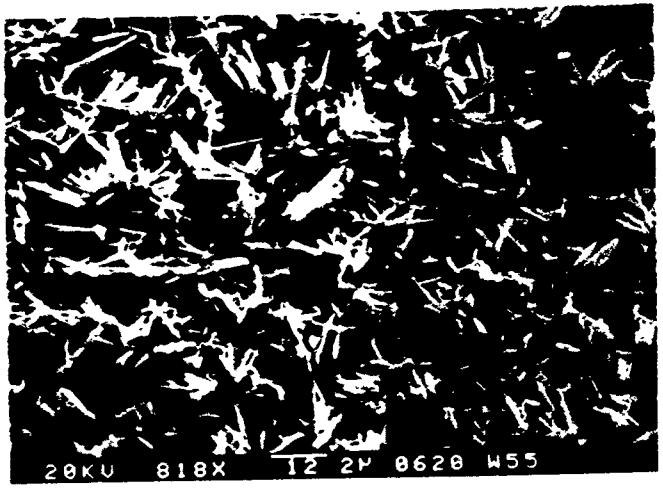

8 w/o Y_2O_3-ZrO_2

Fig. 2 Surface of scandia-stabilized (SSZ) and yttria-stabilized (YSZ) pellets coated with 10 mg/cm^2 of $NaVO_3$ and exposed 475 h at 700°C. Compare unreacted $NaVO_3$ film on SSZ with massive YVO_4 crystal formation on YSZ.

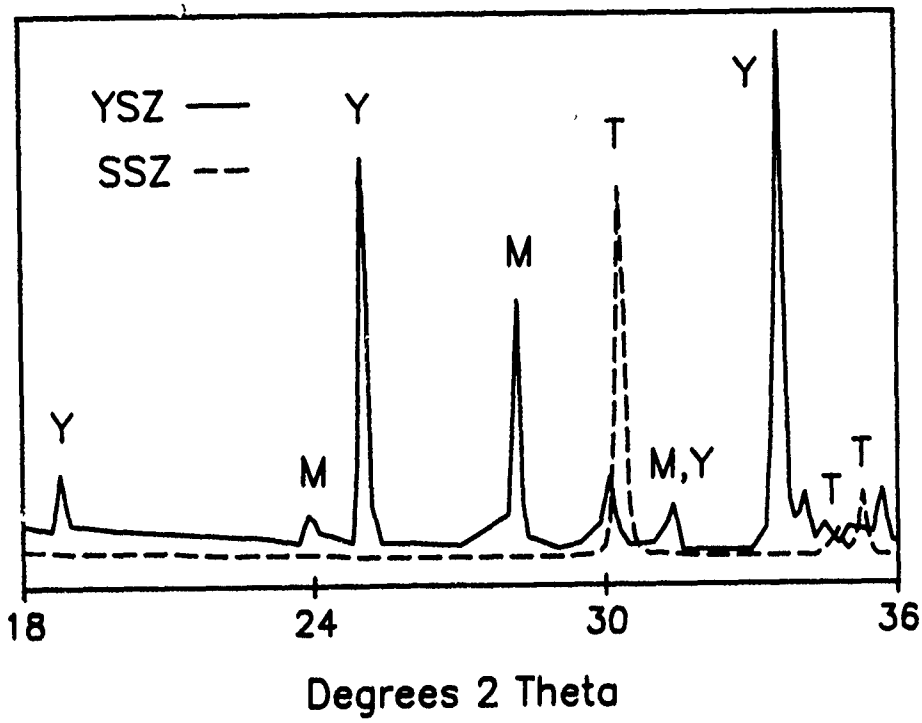

Fig. 3 X-ray diffraction patterns from SSZ and YSZ pellets after 175 h exposure to 900°C $NaVO_3$. See text for explanation of peak labels.

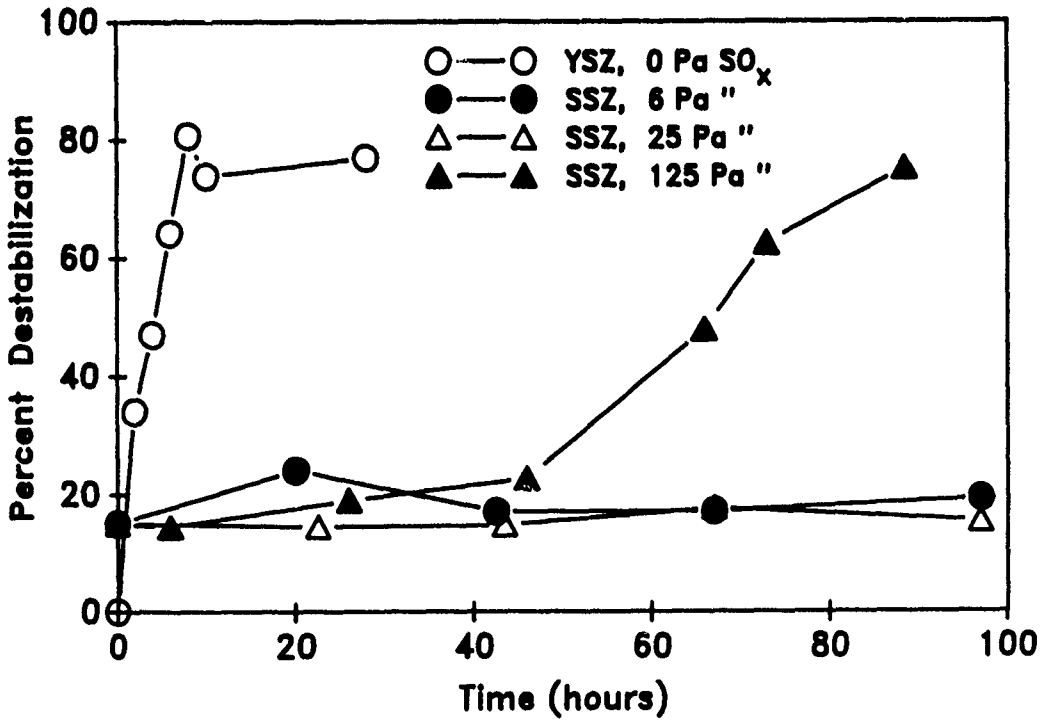

Fig. 4 Influence of SO_x (SO_x = SO_2 + SO_3) in air on destabilization of SSZ and YSZ in 50 mole-percent $NaVO_3$-Na_2SO_4 at 850°C. See text.

FAILURE ANALYSIS IN CARTRIDGE-PNEUMATIC STARTER BREECH CHAMBERS

D.M. Egle, A.S. Khan, R.D. Daniels, A.G. Striz
School of Aerospace and Mechanical Engineering
University of Oklahoma
Norman, Oklahoma

and A.B. Gillies
Oklahoma City Air Logistics Center
Tinker Air Force Base, Oklahoma

ABSTRACT

Premature failures in the breech chambers of cartridge-pneumatic starters occur infrequently but the damage that ensues is extensive enough to warrant serious concern. These failures have occurred well below the manufacturer's rated life of the chambers and in some cases after only a few firings.

Factors which might affect the failures are: (1) inaccurate knowledge of stresses existing in the chambers, (2) pressure overloads due to rapid burning of flawed cartridges, (3) higher than expected temperatures encountered in the combustion process and (4) stress corrosion cracking, perhaps aided by residual stresses, occurring between firings and significantly shortening the life of the chambers.

A comprehensive study was undertaken to determine which of these factors were involved in the failures. Finite element analyses, as well as service pressure, temperature, and residual stress measurements were performed on both used and unused chambers. Acoustic emission, ultrasonic, and eddy current NDT methods were explored to locate potential failure origins.

The results showed that FEM predicted stresses were within 15% of measured values at normal pressures and temperatures. Dynamic pressure measurements in the chambers during firings showed normal to below normal values apparently due to variations in the burning characteristics of the cartridges. Although residual stresses were negligible, moisture was shown to accelerate the corrosion process brought on by the presence of the combustion residue in the chamber. NDT techniques were shown to be capable of locating pitting from the outside of the chamber.

I. INTRODUCTION

Cartridge-pneumatic starters are mechanical systems used to accelerate jet engine rotors to a speed sufficient for starting the engine[1]. The starters are used in two modes: first the cartridge mode, in which a rapidly burning charge is ignited within a closed chamber(breech chamber) and the expanding gasses are used to provide the energy to rotate the engine; and secondly, the pneumatic mode, in which air from another engine or ground support compressor provides the necessary energy. The cartridge mode has two distinct advantages: it is self-sufficient, thus independent of ground support, and it provides quick start capability.

In recent years, premature failures in breech chambers have been prevalent enough to cause concern. Metallurgical studies[2,3] have identified stress-corrosion cracking in the 4340 steel forged chambers as a possible failure mechanism. These failures have occurred at a number of firings well below the manufacturer's rated life and occasionally have occurred after only a few firings.

The goal of the work reported here was to provide a comprehensive analysis of the starter breech chamber to determine the cause or causes of failure and to suggest a solution for preventing the failures. In addressing this goal, the following tasks were conducted:

1. The temperatures, pressures, and selected stresses which occur in the chambers during firings were measured.

2. A finite element stress analysis using the actual pressures and temperatures in the chambers was conducted.

3. The propensity of the material to initiate and propagate cracks under the combined influence of stress and corrosive residue left after firing was determined. The likelihood of stress corrosion cracking occurring between firings was addressed.

4. Residual stresses in new and used chambers were measured.

5. A defect detection technique to locate flaws which may have grown in the chambers as a result of use or storage was sought.

6. An algorithm for predicting the remaining life in a chamber was developed.

II. RESIDUAL STRESS MEASUREMENT

Concern about the role of residual stresses which may arise from manufacturing or from service induced loads led to an experimental study of the residual stresses in both used and new chambers. The technique chosen for this study was the hole-drilling method, a semi-destructive method for measuring the residual stresses near the surface of a material. The method requires the placement of a three element strain gage on the surface, drilling a small hole at the center of the gages, and measuring the relaxation strains induced by the drilled hole. The require.nents of the hole-drilling method are spelled out in an ASTM standard[4].

Both the finite element analysis and previous examinations of failed chambers indicated

that the highest stresses occurred on the inside surface of the chambers. A procedure was established for removing the heat shields by carefully machining the welds bonding the shields to the chambers. A special fixture was designed and constructed to drill the hole in the chamber from the inside surface while maintaining the drill normal to the chamber wall. A drawing of the hole-drilling fixture is shown in figure 1. A small air turbine drill, which was designed for dental uses and which was capable of up to 350000 rpm, was used to drill the holes. Use of the high speed and dental burrs have been shown to minimize the effect of induced machining strains. Further details of the hole-drilling fixture and techniques used in this study are available in the literature[5].

To calibrate the technique and to determine the effects of several potential error inducing factors on the accuracy of the residual stress measurements, several preliminary experiments were conducted. Four mild steel specimens(0.103 x 1.45 x 12 in) were annealed at a temperature of 475 ° F for three hours to relieve residual stresses. These four specimens were used to evaluate the effects of machining strains. During these experiments, the largest induced strain was observed to be 31 μs but the average absolute value of all the induced strains was 16 μs. With this evidence, the inaccuracy in stress due to induced machining strains may be assumed to be less than about 1 ksi.

Several flat specimens(0.090 x 2 x 14 in) were machined from a 0.5 x 4 in bar of 4340 steel and heat treated commercially to hardness of Rc 43. These specimens were used to determine the calibration constants used in the residual stress measurement algorithm(1). An analytical technique for estimating these calibration constants[6] was also used to check the measured values. The two sets of constants agreed to within 10%.

All residual stress measurements were corrected for the drilled hole offset. Although precautions were taken to reduce the offset, errors on the order of 0.005 in could not be avoided. The offset was measured by microscope after the hole was drilled and the residual stress calculations corrected[7] for the offset.

Table 1. Results of the Residual Stress Measurements.

Chamber No.	Distance from Chamber Center (in)	Principal Residual Stresses (psi)	
2 (used)	1.69	2580.	2060.
2 (used)	2.69	830.	1820.
7 (new)	1.65	530.	350.
7 (new)	2.60	210.	2220.
7 (near nozzle)	2.63	-75.	2300.
3 (after failure) (near nozzle)	2.63	34042.	19182.

Residual stresses were measured at locations in three different chambers. The results are shown in Table 1. The first four measurements on chambers 2 and 7 were made at the indicated radii approximately 180° from the exit nozzle. The last two measurements were made in the vicinity of the nozzle. The measurement on chamber 3 was made after it had been fired several times and had failed near the exit nozzle. The chamber wall had bulged but was not cracked; however a crack was evident near the weld in the nozzle.

Aside from the measurement in the failed chamber, the results indicate that the levels of residual stresses in the chambers were very small and would have a negligible effect on the failure of a chamber.

III. STRAIN AND TEMPERATURE MEASUREMENT

The gas pressure and the temperature at various locations in a chamber were measured during firing of the cartridge. A breech starter assembly and nozzle ring were permanently supported in a test cell suitable for firing and discharge of the hot gasses. A pressure transducer built from a steel tube and four 5 mm single element strain gages, arranged in a four active arm Wheatstone bridge, was used to sense the pressure in the chambers. After being amplified with a single conditioner, the output of the pressure transducer was recorded with a strip chart recorder or digital transient recorder.

Solid wire thermocouples located on the outer surface and in the bottom of a 0.080 in deep drilled hole were used to measure the temperature on the outer and near-inner surface of the chamber. The thermocouples were bonded to the surfaces with a ceramic cement capable of withstanding temperatures up to 2800 °F. The thermocouple output was monitored directly with a strip chart recorder.

Strain measurements were also made on some of the tests. Three element rectangular rosettes were mounted on the outer surface of the chamber with epoxy based cement. Each of the gages were connected in a single active arm bridge with three passive resistors. The output of the bridges, after being amplified with a suitable signal conditioner, were recorded with a strip chart recorder or with a digital transient recorder.

Typical results for temperature, pressure and stress are shown in figure 2. The values shown in the inset of figure 2a are maximum temperatures which were recorded after the firing cycle was completed. The pressure history reaches its nominal value in approximately one second but may fluctuate somewhat during the remaining cycle time. As shown in figure 2b, the stress history at a point on the outside of the chamber tracks the pressure very well.

IV. FINITE ELEMENT ANALYSIS

Various finite element models were used to compute the stresses in the chamber when subjected to the pressures measured in the tests described above. The chamber was modeled both as an axisymmetric and as a three-dimensional shell structures. Two finite element codes, SAP IV and MSC/NASTRAN, were used to compute the static stresses due to the internal pressure in the chamber[8].

Three different 3-D models were constructed in the course of this study: a coarse mesh model using 2254 nodal points, 380 elements, and one layer through the thickness; a medium mesh model using 2254 nodal points, 526 elements, and two layers through the thickness; and a fine mesh model using 3369 nodal points, 902 elements, and four layers through the thickness at the top of the chamber. A drawing of the final model is shown in figure 3.

Results of the finite element computations are shown in figures 4 and 5. The stress

distributions shown are on the inside and outside surfaces of the chamber dome along a line extending from the apex of the dome toward the side wall in a direction 180° from the nozzle. These locations, especially from 2 to 3 in from the apex, are the approximate positions of the apparent origins of failure detected in the field. Surface stresses measured experimentally are also plotted in the figure for comparison.

The finite element models examined here show good agreement with each other and with the experimental results. The experimental results are within 10% of the FEM calculation on the upper surface and with 15% on the lower surface. The differences are in part due to the differences in thickness of the chambers used in the experiments which were measured to be a few mils thicker than the nominal 0.090 in used in the analysis.

The maximum stresses on both the inside and the outside surfaces occur very close to the region of maximum curvature in the dome of the chamber. This is attributed to the strong bending action caused by the relatively flexible dome being attached to a rather rigid cylinder. Further computations showed that these stresses could be reduced by decreasing the chamber thickness just below the region of intersection.

Thermal effects were also included in some of the calculations. Two different temperature profiles were examined. The first was taken from temperatures measured on the inside and outside surfaces of the dome about 5 sec after ignition in the experimental phase of this project. This temperature profile, shown in figure 6, represents the steepest gradient obtained through the thickness of the dome during the burn. The temperature was assumed to vary linearly through the thickness and was assumed constant on the side wall. The second profile was derived from measurements made about 19 sec after ignition and which showed a negligible thermal gradient through the wall.

Comparisons of the principal stress distributions between the ambient (70 °F) and elevated temperature cases showed different effects of temperature on the stress. The stresses computed for the model with temperature profile 1 showed a reduction of stress on the inside surface and an increase on the outside surface. This is attributed to the counteracting flexural stresses caused by the higher inside surface temperatures. The stresses associated with temperature profile 2 were slightly lower than those in the ambient case.

V. NON-DESTRUCTIVE TESTING FOR DETECTING FLAWS

Acoustic emission tests were conducted on several chambers to determine if cracks in the chambers could be detected during the normal maintenance procedure which included a pressure proof test of the chamber. Tests were conducted on new chambers which had never been installed or fired; on used chambers which were pulled from service at random for these tests and which had been fired but not recently; and 'fired' chambers, a designation for new chambers fired in our facility within a few days of AE testing.

The AE tests utilized a commercial four channel computer based instrument (PAC 4000) which could provide location of the AE sources and could store many thousands of AE events on floppy disk. The transducers used for these tests were 150 kHz resonant units and the signals were filtered in the preamplifiers by bandpassing the frequency range 100 - 300 kHz. The transducers were in all cases coupled to the parts with a viscous resin(Dow Chemical V9) customarily used for this purpose and were held in place with rubber bands.

In all of the AE tests one of the transducers was mounted on an inactive part(block of aluminum) in order to monitor false events due to electromagnetic sources.

The first series of tests simply monitored unpressurized new and used chambers to determine if AE activity could be detected without further stimulus. Two chambers, one new and one used, were alternately monitored for periods ranging from 12 to 96 hours. The results showed considerable AE activity from the used chamber early in the tests with almost no activity from the new chamber. The AE from the used chamber did decrease over the period of one month but remained substantially higher than that from the new chamber. This decrease in activity was attributed to a gradual drying of the combustion residue in the used chamber. Subsequent tests of used chambers subjected to alternate cycles of oven drying and injection of water in the space between the dome and the heat shield led to the realization that the moisture accelerated corrosion process could be 'heard' with sensitive AE equipment.

A second and longer series of tests utilized several new, used, and fired chambers monitored under a variety of conditions. One used chamber was sawn in half to allow comparative test on the two halves under different conditions. Table 2 shows the results of several of these AE tests. It is evident that the oxide layer and the moisture interact to produce the AE signals. An analysis of the signal levels and energy indicate that there are a few high energy signals apparently associated with a cracking mechanism, probably with cracking of the oxide layer but possibly due to stress corrosion cracking, and a larger number of signals associated with a corrosion mechanism.

Table 2. Results of the Split Chamber AE Tests.

No.	Experiment	Half	Events	Counts	Time	Counts/hr
1	Chamber split into two	A	9	320	3.8	84.2
	dry halves. No moisture	B	33	2150	3.8	565.8
2	Tap water added to	A	92	3000	18.5	162.2
	both halves	B	83	23000	18.5	1243.2
3	Oxide layer in B	A	46	2850	11.6	245.7
	mechanically removed	B	18	2350	11.6	202.6
4	B washed with Alcanox	A	6	1100	9.2	119.6
	Both halves dried	B	0	0	9.2	0.
5	Both sprayed with	A	20	680	10.5	64.7
	distilled water	B	6	550	10.5	52.4

A procedure using conventional ultrasonic equipment was developed for scanning the dome of the breech chambers with a water-coupled, normal-incidence ultrasonic transducer. Both focussed and plane UT transducers were used. The scanning was accomplished with a three-axis computer-controlled bridge coupled to a custom designed and built mechanism to move the transducer in a circular pattern. A high speed digitizer was used to capture the ultrasonic signals which were transferred to a computer and processed digitally. A computer program was used to control the scanning, capture the date, process it, and store

the data for later use. It was established that a pit with a diameter of 12 mils could be resolved with a focussed 20 MHz transducer.

VI. STRESS CORROSION STUDIES

A continuing concern throughout this project had been the characterization of the environment within the breech chamber that is responsible for the sever corrosion problem on the inside surface of the dome. Removal of the heat shields from several new chambers indicate that the inner surface of the dome is only partially plated with electroless nickel, covering only a fan shaped area about 3 in. in radius about the gas exit nozzle. Heavy pitting of the inside surface is a characteristic of the corrosion process. In some failed chambers, pits as deep as 40-50% of the wall thickness were found, and fracture of the dome was directly related to cracks initiated at the base of the corrosion pits.

Breech chambers cut open for analysis of failures provided samples of the 'corrosion product' residue which is a combination of the products of corrosion of the steel chamber and some of the solid combustion products of the breech chamber cartridges. X-ray elemental analysis on the SEM indicated the presence of chlorine and sulphur but otherwise was not helpful in identifying the compounds present in the residue. X-ray diffraction analysis show the presence of the following compounds: KCl, NH_4NO_3, Fe_3O_4, FEOOH, and $FeCl_2$. The NH_4NO_3 in the corrosion product residue is known to cause stress corrosion cracking in high strength steels. Additionally, the pH of the typical residue is 2.8 indicating that a hydrogen-assisted cracking process is also possible.

The susceptibility of the breech chamber steel(AISI 4340, heat treated to a hardness of R_c 40) to stress corrosion cracking in the environments produced in the chambers was evaluated by a constant extension rate test. The CERT method has been shown to be very effective in determining whether or not a material is susceptible to SCC in a given environment. The method involves application of a constant extension rate on the order of 10^{-5} to 10^{-8} in/sec to a tensile specimen and the determination of the ductility of the specimen subjected to the test environment. Susceptibility to SCC is demonstrated if there is a ductility minimum at a particular extension rate.

Results of the CERT tests of 4340 steel specimens in a paste made from the corrosion product residue are shown in figure 7. The ductility is presented as the reduction in area in the paste normalized by the reduction in area in oil at the same extension rate. The minimum that occurs at a rate of 10^{-6} in/sec indicates that the 4340 is susceptible to stress corrosion cracking in this combustion product residue.

VII. FATIGUE LIFE PREDICTION

The goal of this portion of the project was to integrate the information obtained in the other tasks to predict the remaining life of a chamber. To do this the flaw shape and size must be known. Predictions are based on two types of flaws: a semi-ellipsoidal cavity and a semi-elliptical crack. Stress intensity factors were determined from standard sources[9,10] and a correction factor was calculated from a finite element analysis of a three dimensional semi-ellipsoidal cavity in the chamber. The plane strain fracture toughness was assumed to be 50 $ksi*in^{1/2}$ and a crack growth rate equation of the form

$$da/dN = 4.0786 \times 10^{-9}(\Delta K)^{2.4302}$$

was used, where a is the crack length in inches and ΔK is the amplitude of the stress intensity factor in ksi*$in^{1/2}$.

The calculated iife shows predictably that, as the crack depth to chamber dome thickness increases, the fatigue life decreases. For a crack with a depth to width of 0.2, the critical crack length is less than 0.3 times the depth of the chamber dome. Extensive calculations of the predicted life as a function of crack depth and aspect ratio may be found in the project report[11].

VII. CONCLUSIONS

The maximum stress in the chamber occurs on the inside surface near the intersection of the spherical cap and the cylindrical side wall. For an internal pressure of 1200 psi, the maximum stress is 165 ksi. The elevated temperatures present during firing reduces the maximum stress slightly. The maximum stress could be lowered by redesigning the thickness distribution of the chamber wall.

Measurement made on chambers during firings showed outside to inside wall temperatures ranging from 500 • F to 800 • F and variations from 840 to 1200 psi in the peak pressure. The residue deposited on the chamber dome is highly acidic and contains Ammonium Nitrate and Potassium Chloride. The 4340 steel chamber material is susceptible to stress corrosion cracking in this environment which produces pitting. Cracks initiate at these pits and moisture accelerates and may be necessary for initiation of the corrosion process.

The SCC mechanism can be monitored with acoustic emission and active flaws can be detected at pressures well below the failure pressure. Both ultrasonic and eddy current NDT techniques can detect pitting from the outside of the chambers. The UT is more sensitive and capable of detecting pits as small as 12 mils. A life cycle analysis was developed but more information on fracture toughness and fatigue crack propagation of 4340 in the corrosive environment is needed to make accurate predictions of the life of the chambers.

REFERENCES

1) Anderson, J.A. and Galasinski, C.R., "Jet Engine Starters, Cartridge-Pneumatic," ASME Paper No. 67-GT-49, presented at the ASME Gas Turbine Conference and Products Show, Houston, TX, Mar 5-9, 1967.

2) Coleman, W.R., Block, R.J., and Daniels, R.D., "Corrosion Problems in Aircraft Components -- Case Studies of Failures," Proc 1980 Tri-Service Corrosion Conference, AFWAL-TR-81-4019, vol II, 1981, pp 241-270.

3) Perkins, P.C., Daniels, R.D. and Gillies, A.B.," Failure Analyses of Steel Breech Chambers Used with Aircraft Cartridge Ignition Starters," Analyzing Failures: The Problem and the Solutions, ed., V.S. Goel, ASM, Metals Parks, OH, 1986, pp 143-149.

4) ... "Standard Method for Determining Residual Stresses by the Hole-Drilling Strain-Gage Method," ASTM Designation: E837-81.

5) Koshti, A. and Egle, D.M.,"An Alternate Technique for Implementing Center-Hole Drilling/Residual Stress Measurements," Experimental Techniques, vol 9, no 12, Dec 1985, pp 28-30.

6) Nawwar A.M., McLachlan, K., and Shewchuck, J., "A Modified Hole-Drilling Technique for Determining Residual Stresses in Thin Plates," Experimental Mechanics, vol. 16, no. 6, 1976, pp.226-232.

7) Sandifer, J.P. and Bowie, G.E., "Residual Stress by Blind Hole Method with Off-Center Hole," Experimental Mechanics, vol 18, no 5, 1978, pp 173-179.

8) Striz, A.G. and Brueckner, F.P., "Finite Element Analysis and Redesign of Jet Engine Starter Breech Chamber," ASME Paper No. 86-WA/DE-20, presented at the ASME Winter Annual Meeting, Anaheim, CA Dec 1986.

9) Hertzburg, Richard W., Deformation and Fracture Mechanics of Engineering Materials, Wiley, 1983.

10) Broek, David, Elementary Engineering Fracture Mechanics, Sijthoff and Noordhoof, 1978.

11) Egle, D.M., Khan, A.S., Striz, A.G. and Daniels, R.," A Comprehensive Stress and Life-Cycle Analysis of Jet Engine Starter Breech Chambers," Report on USAF-OCALC Contract F34601-83-C-3448, Report No AMNE-85-5, May 1985.

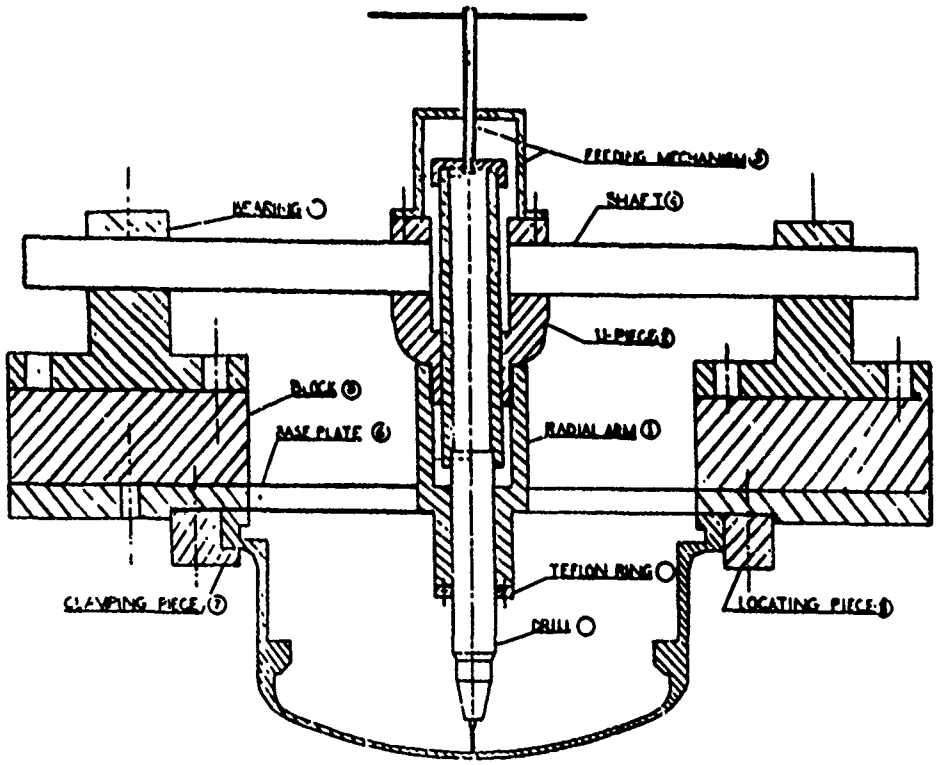

Fig. 1: Hole Drilling Fixture for Residual Stress Measurements.

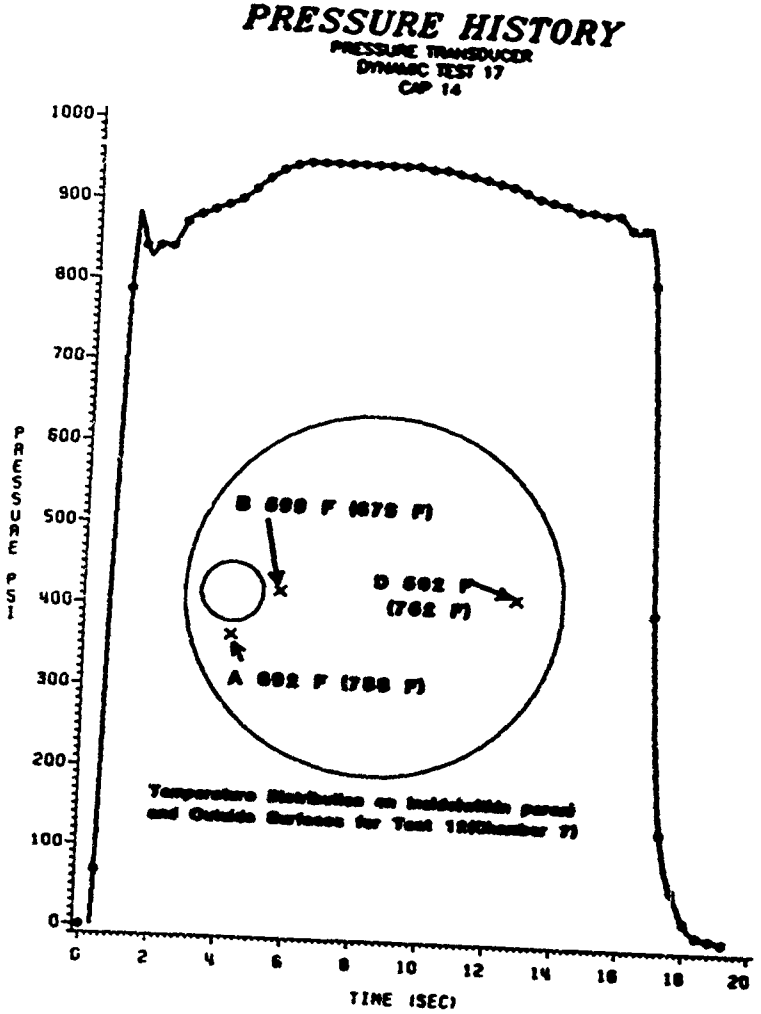

Fig. 2a: Typical Pressure History and Temperature Measurements.

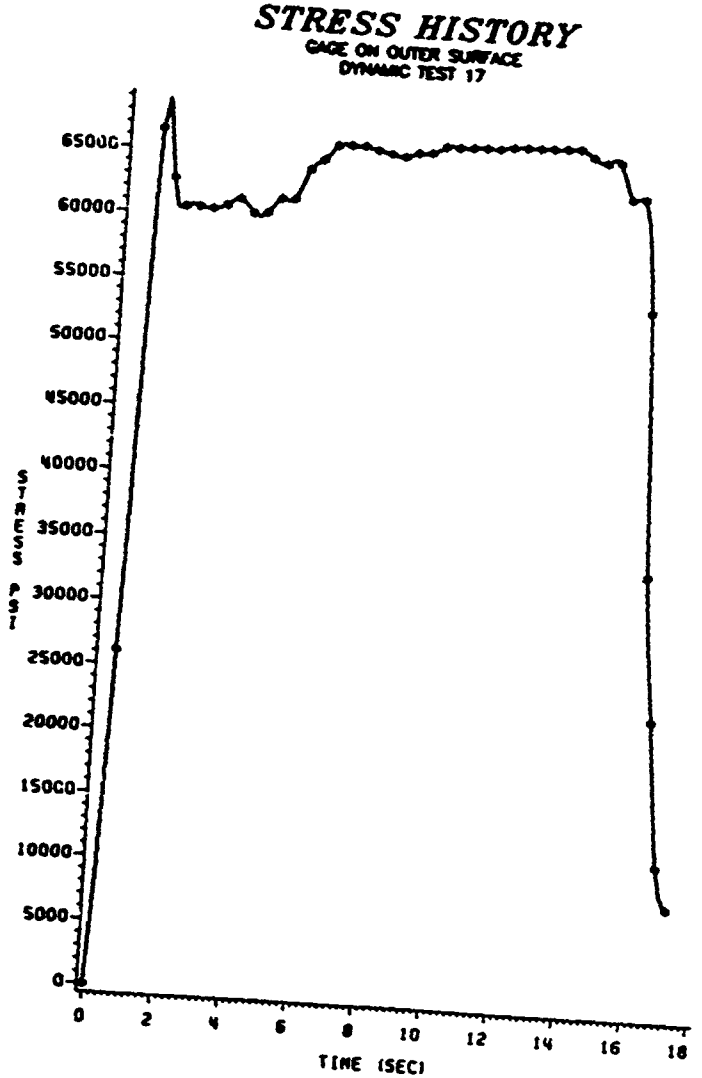

Fig. 2b: Maximum Principal Stress History.

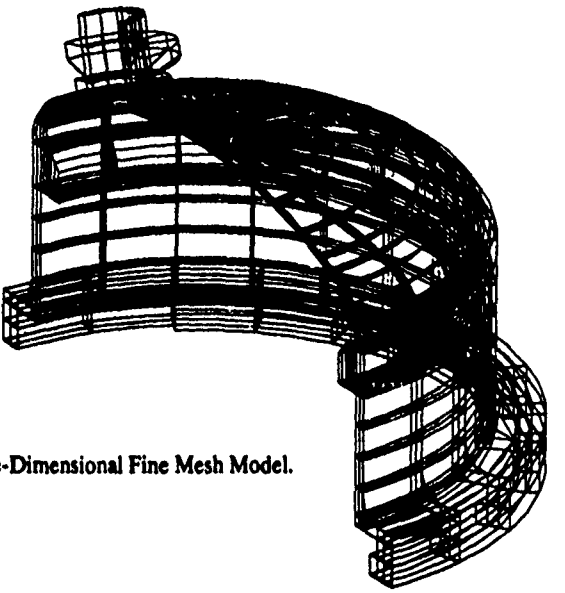

Fig. 3: Three-Dimensional Fine Mesh Model.

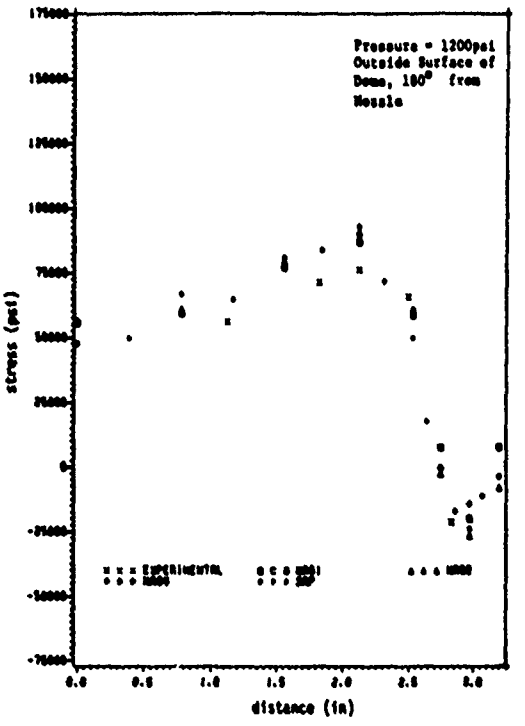

Fig. 4: Comparison of Stress Distributions from Strain Gage Measurements, MSC/NASTRAN and SAPIV FEM on Outside Surface ofDome.

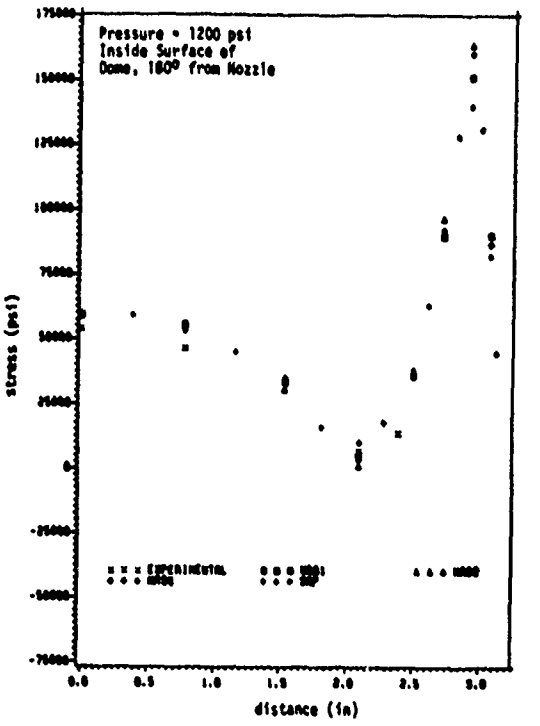

Fig. 5: Comparison of Stress Distributions from Strain Gage Measurements, MSC/NASTRAN and SAPIV FEM on Inside Surface of Dome.

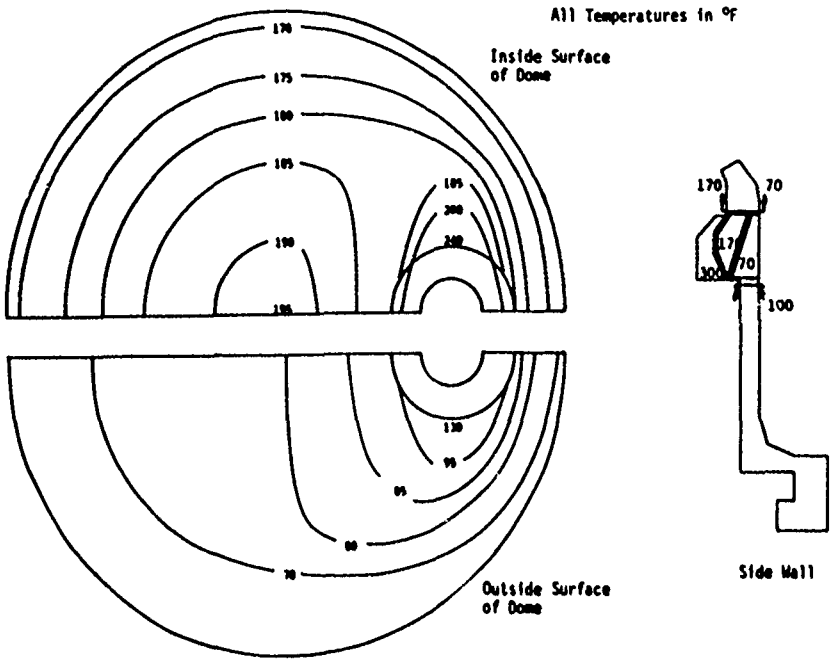

Fig. 6: Temperature Profile 1 for FEM Analysis.

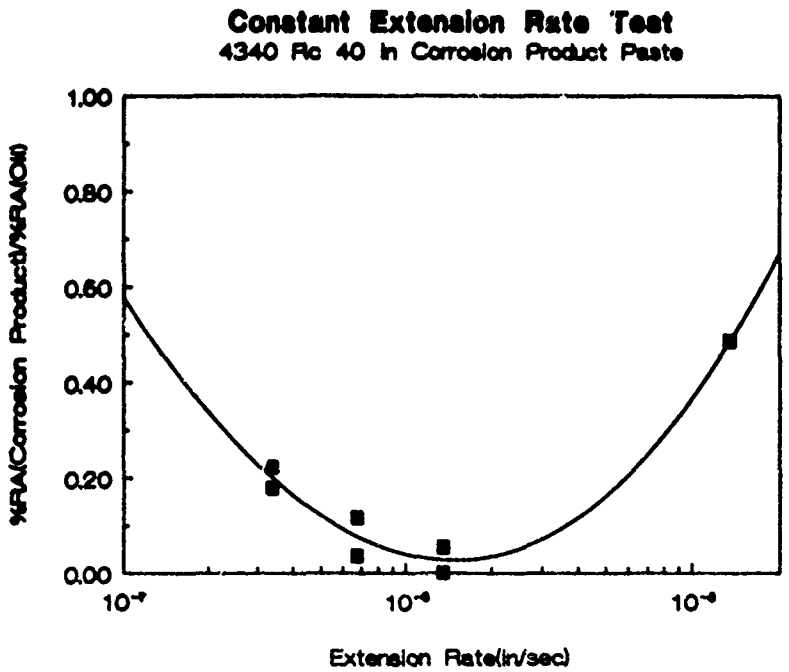

Fig. 7: Constant Extension Rate Test Results.

THE EFFECT OF VOC REGULATIONS ON PROTECTIVE COATINGS USED BY THE NAVY, ARMY, and AIR FORCE

Stephen D. Rodgers
ARINC Research, Inc.
and
James A. Ellor
Ocean City Research Corporation

ABSTRACT

Recently promulgated regulations limit emission to the atmosphere of volatile organic compounds (VOC) from protective coatings. These regulations represent a portion of a large regulatory effort enforcing the Clean Air Act. The VOC regulations have affected the protective coatings specified by the Navy, Army and Air Force. The subject discussion presents a synopsis of the VOC regulatory impact upon the Navy, Army, and Air Force. The discussion is divided into three areas. The first is a summary of VOC regulation having the greatest effect on the military. The second area presents specific, widely used, military coatings or coating procedures affected by the regulation. The third area discusses efforts to comply with the regulations including coating reformulation, coating substitution, and coating process modifications.

[Manuscript Not Available at the Time of Printing]

AN ANALYSIS OF CORROSION PROBLEMS ON THE LACV-30

Patricia Farrell Donahue
ARINC Research Corporation
a Subsidiary of Arinc Incorporated
2551 Riva Road
Annapolis, Maryland 21401

Mario Lipari
U.S. Army Troop Support Command
4300 Goodfellow Boulevard
St. Louis, Missouri 63120-1798

ABSTRACT

During the past 12 years, it has been necessary for the U.S. Army to correct several design deficiencies that were causing extensive corrosion problems on the Lighter Air Cushion Vehicle, 30-Ton (LACV-30). The Army tasked ARINC Research Corporation to analyze the current LACV-30 corrosion-prevention maintenance procedures and replacement materials. The analysis found that many of the vehicle's subsystems were not designed to withstand the marine environment. The analysis also addressed the issues of corrosion-prevention training, depot and field facilities, and resupply of parts. This paper summarizes the analysis and describes techniques for correcting the problems identified. It also presents recommendations for improving the procurement and maintenance of amphibious vehicles.

INTRODUCTION

The Lighter Air Cushion Vehicle, 30-Ton (LACV-30) is an amphibious vehicle capable of transporting 30 short tons of cargo (Figure 1). Its operational role is to convey cargo from supply ships at anchor to shore facilities. Typically operated by a crew of three—operator, navigator, and crewman—the vehicle rides on a cushion of air formed within a neoprene-fabric skirt assembly. It is capable of traversing a variety of terrains, from surf to sand to pavement. Four engines enable it to attain speeds of above 57 miles per hour in calm waters, over a range of 300 miles. The engines drive two lift fans, which fill the skirt assembly with air; and two propellers, which push the vehicle forward. The rudders and propeller pitch provide directional control. The hull is constructed of 15 modular aluminum units joined by rivets. Watertight compartments in the hull give the vehicle its positive buoyancy in water.*

Bell-Textron, which developed the two LACV-30 prototypes for the Army was awarded the contract for the first 12 LACV-30s in 1978. Construction for that purchase was completed in 1983. A second contract was awarded to Bell-Textron in 1981 for another 12 vehicles. The last LACV-30 was delivered to the Army in 1986. The vehicle was purchased as a nondevelopmental item (NDI), although changes were made to the original design to accommodate Army requirements. The Army currently owns 26 LACV-30s: 2 stationed at the Army Charleston Storage Activity in South Carolina and 24 stationed at Ft. Story, Virginia. The 8th and 331st Army Transportation Companies operate and maintain them, performing both field and intermediate-level maintenance. Heretofore, depot overhaul was performed at the Charleston facility, but the depot facility will be moved this year to Ft. Story. Engine rework is performed by the Naval Air Rework Facility, Cherry Point, North Carolina.

**Operator's Manual for the Lighter Air Cushion Vehicle, 30-Ton (LACV-30), NSN 2305-01-061-6230, TM 55-2305-001-10.* Washington, DC: Department of the Army, April 1987, pp. 1-1 and 1-2.

HISTORY OF CORROSION PROBLEMS ON THE LACV-30

During the past 12 years, the readiness posture of the LACV-30 fleet has continually been threatened by corrosion damage. Both complex and simple subsystems have experienced high replacement rates. It has been necessary to redesign several subsystems, at considerable cost to the Army. In March 1988 ARINC Research Corporation was tasked to conduct a corrosion survey of the LACV-30 fleet. The survey found corrosion problems on the vehicles purchased under both the first and second contracts. The corrosion on the newer vehicles, was excessive in the light of their relatively short period of service.

In July 1988 ARINC Research was tasked to conduct a corrosion engineering analysis of the LACV-30. The objective was to review the existing corrosion-prevention materials and procedures, suggest improvements to correct the problems where necessary, and develop a corrosion-control manual based on the findings of the engineering analysis.

DATA COLLECTION

Different types of data were needed to conduct the corrosion engineering analysis. The first type encompassed the corrosion or deterioration problems identified in maintenance and survey reports. The descriptions and photographs in these reports defined the scope and pattern of corrosion on the vehicles.

It was also necessary to obtain data on current maintenance materials and practices. The LACV-30 procurement history had a significant impact on these data. The vehicle was purchased as an NDI. As in many such procurements, the original drawings, and thus the materials information, were not freely available. In addition, since there had been a redesign of the vehicle for the second purchase, some of the materials used on its subsystems differed from the earlier version.

Approved corrosion-prevention maintenance practices are defined in the maintenance, inspection, and supply manuals. Depending on the complexity of the system, there can be several maintenance and inspection levels, from field repair to full overhaul and rework. The documentation for each level of maintenance was reviewed.

The third type of data was gathered from interviews with maintenance personnel and engineers. Interviews with the maintenance personnel focused on their use of existing manuals and their ability to execute required procedures. They also provided an indication of the maintenance personnel's level of corrosion-prevention training. The interviews with engineers centered on design history and maintenance policies, as well as anticipated changes to the LACV-30 maintenance policy and capabilities.

After the LACV-30 documentation was collected, the cause of each corrosion or deterioration problem was determined. The assessment was based on survey photographs, available materials information, component configuration, and known corrosion and deterioration mechanisms. In developing a recommended solution to a specific problem, ARINC Research engineers considered the type of repair equipment available at Ft. Story, the training and availability of maintenance personnel, and the current procedures and products used for LACV-30 maintenance.

LACV-30 CORROSION TRENDS

Thirty-three specific corrosion problems were addressed in the LACV-30 corrosion analysis. These problems have affected 25 of the vehicle subsystems as listed in Table 1. Analysis of these problems identified several trends First, carbon steel fasteners were frequently used to secure aluminum mating surfaces. This caused surface corrosion and pitting to develop around the fastener area. Part of the solution to the problem was to change the fastener metal to corrosion-resistant (CRES 316 or 304) stainless steel.

Table 1. LACV-30 Subsystems Affected by Corrosion

Life Rails	Battery Compartments
Fin-Rudder Assembly	Rudder Bar Assembly
Exciter Ignition	Cabin Heater Assembly
Oil System	Exhaust Pipe Assembly
Horn System	Electrical Connectors
Antenna	Deck Hardware
Fenders	Splice Plates
Cargo Fittings	Puff Port Actuator
Skirt Hinge Pins	Bifurcated Duct
Fuel System	Auxiliary Power Unit
Nacelle Strut Support	Plenum Air System
Engine Roof Assembly	Lift Fan Assembly
Air Conditioner	

In addition, the hard, stiff polysulfide sealant that was applied to the fasteners often cracked, allowing water intrusion into the fastener crevice. The sealant was replaced with an antiseize compound that contained corrosion inhibitors. This compound was particularly recommended for fasteners that are adjusted or removed frequently. The application of water-displacement compounds to unexposed metal surfaces near fasteners was also recommended.

Finally, many of the corroded stationary metal structures either were bare or were painted with an aviation coating system. The recommended solution for many of these parts included painting the surface with a marine epoxy paint, MIL-P-24441. Most of the recommended solutions involved changes in both the fastener metal and the protective coating. More frequent inspections and maintenance were also strongly recommended.

ADDITIONAL BENEFITS OF THE CORROSION ENGINEERING ANALYSIS

The LACV-30 corrosion engineering analysis also provided a comprehensive second look at the system's design. As a result of the analysis, recommendations were made to change the current maintenance schedule, lubrication schedule, and installation method for electrical connectors. Suggestions were also offered for redesigning several structural components to reduce safety hazards or to eliminate costly repairs.

In addition, a significant amount of supply information was obtained and reviewed. Much of this information identified the metals used to fabricate the fasteners and delivery systems used on the LACV-30. For instance, many of the part numbers listed in the resupply list identify the components by military or industrial specification nomenclature, such as MS_ _ _, NAS_ _ _, AN_ _. Most of these specifications, which are available on either microfiche or microfilm in Army libraries, list the metals and coatings used by manufacturers. The compilation of these standard fastener data for most Army systems could assist the engineers in the evaluation of corrosion or structural problems. This information could also help maintenance personnel to better understand how resupply parts are selected and the importance of various maintenance procedures.

The corrosion engineering analysis also found several instances in which the manufacturer assigned a commercial part number rather than a standard specification number. Sometimes no specification exists, because the component is a proprietary product. For several LACV-30 components, however, specific vendors and part numbers are assigned to commonly available components. In particular, the electrical connectors, rivets, and sealants were assigned vendor part numbers even though several qualified vendors are available. The commercial part numbers listed in the LACV-30 supply list should be reexamined to determine whether there are corresponding federal or military specifications. There may be several manufacturers who can supply equivalent or better quality products, at lower costs.

RECOMMENDATIONS FOR IMPROVED MAINTENANCE CAPABILITIES

Training

The corrosion surveys found that training was needed to improve several areas of the LACV-30 maintenance. The LACV-30 has a unique, aircraft-like construction; yet it operates as an amphibious craft. It is difficult to find maintenance personnel with both the aircraft and marine maintenance experience and training necessary to maintain this vehicle. As a result, many of the maintenance procedures performed on the LACV-30 are learned "on the job." This approach can introduce improper procedures and replacement materials. The maintenance procedures described in the LACV-30 manuals need reinforcement with on-site training.

Further, the maintenance personnel should be given specific corrosion prevention and control (CPC) training. Because there is little CPC training available to Army enlisted personnel, only a few of the LACV-30 maintenance personnel have learned corrosion-prevention techniques. The development of a proposed LACV-30 Corrosion Control Technical Bulletin is a significant step toward providing CPC training. Any instruction must address the unique construction and operation of the LACV-30, as well as general CPC theories and principles. These techniques can be taught by videotape, formal courses, certification programs, or a combination of these methods.

Finally, it is necessary for LACV-30 maintenance personnel to learn how to apply and touch up different paint systems. They should have an understanding of the differences in paint types, proper surface preparation, paint preparation and mixing, handling of spray gun equipment, and use of personal protective equipment. Proper paint application can significantly improve the readiness profile and reduce the maintenance requirements of the LACV-30.

Use of Longer-Lasting Coatings

The corrosion engineering analysis determined that many LACV-30 corrosion problems could be resolved by using longer-lasting coatings. The first recommendation was to use marine paint formulations for the exterior and nonskid paint systems. The second was to use two specialty coatings for selected structural components: flame spraying and powder coating. All of these paint systems require depot-level facilities.

A polyurethane paint is currently used to protect the exterior surfaces of the vehicle. The corrosion surveys showed that this paint is peeling from the surfaces of the vehicle, providing little protection from corrosion. The recommendation was to change the exterior coating to a marine epoxy system. Marine paints are commonly used to prevent corrosion on equipment that is exposed to humid coastal environments. The MIL-P-24441 system has demonstrated superior performance on Navy ships over the past 15 years. This specification was recently reformulated to comply with environmental regulations for volatile organic compounds (VOCs).

The current nonskid coating is formulated by mixing sand into the specified polyurethane system. The mixture is applied to the aft decks of the vehicle. Like the exterior coating, this coating is peeling off of the decks, providing little protection from slipping. It was recommended that the existing nonskid system be changed to a more resistant, longer-lasting marine-based system, DOD-C-24667 (with QPL-24483 being used until a qualified parts list [QPL] is available for DOD-C-24667).

It was also recommended that structural components in hard-to-reach areas on the LACV-30 be coated with either a flame-sprayed or powder coating. It is difficult to inspect or maintain these components even when the vehicle is undergoing intermediate maintenance. The surveys showed that many of these components were experiencing extensive corrosion.

The flame spraying process for corrosion control typically involves applying an aluminum or zinc coating to steel structural surfaces. A marine topcoat paint is applied over the flame-sprayed coating to seal it. Aluminum is the preferred metal in flame spraying for marine applications. The metal coating protects the steel by serving as a sacrificial anode (the aluminum coating will corrode instead of the steel structure). Flame-sprayed coatings are very durable and corrosion-resistant. Flame spraying can also be used to rebuild worn surfaces. By refurbishing used parts, flame spraying can reduce the cost of parts replacement.

A flame spraying facility consists of a special application booth and support equipment. Training instruction and manuals are usually developed to support the implementation of this maintenance procedure. DOD-STD-2138 addresses the use of flame spraying for corrosion control. MIL-STD-1687 addresses its use for machinery repair. The one drawback to flame spraying is that it is very expensive in comparison with other paint processes.

Powder coating electrostatically attaches paint powder to the surface of a part. The part is then placed in a heated oven and baked until the powder becomes a solid coating. Many different types of paints, such as epoxies, polyesters, and polyethylenes, can be applied by powder coating, with epoxies often being used for marine applications. A powder coating facility typically consists of a special application booth, support equipment, and a large oven. Training courses and manuals will be needed to support the implementation of this process.

The principal advantage of powder coating is that it limits the exposure of workers and the environment to hazardous solvents. Powder coatings are not as durable as flame-sprayed coatings, but are much less expensive to apply. Compared with conventional coatings, the powder coatings are more durable, more corrosion-resistant, and only slightly more expensive to apply. However, their use is limited. The candidate parts must be amenable to oven heating for a short period without detrimental effect to their structures, be small enough to fit in the available ovens, have no moving elements, and not be subjected to erosion. Yet, even with these limitations, there are many LACV-30 parts that could be powder-coated.

Structural Repair

Army weapon systems and support equipment are now being fabricated from a wider variety of materials than ever before, including aluminum alloys and composite materials. The repair techniques for these newer materials are very different from those used on steel. Aluminum, for example, is much more difficult to weld than mild steel; it requires special temperature control and more exacting welding procedures.

Recently cracks have developed on the aft decks of several LACV-30s. They can be attributed to a combination of the aluminum alloy used, the stress profile of the deck, and the operating environment. The maintenance crews have tried to repair these cracks with welds and threaded fasteners but have not effectively corrected the problem. The LACV-30 maintenance personnel need intensive instruction and the appropriate equipment and facilities if they are to perform welding repairs on the aluminum structure. Improper welding practices can introduce more problems than they correct.

The approach to repairing composites varies with the type of composite used. The LACV-30 has fiberglass ducting, as well as a disk system constructed of aluminum honeycomb sandwich material. Both of these subsystems experience erosion damage. The disks are also damaged by corrosion. The existing protective coating and sealant provide only temporary protection. Unique procedures, sealants and bonding materials, and training are required to maintain both of these subsystems.

LACV-30 CORROSION CONTROL TECHNICAL BULLETIN

In the spring of 1989, the U.S. Army Troop Support Command (TROSCOM) was planning to issue the recommended corrosion control procedures to LACV-30 maintenance personnel in the form of a technical bulletin. The approach to preparing a corrosion control technical bulletin includes selecting the most useful information for the maintenance personnel and then deciding on a logical order for presentation. Interviews with LACV-30 maintenance personnel indicated a need for them to learn how to recognize corrosion and deterioration on a variety of materials. Thus it would be necessary for the bulletin to emphasize the detection of corrosion and deterioration and the identification of metals. The theory of corrosion would be offered in the appendixes as reference information.

The surveys showed that several corrosion problems could be attributed to improper fastener selection, inadequate surface preparation, or improper coating application. The maintenance personnel need to learn the important role of proper surface preparation in the adhesion of paint or preservative. The manual was therefore planned to provide general guidance for the selection and maintenance of fasteners, preservatives, and paints, as well as instruction in surface preparation and the application of preservatives and paints.

The proposed technical bulletin would address corrosion prevention on specific LACV-30 components. Each problem would be presented in a "problem summary," which identifies the corroded parts, states the current maintenance procedures, and then recommends new maintenance procedures and replacement material.

It is also recommended that the current Lubrication Order be revised to encompass more frequent lubrication and the use of more corrosion-resistant lubricants. The recommended schedule for lubrication is based on either operational hours or calendar days. Providing both operational and calendar-based scheduling is essential to improving current military inspection and maintenance schedules.

The appendixes to the technical bulletin would provide reference information on corrosion theory and technical terms. In anticipation of the Ft. Story facility's acquiring full depot maintenance capability, it is considered important that the maintenance crews begin learning how to maintain marine paint systems. Thus one of the appendixes would describe the procedures for applying marine paint with compressed-air and airless spray guns.

SUMMARY

Most of the galvanic corrosion and paint deterioration problems found on the LACV-30 were due to improper material selection during the design phase. Further, the design did not provide proper access or enhanced corrosion protection for all areas of the vehicle. Finally, the surveys indicated that the maintenance personnel need on-site corrosion, coating application, and maintenance training. TROSCOM has taken that first important step to addressing these problems by providing a corrosion resource for use by LACV-30 maintenance personnel.

The Army Material Command has directed that all of its major subordinate commands (MSCs) incorporate CPC techniques into their maintenance documentation. The recommendations made for improving the maintenance of the LACV-30 could be applied by other MSCs to several military weapon systems and support equipment. Only a few of the corrosion problems are unique to the design and operation of the LACV-30. Incorporating CPC techniques into existing maintenance documents is only the first step to improving the readiness of military equipment. CPC principles need to be applied throughout the life cycle of the equipment, from design to decommissioning.

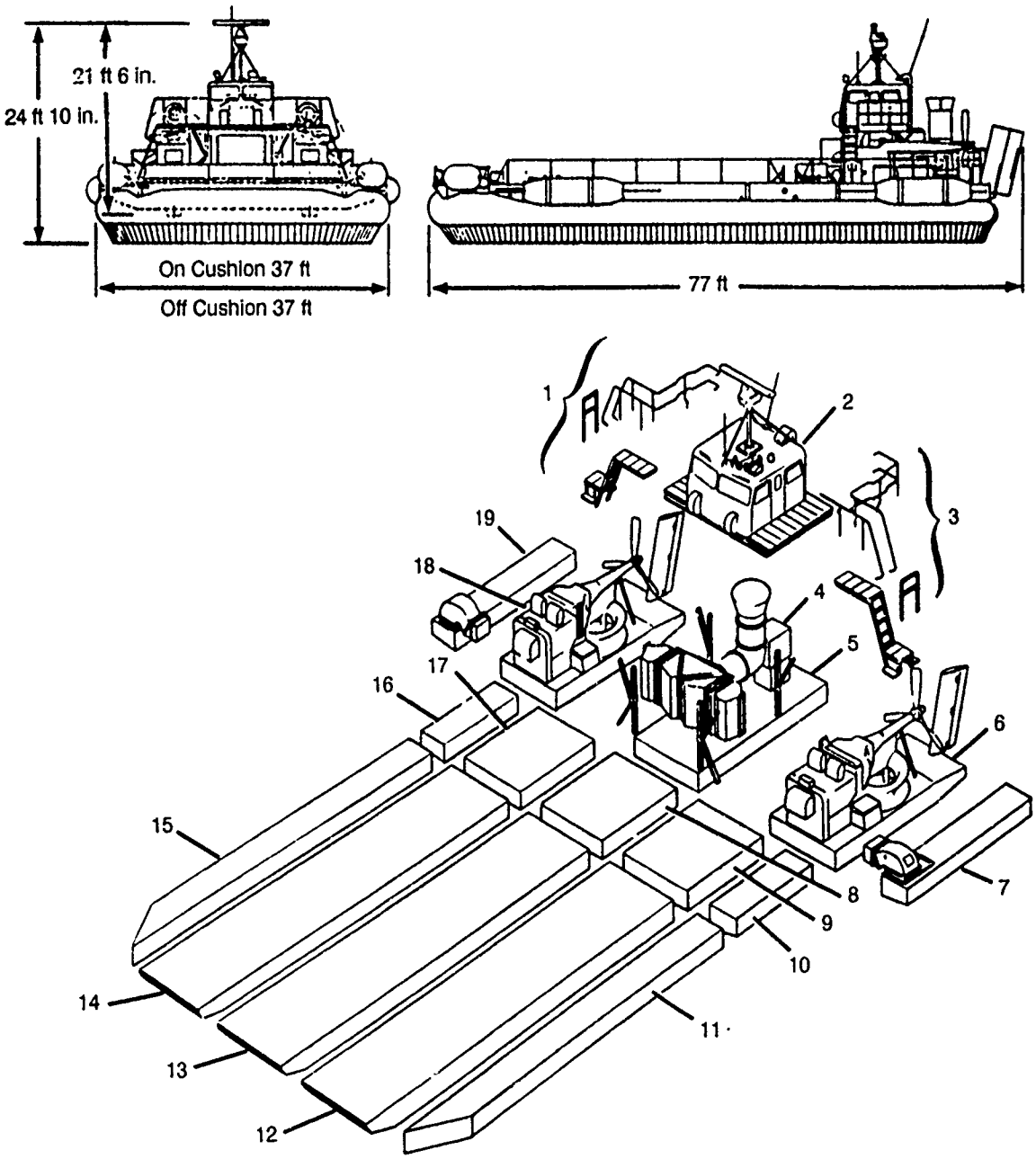

Source: Operator's Manual for Lighter Air Cushion Vehicle: 30-Ton (LACV-30), NSN 2305-01-061-6230, TM 55-2305-001-10

Figure 1. The Dimensions and Modular Construction of the LACV-30

EXPERT SYSTEM FOR CORROSION OF AIRCRAFT

Dr. Chris Westcott
Atomic Energy Research Establishemnt
AIRE, Harwell, U.K.

ABSTRACT

An expert system has been developed for the Air Force for use in aircraft design using the SPICES rule based programming language written in PROLOG. The expert system contains a free test database information retrieval system using STATUS. The expert system can be operated on personal computers. The expert system used an AGARD corrosion handbood for source material. For further information please contact Mr. Fred H. Meyer at (513) 255-5117.

[Manuscript Not Available at the Time of Printing]

FAILURE ANALYSIS/CORROSION of STRUCTURAL MATERIALS

R. Williams and F.H. Meyer
USAF - WRDC
Wright-Patterson AFB, Ohio

ABSTRACT

The Structural Failure Analysis Group of the Air Force WRDC Materials Laboratory performs numerous analysis on field weapons syustem structural failures. This paper presents a number of representative completed studies including recommended action to prevent future occurrences.

[Manuscript Not Available at the Time of Printing]

PERMEATION MEASUREMENTS OF HYDROGEN TRAPPING IN SOME HSLA STEELS

J. A. Smith
Code 6327
Naval Research Laboratory, USA
Washington, D.C. 20375-5000

ABSTRACT

The polarization behavior, H-permeation (electrochemical), and slow strain rate test (SSRT) fracture behavior of six HSLA steels were studied in 0.6N NaCl solutions. Three types of HSLA steels at high and low sulfur contents were utilized. On the basis of the results obtained it is confirmed that increased trapping causes greatly reduced diffusivity and low stress corrosion cracking (SCC) and/or hydrogen assisted cracking (HAC) resistance. The HAC mechanism, contrary to popular belief, is not related to grain boundary segregation of sulfur. A mechanism of the phenomenon is proposed.

INTRODUCTION

The phenomenon encountered in steel called hydrogen embrittlement, or better termed hydrogen assisted cracking, has long been debated, and at this writing is still far from being totally understood. What is understood is that the phenomenon is characterized by a loss in metal/alloy mechanical properties induced by the entrance of hydrogen into the metal system [1-8]. The sources of the hydrogen may vary from humid air to cathodic protection schemes. Whatever the source hydrogen as adatoms enters the metal or alloy and diffuses through it. Most of the hydrogen adatoms will diffuse through the metal, and form hydrogen gas at the outer free metal surface. However, in the course of diffusing through the metal or alloy, any crystalline defect, in homogeneity, or precipitate may interact with the hydrogen and serve as a pseudo-free surface or trapping site. An indication of the comparative strengths of some of pseudo-free surfaces or traps for hydrogen are given in Table 1 [9,10].

TABLE 1- Trapping Sites and their Trapping Energy in Iron Base Alloys

Trapping Site	Trap Energy kJ/mol	Ref.
TiC interfaces	87	43
Al_2O_3 interfaces	79	45
MnS interfaces	72	44
Microvoids	40	41
Dislocations	26	42
Grain boundaries	18	42

This paper describes observations of cathodic hydrogen trapping in HSLA steels, in which the influence of microalloying additions and various sulfur levels are considered.

EXPERIMENTAL PROCEDURES

The composition and characteristics of the HSLA alloys used in these studies are shown in Table 2, and examples of their microstructures are shown in Figs. 1-3.

Electrochemical polarization/permeation experiments performed to analyze the trapping of hydrogen in these HSLA steels utilized an adaptation of Devanathan and Stachurski cell [11] and is shown in Figure 4. The experiments were performed on alloy membranes vacuum annealed for two hours and then furnace cooled. These specimens were then surface ground through 600 grit emery paper and cut to provide 1.27 mm thick specimens with input/output diameters of 19mm. Complete details of the procedures are given elsewhere [12].

TABLE 2- Composition (wt. %) and Yield Strength.

STEEL													
HY 80	1.63	2.40	.37	—	.31	.23	.04	.002	.006	.017	.0120	.190	586.7
HY 82	1.58	2.71	.27	—	.28	.22	.14	.001	N/A	N/A	.0015	.148	592.8
HY 100	1.27	2.88	.28	—	.29	.26	.15	.003	.003	.004	.015	.147	900.8
HY102	1.44	3.40	.29	—	.30	.21	.29	.001	N/A	—	.0019	.191	900.8
A710-1	.71	.97	.19	.046	.56	.36	1.22	—	--	.010	014	.06	677.3
A710-3	.63	.92	.19	.040	.69	.24	1.20	—	—	.010	.004	.05	623.6

In the slow strain rate (SSR) tests utilized in this study LT tensile specimens 127 mm long and 2.8 mm in diameter were pulled to fracture at a strain rate of 1.45×10^{-6} /sec. The tests were carried out at open circuit and various controlled potentials. After testing the SSR specimens were examined metallographically and by scanning electron microscopy. Selected fracture surfaces were examined with auger spectroscopy to analyze for impurity segregation on or near the fracture surface.

RESULTS

A. Polarization Curves

Figures 5-7 show that the anodic currents of alloys HY 80 and HY 82 are clearly lower than those in either the HY 100 and HY 102 alloys or the A710-1 and A710-3 alloys.

B. SSR Behavior

Susceptibility to hydrogen assisted cracking is evaluated using the ratio of percentage reduction in area at failure of alloy materials tested under specified conditions to that of the same alloy tested in air. Figure 8 shows the ratio values for the alloys tested in 0.6N NaCl solutions at open circuit, -850 mV, and -1000 mV potentials. In these 0.6N NaCl solutions all of which have a pH of 6.3, the hydrogen evolution potential ($E_{H/H2}$) calculated by the Nernst equation is approximately -610mV. Although the hydrogen is thermodynamically possible at -610mV, generally only a small portion enters the metal. The extent of hydrogen entry depends on many factors such as alloy composition, surface conditions, chemistry of the electrolyte, pressure, temperature, etc.. It is the formation and absorption of atomic hydrogen into an alloy that represents the initial step in the HAC mechanism. At the test potentials of -850 mV and -1000 mV, the conditions are considered cathodic enough to cause detectable amounts of absorbed hydrogen. The fractograph of alloy HY 80 tested at 1.45×10^{-6}/sec. and shown Figure 9 represents a typical example of the hydrogen environmental effect viewed in these alloys.

C. Permeation Behavior

Hydrogen permeation data obtained from straining electrode tests conducted at -1000 mV are given in Table 3. These data are the average of three tests performed under the same conditions. The data obtained at a straining rate of 1.45×10^{-6}/sec. show significant increases in the permeation current density in the plastic strain range. These increases indicate that for the alloys studied, plastic deformation influences hydrogen transport. This influence is thought to be a hydrogen-dislocation interaction with subsequent hydrogen sweep-in via dislocation motion. No observable increase in permeation values were detected within the elastic range.

TABLE 3- Hydrogen Permeation data obtained at -1000 mV for straining alloy

STEEL	YIELD STRENGTH MPA	H-PERMEATION @50%ys,MA/M2	H-PERMEATION @120%ys,MA/M2	D*10+11 M2/sec	Ecorr mV(SCE)	Co Mole-H/M3
HY 80	585.7	36.6	54.1	0.982	-753	5.47
HY 82	592.5	35.3	44.1	3.15	-742	2.68
HY 100	592.5	7.3	41	0.122	-742	56.6
HY 102	592.5	19.6	83.4	3.73	-722	3.33
A710-1	677.3	17	27.1	0.143	-768	26.1
A710-3	623.5	59	89	1.24	-728	9.1
Fe	--	169	--	139	-849	--

DISCUSSION OF THE PRESENT RESULTS

Previous investigations of HAC in steels have established that the evolution and adsorption of hydrogen at the metal/solution interface may be represented by the following reaction sequence [13]:

$H_2O + e^- = OH^- + H_{ad}$ Charge Transfer Reaction (CTR)

or

$H_3O^+ + e^- = H_2O + H_{ad}$

The adsorbed hydrogen atoms produced by the (CTR) reaction may combine to form hydrogen gas (H_2) by the Tafel reaction:

$H_{ad} + H_{ad} = H_2$

or the electrochemical Heyrovsky reaction

$H_3O^+ + H_{ad} + e^- = H_2 + H_2O$

or

$H_2O + H_{ad} + e^- = H_2 + OH^-$

or they can be absorbed by the alloy: $H_{ads} = H_{abs}$

Assuming the charge transfer step is the rate-determining step, then the absorption reaction (Hads = Habs) for a electrochemically charged membrane may be expressed with Fick's first law as follows: $J = -D\ dc/dx$ (1)

where (D) is the diffusion coefficient.

At steady-state the differential equation becomes $J_{oo} = DC/L$:

(C) is the hydrogen solubility just below the cathodic surface of the membrane, (L) is the membrane thickness, and (D) is the diffusion coefficient. (D) is calculated using the following equation: $D = L^2/6t_L$

where t_L is the time lag for hydrogen to reach the exit surface.

The data in Table 3 suggests that hydrogen diffusivities in these alloys depends on impurity content. A decrease in diffulsivity is noted in going from the pure iron value (Do) to the diffusivity values for the HSLA alloys (D). This reduction in diffusivity is considered proportional to trap strength and trap density. Based on this consideration a equation describing the trap dependent diffusion of hydrogen in an alloy was derived by McNabb and Foster[14].

$$dC/dt = Nt\ dn/dt \quad (2)$$

where Nt is the density of traps.

and dn/dt = trapping rate = $kCL(1-n) - pn$ (3)

where n = fractional occupancy of traps;

CL = lattice concentration of hydrogen;

k = transition probability for hydrogen transport from lattice site to trap;

p = transition probability for hydrogen transport from trap to lattice site.

Traps may be classified as fixed such as a precipitate or a grain boundary and these are considered saturable traps. Or they may be classified as not fixed such as voids where the trap type is termed unsaturable. If the rate constants k and p are large the traps are called reversible. However, if they are small such that equilibration does not occur within the relaxation time ,T, for lattice hydrogen to diffuse through the alloy lattice then the traps are irreversible. For reversible traps the alloy's effective diffusivity (D) is lowered during permeation testing while irreversible traps are considered to saturate at steady state and not affect alloy diffusivity.

In our tests, the initial transients of the alloy electrochemical permeation tests are nonreproducible in both breakthrough time and rise to saturation. However subsequent transients are reproducible. The shifts in breakthrough time and rise to saturation are considered to be the result of strong irreversible traps. These traps fill during the first transients and retain their hydrogen during subsequent transients. At steady state the McNabb and Foster equation predicts that permeation through a material with traps has the same value as a trap free material. Thus for reversible traps characterized by a single energy value the McNabb and Foster solution for equation (2) is:

$$t_T = t_L(1 + 3a/B + 6a/B^2 - 6/B^3(1 + B)\ \ln(1 + B) \quad (4)$$

where $a = N_T k/p$ trapping parameter

$B = C_O k/p = n/1-n$ activity of hydrogen in trap

C_O = lattice hydrogen

N_T = number of traps

t_T = lattice time lag

L = membrane thickness

Kumnick and Johnson [15] discuss the above equation in light of the two limiting forms of the McNabb-Foster expression. For low trap saturation equation (4) becomes------$t_T/t_L = 1 + oo$ (5). While for high saturation equation (4) becomes--$t_T/t_L = 1 + 3N_t/C_O = D_O/D$ (6). where t_L = time lag for trap free material. Because the time of the experiments are relatively long, high saturation conditions are judged applicable in these tests.

TABLE 4- Trapping densities for HSLA alloys.

STEEL	YIELD STRENGTH MPA	H-PERMEATION @50%YS,MA/M2	H-PERMEATION @120%YS,MA/M2	D*10+11 M2/sec	Co Mole-H/M3	Do/D	TRAP DENSITY Nt*10-25
HY 80	586.7	36.6	54.1	0.082	5.47	144.5	15.8
HY 82	592.6	35.3	44.1	3.16	2.68	44.1	2.32
HY 100	592.6	7.3	41	0.122	56.8	1139.3	1300
HY 102	592.5	19.8	83.4	3.73	3.33	37.3	2.43
A710-1	677.3	17	27.1	0.143	25.1	972	489
A710-3	623.5	59	89	1.24	9.1	112.1	20.4
Fe	--	109	--	139	--	--	--

TABLE 5- Cathodic Drift experienced by alloys during SSR testing at open circuit potential.

MATERIAL	POTENTIAL RANGE,mV	CATHODIC DRIFT
HY 80	-666 to -697	46
HY 82	-653 to -702	49
HY 100	-583 to -731	148
HY 102	-563 to -634	71
A710-1	-646 to -736	90
A710-3	-661 to -709	48

The data on trap density determined from equation (6) is presented in Table 4. For a dynamic straining electrode which would occur during SSR testing, hydrogen transport would not only be affected by the accumulation of hydrogen at grain boundaries, matrix/precipitate interfaces, the tortuous path established in the alloy during the deformation process, and the chemistry of the internal surfaces, but also by the accumulation of hydrogen at mobile dislocations and its subsequent sweep into the lattice. All of these factors tend to alter the permeation behavior of an alloy, the former would tend to decrease the permeation current and the later would tend to increase it.

One of the most important symptoms of hydrogen involvement in the cracking process of metals and alloys, i.e. hydrogen embrittlement, is the loss of plasticity. H-embrittlement affects almost all of the mechanical properties of an alloy (ductility, yield strength, etc.) The influence of hydrogen on the aforementioned properties is based on the initial properties of the metal and the parameters of hydrogen absorption. At -1000mV, hydrogen greatly reduces the ductility of these alloys and has a modest effect on their strength. This is apparent in the low sulfur alloys and is seen in Figure 10-12 where increases in the amount of absorbed hydrogen (electrochemically produced at -850 mV and -1000 mV) generally reduces the ultimate strength and increases the yield strength of the tested material. In the case of the high sulfur alloys, the story is mixed showing evidence of work hardening, and a reduction in yield strength for alloys HY 80 and A710-1. For HY 100 work softening and a reduction in yield strength is revealed. These observations suggest higher trapping in the HY 100 alloy as indicated by the data in Table 4. Additionally, observations of alloy response to slow strain rate deformation at the alloy corrosion potentials show a trend toward increased negative electrochemical potential during testing, Table 5. This trend strongly suggests that the behavior of the metal/solution interface during deformation continuously adjusts itself to the shifting electrochemical characteristics of the interface. According to present theory a fixed charge exists on the surface of an alloy membrane in solution that is determined by the preferentially adsorbed ions on the alloy surface. Ideally at open circuit potential this fixed charge in the unstressed alloy is zero and the corresponding potential is called the potential of zero charge (PZC) [16,17]. Potentials to the right of PZC would produce cathodic charges and to the left anodic charges. Any surface disturbances produced during slow straining tend to cause cathodic drifts in freely corroding alloys and cathodic current increases in cathodically potentiostated alloys. Such occurrences would increase the cation (e.g. H^+) selective tendencies of the surface. Consequently, the alloy possessing the greatest cathodic drift or cathodic current increase would be expected to possess the greatest near surface hydrogen concentration. Hence, discernable increases in permeation current density should occur in these alloys if not complicated by trapping (e.g. HY 100).

Since the fracture mode is transgranular in all specimens whether charged with hydrogen or uncharged, the loss in ductility is apparently not caused by embrittlement of the grain boundaries. Thus other sites such as copper rich dispersoids, impurity inclusions (MnS), etc., must serve as nuclei for HAC/SCC fracture. Observations of metallographically prepared specimens of alloy A710-3 clearly show the total number of voids and the void size increased in this high copper, low sulfur alloy after hydrogen charging suggesting that the

primary effect of hydrogen in this alloy is microvoid nucleation. According to a model proposed by Leblond and Dubois [18] this increase in void number and size may be the result of a decreased hydrogen solubility in the lattice of the high copper, low sulfur alloy. In the high copper, high sulfur alloy, A710-1, particle-matrix separation together with some microvoid nucleation is considered the main function of hydrogen involvement. The role of copper in the HAC/SCC behavior of HSLA alloys HY 82 and HY 102 is also noted. Here the alloys are as identical as possible except for their copper content. The ductility index of HY 102 is found to be slightly less than half that for HY 82 in slow strain rate tests at -1000mV. However, failure times are practically the same for both alloys. No clear effects are discernable because of other interactions and factors such as work hardening, etc.

In observing the possible involvement of other microalloying elements it is noted that manganese is present in sufficient amounts to fulfil its primary purpose of tying up the sulfur as MnS inclusions. These inclusions are present as both elongated and spherical particles. The former are predominate in the high sulfur alloys and hydrogen assisted cracking in the high sulfur alloys is found to be associated with these inclusions. Transgranular fracture features existent in these alloys appear to result from mechanically induced separation along the inclusion/matrix interfaces [19]. Since the normal stress is not believed to be large enough to fracture at the grain boundaries a "woody" fracture appearance results. In accord with the findings of L'Ecuyer et al. [20] there is some evidence that Mo rich precipitates have a tendency to segregate around MnS inclusions; however, our present knowledge is insufficient to tell the effect or nature of these precipitates, i.e. whether they serve as innocuous hydrogen traps capable of diverting hydrogen away from the nocuous MnS traps or possess some other function.

The pattern unfolding for these alloys is as follows. The alloy/solution interface properties appear to be less important in determining HAC/SCC behavior than the weakening of precipitate/matrix interfaces and the embrittlement of surrounding material by absorbed hydrogen. Copper gives some indication of promoting void growth in high copper-low sulfur alloys (A710-3). However, in high copper-high sulfur alloys (A710-1) the sulfur appears to moderate or eliminate any involvement of copper in the cracking process.

CONCLUSIONS

Experiments were carried out to study the effects of sulfur and microalloying on the hydrogen assisted cracking behavior of some HSLA steels. Particular attention was paid to hydrogen permeation and hydrogen trapping effects. The major conclusions of this work are:

1. Cracking is transgranular cleavage and is not related to sulfur at grain boundaries.
2. Increased trapping in high sulfur HSLA steels caused a reduction in diffusivity and low HAC/SCC resistance.
3. No conclusive special HAC/SCC effects are found for the microalloys of Cu and Mo.

REFERENCES

[1] M. Smialowski, Hydrogen in Steel, Pergamon, London, 1962.
[2] A.R. Troiano, Trans. ASM, Vol. 52, 1960, p.54.
[3] N.J. Petch and P. Stables, Nature, Vol. 169,.1952, p.842.
[4] R.A. Oriani, Hydrogen in Metals, I.M. Bernstein and A.W. Thompson, Eds., NACE, Houston, 1969.
[5] C. Zapffe and C. Sims,.Trans. AIME, Vol. 145, 1941, p.225.
[6] P. Bastien and P. Azou, Proc. First World Met. Cong., ASM, Cleveland, 1952, p.535.
[7] B.F. Brown, Metallurgical Review, Vol. 13, No. 129, 1968, pp. 171-183.
[8] W. Beck, E.J. Jankowsky and P. Fisher, Naval Air Development Center Report No. NADC-MA-7140, 1971.
[9] J. Hirth, Met Trans. A, Vol. 11A, 1980, pp. 861-889.
[10] C. Paes de Oliveira, M. Aucouturier, and P. Lacombe, Nat. Assoc. of Corr. Engs., Vol. 11A, 1980, pp. 861-889.
[11] M.A.V. Devanathan and Z. Stachwiski, Proc. Roy. Soc. A270, 1960, p. 90
[12] J.A. Smith, Proc. of the 4th International Conference on Hydrogen and materials, Beijing, China, 1988.
[13] A.R. Troiano, Hydrogen in Metals, I. M. Bernstein and A.W. Thompson,Eds., American Society for Metals, 1974.
[14] A. McNabb and P.K. Foster,Trans. AIME., Vol. 227, 1963, p. 618.
[15] A.J. Kummick and H.H. Johnson, Met. Trans, Vol. 5, 1974, pp. 1199-1205.
[16] N. Sato, Corrosion Sci., Vol. 27, No. 5, 1987, pp. 421-433.
[17] G.S. Frankel and R.M. Latanision, Met. Trans., Vol. 17A, 1986, pp. 861-875.
[18] J.B. Leblong and D. Dubois, Acta Metall, 31, 1983, pp. 1459-1471
[19] J. Chine, J.O. Garcia, C. Paes de Oliveira, M. Aucouturier, and P. Lacombe, J. Mic. Spect. Elect., 4, 1979, p. 37.
[20] J.D. L'Ecuyer, G. L'Esperance, M.G. Akben, and B. Bacroix, Acta Metall., 35, No. 5, 1987, pp. 1149-1158.
[21] T.P. Hoar, Electrochem. Society, Vol. 117, 1970, pp. 17C-22C.
[22] B.E. Conway, Theory and Principles of Electrode Processess, Ronald Press, New Press, 1970
[23] J.O.M. Bockris and A.K.N. Reddy, Modern Electrochemistry, Vol. 2, Plenum Press, New York, 1970.
[24] D.A. Meyn, P.G. Moore, R.A. Bayles, and P.E. Denny, in Automated Test Methods for Fracture and Fatigue Crack Growth ASTM STP 877, W.H. Cullen, R.W. Landgrof, L. Kaisand and J.H. Underwood,Eds., American Society for Testing Materials, Philadelphia,PA, 1985, pp. 27-43.
[25] M.F. Stevans, ONR Text Report 036-099-19, Carnegie-Mellon Univ., 1984.
[26] G.M. Pressouyre and I.M. Bernstein, Met. Trans., Vol. 9A, 1978.
[27] S.M. Lee and J.Y.Lee, Acta metall., Vol. 35, No.11, 1987, pp. 2695-2700.
[28] I.M. Bernstein and A.W. Thompson, Alloy and Microstructural Design, J.K. Tien and G. Ansell,Eds., Academic Press, New York, 1976.
[29] J.L. Lee and J.Y. Lee, Metal Sci., Vol. 17, 1983, p. 462
[30] R. Gibala and D.S. Demiglio, Hydrogen Effects in Metals, I.M. Bernstein and A.W. Thompson,Eds., AIME, Pittsburgh,PA, 1980.
[31] M. Smialowski, Hydrogen in Steel, Pergamon, London, 1962.

[32] A.R. Troiano, Trans ASM, Vol. 52, 1960, p. 54.
[33] N.J. Petch and P. Stables, Nature, Vol. 169, 1952, p. 842.
[34] R.A. Oriani, Hydrogen in Metals, I.M. Bernstein and A.W. Thompson,Eds., NACE, Houston, 1969.
[35] C. Zapffe and C. Sims, Trans. AIME, Vol. 145, 1941, p. 225.
[36] M.P. Bastien and P.Azou, Proc. First World Met. Cong., ASM, Cleveland, 1952, p. 535.
[37] Y. Yoshino, Corrosion, 38, 1982, pp. 156-167.
[38] B.D. Craig and G. Krauss, Metall. Trans. A, 11A, 1980, pp. 1799-1808
[39] C. Paes de Oliveira, M. Aucouturier, and P. Lacombe, Corrosion, 36, 1980, p. 53.
[40] R.Gibala, Trans. Met. Soc. AIME, Vol. 238, 1967, p. 1576.
[41] W.Y. Choo and J.Y. Lee, Metall. Trans., 13A, 1982, p. 135
[42] H.G. Lee and J.Y. Lee, Acta metall., 32, 1984, p. 1311.
[43] J.L. Lee and J.Y. Lee, Metal Sci., 17, 1983, p. 462.
[44] J.L. Lee and J.Y. Lee, Metall. Trans., 1986.

(A) HY 80, NORMAL S

(B) HY 82, LOW S

FIG. 1 - The Microstructures of HY 80 (high sulfur) and HY 82 (low sulfur).

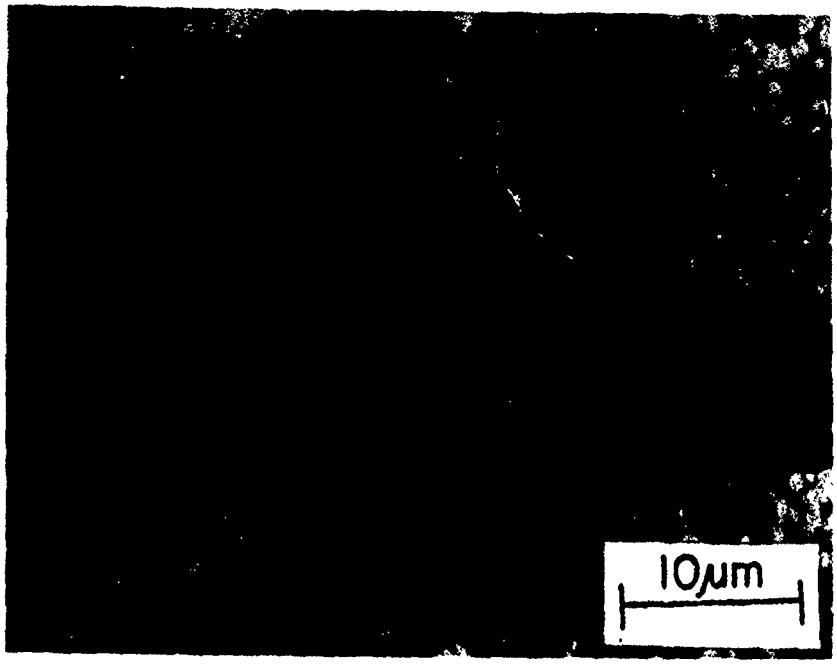

(A) HY 100, NORMAL S

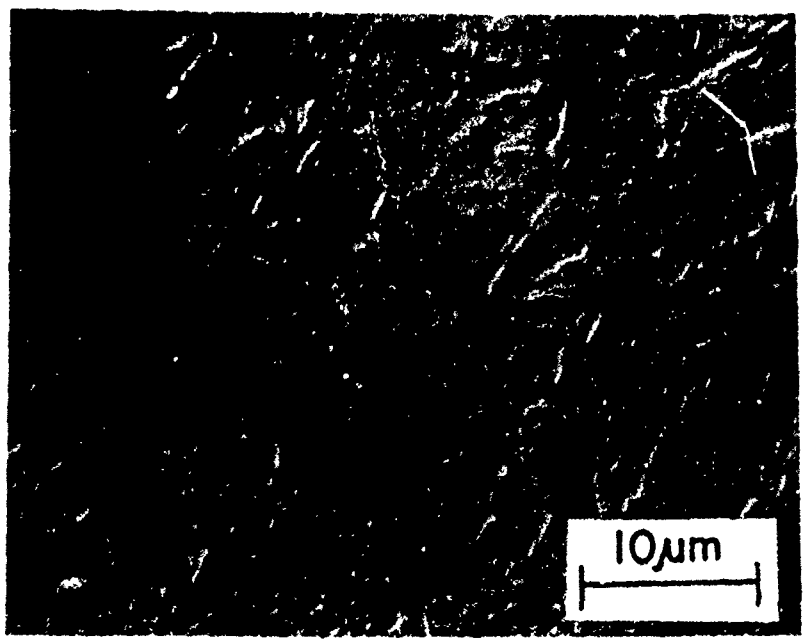

(B) HY 102, LOW S

FIG. 2 - The Microstructures of HY 100 (high sulfur) and HY 102 (low sulfur).

(A) A710-1, NORMAL S

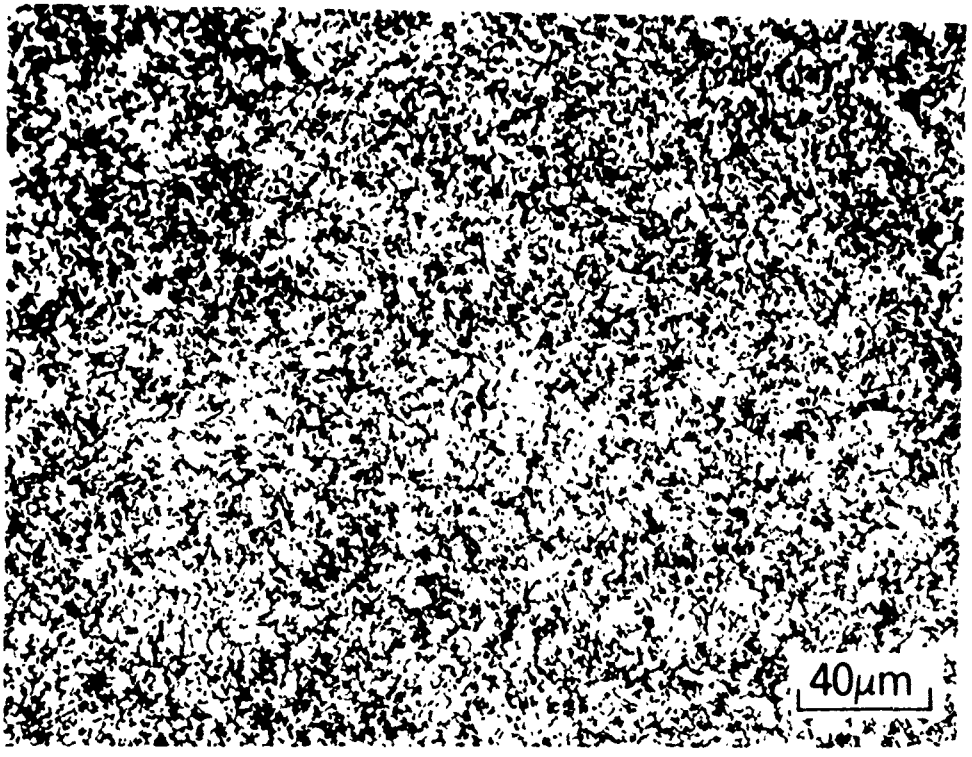

(B) A710-3, LOW S

FIG. 3 - The Microstructures of A710-1 (high sulfur) and A710-3 (low sulfur).

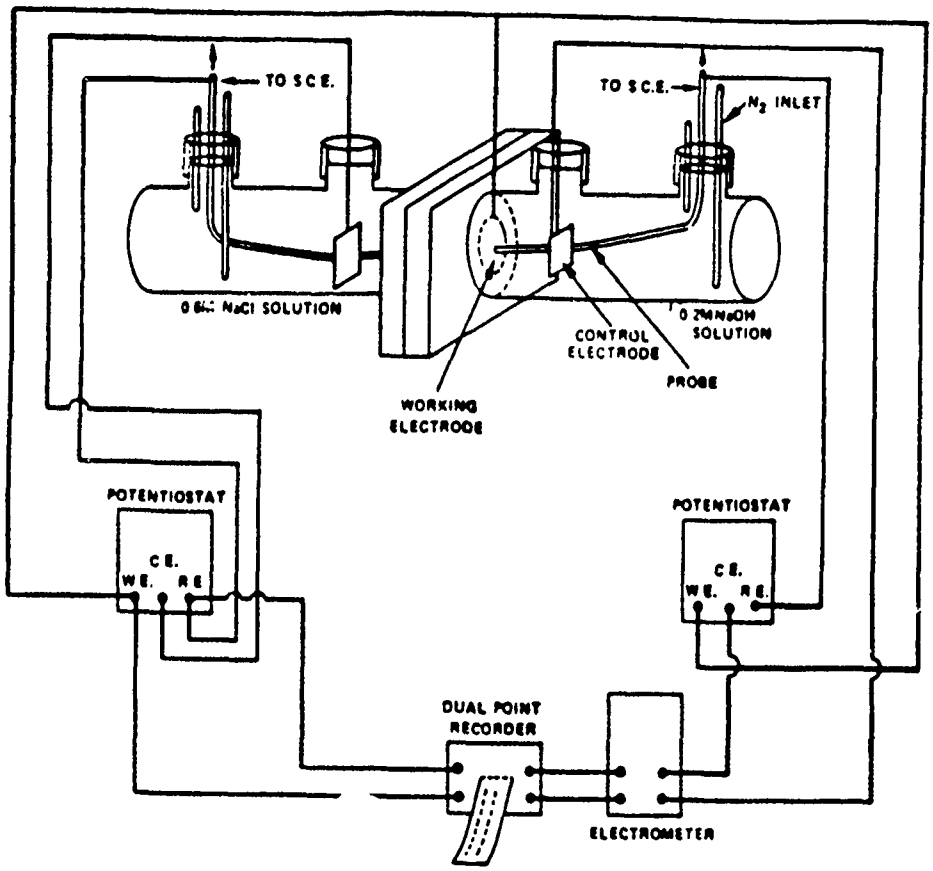

Figure 4. Schematic diagram of the electrochemical permeation cell

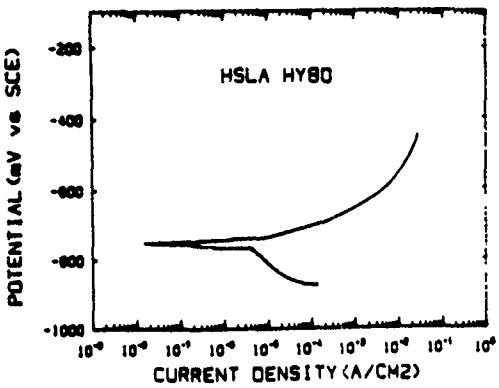

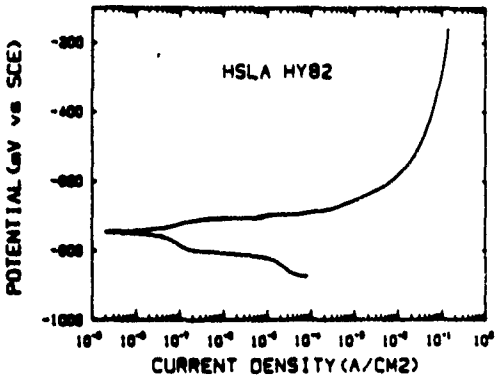

FIG. 5 - Anodic Polarization curves for HY 80 and HY 82.

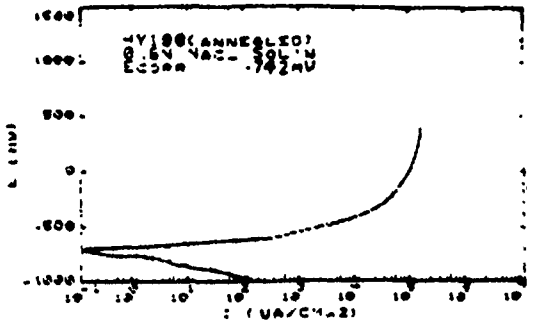

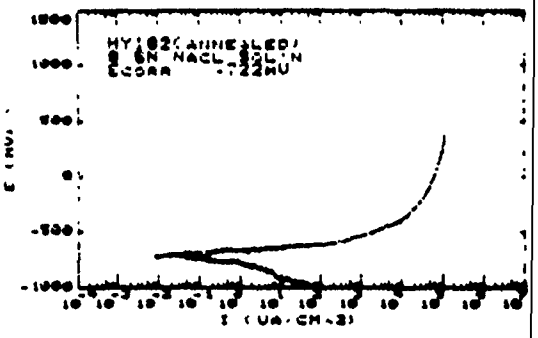

FIG. 6 - Anodic Polarization curves for HY 100 and HY 102.

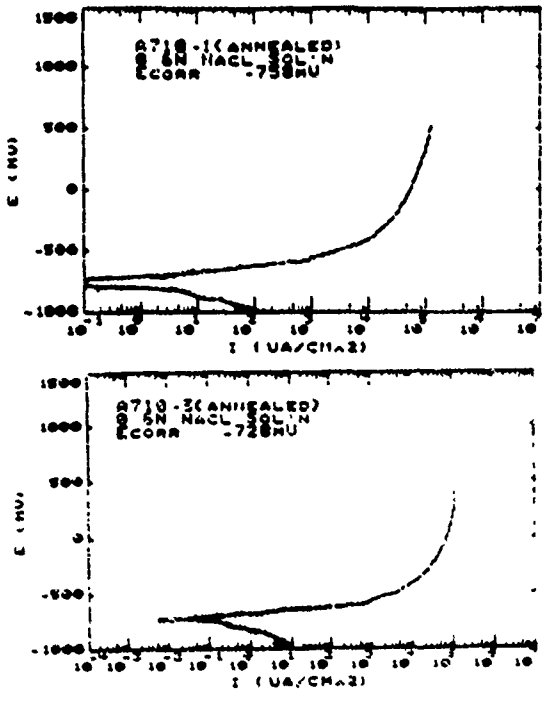

FIG. 7 - Anodic Polarization curves for A710-1 and A710-3.

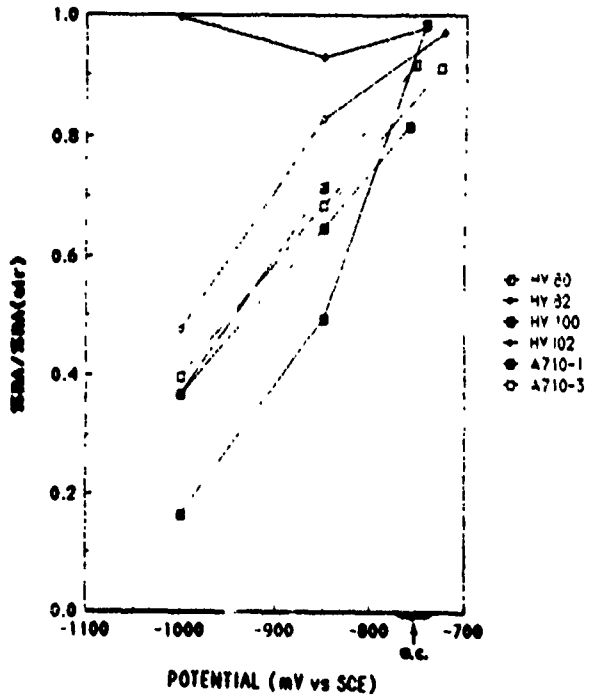

FIG. 8.- Ductility index (%RA(sol.)/%RA(air)) for HSLA alloys as a function of potential.

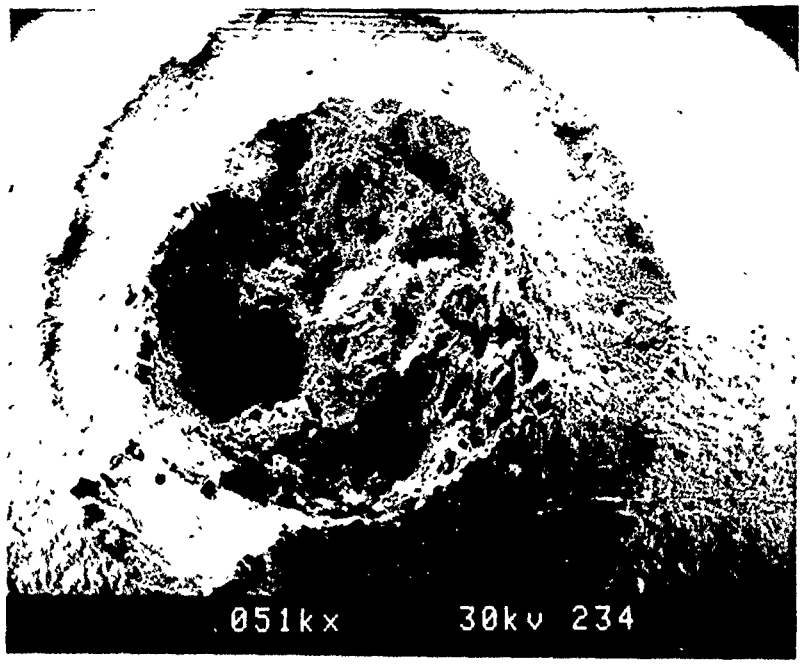

open circuit potential

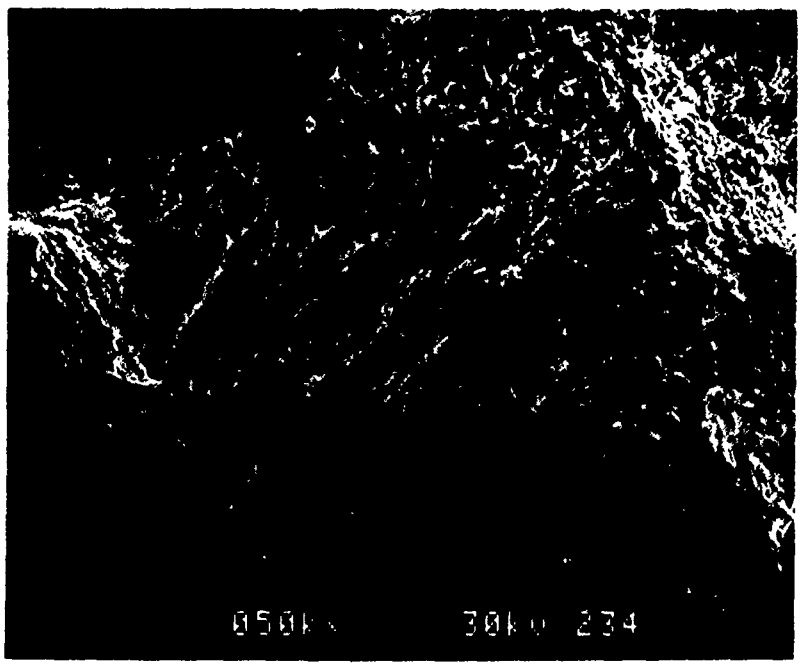

FIG. 9 - Fractographs of Hydrogen embrittlement effect in alloy A710-3.

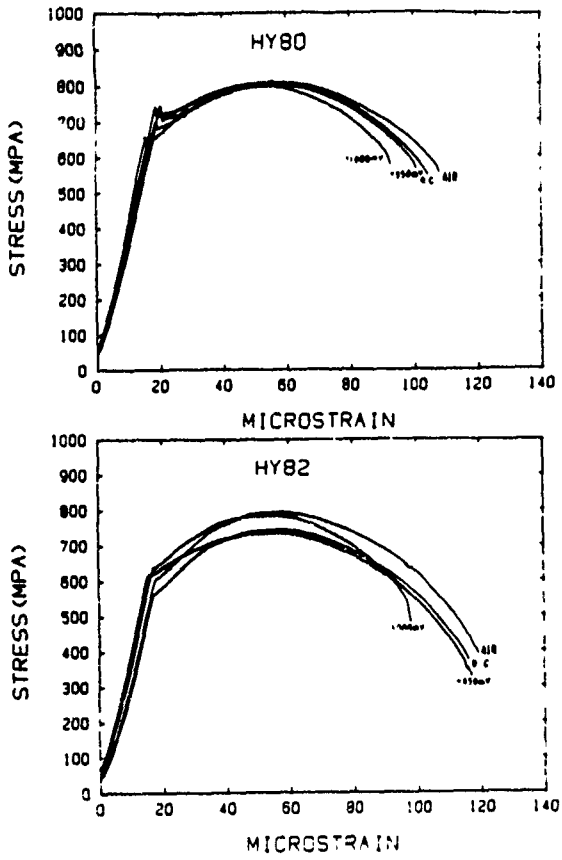

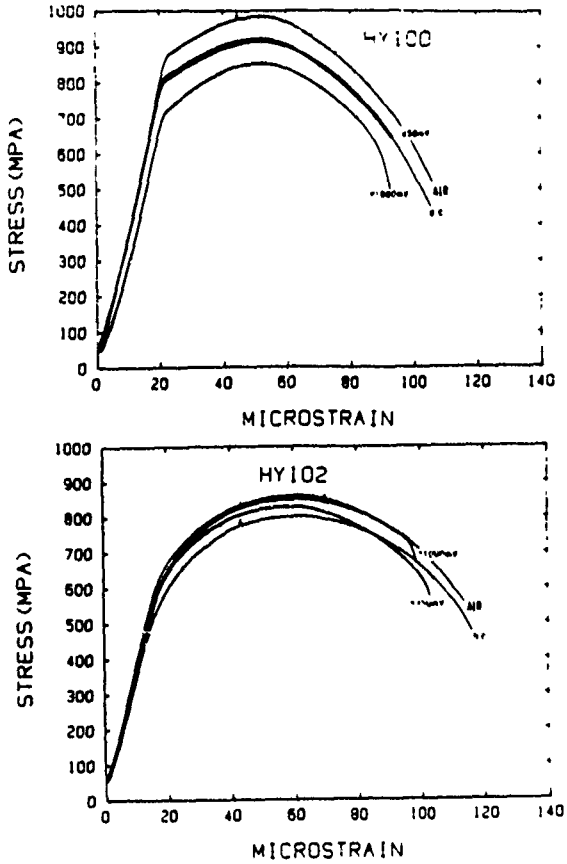

FIG. 10 - Environmental effects on the stress-strain behavior of HY 80 and HY 82

FIG. 11 Environmental effects on the stress strain behavior of HY 100 and HY 102

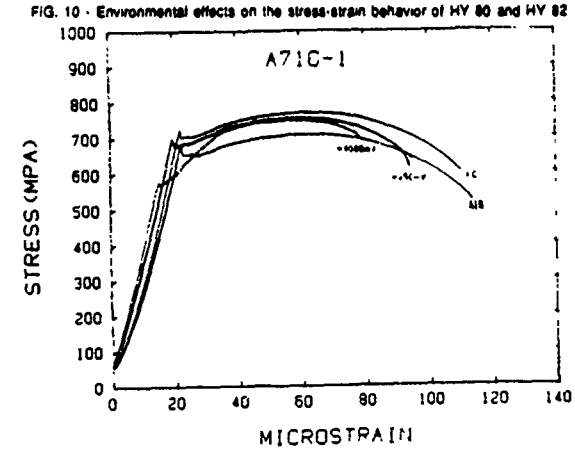

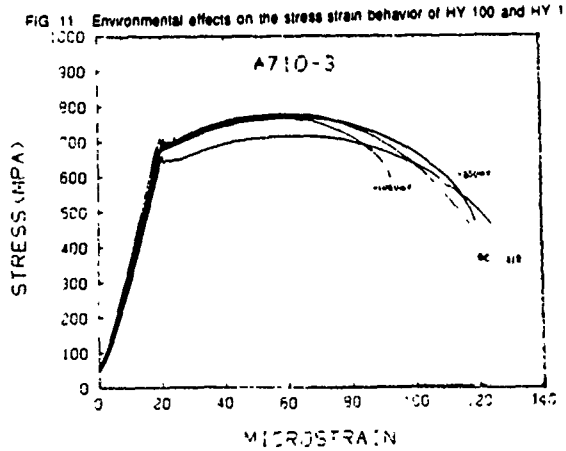

FIG. 12 - Environmental effects on the stress strain behavior of A710-1 and A710-3

ION IMPLANTATION OF 4340 ESR STEEL TO REDUCE HYDROGEN EMBRITTLEMENT

R. Brown
U.S. Army Materials Technology Laboratory
Watertown MA
and
L. Pruitt
Department of Chemical Engineering
University of Rhode Island, Kingston, RI 02881

ABSTRACT

Boron, nitrogen and platinum were ion implanted into Rc 38 and Rc 55 4340 ESR steel discs and circumferentially notched tensile samples to investigate their role in retarding hydrogen embrittlement. Hydrogen uptake studies were conducted by a Barnacle electrode after charging in 3.5% NaCl to determine the relative efficiencies of the implanted species in retarding hydrogen uptake. In all cases, hydrogen uptake was markedly reduced by ion implantation. The microstructural changes to the near surface layers of the steel due to ion implantation were investigated by transmission electron microscopy and related to the uptake data. Slow strain tensile tests in 3.5% NaCl with a crevice in the notch were conducted and failure load measured to detail the effect of ion implantation on mechanical strength. A relative ranking of boron being worst to platinum being the best in mitigating hydrogen embrittlement was determined by this testing. A rationale for this strength ranking and a comparison with the uptake data will be discused.

[Manuscript Not Available at the Time of Printing]

TOW MISSILE STRESS CORROSION STUDY
(RING SPECIMENS)

Wayne M. Bethoney[1], Joseph A. Falco[1], Charles F. Hickey, Jr.[2]

U.S. Army Materials Technology Laboratory
ATTN: SLCMT-MRM
Arsenal Street
Watertown, Massachusetts 02172-0001

ABSTRACT

This report addresses a stress corrosion study on 300 grade, 18% cobalt-containing, maraging steel (C-300) and the 250 grade, cobalt-free, maraging steel (T-250) TOW missile motor cases. In the early 1980's cobalt became a strategic element. This event led to the implementation of the use of T-250, in place of C-300, in this missile system. This paper attempts to establish relative differences in stress corrosion susceptibility between the two materials in the component fabricated condition.

The specimens used in this study were ring type specimens which were machined from along the length of the actual rocket motor cases. Each specimen was notched, precracked, and tested in a salt water environment. Load versus time to failure data was obtained. Also investigated was the possible effects of residual stress on the load versus time to failure data.

Results indicate significant scatter in the data, which could be attributed to the residual stresses along the length of the rocket cases. There was no significant difference in time to failure between the two steels.

INTRODUCTION/BACKGROUND

In 1984, the U.S. Army Missile Command (MICOM) requested the U.S. Army Material Technology Laboratory (MTL) to do a feasibility study on obtaining fracture toughness values (KIc) on TOW rocket motor cases. The wall thickness of the missile motor case (0.072 inches) was found to be too thin for obtaining a valid

[1]Mechanical Engineer, [2]Metallurgist

fracture toughness value. Therefore, only a fracture toughness indicator (Kq) could be addressed. In order to obtain Kq values, the cylinders were precracked using a method developed by MTL. This method involved the use of a series of ring specimens taken from four TOW missile cases fabricated by the shear spinning method. The specimens were electro-discharge machined (E.D.M.) to a depth that did not penetrate the cylinder wall. The ring specimens were then subjected to a slowly increasing internal pressure until the crack propagated through the cylinder wall causing specimen failure. All loads and deflections were recorded. However, no relative values for fracture toughness could be determined. The results of the testing displayed the need for further study of this problem.

Since the notch sensitivity was important, a test to determine this criterion for the missile case was undertaken before any other testing for material properties could be accomplished. A notch running across the face or width was machined into each of the specimens. The notch depth of a number of ring specimens was varied (i.e. specimen #1 had a notch depth of 0.020 inches, specimen #2 had a notch depth of 0.025 inches etc.). These specimens were then tested with the notch in tension using a split "D" ring test fixture (Figure 1). A constant dead weight load was applied to the fixturing using a load rupture machine (Figure 2). This test not only gave an indication of the material's notch sensitivity, but also indicated that there may be significant residual stresses in the missile cases. These residual stresses may have some effect on the material fracture toughness.

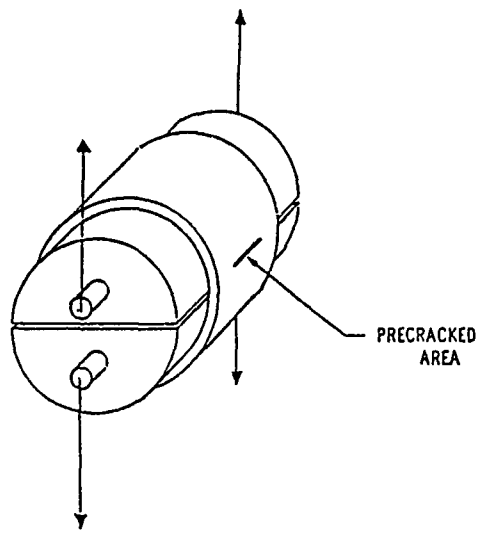

NOTE: arrows indicate loading

Figure 1. Split "D" ring test fixture with specimen.

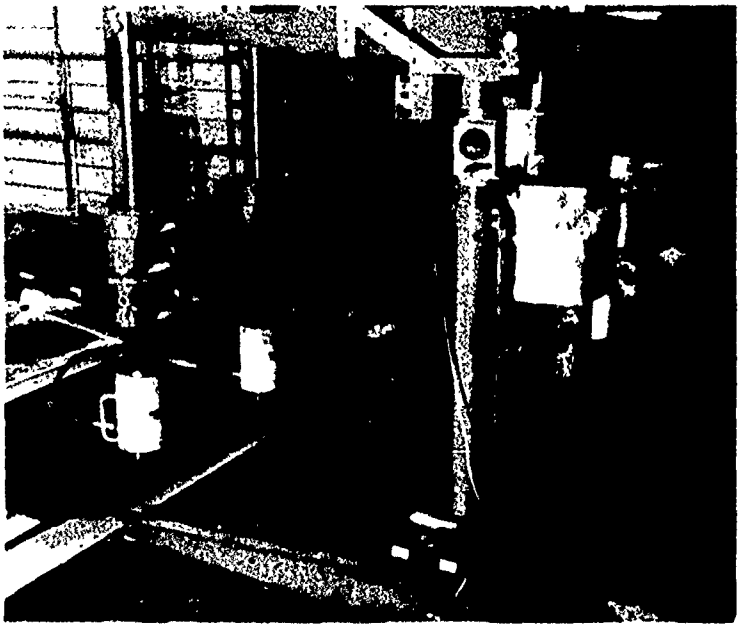

Figure 2. Load rupture machine.

In 1987, a study on the stress corrosion susceptibility of the material used in the TOW missile motor cases was initiated. Two types of stress corrosion tests were performed. The cantilever bend type specimen was used to define the susceptibility to stress corrosion cracking (KIscc) in plate form for the C-300 and T-250 material. The results of that work are reported by Scanlon and Hickey of MTL [1]. This paper addresses the relative susceptibility to stress corrosion cracking of fabricated missile cases using the previously described ring type specimens. The specimens were tested in a 3.5% sodium chloride (NaCl) distilled water solution with load versus time data being obtained.

The possibility of residual stresses playing a major role in the time to failure data was considered. An attempt to measure the residual stresses acting on the rings was made using non-destructive techniques. American Stress Technologies Inc. of Pittsburg, PA performed a series of Barkhausen noise tests for MTL. These rings were supplied to MTL by MICOM. Adjacent rings were destructively tested for residual stresses by MICOM using a milling machine and a strain gage rosette.

[1] Scanlon, J. F. and Hickey, C. F., Jr. "Stress Corrosion Cracking of Maraging Steels", MTL Technical Report

TEST PROCEDURE

A total of four cases were cut into cylindrical ring specimens. Two of the missile cases were fabricated from T-250 cobalt-free maraging steel and the remaining two cases were fabricated from C-300 cobalt-containing maraging steel. Ten one inch wide specimens were cut from each case (Figure 3). This provided twenty T-250 ring specimens and twenty C-300 ring specimens for testing. A slot, 0.50 inches in length and 0.025 inches in depth, was centered across the width of each specimen using an electro-discharge machine (E.D.M.) machining process. The purpose of this notch was to initialize the propagation of a crack in the specimen. To propagate the crack, each specimen was internally pressurized with an oil and water solution. This internal pressure applied to the cylinder walls provided the necessary means for generating the hoop stresses needed to propagate the crack. The pressure was cycled between 500 psi and 3000 psi at a frequency of 15 Hz. until a through wall crack developed causing a loss of internal pressure. Once the specimen was precracked in this manner, it was then statically loaded in the load rupture machine with the crack in tension until it failed.

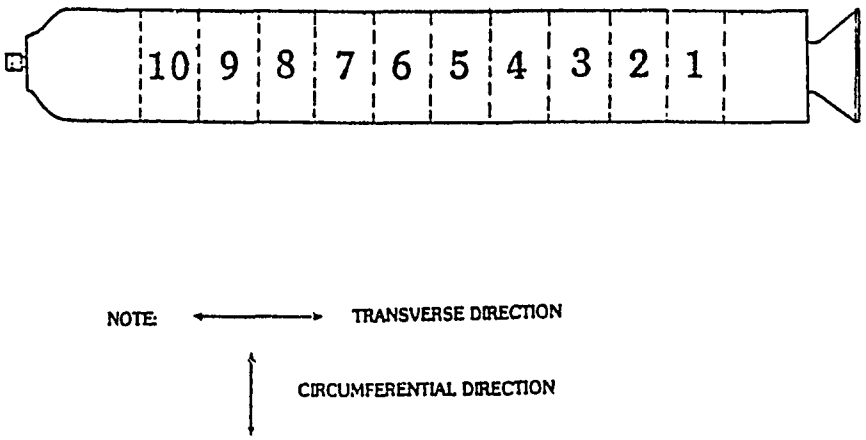

Figure 3. Location of specimens from motor case.

The load rupture machine has two separate split "D" ring fixtures, making it capable of testing two specimens at the same time and recording their times to failure as a function of the constant load. A specimen is placed into the split "D" ring fixture which is located within the salt bath. The tensile load is applied to the specimen using the mechanical lever principal which employs a beam with a dead weight on one end. Due to the location of the fulcrum point of the beam, the specimen is loaded with a weight equal to eight times the applied dead weight load.

EXPERIMENTAL RESULTS

The results from the stress corrosion tests indicate no appreciable difference between the T-250 and C-300 steels. Figure 4 shows that both steels behave the same as a function of the same load. The time to failure did not significantly change between the two materials.

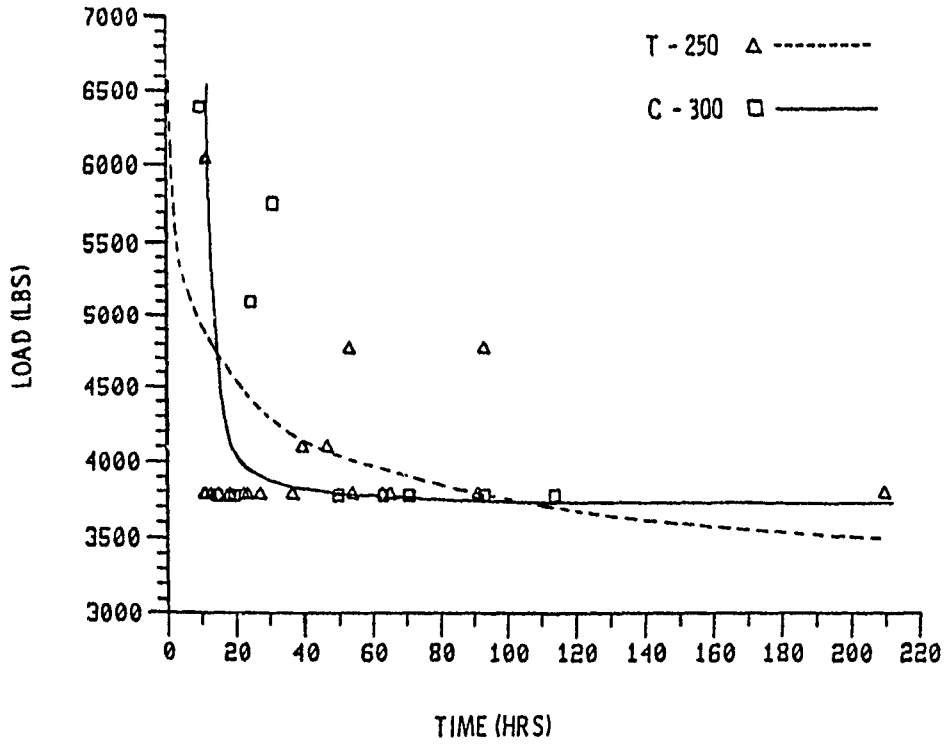

Figure 4. Stress corrosion of T-250 and C-300 steel ring specimens.

Tables 1 and 2 display the actual numbers for the load vs. time to failure. For the T-250, the average time to failure was 48.5 hours while the C-300 had an average time to failure of 58.6 hours. These averages include the results of 15 specimens from each material group of 20 specimens. The first five specimens from each group were used to establish a load versus time to failure data base. The loads for the T-250 (3776 lbs.) and C-300 (3768 lbs.) were chosen as a base for the average time to failure at 50 hours. Each specimen was examined after failure and the percent precracked area was calculated. The average percent precrack area of both materials was within 2-3 percent. This was the basis for taking the average times to failure as the governing criterion for the comparison of both materials.

Table 1
Stress Corrosion Data
T-250 Maraging Steel

Load (lb)	Time (hr)
6030	11.7
4752	93.0
4752	53.5
4088	46.5
4088	39.5
3776	209.4
	53.9
	90.8
	18.1
	62.9
	65.1
	36.7
	22.2
	11.4
	15.0
	27.3
	12.9
	23.5
	10.8

Table 2
Stress Corrosion Data
C-300 Maraging Steel

Load (lb)	Time (hr)
5744	221.5
6384	10.1
5744	31.1
5088	24.7
3768	93.1
	113.7
	70.5
	63.1
	18.4
	18.5
	14.8
	49.9
	19.6
	71.1

Typical fracture surface appearances of failed specimens are displayed in Figure 5 and Figure 6. The C-300 typically showed a textured fracture appearance while the T-250 had little or no textured appearance.

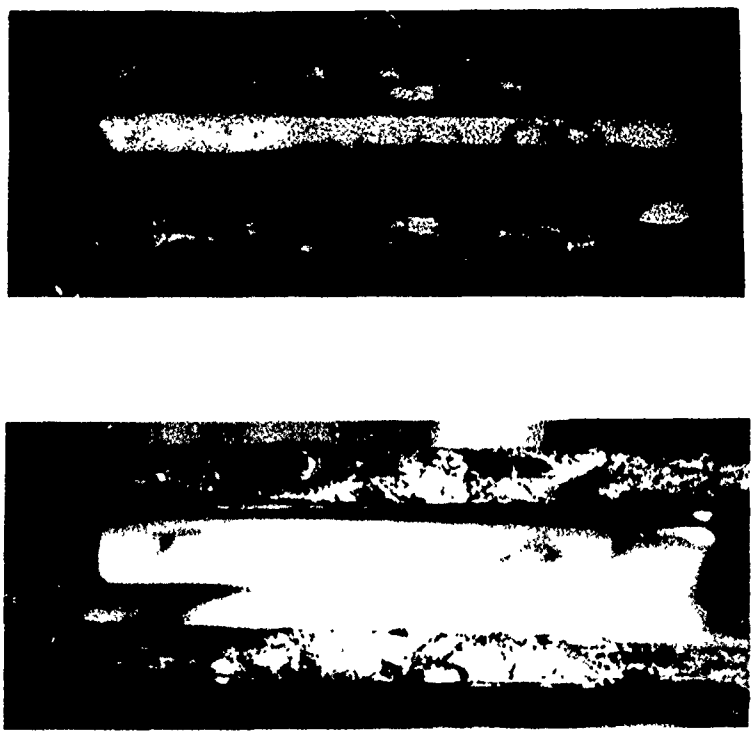

Figure 6. Fracture surface appearance - T-250.

When the failed specimens were examined, an offset in the fracture was observed. One explanation for this offset was due to the possibility that large residual stresses were present. If these stresses are of a tensile nature and are acting on the notch, premature failure due to stress corrosion may take place. Measurement of these stresses could be made using a non-destructive testing technique called the Barkhausen Noise method. In using this method, a probe (coil) is placed in contact with the surface of the specimen. The probe emits a magnetic field that measures the alignment of the lattice structure. This nondestructive evaluation (NDE) technique was performed by American Stress Technologies Inc. on specimens provided by MTL. Tables 3 and 4 are those results of the testing as function of depth. The tables do not provide actual stress values, but show increases and decreases in the noise level as the stresses change magnitudes. Actual stress values could be obtained if a calibration specimen was available. These noise levels do show a similar stress pattern, however, with those obtained by the residual stress measurement techniques used at MICOM.

Table 3
Measurement of Residual Stress
(Barkhausen Noise Method)
Small Ring

Location	Depth[1] (mm)	Direction of Scan	Attenuation (dbm)	Type
OD	0.02	Transverse	24.2	Compression
	0.07	Transverse	11.1	Compression
	0.02	Circumferential	35.0	Low Compression
	0.07	Circumferential	72.0	Tension
ID	0.02	Transverse	62.0	Low Tension
	0.07	Transverse	100.0	Tension
	0.02	Circumferential	9.8	Compression
	0.07	Circumferential	7.4	Compression

Table 4
Measurement of Residual Stress
(Barkhausen Noise Method)
Large Ring

Location	Depth[1] (mm)	Direction of Scan	Attenuation (dbm)	Stress Type
OD	0.02	Transverse	21.0	Compression
	0.07	Transverse	9.0	Compression
	0.02	Circumferential	50.0	No Stress
	0.07	Circumferential	82.0	Tension
ID	0.02	Transverse	83.0	Tension
	0.07	Transverse	55.0	No Stress
	0.02	Circumferential	11.0	Compression
	0.07	Circumferential	8.0	Compression

[1]Conversion factors: 0.02 mm = 0.0008 in., 0.07 mm = 0.0030 in.

SUMMARY AND CONCLUSIONS

This report contains the results of a qualitative investigation as to the susceptibility to stress corrosion cracking between the C-300 and T-250 TOW missile motor cases. Load versus time data was obtained from ring type specimens which were machined from missile cases of both materials, and tested in a 3.5% NaCl environment. The effect of residual stress on the time to failure data is also addressed. The conclusions from this paper are as follows:

1. Time to failure data indicates no appreciable difference between the T-250 and C-300.

2. The residual stresses in the rocket motor cases in the vicinity of the cracks may have played a role in time to failure in the corrosive environment.

3. A larger population of specimens is needed to better determine differences between the two materials.

4. A fracture toughness math model for thin-walled cylinders should be developed.

STRESS CORROSION CRACKING OF MARAGING STEELS

James F. Scanlon and Charles F. Hickey, Jr.
U.S. Army Materials Technology Laboratory
Watertown, MA 02172-0001

ABSTRACT

The 250 and 300 grades of the 18% Ni cobalt-containing (C) and cobalt-free (T) maraging steels were tested in 3.5% NaCl solution in a cantilever bend apparatus to determine their susceptibility to stress corrosion cracking. These alloys represent current or candidate materials for missile motor case applications. In recent years, since cobalt is a critical and strategic element, emphasis has been placed on the suitability of substituting the T versions for the C versions in the TOW and Stinger missile systems. One questiion which has arisen and is addressed in the study is the difference in susceptibiltiy to stress corrosion cracking between the C and T versions. This study has determined that the values of K_{Iscc} for C-250, T-250, C-300 and T-300 are 29, 21, 18 and 16 ksi$\sqrt{in}$, respectively. Electron and optical microscopy were used to investigate the mechanisms of failure. Electrochemical methods were also employed to characterize the general corrosion behavior of the alloys.

[Manuscript Not Available at the Time of Printing]

DESIGNING CONDUCTIVE SEALS FOR NAVAL AIRCRAFT: A CASE HISTORY

J.J. Thompson, W.W. Lin, and D.P.W. Thomas
Naval Air Development Center
Warminster, PA 18974-5000

ABSTRACT

Naval aircraft pose a special challenge to the designers of conductive seals. Conductive seals are required to shield flight critical avionics from electromagnetic interference (EMI); yet, present designs have caused severe structural corrosion damage. Design criteria for conductive seals are often conflicting, requiring compromises for optimum performance in hostile electromagnetic and marine environments. The challenge is exemplified by the series of seal design changes required on a naval fighter aircraft. Early designs ensured conductivity by using noble metals, but caused deep pitting of the aluminum structure. The latest design successfully provides corrosion protection by double encapsulation of noble metal in sealant. The conductive seal operating environment and design criteria are discussed with respect to naval aircraft needs of performance, inspectability, and maintainability.

INTRODUCTION

Modern aircraft are dependent upon avionics for almost every facet of operation. For example, dramatic weight savings and capability improvements have been achieved by replacing hydraulics with electronics and using wires and integrated circuits in advanced flight controls. This control concept is known as "fly by wire".

As avionics technology has moved from vacuum tubes to integrated circuits, the sensitivity of electronic components to electromagnetic interference (EMI) has dramatically increased. Modern circuits operate at low power levels which can be disrupted with low level noise. EMI can affect avionics by introducing garbled and false signals, disrupting memory, and destroying circuits. With the increase in susceptibility has come a concurrent increase in the power and number of EMI sources. The proliferation of long range radar and communication systems has produced a severe electromagnetic environment.

Shielding is used to protect avionics from the electromagnetic environment. Shielding is accomplished by enclosing electronic equipment in a conductive shell (a Faraday shield). The shell reduces the incident EM energy to tolerable levels through reflection and absorption. Joints and seams provide a point for EMI leakage. Conductive gaskets are used to provide electrical continuity across

joints to ensure a continuous protective shell. Conductive gaskets also aid lightning strike protection by providing a conductive path.

Corrosion is a major cause of shielding deterioration. Corrosion protection has traditionally relied upon oxides, organic coatings, and other non-conductive films to act as a barrier to the environment. Conversely, EMI gasketing has traditionally relied upon non-oxidizing, conductive noble metals. EMI seals eliminate corrosion protective coatings to ensure a conductive path across a joint. A typical low electrical resistance joint of silver and aluminum is a dissimilar metal couple with a large galvanic driving force for corrosion. Corrosion produces non-conductive films allowing EMI intrusion, and degrades the load bearing capabilities of a structure.

The Navy maintains a data base of electromagnetic compatibility (EMC) problems entitled AMITS (Air Systems EMI Corrective Action Program (ASEMICAP) Management Information and Tracking System). The following are examples of the kinds of problems that can result from inadequate, deteriorated shielding. Aircraft and helicopters can jettison bombs while taking off from an aircraft carrier due to the response of bomb release circuits to carrier transmitters. Helicopter rotor blades and aircraft wings can inadvertently fold when illuminated by radar. Shipboard EMI can cause aircraft computers to "dump" programs necessary for the operation of mission essential equipment.

Combining corrosion protection with EMI shielding in a severe corrosive and EM environment poses a significant challenge in designing and maintaining conductive seals. This paper discusses EMI seal requirements of naval aircraft by examining the operating environment and the corrosion driven redesign of a conductive seal.

NAVAL AIRCRAFT OPERATIONAL ENVIRONMENT

Naval aircraft deployed on an aircraft carrier encounter a combination of high humidity, temperature, atmospheric salt content, and stack gases. Communication and radar systems require use of a wide range of frequencies at high power levels. The severe environment aboard aircraft carriers necessitates extensive protective measures.

Corrosive Environment

Corrosion is most active while the aircraft is at sea level. Naval aircraft spend considerable time on the flight decks of aircraft carriers exposed to sea spray and sulfur-bearing stack gases. Atmospheric salt concentration in marine tropical environments[1] is approximately $2.5 \times 10^{-4} g/m^3$. Deployed aircraft encounter temperatures of 90°F (32 C) and 90% relative humidity for months at a time. Measurements made of surface moisture from aircraft on flight decks determined the pH to be between 2.4 and 4.0, and also detected the presence of sulfate ion.[2] The carrier environment can be considered to contain salt spray with weak sulfuric acid. The severity of the shipboard environment compared with other marine environments is shown in Figure 1.[3]

The proximity to a marine environment obviously poses major corrosion problems for the aircraft exterior. Not so obvious is the intrusion of saline moisture into avionic equipment and systems installed in apparently protected areas.[4] Salt laden moisture can be rapidly driven into cracks and crevices by 40 mph winds during normal flight operations. Experience has indicated the wide range of flight loads, inherent airframe flexing, and inevitable seal deterioration make a water-tight airframe unobtainable. The effectiveness of a seal in minimizing moisture intrusion depends upon the structural stiffness of the airframe, the thickness, compressibility, permeability and freedom from voids in the gasket, and spacing of the fasteners. Weight and maintainability considerations have led to doors with little design margin for less than optimum conditions. Seal deterioration arises from dimensional changes, periodic maintenance actions, and attack by various fluids, heat, ozone, etc. Fastener areas can be important points for water intrusion. Maintenance actions requiring access door removal and replacement can cause the fastener holes to elongate and increase diameter.

While efforts continue to improve the moisture resistance of airframes, judicious design should be based on the assumption that the corrosive exterior environment will be present both outside and inside a naval airframe.

Electromagnetic Environment

Communications and radar systems have dramatically increased the power and frequency range of electromagnetic waves used in commercial and military applications. A naval battle group uses a frequency spectrum from 10 kHz to 40 GHz at power levels for individual emitters of almost 14,000 V/m.[5] Actual power levels of seven of the frequently used radar systems have been measured aboard an aircraft carrier.[6] With only one system operating, the power levels for most of the flight deck exceeded the commonly specified level of 200 V/m used for Navy qualification testing.[7] Older aircraft and avionics presently operational were tested at field strengths up to 20 V/m.[8]

Shielding is used to attenuate the external field to a level where the avionics are not susceptible. The equation for shielding effectiveness is given as follows:

$$SE = -20 \log (E_i/E_o)$$

where SE is shielding effectiveness in decibels (dB), Ei is the incident field strength, and Eo is the transmitted field strength.[9] For example, to shield avionics of older aircraft tested at 20 V/m from an external field of 1000 V/m, 34 dB attenuation is required. The trend towards increasing emitter power, microcircuits sensitivity, and avionics dependence will increase future shielding requirements.

CASE HISTORY OF CONDUCTIVE SEAL DESIGNS ON A NAVAL AIRCRAFT

Modern naval aircraft are typically carrier based, multi-mission, and are under fly-by-wire control. They are designed so the airframe acts as a conductive

shell to partially shield the internal avionics. The fuselages consists largely of graphite/epoxy and aluminum access doors over an aluminum frame. EMI seals on door joints in the dorsal region protect flight control wire bundles necessary for safety of flight. EMI seals have required several redesigns because of extensive corrosion of the aluminum structure. The potential corrosion problem was recognized in design,[10] but at the time the environment was not well characterized making it difficult to determine performance standards, testing, and establishment of corrosion control methods. These factors, to a large degree, still hold true.

Initial Seal Design

A design for one aircraft originally used noble conductive materials and relied on environmental seals to protect the dissimilar metal couples. The composite door was electrically bonded to the aluminum longeron by a round compressible EMI gasket (see Figures 2 and 3). The gasket consisted of monel wire mesh knitted around a silicone sponge core. Titanium rub strips were used on either side of the knitted wire mesh to prevent galling. The rub strips were bonded to the aluminum longeron with a silver-filled epoxy adhesive. The Ti/Ag/Al dissimilar metal interface was covered with polysulfide form-in-place (FIP) seal to provide environmental protection. The EMI gasket was spot bonded to the rub strip at one inch (25 mm) intervals with a non-conductive epoxy adhesive.

After three years service an aircraft undergoing thorough inspection was observed to have pits up to 70 mils (1.8 mm) deep in the aluminum longeron beneath the Ti rub strip (Figure 4).[11] In this area corrosion damage 10 mils (0.25 mm) deep causes concern. Damage was not noted before this inspection because the area was hidden beneath the rub strip and FIP seal. The damage was particularly severe at low points in the scalloped longeron where the width of the FIP seal was less than one-eighth inch (3 mm).

Second Seal Design

The damage severity and unknown loss in EMI shielding forced prompt action. A two prong approach was used. Similar EMI seals on the accessible radar bulkhead were sprayed with an electronics grade water displacing coating[12] each time the bulkhead was opened. On the dorsal longeron, the EMI seals were redesigned (Figure 5a) to replace the dissimilar Ti/Ag/Al interface. The monel knitted wire mesh was replaced by steel wire electroplated with a copper flash followed by tin. The plated wire mesh is soft and allowed the removal of the Ti rub strips. Other composite-skinned aircraft effectively utilize a metal-sprayed coating consisting of 80% Sn/20% Zn for EMI shielding. Measurements of electrochemical rest potential indicated Sn/Zn metal spray is compatible with aluminum. Metal spraying can be performed aboard ship, allowing any damage in the seal area to be inspectable and repairable. These advantages made the plated wire mesh and Sn/Zn coating appear to be an ideal solution.

One year and one deployment after implementing the second seal design,[13] pits up to 30 mils (0.8 mm) deep were observed in the longeron. Testing in SO2 salt spray (ASTM G85.A4) and electrochemical studies utilizing the zero impedance ammeter

technique showed the Sn/Zn coating initially cathodically protects the aluminum through Zn and Sn dissolution. However, a dealloying process occurred with time. A Sn rich coating formed which was electrochemically incompatible with aluminum. The rest potential shifted from that of zinc (compatible with Al) to that of Sn (incompatible with Al). The porous nature of the metal-sprayed coating allowed the environment access to the longeron substrate almost immediately. Also, the non-conductive spot adhesive formed hard spots which prevented the door from closing tightly to the FIP seal. The wire knitted mesh exhibited extensive red rust. The water-displacing compound was found in lab testing to effectively protect the Sn/Zn coating for up to two weeks.

The galvanic incompatibility of tin with aluminum is consistent with previous testing of EMI joints aboard ships.[14] In contrast, other studies[15] have shown a good quality tin plating provides the best overall performance, but noted results between geographical locations are highly variable.

Present Seal Design

After two unacceptable designs, corrosion became the dominant concern. To address this, the corrosion prone knitted wire braid and tin/zinc metal spray coating were eliminated. Instead, a fluorosilicone elastomer rope filled with silver coated aluminum particles was bonded onto the structure using a fluorosilicone room temperature vulcanizing (RTV) compound (Figure 5b). The RTV and FIP seal completely covered the conductive gasket/structure interface, preventing moisture ingress.

There were some initial concerns about the corrosion resistance of this design. First, the conductive particles are silver coated creating a large electrochemical potential difference between the aluminum longeron and the gasket. Secondly, the fluorosilicone RTV adhesive evolves acetic acid during curing, which is known to accelerate corrosion. Detailed examination of other aircraft of this type which had been deployed to the Indian Ocean for 7-8 months showed only minor and isolated pitting corrosion, no more than 2 mils (0.05 mm) deep. However, other problems were observed developing from the design, materials, and personnel training. The primary problems were electrical contact, and maintenance considerations.

Poor electrical contact between the conductive gasket and the longeron was the primary problem of this design. This arose from pressing the conductive rope through the RTV and from joint unevenness. A non-conductive skin formed between the gasket and the longeron if the conductive gasket was not applied quickly. Large joint unevenness due to door bowing, production tolerances, and corrosion removal cannot be compensated by the uniform diameter of the conductive gasket rope.

Poor electrical contact also arose from joint unevenness which caused permanent deformation of the gasket. Damage to the conductive rope resulted in areas where pressure exceeded the maximum pressure limit of the material. The mechanical properties of the fluorosilicone, and the maximum pressure limit, are reduced by loading conductive particles into an elastomer. Compression set degraded both the EMI and environmental seal capabilities.

Maintenance considerations also have been an issue. This seal was designed to be maintained aboard a carrier deck. Because shielding of this location is considered necessary for safety of flight, an aircraft with a damaged seal is grounded until the EMI seal is repaired. A procedure exists for seal repair aboard ship, but the skill required for proper installation has made repair feasible only at a depot facility when the carrier returned to port. The fluorosilicone RTV in an enclosed area requires four to eleven days to cure. Even if this design had been repairable on a carrier, seal repair would require (theoretically) an aircraft to be grounded until the RTV cured.

Other concerns were the poor adhesion of the RTV to both the polysulfide and conductive rope, and incomplete coverage of the structure with the RTV. Both situations could allow moisture to penetrate to the conductive gasket/longeron interface and cause corrosion. Poor adhesion may have been caused by inadequate surface preparation or by using a RTV beyond its shelf life. These two problems may be alleviated by increased training and experience of maintenance personnel.

Potential Seal Design and Materials

The design complexity and large joint mismatch made conductive gaskets, which are cured before installation, inappropriate for this application. Conductive form-in-place (CFIP) seals (Figure 5c) combine EMI seals with an environmental seal. CFIP seals are elastomers filled with conductive particles which are cured directly on the aircraft. This best compensates for large joint unevenness and provides improved electrical contact. Using CFIPs instead of pre-formed gaskets would eliminate an intermediate, non-conductive adhesive between the conductive seal and the structure. Under current investigation is a polythioether sealant filled with nickel coated carbon and a chromate inhibitor.

The major problem with using CFIP seals is the consistency of seal properties after installation. Similar to other aircraft sealants, CFIP seal properties are dependent on the cure environment and mixing procedure. Proper mixing procedure is essential to obtain uniform properties. Conductive gaskets have more consistent properties because they are made in a controlled manufacturing environment where the quality of the material can be assured before use. CFIP application draws upon the experience and training fleet personnel presently have with conventional sealants. CFIPs have great potential to meet the need for EMI seals in joints with large unevenness and difficult operational requirements.

Another approach to forming conductive materials uses chemical bonding agents (CBAs). The CBAs are mixtures of chelating and reducing agents which reduce oxides. The resulting elemental metal and metal complexes form a conductive medium. Corrosion protection is provided by scavenging oxygen, and through formation of a hermetic barrier coating. This approach has been found effective with steel for intermodulation interference (IMI) applications aboard ships.[16] For EMI applications involving aluminum, a conductive elastomer has been developed consisting of adiprene, ascorbic acid, and zinc carbonate.[17]

CONDUCTIVE SEAL DESIGN CONSIDERATIONS

The lessons derived from a naval aircraft EMI seal redesign provide insight into general conductive seal guidelines. These fall into two categories: (1) properties which should be incorporated into seal design and tested; and, (2) inspection and maintenance procedures to ensure optimum operation.

Design Guidelines for Conductive Gaskets

Conductive gasketing is used to provide an electrical ground and EMI shielding across a joint, and often employs an environmental seal. They are used on temporary apertures such as access panels. These panels have seams that must be electromagnetically sealed. The form of a gasket is determined by attachment methods, force available, joint unevenness, available space and the EMI shielding criteria. The major material requirements for EMI gaskets include:

(1) Good electrical properties - Good conductivity is taken as an rough, indirect measure of EMI shielding. In addition, a contact resistance of 2.5 milliohms is specified across joints for grounding, lightning strike protection.[18]
(2) Corrosion resistance of gasket material - Properties should not change with service, e.g. corrosion which produces an insulating layer of material.
(3) Compatibility with the mating surface - Electrochemical compatibility to prevent galvanic corrosion.
(4) Good adhesive qualities - Required for electrical contact and environmental sealing.
(5) Chemical resistance to solvents - Properties should not change with exposure to operational chemicals e.g. fuel, paint stripper, hydraulic fluid, etc.
(6) Resilience - Resistance to compression required for electrical contact and environmental sealing. Long term pressure should not cause permanent deformation (compression set). Normal deflection for solid rectangular elastomer seals range from 5 to 15%.
(7) Wear resistance - Important when the gasket is repeatedly compressed and depressed.
(8) Conformability - Accommodate joint unevenness

The often conflicting material requirements create difficulties in seal design. For example, replacing the monel wire mesh with plated steel wire mesh allowed the Ti rub strips to be removed, but aircraft vibration wore away the tin plating and exposed the vulnerable steel substrate.

Some of the important lessons learned during the design evolution concerned corrosion test methods. The initial test samples consisted of a sandwich of graphite epoxy, environmental seal, and aluminum encapsulating the EMI seal. All aspects of the simulated seal were perfect. The significance of test results was biased toward neutral salt spray (ASTM B117) results. Experience showed these assumptions were incorrect. Environmental seals leak, the EMI seal was exposed to a corrosive environment. The naval operating corrosive environment was found to be more closely represented by SO_2 salt spray (ASTM G85). Later test samples

were open to the environment, contained reasonable flaws, and were tested up to four weeks in SO_2 salt spray.

Recommended Inspection and Maintenance Requirements

Aircraft requirements are well reviewed in a manual[19] on EMC theory and practice issued by NAVAIR for the naval maintenance community. EMI gaskets should be periodically checked to ensure they are continuing to provide their intended functions. Inspection intervals should balance the need for proper operation and the environment, with the destructiveness caused by surface wear of gaskets with opening and closing. Gaskets may deteriorate through attack by operational chemicals, corrosion, and wear. Therefore, inspection should include the following guidelines:

(1) Check for corrosion products, pitting of the aluminum surface, or bulges in the sealant due to corrosion beneath the gasket.
(2) Check the bonding of the gasket to the structure to prevent moisture ingress.
(3) Check for loss of electrical conductivity of the gasket,[20] or its electrical bond to the aircraft.[18]
(4) Check for wear and swelling of the gasket.
(5) Check for compression set of the seal.
(6) Check maintenance procedures are being followed, e.g. avoid cleaning solvents which can wash away conductive particles.

If the gasket shows deterioration, the design should allow easy repair and/or replacement.

A chattering relay test based upon MIL-STD-462[21] is under investigation as a method to inspect EMI shielding integrity. With a battery powered EMI source inside an aircraft and a portable receiver outside, the EM field is measured with the door open and closed to determine attenuation. Portability requirements for the receiver limit the frequency range which may be measured.

CONCLUSIONS

The recognized need to shield against a severe EM environment in a corrosive atmosphere has been met with only partial success. Current practices are either too short lived or too labor intensive to ensure the shielding needed for long term survivability in the hostile carrier environment. Problems experienced with EMI seals are illustrated by the corrosion driven design evolution on a naval aircraft. The major problems were determined to be maintaining conductive seal performance due to electrochemical incompatibility, joint unevenness, mechanical degradation, and repair difficulties. Seal design for naval applications should consider the need for inspecting and maintaining performance, and assume the impossibility of sealing from the corrosive marine environment. Failure to consider these lessons learned will result in aircraft EMI susceptibility and potential catastrophic consequences.

REFERENCES

1. H.J. Singletary, "Aircraft Service Life Extension Through Corrosion Control, "CORROSION/73, Paper No. 217, National Association of Corrosion Engineers, Houston, TX, March 1987.
2. S.J. Ketcham and E.J. Jankowsky, "Developing and Accelerated Test: Problems and Pitfalls," Laboratory Corrosion Tests and Standards, ASTM STP 866, G.S. Haynes and R. Baboian, Eds., ASTM, Phila., p. 14, 1985.
3. E.J. Jankowsky and S.J. Ketcham, "Shipboard Exposure Testing," Naval Air Development Center Report No. NADC-81075-60, Sept 1981.
4. NAVMAT P 4855-2, "Design Guidelines for Prevention and Control of Avionic Corrosion, June 1983.
5. R.G. Siefker, "Tailoring MIL-STD-461B For Naval Avionics Applications, "Symposium Record of IEEE International Symposium on Electromagnetic Compatibility, 16-18 Sept 1986, San Diego CA, pp. 387-395.
6. R. Lowry, "USS Constellation (CV-64) EMC Measurements," Electromagnetic Compatibility Analysis Center Report No. ECAC-CR-85-002, March 1985.
7. MIL-STD-461C, Electromagnetic Emission and Susceptibility Requirements for the Control of Electromagnetic Interference, 4 Aug 1986.
8. MIL-STD-461A, Electromagnetic Interference Characteristics, Requirements for Equipment, 31 July 1967.
9. D.R.J. White, "Electromagnetic Shielding: Materials and Performance," Don White Consultants, Inc., Gainseville VA, p. 1.14, 1980.
10. A.W. Morris and J.J. Reilly, "Corrosion Control Methods for Electrically Bonded Joints in Aircraft," Materials Performance, Vol. 14, No. 1, p. 9 (1975).
11. G.S. Peranteau, "F/A-18 Aircraft First Cruise Post-Deployment Corrosion Inspection," Naval Engineering Support Office Report No. NESO-001-86, 9 May 1986.
12. MIL-C-81309D Class III, Corrosion Preventive Compound, Water Displacing, Ultra-thin, Soft Film.
13. V.S. Agarwala, R.C. Paciej, and J.J. Thompson, "A Study of Zn/Sn EMI Seal Material," Naval Air Development Center Report No. NADC-87014-60, April 1986.
14. E.J. Jankowsky, "Shipboard Exposure Testing of F/A-18 Finish Systems," Naval Air Development Center ltr 6062, 1 Dec 1982.
15. B.L. Cain, "EMI/RFI Gasketing for Tactical Shielded Shelter Door Seam Application," Report No. AFWAL-TR-83-4127, February 1984.
16. J.C. Cooper, Rm. Panayappan, and R.C. Steele, "Chemically Suppressing Rusty -Bolt Intermodulation Interference," Proceedings of IEEE National Symposium on Electromagnetic Compatibility, Institute of Electrical and Electronics Engineers, Piscataway, NJ, p. 233, 1984.
17. J.C. Cooper, Naval Research Laboratory, Washington D.C., Private communication, 1988.
18. MIL-B-5087 Bonding, Electrical, and Lightning Protection for Aerospace Systems.
19. NAVAIR 5161/653-1988, "Electromagnetic Compatibility Theory and Practice Manual for Naval Aviation Depots," May 1988.
20. MIL-G-83528 Shielding, Gaskets, Shielding, Elastomer Electrical, EMI/RFI, General Specification For.
21. MIL-STD-462 Electromagnetic Interference Characteristics, Measurement of.

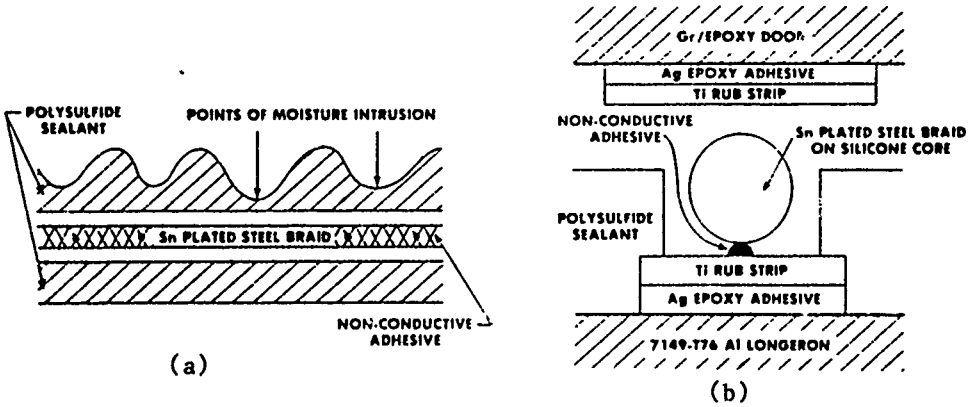

Figure 3. Initial Conductive Seal Design in (a) Longitudinal and (b) Cross Sectional Views

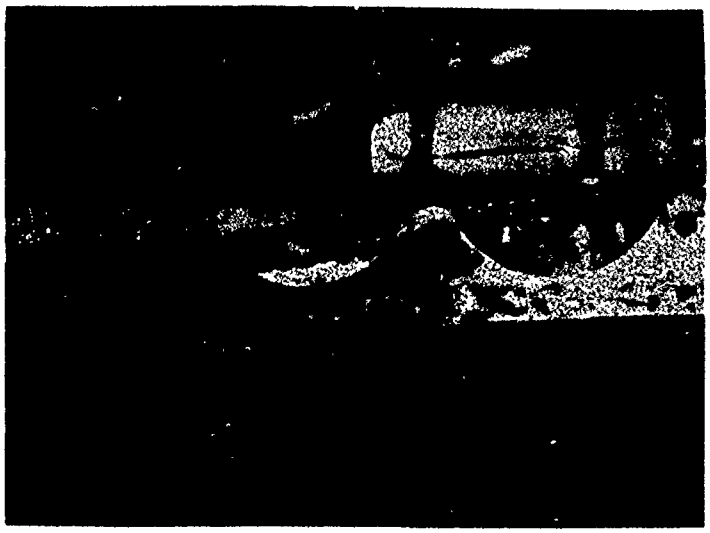

Figure 4. Corrosion of Aluminum Longeron Beneath Initial Conductive Seal Design

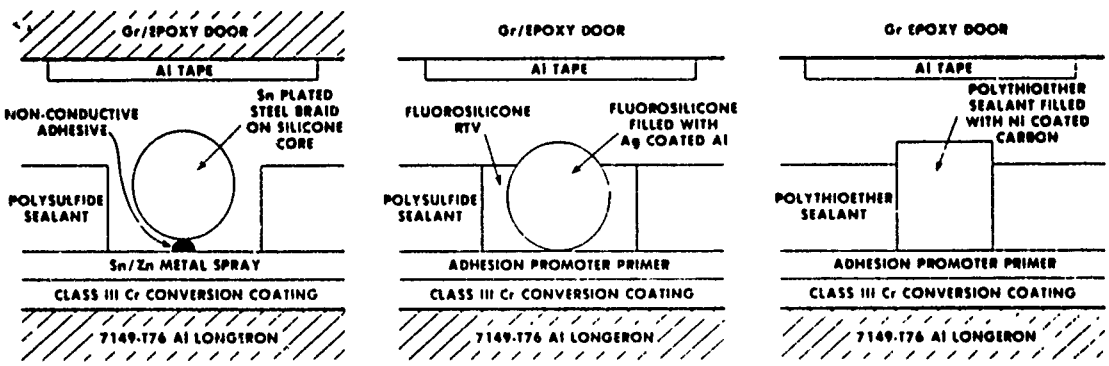

Figure 5. Cross Sectional Views of (a) Second, (b) Present, and (c) CFIP Conductive Seal Designs

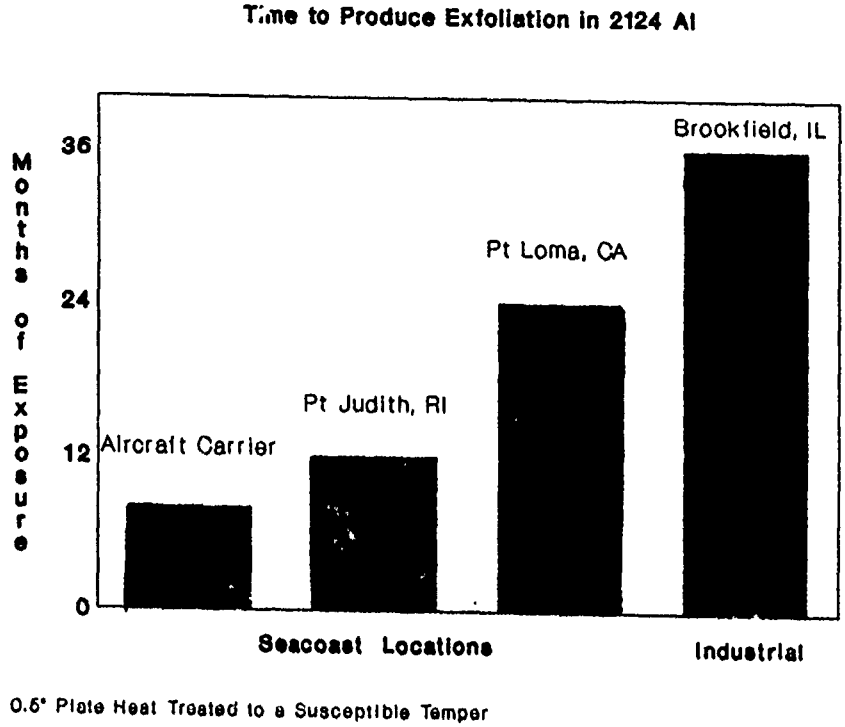

Figure 1. Comparative Corrosivity of Environments

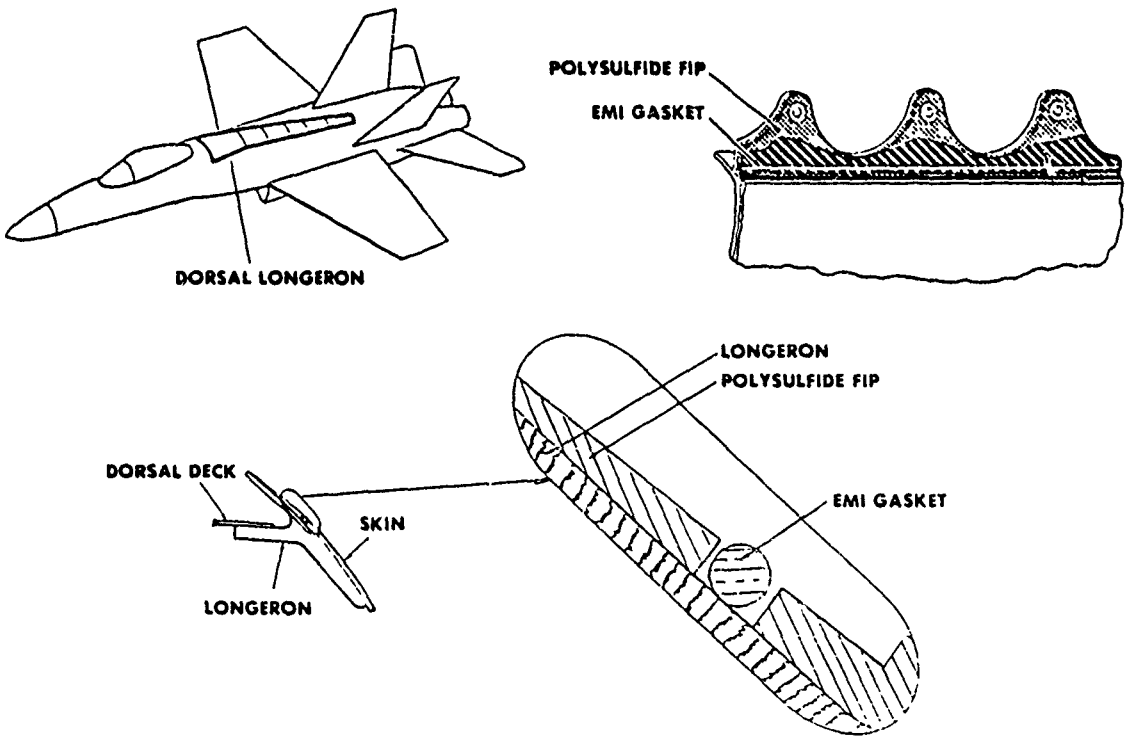

Figure 2. Location of Dorsal Longeron Conductive Seal

EFFECT OF APPLIED DIRECT AND ALTERNATING CURRENTS ON THE CORROSION BEHAVIOR OF 90/10 Cu-Ni

R. K. Conrad and J. F. McIntyre

Naval Surface Warfare Center
Materials Division
Electrochemistry Branch
10901 New Hampshire Avenue
Silver Spring, MD 20903-5000

Corrosion failure of 90/10 Cu-Ni seawater piping is a recognized problem in the Navy. Many corrosion failures have been attributed to erosion/corrosion, impingement, and cavitation effects. To mitigate these types of attack, it is necessary to carefully control flow velocities and optimize piping geometries. Another potential contribution to seawater piping failure is accelerated attack by stray-currents. A laboratory investigation was conducted to study the effects of applied direct and alternating currents on the corrosion behavior of 90/10 Cu-Ni. Corrosion behavior was determined by weight-loss measurements. Both direct and alternating currents were applied by two methods: internal and external. External currents were forced across the metal/solution interface and internal currents were applied through the bulk of the alloy. The influence of impingement attack was also studied with and without the application of direct currents.

INTRODUCTION

Preliminary laboratory results on the effect of applied direct currents (DCs) and alternating currents (ACs) on 90/10 Cu-Ni (CN) are reported herewith. This research was conducted to support the Naval Surface Warfare Center's task to determine the effect of stray currents on the corrosion behavior of navy seawater cooling pipes. Potential-drop measurements made on several ships revealed that DCs and ACs were present in CN seawater piping. Subsequent measurements determined that ACs were introduced into the seawater piping by pumps located on the ship's cooling skid. However, during these measurements, the source of DCs was not ascertained. Laboratory tests were conducted concurrently with shipboard measurements to aid in establishing the corrosion behavior of CN piping in the presence of stray currents.

BACKGROUND

The action of stray currents on metallic structures can lead to accelerated failures. Stray currents enter a structure at a point of low

electronic resistance and often travel for some distance before exiting at a point of least resistance. The place where stray currents exit the structure acts as the anode and preferentially corrodes at a high rate. This phenomenon has been associated with buried pipe lines and ship hulls. Stray currents originate from faulty cathodic protection systems on buried pipe lines or leakage of current from nearby power stations. Stray-current corrosion on steel ship hulls originates almost exclusively from poor grounding of welding equipment. The current return path to the welding equipment is through the ship's hull, exiting at the water/steel interface, and returning to welding equipment on shore. A number of articles can be found in the literature on stray current corrosion.[1-9] A schematic of this mechanism is illustrated in Figure 1.

The present understanding of the stray current corrosion mechanism suggests that this form of corrosive attack should not be problematic in seawater piping, provided piping runs are not electrically isolated. Although ACs and DCs are present in the pipes, the chance that premature failures are caused exclusively by stray currents is minimal. The presence of an insulating material, e.g., high impedance oxide or other dielectric substance, in the electrical current path would be necessary for stray currents to affect corrosion. In the absence of an insulator, which blocks current passage, the movement of currents through the piping system should proceed unimpeded. It is unknown what effect stray currents will have on the corrosion behavior of pipes locally thinned by erosion-corrosion, impingement, or cavitation. Laboratory investigations hav been designed to focus on this unanswered question. Laboratory tests will be complemented by controlled dock-side tests on CN piping, where the individual effects of flow velocity, stray currents, and microbial attack will be investigated.

EXPERIMENTAL

Corrosion behavior of CN was determined by weight-loss (WL) measurements. Samples were machined into 1" diameter disks from 1/16" sheet supplied by Metal Samples, Inc. The elemental composition for CN is given in Table 1.

TABLE 1. ELEMENTAL COMPOSITION OF 90/10 Cu-Ni

Cu	Ni	Fe	Mn	Zn	Pb	P	C	S
88.15	9.51	1.53	.605	.098	.005	.005	.003	.002

All samples were wet-ground down to a 400 grit SiC finish, rinsed in distilled water (DW), the surface cleaned with a cotton swab, rinsed with DW, and dried in a stream of air. Samples were weighed to the nearest 0.1 mg using an analytical balance. All samples were exposed to ASTM synthetic

seawater for 7 to 14 days. At the conclusion of exposure testing, samples were cleaned with DW, corrosion products were removed by a 1-2 minute soak in deaerated 50 v/o HCl, and reweighed to obtain the experimental WL. Blank samples were subjected to the same chemical post-treatment to attain WL induced by the stripping solution. A plot of WL against time of exposure to the cleaning solution is shown in Figure 2. No correction on the WL data was necessary because actual samples were exposed to the stripping solution for 1-2 minutes, which is less than the time required to produced noticeable WLs. Corrosion rates were calculated from the WL data and are reported as mils per year (mpy).

ACs and DCs were applied to a given sample by either an internal or external method. External application of AC or DC involved forcing a current across the metal/solution interface using a graphite rod, as an auxiliary electrode, and a DC power source or an AC wave generator (see Figure 3). The internal method involved application of ACs or DCs through the bulk of the metal. A sample holder was constructed from polyethylene and designed so that the metal sample was exposed on two sides. The sample configuration was similar for both externally and internally applied currents. For application of internal currents the test sample was sandwiched between two copper o-rings; current entered through the first copper o-ring, passed through the bulk of the metal, and exited through the second copper o-ring (see Figure 4).

Preliminary tests were also initiated to study the influence of solution impingement on the corrosion behavior of 90/10 Cu-Ni in the absence and presence of applied internal DCs. A schematic of the test apparatus is shown in Figure 5. The same sample holders were used in this round of testing as were used for previous tests. The sample was held at a fixed distance from a 1/8" diameter orifice, which created a jet impingement on the sample. ASTM synthetic seawater was used for impingement tests. A flow velocity of 1000 ml/min was maintained with a Master Flex® peristaltic pump.

RESULTS

The corrosion rate of CN alloy in the absence of applied currents is summarized in Table 2 for 7-14 day exposures. It can be seen that the corrosion rate at 7 days was identical to that at 14 days. All samples were uniformly attacked and covered with a thin, dark, adherent oxide layer.

The application of external DCs and ACs resulted in greatly accelerated attack. A summary of corrosion rates for externally applied currents can be seen in Tables 3 and 4. In comparison the corrosion rate for CN increased significantly with the application of either external DCs or ACs. As compared to freely corroded CN samples, the corrosion rate was about an order of magnitude higher for 0.49 mA/cm^2 DC and AC and two orders of magnitude higher for 5 mA/cm^2 DC. Corrosion rates were higher for applied DCs than for ACs. The corrosion rate decreased as the

TABLE 2. CORROSION RATES FOR 90/10 Cu-Ni EXPOSED TO ASTM SYNTHETIC SEAWATER

Days	WL (mg)	MPY
7	2.2	2.06*
14	4.1	1.94@

* average of six tests
@ average of three tests

TABLE 3. CORROSION RATES FOR 90/10 Cu-Ni EXPOSED TO ASTM SYNTHETIC SEAWATER FOR 7 DAYS WITH APPLIED EXTERNAL DCS

Current Density (mA/cm^2)	WL (mg)	MPY#
0.05	4.6	23.4
0.50	39.5	37.0
4.90	378	354

\# average of three tests

TABLE 4. CORROSION RATES FOR 90/10 Cu-Ni EXPOSED TO ASTM SYNTHETIC SEAWATER FOR 7 DAYS WITH APPLIED EXTERNAL ACS

Current Density (mA/cm^2)	Hz	WL (mg)	mpy*
0.50	10	23.3	22
5.10	10	22.8	23
0.50	30	23.6	24
5.10	30	27.8	28
0.05	50	9.4	9
0.50	50	24.5	23
5.10	50	11.3	11
0.50	60	14.7	14
5.10	60	3.6	3
0.50	300	10.0	8
5.10	300	34.1	28

* average of two tests

frequency of the AC signal increased, with an exception at 300 Hz for an applied AC of 5 mA/cm^2. This anomaly occurred because of severe crevice corrosion between the o-ring seal and the sample surface. All test samples were covered by a two layer film: an inner, dark, tightly adherent film and loosely adherent outer blue-green layer.

The application of internal DCs and ACs to exposed CN samples showed no change in the corrosion rate as compared to those with no applied currents. The results for internally applied currents are summarized in Tables 5 and 6. A comparison of the corrosion rates for CN without applied currents and those samples subjected to internal currents are nearly identical; in fact, it appeared as though the application of internal DCs and ACs reduced the rate of attack. All surfaces were uniformly attacked and covered with thin dark adherent oxide layer.

Several samples were subjected to vigorous agitation using a magnetic stirring device. This test was conducted to determine whether increased flow across the sample surface would increase the corrosion rate. The magnitude of the solution flowing past the sample was not measured. Results indicated that the corrosion rate remained unaffected by increased agitation for samples with no applied currents. A sample with an applied internal DC of 10.2 mA/cm^2 exhibited a slight increase in the corrosion rate when exposed to an agitated solution (see Table 7).

TABLE 5. CORROSION RATES FOR 90/10 Cu-Ni EXPOSED TO ASTM SYNTHETIC SEAWATER FOR 7 DAYS WITH APPLIED INTERNAL DCS

Current Density (mA/cm^2)	WL (mg)	MPY*
0.50	1.25	1.2
4.95	0.85	0.8
10.2	1.15	1.1

* average of 2 tests

TABLE 6. CORROSION RATES FOR 90/10 Cu-Ni EXPOSED TO ASTM SYNTHETIC SEAWATER FOR 7 DAYS WITH APPLIED INTERNAL ACS

Current Density (mA/cm^2)	Hz	WL (mg)	MPY
0.50	10	1.9	1.8
5.10	10	0.5	0.5
0.50	30	0.1	0.01
5.10	30	3.0	2.8
0.50	50	0.0	0.0
5.10	50	0.5	0.5
0.50	60	2.1	1.85
5.10	60	1.9	1.7

TABLE 7. CORROSION RATES FOR 90/10 Cu-Ni EXPOSED TO ASTM SYNTHETIC SEAWATER FOR 7 DAYS WITH SOLUTION AGITATION

Condition	WL (mg)	mpy*
No Applied Currents	1.84	2.0
Applied Internal DC (10.2 mA/cm^2)	2.63	2.9

* average of two tests

DISCUSSIONS

At a uniform corrosion rate of 2 mpy (the rate of freely corroded CN), it would take approximately 45 years for a 3" diameter CN pipe of .095" thickness to fail. However, stray DCs of 0.5 or 5.0 mA/cm^2 would lead to failure in 2.5 years and 3.25 months, respectively. This assumes that stray current corrosion can be represented by the external current application tests of this study. A similar increase in failure time can be expected for low frequency, i.e., <60 Hz stray ACs.

CN seawater pipes have failed in 3 to 6 months on a number of ships, this corresponds to corrosion rates of between 190 and 350 mpy. From potential drop measurements made on navy ships, the magnitude of DCs was approximately 5 mA (2.8 mA/cm^2 for a 3" diameter pipe). If all of this current exited the pipe at one localized spot, e.g., a 0.5 cm^2 area, the resulting 5.6 mA/cm^2 DC would be sufficient to cause a leak in the pipe in 3 months. However, this could only occur in the vicinity of an insulator in the CN pipe. Because no insulators are used in CN seawater piping, i.e., at flange connections, it is unlikely that stray currents will cause premature failure.

A current flowing in pipes containing water usually causes no accelerated corrosion to the inside of the pipe.[10] The high electrical conductivity of CN compared to water (or seawater) makes it nearly impossible to generate corrosion currents across the pipe/water interface which are sufficient to accelerate corrosion. For example, as described by Uhlig:[10]

> ... since the resistance of any conductor per unit length equals ρ/A where ρ is the resistivity and A is the cross-sectional area, then the ratio of current carried by a metal pipe compared to that carried by the water it contains is equal to $\rho_w A_m/\rho_m A_w$, where subscripts w and m refer to water and metal, respectively. For iron, $\rho_m = 10^{-5}$ $\Omega\cdot$cm and for potable water ρ_w may be 10^4 $\Omega\cdot$cm. Assuming that the cross-sectional area of water is 10 times that of the steel pipe, it is seen that if current through the pipe is 1 A, only about 10^{-8} A flows through

the water. This small current leaving the pipe and entering the water causes negligible corrosion. If seawater is transported instead, with ρ_w = 20 Ω·cm, the ratio of currents is 2 X 10^5, indicating that even in this case most of the current is carried by the metallic pipe and there is very little stray current corrosion on the inner surface.

Accelerated corrosion of CN seawater piping can be attributed to other failure mechanisms: erosion/corrosion, cavitation, impingement, or microbial attack. The interaction of these modes of failure with stray-currents is not well understood. It has not been determined whether stray-currents in pipes exacerbate erosion/corrosion, cavitation, or impingement failures.

Preliminary tests to investigate the effect of solution impingement on the corrosion behavior of CN in the absence and presence of applied internal DCs indicated that the corrosion rate was significantly increased by solution impingement (see Table 8). In fact initial results indicate that the corrosion is further exacerbated by applied internal DCs. No explanation for this behavior has been proposed.

TABLE 8. CORROSION RATES FOR 90/10 Cu-Ni EXPOSED TO ASTM SYNTHETIC SEAWATER FOR 7 DAYS WITH AND WITHOUT APPLIED INTERNAL DCS AND SUBJECTED TO JET IMPINGEMENT

Condition	WL (mg)	mpy*
No Applied Currents	7.9	10.6
Applied DC Internal (10 mA/cm^2)	14.7	25.7

* average of three tests

CONCLUSION

The uniform corrosion rate of CN exposed to synthetic seawater is small and pipe failures, in the absence of highly localized attack, should not occur for many years. Because of the deleterious effects of high flow velocities, impingement, and cavitation, highly corrosion resistant CN is susceptible to accelerated failures. Induced external DCs or ACs leads to rapid corrosion of CN, which should be indicative of active stray-currents. However, the presence of currents flowing through the bulk of CN test samples did not promote accelerated corrosion. The application of internal DCs or ACs should be representative of currents found in the CN seawater piping. It is proposed, in the limit of this investigation, that

currents which remain in the bulk of the pipe will not result in premature failures. It remains unclear as to the nature of the interaction which occurs between stray currents found in the CN piping and the mechanically induced acceleration of CN piping corrosion caused by high flow velocities, impingement, or cavitation.

REFERENCES

1. Lennox, T. J. and Peterson, M. H., "Stray Current Corrosion of Steel," Naval Engineers Journal, Feb, 1976, p. 45.

2. Lennox, T. J. and Peterson, M. H., "Stray Current Corrosion of Aluminum," Naval Engineers Journal, Aug, 1977, p. 73.

3. Cornet, I., Pirtz, D., Polivka, M., Gau, Y., and Shimizu, A., "Laboratory Testing and Monitoring of Stray Current Corrosion of Prestressed Concrete in Seawater," Corrosion of Reinforcing Steels in Concrete: ASTM STP 713, 1978, p. 78.

4. G.D. Sump and M.D. Schrantz, "Stray Current Corrosion During Platform Welding Operations Offshore," Offshore Technology Conference: Vol. 4, Dallas, TX, pp. 443 (1977).

5. Lennox, T. J. and Peterson, M. H., "The Effect of Stray Direct Current on Yellow Brass," National Association of Corrosion Engineers Conference, Paper No. 95 (1977).

6. Sibila, J., "Some Aspects of Determining Corrosive Conditions of Underground Structures in Stray Current Areas," National Association of Corrosion Engineers Conference, Ontario, Canada, Paper No. 81, 1981.

7. Schwalm, L. H. and Sandor, J. G., "Stray Current- The Major Cause of Underground Plant Corrosion," Materials Protection, June, 1969, p. 39.

8. Grosz, O. L., "Evaluation of Corrosion Damage Due to Improper Grounding of Welding Unit on Offshore Platforms," National Association of Corrosion Engineers Conference, Paper No. 179, 1976.

9. Meany, J. J., "A History of Stray Traction Current Corrosion in the United States," National Association of Corrosion Engineers Conference, Paper No. 152, 1974.

10. Uhlig, H. H. and Revie, R. W., Corrosion and Corrosion Control: An Introduction to Corrosion Science and Engineering, John Wiley, & Sons, New York, NY, 1975, pp. 212-213.

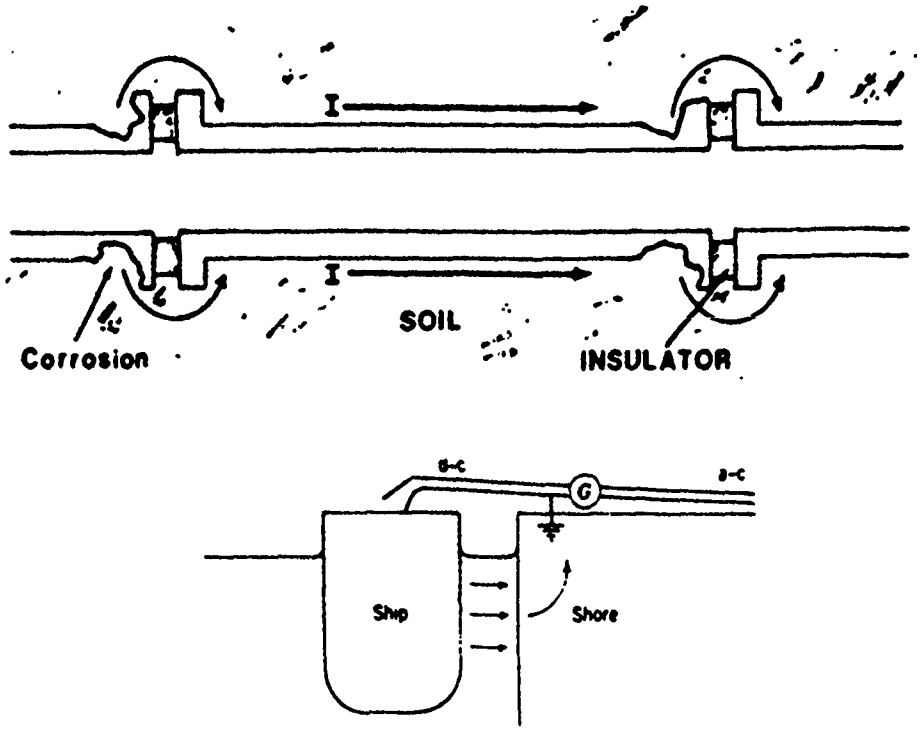

FIGURE 1. SCHEMATICS OF STRAY CURRENT CORROSION

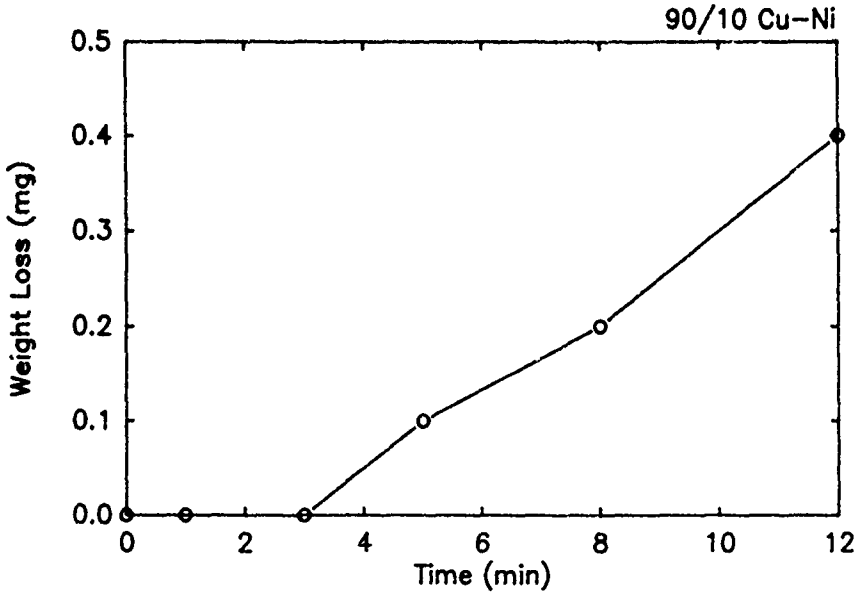

FIGURE 2. Effect of Stripping Solution on Weight-Loss

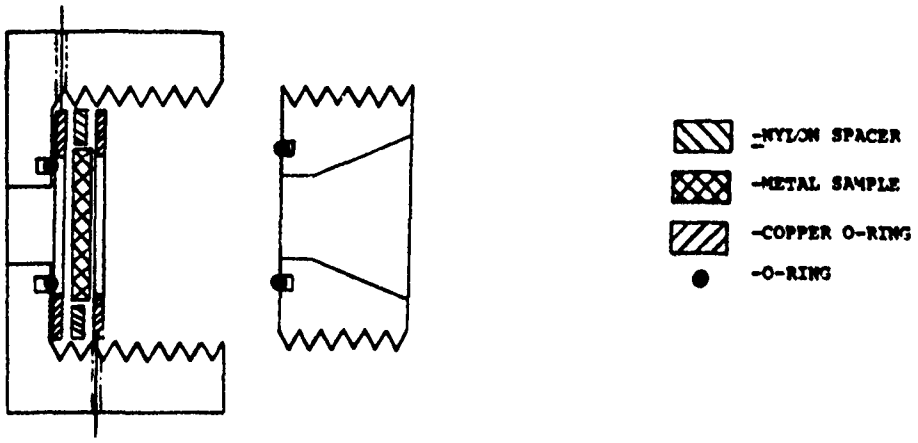

FIGURE 3. SCHEMATIC FOR APPLICATION OF EXTERNAL CURRENTS

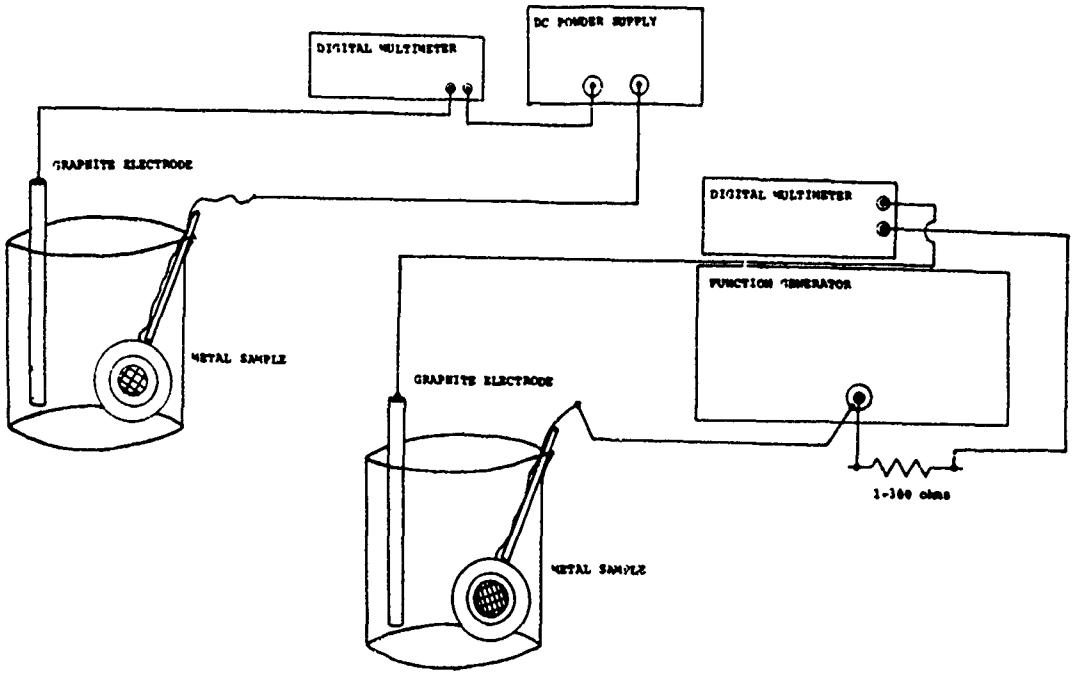

FIGURE 4. CELL HOLDER FOR APPLICATION OF INTERNAL CURRENTS

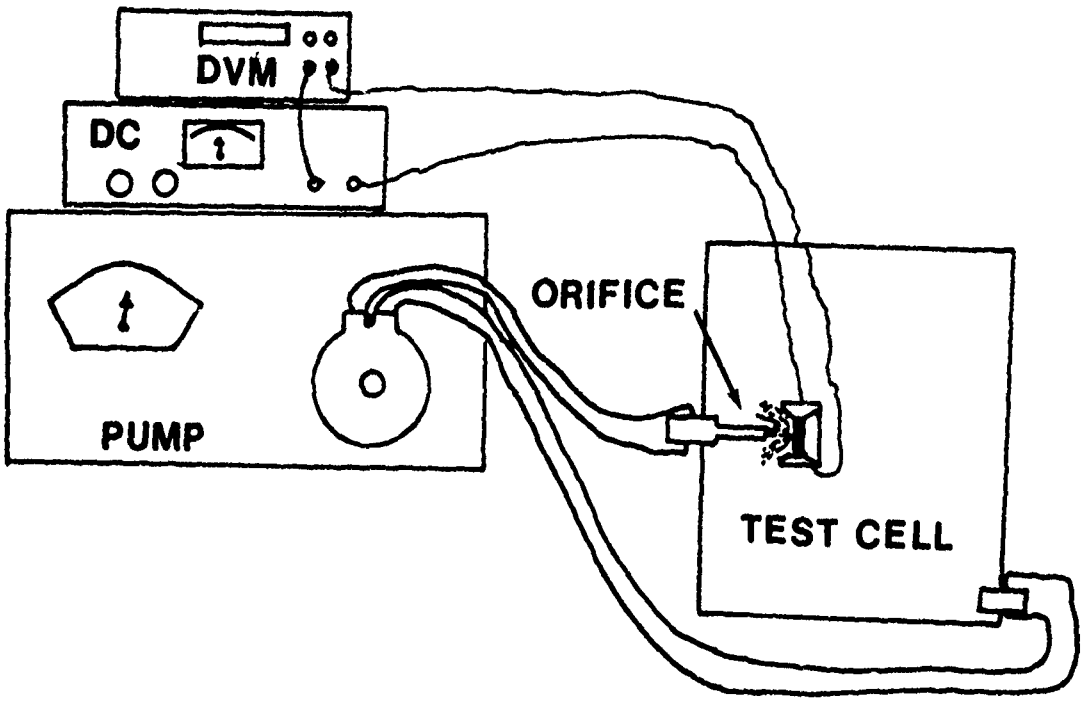

FIGURE 5. SCHEMATIC OF JET-IMPINGEMENT TEST

APPLICATION OF CORROSION-CONTROL TECHNOLOGIES TO EMP-HARDENING FITTINGS AND OTHER DEVICES IN THE NAVAL TOPSIDE ENVIRONMENT

N. Andrew Greig
ARINC Research Corporation
a Subsidiary of Arinc Incorporated
2551 Riva Road
Annapolis, Maryland 21401

ABSTRACT

The U.S. Navy is retrofitting major combatant warships to enclose exposed topside cables in shielded conduit to protect low-power solid-state electronics from disruption or damage due to a nuclear electromagnetic pulse. Metal fittings are used to connect conduit to topside electrical penetrations and enclosures. Inappropriate material selection, inadequate weather sealing, and poor mechanical design led to corrosive failure of these fittings. Marine environmental exposure testing of typical fitting assemblies confirmed that incipient corrosion destroys the low-resistance electrical ground path required for EMP hardening. This paper presents recommended short-term and long-term improvements in materials selection, fitting mechanical design, and weather-sealing materials and techniques to improve the life-cycle performance of EMP-hardening fittings. It describes recent efforts to develop corrosion-resistant materials and components for EMI/EMP applications in the marine environment.

INTRODUCTION

The naval topside environment includes both natural conditions, such as salt-water splash/spray, thermal cycles (-40 to 150°F), ultraviolet radiation, and man-made influences such as SO_2 stack gas, solvents, detergents, fuels, and lubricants. Deterioration of naval topside equipment due to the effects of these environmental conditions is unlikely to be forestalled by routine maintenance, because of the time, manpower, and material constraints typical of warships at sea. Topside equipment must be designed to resist environmental conditions if acceptable life-cycle performance is to be achieved.

Naval topside equipments also are exposed to a wide and powerful spectrum of electromagnetic energy, the sources of which must be considered. Failure to protect complicated electronics against the effects of electromagnetic interference (EMI) has led to operational failures. For example, high-frequency radio transmissions have caused shutdown of main propulsion turbines in FFG-7 Class frigates[1] and severe disruption of avionics.[2]

Another, more ominous source of electromagnetic energy is the electromagnetic pulse (EMP) generated by an exo-atmospheric nuclear detonation. The peak field energy is believed to be 50,000 volts per meter over a broad frequency band (1 Hz through 1 GHz).[3] Department of Defense (DoD) Directive 4245.4, of 25 July 1988, directs all DoD components to "...ensure that the nuclear survivability of non-major systems is evaluated for possible impacts on critical functions supporting vital missions..." and to ensure that consideration is given to cost-effective means of achieving nuclear survivability, including EMP hardening. The EMP environment is defined in DOD-STD-2169A.

Hardening encompasses measures for attenuating the transfer of EMI/EMP energy to an electronic or electrical system to prevent disruption of or permanent damage to the affected system. The U.S. Navy has employed external shielding to harden topside cables. The cables are encased in shielded conduit, and mechanical fittings are

used to attach the conduit to an electrical enclosure, stuffing tube, or connector backshell. External shielding enables the conduit to absorb the EMI/EMP energy and shunt most of it to the ground plane (ship structure) through the fittings. The fittings, also called shielded ground adapters (SGA) or conduit ground adapters (CGA), must be grounded 360° at the termination points. Broadband attenuation of 80 decibels (dB) is considered the minimum necessary to achieve EMP hardening with shielded conduit.

The most widely used conduit consisted of galvanized steel interlocking convolute containing an integral, helical copper ground wire. This flexible metallic tube was covered with extruded thermoplastic for watertightness. Fittings consisted of mechanically deposited zinc-coated steel or malleable iron bodies with tapered national pipe thread (NPT) ends; a toothed jam nut for installation into electrical enclosures; a zinc-coated steel grounding ferrule that threads into the inner diameter of the metal convolute; and a female NPT cap nut to maintain contact between the ferrule and fitting body and to compress a plastic sealing ring against the conduit jacket, thereby excluding water.

Stuffing tubes are used topside for cable penetrations through bulkheads or decks. These stuffing tubes contain packing compressed with gland nuts to provide a moisture- and gas-tight seal between weather areas and ship interior spaces. Specially manufactured adapters were required to replace the stuffing tube gland nuts and accept the conduit ground fittings. The same material specified for stuffing tube gland nuts was used to manufacture these adapters: brass for steel stuffing tubes, and aluminum for aluminum stuffing tubes. The aluminum adapters were cadmium-plated and chromate-treated to achieve an olive drab finish in accordance with Federal Specification QQ-P-416, Type II, Class 3.

This commercial hardware was inadequate to withstand the corrosive environmental threat to topside equipment. In December 1986, the Board of Naval Inspection and Survey reported corrosive deterioration of recently installed EMP-hardening fittings before completion of ship overhaul while the ship was still in drydock. Field inspections confirmed corrosive deterioration, including general corrosion, galvanic corrosion, and failure of corrosion-resistant plating. Weather-sealing attempts were nonuniform and ineffective.

EXPERIMENTAL APPROACH

ARINC Research Corporation performed a marine atmospheric exposure test to verify the corrosion mechanisms observed aboard ship and to determine whether incipient corrosion actually impaired the functional performance of EMI/EMP-hardening fittings. The deleterious effects of incipient corrosion on electronics are well known.[4,5] Corrosion-product buildup has been reported to increase impedance enough to destroy EMP hardness.[6]

For baseline testing, the same types of commercial conduit, fittings, and adapters identified during field inspections were assembled into military specification stuffing tubes and electrical enclosures. A 12-inch length of conduit was used in all assemblies for consistency among test assemblies. Three corrosion-resistant steel (CRES) 316 fittings were tested to compare performance with four CRES 303 fittings of the same design. Five sealant systems were selected for evaluation. Ninety-degree box elbows made of zinc-coated malleable iron were used for sealant evaluations, because they exhibited extensive shipboard corrosion and would be the most difficult to seal. Table 1 lists the fittings, sealants, and shipside connections examined in this experiment.

The sealants selected for evaluation represented current U.S. Navy technologies, with one exception: a proprietary gelatinous strip product (Raychem GelTek™) designed to provide a flexible, water-occlusive seal. Fiberglass had been used to weatherseal EMP fittings at one shipyard, and good short-term results had been reported. RTV silicone (MIL-A-46146) and heat-shrinkable cable repair sleeving (MIL-I-23053/15) are sealant techniques specified in Navy standards for electrical equipment. Polysulfide sealant (MIL-S-81733, Class I-2) has been employed to seal avionics enclosures and is used for sealing topside fasteners. This material also was selected because it was available in the federal stock system, could provide a flexible long-term seal, and contained chromates for inhibiting corrosion if moisture penetrated the seal.

TABLE 1

FITTINGS, ATTACHMENTS, AND SEALANTS

Shipside Fitting Type	Boxes			Stuffing Tubes	
	Brass	Steel	Aluminum	Steel	Aluminum
Group 1: Baseline Hardware					
Zinc/Steel Box Fitting	2	1	1		
Brass T-Type Adapter				2	
Aluminum T-Type Adapter				1	2
Aluminum Adapter				1	1
CRES 303				2	2
CRES 316	1			1	1
Group 2: Sealants					
Polysulfide	2	2	1		
Fiberglass	1	1	1		
Silicone	1	1	1		
Gelatinous Strip	2	2	1		
Heat-Shrink Boot	1	1	1		

Quantitative data were obtained by measuring the change in dc electrical resistance through the specimen assemblies during the 11-month exposure period. A study of electrical-enclosure cover panels confirmed that dc resistance on the order of 2.5 milliohms was required (but was not the sole criterion) for ensuring the effectiveness of low-impedance EMI/EMP shielding.[6] The study also related increases in dc resistance to the onset and progress of corrosive attack at the junction of the cover plate and the enclosure. The dc resistance has been shown to be consistent with low-frequency ac impedance measurements on similar fittings.[7]

The test assemblies were mounted on a test stand at the Ocean City Research Sea Isle test site in New Jersey. The test site is approximately 150 feet from the shoreline. To accelerate the simulated naval topside environment, the test assemblies were sprayed with natural seawater three times a day, weather permitting. Exposure testing began in mid-November 1987. CRES fittings were added to the test stand in January 1988. A photograph of the test stand is presented in Figure 1.

Resistance measurements were taken by using a four-terminal Kelvin bridge device (GenRad Model 1666 dc resistance bridge). Test probes were soldered inside the box, inside the elbow, and at the end of the 12-inch length of conduit—an arrangement that permitted measuring resistance across both the fitting-to-box junction and the fitting-to-conduit junction. The test-probe locations were similar for stuffing-tube assemblies, except that no probe could be installed inside the adapter, because of the need to insert a dummy 0.5-inch cable inside these assemblies. Figure 2 illustrates the specimen arrangements and resistance-measurement wire-solder points. Conduit from the baseline stuffing-tube adapters was installed into the steel and brass boxes with baseline metal-box fittings. The conduit test probes were soldered to the box-fitting body instead of the conduit, adding another junction that could suffer corrosion damage; the junction is included in the stuffing tube-to-conduit resistance measurements. The test probes for the CRES stuffing-tube fittings were installed as shown in Figure 2.

OBSERVATIONS

Initial dc resistance measurements were taken in mid-November 1987, following assembly of the test stand and specimens. The dc resistance across the electrical box-to-fitting junction was more than an order of magnitude

lower than resistance between the fitting and 12 inches of conduit. This low contact resistance (0.0002 to 0.002 ohm) is attained by direct metal-to-metal contact between tapered pipe threads and a toothed jam nut that cuts into the inside wall of the junction box. The higher circuit resistance can be attributed to the more passive contact fitting-to-conduit junction or to the line resistance over 12 inches of conduit, or to both. The initial contact and circuit resistances were comparable among all assemblies irrespective of box, stuffing tube, or fitting material.

Figure 3 is a compilation of junction-box/sealant resistance measurements taken at approximately one-month intervals. Fittings installed in electrical boxes made of three different materials—aluminum, steel, and brass—were tested. Only 2 of the 24 specimen assemblies have exhibited significant increases in dc resistance. For all electrical boxes, the elbow-to-box resistance values have remained uniformly low (0.001 to 0.09 ohm) and exhibit a very gradual increasing trend for all specimens. This gradual aging trend also is observed for the conduit-to-box resistance readings.

Figures 3(a) and 3(b) indicate no gross failures of fittings installed in the aluminum junction box. Unlike the other two junction boxes, this box is a heavy wall casting that is more rigid at the fitting junction. Aluminum boxes also provide a large anode-to-cathode area ratio, reducing corrosion rates.

Figures 3(c) and 3(d) for the steel junction box indicate that the fitting sealed with heat-shrink sleeving has failed electrically. Comparison of the curves for this specimen on the two figures indicates that the failure is at the fitting-to-box junction. In contrast, the failure of the heat-shrink-sleeved specimen installed in the brass junction box shown in Figure 3(e) appears to be at the fitting-to-conduit junction, since the Figure 3(f) curve at the fitting-to-box junction is flat.

Figure 4 presents the data for dc resistance between aluminum and steel stuffing tubes and 12 inches of conduit, including various adapters. Except for the CRES fittings, these data also include the resistance across the conduit-to-fitting junction for the box fitting attaching the conduit to the underside of the steel or brass box. Resistance measurements for the aluminum stuffing tube are in the range of 0.04 to 0.2 ohm except for the two aluminum T-type special adapter assemblies, both of which failed. While the zinc coating on the steel cap had powdered, the Iridite coating on the adapter body appeared sound. Subsequent disassembly inspection revealed more extensive corrosion of the box-fitting grounding ferrule than of the adapter grounding ferrule. The steel-stuffing-tube data of Figure 4(b) show one failure of the aluminum adapter specimen, which exhibited the highest dc resistance observed (20 ohms). These results were expected, inasmuch as field inspections revealed extensive corrosion of aluminum adapters. However, the failure may have occurred in the box fitting rather than at the aluminum adapter.

The CRES 303 stuffing-tube fittings had rust stains over 80% of the surface, while the CRES 316 fittings of the same design had only 20% surface staining. None of the CRES stuffing-tube adapters exhibited dc resistance fluctuations in either steel or aluminum stuffing tubes.

All baseline fitting surfaces not covered with sealant or residual zinc-dust antiseize thread lubricant were corroded. The uncoated control specimens all had corrosive powdering of the zinc coating and varying degrees of running rust. The appearance of these fittings would be expected to deteriorate, consistent with field inspection observations. Vinyl tape on the gelatinous strip was unraveling. The RTV silicone sealant had discolored and would be expected to become brittle because of the effects of UV radiation. The polysulfide coating had the best post-exposure appearance.

The key finding of these tests is that incipient corrosion can defeat the purpose of EMP hardening in as little as two months after installation. Further, the severity of visible corrosion could not be correlated with electrical grounding failure. Thus visual inspection cannot determine whether or not an installed EMP-hardening fitting is functional.

DISCUSSION AND RECOMMENDATIONS

The following discussion of the performance of EMP-hardening fittings is based on corrosion engineering inferences drawn from field inspection and exposure testing data described herein and from related studies reported

in the literature. Recommendations are presented separately, but the interrelationship of the technical factors discussed below should be considered in developing new generations of EMP-hardening fittings.

Materials

Ship inspection data and results of the environmental exposure testing confirm the obvious: construction materials for EMP-hardening fittings must be inherently corrosion-resistant and must be galvanically compatible with the shipside electrical equipment to which the fittings are grounded.

Brass-alloy or bronze-alloy fittings would be satisfactory with the numerous brass electrical enclosures employed, because these alloys are corrosion-resistant and machinable. Aluminum alloy 6061 is also corrosion-resistant and offers the advantage of light weight for fittings used in aluminum electrical enclosures and stuffing tubes. However, using either of these fittings with an incompatible electrical enclosure would lead to grounding and corrosion failure in a short period, unless the fittings were completely sealed from the environment.

CRES alloy 316 (17% Cr, 12% Ni, 3% Mo) may be suitable as either a box or stuffing-tube fitting material. The passive-film behavior of CRES makes this material reasonably compatible even with aluminum. CRES 316 is more expensive and harder to machine than some other alternatives, but the life-cycle benefits outweigh the marginally higher (10% to 30%) unit costs.

Metal Plating and Conversion Coating

Active-metal plating materials, such as cadmium and zinc, have been shown to be ineffective by field inspections and controlled observation of environmental exposure tests. On the basis of acid salt fog testing, a dual plating of cadmium and electroless nickel over either CRES 316 or aluminum was considered effective for aircraft fittings subjected to high marine humidity.[8] These plating combinations are specified for heavy-duty connectors in accordance with MIL-C-28840.

Mechanical Design

Field inspections identified at least two mechanical design features that should be avoided. First, the single revolution of thread contact of toothed jam nuts is insufficient to maintain box-fitting connections. Second, tapered pipe-threaded fittings used with aluminum adapters impart tensile stress, which, in combination with aluminum-corrosion-product expansion, is sufficient to split the adapter.

These observations suggest that fittings having low-stress machine threads with adequate thread engagement should be employed. A toothed or serrated jam nut is necessary to cut through any paint or conversion coating on the inside surface of thin-wall electrical enclosures to assure grounding. Locking mechanisms are necessary to ensure that thread preload can withstand the mechanical pounding and vibration imparted to topside equipments. Environmental seals should be employed at each junction to protect the grounding paths from oxidation due to moisture.

For standardization, the conduit-to-fitting connection should be compatible with any qualified EMP-hardening shielded conduit. A study[9] of several fitting-to-conduit connection designs, including iris rings and five dual-cone arrangements, concluded that surface transfer impedance was controlled by the shield braid. As a result, this study suggested that factors other than minimizing impedance could be used to select fitting-to-conduit connection designs. These factors could include watertightness, integrity under vibration, ease of use, and ease of assembly. The compatibility matrix of Table 2 suggests that either iris rings or dual-cone connections have the broadest applicability.

Sealants

The ideal sealant would be easy to apply, capable of sealing close and difficult geometries, and environmentally stable; and it would retain flexibility for many years. None of the sealants investigated has all of these characteristics.

TABLE 2

COMPATIBILITY OF FITTING JUNCTIONS WITH EMP CONDUIT

Fitting Junction	Conduit Construction		
	Metal Convolute	Braid Over Metal Convolute	Braid Over Plastic Core
Grounding Ferrule	Yes*	Yes*	No
Iris Ring	Yes	Yes	Yes**
Dual Cone	Yes†	Yes	Yes
CRES Cinch Band	No	Yes	Yes
"Light Bulb" Threads	No	Yes	Yes
Solder	Yes‡	Yes	Doubtful

* Not interchangeable, because of incompatible thread forms.

** Iris rings probably would work, but they have not been tested with this conduit. The plastic core may be too flexible to ensure sufficient compression of the iris ring between the fitting wall and the shielding braid.

† Dual-cone junctions probably could work, but they have not been tested with metal-convolute-only EMP conduit.

‡ No data on convolute-only. Heat-input controls are required to prevent melting of plastic core and damage to internal cable.

The wrap-type sealants, including heat-shrinkable sleeving, gelatinous strip, and fiberglass, were difficult to apply to the closely spaced elbows. Fiberglass is brittle and does not adhere to the thermoplastic conduit jacket. Heat-shrinkable boots or cable repair sleeving may be appropriate for weather-sealing straight-run fitting arrangements, but care must be taken to ensure that the wrap is completely sealed at both ends.

The air-curing compounds, including polysulfide, silicone, and fiberglass, were somewhat messy and difficult to apply. Polysulfide was the most difficult compound to handle, because it is a two-part mixture having a limited application period (two hours). The silicone sealant required no pre-mixing. However, silicone sealants have exhibited deterioration in topside environments and should be used only in conjunction with an overwrapping of either electrical tape or vinyl tape, or both.[8]

Polysulfide sealant exhibited the best post-exposure performance and is recommended because of its environmental stability, resistance to fuels and detergents, and flexibility. Since polysulfide is extremely adherent, it should be applied only to fittings that are not routinely disconnected for maintenance.

Torque

Several studies have noted the importance of controlling torque to assure adequate grounding of SGAs, electrical enclosures, and other cable-shielding assemblies such as pipe and conduit.[6,7,10,11] Previous studies have shown that connector transfer impedance is inversely proportional to assembly torque and that use of nonconductive thread lubrication is necessary to ease assembly and achieve consistent electromagnetic measurements.[12] The application of a zinc-dust antiseize compound on all threaded peices is recommended to prevent galling. The zinc-dust will also act to mitigate corrosion if moisture penetrates the threaded joint; it is recommended for all threaded connections, regardless of material.

NAVY ACTION TO MITIGATE CORROSION OF EMP-HARDENING FITTINGS

With respect to EMP hardening, the Navy has acted to mitigate corrosive deterioration by issuing Technical Report 407-TR-0001 and revision E of the "Grounding and Bonding Standard," MIL-STD-1310. Both

documents require the use of fittings that meet MIL-C-28840 requirements for materials and finishes, selection of fitting material for galvanic compatibility with the shipside equipment, treatment of threads with antiseize, and weather sealing with polysulfide sealant in accordance with MIL-S-81733. The Navy also is preparing a procurement specification for EMP-hardening conduit and fittings, MIL-C-XX254. This specification will provide long-term remedies by standardizing hardware; encouraging use of corrosion-resistant materials and integral weather seals; and imposing qualification testing to demonstrate adequacy of mechanical design, corrosion resistance, and electrical performance. These actions implement many of the specific findings reported in this paper.

The clear lesson from the ship EMP-hardening experience is that environmental effects on system functional performance must be considered during initial design. Encouragingly, recent Navy-sponsored efforts to design new grounding devices reflect healthy consideration of corrosion control. Two efforts are described here.

Conduit Ground Adapters

The Naval Underwater Systems Center (NUSC) has been tasked by NAVSEA to develop a conduit ground adapter (CGA) for electrically grounding EMP-hardening conduit to stuffing tubes. NUSC assembled a multidisciplinary team—consisting of mechanical, electrical, and materials engineers—to attack this problem. Using empirical research[7] and newly developed analytical models, the NUSC team has designed its CGA from first principles. The NUSC CGA employs corrosion-resistant materials and integral weather seals. This design avoids the thread-conductive-path problem by using iris rings to couple the CGA to the outside of the stuffing tube. This iris ring arrangement shunts current to the outer skin of the stuffing tube, since the NUSC CGA analytical model showed that this was the most effective way of shielding the conduit-encased cable. Photographs of the design are presented in Figure 5.

Bond Straps

Heavy-duty bond straps shown in MIL-STD-1310 typically are multistrand copper wires crimped into aluminum or CRES lugs. The lugs are either welded or bolted to ship structures. Not surprisingly, these bond straps suffer rapid corrosive failure and mechanical damage, requiring frequent replacement.

NAVSEA tasked the Naval Coastal Systems Center (NCSC) to develop a more corrosion-resistant bond strap for naval topside environments. NCSC also assembled a multidisciplinary team of engineers and used analytical modeling to design a new bond strap from first principles. The new bond straps are provided in complete kits with instructions, as shown in Figure 6. Seaside corrosion testing confirmed the efficacy of the design.[13]

INTEGRATED SYSTEM DESIGN

The preceding sections have addressed the desirability of accounting for environmental factors in electronic component design. Better reliability and lower life-cycle costs can be achieved by imposing consideration of environmental factors during the design of entire weapon systems. Specific attention to corrosion control is implemented by the Army through the Corrosion Prevention and Control Program and by the Navy through the Shipboard Corrosion Control Program. These programs are having positive impacts on the design and production of military aircraft and ships. However, a more comprehensive analysis of the Total Threat Environment (TTE) is required.

TTE addresses all environmental conditions, both natural and combat-related, against which a military system must be expected to survive and continue its mission. Merely identifying the TTE for a new system is a significant task, because requirements may be specified in an array of different and conflicting military standards and top-level instructions. Threats can include electromagnetic influences (EMI, EMP, TREE), overpressure from nuclear or conventional weapon blasts, thermal transients from nuclear blasts, both operational and weapons-detonation multiaxial shock and vibration, and resistance to NBC agents and decontamination treatments. The various levels of subsystem degradation due to TTE factors must be defined and assessed in the design phase.

It is necessary to coordinate policy guidelines and requirements related to TTE analysis. Many factors may be found to overlap, permitting definition of environmental envelopes. For example, EMP considerations dominate up to 1 GHz, but EMI considerations dominate beyond 1 GHz. Other requirements may conflict; for example, the dielectric-isolation requirements for corrosion control have been found to be in conflict with the grounding requirements for EMI/EMP hardening in specifications for DDG-51 Class destroyers. Coordination is even more important for common equipments used by more than one service, such as some communications sets and helicopter airframes.

SUMMARY

The dc electrical resistance measurements of 35 EMP-hardening fitting assemblies exposed to a simulated naval topside environment confirm that incipient corrosion can destroy functional performance in several months. Functional deterioration can occur before there is any visible corrosion-induced cosmetic or mechanical failure of the EMP-hardening fitting. Future hardening retrofits should use corrosion-resistant fitting materials such as bronze or CRES 316, specify proper installation torque using zinc-dust antiseize thread lubricants, and use polysulfide sealant. Recent service-sponsored component development programs demonstrate the efficacy of addressing corrosion control during the initial design of topside electrical devices and treatments. Further coordination is required for the proper design of military equipment to withstand the Total Threat Environment, which includes natural and combat-related electrical, chemical, and mechanical conditions.

ACKNOWLEDGMENTS

This paper summarizes a report[14] funded under Contract N00024-86-D-4306; Mr. A. R. Parks (NAVSEA 05M1) is the Contracting Officer's Technical Representative. Technical direction has been provided by Myer Berman, Kenneth Carrigan, and James Kudzal, Naval Sea Systems Command (NAVSEA 06D442). The author is indebted to James A. Ellor, P.E., Ocean City Research, for his valuable contributions. The NUSC Conduit Ground Adapter study[7] was supported by the EMP Ship-Hardening Techniques Program, Mr. Harold Smith (PMS423), Program Manager, and by the OCNR/ONT Submarine Technology Program Element, Mr. Gene Remmer (NUSC Code 233), Program Manager, and Mr. Lincoln Cathers (DTRC Code 0144), Block Program Manager.

REFERENCES

1. J. Monr ., "Electromagnetic Interference," *Deckplate*, Vol. 7, No. 1, January-February 1987.
2. R. Garbely, "Shielding Electronic Components from Nuclear Effects," *Defense Electronics*, Vol. 19, No. 5, May 1987.
3. *Electromagnetic Pulse (EMP) Protection for U.S. Navy Ships, Materials and Methods for*, NAVSEA Technical Report No. 407-TR-0001, September 1987.
4. J. D. Gutenplan, "Corrosion in the Electronics Industry," *ASM Metals Handbook*, advance copy chapter of Corrosion volume.
5. "Design Guidelines for Prevention and Control of Avionics Corrosion," NAVMAT Publication P-4855-2, June 1983.
6. J. W. Gooch and John K. Daher, "Shielding Effectiveness of Metallic Joints Versus Corrosion Protection," *Proceedings of the 1987 Tri-Service Conference on Corrosion*, Air Force Wright Aeronautical Laboratories Publication AFWAL-TR-87-4139, Vol. 1, May 1987.
7. D. S. Dixon, S. I. Sherman, and M. Van Brunt, "An Evaluation of the Long Term EMI Performance of Several Shield Ground Adapters," *Proceedings of the 1987 IEEE Conference on EMI/EMP.*
8. E. J. Jankowski, *Coatings for Electrical Connector Shells*, Naval Air Development Center Report No. NADC-76274-30, 13 August 1976.
9. J. E. Merrel, L. O. Hoeft, and J. S. Hofstra, "Measured Surface Transfer Impedance/Shielding Effectiveness of RFI/EMI Backshell Terminations for Circular Connectors," *Record of the 19th Annual Connectors and Interconnection Technology Symposium*, 7-9 October 1986.

10. D. J. Leverence, P. H. Nielson, and R. G. McCormack, *EMP Shielding Properties of Conduit Systems and Related Hardware*, Army Construction Engineering Research Laboratory Report CERL-TR-C-19, June 1975.

11. D. Fromme, T. Peterson, G. Ross, and E. Peterson, *Condulet Test Report*, JAYCOR Report No. JTN-CS-5029, 19 September 1986.

12. L. O. Hoeft and J. S. Hofstra, "Measured Surface Transfer Impedance of Various Connector/ Backshell Interfaces," *Record of the 20th Annual Connectors and Interconnection Technology Symposium*, 19-20 October 1987.

13. F. J. Higgins, S. Mahan, T. Pruit, and M. Glasser, *Improved Bond Strap Investigations*, Naval Coastal Systems Center Report No. U345-86-005-3OU53, 3 November 1986.

14. N. Andrew Greig, *Corrosion of EMP-Hardening Fittings in the Naval Topside Environment*, ARINC Research Publication 3547-02-02-4839, December 1988.

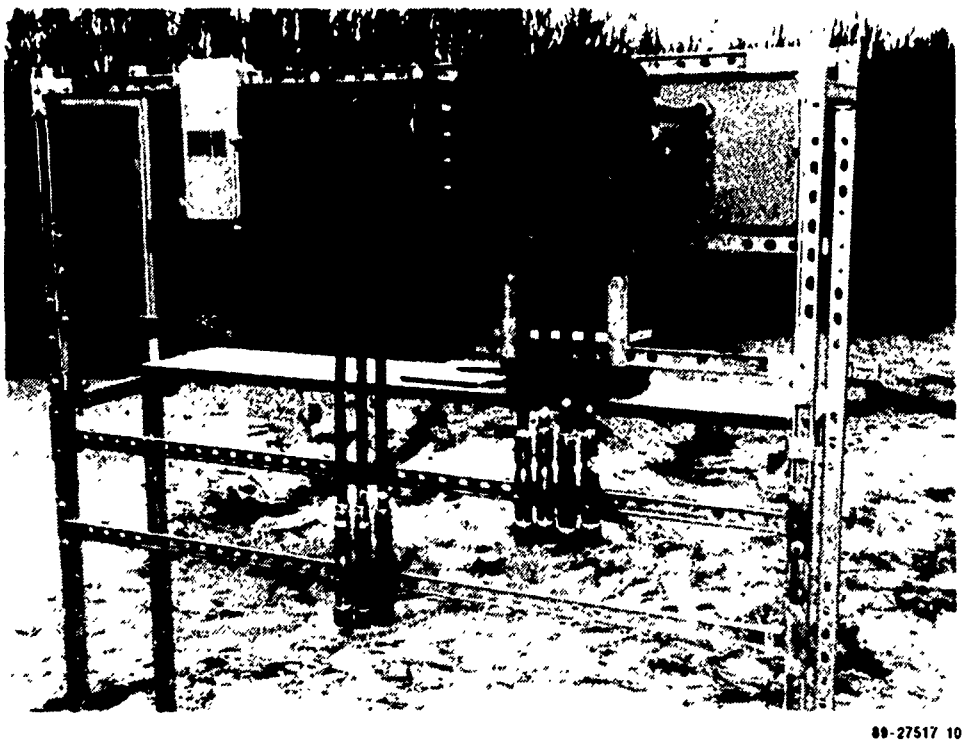

Figure 1. Test Stand Supporting Aluminum, Steel, and Brass Electrical Enclosures and Aluminum and Steel Stuffing Tubes with Installed EMP-Hardening Fittings and Conduit

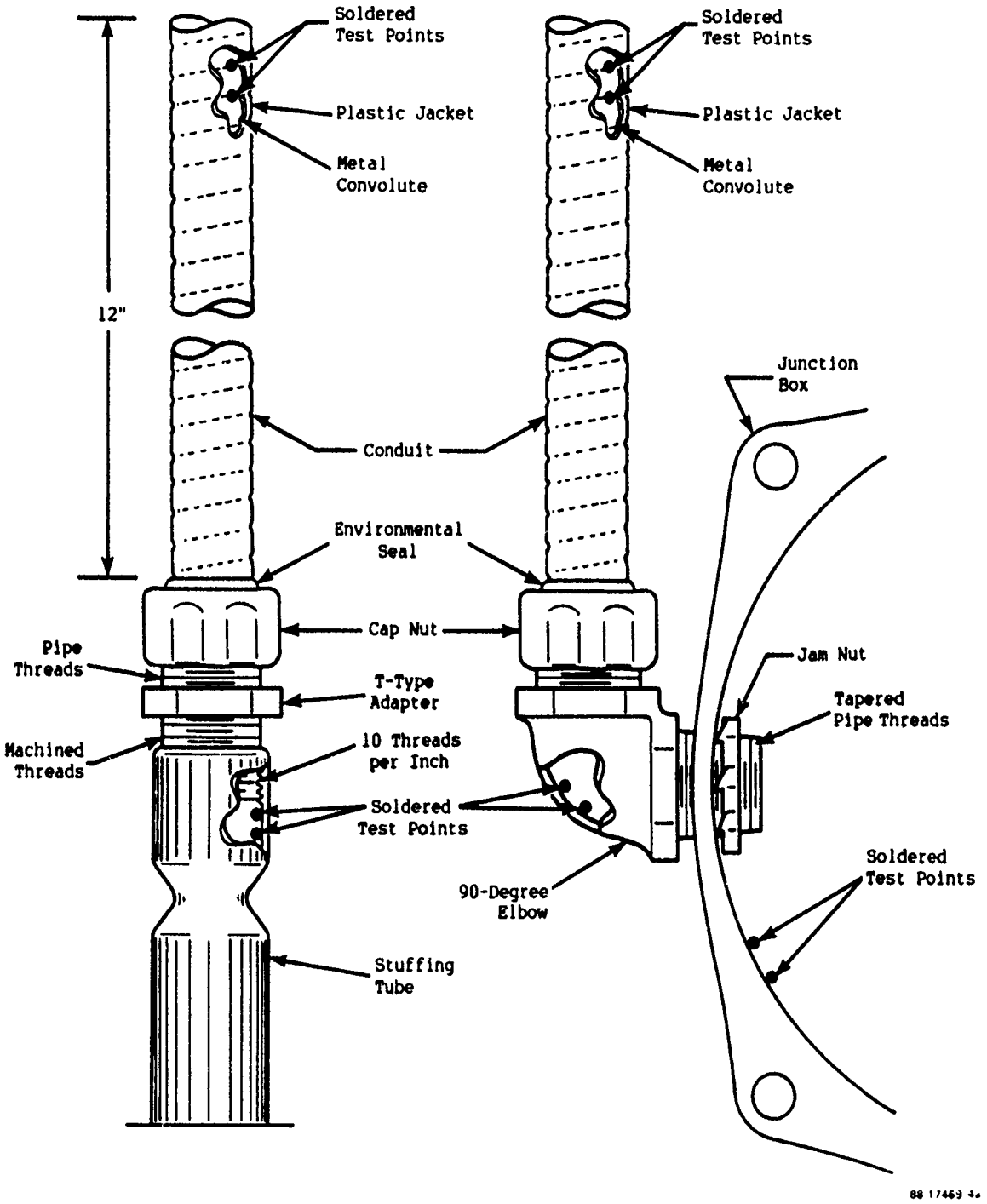

Figure 2. Stuffing Tube and Junction Box Specimens

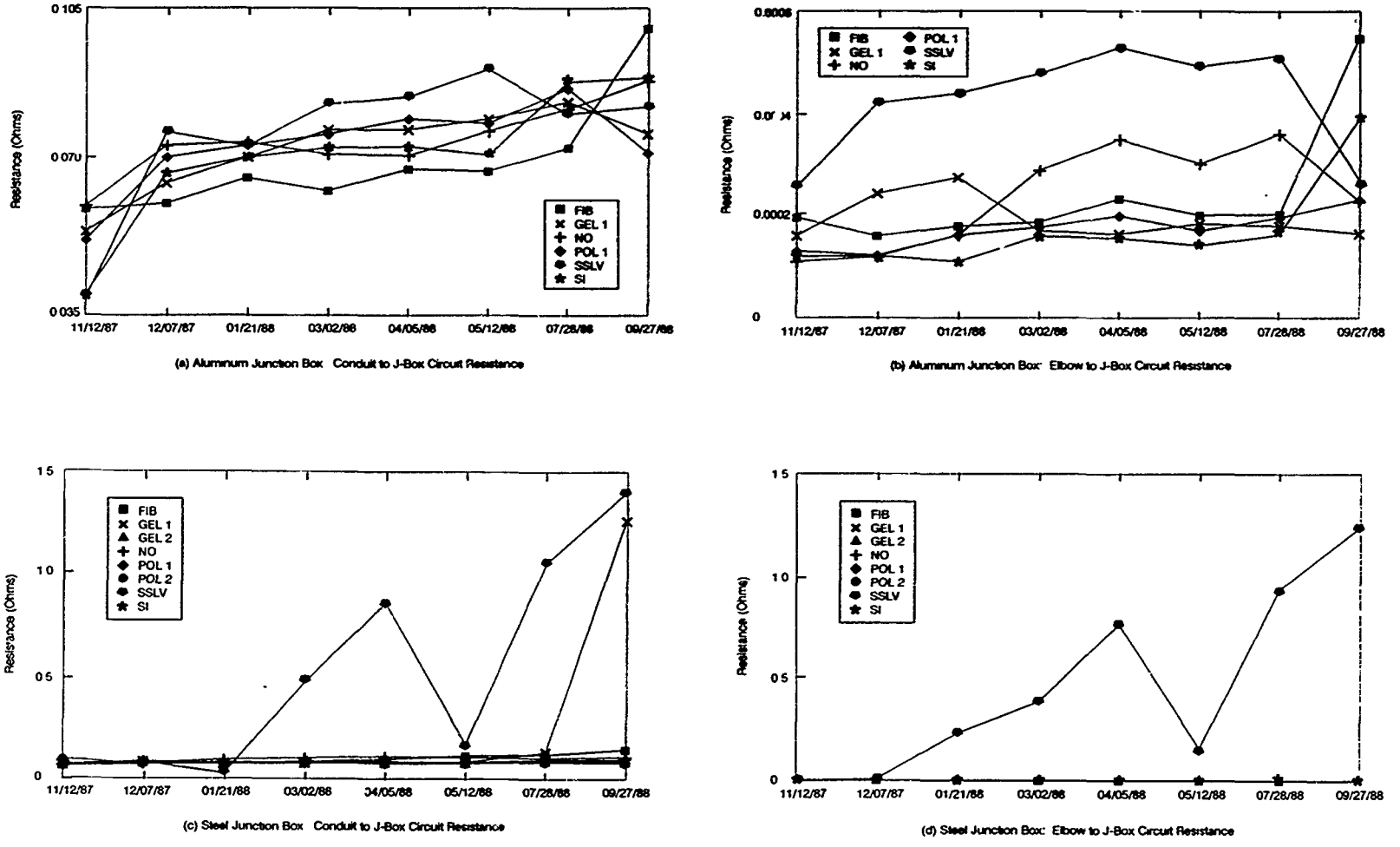

Figure 3. Environmental Exposure Data for Box Fittings

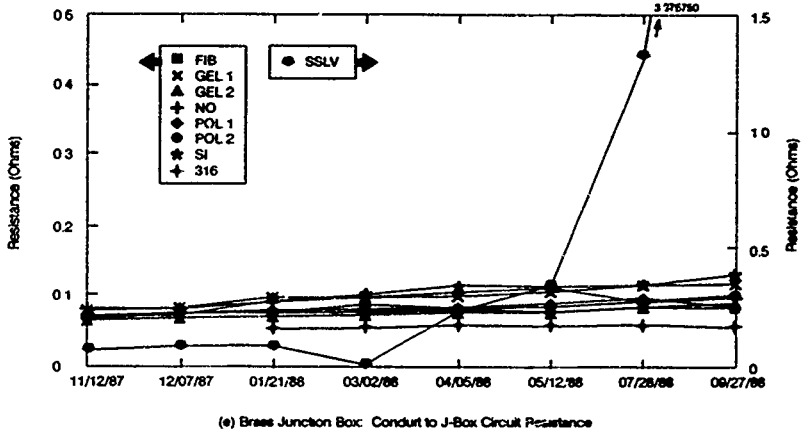

(e) Brass Junction Box: Conduit to J-Box Circuit Resistance

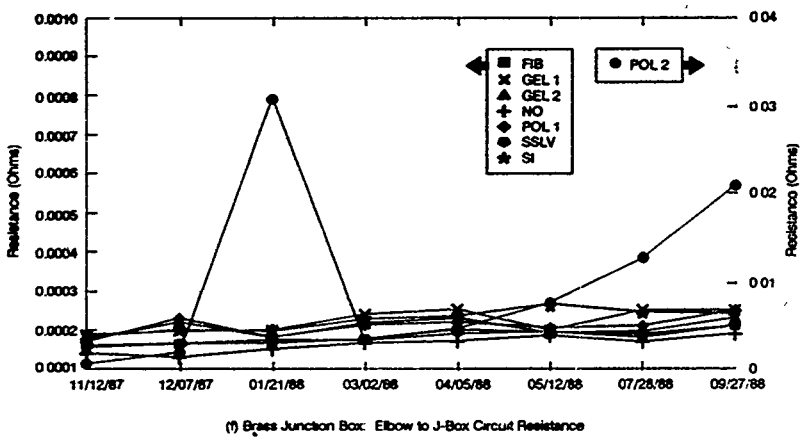

(f) Brass Junction Box: Elbow to J-Box Circuit Resistance

Figure 3 (continued)

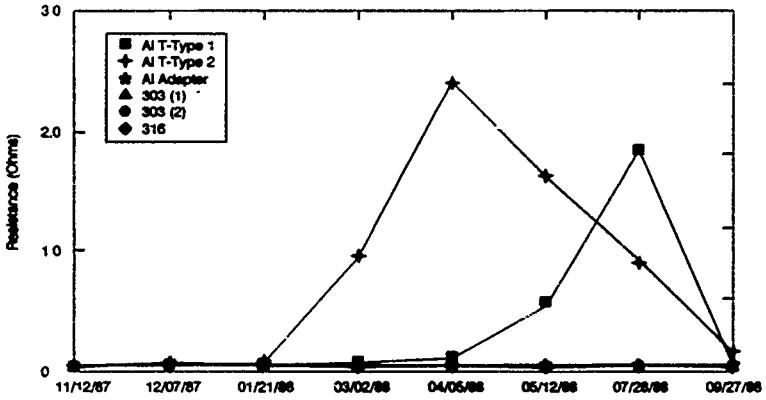

(a) Aluminum Stuffing Tubes: Conduit to Stuffing Tube Circuit Resistance

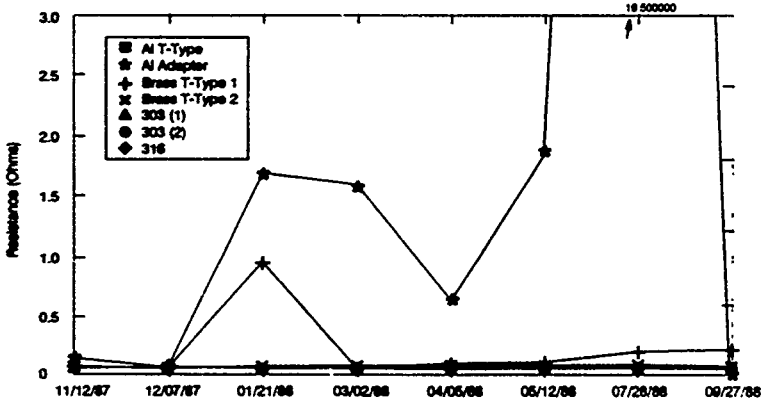

(b) Steel Stuffing Tubes: Conduit to Stuffing Tube Circuit Resistance

Figure 4. Environmental Exposure Data for Stuffing-Tube Adapter

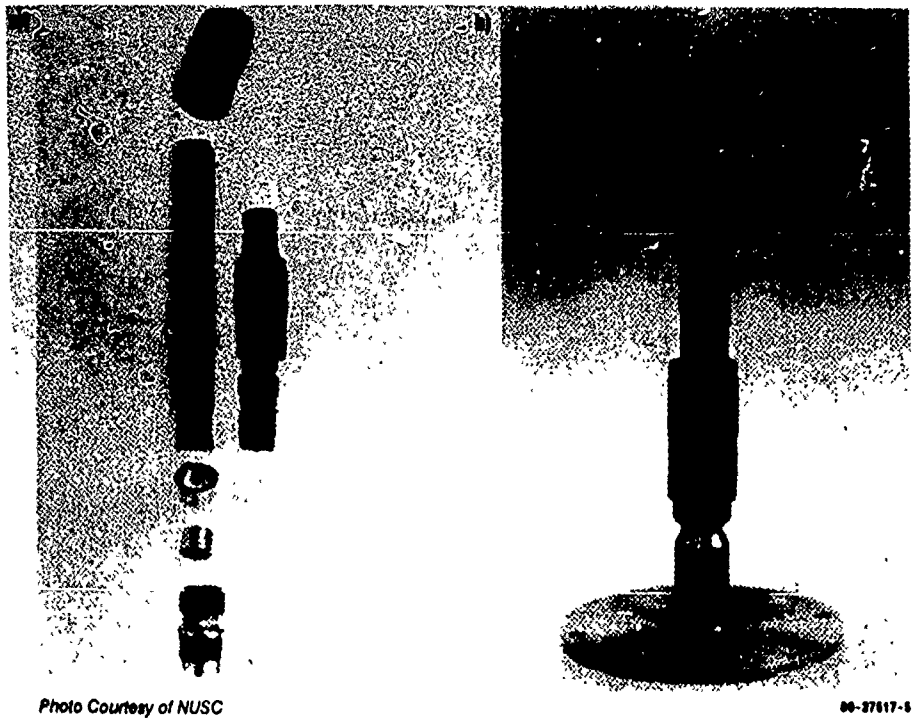

Figure 5. NUSC CGA Prototype V: a) Part of Aluminum Adapter and Partially Assembled Brass Adapter; b) Aluminum Adapter Installed on Aluminum Stuffing Tube (Flange is Part of EMP Shielding-Effectiveness Test Apparatus)

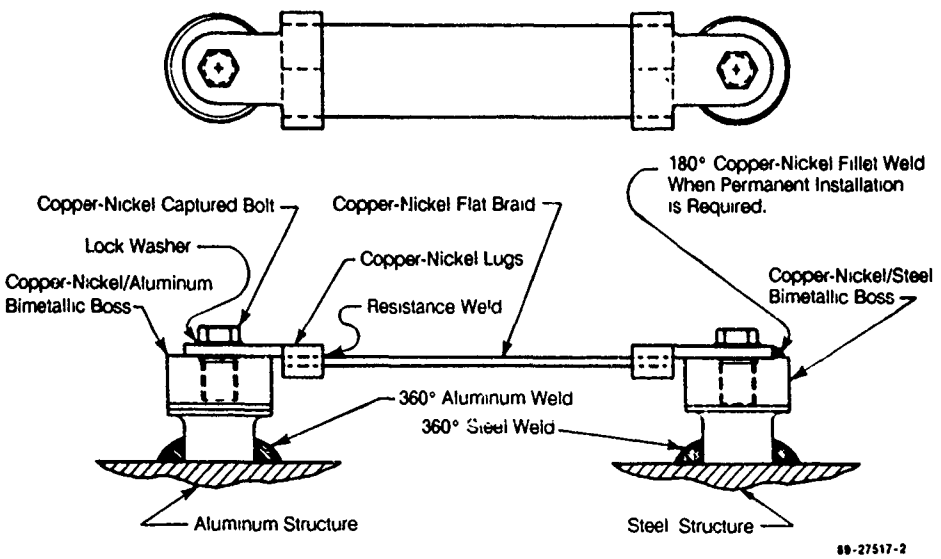

Figure 6. NCSC Corrosion-Resistant Bond Strap

AVIONIC CORROSION: CASE HISTORIES

Edward White, George Slenski, Michael Marchese, Bill Dobbs
Wright Research & Development Center
WRDC/MLSA
Materials Laboratory
Wright-Patterson Air Force Base, Ohio

John Ziegenhagen
University of Dayton Research Institute

Abstract

Investigations by the Wright Research & Development Center Materials Laboratory Equipment Failure Analysis Group of corrosion related problems in Air Force avionic equipment will be presented. Case histories of component failures will be discussed in the following areas: connector pins, antennas, RAM modules, potentiometers, proximity switches, IC components, electronic hybrid modules and wire braiding. Past experience indicates that approximately 20% of the failure investigations performed are related to corrosion.

Introduction

New Air Force aircraft, missiles and space systems are increasingly more complex. This makes high reliability more difficult to attain. When electrical failures degrade system performance, the Air Force mission is hindered by increased maintenance, safety of flight issues and fault isolation. The reliability and maintainability of military electronic systems rests heavily upon an ability to isolate part failures, establish the cause of failure and recommend corrective action to insure improved performance. The Electrical/Electronic Failure Analysis Group of the System Support Division of the Materials Laboratory, Wright-Patterson AFB, has the facilities and expertise to investigate specific component failures on Air Force weapon systems. The Failure Analysis Group has investigated a large number of electronic and electrical failures. It has been established that while eighty percent of these failures are caused by materials and manufacturing process defects, about twenty percent of the failures are caused by corrosion problems. A few of the case histories of electronic failures associated with these corrosion problems will be presented along with recommended corrective actions and a discussion of the benefits of these analyses. The discussion includes a wide range of electronic applications which have been proven susceptible to corrosion. Topics consist of connector pins, an airborne antenna, several integrated circuits (ICs), discrete components, hybrids and finally aircraft wiring.

Backpanel Connector Pins

After backpanel pins were found to have a black appearance on their tips during an inspection, the manufacturer submitted the pins for an evaluation of the corrosion and contamination. The manufacturer claimed that the black

material was the result of contamination corroding the gold plating on the pins (Figure 1). The contaminants were identified as containing chlorine and potassium.

Initially, the pins were metallurgically mounted and cross-sectioned for examination in the scanning electron microscope (SEM). The associated energy dispersive x-ray analysis was used to determine the elemental composition of the pins. The base material of the pins was a phosphor bronze containing copper (Cu), tin (Sn) and phosphorus (P). The base metal was then plated with a 50 microinch thick coating of nickel (Ni). The final material deposited on the nickel was gold (Au). Figure 2 is an SEM micrograph of a cross-sectioned pin showing the base metal and the two platings. Measurements of the plating thicknesses indicated conformance to the corresponding plating specifications.

Optical examinations of the pins were conducted and several anomalies were found. A green material was found on the tips and sides of several pins (Figure 3). Elemental x-ray analysis of this area identified copper and chlorine. Therefore, the green material was suspected to be a copper chloride compound. The chlorine contamination was suspected to have come from the city tap water used in the final rinse cycle of the plating process. There was no corrosion of the pin's gold plating from the potassium or chlorine contamination.

White deposits were found on the board (Figure 4) and on the pins (Figure 5). Analysis in the SEM and chemical analysis by infrared (IR) spectroscopy of the white residue identified potassium on the pins and a metal carbonate on the board. The IR spectrum resembled that of lead carbonate. The presence of a carbonate indicated that the boards were being inadequately cleaned and that organic contaminants may have been present. These organics (possibly flux residues) combine with moisture and form weak acids which leach lead out of tin/lead solder found in the board holes. Potassium was a major constituent in the vendor's plating process and was identified as the source of contamination on the pins.

Physical damage to the pin platings (as seen by flattening of the pin tips) as a result of misregistration of the board holes, during the pin insertion process, exposed the base phosphor bronze material on the pins (Figure 6). This allows the bronze base material to be attacked by contaminants (Figure 7). This corrosion of the phosphor bronze material also caused defoliation of the nickel and gold platings (Figure 8). Continued delamination of the platings exposed more of the pin base material and allowed oxidation of the copper to occur. This oxidation product, observed to be the blackened pin tips, is suspected to be a copper oxide (Figure 9). To alleviate the physical damage to the pins during the insertion process, a softer phenolic backplate material has been used. This, in conjunction with making the holes larger, appears to have eliminated plating damage due to board expansion and hole misregistration.

The corrective action taken by the pin vendor to eliminate the pin contamination was the implementation of a high pressure deionized water rinse. To date, this appears to be an adequate fix in removing pin

contamination. Finally, the board cleaning procedures were reviewed at the board manufacturer's facility to insure proper removal of all organic and inorganic contaminants.

Airborne Antenna

An airborne antenna was submitted for failure analysis after exhibiting corrosion in the field during aircraft inspection. Figure 10 is a photograph of the disassembled antenna as received. The antenna assembly consisted of three pieces: the horn (largest piece), waveguide (smaller rectangular piece), and the matching assembly (tubular piece).

Several corrosion sites were found on the horn and waveguide components. One of the larger corrosion sites found on the horn is shown in Figure 11. A typical corrosion site on the waveguide component is shown in Figure 12. Also found on the bottom of the waveguide was an area indicating the presence of subsurface corrosion. This blistered area is shown in Figure 13.

Chemical analysis of the antenna material indicated the antenna was fabricated from aluminum and plated with copper, then tin. Literature indicated the base metal composition was similar to 6061 aluminum alloy. While this alloy has a high resistance to corrosion because of the thin oxide film which forms on the surface, contact with other metals (copper in this case) should be avoided as the resulting galvanic couple could initiate corrosion.

Examination of the eroded areas on the horn and the waveguide components indicated that the corrosion initiated from the surface of the aluminum beneath the plating. The copper and tin platings eventually flake off. This is verified in Figure 14 where the corrosion area is between the aluminum and copper plating. The area f the waveguide where the plating was intact, but had a bubbled appearance due to subsurface corrosion, was an earlier stage of the corrosion process. There was no separation or corrosion between the copper and tin platings.

In order to determine the effects of the corrosion on the antenna's electrical operation, surface resistivity measurements were made using the 4-point probe method. Surface conductivity of both intact and corroded areas of the antenna were measured and compared. A polished copper plate was used as a standard to compare the test results with that of a relatively conductive surface. A number of readings were taken in each case and an average resistance value was calculated. The measurements of uncorroded areas ranged from 0.0029 to 0.003 milliohms while corroded areas ranged from 0.2930 milliohms to nonconductive. The typical requirement is 2.5 milliohms between probe points. Therefore, the corrosion was affecting the surface conductivity and eventually the surface became nonconductive. Since the signal in an antenna travels close to the surface (skin effect), the corrosion could attenuate the signal and degrade the electrical operation of the antenna.

The corrosion products were chemically analyzed and the closest match was the reference spectrum of aluminum oxide hydroxide (AlOOH). The AlOOH is

typically produced when Al forms a galvanic couple with a dissimilar metal, Cu in this case, in the presence of moisture. Aluminum is anodic and copper is cathodic. The AlOOH is insoluble in water and is nonconductive.

Therefore, the corrosion may be attributed to two factors. The first factor was the use of conductive platings on the aluminum base metal which promote corrosion under certain environmental conditions. The second factor was the intrusion of moisture into the antenna housing. There could have been flaws in the surface of the plating which could have allowed moisture or other contaminants to penetrate. Poor plating integrity may also have been due to improper aluminum surface preparation.

A repair procedure to fix antennas in the field was investigated. Initially, an attempt to remove the corrosion by gritblasting was successful (Figure 15). The treated surface was shown to be electrically conductive (0.0045 milliohms). Next, a conductive and corrosion resistant coating was analyzed. It was decided to follow the corrosion removal by gritblasting with a chromate conversion coating on the eroded areas. The conversion coating would protect the bare aluminum surface from further degradation as well as provide the necessary electrical conductivity. The suitability of this technique was determined by treating a section of the antenna in this manner and leaving an adjacent section of the antenna untouched. The chromate conversion coating procedure conformed to MIL-C-5541 Class III conductivity requirements. Surface resistance measurements were then taken of the treated and untreated surfaces on the coupon. The coupon containing both areas was placed in a salt fog/spray environment conforming to ASTM B117 to determine corrosion resistance. The duration of the test was 168 hours. The surface conductivity of the two areas was measured at the completion of the environmental exposure. Surface conductivity was relatively consistent throughout the treated region. The resistivity of the treated surface changed from 0.0038 milliohms to 0.0056 milliohms after 168 hours of salt spray exposure. This is well under the 2.5 milliohms maximum requirement. When measurements were taken on the treated area, results varied from relatively low resistivity initially (0.0043 milliohms) to comparatively high values (5906 milliohms). Some areas were nonconductive. Figures 16 and 17 are photographs of the test coupon before and after it was removed from the salt spray exposure. There was a lack of corrosion in the area treated by gritblasting and conversion coating. The plating peeled off on the corners on the untreated base metal. Therefore, gritblasting to remove corrosion and then coating the surface with chromate conversion coating according to MIL-C-5541 seems to be an adequate repair procedure. If left untreated, the platings will eventually flake off leaving a non-conductive surface. The chromate conversion coating provided more than adequate protection from further corrosion, as well as adequate surface conductivity. It is also important to insure complete removal of the platings, especially copper, on the antenna prior to coating. This coating is for Al only and does not adhere to copper as Figure 16 indicates.

RAM Modules

Three RAM (random access memory) models, which were experiencing thermal failures, were submitted for analysis. These RAM modules developed

corrosion when constant current was applied during the accumulation of burn-in cycles. The corrosion mechanism was believed to be moisture related based on previous testing conducted by two other laboratories. A representative RAM module is shown in Figure 18.

Initially, the RAM modules were examined externally. Areas of corrosion were found on all three of the RAM modules. Close-ups of a sample of the corroded areas are shown in Figures 19 through 22.

Samples from two corroded areas were analyzed chemically using infrared techniques. The corrosion sample's IR spectrums most resemble the IR spectrum of lead carbonate ($PbCO_3$). The corrosion was always associated with areas that have tin/lead solder. Because of this, it was determined that the source of lead was the lead contained in the solder. It was suspected that there was a contaminant present which leaches the lead from the solder. Once exposed, this lead is oxidized to lead oxide (PbO). Lead oxide, combined with moisture and carbon dioxide from the air, which form carbonic acid (H_2CO_3), react to form lead carbonate ($PbCO_3$). This hypothesis was supported by the experimental evidence of the corrosion appearing during the burn-in cycle when moisture was present.

The contaminant which leached the lead from the solder was likely one of the rinse solutions in the soldering process. The contaminant was also organic in nature. Organic materials, namely organic acids, have been known to react with the lead in solder tinned leads.

The probable cause of the excessive currents during the ATP burn-in cycle is the leakage currents caused by the presence of the $PbCO_3$ between the leads. It was recommended to review the rinsing solution used during the soldering process to insure no contaminants are present which would leave residues on the RAMs. Also the humidity testing should be done without biasing the RAMs to verify that moisture triggers the corrosion process once PbO is formed. The vendor suggested conformally coating the RAMs. This is not recommended since the contaminant would be sealed inside. Conformal coating is only a time barrier to moisture. Corrosion would still occur unless the contaminate was removed. The corrosion process would just take longer.

Resistor Potentiometers

Another example of hardware examined in the Electronic Failure Analysis Laboratory was resistor potentiometers. The manufacturer submitted eight potentiometers for failure analysis (Figure 23).

Each of the resistive components of the potentiometers was examined optically. On several of the components, cracks or discontinuities were observed in the silver epoxy where the brass pin protrudes from the surface of the disk (Figure 24). The resistance between pins was then measured, and several opens were measured, especially where severe cracks in the epoxy were found. These cracks were analyzed with elemental x-ray analysis in the SEM and found to contain sulfur (Figure 25).

Since the manufacturer suspected thermal shock as the mode of failure, attempts were made to reproduce the failure. Using a solder iron similar to one used in the factory environment, a thermal shock test was performed reaching temperatures of 585°F, but no failures resulted. A liquid nitrogen test -195°C), where the potentiometers were submerged in liquid nitrogen, was also performed and no failures could be produced.

The silver epoxy was then contaminated with sulfur compounds, and the potentiometers were baked at 640°F for five minutes. This resulted in severe cracks similar to the field failures (see Figures 26 and 27). It was then concluded that thermal shock alone was not the cause of cracks in the resistive element of the potentiometer, but the presence of sulfur was also required. Cigarettes proved to be the source of sulfur contamination.

Recommendations to the manufacturer included eliminating sulfur contamination from the potentiometer environment and to heatsink the potentiometer during soldering.

Wiring Braiding

A sample of contaminated organic braiding and shield conductor from an aircraft and a bottle of concentrated flame retardant were submitted for analysis. After noting severe corrosion on the structure of several recently produced aircraft, an investigation was performed that revealed the submitted braiding was the source of corrosive materials. Specifically a flame retardant product used on the fabric wire braiding was suspected of containing the corrosive materials. The submitted braiding material is shown in Figure 28. Chemical analysis indicated the braiding was a polyester. The material was also found to be flammable. The white contamination product was identified as a polycarbonate. The source of the white residue found on the braiding could not be determined. The ammonia salts added to the braiding for flame resistance were not found in the polyester fabric. The shielded conductor next to the polyester braiding exhibited corrosion damage (Figure 29).

The corroded shielding was examined in the SEM with elemental x-ray analysis (Figure 30). The shielded conductor was identified as copper (Cu) with tin (Sn) plating. The green and white corrosion product contained the following elements: aluminum (Al), bromine (Br), phosphorus (P), and sulfur (S). This shielded conductor exhibited galvanic corrosion which was accelerated by moisture and the presence of contamination made up of bromine, phosphorus and sulfur. The exposed copper had been corroded by the tin and copper galvanic couple. The source of contamination was most likely the flame retardant treated braiding which was in physical contact with the shielding. The chemical analysis supported this since the flame proofing compounds were identified as ammonium phosphate, ammonium sulfamate and ammonium bromide. These salts are amphoteric and form either weak acids or bases when exposed to moisture or high humidity.

The flame retardant material was evaluated in a sandwich corrosion test (SAE ARP-1512) and immersion corrosion test (ASTM-F 485). Bare aluminum 7075-T6 samples were used in both tests. After 168 hours, the panels with the flame

retardant exhibited severe corrosion as shown in Figures 31 and 32. After 168 hours at 95°F in the immersion test, the flame retardant had lost half of its volume and solidified into a milkly white mass. The samples remaining in the fluid exhibited corrosion pits. It was concluded from these two tests that the flame retardant is severely corrosive to aluminum in the humid atmosphere. Based on the analysis, it was recommended that the use of ammonia salt based materials should be discontinued in this application.

Integrated Circuits

A large group of integrated circuits were submitted for analysis after a white residue was noted between the package leads. The devices were UV-PROMs in ceramic dual-in-line packages.

The white residue was present at the glass frit and lead interface (see Figures 33-35). The residue was analyzed using energy dispersive x-ray analysis. The following elements were identified: lead, tin, silicon, and sulfur. The overlapping of the sulfur and lead energy peaks prevented positive identification of sulfur. The residue was examined with infrared and Auger spectroscopy. The infrared analysis matched the residue to lead sulfate basic ($2PbSO_4PbO$). The Auger analysis identified lead, sulfur, carbon, oxygen and tin. The three analysis techniques provided sufficient evidence that the white residue was lead sulfate. The lead sulfate was found to be sufficiently soluble in water to cause excess leakage currents to develop between the PROM leads. The lead was most likely leached from the tin/lead solder. The source of sulfur was most likely from sulfuric acid. It is speculated that the components were exposed to sulfur dioxide. This compound is produced by car exhaust and other pollution sources. The components had been stored for approximately a year in an uncontrolled environment. During this period of time, the components were removed from printed wiring boards and exposed to temperatures in excess of 500°F for up to five minutes. Hot water and mechanical cleaning was found to remove a large amount of the white residue. This process, however, degraded the solderability of the component leads. The presence of the white residue and several other unrelated anomalies resulted in all of the PROMs being scrapped.

Conclusion

The penetration of moisture and contaminants into electronic systems has many detrimental effects including corrosion. Corrosion is becoming an even more significant factor in the reliability of electrical and electronic equipment. This is caused by many reasons. One is that in most electronic systems, dimensions have been reduced for faster signal processing and higher density. This means that most metallizations are thin or small in cross-sectional areas and the individual metallizations are closer together. In such systems, only trace amounts of moisture or contaminants can create favorable conditions for corrosion. Another factor is the exposure of electronics to harsher environments. Corrosion occurs during manufacturing, storage, shipping and service. With this in mind, methods for minimizing or preventing corrosion should be considered at the beginning of

the design stage. Corrosion engineers, as well as electronic engineers, should be a part of the design stage. These designs should usually be based on the worst case scenarios and the assumption that moisture will be present in the intended application. Metals should be used in their most corrosion-resistant form. Therefore guidelines in MIL-STD-1250 and MIL-STD-454 should be followed. If it can be avoided, dissimilar metals (one anodic the other cathodic for example) as defined in MIL-STD-889 should not be used in contact with each other. Otherwise plate with a metal to reduce the potential difference of the couple. All aluminum, unless plated, should be coated with a chemical film in accordance with MIL-C-5541 or anodized in accordance with MIL-A-8625. Cleaning solutions should be used to insure complete removal of residues such as flux or processing solutions. In a hermetically sealed packet, it is important to properly cure materials inside the package to prevent outgassing of potential contaminants. Remember, it is always less expensive to redesign or choose an alternate material on the drawing board than to analyze the cause and or replace fielded equipment. Paraphrasing the old addage "an ounce of prevention is better than a pound of cure."

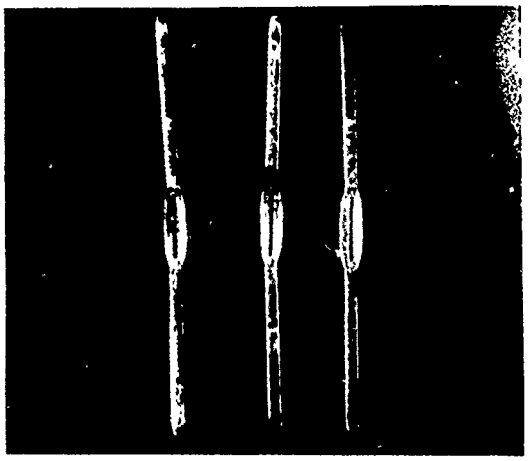

Figure 1: Backpanel pins submitted for examination. MAG: 4X.

Figure 3: Close-up view of a pin tip with the green contamination, suspected to be a copper chloride compound. MAG: 51X.

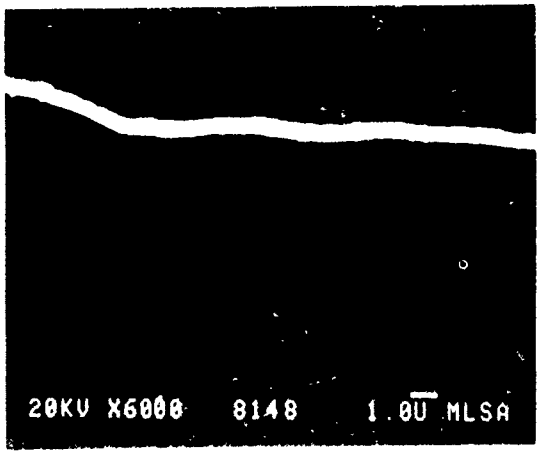

Figure 2: SEM micrograph showing the base phosphor bronze material and the nickel and gold platings. MAG: 600X.

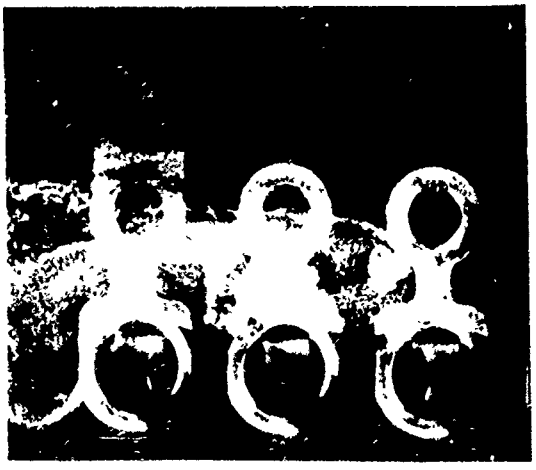

Figure 4: White deposit found on backpanel board which was analyzed to be a metal carbonate. MAG: 12X.

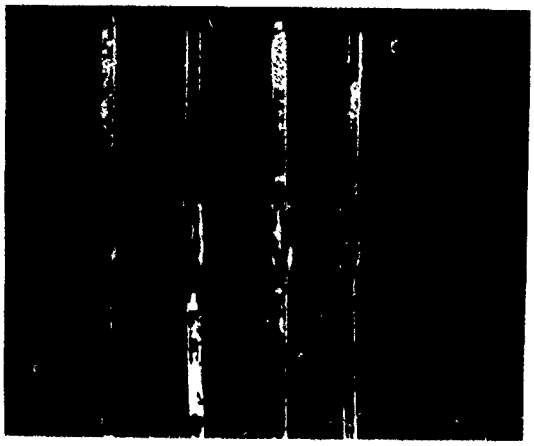

Figure 5: Example of white residue found on pins which was examined elemental x-ray analysis and found to be postasium rich. MAG: 4X.

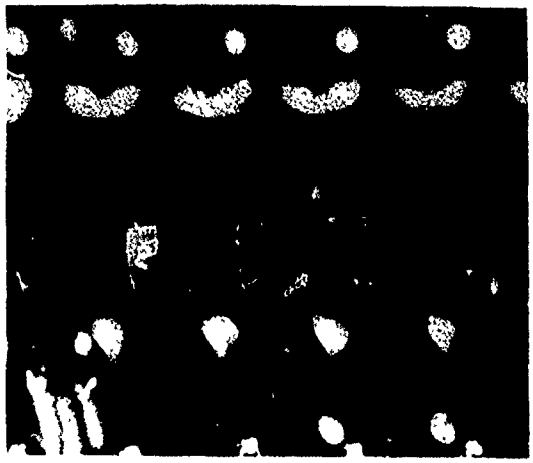

Figure 7: Example of pins with plating damage, green contamination and plating defoliation. MAG: 10X.

Figure 6: A comparison of two pins. The one on the left displaying a flattened tip and complete removal of the nickel and gold platings and the one on the right is undamaged. MAG: 45X.

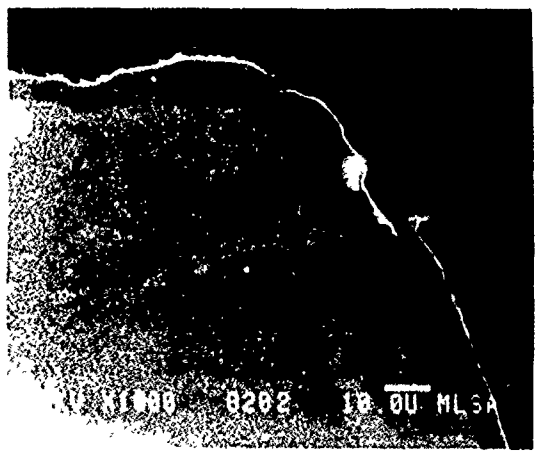

Figure 8: SEM micrograph showing eroded base material and defoliation of the two platings. MAG: 1000X.

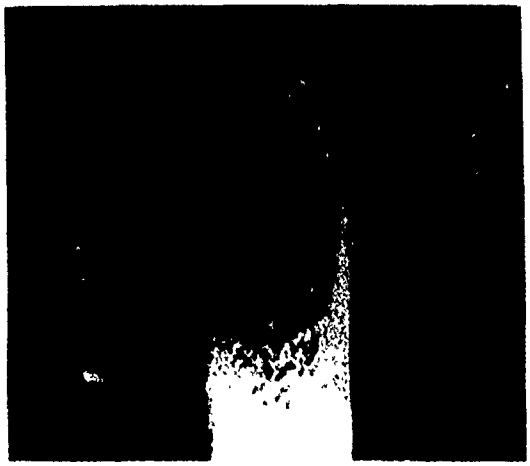

Figure 9: Blackened pin tip which was examined using elemental x-ray analysis. MAG: 44X.

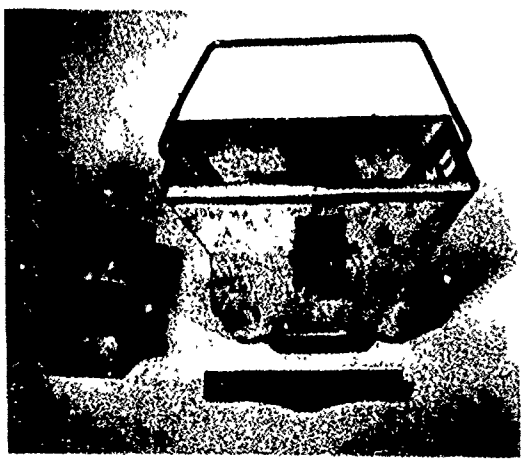

Figure 10: Antenna assembly as received. MAG: 0.2X.

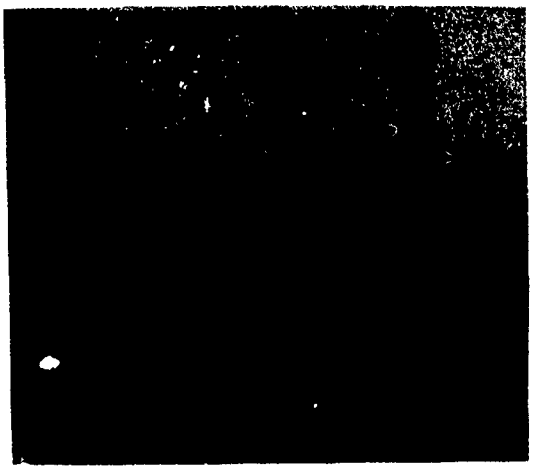

Figure 11: Close-up of a corrosion site on the horn. MAG: 1.7X.

Figure 12: Close-up of a corrosion site on the waveguide. MAG: 1.5X.

Figure 13: Area on waveguide revealing subsurface corrosion. MAG: 2.5X.

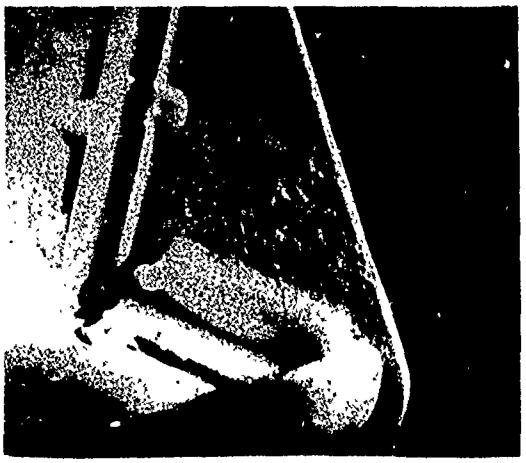

Figure 15: Corroded area after grit-blasting treatment. MAG: 2.0X.

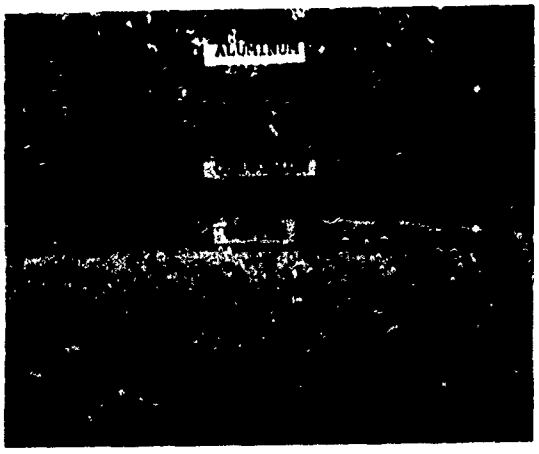

Figure 14: Cross-section of area of subsurface corrosion (SEM photomicrograph). Note the Sn and Cu platings and the corrosion. MAG: 900X.

Figure 16: Coupon after chromate conversion coating applied and before salt spray exposure. The arrow points to the converted area. The reddish brown area is copper where the chromate conversion coating did not adhere. MAG: 1.6X.

Figure 17: Coupon after chromate conversion coating applied and after salt spray exposure. The arrow points to converted area. MAG: 1.1X.

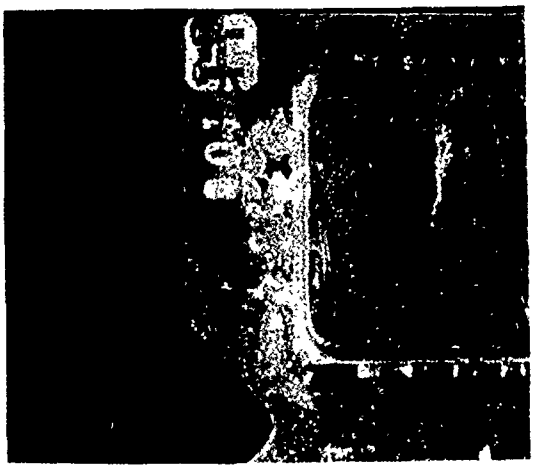

Figure 19: Corrosion located at the end of the RAM around the castellations and on the coding. MAG: 7.64X.

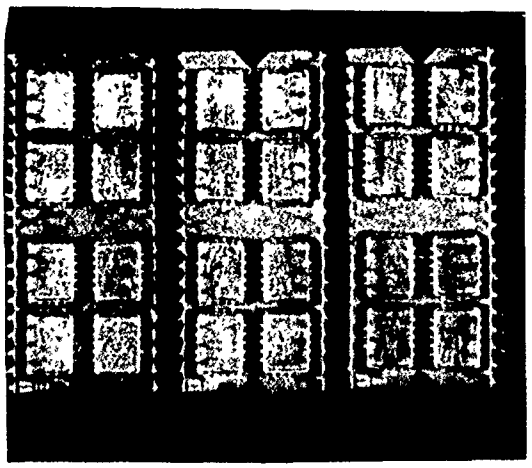

Figure 18: Bottom view of RAM modules as received. MAG: 1.63X.

Figure 20: Corrosion area found around the package lead. MAG: 6X.

Figure 21: Close-up of the corrosion shown in Figure 20 that was chemically analyzed. MAG: 66X.

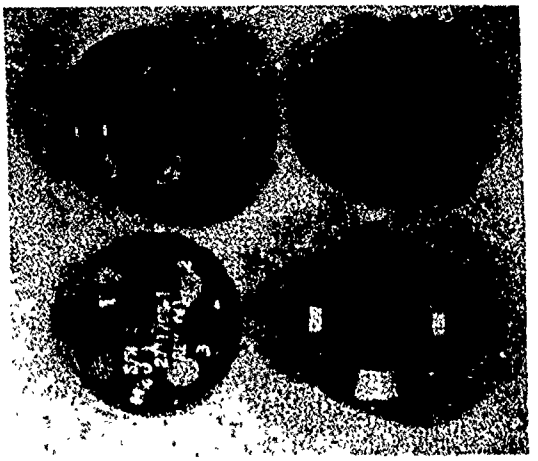

Figure 23: Top (left) and bottom (right) views of potentiometers as received. MAG: 1.1X.

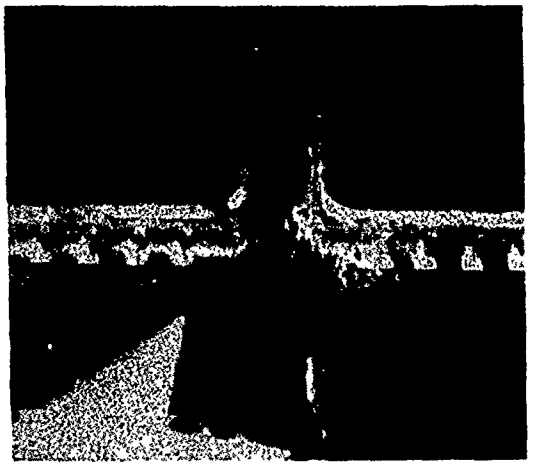

Figure 22: Photograph showing the extent of the corrosion around and between the castellations of the leadless chips. This was likely responsible for the leakage currents and excessive currents during the ATP burn-in cycle. MAG: 6X.

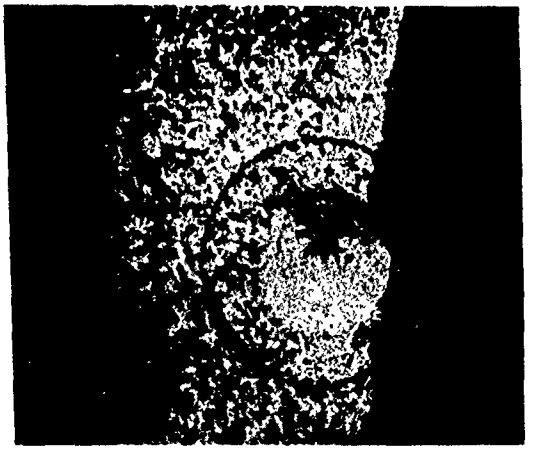

Figure 24: Example of pin showing blackish tint discoloration in a severely cracked pin. MAG: 27.5X

Figure 25: SEM micrograph of cross-section of cracked pin showing contamination. MAG: 1000X.

Figure 27: View of pin showing severe cracking after sulfur contamination and bake. MAG: 27.5X.

Figure 26: View of pin showing condition before sulfur contamination and bake. MAG: 27.5X.

Figure 28: The braiding material as received. Note the surface desposites (light area). MAG: 0.6X.

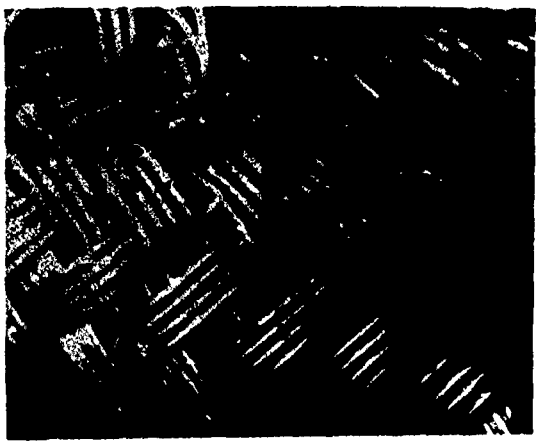

Figure 29: Close-up of the shielded conductor. Note the exposed copper conductor and green and white corrosion products. MAG: 13X.

Figure 31: Sandwich corrosion test samples after 168 hours. The sample on the right was the control and the left sample was exposed to flame retardant. Note the pitting corrosion (black spots) on the left sample. MAG: 0.84X.

Figure 30: SEM micrograph showing corrosion damage to the copper conductor (see arrow) and corrosion product (upper right corner). The corrosion product contained aluminum, copper, tin, bromine, sulfur and phosphorus. MAG: 320X.

Figure 32: Close-up of the pitting corrosion on the left sample from Figure 31. Note the structural damage to the surface. MAG: 16X.

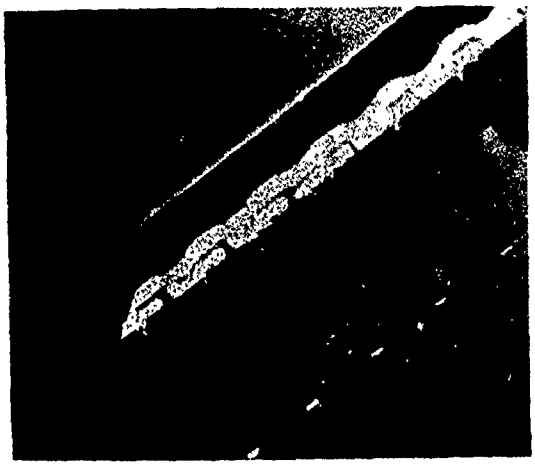

Figure 33: White residue found on the glass frit of a PROM. MAG: 6.5X.

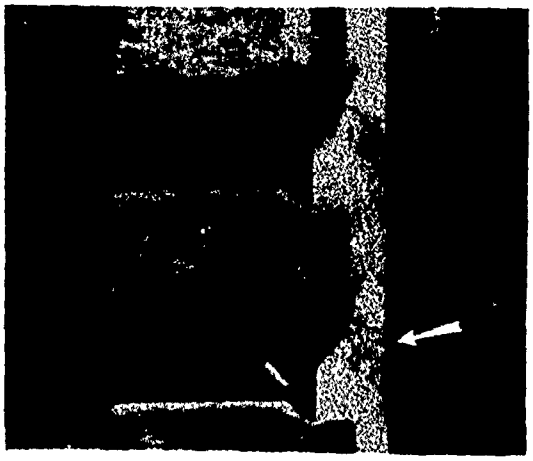

Figure 35: White residue found on the glass frit of one of the PROMs. Note that the residue can be mechanically removed (arrow). MAG: 16X.

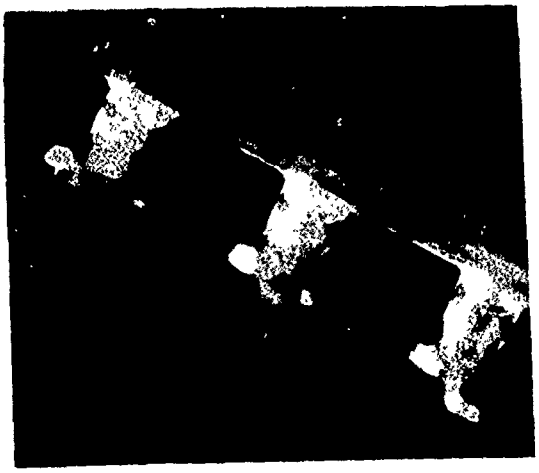

Figure 34: Underside of the PROM glass frit and lead interface. Note the accumulation of the white resudue. MAG: 20X.

A NEW TECHNIQUE FOR DETERMINING CORROSION RESISTANCE BEHAVIOR OF LUBRICANTS

P. J. Kennedy and V. S. Agarwala
Naval Air Development Center
Warminster, PA 18974

ABSTRACT

A method, based on a new corrosion sensor, has been developed to quantitatively determine the corrosion resistance behavior of lubricants, hydraulic fluids, greases and solid films. It is based on the electrochemical concept of measuring the corrosion current generated by a galvanic couple underneath a thin oil film. The magnitude of this current was directly related to the effectiveness of the oil film in preventing corrosion. The corrosion resistant properties of the lubricants have been related to the chemical structures of the film, the type of contaminant and composition of the additive. It was shown that the steel coated with a thin film of turbine engine oil corroded at a maximum rate of 0.01 mdd where as the oil contaminated with 100 ppm sea salt increased the corrosion rate by a factor of 300. Conversely, the maximum corrosion rate could be reduced further to 0.0008 mdd by addition of an appropriate corrosion inhibitor to the oil.

INTRODUCTION

The primary function of a lubricant, as the name implies, is to reduce friction and wear. Presently, operation of Naval aircraft require turbine engine oils, transmission oils, various special lubricants, hydraulic fluids, specially formulated greases and solid film lubricants. All of these lubricated areas are essentially unprotected and potential corrosion areas, except for the protection provided by the oil itself. For example, corrosion protection of hydraulic pistons, engine components and bearings rely to a great extent on the formation and stability of thin oil films. This investigation was a result of a reported problem concerning corrosion of naval aircraft turbine engine bearings (1). These bearings are lubricated with a neopentyl polyol ester type of turbine engine oil that corresponds to the requirements of the Mil-L-23699 military specification. Polyol esters type fluids were chosen for this application since these fluids exhibit a much higher thermal stability

than most lubricating oils; however these esters are more polar and exhibit a stronger affinity for water. These latter characteristics suggest that the turbine oil films would be less hydrophobic and, therefore, less effective in preventing corrosion than petroleum oils. The particular corrosion process that was initially studied involved pitting that occurred on the raceways of naval aircraft ball and roller bearings. The studies suggest that this pitting is associated with the low level contamination in the turbine engine oil with the ingestion of salt laden air of the marine environment (2). The initial approach to this problem was to develop a rust inhibited version of the turbine engine oil. Thus, a rust inhibiting system was incorporation into the turbine engine oil; however, competitive adsorption effects resulted in a trade-off in wear resistance. Therefore, this study was initiated to better understand the corrosion mechanism.

Conventional procedures for estimating corrosion inhibiting characteristics of a thin oil film involve either visually monitoring a steel plate coated with an oil film for the first signs of corrosion (3) or measuring the weight loss associated with corrosion (4). These test procedures are designed to study the practical condition where a thin oil film (in the process of draining from a metal surface) provides corrosion protection by acting as a barrier to a hostile environment. However, these methods lack in sensitivity for detecting micro-corrosion effects that would result in response to a change in environmental conditions. The intent of this investigation was to develop a quanitative test procedure having sufficient sensitivity to study rusting under thin oil films. Oil films that were studied as part of this investigation include turbine engine oils, salt contaminated oils, additive free and additive containing petroleum oils.

EXPERIMENTAL

The technique developed consisted of a corrosion monitoring probe which is essentially a galvanic cell formed by the alternate stacking of rectangular plates of copper and steel. The copper and steel plates were approximately 140 mm in length, 25 mm in width and 0.80 mm in thickness. Actual construction involved alternately placing the copper and steel plates in an aluminum mold so that the final spacing was approximately 0.8 mm. After soldering wire leads to each plate, the assembly was potted using a two part epoxy system. The epoxy was built-up around the metal plate assembly so as to encase the five interior sides of each plate leaving only one exterior edge face exposed. All electrical leads were also encased in the epoxy block. The epoxy block was then polished to expose only the side faces of the copper and steel plates and further shaped to provide a 60 degree angle

with the resting surface. The construction of the corrosion probe can be seen in Figure 1.

The concept for using a corrosion monitor for studying the corrosion process in thin oil film systems evolved from the use of similar type probes on naval aircraft carriers (5-6). Of course, the probe shown in Figure 1 has undergone considerable design modifications related to construction materials, shape and auxiliary cooling capability in order to allow its use in oil systems (7). The original corrosion monitoring probes was based on a design that used teflon spacers (1). Its primary function was to monitor the corrosivity of sea environment due to moisture and salt in the absence of any protective films. The developmental history of this probe and related theory have been reported elsewhere (5,8). In operation, a thin film of water condenses on the dry probe such that it spans the spacer material and acts as pathway for ion flow between steel and copper surfaces. In other words, this condensed film acts as an electrolyte to complete the galvanic cell and allows a flow of current. The principles involved in using this probe as a corrosion monitor were reported previously (5). Usually, the cathodic metal (e.g., copper) corrodes very little or not at all and corrosion of the anodic metal (e.g., steel) is increased significantly. The driving force for this couple is the galvanic potential developed between the two dissimilar metals in the environment. The magnitude of the corrosion current is dependent upon this potential which in turn is dependent upon three important environmental variables, temperature, relative humidity and the corrosive elements of the environment. In this study, the three environmental variables are held constant and therefore the electrochemical response of the probe, in the absence of any complicating factors, should be reproducible.

The significant aspect of this study is that the surface of the probe are coated with thin films of oil that insulate the probe from contact of the corrosive environment. Thus, the initiation of corrosion marks the break-down point of the oil film, and the magnitude of the corrosion sheds light on the corrosive nature of the oil film and environment. Usually, the break-down point of the oil film is marked by a sharp increase in corrosion current. This current was recorded on an hourly basis using an electronic device consisting of a zero resistance ammeter (ZRA), an analog to digital converter and a data logger. The ZRA was constructed using a potentiostat (Aardvark Model PEC-1) in which the current between the working and counter terminals were adjusted to zero. A standard resistance box was connected between the reference and counter terminals to convert the current into a potential drop for amplification and recording. The digital data logging system was a commercially available instrument from Precision Digital (Model 1040). The primary advantage of this type of recording system was that current variations

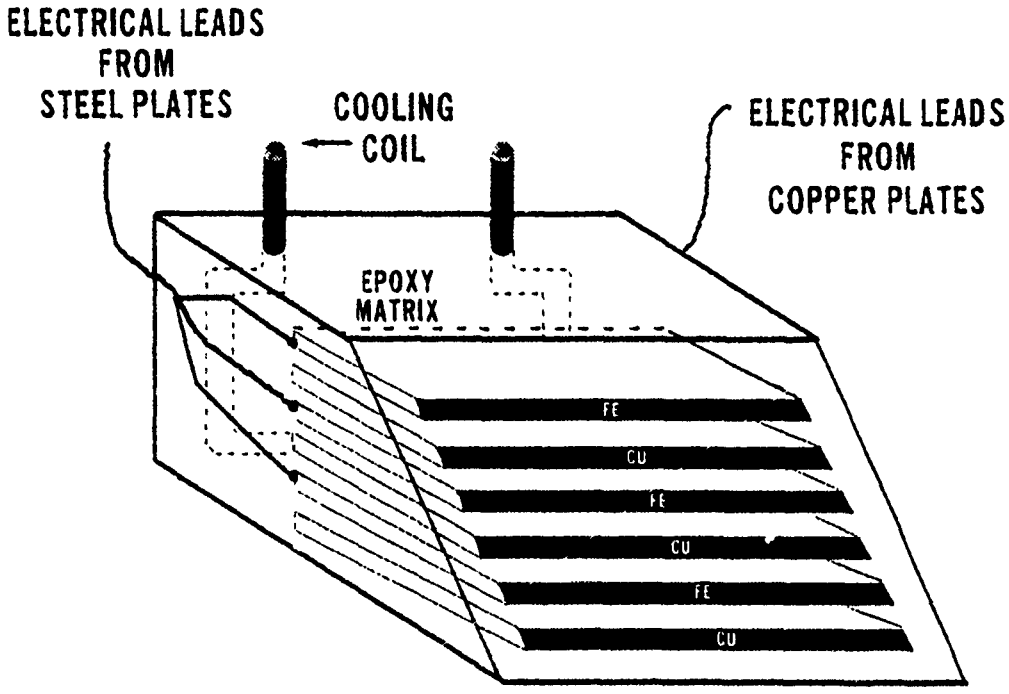

Figure 1 - Schematic of corrosion probe showing copper and steel plates embedded in an epoxy matrix.

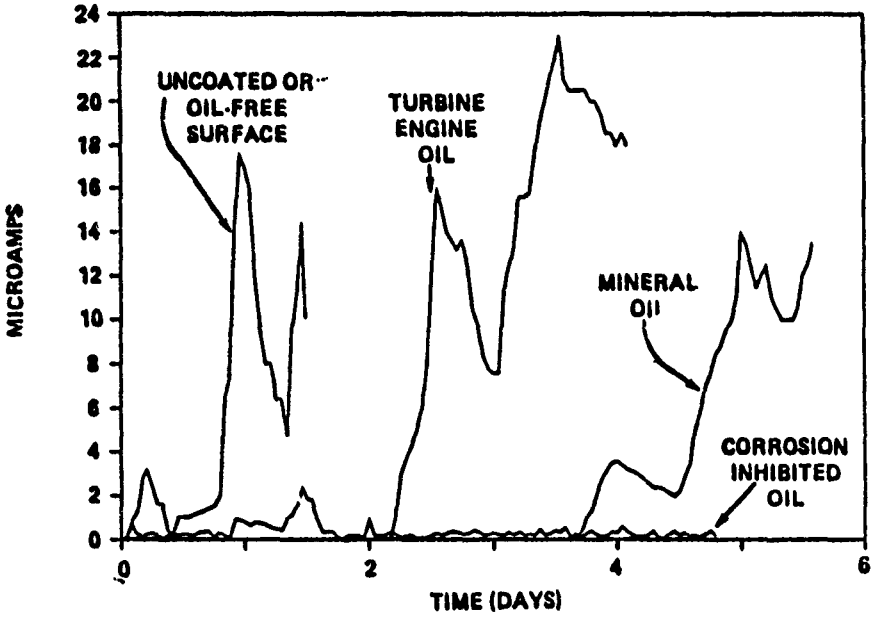

Figure 2 - Typical current transients from an uncoated probe versus the probe coated with various lubricant films using an ambient temperature probe in a mist environment.

of up to three orders of magnitude could be easily recorded without changing the resistance between the reference and counter terminals. A 100 K Ohm resistor was adequate to measure current in the range of 0.01 to 10 microamps.

Turbine engine oils, hydraulic fluids and mineral oils were investigated for corrosion inhibiting ability in the absence and presence of contaminants. The turbine engine oil used in this study conformed to the Mil-L-23699 specification. The effect of salt contamination on the effectiveness of this oil in inhibiting corrosion was investigated by doping the oil with a 10% aqueous sea salt solution. One of the corrosion inhibited turbine oils used was an experimental commercial product. The other corrosion inhibited turbine engine oil was prepared in this laboratory and contained a mixture of quaternary compounds of dichromate, nitrite, molybdate and borate, called DNBM, at about 4% concentration. The light mineral oil was a laboratory grade paraffin with a viscosity of 125 SUS, the heavier oil was a typical pharmaceutical oil with a 340 SUS viscosity.

Oils were evaluated in an environmental chamber maintained at 100% relative humidity and ambient laboratory temperature. Occasionally a fine mist was necessary to produce quick condensation on the monitoring probe. Testing involved both the use of uncoated probes and oil coated probes. The surface preparation involved hand polishing with 360 and 600 grade silicon carbide paper, alcohol cleaning and a surface deactivation step that involved coating the exposed surface with a film of distilled water for 5 minutes. The surface of the probe was then towel dried and coated with an oil film for a five minute interval and then allowed to drain off of the surface in the environmental chamber.

RESULTS AND DISCUSSION

The probe used in the initial part of this study was cylindrical and consisted of alternating copper and steel plates separated by teflon spacers. This assembly was mechanically held together by two brass bolts which acted as electrical pathways for the cell. This cell was illustrate in a previous paper (1). The major problem with this type of construction was a significant loss in internal resistance during and after testing due to oil/water diffusion at the teflon/metal interfaces. Other problems involved the relative slowness of the probe to develop corrosion and general difficulties in polishing and reproducing identical drainage characteristics. The initial difficulty with probe contamination was resolved by casting the plates in epoxy. More realistic drainage conditions were obtained by using a face angled at 60 degrees to the surface. One other significant improvement involved using a cooling coil in the top portion of the probe to insure continuous condensation on

the probe. A further improvement in probe performance was achieved by placing the cooling coil behind the body of the probe rather than on top of the probe.

Preliminary studies involved the use of a probe that was operated at room temperature (1). It was similar to the one shown in Figure 1 except that this probe was not equipped with a cooling coil. Typical data are shown in Figure 2 for the ambient temperature operation of the probe. Under the standard test conditions, approximately 24 hours were required before significant corrosion was observed on the uncoated or oil-free probe. Visual observations indicated that several hours were required before the build-up of small droplets on the probe surface and several additional hours were required for these droplets to grow to the critical size necessary to span the gap between two metal plates. This initial condensation can be attributed to the presence of saturated air at a temperature a few degrees above that of the probe. Figure 2 indicates that thin films of turbine engine oil, a light paraffin oil and a corrosion inhibited oil vary in their effectiveness in protecting the steel surface from the surrounding environment. The general corrosion process does not appear to be gradual but rather fairly abrupt. The large peaks and valleys in the corrosion current versus time curves are probably related to the make and break in the surface film due to fluctuations in temperature, and condensation developing with time on the lid of the environmental chamber which produce droplets, and eventually grow to a critical size and rain down on the probe. After such an occurrence, the droplets evaporate or run off of the surface and thus create a relatively dry surface condition for a while.

The reproducibility of data is an important consideration. Figure 3 shows corrosion current tracings for 3 separate evaluations that involved coating the probe with thin films of mineral oil. Reproducibility in the case of mineral oils is very good. During testing, the oil is allowed to drain away from the surface. Figure 3 suggests that the amount of oil or the emulsified condition of the oil remaining on the surface of the probe after three to four days is insufficient to provide any significant level of corrosion protection. The data illustrated in Figure 3 required approximately 3 weeks to collect. Since the large variations in peaks and valleys were believed to be due to laboratory temperature variations, it was decided that more meaningful data could be obtained if the probe was equipped with an cooling coil. A circulating bath containing antifreeze at 15^{o} C was used to force coolant through the probe and thus cause condensation directly on the unprotected plate edge face of the probe or directly onto the protective oil film. Results obtained using the cooled probe are shown in Figure 4. A comparison of these data with data in Figure 2 indicates a significant difference in corrosion current transients. Data in Figure 4 indicates that mineral

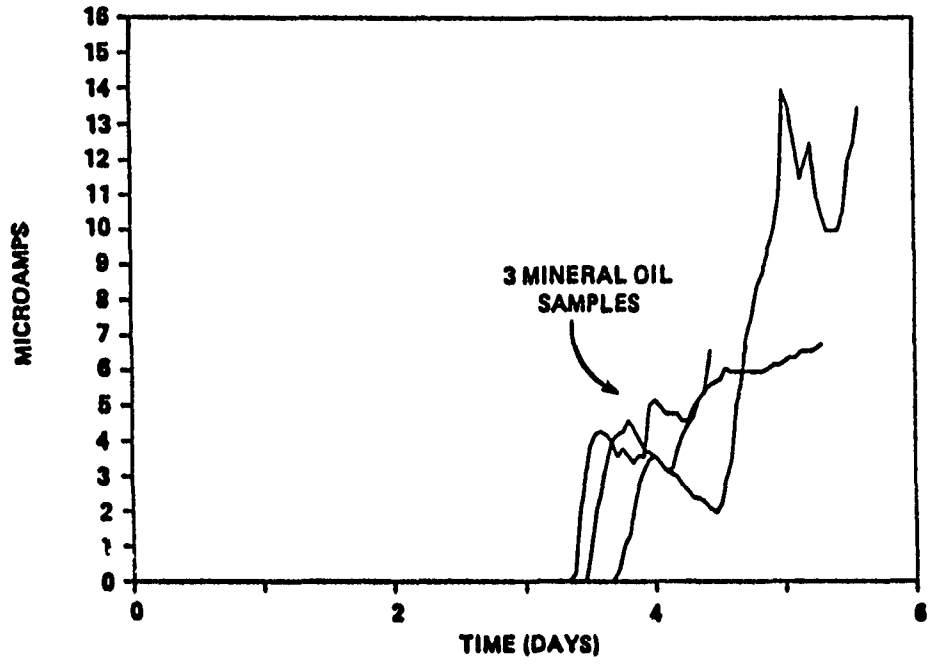

Figure 3 - Three consecutive transients showing reproducible behavior of ambient temperature probe coated with thin films of mineral oil and operated in mist environment.

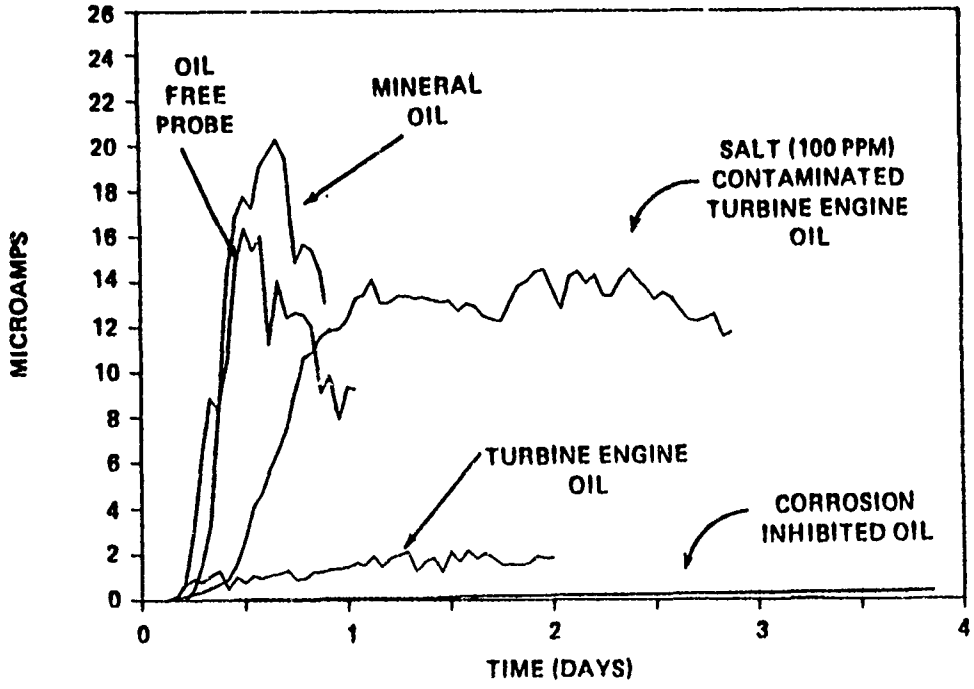

Figure 4 - Typical current transients from a cooled probe (15° C) operating in a mist environment at ambient temperature and coated with thin films of various oils.

oil is less effective in preventing corrosion relative to turbine engine oil under cooled probe conditions as compared to ambient probe conditions (cf Figure 2). The corrosion accelerating effects of 100 ppm sea salt contamination in turbine engine oil is also illustrated. The corrosion inhibited turbine engine oil was also effective in preventing corrosion under cooled probe operating conditions. This may be related to the observation that droplet condensation does not occur on the lid of the environmental chamber under cooled probe conditions.

The corrosion behavior transients of a series of light and heavy mineral oil is shown in Figure 5. This evaluation was done using the cooled probe; reproducibility was excellent. Here, four of the five mineral oils were paraffin oils in the 125-130 SUS viscosity range whereas the fifth oil was a pharmaceutical grade oil in the 340-365 SUS range. The heavier oil is indistinguishable from the lighter oil and thus shows that viscosity effects are insignificant under these test conditions. The transients in Figure 5 suggest that corrosion currents initiate within two to four hours of exposure and rapidly increase to a high current density of approximately 1 $\mu A/cm^2$ within 9 to 10 hours, based on the steel surface area of 16 cm^2. The corrosion current then decreases to a steady-state current density of $< 0.1\ \mu A/cm^2$. The general reduction in peaks and valleys due to the cooled probe can also be observed in the transients.

The results on the effect of thin hydrocarbons films on the corrosion of steel are also presented in Table 1. The data is given for two cooled probes operated at 15^{o} C. These probes were similar but were of different construction with regard to the placement of the cooling coils. The time required for the maximum corrosion current to develop and the cumulative amount of iron oxidized per square cm of steel surface after 24 hours of testing were considered critical parameters in defining the corrosion process and are listed for both probes in this table. The data from blank runs or tests that were made using probes that were free of oil films are also shown. The average maximum corrosion current was about 7 uA and required approximately 12 hours to develop. After one day of testing, the cumulative amount of corrosion was severe and was approximately 7 $\mu g/cm^2$. This data was based on four separate evaluations for each probe and showed a high degree of consistency.

It seems reasonable to assume that coating the probes with thin films of mineral oil would provide some degree of corrosion protection. A limited amount of corrosion protection was observed to occur as shown in Figure 2 when the probe was operated at room temperature but did not appear to occur when the probe was cooled as in Figure 4. Cooling the probe greatly increases the rate of condensation on the surface of the oil coated probe and decreases the time

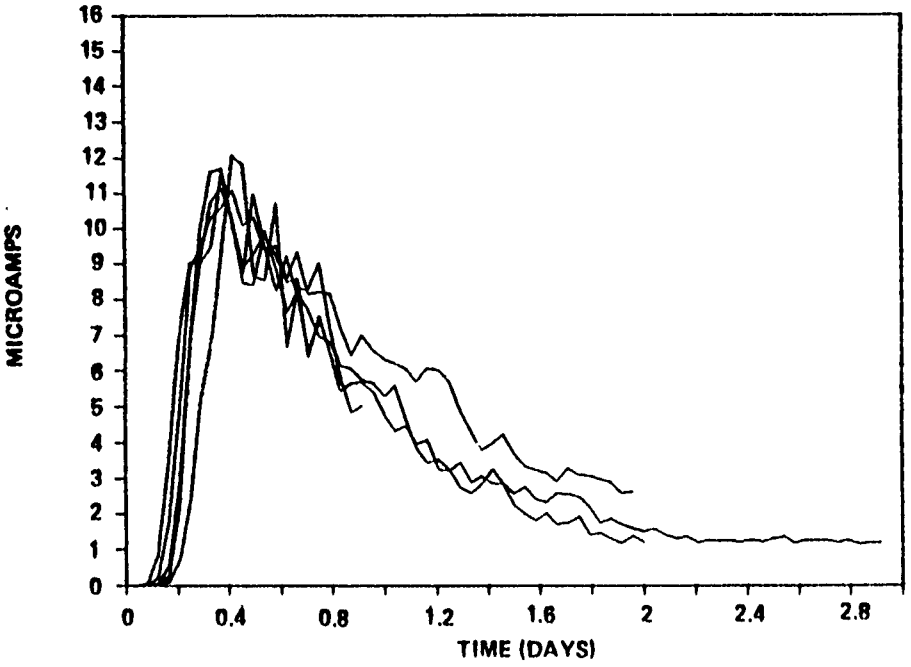

Figure 5 - Results showing reproducibility of the cooled probe coated with thin films of various mineral oils.

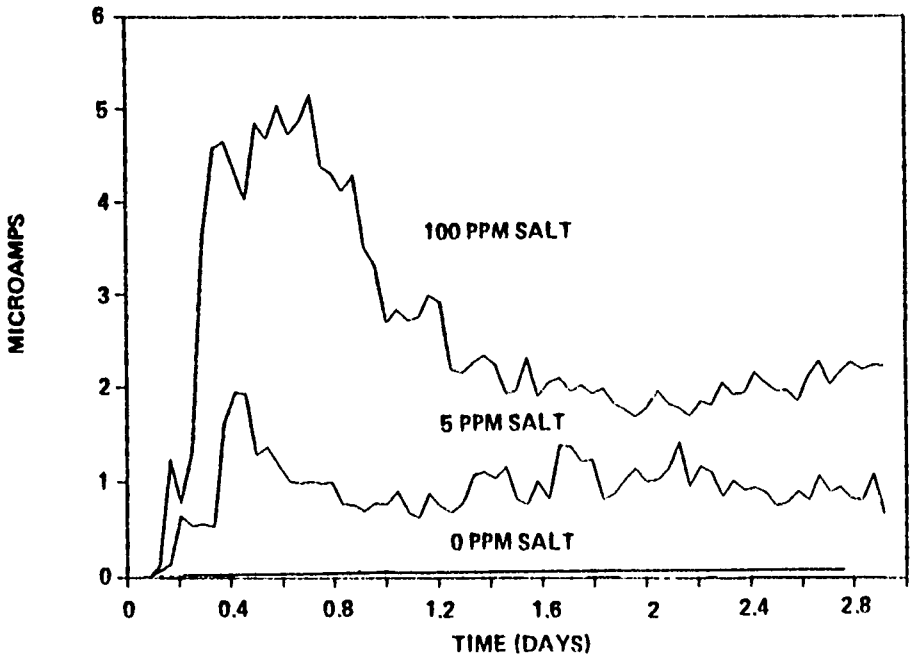

Figure 6 - The effect of sea salt contamination level in turbine engine oil on the corrosion rate of steel.

required for corrosion initiation from 3.5 days to nearly two hours. From Table 1, it can be inferred that paraffin oil is not a corrosion inhibiting lubricant. Lighter molecular weight hydrocarbons such as octene, octane and dodecane are readily evaporated from the surface of the probe. The results (Table 1) show a significant reduction in cumulative corrosion current or total amount of iron oxidized due these light hydrocarbons. One possible explanation would be that evaporation of these hydrocarbons leaves behind a residue-film of higher molecular weight oxidation products which are of protective nature.

This corrosion probe evolved out of a study concerned with factors responsible for the corrosion of turbine engine bearings. The primary factor appears to be related to low level salt water contamination of the turbine engine oil as a result of operating in the marine environment. Figure 6 shows the effect of salt contamination on corrosion rates and illustrates that salt concentrations of even 5 ppm can significantly accelerate corrosion rates. Concentrations of salt in the 5 ppm range have already been reported in fleet studies and this data illustrates that this low level contamination can contribute significantly to rusting. The effect of salt is more clearly illustrated in Table 2. The turbine engine oil provides a significant level of corrosion inhibition when compared with the uncoated probe or probe coated with mineral oil. Adding as little as 5 ppm sea salt produced a 50 fold increase in the corrosion rate. A further increase in salt concentation to 100 ppm produced even a more significant increase in the total amount of iron oxidized after 24 hours of testing (cf. Table 2).

One approach to this problem would be to use commercial organic corrosion inhibitors in the turbine engine oil. The corrosion current transients in the presence of a rust inhibitor were very sporadic but very small in magnitude, average less than 0.01 μA at steady-state. Perhaps, it can be assumed that a close-packed monolayer of rust inhibitor with fairly strong bonds to the surface would form under these conditions. This monolayer would be expected to act as a barrier protecting the surface from the environment. Quite often, corrosion inhibited oils fail by initially forming several extremely small corrosion spots of < 1 mm in diameter. After several days of exposure to high humidity conditions, these spots would tend to slowly increase in size. It appears that either a passive film develops or that the monolayer is capable of repairing itself within a matter of a few hours since the corrosion current shows a tendency to return to the base line value.

The use of an organic corrosion inhibitor in a turbine engine oil formulation is questionable since organic materials are generally thermally unstable at the bearing operating temperatures. A possible solution would be to use an

TABLE 1. CORROSION OF STEEL IN THE PRESENCE OF HYDROCARBON FILMS

HYDROCARBON FILM	RUN #	PROBE #1 MAX. CURRENT (μA)	PROBE #1 (TIME) (days)	PROBE #1 AMT. Fe OXIDIZED *	PROBE #2 MAX. CURRENT (μA)	PROBE #2 (TIME) (days)	PROBE #2 AMT. Fe OXIDIZED *
BLANK (NO OIL FILM)	1	5	0.4	4.0	7	0.9	6.0
	2	6	0.4	5.0	8	0.8	7.0
	3	12	0.5	12.0	8	0.5	8.0
	4	6	0.5	6.0	4	0.8	5.0
AVERAGE		**7.2**	**0.5**	**6.8**	**6.8**	**0.7**	**6.5**
PAR-AFFIN OIL	1	11	0.40	8.5	1	0.40	1.0
	2	10	0.45	8.5	5	0.45	5.0
	3	15	0.35	12.0	7	0.35	7.0
	4	11	0.40	10.5	6	0.40	5.5
	5	12	0.45	9.0	9	0.35	8.0
	6	11	0.45	11.0	8	0.35	6.0
	7	12	0.35	10.0	9	0.35	9.5
	8	12	0.40	9.8	8	0.50	7.8
AVERAGE		**12**	**0.40**	**9.9**	**7**	**0.40**	**6.2**
OCTENE	1	1	0.5	0.65	2.3	1.8	0.14
OCTENE	2	1	1.2	0.50	1.2	0.4	0.60
AVERAGE		**1**	**0.8**	**0.60**	**1.8**	**1.1**	**0.37**
OCTANE		**1**	**1.6**	**0.70**	**1.4**	**0.6**	**0.70**
DODECANE		**3**	**1.6**	**2.20**	**0.2**	**0.4**	**0.15**

* $\mu g/cm^2/day$

TABLE 2. THE EFFECT OF SALT CONTAMINATION ON THE RUST INHIBITING PROPERTIES OF TURBINE ENGINE OIL.

FLUID TYPE	RUN #	MAX. CURRENT (μA)	(TIME) (days)	AMT. Fe OXIDIZED ($\mu g/cm^2/day$)
TURBINE ENGINE OIL (NO ADDED CONTAMINANT)	1	2.40	12	-.001
	2	0.45	7	-.020
	3	0.30	8	-.005
	4	2.40	9	-.004
AVERAGE		**1.39**	**9**	**-.008**
TURBINE ENGINE OIL WITH 5 PPM SEA SALT	1	1.30	4.5	0.010
	2	0.50	0.5	0.200
	3	1.20	0.5	1.000
	4	1.00	1.0	0.200
	5	0.50	6.0	1.000
AVERAGE		**0.90**	**2.5**	**0.480**
TURBINE ENGINE OIL WITH 100 PPM SEA SALT	1	13.00	0.5	10.000
	2	6.00	1.0	4.000
	3	6.00	0.5	5.000
	4	2.60	5.0	1.000
	5	0.50	6.0	0.200
AVERAGE		**5.60**	**1.4**	**4.000**
TURBINE ENGINE OIL WITH 4.2% DNBM	1	0.005	0.5	0.0016
	2	0.003	0.2	0.0005
AVERAGE		**0.004**	**0.4**	**0.0010**
ENGINE OIL WITH 4.2% DNBM + 100 PPM SALT	1	**0.800**	**0.5**	**0.0350**

inorganic system to provide corrosion protection. One such system is DNBM which is a blend of dichromate, nitrite, borate and molybdate quaternary ammonium salts. The corrosion inhibiting properties of the DNBM system on steels have been reported elsewhere (9). The data in Table 2 show that the DNBM does significantly improve the corrosion inhibition characteristics of turbine engine oil. One surprising finding came in a study of the affect of adding the DNBM to a turbine oil made highly corrosive through addition of 100 ppm of sea salt. This can be seen in Table 2 by comparing the corrosion rates in turbine engine oil containing 100 ppm sea salt in the presence and absence of DNBM inhibitor. The net effect of DNBM was a reduction of corrosion rate by two orders of magnitude. The galvanic currents measured with the probe were in fact negative in polarity. This suggests that in the galvanic probe, copper had become an anode and steel behaved like a cathode. In other words the steel surface became passive due to the DNBM. The overall corrosion currents were extremely small suggesting that this particular inhibitor system may provide a practical solution to this problem.

CONCLUSIONS

The electrochemical method (galvanic probe) represents an interesting alternative to standard test procedures that are now being used to determine the corrosion inhibiting characteristics of thin oil films. Some of the advantages in the use of this probe over alternative techniques are the quanntitative nature of the probe, ease in accelerating the test procedure and extremely high sensitivity. It represents an important tool, along with such approaches as AC impedance spectroscopy, in studying corrosion under thin oil films.

ACKNOWLEDGMENT

The authors thank M. S. Ruzansky for his assistance in fabrication of the probe and carrying out the experiments.

REFERENCES

1. L.Stallings, P.Kennedy, N.Rebuck and V.S.Agarwala, "Electrochemical Evaluation of Corrosivity in Turbine Engine Oils", in Aviation Gas Lubricants - Military and Civil Aspects, Aviation Fuel and Lubricant Performance Testing, SAE Technical Paper Series SP-633, 1985, p.103.

2. M.J.Bieberich, C.L.Brown and J.C.Limpert, David Taylor Naval Ship R & D Center Report No. DTRC/SME-80/36,1980.

3. 1985 Annual Book of ASTM Standards, Section 5, Petroleum

Products, Lubricants and Fossil Fuels, Vol 05.02, Method D1748-83, p.50 (1985).

4. P.A.Warner, G.C.Brown, R.J.Meehan and W.J.Purvis, Air Force Wright Aeronautical Laboratories Report No. AFWAL-TR-81-4028, "Corrosion Inhibiting Engine Oils"(1982).

5. V.S.Agarwala," A Probe for Monitoring Corrosivity in Marine Environments" Atmospheric Corrosion, W. H. Ailor, Ed., J. Wiley Interscience, N.Y. 183-192 (1982).

6. V.S. Agarwala, "Corrosion Monitoring of Shipboard Environments" in Degradation of Metals in the Atmposhere, ASTM STP 965, S.W. Dean and T.S. Lee, Eds., American Society for Testing and Materials, Philadelphia, PA, 1988, pp. 354-365.

7. P.J. Kennedy, M.J. Ruzansky and V.S. Agarwala, Corrosion, 45(2), 160-165 (1989).

8. P.J.Sereda, ASTM Special Technical Presentations on Corrosion in Natural Environments, 555, 239 (1974).

9. V.S.Agarwala, " Modification of Crack Tip Chemistry to Inhibit Corrosion" in Embrittlement by the Localized Crack Environment, R.P. Gangloff, Ed., AIME Publication, 1984, pp. 405-419.

DUAL MODE CORROSION MONITORS

Frank Ansuini, Technical Director

Electrochemical Devices, Inc.
PO Box 31, Albion, RI 02802
Telephone 401/333-6112

This paper describes a prototype dual mode corrosion monitor capable of measuring both instantaneous corrosion rate and the cumulative corrosion loss in atmospheric environments. The system consists of two components: a small flat sensor to be located in the area to be monitored and a battery powered meter unit to query the sensor. The sensor element is made of steel which is far more sensitive to atmospheric corrosion than most other metals; thus the sensor will react before significant damage has been done to other materials. The sensor itself is actually two discrete sensors on the same substrate and photo-etched from the same foil. Corrosion rate is measured using two-electrode Linear Polarization Resistance (LPR) while cumulative loss is measured by the Electrical Resistance (ER) method. The meter has been designed for operation by personnel with minimal corrosion knowledge. Its primary purpose is to alert an operator of the existence of corrosive conditions, thereby allowing remedial action to be taken before extensive corrosion damage has occurred.

INTRODUCTION

Two quantities are of interest in the field of corrosion monitoring: instantaneous corrosion rate occurring at the time of measurement and cumulative corrosion loss which has occurred over some extended time interval. Both types of measurements are needed to properly monitor corrosion. Rate measurements define the severity of a corrosion problem and are often the first indication of an abnormal situation. Loss measurements serve as a back-up for rate measurements by maintaining a record of the total amount of corrosion damage which has occurred.

Corrosion rate is frequently monitored by using the Linear Polarization Resistance (LPR) technique. An LPR sensor typically consists of three electrodes: a working electrode which is the metal of interest, a reference electrode whose potential remains constant throughout the test, and a counter electrode through which a biasing current flows to the working electrode. This bias current should be sufficient to cause the potential of the working electrode to shift a small amount, typically 10 mV, relative to the reference electrode. The ratio between the potential shift and the current required to cause it is termed the polarization resistance and is inversely proportional to the instantaneous corrosion rate.

A simplification of this method involves using only two electrodes, both made of the same metal. One remains the working electrode, the other combines the functions of the reference and counter electrodes. As with the three electrode method, the voltage/current ratio is inversely proportional to the instantaneous corrosion rate.

Cumulative corrosion loss is often determined by the Electrical Resistance (ER) method. The electrical resistance of a single electrode exposed to the environment is measured. As this electrode thins from corrosion, its resistance increases proportionately. Temperature variations in resistivity are compensated by providing a second electrode of the same material and initial resistance but shielded from the environment. The measurement circuit measures the increase in the resistance of the active electrode relative to that of the dummy electrode.

Most corrosion monitoring equipment will typically use only one of these techniques. If both rate and loss information is desired, it is necessary to install two separate monitoring systems. The cost of corrosion monitoring could be reduced if a single corrosion sensor could be designed which was capable of measuring both rate and loss. We had proposed that such a sensor could be made using the photo-fabrication process. The sensor itself is actually two discrete sensors on the same substrate and photo-etched from the same foil. The fact that all electrodes in the sensor originated from the same piece of metal greatly minimizes any errors resulting from individual electrodes having slightly different compositions or processing histories.

A dual mode sensor would prove particularly advantageous when used as corrosion detectors in nominally "dry" areas such as ordinance storage sites or electronic enclosures. In the ER (loss) mode, the sensor will record all corrosion which occurs including normal indoor atmospheric oxidation. In the LPR (rate) mode, the sensor will fully respond when the surface is wet, such as would occur if atmospheric moisture condensation has occurred, and will partially respond when the humidity is high enough to

permit electrochemical activity. The presence of a surface film of moisture can accelerate corrosion by orders of magnitude over that which would occur in the absence of the surface film. The practical implications of a sensor's ability to discern between condensing and non-condensing conditions is that it can be used to determine the integrity of hermetically sealed or otherwise intentionally dry environments.

Any reading from the sensor in the LPR mode would be indicative of high humidity or condensing conditions and therefore necessary corrective actions should be immediately initiated. High readings in the ER mode only would be indicative of prior, but not present, existence of corrosive conditions. This would also warrant investigation. It is conceivable that the ratio between the corrosion rates measured by the LPR and ER modes can be used to infer the amount of time the sensor surface was wet, but the relationship certainly will not be linear. There will also be a rough correlation between the corrosion rate of the metal used for the sensor element and that exhibited by other metals in the same environment. Such correlations are best determined empirically and in specific environments.

SENSOR DESIGN

Feasibility Tests - During a Phase 1 SBIR contract the feasibility of producing dual mode sensors was demonstrated [1]. Sensors made by etching a proprietary pattern into foils of zinc, aluminum, copper and steel were tested in an Accelerated Atmospheric Corrosion Test Chamber modeled after one described in the literature [2]. Weight loss panels concurrently exposed with the prototype sensors permitted direct comparisons to be made of the corrosion rates as determined by each of the specimen types. The results of this project, and a subsequent project involving copper nickel and steel sensors in synthetic seawater [3], showed that good agreement exists on corrosion data obtained by all three test methods.

One of the findings of the Phase 1 project was that sensors made of steel were significantly more sensitive than those made of the other metals tested. This suggested that steel element sensors could be adapted to serve as corrosion monitors in very benign environments. The output of the sensors, when used as corrosion detectors, must be considered qualitative in nature since only steel is being used as the sensing element. In order for the sensors to be quantitative, the sensing element obviously must be made of the same metal as the structure of interest.

Sensor Design Refinement - A major part of a follow-on Phase 2 SBIR contract was devoted to refining the design of the sensor to effect both an overall size reduction as well as optimizing details of the various features of the sensing trace. Working

patterns for each portion of the sensor were prepared so that they could be evaluated independently. A composite pattern combining the features of the preferred ER and LPR working patterns would be prepared as the final pattern.

Previous work on kinetics of atmospheric corrosion has shown that virtually all corrosion activity occurs during periods when the surface wet. For this reason, all optimization testing was conducted with sensors immersed in aerated distilled water. The corrosion rate of steel, as measured by weight loss panels, was about 5 mpy. ER specimens were designed to evaluate the effect of aspect ratio (trace width:trace thickness) on the response of the sensor. High aspect ratio specimens were preferable as they minimize error when using a simple data reduction model which presumes all metal loss occurs on the top surface. ER sensors consistently report higher corrosion losses than weight loss panels. This is normal as the data reduction model presumes a uniform loss of metal while in actuality the corroded surface is rough and irregular. The effect is that the measured resistance reflects and reports the lesser amount of metal remaining under the deeper gouges. In an extreme case, where the trace is virtually severed by a single corrosion pit, the ER method would report a loss equal to the trace thickness. In some cases, the enhanced sensitivity of the ER method would be advantageous.

Variables evaluated on the LPR sensor were trace width and gap width. Sensitivity is increased by reducing both dimensions as this reduces the effect of solution IR drop over the surface of a given electrode and between electrodes. In addition, fine geometry sensors have an actual exposed area which can be significantly higher than the apparent exposed area (footprint) due to contributions from the sidewall. Since the measured current is dependent, in part, on the exposed area, fine geometry sensors will give a stronger signal than a coarse geometry sensor of the same apparent area.

The redesigned corrosion sensor, shown in Figure 1, incorporates those features shown to be beneficial in earlier work. The electrical resistance trace (loss measurement) was designed with a high aspect ratio (9:1) to minimize sidewall effects. The linear polarization resistance sensor (rate measurement) was designed with narrow electrodes (6 mil) separated by narrow gaps (3 mil). The sensor, photoetched from 1 mil steel foil, consists of two discrete patterns. The main pattern contains the LPR trace and the ER, active trace while the back pattern contains the ER, dummy trace. The main pattern is partially masked during final lamination so only the active portions of the trace are exposed; the back pattern is completely masked. Double sided adhesive tape is applied to the underside for attaching the sensor to a surface. The patterns terminate in six contact pads to which a ribbon cable is soldered.

ELECTRONICS DESIGN

Corrosion Rate Circuit - The corrosion rate circuit (Figure 2) is essentially a mini-potentiostat. It supplies whatever current is necessary, within the limits of the components, to keep the signal electrode at a preset bias voltage referenced to common. Since the other electrode is at common, the bias voltage is, in effect, applied between the electrodes. A 20 mV bias voltage is preset at trimmer VR4; this is within the range of bias potentials for which the resultant current flow bears a linear relationship to instantaneous corrosion rate. Higher bias voltages can be used, but in these cases the resultant current flow will be proportional to the conductivity of the electrolyte covering the sensor rather than the sensor's corrosion rate.

An operational amplifier (U7), set up as a current to voltage converter, supplies current to keep the LPR electrodes at the preset bias voltage. A voltage proportional to this current is generated across R6. An instrument amplifier (U8) re-references this signal to common, backing out the bias voltage. The display driver (U4) has a logarithmic scale so that the total response range of the display is just under two orders of magnitude. LED Bar Graphs operating in the dot mode were selected as the display in order to provide for a display which is easily absorbed and interpreted by operating personnel without extensive training in corrosion. It provides data with only one significant digit of accuracy; for monitoring purposes, this is usually adequate. If more precise data is required, the actual applied bias voltage and the resulting current flow can be measured at test points on the circuit board.

Corrosion Loss Circuit - The corrosion loss circuit (Figure 3) is a standard resistance bridge of the type used to query resistance based transducers. Since the resistance of each sensor trace is also affected by temperature, the circuit has been set up to measure the difference in resistance between the traces, thus removing the temperature effect. The active and dummy resistance traces form two legs of the bridge, a pair of resistors on the circuit board, R5, form the other two legs. On a new sensor, when the resistance of the active trace equals that of the dummy trace, the voltage drop across both traces would be equal. As the resistance of the active trace increases due to thinning from corrosion, the voltage drop across the two sensor traces becomes unequal. An instrument amplifier (U9) senses this inequality and responds with an amplified signal proportional to it.

Linear display drivers (U5 and U6) activate an LED on the bar graph array which is proportional to the resistance increase of the active trace and hence the loss of thickness of this trace due to corrosion. A cumulative corrosion loss on the sensor of

about a quarter mil will cause an LED dot in the middle of the range to light. When this level of loss is reported, it is safe to assume that serious corrosion damage has likely occurred to sensitive parts in the same environment. These parts should be inspected and a new sensor installed after the inspection.

Electronics Operation - The meter is shown in Figure 4. To query the sensor, the sensor cable is first plugged into the meter. Battery level is checked by pushing the black button, if the batteries are fine, a green LED will light in the hole marked "OK". If no light shows, the batteries are weak and should be replaced. Corrosion rate on the sensor is checked by pushing and holding the toggle switch down. It should be held about 30 seconds for an accurate reading. The upper bars will light if the sensor surface is partially or fully wetted. The middle bars will light if the humidity level near the sensor is high enough to be of concern. The lower bars will light if the atmosphere is not overly corrosive. Cumulative loss is checked by pushing and holding the toggle switch upward. Each succeeding higher bar corresponds to a thickness loss of about 0.025 mils (0.000025") of steel lost from the sensor surface.

SYSTEM RESPONSE

Meter Correlation - The rate part of the meter was correlated by replacing the sensor with a variable resistor. A 20 mV bias voltage was placed across the resistor and the resistance varied to determine the LED shift points. The current at these shift points was treated as a measured current from a sensor which was converted to corrosion rate. The following values were used for the constants:

Electrochemical Equivalent: EE = 27.92 (Based on iron going to the double valence oxidation state.)

Polarization Constant: B = 25 mV (An estimate; for a rigorous conversion, this should be experimentally determined.)

Density: 7.86 gm/cc (Handbook value.)

Units Conversion Constant: K = 0.1288 (For adjusting the units from uA/sq.cm. to mpy)

Area: A = .884 sq.cm. (Calc. from sensor dimensions)

Applied Bias Voltage: Vb = 20 mV

The results of these calculations are shown in Figure 5. On the meter label, the following terms were arbitrarily assigned to steel corrosion rates: High - 4 mpy, Moderate - 1.5 mpy, Low - 0.5 mpy.

Sensor Response - Polarization Resistance is defined as the slope of the potential/current density curve in the vicinity of the free corrosion potential. In the following discussion, the term is used to refer to the slope of a potential/current curve, i.e. an adjustment was not made for the area of the sensor. Since all the sensors were identical, this mathematical short-cut will not have any effect on results where relative corrosion rates are compared. The area of the sensor must be taken into account when the data is converted to an absolute corrosion rate.

Sensors were tested at several bias levels and in solutions with various conductivities (distilled, tap and salt waters). Bias voltages ranged from 0 to 100 mV and it took about a minute after application of the voltage for the current to stabilize. The sensor has a direct linear response with the applied bias voltage, Vb, and an inverse linear response with the logarithm of the electrolyte resistivity. This is in line with the expected behavior of these types of sensors.

Ultimately, the quantity being measured is the corrosion rate which varies inversely as the polarization resistance, Rp, which is defined as dE/dI, i.e. CR = K(1/Rp) where K is a constant accounting for the sensor material and exposed area. Since one of the two bias voltages used was zero, dE = E so Rp = E/dI. The problem comes with response current; the two electrodes may spontaneously develop a small bias between them due to local inhomogenieties in the metal. Therefore, E = 0 is actually an applied bias and hence there could be a response current. To precisely calculate Rp, one should use dI (I @ Vb - I @ 0). However, this would increase the complexity of the circuitry by requiring either a microprocessor or alternate means to store the first reading. Since a goal of this project is to keep the electronics simple, we determined the difference in measured rates which would occur if the erroneous assumption was made that I = 0 at E = 0 so Rp = E/I. It turns out that this creates an error at low bias voltages which decreases as Vb increases.

Figure 6 shows the log of the inverse polarization resistance at several bias voltages calculated by both methods. Two things are apparent on examining this figure. First, for applied bias voltages greater than 20 mV, the difference in measured rates between the two modes of data reduction becomes minimal; it is about the same magnitude as the inter-sensor variation. Second, the error has the effect of reporting a slightly higher corrosion rate (inverse polarization resistance) which is preferable to understating the rate. It appears,therefore, that a functional monitoring unit can be made by setting Vb = 20 mV.

Further verification of the single point technique of doing linear polarization measurements as versus the conventional two

point technique was obtained in another experiment. During each measurement event, the polarization resistance was calculated by the two point method at +/- 10 mV. Figure 7 shows the value of 1/Rp plotted against current measured by the single point method for the same reading. The data lie in close to a straight line with a slope of close to one (0.93). Regression analysis shows the correlation coefficient to be 0.975 (1.0 means perfect correlation). These data demonstrate that the single point technique, as used in the dual mode sensor electronic meter, can provide corrosion rate data for monitoring purposes equivalent to that obtained with more sophisticated instruments using two point techniques. The range of rates measured in this test was approximately six orders of magnitude and span the range likely to be encountered in service.

FUTURE WORK

Based on the work to date, several areas for modifications and improvements to both the sensor and the meter have been identified. Designs exist for a single layer sensor which will allow further size and cost reductions. The meter display is being converted to LCD to reduce power consumption and permit continuous monitoring. Alarm circuits, provision for line power and the ability to export data to a logger will also be added.

Mixed-gas environmental chambers are increasingly used to simulate indoor corrosion. To date, much of the work done in these chambers has involved exposure of fabricated parts (connectors, contacts, etc.) which were tested before and after exposure to the chamber. A direct and quantitative comparison of the effects of various atmospheric gas mixes on the corrosion behavior of common metals can now be obtained through the use of these new sensors. Sensors manufactured in each of the metals of interest can be concurrently exposed in a mixed gas chamber and the corrosion rate continuously logged.

REFERENCES

[1] "Feasibility of Producing Low Cost Atmospheric Corrosion Sensors"; F. J. Ansuini and R. E. Howe; Final Report under U. S. Air Force Contract No. F33615-83-C-5104; June, 1984.

[2] "An Accelerated Atmospheric Corrosion Test (AACT)"; R. D. Smith; ASTM STP 646; June, 1978.

[3] "Low Cost Seawater Corrosion Sensors"; F. Ansuini; Final Report to NSWC, Contract N60921-85-C-0015; October, 1985.

[4] "Optimization of Sensor Geometry"; F. Ansuini; Int. Report, to AFWAL/MLSA, Contract No. F33615-85-C-5069; December, 1986.

Figure 1

View of corrosion sensor (Approx 1.5X)

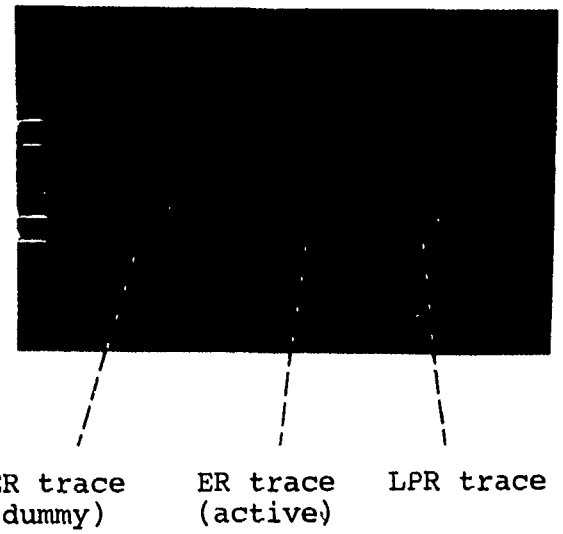

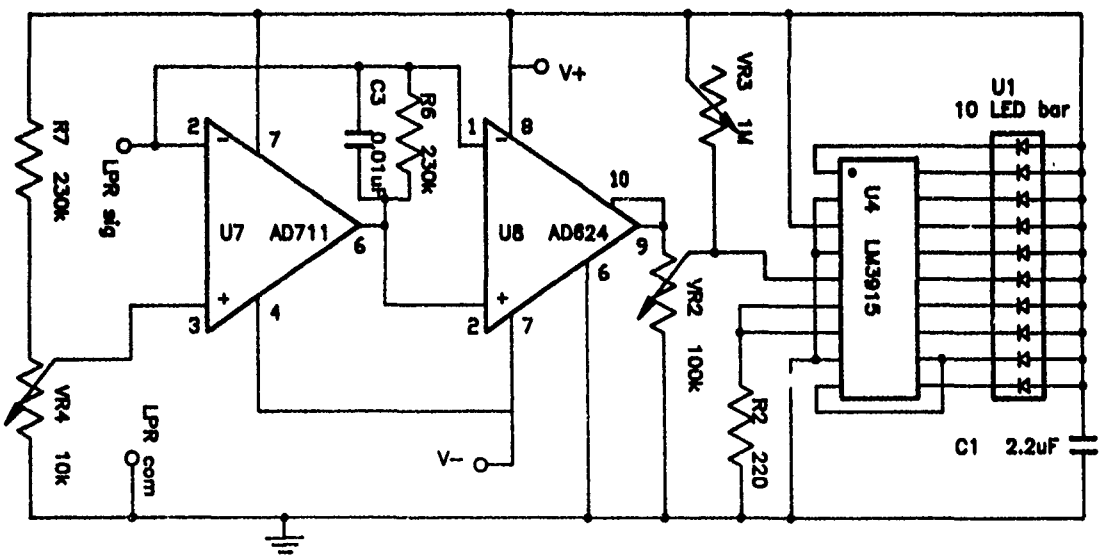

Figure 2 Linear Polarization Resistance Sensor (Instantaneous Corrosion Rate) Measurement and Display Circuit

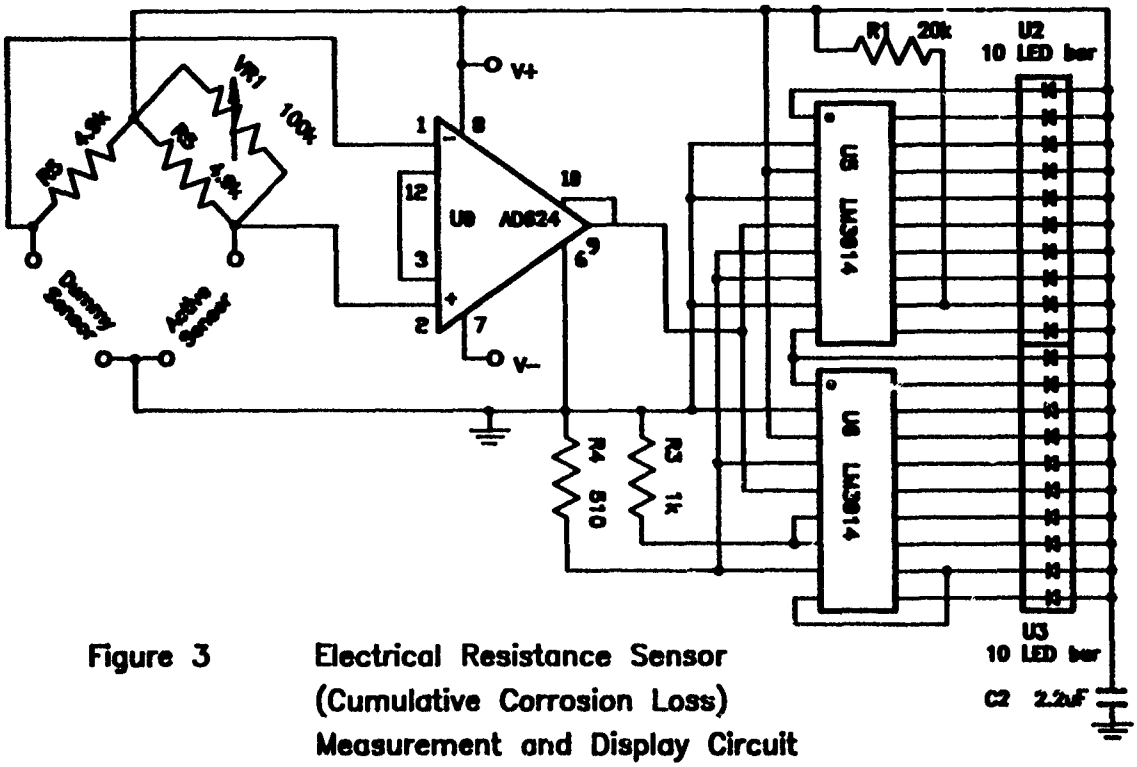

Figure 3 Electrical Resistance Sensor (Cumulative Corrosion Loss) Measurement and Display Circuit

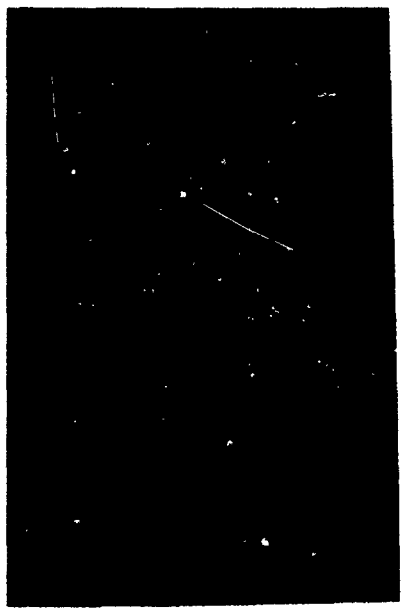

Figure 4

View of Dual Mode meter
(Approx 0.4X)

Figure 5

Correlation between corrosion rate and meter display.

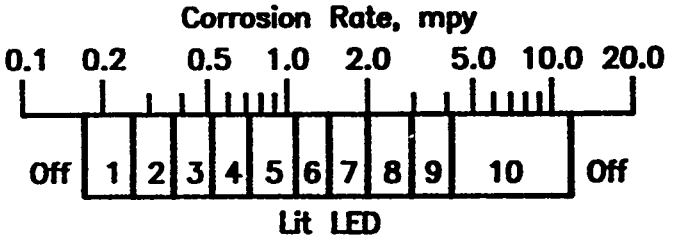

Figure 6

Sensor response in distilled, tap and salt water at various applied bias levels. The effect of both data reduction models is shown (see text).

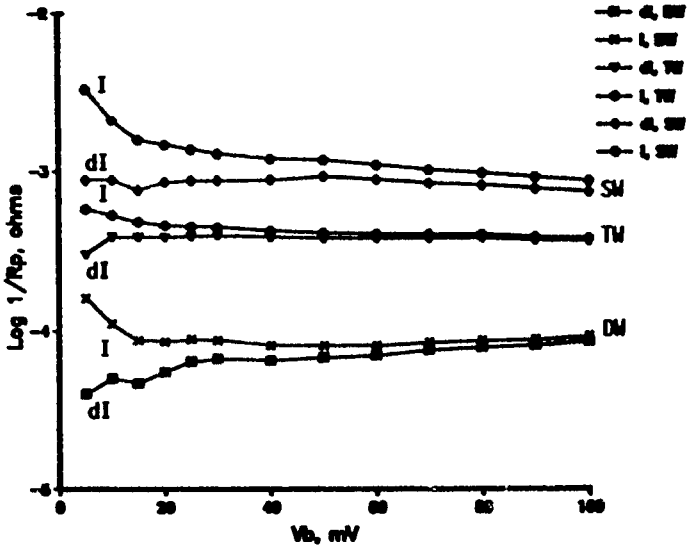

Figure 7

Correlation between 1/Rp as determined by the two-point method and the measured current (single-point method).

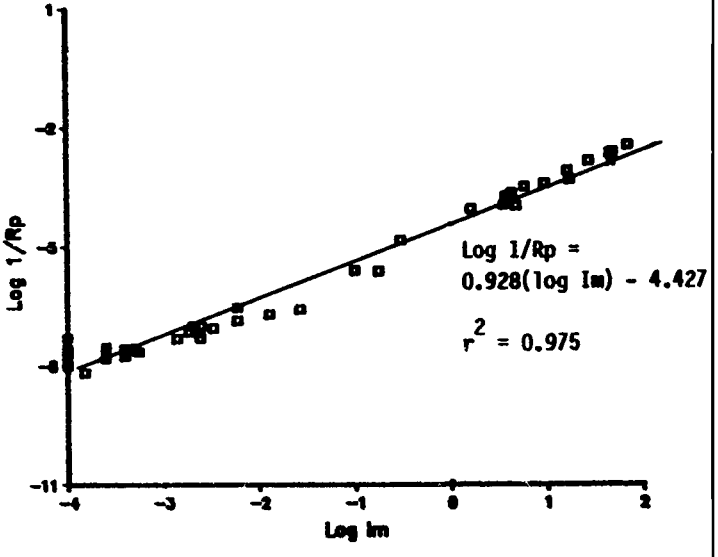

MONITORING CORROSION WITH AN AUTOMATED ELECTRICAL RESISTANCE CORROSION PROBE MONITORING SYSTEM

John T. Stropki, Gerhardus H. Koch, and Mark T. Byrne
Battelle
505 King Avenue
Columbus, Ohio 43201

ABSTRACT

The ability to automatically detect and/or monitor the corrosion of structural components, located within difficult-to-access areas on aging military aircraft and equipment, could contribute to a significant reduction in the annual depot maintenance expenditures of the United States Air Logistic Command Centers. Reductions in the frequency of PDM overhauls, corrosion inspections, and unanticipated structural rework/repairs could be achieved if a system were available to accurately monitor the corrosion of components within these areas.

During the past several years, Battelle engineers have concentrated on improving the electrical resistance (ER) corrosion probe monitoring system. The results of these efforts have confirmed that the ER system is capable of accurately measuring the (1) level of corrosivity, and (2) relative magnitude of corrosion attack on structural components located within the difficult-to-access areas of fixed and rotary winged aircraft systems. The most recent development of an automated data acquisition/logging system, which electronically interfaces with the ER corrosion probe, represents a further step in optimizing the operational reliability and efficiency of the system.

INTRODUCTION

Substantial expenditures of manpower and money are disbursed annually by the United States Air Force for the inspection and subsequent repair of corrosion which occurs on airframe components that are located in difficult-to-access areas on both fixed and rotary-winged military aircraft systems. Quite often, these areas contain crevices, grooves, pockets, and/or sharp corners which tend to entrap and accumulate moisture and organic/inorganic contaminants. Increases in the concentration of these contaminants, in combination with the extreme atmospheric conditions (i.e., humidity and elevated temperatures) that are characteristic to some geographic locations, will contribute to an appreciable decrease in a components inherent corrosion resistance, increasing the frequency and magnitude of pitting and/or intergranular corrosion attack which occurs on the "exposed" surfaces of the components. If this condition remains undetected, which is normally the case in many of these difficult-to-

access areas, the component and/or surrounding system will prematurely fail as a result of corrosion. Any ability to automatically detect the initiation, and monitor the growth of the corrosion attack within these areas, would certainly reduce the level of effort and funds expended to inspect and repair/replace the components that have corroded.

Additional reductions in aircraft maintenance expenditures would also be realized if the costs associated with performing routine corrosion related inspections were minimized. Specifically, extensive amounts of time and effort are required to disassemble, remove and reassemble airframe structures and/or systems which surround many difficult-to-access areas. These procedures, as well as the actual inspections are quite costly if the magnitude of corrosion attack in these areas is minimal at one inspection interval, and extensive at another. This inability to conclusively quantify the degree of corrosion-related damage on the airframe components in the difficult-to-access areas, without performing the time consuming visual inspections, necessitates the need to develop a reliable, inexpensive corrosion probe monitoring system.

BACKGROUND

Battelle-Columbus has used a commercially available Corrosometer®/CK-3® corrosion probe monitoring system during several USAF/WR-ALC sponsored research programs to monitor the corrosion of airframe components located in difficult-to-access areas on two C-141 transport aircraft.[1,2,3] As expected, the results from each of the programs confirmed that the electrical resistance (ER) measurement technique represents a feasible method of monitoring the (1) environmental corrosivity, and (2) relative level of corrosion developing on airframe structures located within these areas. However, from these programs, it was determined that there were inherent problems associated with the design and operation of this particular system. Specifically, the manual operation of the data logger and limited sensitivity of the corrosion probes restricted the performance quality and/or operational efficiency of this system.

In response to the limitations associated with the Corrosometer/CK-3 system, Battelle was contracted by the USAF/WR-ALC to design, and fabricate an improved or automated version of the ER corrosion monitoring system. Such a system was developed, and comparatively tested against the manually-operated Corrosometer/CK-3 system in a series of three environmentally controlled laboratory experiments. The results acquired from each of these test exposures confirmed that the system was capable of automatically detecting and monitoring the relative rates of corrosion attack occurring on both uncoated and coated test elements of commercially available ER corrosion probes.

In addition to laboratory experimentation, a prototype version of the automated ER corrosion probe monitoring system was instrumented on a USAF H-53 helicopter. At the time of installation, this aircraft was undergoing extensive rework during a scheduled PDM interval at the PNARF facility in Pensacola, Florida.

MONITORING SYSTEM

Corrosion Probes

In principle, the electrical resistance (ER) method of corrosion detection operates on the fundamental principle that the electrical resistance of a metallic conductor increases as its cross-sectional area decreases. Therefore, the backbone of any ER monitoring system is an electrical resistance corrosion probe.

The ER corrosion probes used by Battelle in all field and laboratory exposure tests were manufactured by Rohrback Cosasco Systems. Each probe was thin (approx. 0.125 inch) and composed of two 0.009 inch thick 7075-T6 Al elements. Approximate dimensions of a typical ER corrosion probe are documented in Figure 1. As shown, one of the elements on the probe is protectively sealed in a glass coating. This element is referred to as the **reference** element, whereas, the second element, which is uncoated, is considered the **test** element. Since both elements are identical in size, shape, and composition when the probes are manufactured, the nominal resistances of the two elements are assumed to be identical.

Exposure to a suspected corrosive environment causes the test element of a standard ER corrosion probe to corrode. Subsequently, the resistance of this element increases. The resistance of the reference element remains constant throughout the duration of the service exposure. Continuous and/or intermittent monitoring of the change in resistances, measured as a ratio of the resistances between the two elements, gives an indication of the inherent corrosivity of the environment and magnitude of corrosion attack occurring on the surfaces being monitored.

Data Logger/Acquisition System

Many of the measurement systems which are available for monitoring the ratio of resistances between two elements on a ER corrosion probe make use of a manually-balanced resistance bridge. In numerous studies,[4,5,6] this technique has been an effective method of measuring the minute resistance changes that are inherent to a corroding probe. However, many of the portable data logger/acquisition systems which are available for acquiring and storing these probe measurements are manually operated. This mode of operation is suspected of reducing the operational reliability and overall efficiency of the system.

Battelle improved the efficiency and reliability of the ER corrosion monitoring system by designing and fabricating an automated data logger/acquisition system. This system, which is interfaced with multiple ER corrosion probes, is small, programmable and inexpensive to operate and maintain. During "active" monitoring, the system automatically controls, acquires and stores all response

signals which are emitted from a maximum of ten ER corrosion probes. Actual data manipulation and/or corrosion rate calculations, for the individual probes, are processed within the data logger or via an IBM-PC computer system.

The following textual summary serves to define the basic operation of a "prototype version" of the automated data logger/acquisition system. The block diagram in Figure 2 serves to illustrate the placement of the various subsystems within the laboratory prototype that is currently instrumented onboard an H-53 helicopter.

Operation

By design, the automated system has three separate operating modes: dormant, warm-up, and data acquisition. Most of the time, the system will be dormant, drawing approximately 100 μA from the available power source. At pre-programmed time intervals, the system will power up for a one hour "warm-up" period. During this period, all subsystems, except the current source will draw power. The expected current drain during this period will be 50-100 mA. At the end of the warm-up cycle, the current source turns on, and the (1) Squirrel*, and (2) Tattletale** systems begin logging data from each of the corrosion probes. For this mode, an additional 100 mA of current is required. Following data acquisition, the system turns off until the next scheduled power up cycle. As a result of these three discrete operating modes, the effective battery drain is minimized, thus, extending the operational service life of the system. In most instances, it is assumed that there will be only one "active" power-up cycle per 24 hour period. Additional cycles are possible, however, increasing the number of cycles will substantially reduce the effective service life of the system's power supply.

---

* The Squirrel® data logger is being used as a back-up acquisition system in the prototype version of the monitoring system. The replacement of this data logger with the Tattletale computer is imperative, because of size, weight and cost reduction requirements.

** The Tattletale® Model IV single board computer was selected to serve as a controller and primary data logger for the monitoring system. As packaged, this inexpensive unit features a BASIC language interpreter for easy programming, an onboard 10-bit A/D converter, 16 programmable digital I/O lines, small (2.25 X 3.75 inches) size, and a low (2-15 mA) power operating mode. A typical unit is capable of being programmed to control the (1) zero calibration, (2) power supply, and (3) current source circuits that are incorporated into a standard monitoring system. In addition, each unit is capable of storing data onto a 32K x 8 RAM chip. A single 512K datafile expansion board has been installed as a complement to the memory storage that is standard for the basic unit.

EXPERIMENTAL PROCEDURES

In earlier experimental programs[1,2,3], the feasibility of monitoring the (1) level of environmental corrosivity, and (2) relative magnitude of airframe corrosion attack, was determined by characterizing the performance of the ER corrosion probe monitoring system as a function of exposure to several difficult-to-access areas on USAF transport aircraft. Conversely, the performance of the automated ER corrosion probe monitoring system was evaluated in both the laboratory and the field environments.

Laboratory Environment

Three standard accelerated corrosion tests were performed in the laboratory to comparatively evaluate the operational performance of the (1) manual Corrosometer/CK-3 monitoring system, and (2) automated ER corrosion probe monitoring system. An abbreviated description of the testing protocol for each of these tests, as well as a listing of the number and types of ER corrosion probes exposed within each test is summarized in Table 1. As tested, all corrosion probes were positioned at approximately 30 degrees from vertical in the salt fog test chamber.

Measurements from the individual corrosion probes, using both the manual and automated systems, were recorded three times a day throughout the duration of the scheduled exposure period. Individual corrosion rate profiles were generated directly from these measurements, along with temperature profiles that were produced from the temperature data recorded for inside and outside the salt fog chamber. Collectively, these individual profiles were used to characterize the sensitivity, accuracy and reliability of the response data acquired from each of the monitoring systems.

Post-test optical microscopy and metallographic cross-sectional analysis techniques were used to characterize, as well as quantify the corrosion attack which was noted on both the test and reference elements of the individual corrosion probes. Also included in the analyses was an assessment of the level of protection afforded by each of the coating systems that were applied to each of the tested probes.

Aircraft Environment

The "in-service" performance quality of a prototype version of the automated ER corrosion monitoring system was to be determined after 15 months of exposure onboard a single H-53 helicopter (S/N 69-5784). This particular aircraft was selected by the Air Force because of the following:

- It was undergoing major depot maintenance at the Pensacola Naval Air Rework Facility (PNARF) in Pensacola, Fl.

TABLE 1. SUMMARY OF ACCELERATED CORROSION TESTS USED TO CHARACTERIZE THE PERFORMANCE QUALITY OF ER CORROSION MONITORING SYSTEMS

	Test Method	Test Mode	Test Duration	Test Solution	pH	Solution Temperature	Probes
Test 1	ASTM B117	Continuous	500 hrs.	5% NaCl	6 - 6.5	98 F +/- 2 F	1 chromate conversion coated (MIL-C-5541) 2 chromate conversion coated, primed (MIL-P-23377) 1 chromated, primed, and topcoated (MIL-C-83286)
Test 1	ASTM B117	Cyclic	500 hrs.	5% NaCl	6 - 6.5	98 F +/- 2 F	1 chromate conversion coated (MIL-C-5541) 2 chromate conversion coated, primed (MIL-P-23377) 1 chromated, primed, and topcoated (MIL-C-83286)
Test 3	ASTM B368	Continuous	500 hrs.	5% NaCl, $CuCl_2$, CH_3CO_2H	3.1 - 3.2	115 F +/- 3 F	2 chromate conversion coated (MIL-C-5541) 3 chromated, primed (MIL-P-23377) 3 chromated, primed and topcoated (MIL-C-83286)

- It was to be commissioned to a seacoast installation where the corrosivity index will be higher than most inland installations.

- It contained several corrosion prone areas or "hot spots", which are difficult to access during routine inspection intervals.

In addition, the corrosion probes and monitoring system would be subjected to the adverse operating conditions (i.e., vibration, shock and salt water contamination) which are characteristic to many rotary winged aircraft.

A total of four ER corrosion probes, three temperature thermistors and one data logger/acquisition system were instrumented on the H-53 helicopter. Figures 3a and 3b serve to document the placement of two corrosion probes (one chromated only and one chromated/primed/topcoated) and one thermistor on the internal surfaces of the structural skins (F.S. 320 - W.L. 90) of the RH sponson tank. A second set of two probes (one chromated and one chromated/primed) and one thermistor were mounted to the internal surfaces of fuselage panels which are located beneath the center floor section of the aircraft. Figures 4a and 4b document the location (i.e., F.S. 520 - W.L. 87), as well as orientation and placement of the probes within this section of the aircraft. As shown in Figure 4a, this area is adjacent to the hinged section of a cargo ramp, which entraps a significant amount of moisture (i.e., seawater and condensate) during normal service. A review of the maintenance records for this aircraft indicated that the airframe structures in this latter area and the area beneath the fuel bladder (RH sponson tank) incur appreciable amounts of corrosion attack after limited service exposures.

The orientation and placement of the data acquisition system and/or cabinet within the cabin section (i.e., F.S. 422-442 and W.L. 140) is detailed in Figure 5. As shown, the hermetically sealed cabinet was securely mounted to a pair of stabilizer webs which were riveted to both the fuselage panel and two support stringers. The electrical connector (probe and thermistor) ports are located at the bottom of the cabinet.

RESULTS AND DISCUSSION

Laboratory Environment

All corrosion probe measurements that were recorded by the two monitoring systems, during each of the three accelerated laboratory tests, are graphically summarized in Figures 6 to 8. As presented, the measurements are plotted as a function of exposure time.

A review of the data summarized within each of the summary plots yields several obvious conclusions. Specifically, the monitoring systems confirmed that the test elements on the chromated (MIL-C-5541) corrosion probes, exposed to Tests 1 and 3 (Figures 6 and 8), incurred significant corrosion attack. As

shown in Figure 6a, the single probe tested in the ASTM B117 test environment began to detect corrosion attack after 250 hours of continuous exposure. The photomicrographs in Figures 9a and 9b serve to illustrate the level of pitting and/or intergranular corrosion attack, which was confined within two separate metallographically cross-sectioned areas on the test element of this probe. As shown, the upper and lower surfaces of the element had incurred corrosion attack after the scheduled exposure period. By comparison, both of the "chromated-only" probes tested in the ASTM B368 test (i.e., Test No. 3) detected the onset of corrosion after only 30 hours of exposure. These probes were removed from the test chamber after 200 hours of exposure, and metallographically cross-sectioned. Figures 10 and 11 serve to document the level of attack to both test elements from these probes.

The data recorded for the chromated probe, which was exposed to the corrosive environment of Test No. 2, indicates that the test element on this probe did not corrode during the scheduled 500 hour test exposure. The suspected reason for this observance is related to the cyclic nature of the test exposure. Specifically, the dryout period that was included in each 1-hour test cycle caused all corrosion products and/or films which formed on the surface of the probes element to dry. This intermittent drying served to retard both the initiation and growth of corrosion attack on this probe's test element, as well as the test elements for the balance of the probes (i.e., primed and primed/topcoated) that were exposed to this particular corrosion test.

The data scatter measured by the automated monitoring system, during Tests 1 and 2 for the 0-100 hour measurement interval, was related to (1) temperature fluctuations within the test chambers, and (2) externally induced electrical noise generated by various electronic test instruments. Specifically, several strip-chart recorders, in-line filters, and electrometers were connected, disconnected and reconnected to the interface circuits during this particular time period. The measurements made using this equipment served to calibrate the monitoring system, and also adjust its measurement sensitivity as a function of environmental variability.

The response measurements recorded for the coated (i.e., chromated/primed and/or chromated/primed/topcoated) probes that were exposed to the two ASTM B117 tests (i.e., Tests 1 and 2) suggest that the test elements on these probes had incurred a minimal amount (i.e., 0.05 mpy) of corrosion attack. This result was confirmed by both corrosion probe monitoring systems and the post-test examinations (visual and microscopic) that were performed on the individual probes. Conversely, there were areas of localized pitting and/or intergranular corrosion attack detected on the coated elements of several corrosion probes that were exposed to the ASTM B368 corrosion test. The results attained from this latter test were expected when considering the aggressiveness of the test solution.

Aircraft Environment

To date, no corrosion probe data has been retrieved from the automated ER monitoring system that was installed on the H-53 helicopter selected to

participate in this program. The reasons for this limitation are related to the fact that at this time the aircraft has not yet been commissioned to "active" flight status.

CONCLUSIONS

The results from the laboratory testing that was conducted on the two ER corrosion probe monitoring systems confirm that the automated system is capable of automatically monitoring the corrosivity of an environment, as well as detecting corrosion attack. Actual response data recorded using this system were statistically similar to the data recorded by the manually-operated Corrosometer/CK-3 monitoring system. The data suggests that the automated system is sensitive to moderate temperature and time-of-wetness fluctuations, which are inherent to highly corrosive environments. The scheduled installations of several prototype versions of the monitoring system into "flight-active" aircraft systems will verify the systems operational performance accuracy and reliability.

REFERENCES

(1) Stropki, J.T., Byrne, M.T., Woodruff, K.R., "Evaluating and Modifying Techniques for Detecting Corrosion in Inaccessible Areas on Military Equipment", WR-ALC Contract No. F-09603-86-R-1033, October 1988.

(2) Stropki, J.T., and Koch, G.H., "Investigation of Metal Probes or Metal Strips to Detect Corrosion in Difficult-to-Access Regions", WR-ALC Contract No. F-09603-83-G-1271-0003, October 1986.

(3) Koch, G.H., Diegle, R.B., and Berry, W.E., "Monitoring Corrosion on C-141 Cargo Planes", WR-ALC Contract No. F09603-80-G-0420, June 1982.

(4) Bergstrom, D.R., "Case Histories - Electrical Resistance Probes Control Corrosion in Chemical Industry", Materials Performance, Vol. 20, No. 9, (1981), pp. 17-20.

(5) Freeman, A.J., and Dravnieks, A., Corrosion Vol. 14 (1958) p 175.

(6) Dept. of Industry, "Industrial Corrosion Monitoring", HMSO, UK (1978).

ACKNOWLEDGEMENTS

The authors express appreciation to the technical personnel at HQ-MAC, WR-ALC/MMEA and PNARF, for their assistance in coordinating and monitoring all programs related to the development of the automated ER corrosion probe monitoring system.

FIGURE 1. PHOTOGRAPH OF CORROSOMETER® ELECTRICAL RESISTANCE (ER) CORROSION PROBE

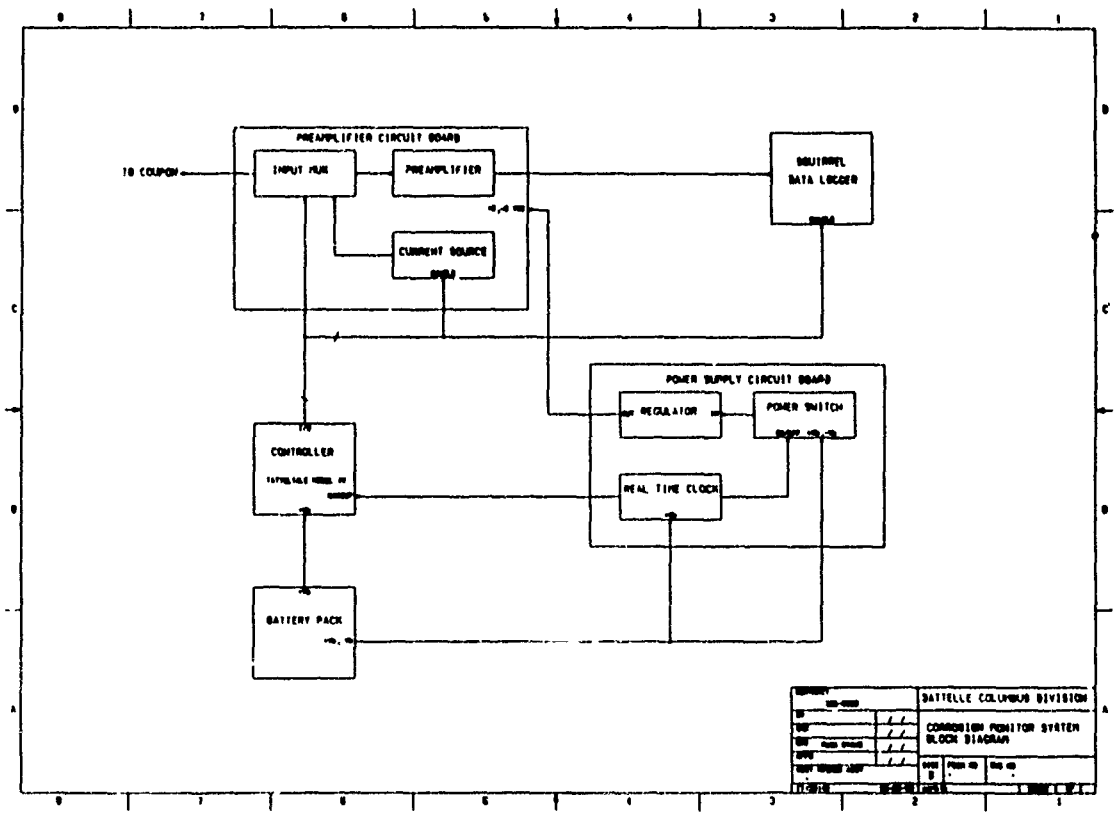

FIGURE 2. FUNCTIONAL BLOCK DIAGRAM OF ELECTRONIC DATA LOGGER/ACQUISITION INSTRUMENT USED BY AUTOMATED CORROSION PROBE MONITORING SYSTEM

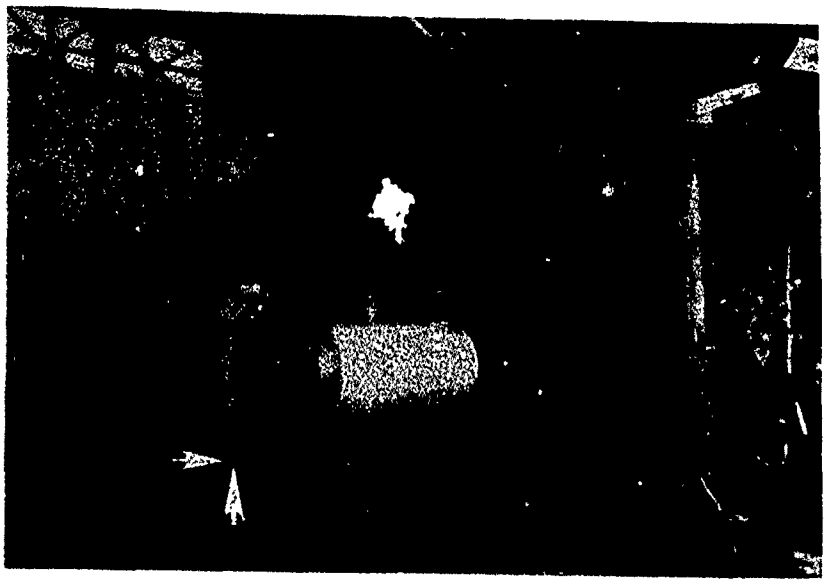

(a) R.H. Sponson Tank (Arrows Indicate Placement of Corrosion Probes)

(b) Coated and Uncoated ER Corrosion Probes

FIGURE 3. PHOTOGRAPHS DOCUMENTING PLACEMENT AND ORIENTATION OF ER CORROSION PROBES WITHIN THE R.H. SPONSON TANK OF AN H-53 HELICOPTER (S/N 69-5784)

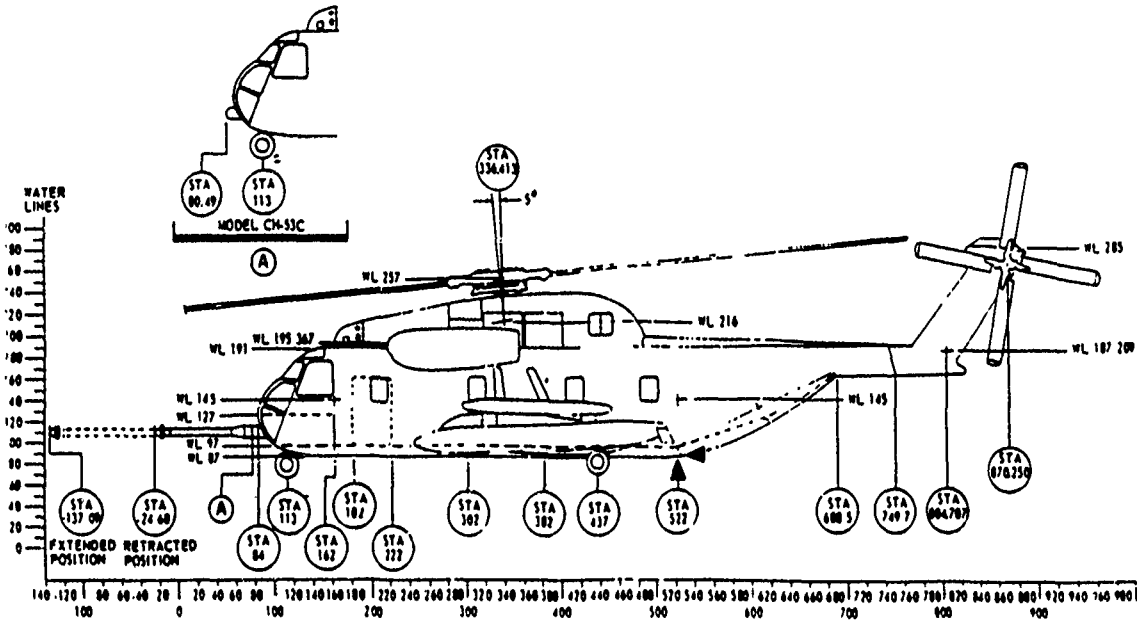

(a) Schematic Diagram of H-53 Helicopter (Arrows Indicate Location of ER Corrosion Probes)

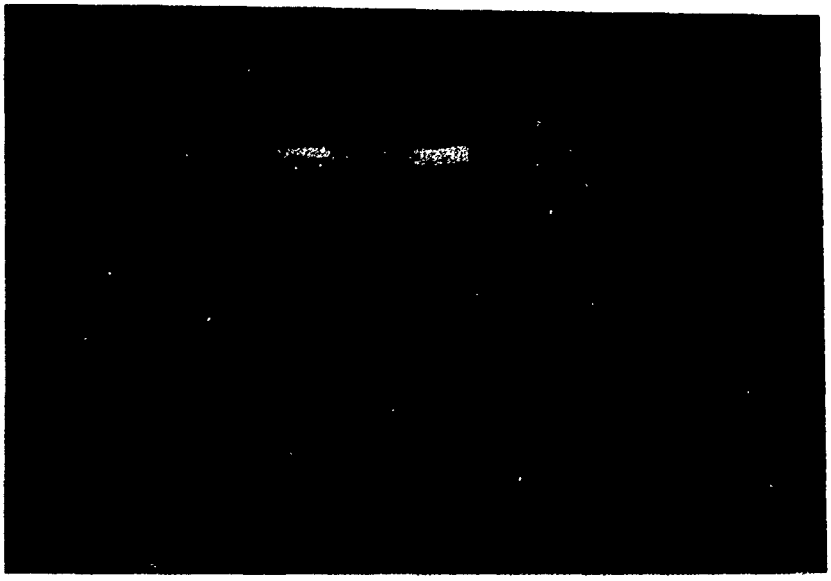

(b) Coated and Uncoated ER Corrosion Probes

FIGURE 4. PHOTOGRAPHS DOCUMENTING PLACEMENT AND ORIENTATION OF ER CORROSION PROBES WITHIN THE LOWER FUSELAGE SECTION OF H-53 HELICOPTER (S/N 69-5784)

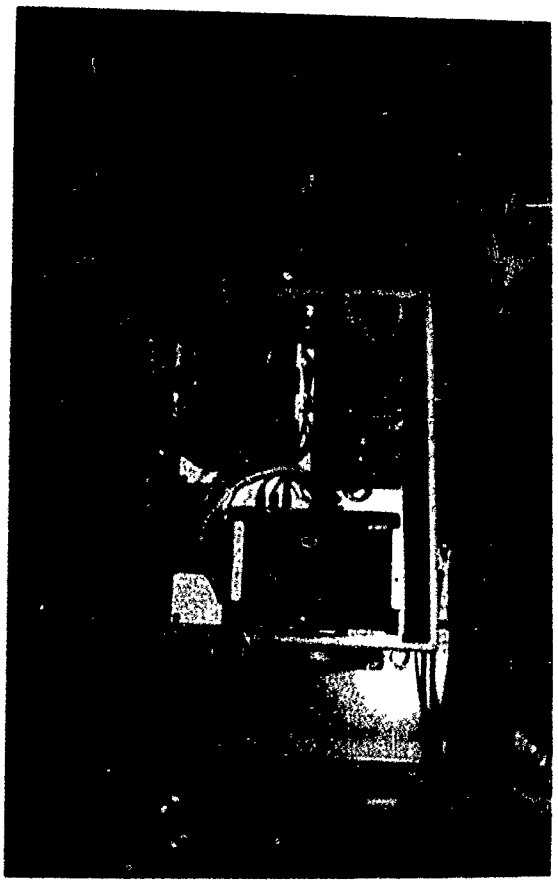

FIGURE 5. PHOTOGRAPH DOCUMENTING ORIENTATION AND LOCATION OF DATA ACQUISITION SYSTEM WITHIN CABIN AREA OF H-53 HELICOPTER

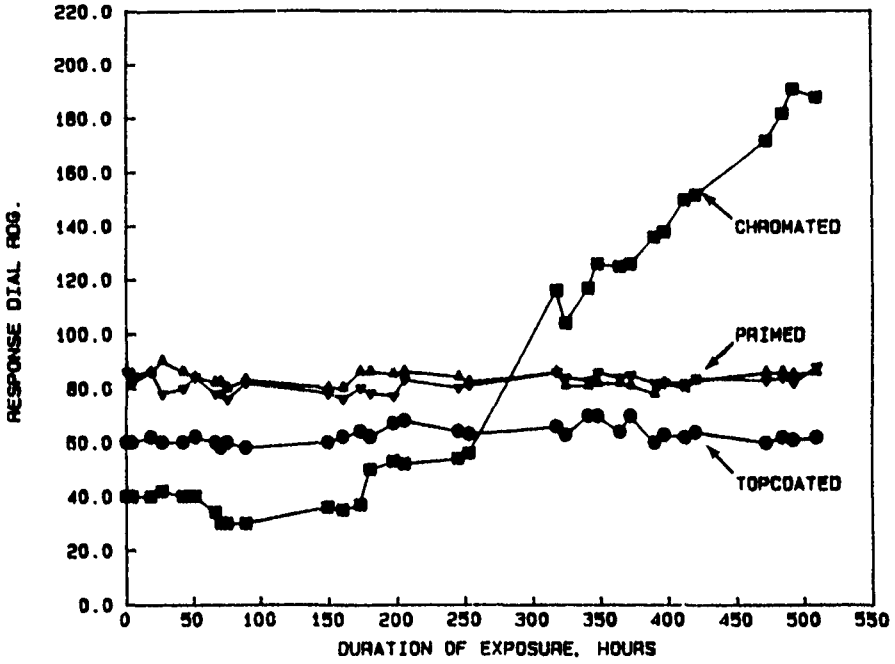

(a) Manual Corrosion Monitoring System

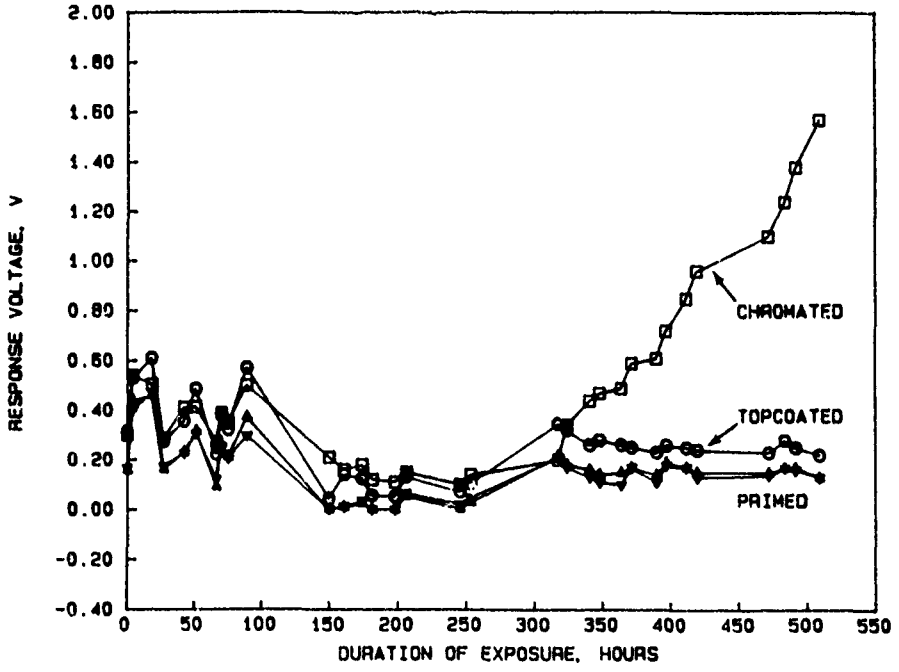

(b) Automated Corrosion Monitoring System

FIGURE 6. GRAPHICAL SUMMARIES OF CORROSION PROBE RESPONSE DATA RECORDED BY MANUAL AND AUTOMATED ER CORROSION MONITORING SYSTEMS DURING TEST NO. 1

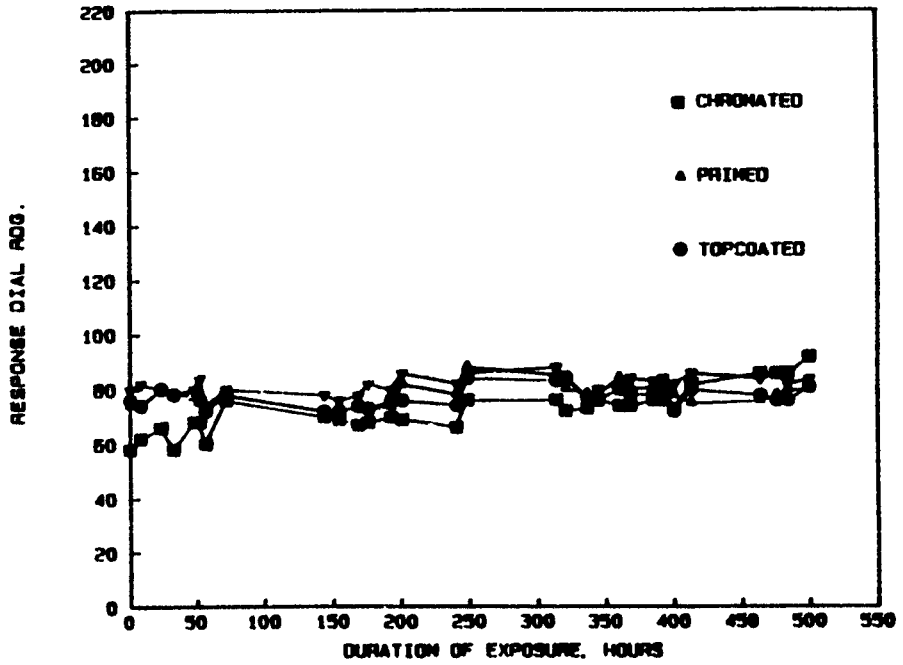

(a) Manual Corrosion Monitoring System

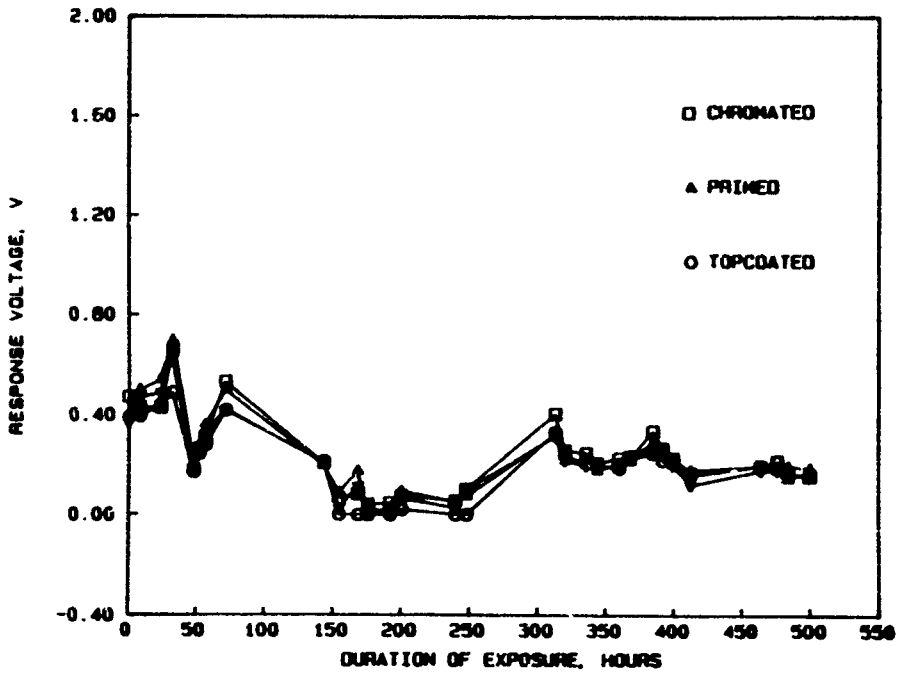

(b) Automated Corrosion Monitoring System

FIGURE 7. GRAPHICAL SUMMARIES OF CORROSION PROBE RESPONSE DATA RECORDED BY MANUAL AND AUTOMATED ER CORROSION MONITORING SYSTEMS DURING TEST NO. 2

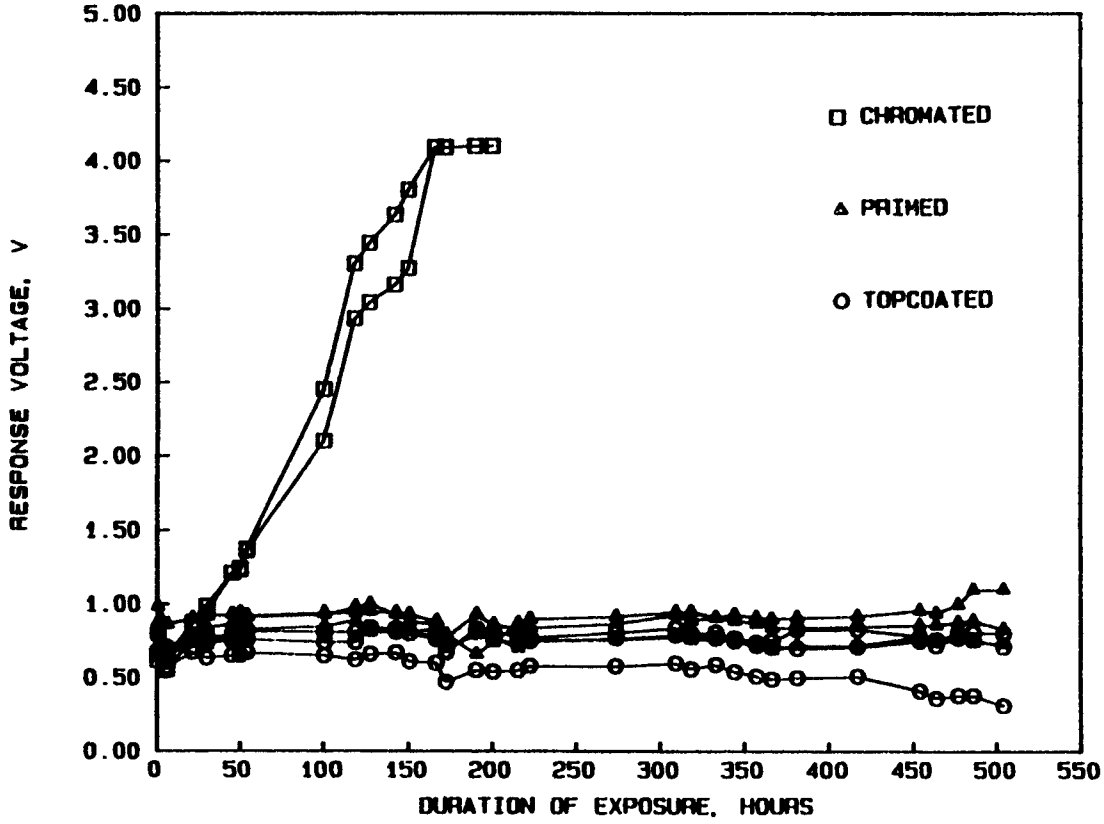

FIGURE 8. GRAPHICAL SUMMARY OF CORROSION PROBE RESPONSE DATA RECORDED BY AUTOMATED ER CORROSION MONITORING SYSTEM DURING TEST NO. 3

(a) Cross-Section of Chromated Only Test Element

(b) Severity of Pitting and Intergranular Attack

FIGURE 9. MICROGRAPHS DOCUMENTING CORROSION ATTACK TO TEST ELEMENT OF CHROMATED CORROSION PROBE, AFTER 250 HOURS OF ASTM B117-85 CORROSION TESTING

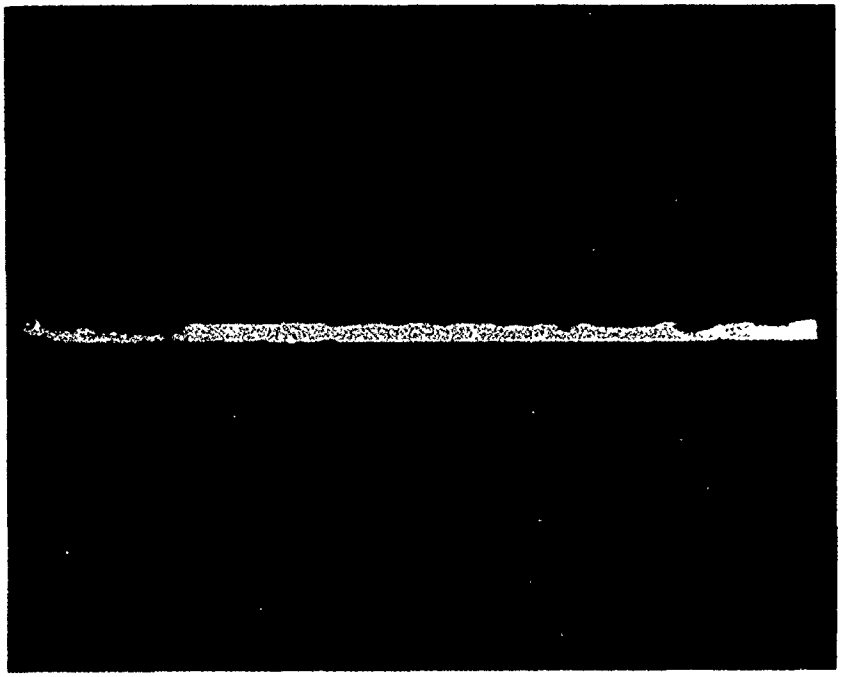

FIGURE 10. MICROGRAPH OF PITTING AND INTERGRANULAR CORROSION ATTACK THROUGH CROSS-SECTIONED AREA OF PROBE NO. 5, AFTER 30 HOURS OF ASTM B368-85 CORROSION TESTING

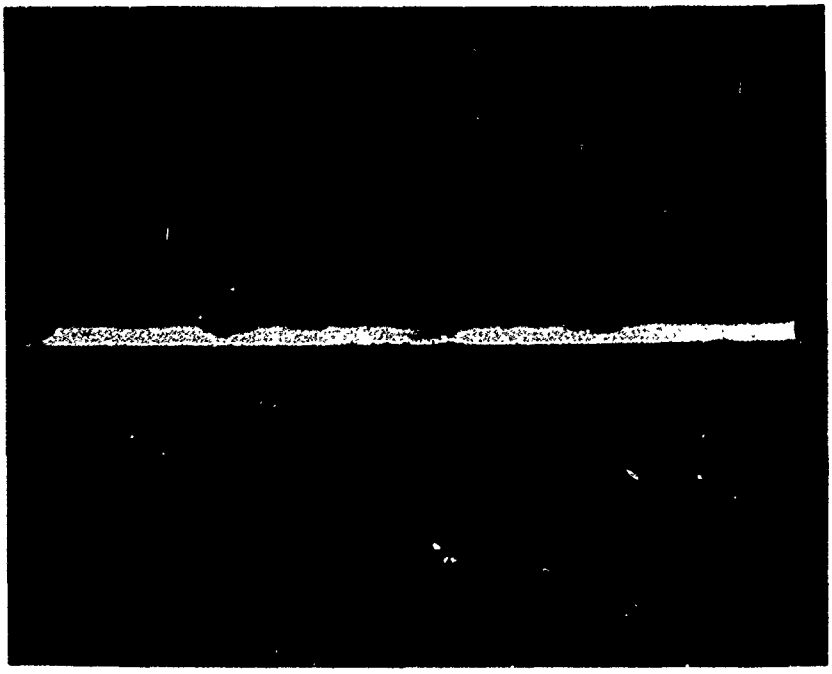

FIGURE 11. MICROGRAPH OF PITTING AND INTERGRANULAR CORROSION ATTACK THROUGH CROSS-SECTIONED AREA OF PROBE NO. 6, AFTER 30 HOURS OF ASTM B368-85 CORROSION TESTING

DEVELOPMENT OF A MULTIPLE ELEMENT SENSOR FOR LOCALIZED CORROSION OF STAINLESS STEEL

Timothy P. Anguish, Paul V. Janavicius, Joe H. Payer

Department of Materials Science and Engineering
Case Western Reserve University
Cleveland, Ohio 44106

ABSTRACT

Sensors manufactured by microelectronic fabrication techniques can measure corrosion rates directly or determine effectiveness of corrosion control systems. Various sensor elements are described. The combination of multiple-element sensors and data bases for corrosion behavior provides a powerful technique to enhance durability and reliability of equipment and structures. An application of this technology for localized corrosion is described.

INTRODUCTION

The annual cost of corrosion for the United States is estimated to be 4.2 percent of the Gross National Product.[1] Improved methods to monitor corrosion and to forewarn of corrosive conditions could greatly reduce the costs of corrosion. Projects are underway at Case Western Reserve University to develop corrosion sensors using microelectronic techniques.

Recent advances in microelectronic fabrication make it possible to reproducibly manufacture planar sensor elements. Typical fabrication methods include etching, vacuum deposition, crystal growth, diffusion, and micromachining. Photolithography for chemical etching and the use of stencils and masks for film deposition provide precise control of the size and geometry. Miniaturized devices based on conductors, semiconductors, and dielectrics can be made by both thick film and thin film techniques.[2] Typical devices include Ag/AgCl chloride sensors, Nafion coated Ag/AgCl reference electrodes, thermistors, resistance temperature detectors, Pd/PdO pH sensors, and ion selective field effect transistors.

Corrosion processes are controlled by the combination of the corrosion resistance of the metal and the corrosivity of the environment. The corrosivity can be defined by several parameters. Where a data base for the corrosion behavior of a metal is available in terms of these parameters, sensors to monitor the environment can be used to warn of incipient corrosion. For stainless steel in chloride solutions, the critical parameters are temperature, pH, chloride concentration, oxygen concentration and oxidizing potential. This paper describes the development of a multi-element sensor to monitor corrosion of stainless steel in chloride solutions.

Multiple Controlling Parameters Determine Corrosion Rate

Multiple controlling parameters control most corrosion reactions. Typical parameters include potential, temperature, pH, chloride concentration, and oxygen concentration. The effects of these parameters on corrosion rate are discussed below.

Pitting of stainless steel in chloride solutions increases as the solutions become more acidic. Figure 1 shows the effect of pH on critical pitting potential for 18-8 stainless steel.[3] The pitting potential is lowest for pH to 6 and then rises rapidly with increasing pH. The potential-pH (Pourbaix) diagrams for a metal provides an indication of the effect of pH on the corrosion behavior of a metal.[4]

The potential of a metal in solution can indicate its tendency to corrode. The potential is governed by both the specific oxidizing power of the constituents and by the concentration of the constituents in solution. Changes in the concentration can stimulate the formation or dissolution of protective films. Figure 2

illustrates the typical relationship between potential and corrosion rate of an active metal.[5] As the potential becomes more positive, the corrosion rate of the metal increases. The relationship between potential and corrosion rate for an active-passive-transpassive metal is shown in Figure 3.[6] Where the anodic polarization curve is known, the potential of the metal in the solution can be monitored to determine the corrosion state.

Temperature affects a corrosion reaction in a number of ways.[6] The solubility of species important to the corrosion reaction is temperature dependent, and a change in temperature can have a prominent effect on the concentration. The corrosion of iron in a system open to the atmosphere is shown in Figure 4.[3] The corrosion rate increases linearly with temperature to near the boiling point where the corrosion rate decreases sharply. This decrease is attributed to the decreasing solubility of oxygen at boiling, and the resultant decrease in rate of the cathodic process. Corrosion reactions that are controlled primarily by the process of metal oxidation will have a temperature dependence which is reflected by an Arrhenius expression.

$$r = A \exp(-E/RT)$$

Where r is the corrosion rate, A is a constant, E is an activation energy, R is the gas constant, and T is the absolute temperature. This behavior is shown in Figure 5.[3] A rule-of-thumb is that the corrosion rate doubles for each 10°C increase in temperature.

The effect of chloride on the corrosion of stainless steels is shown in Figure 6. Increasing chloride concentration decreases the pitting potential of 18-8 stainless steel.[4] The corrosion of carbon steels in the presence of oxygen is another example of the effects of solution chemistry. As the amount of oxygen in solution is reduced the corrosion rate is reduced.

The complexity of the interdependence of variables in a corrosion reaction is apparent. It is difficult to predict corrosion behavior in dynamic situations. This makes it necessary to monitor the relative corrosivity of the solution in order to avoid the degradation and eventual failure of component materials. The use of multiple sensors in conjunction with the currently available databases can be used successfully to prevent unexpected failures. Presently there is a large database on corrosion behavior. The corrosion behavior of commonly used metals has been well documented. These data are useful in determining the regions of safe and unsafe operation with respect to solution corrosivity.

Microelectronic Sensors Monitor The Controlling Parameters

A sensor is one or more transducer elements used to monitor a system. Transducer elements are devices that convert physical, chemical, or electrochemical characteristics of a system to electrical signals.

For corrosion applications, transducers sensitive to temperature, concentration of aggressive species, pH, aeration conditions, electrode potential, changes in weight, etc. are of interest. For any corrosion system an array of various transducers can be arranged to generate electrical responses that give information on the corrosion conditions in the system at any time. If real-time information on the corrosion conditions is obtained, corrective actions can be initiated before serious damage to the system occurs. The use of such sensors prevents damage to equipment and results in savings from reduced replacement costs and shorter down times.

There are two types of transducers in a corrosion system, inactive and interactive elements. An inactive element takes input from the system and generates signals. Interactive sensing elements are output/input devices which perturb the system while measurements of the response are made. The two types of elements require different circuitry. Inactive elements only require electronic measurement circuitry, while interactive elements require signal generation and measurement circuitry. A transducer element for real-time measurements of corrosion is a direct sensing element. Indirect measurements determine corrosion based upon environmental variables rather than direct measurement of corrosion.

Two approaches apply to the manufacture of a multi-element sensor, modular or integrated. In a modular design, individual elements are manufactured separately and are combined by fixing to a support structure. An integrated design manufactures the elements directly on a common substrate. Advantages of modular

design include the ability to combine a wide variety of devices; each manufactured by a fairly simple process. Modular design avoids the affect of the production of one element having a detrimental effect on another element. An integrated design on the other hand would be advantageous for high production runs and can favor smaller sensors.

Several sensing elements are described here. A working electrode on a sensor can be made of the metal of interest. A surface of the equipment can be monitored, the metal can be deposited on an inert substrate by either thick or thin film techniques, or the metal electrode could be cut from a bulk sample and attached to an inert substrate.

The potential is an important piece of information for determining corrosion of a metal. The potential is measured with respect to a reference electrode. A common reference electrode involves a "MetalIInsoluble Metal Salt Ionic Solution (reversible species)" reaction, e.g.

$$MAn + e = M + An^-$$

where M is a metal atom and An is an anion and e is an electron.
The potential of an electrode is given by the Nernst equation

$$E = E_o - (2.303RT/F)\log a_{An}$$

where E is the potential, E_o is the standard half cell potential with respect to hydrogen, R is the gas constant, T is the Kelvin temperature, F is Faraday's constant, and a_{An} is the activity of the anion in the solution. Large, conventional, reference electrodes maintain solutions with known ionic activity. When electrode size is reduced, a problem arises in maintaining a known ion concentration around the electrode while having conductivity with the corrosive solution. A remedy to this problem is to use a polymer coating on the metal which immobilizes the anions but is permeable to cations.[7] The polymer is saturated with a known concentration of anions to keep the activity constant. The life of many currently available reference electrodes is short, but further development of electrodes and membranes will extend lifetimes.[8] An example of a reference electrode currently used is the silver/silver chloride (Ag/AgCl) system. A silver substrate is polarized in 0.1N HCl at 1.0 V for 30 seconds to produce AgCl on the surface of the Ag electrode.[2] A coating of Nafion saturated with NaCl can cover the electrode to maintain a constant activity of chloride ions.

There are several single-component sensors currently available which give information on specific aspects of the corrosivity of an environment. These include temperature, pH, chloride, oxygen, and other ion-sensitive sensors. By selecting individual elements a wide variety of conditions can be monitored in almost any corrosion system.

Several different transducers can be used to measure temperature. Diodes, transistors, integrated circuits (IC), thermocouples, resistance thermometers, and thermistors are a few devices currently used for temperature measurements.[9] If a modular design of a multi-element sensor is utilized, any of these devices could be used. A resistance thermometer or resistance temperature detector (RTD) is most suitable in terms of micro-fabrication methods.

A transducer sensitive to pH is based on the potential of a metal/metal oxide reversible reaction. The electrochemical reaction for the reduction of a metal oxide is given by

$$MO + 2H^+ + 2e = M + H_2O$$

where M is a metal atom, and O is oxygen. The potential of this electrode is Nernstian and is controlled by temperature and pH

$$E = E_o - (2.303RT/F)[pH]$$

The metal/metal oxide system chosen for the electrode may be affected by the presence of other aggressive species in the system. An example of this is the palladium/palladium oxide (Pd/PdO) electrode which is

unsuitable in electrolytes containing Cl^- ions since the chloride causes dissolution of PdO. A cation permeable membrane can be used to protect the electrode but the life of the electrode will be limited by the durability of the membrane.[2,10,11]

An ion-sensitive element can be made from a redox system involving the ion of interest. The potential will be Nernstian and will depend on the activity of the ion in solution. For a chloride sensitive element a Ag/AgCl electrode is exposed directly to the electrolyte.[2] Ion-selective electrodes can also be made from monitoring the potential of an inert electrode. The ferric/ferrous ion system is an example of a redox couple which has been monitored by measuring the potential of a gold electrode versus a reference electrode. These two examples are inactive or potentiometric in nature, and the potential of the electrode is measured against a reference electrode.

Interactive sensors can also be used to determine the amount of a species in an environment. A three electrode oxygen sensor has been developed.[12] The sensor consisted of two three pronged gold electrodes and a Ag/AgCl electrode. A square mesh geometry with 24 interconnected gold microelectrodes is fabricated on one electrode. Using the meshed gold electrode as a working electrode, the bare gold electrode as a working electrode and the Ag/AgCl electrode as a reference (chloride concentration was known), the reduction of dissolved oxygen to hydroxyl ions was monitored using polarograms or V-I scans. A plateau was observed in the current which corresponded to oxygen concentration. The current measured at a polarization of 0.8 V for 300 s also corresponded to oxygen concentration.

Other ion-selective elements use FET's that are connected to ion selective membranes. These devices are known as ion selective field effect transistors (ISFET) or chemical field effect transistors (ChemFET). The gate potential of the FET is affected by ion exchange at the membrane anolyte which in turn changes the conductance of the FET. The durability of the ion selective membrane and the packaging of the FET are key factors affecting the application and life of the ISFET.

Two ways to measure corrosion directly are linear polarization and resistance measurements. Linear polarization is an interactive technique in which a small voltage pulse is applied between two electrodes while the current is monitored. The ratio between the voltage and the current is the polarization resistance and can be related to the corrosion current. The corrosion current can be converted to a mass loss rate.[13] Electrical resistance can be used to determine the thickness of a metal foil. Measurement of resistance is straight forward and the resistance change can be converted to weight loss or corrosion rate. Direct measurements of corrosion are useful in cases where uniform corrosion limits the lifetime of the material. Localized corrosion limits the applicability of these methods.

DISCUSSION

A multi-element sensor is being developed to monitor the localized corrosion of 316 stainless steel used in bleaching processes. The high chloride concentration is conducive to pitting, and several studies have been made as to the controlling parameters.[14,15] A model was developed by Matamala relating the pH, temperature, and chloride concentration to the critical pitting potential of 316 stainless steel.[16] This relationship was determined using anodic polarization to measure pitting potentials. Equations relating pitting potential to pH, temperature, and chloride content were obtained using linear regression. An equation is shown below.

$$E_p = 2570 - 5.81T + 0.07\ pH - 0.49\ T \log[Cl^-]$$

Where E_p is the critical pitting potential in millivolts versus a saturated calomel electrode, T is the absolute temperature, and [Cl-] is the concentration of chloride in parts per million. Plotted in three dimensions this equation defines a surface above which pitting occurs and below which pitting does not occur. A diagram of this surface at constant pH is shown in Figure 7. The values of parameters measured by the multi-element sensor can be compared to this surface to indicate the behavior of 316 SS.

The position of the surface boundary between no corrosion and pitting depends upon alloy composition. In general, the surface moves to higher values as the nickel, chromium and molybdenum concentration of the alloy increases. The effect of increasing corrosion resistance of the alloy is shown in two dimensions in

Figure 8. The expected behavior of a series of alloys can be determined where a data base is available for comparison to measured parameters of the solution.

In a bleaching process it is important to avoid conditions conducive to pitting. A sensor containing a working electrode of 316 stainless steel, an RTD temperature sensor, a pH electrode, a coated Ag/AgCl reference electrode, and a Ag/AgCl chloride sensor is in the initial stages of development. A modular design shown schematically in Figure 9 is being used during the developmental stages. An integrated design would be adapted after the proper processing sequence has been determined. The sensor is encapsulated a polymer for protection and ease of placement (Figure 10). The multi-element sensor can be mounted to monitor the behavior of a metal coupon or mounted directly to monitor the behavior of the equipment.

CONCLUSIONS

Sensors can be used to control the high cost of corrosion. Measurements of the corrosivity of the system or direct measurements of corrosion can be made with various transducer elements. Corrosion systems rarely depend on one variable; rather, temperature, pH, concentration of aggressive species, and electrode potential are variables that determine the corrosion behavior of a system.

Multiple measurements of the corrosivity of a solution can be made using an array of transducers which are sensitive to specific parameters of a corrosive system. A modular or integrated design can be applied to the construction of multi-element sensors. Modular design allows the construction of a wide variety of multi-element sensors from a stock of single-component sensors. Integrated design, on the other hand, is suitable for high production runs and sensors of reduced size. Transducers which are currently available have limited lifetimes due to the durability of polymer coatings, interconnects, and adhesives.

The variables that affect the corrosion rate of a specific system can be found in existing data bases prior to sensor design. For 316 stainless steels used in the bleaching processes, pitting is the corrosion process that limits the lifetime of material. The environment in the process can be monitored using a working electrode of 316 stainless steel, a coated Ag/AgCl reference electrode, a temperature transducer, a Ag/AgCl chloride sensor, and a pH electrode. By monitoring these parameters the critical regions where pitting is probable can be avoided. The monitoring of critical parameters can be applied to most corrosion systems, for the control of the high cost of corrosion.

ACKNOWLEDGEMENTS

This work is being conducted under the sponsorship of the Edison Sensor Technology Center at Case Western Reserve University. Microelectronic sensors were fabricated in the Electronics Design Center at CWRU.

REFERENCES

1. J.H. Payer, W.K. Boyd, D.G. Dippold, W.H. Fisher, "NBS-Battelle Cost of Corrosion Study, Parts 1-7," Materials Performance, Vol. 19 (May-Nov. 1980).

2. S.K. Chawla, T. Anguish, J.H. Payer, "Microsensors For Corrosion Control," Corrosion '89, New Orleans, 1989.

3. H.P. Leckie, and H. H. Uhlig "Environmental Factors Affection the Critical Potential for Pitting in 18-8 Stainless Steel," Journal of the Electrochemical Society, Vol. 113, No.12, 1966, pp 1262-1267.

4. M. Pourbaix. Atlas of Electrochemical Equilibria in Aqueous Solutions, National Association of Corrosion Engineers, Houston, 1974.

5. M.G. Fontana, Corrosion Engineering, McGraw-Hill Book Co., New York, 1986.

6. D.C. Silverman and R.B. Puyear. "Effects of Environmental Variables on Aqueous Corrosion," ASM Metals Handbook, 9th edition, Vol. 13, 1987.

7. A. Bettelheim, R. Harth, and D. Ozer. "A New Polymer Ag/AgCl Reference Electrode with No Contacting Electrolyte Solution," Journal of the Electrochemical Society, Vol. 135, No. 4, 1988, pp 1041-1042.

8. J. Janata, and A. Bezegh. "Chemical Sensors" Analytical Chemistry, Vol. 60, No. 12, 1988, pp 62R-72R.

9. C.H. Lin and H. Jadavar. "Interfacing Temperature Sensors," Interfacing Sensors to the IBM PC, Ch. 7, Prentice Hall, NJ, 1988.

10. C.C. Liu, B.C. Bocchicchio, P.A. Overmyer, and M.R. Neuman. "A Palladium-Palladium Oxide Miniature pH Electrode," Science, vol. 27, 11 January 1980.

11. V.A. Karagounis, C.C. Liu, M.R. Neuman, L.T. Romankiw, P.A. Leary, and J.J. Cuomo. "A Pd-PdO film Potentiometric pH Sensor," IEEE Transactions on Biomedical Engineering, Vol. BME-33, No. 2, 1986, pp 113-116.

12. V. Karagounis, L. Lun, and C.C. Liu. "A Thick-Film Multiple Component Three Electrode Oxygen Sensor," IEEE Transactions on Biomedical Engineering, Vol. BME-33, No. 2, 1986, pp 108-112.

13. F. Ansuini. "Low Cost Corrosion Sensors," Proceedings of the 1987 Tri-Service Conference on Corrosion, 1987.

14. A. Garner. "Corrosion Control in the Bleach Plant," Pulp and Paper Canada, Vol. 86, No. 12, 1985, pp T419-T426.

15. M. Kurkela, N. Suttala, and J. Kemppainen. "On the Selection of Stainless Steels in Bleach Plants and White Water Systems," 1986 Fifth International Symposium on Corrosion in the Pulp and Paper Industry, Canadian Pulp and Paper Association 1986, pp 127-132.

16. G. Matamala R., "Correlation Model of the AISI 316 Stainless Steel Potential with Cellulose Bleach Process Variables," Corrosion, Vol. 43 (No. 2), 1987, pp. 97-100.

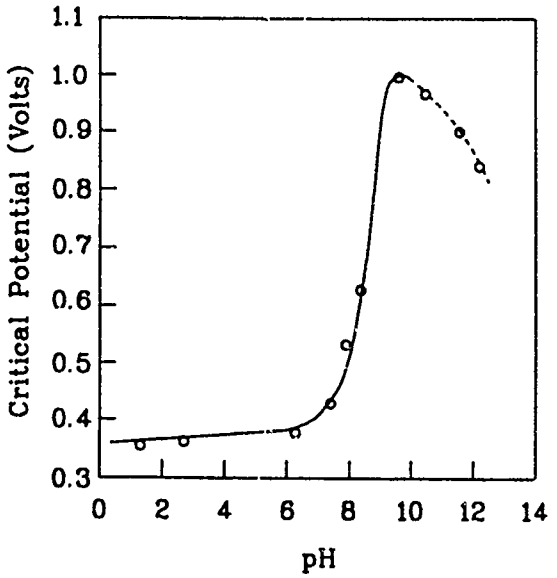

Figure 1 – The effect of pH on critical pitting potential in 18–8 stainless steel. (after Leckie and Uhlig[4])

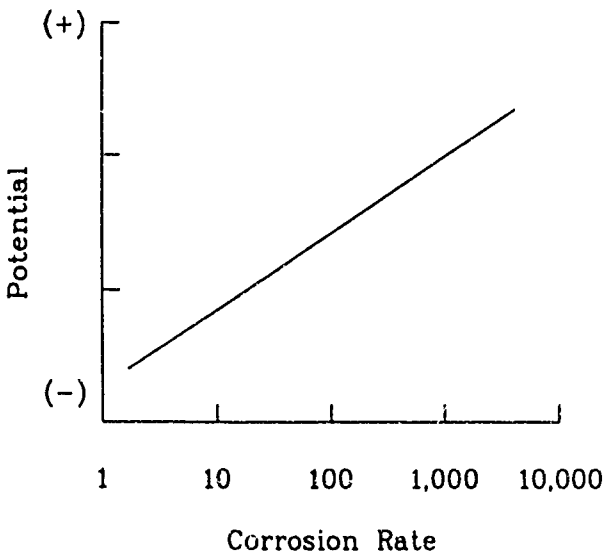

Figure 2 – Effect of potential on corrosion rate of an active metal. (after Fontana[6])

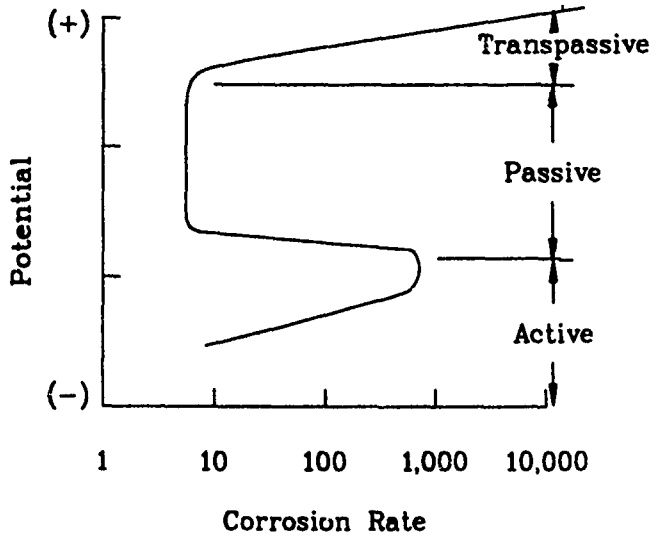

Figure 3 – Effect of potential on corrosion rate of an Active–Passive–Transpassive metal. (after Fontana[6])

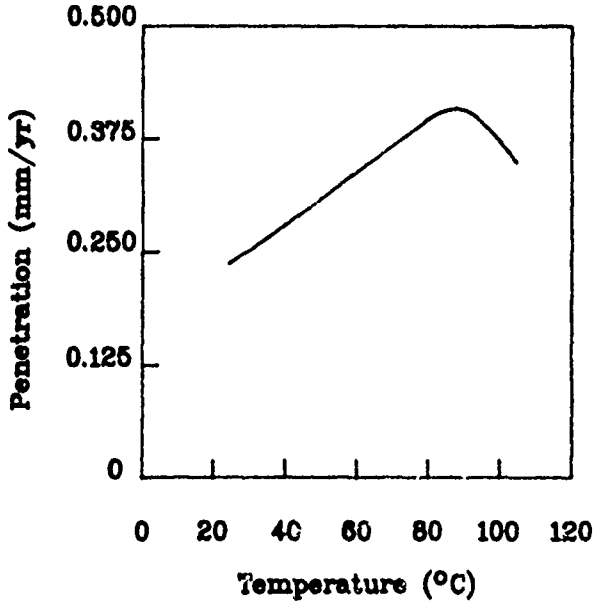

Figure 4 – Temperature dependence of corrosion rate of iron in water open to the atmosphere. (after Tomashov[3])

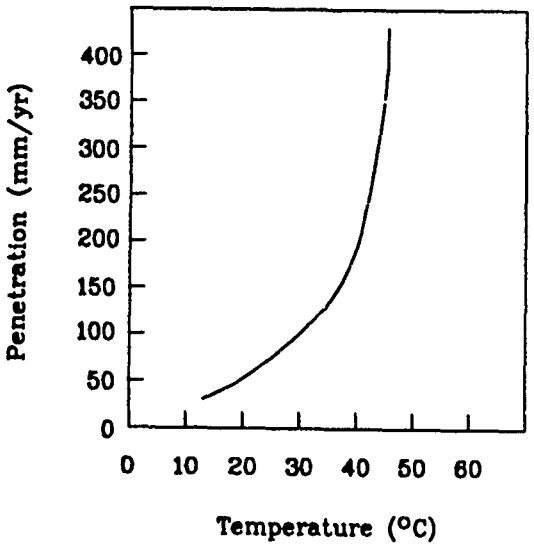

Figure 5 – Typical temperature dependence of corrosion according to an Arrhenius relationship. (after Tomashov[3])

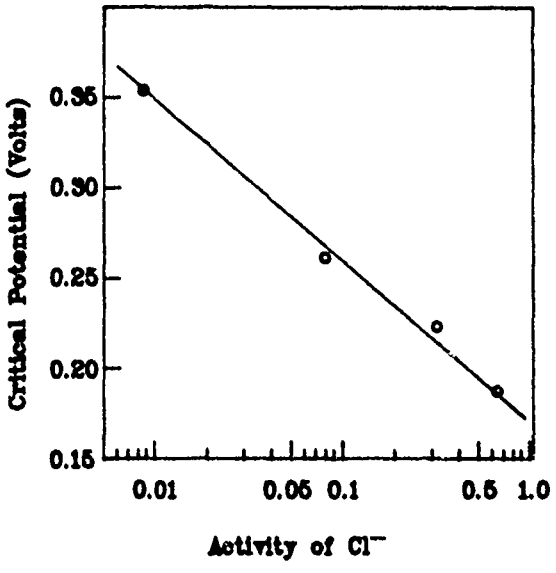

Figure 6 – The affect of chloride on critical pitting potential in 18–8 stainless steel. (after Leckie and Uhlig[4])

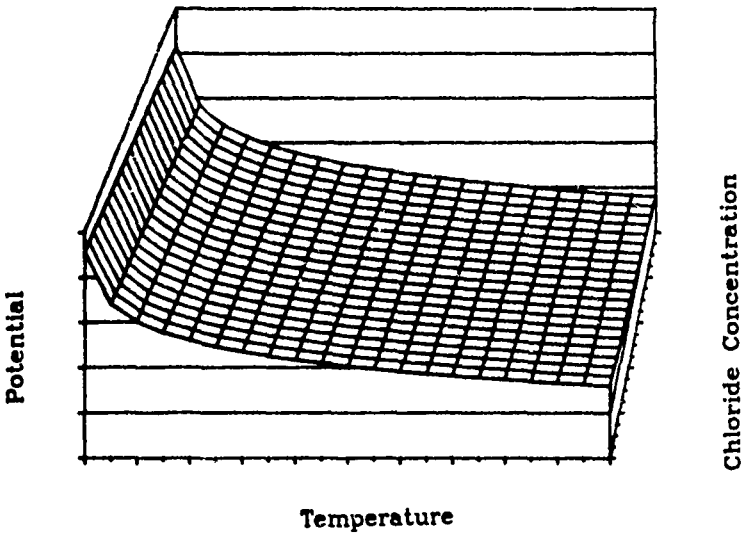

Figure 7 – Three dimensional plot showing the surface of critical pitting potential as a function of temperature and chloride concentration at a constant pH. Based on an equation developed by Manamala.[17]

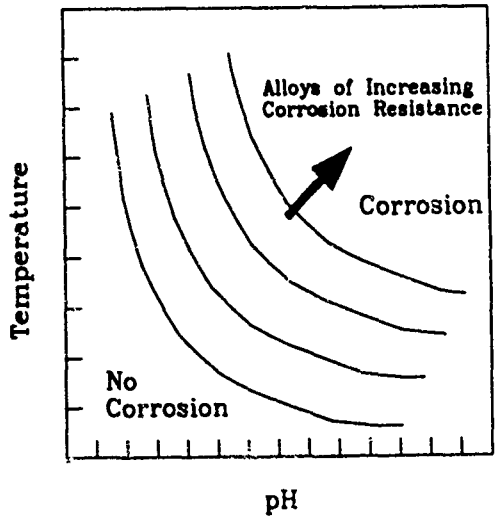

Figure 8 – Schematic showing the effect of alloys with different corrosion resistances on critical corrosion values.

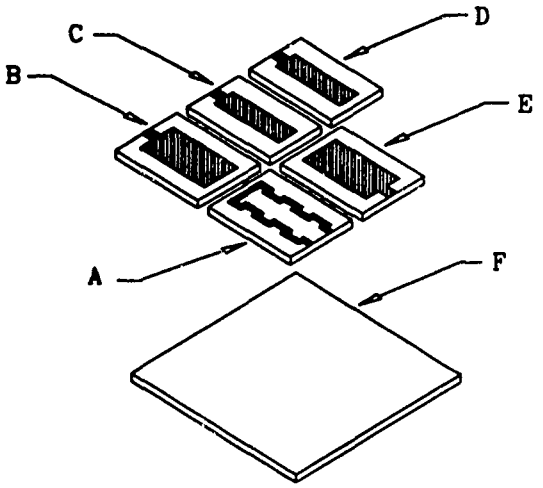

A – Platinum Element Temperature Sensor
B – Paladium/Paladium Oxide pH Sensor
C – Silver/Silver Chloride Chloride Sensor
D – Coated Silver/Silver Chloride Reference Electrode
E – Platinum Element for Measuring the Solution Redox Potential
F – Ceramic Base

Figure 9 – Modular Multi-Element Sensor for localized corrosion.

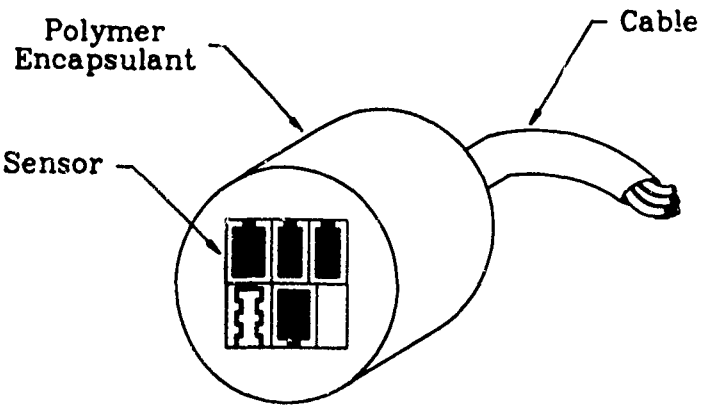

Figure 10 – Schematic diagram of an encapsulated multi-element sensor.

AEROSPACE MATERIALS LABORATORY TRIBOLOGY OVERVIEW

Alfeo A. Conte, Jr.

Naval Air Development Center
Warminster, Pennsylvania 18974-5000

ABSTRACT

A brief overview will be presented on the work performed at the Aerospace Materials Laboratory of the Naval Air Development Center in the area of tribology.

Without functional high temperature lubricant/bearing systems, advances in aerospace propulsion technology will be severely limited. Advanced Naval aircraft propulsion systems will be required to operate at temperatures outside the performance range of metals. Ceramics are being proposed for this application because of their ability to maintain high hardness at elevated temperatures and thus support heavy loads. The tribology of ceramic materials however, has not been as thoroughly explored as that of metals and is still in it's infancy. The fundamental tribological characteristics of ceramics resemble glasses more than metals in that there is a strong tendency for ceramics to fracture rather than plastically deform under impact load. Failure is usually via micro and/or macrofracture processes. A basic understanding of ceramic failure mechanisms and processes that contribute to failure are being studied for rolling, sliding and oscillatory contacts as a function of temperature, motion and load. Silicon nitride, silicon carbide and zirconia have been identified as potentially useful materials for further study.

Lubrication above 350 C will be limited to solids. Several approaches are possible utilizing films, composites, powder lubrication or ion implantation techniques. The primary driving factor for the selection of a lubricating material is long term high temperature (750 C) stability coupled with inherent lubricity especially in oxidative environments.

Other important considerations include strong adhesion of surface films or replenishment techniques which will meet durability requirements. Current widely used lubricating solids are lamellar materials such as molybdenum disulfide and graphite. These materials are deficient in resistance to oxidation (400 C and 600 C), respectively. New directions toward research in the realm of high temperature lubricating materials is urgently needed. Intercalated graphite, phthalocyanine complexes and Schiff's bases are examples of materials with potentially improved lubricating characteristics.

A method based on a new corrosion sensor, has been developed to quantitatively determine the corrosion resistance behavior of lubricants. It is based on the electrochemical concept of measuring the corrosion current generated by a galvanic couple beneath a thin oil film. The magnitude of this current was found to be directly related to the effectiveness of the oil film in preventing corrosion. This method represents an interesting alternative to standard procedures that are now being used to determine the corrosion inhibiting properties of thin oil films. The advantages in the use of the probe compared to alternative techniques are the quantitative nature of the probe, ease in accelerating the test procedure and extremely high sensitivity.

Sensor probes located in the pump housing of an experimental aerospace coolant/dielectric system are malfunctioning causing the system to "shut down". Corrosion of the sensors and possible arcing had been reported. The fluid used in this system is a perfluorinated hydrocarbon conforming to MIL-H-81829 specification. An investigation of used fluid property changes (viscosity, specific gravity, dielectric strength, volume resistivity and hydrolytic stability) revealed that no degradation of the fluid had occurred as a result of system usage or contamination. Qualitative corrosion tests with 52100 steel coupons immersed in fluid contaminated with water showed that water intrusion can cause corrosion and that the fluid by itself does not contribute to corrosion. Examination of a corroded needle valve revealed corrosion at both the "entry" and "exit" ports. Corrosion was more evident on the "entry" port although the "exit" was also considered to be severely corroded. Corrosion progressed outward along the threads to a point where the connecting lines were attached.

The corrosion product (red rust) was found to be similar to that produced in laboratory tests. From the results of this investigation it was concluded that the perfluorinated fluid is stable in the presence of copious quantities of water and, any corrosion observed in the system is considered due solely to water intrusion and not chemical breakdown of the fluid.

A particular US Navy problem which has been at the forefront of maintenance attention for over a decade, involves the use of 2-ethyl-1-butyl silicate ester (2-EBSE) in airborne radar systems. Contamination of the radar system with alcohol and silica called for immediate maintenance procedures to alleviate or eliminate this problem. These costly procedures have controlled the problems somewhat but have not eliminated them. The search for a replacement fluid led the US Navy to propose the use a polyalphaolefin (PAO) based fluid which possessed all of the desirable properties of a good coolant/dielectric fluid and in addition was considered to be hydrolytically stable. Interest in this candidate fluid was also expressed by the US Air Force which also has the identical problem as the US Navy, but not to that great of an extent. As a result of work performed in the area of coolant/ dielectric fluid technology, PAO based fluids are now being proposed as a replacement for currently used silicate ester coolant/dielectric media in US military aircraft radar systems. Silicate esters are known to be hydrolytically unstable, forming solid contamination (SiO_2), which is attracted to electronic components and alcohol, which posses a fire hazard threat. PAO fluids are synthesized hydrocarbons which are hydrolytically stable and offer improved fire-resistance, heat transfer capability and lubricity compared to silicate ester fluids.

Finally, grease lubricated bearing failures due to corrosion will be discussed.

DEVELOPMENT OF LABORATORY TEST TO SIMULATE M60 SALT WATER IMMERSION FIRING TEST

Stephen Whalen
U.S. Army Research, Development and Engineering Center
SMCAR-AET-O, ATD, AED
Picatinny Arsenal, NJ 07806-5000

Abstract

In the performance of qualification testing of weapons lubricants conforming to MIL-L-63460, "Lubricant, Cleaner and Preservative for Weapons and Weapons Systems" (CLP), it was noted that the candidate lubricant's ability to pass standard laboratory salt spray and humidity cabinet tests did not necessarily reflect its ability to pass the "M60 Salt Water Immersion Firing Test". This paper deals with the development of laboratory tests which appear to predict the ability of a CLP type lubricant to prevent failure in the firing test. Steel panels treated with different CLP lubricants were exposed to the ignition by-products of a propellant and subjected to various types of laboratory simulated high humidity conditions in order to assess which test methods would reliably predict the CLP's ability to protect against corrosion due to the propellant by-products.

INTRODUCTION

When a company wishes to have its weapons lubricant qualified under Military Specification MIL-L-63460 "Lubricant, Cleaner and Preservative for Weapons and Weapons Systems" (CLP), the product must successfully meet all requirements of the specification. Two of the laboratory test requirements which gauge a CLP's corrosion prevention ability are the salt spray resistance test described in Federal Test Method Standard No 791 Method 4001 and protection from rust in the humidity cabinet described in ASTM D 1748. Although two candidate CLP lubricants passed all laboratory test requirements in the specification, they did not provide sufficient corrosion protection to the M60 machine gun in the salt water immersion gun firing test requirement. The conducting of live firing qualification tests is a lengthy and expensive process, thus it was decided that a laboratory test to simulate the salt water immersion gun test would be developed to assist in screening out inferior CLP candidate lubricants prior to testing on the M60 machine gun.

Initial investigation revealed that subjecting CLP treated steel panels to heat alone did not serve to duplicate the results observed in the gun firing tests. It was not until treated panels were exposed to the ignition by-products of propellant and exposed to laboratory simulated high humidity conditions that results were seen paralleling the results observed in the salt water immersion gun firing tests.

EXPERIMENTAL PROCEDURES

Test Panel Preparation

Steel panels, as called for in ASTM D 1748 "Rust Protection by Metal Preservatives in the Humidity Cabinet", were cleaned in a heated bath of hexane followed by immersion in a bath of hot methanol. After cleaning, the panels were sloshed in a beaker of the test oil for one minute and allowed to drain for two hours. They were then sloshed in a five percent aqueous sodium chloride solution for one minute and allowed to drain another fifteen minutes. After draining, each panel was suspended, test face down, two inches above a porcelain evaporating dish containing three grams of the double base small caliber propellant WC844. The propellant was ignited, exposing the test face of the panel to the hot propellant by-products. Following this the panels were exposed to the following controlled high humidity conditions:

1. The humidity cabinet described in ASTM D 1748. Temperature was maintained at 120°F.

2. An environmental chamber utilizing wet and dry bulb temperature controls. Both wet and dry bulb temperatures were maintained at 120°F in order to achieve an atmosphere of condensing humidity.

3. Static humidity chambers consisting of distilled water in glass desiccators. Temperatures of the chambers varied during the investigation.

Test Panel Inspection

Upon completion of the exposure in the high humidity environments, the panels were removed, wiped lightly with tissue paper soaked with petroleum ether and observed for rusting on the test faces. Corrosion was considered significant only if the rust spot was 2mm or greater and involved visible pitting or etching of the metal. Rusting of the panels within 1/8 inch of their edges, rust spots smaller than 2mm and staining of the panels were not considered significant corrosion.

The balance of the exposure times of the test panels to the high humidity conditions was for a 96 hour period. A round of testing usually consisted of three panels conditioned with the test lubricant and propellant by-products.

DISCUSSION

The investigation involved the use of four different CLP type lubricants. Two of the test lubricants, labeled A and B, were candidate CLP oils which successfully met the salt spray and humidity corrosion protection requirements of MIL-L-63460, yet failed to pass the salt water immersion gun firing test. The other two lubricants, labeled C and D, successfully met all corrosion protection requirements.

Results With The ASTM D 1748 Humidity Cabinet

Exposure in the humidity cabinet of the panels coated and conditioned with the two inferior CLP lubricants A and B and the WC844 propellant residue failed to produce extensive corrosion on the panels even after an extended period of time (Tables 1 and 2). Because of the poor results obtained with the ASTM D 1748 Humidity Cabinet, its use was discontinued after conducting a few rounds of tests.

Results With The Environmental Chamber With Wet And Dry Bulb Controls

Panels coated with lubricant A and exposed to WC844 propellant ignition by-products consistently showed significant corrosion when conditioned in the environmental chamber. Only one panel in the three rounds of tests conducted failed to show significant corrosion (Table 3). Panels treated with the other inferior CLP lubricant B paralleled these results. As seen in Table 4, only one panel in four rounds of tests did not corrode.

The data for three rounds of tests using panels coated with lubricant C are shown in Tabel 5. No panel exhibited significant corrosion even after eight days exposure in the environmental chamber. As seen in Table 6, results for lubricant D parallel those of the other acceptable CLP lubricant in that no significant corrosion was noted on the test panels even after eight days exposure in the environmental chamber.

Results With The Static Humidity Chambers

The successful use of static humidity chambers to duplicate the corrosion results observed in the salt water immersion gun test is desirable because the commercial companies submitting CLP candidates would have the means to screen their own products at a modest cost prior to submission for qualification testing. The environmental chamber utilizing dry and wet bulb controls is a relatively expensive apparatus not usually found in a commercial company's laboratory.

Static Humidity Temperature of 75°F

The first round of test panels treated with lubricant A and WC844 propellant ignition by-products failed to show significant corrosion even after a period of 14 days in the static humidity chambers (Table 7). It was decided to try this test procedure with the covered desiccators placed in the oven at elevated temperature.

Static Humidity Temperature Of 130°F

Test rounds two, three and four (Table 7) showed that placing covered desiccators containing the lubricant A treated panels in an oven maintained at 130°F resulted in rusting of at least one of the test panels in each of these three rounds, however, the corrosion was not very extensive. In the case of panels coated with lubricant B and exposed to the propellant by-products, Table 8 shows that in the first four rounds of tests, only two test panels in round two exhibited significant rusting.

Static Humidity Temperature Of 130°F and 75°F

To promote corrosion of the treated test panels, it was decided to employ cyclic conditions in the static humidity chamber test procedure. After initially placing the covered chambers in the oven at 130°F overnight, the chambers were removed in the morning, left uncovered at room temperature for six hours, then again covered and placed in the oven overnight. This cycle was performed for the duration of the test.

For the test panels treated with the inferior CLP lubricants A and B, corrosion increased dramatically. For test rounds five and six of lubricant A (Table 7) and rounds five and six for lubricant B (Table 8), only one test panel treated with lubricant B failed to exhibit significant corrosion. However, for test round seven, involving both of the inferior lubricants in the cyclic static humidity chambers, no corrosion appeared on any of the panels.

Test panels treated with the two qualified CLP lubricants C and D showed no significant corrosion after a round of environmental cycling in the static humidity chambers over periods of 13 and 14 days, respectively (Tables 9 and 10).

CONCLUSIONS

Humidity Cabinet Conforming to ASTM D 1748

This method does not serve to duplicate results observed in the M60 machine gun salt water immersion firing test.

Environmental Chamber Using Wet and Dry Bulb Controls

Results of this study show this method to be the best for predicting the ability of a CLP type lubricant to protect against corrosion in the M60 salt water immersion gun test. Results of this method consistently agreed with those observed in the actual M60 qualification firing tests. As a result, this test method was incorporated into the qualification test section of MIL-L-63460.

Static Humidity Chambers

With the exception of the last round of tests performed with the inferior CLP candidates A and B, this method appears to be a reliable alternative to the use of the environmental chamber. However, further testing would be required to be conducted with the four test lubricants in order to have full confidence in this method's ability to consistently predict the ability of a CLP lubricant to prevent corrosion in the M60 salt water immersion firing test.

Table 1. Lubricant A in ASTM D 1748 humidity cabinet

Test round	Test specimen	Test duration (days)	Extent of corrosion
1	1	4	None
	2	11	None
	3	11	None
2	1	18	One rust spot
	2	25	None
	3	25	None

Table 2. Lubricant B in ASTM D 1748 humidity cabinet

Test round	Test specimen	Test duration (days)	Extent of corrosion
1	1	18	None
	2	18	None
	3	18	None

Table 4. Lubricant B propellant in environmental chamber

Test round	Test specimen	Test duration (days)	Extent of corrosion
1	1	4	Rusted area: 16 x 13mm
	2	4	Rusted area: 55 x 13mm
	3	4	Rusted area: 23 x 21mm
2	1	4	17 rust spots
	2	4	20 rust spots
	3	4	20 rust spots
3	1	4	Rusted area: 33 x 32mm and one rust spot
	2	4	Rusted area: 43 x 19mm and one rust spot
	3	4	None
4	1	4	Rusted areas:23 x 10mm 15 x 10mm, 10 x 8mm 6 x 5mm and six rust spots
	2	4	One rust spot
	3	4	Rusted areas: 16 x 10mm and 4 x 2mm

Table 3. Lubricant A in environmental chamber

Test round	Test specimen	Test duration (days)	Extent of corrosion
1	1	4	Rusted area: 50 x 25mm
	2	4	Rusted area: 37 x 14mm
	3	4	Rusted area: 57 x 30mm
2	1	4	Five rust spots
	2	4	Six rust spots
3	1	4	Rusted areas: 10 x 5mm and 9 x 8mm, and three rust spots
	2	4	None
	3	4	Rusted area: 9 x 8mm

Table 5. Lubricant C in environmental chamber

Test round	Test specimen	Test duration (days)	Extent of corrosion
1	1	8	None
	2	8	None
	3	8	None
2	1	8	None
	2	8	None
3	1	4	None
	2	4	None

Table 6. Lubricant D in environmental chamber

Test round	Test specimen	Test duration (days)	Extent of corrosion
1	1	8	None
	2	8	None
2	1	4	None
	2	4	None
	3	4	None
	4	4	None
	5	4	None
	6	4	None

Table 7. Lubricant A propellant in static humidity chamber

Test round	Test specimen	Temperature (^{o}F + 5^{o}F)	Test duration (days)	Extent of corrosion
1	1	75	4	None
	2	75	8	None
	3	75	14	None
2	1	130	6	One rust spot
	2	130	6	Rusted area: 28 x 15mm
3	1	130	4	Two rust spots
	2	130	4	None
	3	130	4	None
4	1	130	4	One rust spot
	2	130	4	Four rust spots
	3	130	4	None
5	1	130,75	4	Rusted area: 11 x 5mm and five rust spots
	2	130,75	4	Rusted areas: 14 x 9mm 9 x 4mm, and five rust spots
	3	130,75	4	Rusted area: 41 x 29mm and three rust spots
6	1	130,75	4	One rust spot
	2	130,75	4	Three rust spots
	3	130,75	4	Rusted areas: 38 x 16mm 4 x 2mm, 10 x 4mm and five rust spots
7	1	130,75	4	None
	2	130,75	4	None
	3	130,75	4	None

Table 8. Lubricant B propellant in static humidity chamber

Test round	Test specimen	Temperature (°F + 5°F)	Test duration (days)	Extent of corrosion
1	1	130	4	None
	2	130	4	None
	3	130	4	None
2	1	130	4	One rust spot
	2	130	4	Four rust spots
	3	130	4	None
3	1	130	4	None
	2	130	4	None
	3	130	4	None
4	1	130	4	None
	2	130	4	None
	3	130	4	None
5	1	130,75	4	Rusted areas: 48 x 18mm 5 x 3mm and two rust spots
	2	130,75	4	Rusted areas: 55 x 21mm 5 x 5mm, and one rust spot
	3	130,75	4	None
6	1	130,75	4	Rusted area: 27 x 13mm and two rust spots
	2	130,75	4	Rusted areas: 17 x 18mm and 13 x 8 mm
	3	130,75	4	Rusted areas: 47 x 22mm 7 x 5mm, and two rust spots
7	1	130,75	4	None
	2	130,75	4	None
	3	130,75	4	None

Table 9. Lubricant C propellant in static humidity chamber

Test round	Test specimen	Temperature (°F + 5°F)	Test duration (days)	Extent of corrosion
1	1	130,75	13	None
	2	130,75	13	None
	3	130,75	13	None

Table 10. Lubricant D propellant in static humidity chamber

Test round	Test specimen	Temperature (°F + 5°F)	Test duration (days)	Extent of corrosion
1	1	130,75	14	None
	2	130,75	14	None
	3	130,75	14	None

EVALUATION OF QUALITY OF COATINGS FOR TRIBO-CORROSION APPLICATIONS

Kirit J. Bhansali
U. S. Army Materials Technology Laboratory, Watertown, MA 02172-0001

Theo Z. Kattamis
Institute of Materials Science
University of Connecticut
Storrs, CT 06268

ABSTRACT

The soundness and comparative quality of various coatings were evaluated with a CSEM-Revetest automatic scratch tester. These coatings were: TiB_2 on MP35N alloy, TiN on PH 17-4 steel, Al_2O_3-SiO_2-Cr_2O_3 on PH 17-4 steel and Plasma Enhanced CVD-processed SiC on 4340 low alloy steel. During scratch testing the acoustic emission signal intensity, the frictional or tangential force and the friction coefficient were plotted versus load, as well as time at various constant loads. Results were interpreted in terms of coating microstructure which was investigated by optical and scanning electron microscopy. The TiN-coated steel specimens exhibited higher coating cohesive and adhesive loads than the others, as well as a lower friction coefficient, which would indicate that they would also exhibit a better abrasive wear resistance. Significant difference in quality and soundness was detected for TiN coatings processed by different methods.

INTRODUCTION

The U.S. Army Laboratory Command (LABCOM) and Armament, Munitions and Chemical Command(AMCCOM) have been developing a new high performance gun that utilizes a liquid propellant charge. This gun, generally referred to as the LP Gun, offers a number of advantages over the conventional gun.This gun uses a proprietary seal design and combustion phenomena known as regenerative technology that allows controlled combustion of a hydroxyl ammonium nitrate (HAN)-based monopropellant to provide superior ballistic performance of the gun. This new design, however, offers significant challenges for materials in general and seal materials in particular. The corrosive nature of the propellant is not only detrimental to materials durability but ensuing corrosion products quite often affect the performance of the propellant. Extreme high temperatures and pressures in combination with thermomechanical fatigue experienced by seals demand performance that no single material can satisfactorily deliver. Consequently, emerging coating technology is being considered for mitigating damage under these severe conditions.Coating processes that can satisfy the need to preserve the heat treatment, the structure and the surface finish of the substrate were given the first priority. Accordingly, thin films deposited by a number of vapor deposition processes were considered. A number of candidate coatings were applied on the substrate structural materials, usually 17-4 PH steel. These coated samples were first screened for compatibility with the LP and the successful candidates were considered for the seals application.

Certain thin films processed by physical vapor deposition (PVD) or chemical vapor deposition (CVD) are extensively used industrially because of their remarkable specific resistance to abrasion, erosion, microwelding and galling, corrosion, high temperature oxidation and radiation damage, and sticking by their lubricity, as well as for their magnetic and dielectric properties. Such coatings

as TiC, TiN, Ti(C, N), $Cr_{23}C_2$, Al_2O_3 and combinations thereof are commonly applied to cemented carbide cutting inserts, high speed steel tools and roller bearing elements used under severe service conditions, of either very high or low temperatures, corrosive environments and where lubrication may be absent. Thin film-coating of tools with TiN is widely practiced because service life between regrinding operations is then lengthened and machine down-time is reduced, hence productivity is increased. Also, the reduced friction characteristics of TiN coatings enable drilling speeds and feeding velocities to be increased in the order of two to three times without significant tool wear. Drilling dynamometer traces confirmed that a coated drill requires less torque and thrust forces (cutting and feed forces) than a conventional steam tempered twist drill [1, 2].

Other common applications of coatings are for electrical contacts, body implants, watches and jewelry (TiN for gold and TiC for silver colors). Deposition of TiN coatings through PVD in vacuum, using evaporation of Ti with an electron beam or arc-discharge, as well as sputtering or atomic bombardment to atomize the target material [3] often leads to poor adhesion to the substrate. This problem can be overcome by plasma-assisted processes, such as PAPVD or PACVD, which yield excellent coatings on a wide range of steel substrates.

It was realized, very early on , that in addition to providing chemical compatibility, the coating process itself played a significant role in the eventual performance of the coating in a 30 mm LP Gun dedicated for seal testing. Hence a screening test for evaluating variations in both the coating process and the resultant coating quality was needed.The structure, integrity, properties and performance of films depend on adhesion to the substrate. Sufficiently good intrinsic cohesive strength of the coating and adhesive strength to the substrate material yield considerably increased tool life and performance of work-pieces. Three significant coating properties are:(1) Elastic strain limit, which is an important parameter related to wear [4, 5]- where a high elastic strain value will inhibit crack initiation and propagation thus reducing wear; (2) hardness, which if high is a dominant property reducing wear (abrasive, adhesive, fretting)- most metal (Al, Ti, W, Hf) nitrides are hard and so are their carbides, borides and oxides; (3) hot hardness which for cutting tools should be as high as possible. Ceramic coatings deposited by PVD or CVD techniques should, therefore, be desirable by providing additional advantages of : (a) Good resistance to abrasion; (b) low friction coefficient, hence good resistance to adhesive wear; (c) low compatibility with substrates, hence greatly reduced possibility of seizure, galling, scuffing and solid solutioning; (d) low thermal conductivity, which makes them good thermal barriers against tool bulk tool heating; (e) good corrosion resistance, such as TiC in sea water and; (f) attractive cosmetic gold color of nitrides, such as TiN, ZrN and HfN. Among these nitrides TiN is the best because of the low cost and the ease of the titanium target manufacturing. ZrN is less hard than TiN and HfN is very expensive.

Coatings deposited by PVD or CVD must meet the following requirements: (1) Good substrate bonding , with no spalling even when the coated substrate is bent by 90°. A higher substrate temperature will limit the formation of columnar crystallites, leading to lower porosity [6]. Good coatings of commercial TiN exhibit a very fine grain size and a high dislocation density; (2) controllable surface topography; (3) uniform coating thickness; (4) high structural integrity and ;(5) reproducible quality through computer-controlled vacuum processing and more rigorous product assurance.

Most of the CVD or PVD-processed thin hard coatings have excellent tribological properties. with a low friction coefficient (μ*) against themselves or steel and are thus very wear resistant [7-11]. Unlubricated bearings with coated balls or rings have been used in high temperature applications [12], or in the high vacuum of outer space [13] very successfully.

The interfacial bond strength or adhesion of the coating to the substrate is a very important property of thin, hard coatings. Poor adhesion leads to "flaking" (adhesive failure), whereas poor cohesion causes chipping (cohesive failure). Adhesion can be evaluated by various techniques some of

which, however, have serious limitations. Among them the "scratch test" first proposed by Heavens [14] and introduced by Benjamin and Weaver [15] has led to consistently meaningful results and is applicable as a quality control tool in production of many different kinds of parts with soft coatings.This method for soft coatings uses other criteria for failure than those pertinent to hard coatings of this study.

A reliable quantitative measurement of adhesion is still elusive [16]. Benjamin and Weaver [15] analyzed the scratch test in detail and showed that the action of the indenter involves plastic deformation of the substrate and that this deformation generates a shearing force at the film/substrate interface around the rim of the indentation produced by the point. This shearing adhesive force was expressed in terms of tip radius, radius of the circle of contact, indentation hardness of the substrate material and critical load, which was defined as the minimum force applied to the stylus that stripped the film cleanly from the substrate leaving a clear channel [14, 15]. Ahn, Mittal and MacQueen [17] established that : (1) A thin film, such as gold on glass may get detached before formation of a cleared track and, conversely an originally clear film may be made optically translucent around the scratch trace without being removed; (2) the form of the track depends on the relative hardness of the film and substrate; (3) stylus size, shape and surface finish, as well as film thickness influence whether failure occurs first in the film, the substrate or at the interface; (4) film detachment often occurs at loads lower than that required for track clearance which appears to depend on film tearing, film pile-up in front of the stylus, as well as the presence of dust and imperfections. The subjectivity of the complete removal criterion led to doubts regarding the quantitative reliability of the scratch test as a measure of thin film adhesion [16, 18]. It was always observed [18] that at stylus loads well below the "critical load" there was some film detachment in spots, within the central portion of the track. Such observations led to the concept of "Threshold Adhesion Failure" (TAF) [16], which occurs if, within the boundaries of a scratch and over its 1-cm path, removal of the film from its substrate can be detected by transmitted light with a microscope at 40X at even one spot, no matter how small. Since each stylus exhibits its own individual scribing and testing characteristics, the TAF mean loads of one thin film sample can only be compared with another or with a "standard", provided that for all measurements the same stylus was used in the same position in the instrument. Stylus loadings should not exceed those levels at which crescent formation of the substrate will occur, if the TAF determination is to be valid.

In scratch testing stresses are introduced at the interface by deforming the surface with a moving diamond tip . The applied load is increased stepwise or continuously until the deformation causes stresses which result in flaking or chipping of their coating. The smallest load at which the coating cracks (cohesive failure) or is detached (adhesive failure) is called the critical load and is determined by optical or electron microscopy, as well as by acoustic emission (AE). Usually, the onset of AE signals and the microscopical observation of the first damage occurring in the coating correlate quite well. The method is used in research as well as in production control. In the automatic scratch test which was developed at LSRH scratches are made at constant translational speed and linearly increasing load, with automatic recording of the AE-Normal Load diagram. The purpose of this work was to use this CSEM-Revetest automatic scratch testing apparatus to compare the quality and soundness of various coatings,and measure their adhesive strength to a given substrate.

EXPERIMENTAL PROCEDURE

The following types of specimens prepared by various processes were used in this investigation: TiB_2-coated MP35N nickel-base alloy specimens; TiN-coated PH 17-4 steel specimens; PH 17-4 steel specimens coated with a ternary Al_2O_3-SiO_2-Cr_2O_3 oxide; and SiC-coated 4340 low alloy steel specimens.

Specimen Preparation

TiB_2-coated MP35N specimens were prepared by a conventional CVD batch process, using a mixture of BCl_3(g) and evaporated $TiCl_4$(l). Deposition temperature was 1000°C and the rate was about 0.6 μm/h.

The TiN film was deposited on PH 17-4 steel specimens by Cathodic Arc PVD, a process using arc evaporation. The advantages of the arc evaporation device are that no molten metal pool is generated and thus the source can be used in any orientation; also the evaporation rate is much higher than with a sputtering source. The process was mainly developed for coating tool and die steels, as well as carbide cutting and forming tools with wear resistant materials. In contrast CVD involves a gaseous chemical reaction and requires elevated substrate temperatures (up to 1050°C) which may be detrimental to the dimensions and metallurgical structure of the components. PVD processes, which are more recent involve vaporizing the coating material inside a vacuum chamber containing the parts to be coated. The process is excellent for parts with critical tolerances because the required substrate temperature is much lower, usually only 150-500°C. For this TiN wear coating applications, the Cathodic Arc PVD process uses multiple arc evaporators to vaporize the coating materials directly from the solid. The vapor energy level is high (50 to 150 eV) and the level of ionization is very high (80-90%). Hence, adhesion is superior. Two different groups of specimens were processed, using different equipment and sets of process variable values.

The Al_2O_3-SiO_2-Cr_2O_3 wear resistant coating was deposited by a CVD batch process on PH 17-4 steel specimens at a temperature of about 1000°C and a rate of about 0.5μm/h. Deposition was followed by heat-treatment to reharden the substructure.

Another type of specimens used herein consisted of SiC-coated 4340 low alloy steel. The SiC coatings were processed through decomposition of silane (SiH_4) and ethylene (CH_2=CH_2) in an RF discharge. The coatings, designated as a-SiC:H invariably contained H_2 and had nominal Si/C ratios of unity, as detected by X-ray photoelectron spectroscopy (XPS). These coatings were partially or totally amorphous. As entrapped hydrogen diffuses out of the coatings resultant shrinkage causes tensile residual stresses in the deposit. It is well established that at elevated substrate temperatures less hydrogen is incorporated in the coatings. Accordingly coatings deposited at elevated temperatures can better retain the compressive stresses generated by ion bombardment than those at low substrate temperatures. Coatings of 0.2, 0.4 and 0.75μm were processed by applying 25W to the substrate electrode at an ion bombardment energy of 90 eV.

Specimen Testing

The soundness and quality of various coatings was evaluated primarily with a CSEM-Revetest automatic scratch testing apparatus (moving diamond tip radius=200 μm and angle 120°), Figure 1a, coupled with an X-Y chart recorder (LINSEIS) with an input impedance Ri >5 KOhm and a sensitivity range S> 1 mV/cm. The apparatus includes a diamond indenter with an original tip radius of 0.2mm, a resonant acoustic emission (AE) detector (Bruel & Kjaer, Denmark) with an AE preamplifier, amplifier and signal converter, a load cell with a load driving motor and a sample table with a driving motor and a screw drive for manual lateral sample stage displacement. Two proximity switches settle the end of the stroke of the sample table and two others limit the end of the stroke of the loading device. Pen-lift of the chart recorder can be achieved either automatically or manually directly from the control unit.

The testing procedure may be summarized as follows: The diamond point first comes down until it touches the surface of the sample. Then the normal load (force Fn) applied to the diamond

immediately starts to increase linearly with time and its instantaneous value is displayed. During the motion of the table the upper load display (min-max) flickers. When this force exceeds the preselected lower load the sample starts to move and continues until the applied force reaches the desired upper load limit.Then the diamond is discharged and lifted-up from the sample surface and the table moves back automatically to its original position, so after lateral translation the equipment is ready for the next test. The adjustable test parameters are: Force range 1-200N, load display: 100 div (full scale= 100/200N), sample table translation speed: 10mm/min and loading rate: 100N/min. Scratch testing is also possible under constant load applied to the diamond point enabling scratching penetration to lie within the coating, at the coating/substrate interface, or within the substrate.

Specimen cross-sections were examined metallographically , Figure 2, to determine film thickness and uniformity of coatings, as well as the presence of porosity or other discontinuities. The free surface of coatings was examined by SEM as was the scratch track morphology.

RESULTS AND DISCUSSION

During a variable load scratch test , Figure 3a, the first acoustic event on an acoustic emission versus load curve corresponds to the crack initiation within the coating at a load L_C (load for cohesive failure). Next the slope of the curve abruptly increases at a load L_A (load for adhesive failure), which corresponds to the propagation of the crack at the coating-substrate interface, causing delamination. Scratch tests were conducted on all specimens. Results may be summarized as follows:

(1) TiB_2 - Coated MP35N Specimens

A photomicrograph of a cross-section of a coated specimen is shown in Figure 2a. The coating thickness is not very uniform and some amount of microporosity is apparent. The results of the scratch test at variable load between 0 and 70N are exhibited ion Figure 3a, where the acoustic emission signal intensi (arbitrary units), the tangential or friction force, Ft (N) and the friction coefficient, μ^* have been plotted versus normal load, Fn (N). The AE curve shows that cohesive failure occurs at a load L_C= 7N and adhesive failure at L_A = 28N. The friction coefficient gradually increases with load from about 0 to 0.75, because of increasing penetration of the diamond point. The same parameters (AE, Ft, and μ^*) have been plotted in Figure 1b at constant load versus time. Selected loads were: 4N (below L_C), 6N (about equal to L_C), 10N (above L_C) where the scratch lies entirely inside the coating and 29N (above L_A) where the scratch penetrates into the substrate. At a load of 4N there is no acoustic emission, because the corresponding stress is below the yield point of the coating material.

Figures 4a-d are scanning electron micrographs illustrating the morphology of the scratch obtained under variable load (0 -70N). A top view of the virgin coating illustrated in Figure 4a and scratch morphology is shown in Figures 4b-d. Figure 4b corresponds to the beginning of the scratch and to a load 35-40N. Some remaining islands of the film are still visible on the nickel-base substrate. Figure 4c corresponds to the middle of the scratch at a load of about 50-55N. All the film has by now been removed and crescent shaped cracks appear on the substrate surface. Figure 4d illustrates the morphology of the end of the scratch.

(2) TiN - Coated PH 17-4 Steel Specimens

Two different types of specimens, I and II, produced by different manufacturers were evaluated by scratch testing. A photomicrograph of a cross-section of specimen I is illustrated in Fig. 2b. The coating thickness is uniform and the coating-substrate interface appears to be sound, hence

adhesion is expected to be good. In Fig. 3b the AE responses of both specimens and the friction coefficients, μ^*, have been plotted versus normal load, Fn, which varied between 0 and 75N. For specimen I L_C=31N and L_A = 37N. For specimen II both the cohesive and adhesive failure loads were substantially lower. The friction coefficient, μ^* is about 0.3 for both specimens. Figures 2c and d show that the coating on specimen II is very thin, of nonuniform thickness and locally discontinuous. It is clear that the friction coefficient of TiN coatings is less than that of TiB_2. The friction coefficient $\mu^* = \mu p + \mu a$, where μp is the ploughing component and μa is the adhesive component. Though the surface of TiN coatings is smoother than that of TiB_2, hence the ploughing component for TiN is expected to be lower than that of TiB_2, it is still believed that the adhesive component for TiN is also much lower than that of TiB_2, hence the abrasive wear resistance of the nitride should be superior to that of boride. Figure 5 illustrates SE micrographs of a scratch on TiN-coated PH 17-4 steel specimen I performed with a variable load between 0 and 70N. Figures 5a and b correspond to two locations at which the loads were 40-45N, 55-60N and 65-70N, respectively. In Figure 5a longitudinal striations appear in the coating. In Figure 5b the remaining islands of TiN are clearly visible with a crescent-like arrangement. Figure 8c shows a scanning electron micrograph of a scratch on TiN-coated PH 17-4 steel specimen II. Removal of TiN coating in the track occurs at a significantly lower load.

(3) (Al_2O_3 - SiO_2 - Cr_2O_3) - Coated PH 17-4 Steel Specimens

The cross-section of this specimen is illustrated in Figure 2e. The coating is thick, uniform and continuous.Figure 3c shows for this coating and for a variable load test, between 0 and 75N, an L_C = 22N and L_A = 38N. The friction coefficient gradually increases with increasing normal load to about 0.3, which is approximately equal to that of TiN. Scanning electron micrographs of a scratch on this coating for a linearly variable load between 0 and 70N are illustrated in Figure 6a for the beginning of the scratch (38 - 53N) and in Figure 6b for the end of the scratch (60-65N).

(4) Plasma Enhanced CVD SiC-Coated 4340 Steel Specimens

AE, the tangential or frictional load and the friction coefficient were plotted versus variable load between 0 and 80N, Fig 3d. In this case L_C = 17N and L_A = 33N. They are both lower than that of TiN, which shows that the latter is a superior coating. The friction coefficient μ^* , of SiC on the other hand is comparable to that of TiN.

SUMMARY

The CSEM-Revetest automatic scratch testing apparatus was used for evaluating the quality and soundness of various coatings: TiB_2 on MP35N alloy, TiN on PH 17-4 steel, Al_2O_3 - SiO_2 - Cr_2O_3 on PH 17-4 steel and PECVD SiC on 4340 low alloy steel. The scratch test gives the acoustic emission signal intensity, frictional or tangential force and the scratching or friction coefficient versus load, or versus time at constant load. It was concluded that TiN-coated PH 17-4 steel specimens of Type I exhibited higher cohesive and adhesive loads than the Type II coated specimen or the other specimens tested, as well as a lower friction coefficient, which would imply that the type I specimens should also.exhibit a better abrasive wear resistance.

REFERENCES

1. R.H. Thornley and D.P. Upton, "The Effect of Titanium Nitride Coatings on Cutting Tools", presented at "Fintech Symposium", Espoo, Finland, March 17-21, 1986.
2. A. Thomas and P. Thomson, "Performance and Wear Characteristics of TiN-Coated Drills" presented at the "Plasma-Assisted Coatings Technology" seminar (Cutting Tools), National Center of Tribology, U.K, June 11, 1986.
3. A. Matthews, Surface Engineering, 1, 93 (1985).

4. T.S. Oberle, J. of Met., 3, 438 (1958).
5. N.P. Suh, Wear, 25, 111 (1973).
6. J. Thornton, J. Ann. Rev. Mater. Sci., 7, 239 (1977)
7. H.E. Hintermann, J. Vac. Sci. Technol. B2, 2, 816 (1984).
8. V. Linial and H. E. Hintermann, in Proceedings of the Conference on "Wear of Materials", K.C. Ludema, W. A. Glaser and S.K. Rhee, eds., ASME, 403 (1979).
9. H.E. Hintermann, Tribol Int., 13, 267 (1980).
10. K.H. Habig, W. Evers and H.E. Hintermann , Z. Werkstofftech, 11, 182 (1980).
11. H.E. Hintermann, Thin Solid Films, 8a, 215 (1981).
12. H.E. Hintermann, H. Boring and W. Hanni, Wear 38, 225 (1978).
13. M. Maillat, H. Boring and H.E. Hintermann, Proceed of the Space Tribology Workshop, Risley, GB, 3 (1980).
14. O.S. Heavens, J. Phys and Rad., 11, 355 (1950).
15. P. Benjamin and C. Weaver, Proc. Royal Society. A 254, 163 (1980).
16. J. Oroshnik and W.K. Croll, in "Adhesive Measurements of Thin Films, Thick Films and Bulk Coatings", ASTM STP 640, K.L. Mittal, ed., ASTM, 158 (1978).
17. J. Ahn, K.L. Mittal and R.H. MacQueen, in "Adhesive Measurement of Thin Films, Thick Films and Bulk Coatings", ASTM STP 640, K. L. Mittal , ed., ASTM, 139 (1978).
18. D.W. Butler, C.T.H. Stoddart and P.R. Stuart, J. of Physics, (D), 3, 877 (1970).

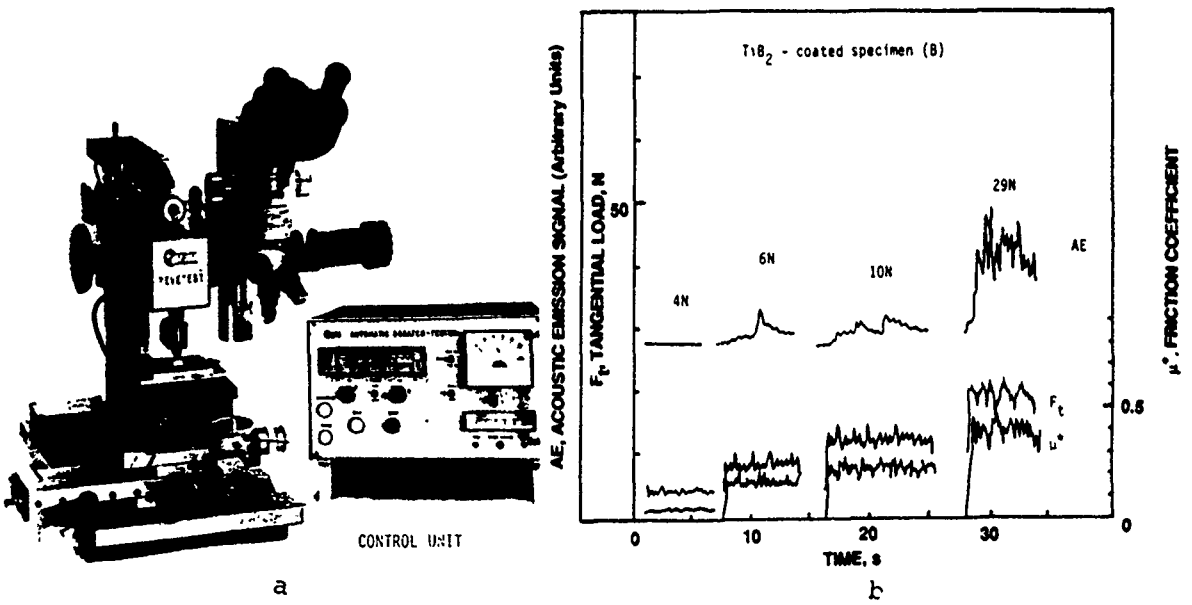

Figure 1: (a) Overall view of the CSEM-Revetest scratch tester. (b) Acoustic emission signal (AE), tangential or frictional load and friction coefficient versus time at various constant loads. TiB_2-coated MP35N specimen.

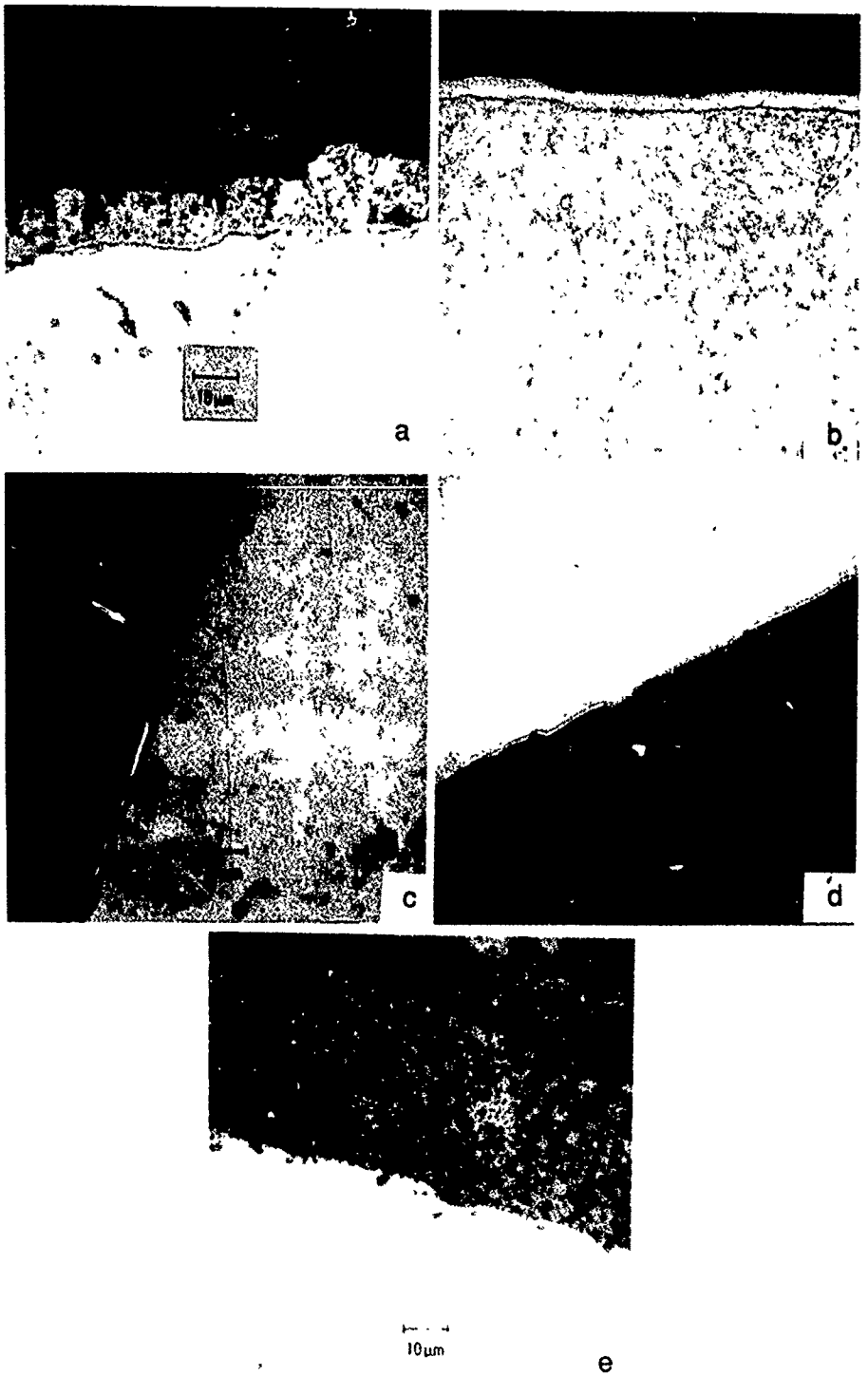

Figure 2: Photomicrographs of cross-sections of various coated specimens. (a) TiB_2-coated MP35N nickel-base alloy, (b) TiN-coated PH 17-4 steel, Type I, etched with picral, (c),(d) TiN-coated PH 17-4 steel, Type II and (e) (Al_2O_3-SiO_2-Cr_2O_3)-coated PH 17-4 steel.

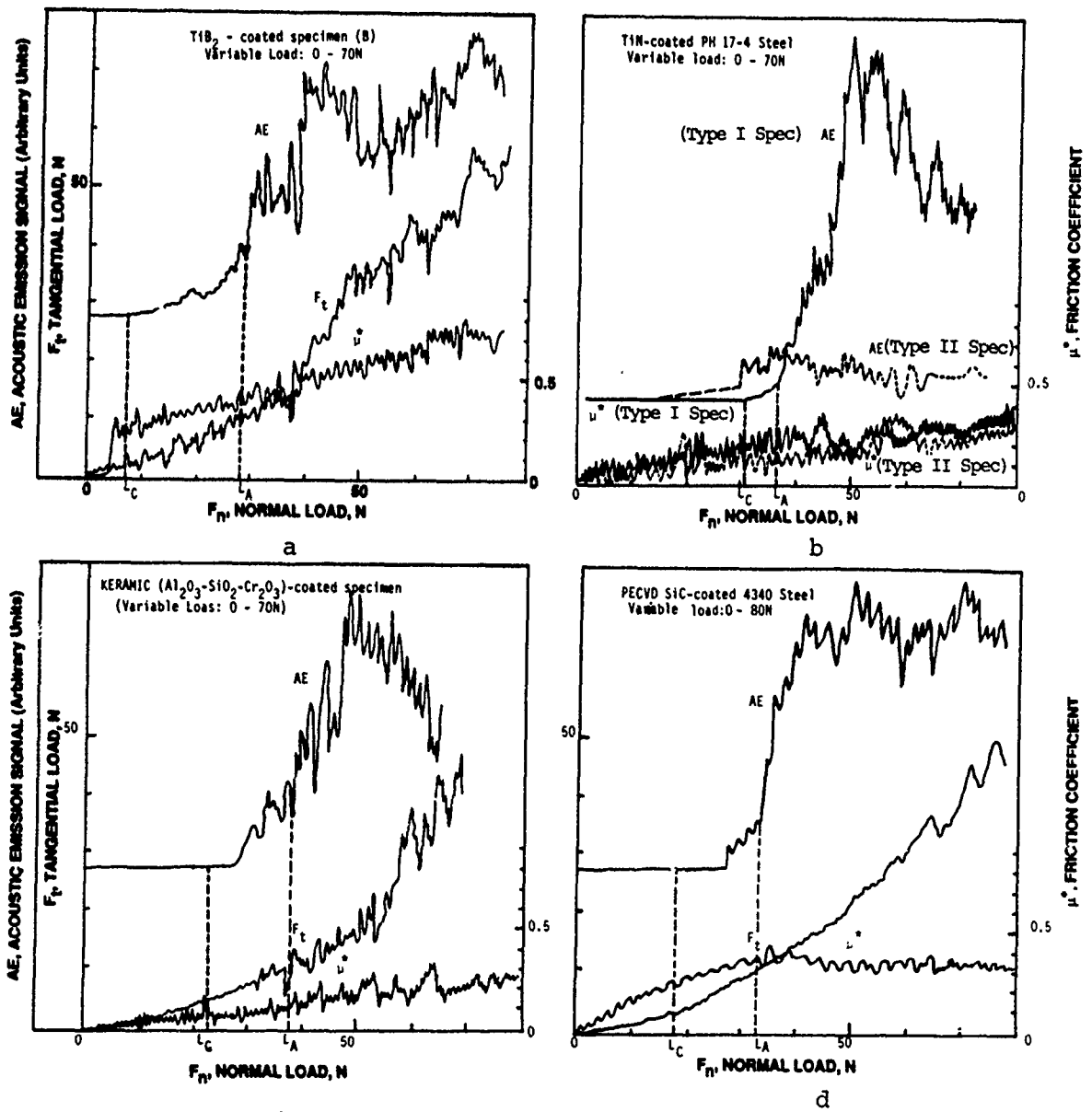

Figure 3: Acoustic emission signal (AE, arbitrary units), tangential or frictional load and friction coefficient versus normal load, variable between 0 and 70N. (a) TiB_2-coated MP35N nickel-base alloy, (b) TiN-coated PH 17-4 steel, Types I and II, (c) $(Al_2O_3-SiO_2-Cr_2O_3)$-coated PH 17-4 steel and (d) PECVD SiC-coated 4340 low alloy steel.

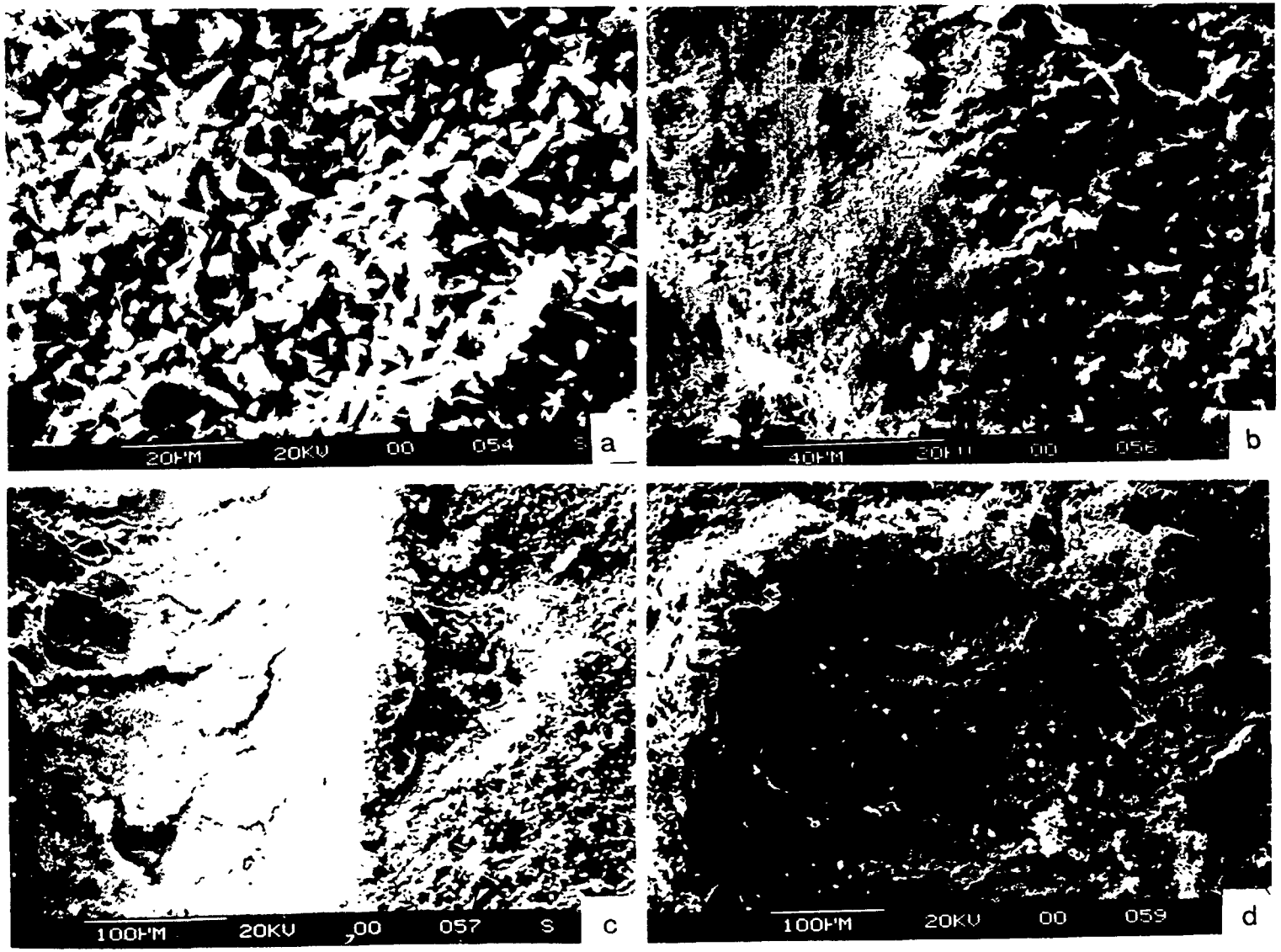

Figure 4: Scanning electron micrographs of the surface of TiB_2-coated MP35N nickel-base alloy (a) and of the scratch near its beginning (b), middle (c) and end (d).

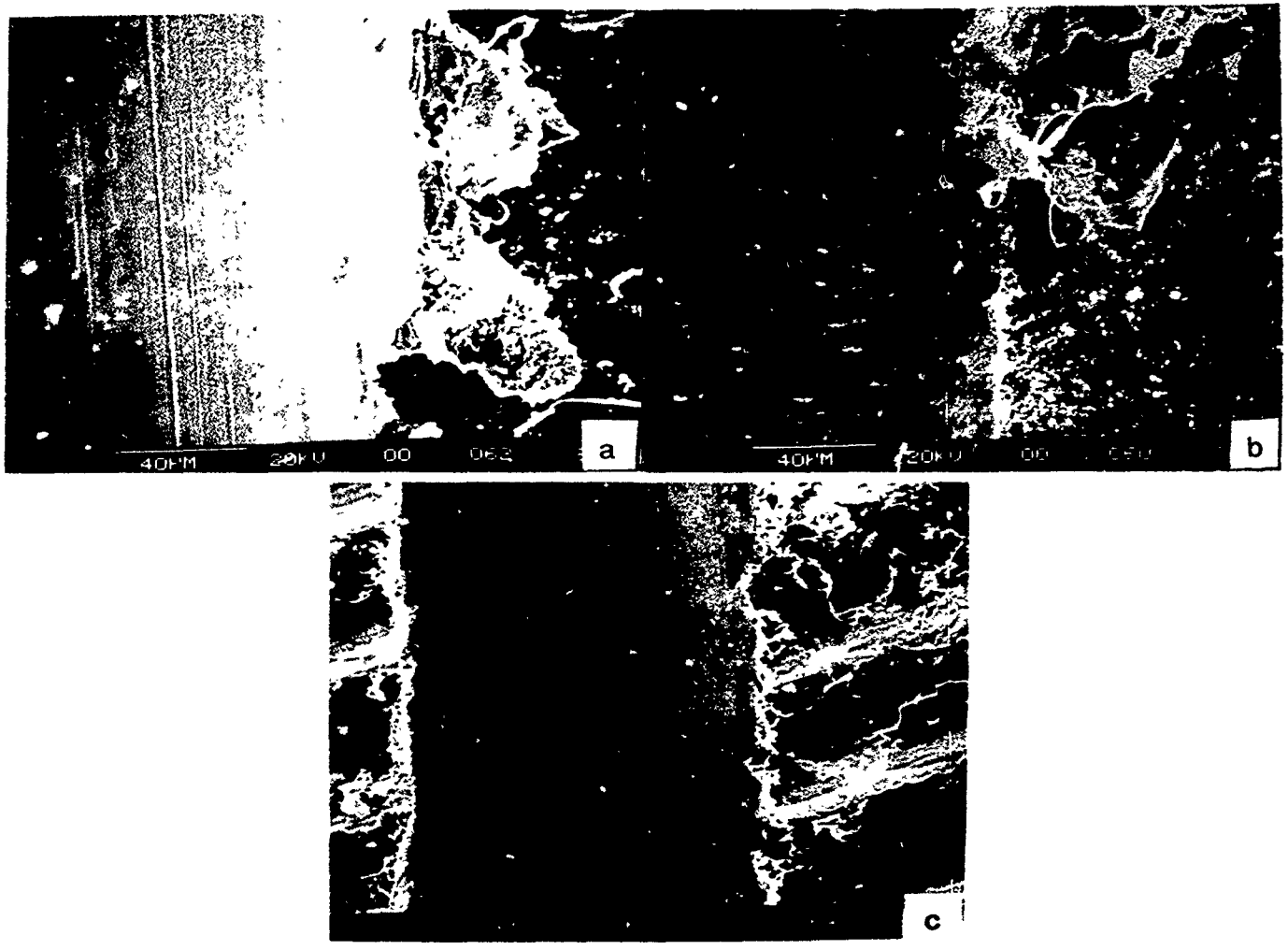

Figure 5: Scanning electron micrographs of scratches in TiN-coated PH 17-4 steel specimens. (a),(b) Type I specimen. Micrograph (a) was taken close to the beginning of the scratch and (b) farther away. (c) Type II specimen. Micrograph was taken very close to the beginning of the scratch.

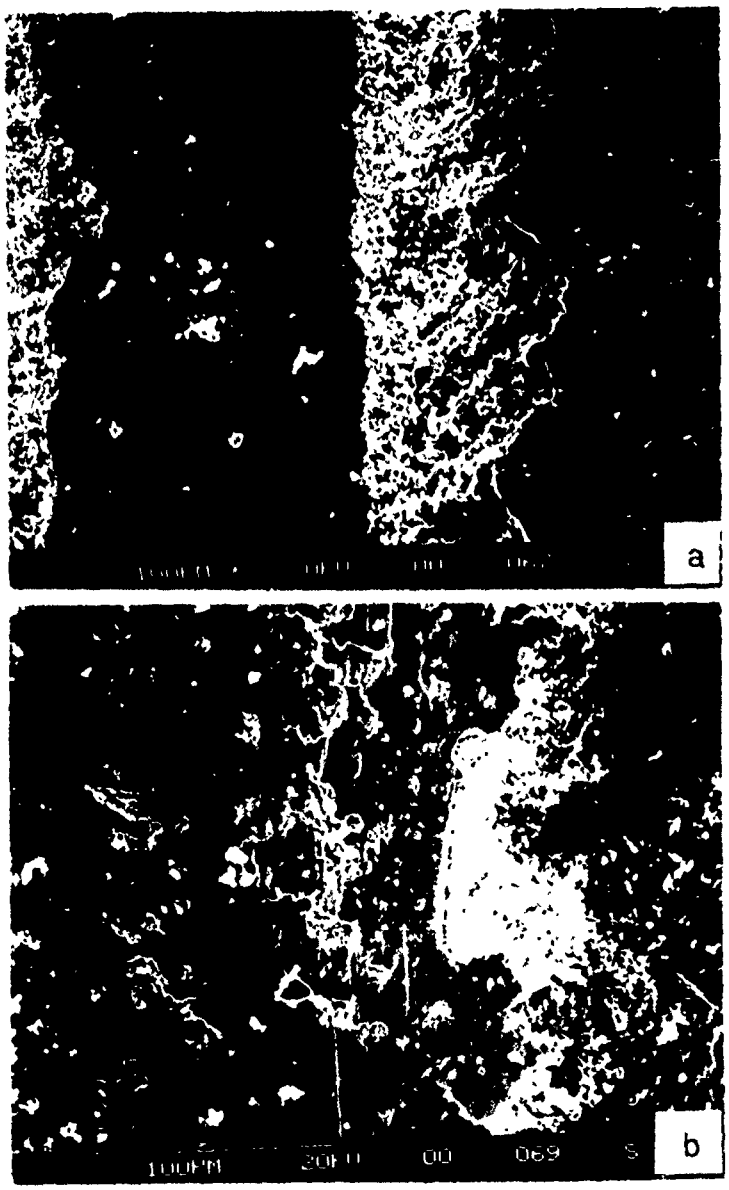

Figure 6: Scanning electron micrographs of a scratch in (Al_2O_3-SiO_2-Cr_2O_3)-coated PH 17-4 steel specimen taken closer to the beginning of the scratch (a) and farther away (b).

ALUMINUM CORROSION CAUSED BY AQUEOUS ZINC ION

Robert Summitt and Rajayya Manesh
Metallurgy, Mechanics and Materials Science
Michigan State University
East Lansing, Michigan 48824

ABSTRACT

Zinc exposed to the atmosphere is coated with a slightly soluble film of basic zinc carbonate; its solubility is increased when atmospheric sulfur dioxide is present. Thus water in contact with zinc contains 90 umol/l or more of zinc ion. Aluminum is anodic to zinc in the electromotive series, and aluminum alloys are anodic to zinc in salt water, consequently aqueous solutions of zinc ion are corrosive to aluminum alloys. Immersion exposure tests and galvanostatic/ potentiostatic measurements have been performed in order to determine the corrosion rates of AA-2024 in the presence of zinc ion. The results show that the use of zinc-coated steel fasteners with aluminum alloys will create a corrosive environment for aluminum alloys if water is present.

[Manuscript Not Available at the Time of Printing]

THE ELECTRON NUMBER DIAGRAM: A NEW TOOL FOR ANALYSIS OF AQUEOUS REDOX SYSTEMS

Michael J. Zappia
John C. Angus
Rebecca Yung

Department of Chemical Engineering
Case Western Reserve University
Cleveland, OH 44106

The electron number diagram is a new kind of phase diagram designed for the graphical display and analysis of complex, aqueous redox systems. In this approach the electrons are treated as a separate chemical component. The resulting diagrams are the electrochemical analog of conventional metallurgical T–x diagrams, long used in process metallurgy. They have many conceptual and practical advantages for analyzing processes that take place in aqueous corrosion, hydrometallurgy and the electrodeposition of compounds, for example, gallium arsenide.

Current research includes the experimental confirmation of computed diagrams for the aqueous sulfur system. A preliminary experimental electron number diagram for the aqueous sulfur system at pH = 2.8 has been constructed.

Algorithms for the construction of diagrams for systems containing two redox elements, such as the Fe–S, In–Sb and U–C systems, have been developed. Three–dimensional equilibrium diagrams for use in complex redox systems have been constructed in three different forms. The results are illustrated using the aqueous Ga–As, Cd–Te and U–C systems. Regimes leading to enhanced solubility of uranium compounds when complexing agents such as fluoride ion are present are illustrated. Conditions under which direct electrodeposition of III–V and II–VI compounds, e.g., CdTe, can be expected are determined.

INTRODUCTION

A phase diagram is a useful means of summarizing large amounts of thermodynamic information in a convenient, compact form. This thermodynamic information can be used to understand the behavior of very complex chemical systems and to plan experiments and interpret experimental data.

Various types of phase diagrams have been developed for electrochemical systems. Potential–pH diagrams are the most familiar and have been applied in corrosion studies, hydrometallurgy, geologic studies and electrodeposition. Potential–pH diagrams display the

stability of chemical species on a field of potential (E) versus pH. The authors have previously developed a thermodynamic framework for systems containing one redox element, which they applied to the calculation and geometric interpretation of Pourbaix diagrams (1) and potential–pH diagrams for complex systems (2). Within this framework, an efficient computational algorithm for the construction of potential–pH diagrams was developed. This algorithm represented a significant departure from previous computer methods (3,4).

However, because potential is not a conserved quantity, the use of potential–pH diagrams is not convenient in all cases. For example, a point cannot be located on a potential–pH diagram from a knowledge of composition. It is also difficult to follow process trajectories on these diagrams. Finally, the relationship between potential and composition is not always clear. Large potential changes sometimes occur over very small composition ranges, while large composition changes can occur at constant potentials.

ELECTRON NUMBER DIAGRAMS

The electron number diagram is a new graphical representation of multiphase equilibrium in aqueous redox systems (5). The electron number diagram is a transformed potential–pH diagram in which potential is replaced by its thermodynamic conjugate, the electron number. The electron number is a measure of the number of electrons per atom of active redox element and thus a conserved quantity. In the case of a system containing a single redox element, such as the aqueous copper system, the electron number of a copper species is numerically equal to its electrochemical valence. Electron number diagrams can be used with potential–pH diagrams to provide a more complete understanding of the thermodynamic structure of an aqueous redox system.

On an electron number diagram, phase stability at a fixed pH is displayed on a field of the logarithm of the activity of the active element versus the average electron number $\bar{z}$ of the active element. Figure 1 shows the electron number diagram for the aqueous uranium system at pH = 4. Electron number diagrams often exhibit features resembling eutectics, peritectics and congruent dissolving points. All of these features appear in Figure 1.

Figure 1 and the other calculated figures in this paper were constructed using tabulated free energy data at 25 °C and 1 bar (6,7,8). Potentials are given with reference to the normal hydrogen electrode. Pure solid phases and ideal aqueous solutions were assumed in calculating these figures. Consequently, activities and concentrations are used interchangeably. While convenient, this assumption is not necessary. The equilibrium calculations yield values of activity; concentrations may then be determined using appropriate activity coefficient data or solution models.

Three types of regions appear on electron number diagrams. In the single–phase aqueous region, no solid phases are stable. In a two–phase region, a single solid exists in equilibrium with the aqueous phase. Notice that in the two–phase regions the constant potential lines also serve as tie lines. Figure 1 (drawn for pH = 4) shows that at $-\log_{10}[U]_{aq} = 8.48$, and E = 0.15 V, solid UO_2, for which z = 4, exists in equilibrium with a solution for which $\bar{z} = 5.65$. In a two–phase region, the relative amounts of uranium in the solid phase and in the aqueous phase can be determined using the inverse lever arm rule along the appropriate tie line. In the inaccessible region, below the lowest–lying horizontal lines, the system cannot exist in equilibrium because solubility limits would be exceeded. Along each of the horizontal lines dividing the two–phase and inaccessible regions, two solids and the aqueous phase are stable. For example, again referring to Figure 1, at $-\log_{10}[U]_{aq} = 1.96$, the solids U and UO_2 are in

equilibrium with an aqueous phase for which $\bar{z} = 3$.

Because electron number is a conserved quantity, graphical material balances can be performed and process trajectories can be followed on electron number diagrams. A process which involves no net transfer of electrons to or from the system takes place at constant $\bar{z}$ and thus lies on a vertical line on an electron number diagram. For example, evaporation paths at constant $\bar{z}$ can be used to predict which solids form as an aqueous solution is concentrated at constant pH. Evaporation and dilution trajectories can be followed at constant potential as well as at constant $\bar{z}$. Processes that involve a net increase or decrease in the number of electrons in a system at constant concentration and pH lie on horizontal lines on an electron number diagram. Mixing processes can also be shown on electron number diagrams; graphical material balances can be used to determine the electron number of the system that results from the combination of systems of known $\bar{z}$ and concentration.

PRELIMINARY EXPERIMENTAL ELECTRON NUMBER DIAGRAM FOR THE AQUEOUS SULFUR SYSTEM

A preliminary electron number diagram for the aqueous sulfur system at 25 °C and pH = 2.8 ± 0.3 has been constructed. The diagram shown in Figure 2 includes experimental data and a solid line indicating the phase boundary predicted by thermodynamic calculations. Inside the two–phase envelope, solid sulfur exists in equilibrium with dissolved sulfur–containing species; outside, sulfur is stable only in the aqueous phase.

Two different types of experiments have been used to obtain the data needed to construct an experimental electron number diagram. In the first type of experiment, solutions of sodium sulfide ($\bar{z} = -2$) and sodium sulfite ($\bar{z} = 4$) are mixed to give a solution for which 0.03 M $\leq [S]_{aq} \leq$ 0.4 M and $-2 < \bar{z} < 2$. Acidification of these solutions into the pH range of interest causes the precipitation of solid sulfur. The distribution of sulfur between the solid and aqueous phases, determined by chemical analysis, is used with sulfur and electron balances to determine the electron number of the aqueous phase in equilibrium with solid sulfur. This gives a point on the two–phase envelope.

The data obtained in this manner agree with the computed diagram on the location of the right side of the two–phase boundary near $\bar{z} = 2$; however, the the data show far greater solubility than the calculations predict at intermediate values of $\bar{z}$, e.g., near $\bar{z} = 0$. See Figure 2. The formation of metastable intermediates and colloidal sulfur, and sluggish kinetics could contribute to this difference. The solutions used in these experiments are similar to Wackenroder's liquid, a complex, metastable mixture of sulfur species including colloidal sulfur (9,10).

The failure to include important species in the database used to calculate the theoretical diagram could also be significant. For example, protonated polysulfides have not been included in the theoretical calculations because of the unavailability of data. Thionates have also been excluded from this calculation.

The second type of experiment is a direct determination of the two–phase envelope by determining whether or not a solid phase precipitates. A solution of known electron number and concentration, which defines a point ($\bar{z}$, $-\log_{10}[S]_{aq}$) on an electron number diagram, is acidified into the range of interest. If the solution remains clear, then the point ($\bar{z}$, $-\log_{10}[S]_{aq}$) is outside the two–phase region; if solid sulfur forms, then the point is inside the envelope. By considering a series of closely spaced solutions, the location of the phase

boundary can be determined.

The data from the direct determinations show a sulfur solubility much closer to that predicted by the calculations. See Figure 2. The major uncertainty of the visual method involves the detection of an extremely small amount of dispersed solid sulfur. This problem is being addressed by directing a laser beam through the solution. Colloidal sulfur, even in very small quantities, causes scattering that is visible as a line through the solution. Preliminary tests with a 5–mWatt He–Ne laser suggest that sulfur solubility is lower than that indicated by the direct determination test data in Figure 2. This would move the experimental two–phase boundary even closer to that predicted by theory.

That the two different types of experiments produce different apparent sulfur solubility curves is not surprising. The sulfur and electron balance experiments use relatively concentrated solutions, which begin to precipitate sulfur at $5 < pH < 7$ and form large amounts of solid S. The formation of large amounts of high molecular weight metastable polysulfides in this environment could account for the large apparent sulfur solubility, greater than that predicted by the calculations. For electron numbers near $\bar{z} = 0$, the direct tests use very dilute solutions and solid S forms in very small amounts (if at all) near pH = 3. Polysulfides are less likely to form in these dilute solutions. Further experimental work and more theoretical calculations using an expanded database will be needed before final conclusions can be drawn.

SYSTEMS CONTAINING TWO REDOX ELEMENTS

Many aqueous systems of great interest, such as Fe–S, In–Sb and U–C, contain two active redox elements. As a logical extension of previous work for systems containing a single active redox element, a thermodynamic framework for the generation of phase diagrams for binary aqueous systems (i.e., systems containing two active redox elements) has been developed (11).

Three independent intensive variables must be fixed to specify equilibrium in a binary redox system at constant pH, temperature and pressure. For a system containing active redox elements M and N, the three intensive variables chosen are the potential E and the chemical potentials of the two redox elements. Once the equilibrium problem has been solved in the computationally convenient space given by E, μ_m/RT, and μ_n/RT, the equilibrium surface can be constructed in this chemical potential space. Figure 3 shows the equilibrium surface for the aqueous U–C system at pH = 4. On the surface of the figure, a single solid phase exists in equilibrium with the aqueous phase. Inside the surface (at lower chemical potentials), a single aqueous phase exists; outside the surface (at higher chemical potentials), the system cannot exist in equilibrium.

The equilibrium surface from chemical potential space can also be reconstructed in other three dimensional spaces, such as $-\log_{10}[M]_{aq}/\ -\log_{10}[N]_{aq}/E$ space or $\bar{z}/\ -\log_{10}[M]_{aq}/\ -\log_{10}[N]_{aq}$ space. These alternative representations are constructed from the same thermodynamic information but can provide further insight into the structure of the aqueous redox system. Figure 4 shows the equilibrium diagram for the aqueous U–C system at pH = 4 in $-\log_{10}[U]_{aq}/\ -\log_{10}[C]_{aq}/$ E space. These diagrams have been drawn using extremely wide concentration ranges to illustrate the structure of the diagrams and to show the extreme insolubility of some of the solids. Also, it should be noted that some regions of the diagrams can exist only with very large H_2 and O_2 pressures. Each constant potential line at constant pH corresponds to fixed pressures of both H_2 and O_2.

The U–C equilibrium diagram in Figure 4 is a surface in three–dimensional space. On the surface, a solid phase is in equilibrium with the aqueous phase. Above the surface, the system is undersaturated, so no solid phases exist in equilibrium; the volume below the surface is inaccessible in equilibrium because the solubility limit is exceeded. Note that two solids can coexist in equilibrium with the aqueous phase along a line formed by the intersection of the equilibrium surfaces of two solids; four phase invariant points, where three solids and the aqueous phase are stable, also appear on the diagram.

Diagrams of this type can be used to compare solubilities of solids as a function of pH and activities of complexing species. For example, this information could be used in the study of the leaching of uranium solids into groundwater. Figure 5 shows the equilibrium surface for the U–C–F^- system at pH = 4 and a fluoride activity of 0.1. Notice the increased solubility of uranium, compared with Figure 4, in which F^- was not included. In the U–C–F^- system shown in Figure 5, fluoride ion is assumed to undergo no redox transitions.

Another application of these diagrams is in the study of the electrodeposition of III–V semiconductors from aqueous solutions. Figure 6 shows the three dimensional equilibrium surface for the aqueous Ga–As system at pH = 13. Notice the low potentials, favoring hydrogen evolution, in the regions where GaAs is stable. Constant $-\log_{10}[Ga]_{aq}$ contours are shown on the surface. Figures 7 and 8 show the equilibrium surfaces for the aqueous Cd–Te system at pH = 2.5 and pH = 10, respectively. In Figure 8, the equilibrium surface for $Cd(OH)_2$, which lies in the $-\log_{10}[Cd] = 5.2$ plane, is not shown, as it would obscure other parts of the diagram. Constant $-\log_{10}[Cd]_{aq}$ contours show the shape of the surface. These diagrams permit one to identify regions which will minimize the co–evolution of hydrogen while GaAs or CdTe is being deposited.

Electron number diagrams for binary systems can be constructed, provided that electron number has been defined for a species containing two active redox elements. The standard formation reaction for a species S_k containing active redox elements M and N and complexing species X and Y can be written as:

$$\left[\frac{\alpha_m}{\alpha_m + \alpha_n}\right]_k M + \left[\frac{\alpha_n}{\alpha_m + \alpha_n}\right]_k N = \left[\frac{1}{\alpha_m + \alpha_n}\right]_k S_k + h_k H^+ + w_k H_2O + x_k X + y_k Y + z_k e^-$$

where α_m is the number of atoms of element M per molecule of species S_k and α_n is the number of atoms of element N per molecule of species S_k. Note that the formation reaction, in this normalized form, is written for a total of one mole of active redox element. Thus, the electron number of a species S_k, containing two active redox elements, can be unambiguously identified with the coefficient z_k in the above equation.

For example, the standard formation reaction for $UO_2(CO_3)_2^{2-}$ is written as:

$$\frac{1}{3} U + \frac{2}{3} C = \frac{1}{3} UO_2(CO_3)_2^{2-} + \frac{16}{3} H^+ - \frac{8}{3} H_2O + \frac{14}{3} e^-$$

where $\alpha_U = 1$, $\alpha_C = 2$, $h = 16 / 3$, $w = -8 / 3$, $z = 14 / 3$, $x = 0$ and $y = 0$.

The equilibrium surface for the aqueous Cd–Te system at pH = 10, shown in Figure 8 in $E/ -\log_{10}[Te]_{aq}/ -\log_{10}[Cd]_{aq}$ space, can be replotted in $\bar{z}/ -\log_{10}[Te]_{aq}/ -\log_{10}[Cd]_{aq}$ space. The three dimensional electron number diagram for the aqueous phase in equilibrium with solid

CdTe is shown in Figure 9. Contours of constant $-\log_{10}[Cd]_{aq}$ have been plotted to show the curvature of the surface. Each point on this aqueous surface is in equilibrium with CdTe. A complete diagram would therefore show tie lines between the aqueous surface and CdTe, i.e., the $\bar{z} = 0$ plane. These tie lines have been omitted for purposes of clarity. Notice how the composition of the solution in equilibrium with CdTe changes over the range of the solid's stability.

CONCLUSIONS

The electron number diagram, a new graphical representation of phase equilibrium in aqueous redox systems, has been developed. The use of electron number, a conserved quantity, as a variable allows graphical material balances to be performed on the diagrams. Process trajectories can also be followed on these diagrams, which are the electrochemical analog of conventional metallurgical T–x diagrams. Electron number diagrams provide information complementary to that given by potential–pH diagrams and have applications in many areas including corrosion studies, hydrometallurgy, geologic studies and electrodeposition.

A preliminary experimental electron number diagram has been constructed for the aqueous sulfur system at pH = 2.8. Two types of experiments have been used to map out the boundary of the two–phase envelope in which solid sulfur and the aqueous phase coexist in equilibrium. Current experimental data show greater solubility than predicted by theory, but more sensitive experimental methods and an expanded database for the computed diagrams are being investigated.

A thermodynamic framework for the generation of electrochemical phase diagrams for systems containing two redox elements has been developed. Three–dimensional equilibrium diagrams have been constructed at constant pH in a chemical potential/ electrochemical potential space, in concentration/ electrochemical space and in concentration/ electron number space.

REFERENCES

1. Angus, J.C.; Angus, C.T. *J. Electrochem. Soc.* **1985**, 132, 1014.
2. Angus, J.C.; Lu, B.; Zappia, M.J. *J. Applied Electrochem.* **1987**, 17, 1.
3. Barry, T.I.; in "Thermodynamics of Aqueous Solutions with Industrial Applications"; ACS Symposium Series 133 (edited by Newman, S.A.); ACS: Washington, DC, 1980; 681.
4. Linkson, P.B.; Phillips, B.E.; Rowles, C.D. *Miner. Sci. Eng.* **1979**, 11, 65.
5. Angus, J.C.; Zappia, M.J. *J. Electrochem. Soc.* **1987**, 134, 1374.
6. Wagman, D.D.; Evans, W.H.; Parker, V.P.; Schumm, R.H.; Halow, I.: Bailey, S.M.; Churney, K.L.; Nuttal, R.L. "The NBS Tables of Chemical Thermodynamic Properties: Selected Values for Inorganic and C_1 and C_2 Organic Substances in SI Units"; National Bureau of Standards: Washington, D.C., 1982.
7. Pourbaix, M. "Atlas of Electrochemical Equilibria in Aqueous Solution"; Pergamon: New York, 1966.
8. Langmuir, D. *Geochim. Cosmochim. Acta* **1978**, 42, 547.
9. Nickless, G. "Inorganic Sulphur Chemistry"; Elsevier: Amsterdam, 1968.
10. Karchmer,J.H. "The Analytical Chemistry of Sulfur and its Compounds: Part 1"; Wiley–Interscience: New York, 1970.
11. Zappia, M.J., Ph.D. Dissertation, Case Western Reserve University, 1989.

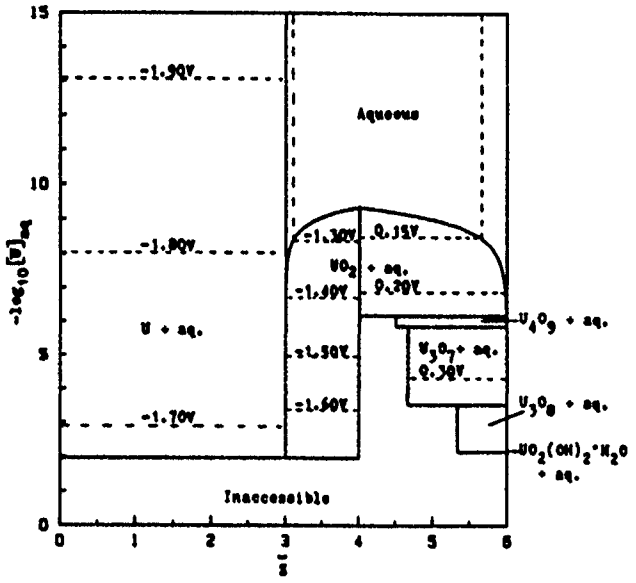

Figure 1. The aqueous uranium system at pH = 4.

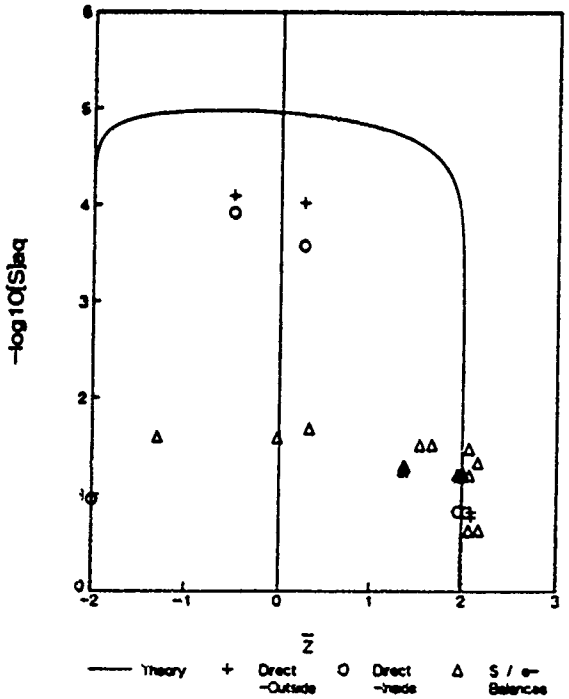

Figure 2. Preliminary experimental electron number for the aqueous sulfur system at pH = 2.8 ± 0.3.

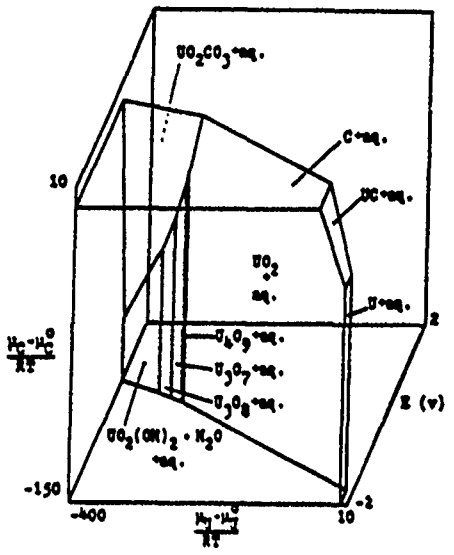

Figure 3. The aqueous U–C system at pH = 4.

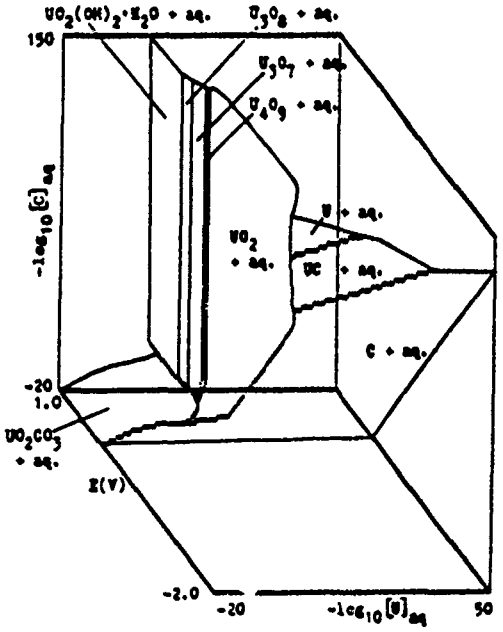

Figure 4. The aqueous U–C system at pH = 4.

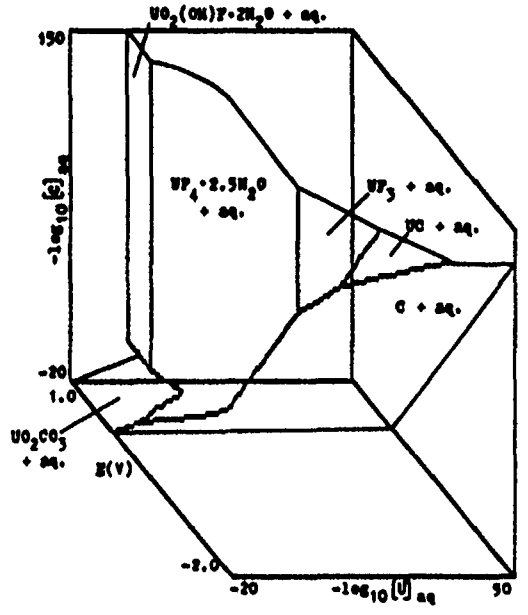

Figure 5. The aqueous U–C–F^- system at pH = 4, $a_{F^-} = 0.1$.

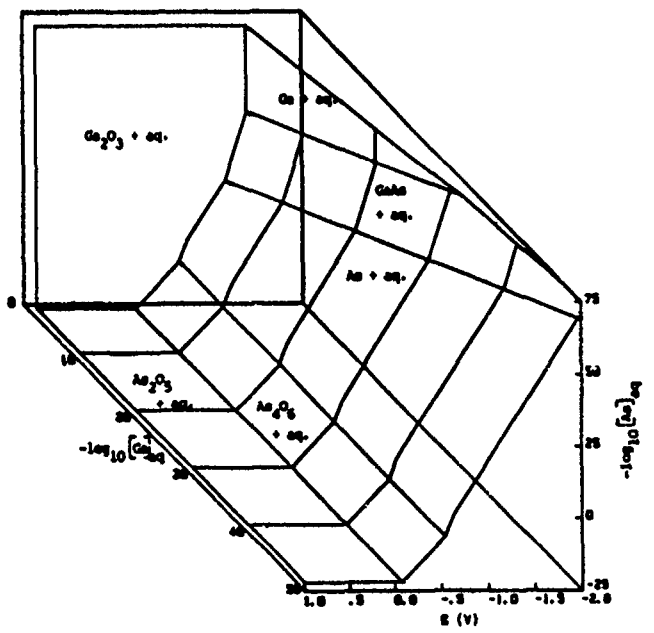

Figure 6. The aqueous Ga–As system at pH = 13.

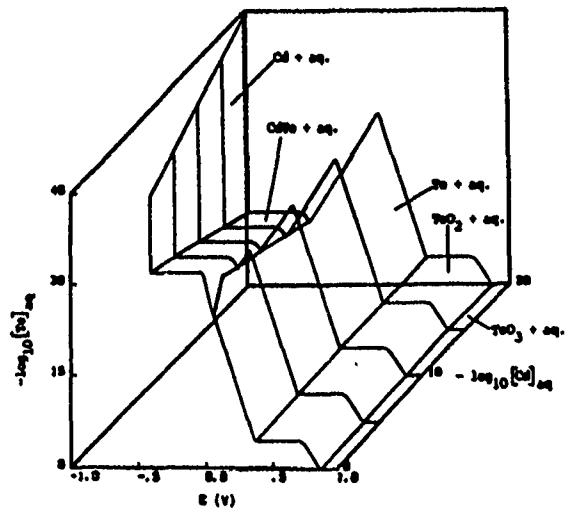

Figure 7. The aqueous Cd–Te system at pH = 2.5.

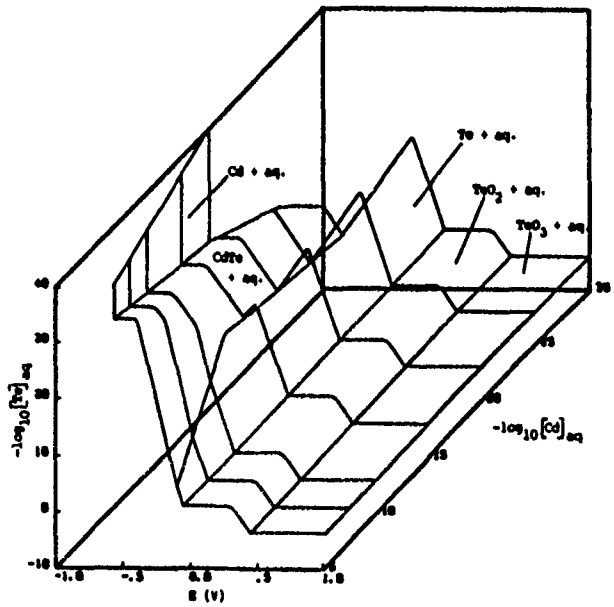

Figure 8. The aqueous Cd–Te system at pH = 10. Stable surface for $Cd(OH)_2$ is not shown.

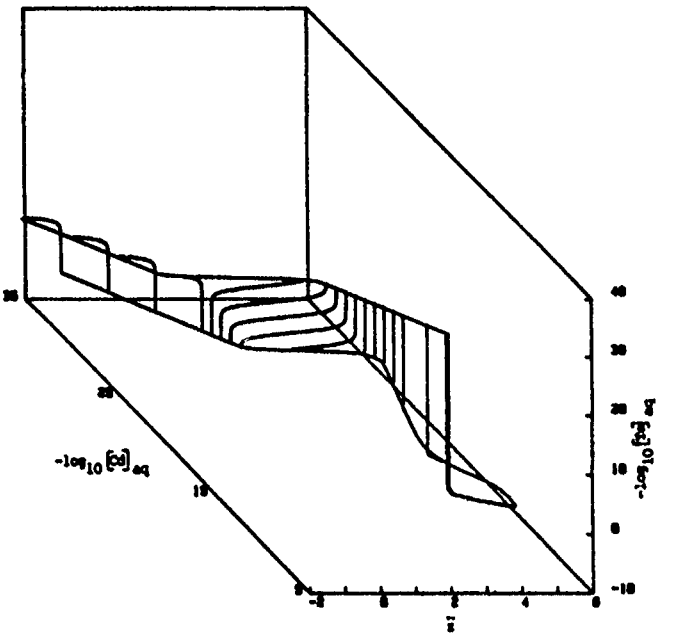

Figure 9. The aqueous Cd–Te system at pH = 10. The surface is the three dimensional electron number diagram for the aqueous phase in equilibrium with CdTe.

COMPUTER ENHANCED TEST METHODOLOGY FOR FATIGUE CRACK GROWTH RATE DETERMINATION IN A MARINE ENVIRONMENT

S.T. Scheirer and G.A. Gehring Jr.
Materials Research & Testing Div
Ocian City Research Corp.

ABSTRACT

Testing methodology was developed to determine crack growth rates at low frequencies in the threshold region for A-710 high strength steel in a marine environment. In order to accurately reproduce service effects, test parameters included a consideration of cathodic protection to mitigate corrosion and an actual seawater test environment. Computer hardware was developed to permit frequency shifting during testing without system perturbations. Compliance gage and electric potential methods were adapted for crack length measurement in the presence of calcareous deposits and cathodic polarization. In the seawater tests deposit formation occurred over the entire crack face, thereby retarding crack growth significantly compared to testing in air or in freely corroding seawater. Retardation effects were most prominent at slower growth rates and low frequencies. A propagating fatigue crack was arrested upon switching from 5.0 Hz to 0.5Hz under conditions of cathodic protection. This occurred at a growth rate of about 8×10^{-8} in/cycle, compared to crack arrest at 2×10^{-9} in/cycle under freely corroding conditions. Results of this program reinforce the desirability of conducting fatigue and other long term material characterization tests in a realistic test environment.

[Manuscript Not Available at the Time of Printing]

DESICCANT WHEEL DEHUMIDIFICATION OF MILITARY EQUIPMENT FOR EFFECTIVE CORROSION PROTECTION

Craig S. Laurent

Munters Cargocaire
Defense Division
79 Monroe Street, P. O. Box 640
Amesbury, MA 01913

ABSTRACT

Moisture induced failures and corrosion significantly degrade weapon system and equipment readiness. Application of Desiccant Wheel Dehumidification technology to operational equipment has increased system Mean Time Between Failure (MTBF) by nearly 300% and reduced operation and maintenance costs by 20% for Scandinavian military forces. Recent test results such as those conducted by the Army of the Federal Republic of Germany have underscored the superb operating capabilities of Desiccant Wheel dehumidification. Main battle tanks were removed from desiccant wheel dehumidified storage after a period of more than eleven years, having received absolutely no maintenance during that period the tanks were like new with no defects or corrosion due to the long term storage.

THE PROBLEM -- CORROSION

Moisture-induced corrosion significantly degrades aircraft and weapon system readiness. It increases life cycle and maintenance support costs. Corrosion can be in the form of rust, water stains, mold, mildew or other types of organic and inorganic degradation. Corrosion reduces productivity--of people and of resources.

The cost of corrosion to the U.S. economy is tremendous. Research conducted by the National Bureau of Standards as well as the U.S. Army Material Technology Laboratory, estimate the 4.2% of the Gross National Product, or around $170 billion in 1988 dollars is the cost of metallic corrosion alone.(1) If one considers the financial impact of corrosion on other types of materials such as electronics, clothing and textiles to name just a few, the numbers are even more staggering. This figure

DESICCANT WHEEL DEHUMIDIFICATION OF MILITARY EQUIPMENT FOR EFFECTIVE CORROSION PROTECTION

Craig S. Laurent

Munters Cargocaire
Defense Division
79 Monroe Street, P. O. Box 640
Amesbury, MA 01913

ABSTRACT

Moisture induced failures and corrosion significantly degrade weapon system and equipment readiness. Application of Desiccant Wheel Dehumidification technology to operational equipment has increased system Mean Time Between Failure (MTBF) by nearly 300% and reduced operation and maintenance costs by 20% for Scandinavian military forces. Recent test results such as those conducted by the Army of the Federal Republic of Germany have underscored the superb operating capabilities of Desiccant Wheel dehumidification. Main battle tanks were removed from desiccant wheel dehumidified storage after a period of more than eleven years, having received absolutely no maintenance during that period the tanks were like new with no defects or corrosion due to the long term storage.

THE PROBLEM -- CORROSION

Moisture-induced corrosion significantly degrades aircraft and weapon system readiness. It increases life cycle and maintenance support costs. Corrosion can be in the form of rust, water stains, mold, mildew or other types of organic and inorganic degradation. Corrosion reduces productivity--of people and of resources.

The cost of corrosion to the U.S. economy is tremendous. Research conducted by the National Bureau of Standards as well as the U.S. Army Material Technology Laboratory, estimate the 4.2% of the Gross National Product, or around $170 billion in 1988 dollars is the cost of metallic corrosion alone.(1) If one considers the financial impact of corrosion on other types of materials such as electronics, clothing and textiles to name just a few, the numbers are even more staggering. This figure

includes approximately $2-$4 billion in estimated annual damage in each of the individual U.S. Military Services.

THE CAUSE -- MOISTURE

In basic terms, three main things must be present in order for corrosion to be created: air (oxygen), moisture and a chemical, or electrochemical, reaction. Take away any one of these and there is no corrosion problem.

Since oxygen is always present in the atmosphere, and few materials are totally corrosion resistant, the variable that determines if corrosion will take place or not is the concentration of moisture. Moisture, however, should not be used interchangeably with precipitation. Scientific experiments carried out actually show no clear relationship between precipitation and the formation of corrosion.[2] Research does, however, clearly indicate a direct relationship between relative humidity and corrosion rates.[3-5] Thus, covered storage alone is not necessarily a key to corrosion prevention.

Relative humidity (RH) is defined as the ratio of the vapor pressure of water in a given mixture compared with the vapor pressure at saturation at the same temperature.[6] In other words, RH is the percentage of moisture in a given sample in relation to the maximum moisture content of air at a specified temperature.

The link between RH and corrosion is not new. As early as 1923 and 1927, W.H.J. Vernon outlined the characteristics of iron in his report to the Atmospheric Corrosion Research Committee of the Faraday Society. Vernon demonstrated that at above 50% RH the rate of corrosion of iron, lead and aluminum changes from a linear to an exponential progression. His research also indicated that the layers formed on the surface of those metals by corrosion tend to accelerate the rate of corrosion rather than to decrease it.[7] Vernon's research may appear to be dated, however, the general conclusions from this research have not changed. These studies are the starting point for all subsequent research on the subject of the relationships between corrosion, humidity and atmospheric contamination.

As evidence of this fact, research conducted by S. Tosto and G. Brusco in 1984 clearly indicated the relationship of increasing relative humidity to increased corrosion in both High Strength Low Alloy and Low-Carbon steel.[8] Their study indicated the rate of corrosion at 55% RH was minute while at 95% RH the rate was very high. In fact, at a high relative humidity, rates of corrosion are 100 - 2000 times greater than corrosion rates at lower humidity values.[9-10]

Research has proven that the rate of corrosion is also influenced by pollutants. The greater the pollution, the higher the rate of corrosion. This is especially true of

THE OPTIONS -- TO STOP CORROSION

Protective Coatings

Protective coatings are widely used to reduce the negative impact of corrosion. Properly used, protective coatings can be moderately effective in reducing corrosion and protecting against its impacts. In certain applications, such coatings may be the only alternative.

Unfortunately, while the use of paints, oil-based preservatives and other coatings is helpful, the process is extremely labor intensive, expensive and the ultimate results often means reduced readiness for that item or material.(21) Coatings can also become ineffective when scratched or otherwise damaged. Corrosion can even be increased if surfaces are not prepared properly. Moisture can actually be sealed into the space or material being coated creating adverse results.

Packaging

The use of traditional packaging for corrosion control is widespread throughout the Department of Defense (DoD) and the economy as a whole. Various types of containers and barrier materials are employed to prevent the movement of moisture across them into the space to be protected. Packaging in water-resistant or water-vapor resistant barriers can be especially effective for items in storage and transit, where no other corrosion prevention alternatives exist. Modern technology has developed a variety of new packaging techniques which can be effective for specific applications. Packaging techniques, while effective, are often extremely expensive.

Packaging techniques do not always prevent moisture-related corrosion and faults. According to the laws of physics, moisture in the form of water vapor will always flow from high vapor pressure to low vapor pressure. In many cases the packaging employed cannot stop nature and moisture damage occurs. Packaging can also be damaged during handling and transportation rendering this corrosion control technique ineffective. The use of desiccant (static) materials such as silica gel and activated alumina can increase the effectiveness of packaging. This material is placed into the container and absorbs moisture when it enters the container or space to be protected. Damage to the container can negate the effectiveness of this packaging approach. Manpower requirements and desiccant replacement increase the overall cost of this option.

Environmental -- Dehumidification

The use of dry air to preserve and protect various materials has been in practice for thousands of years. Natural dehumidification, by locating in a dry climate, is

frequently an optimal solution. The Egyptians have long known the benefits of using the dry desert climate to protect and store their national treasures. Some years ago, a perfectly preserved mummy was removed from its resting place in the desert and brought to a museum in England. The higher relative humidity resulted in immediate decay. But, after placing the mummy in an atmosphere of dry air created by a desiccant wheel dehumidifier, all decay was once again halted. World military forces are also familiar with the benefits of dry air. This explains why the U.S. Air Force has stored aircraft in the desert of Tucson, Arizona.

Since the feasibility of storing all equipment in a dry desert climate does not exist for obvious reasons, a method was developed to bring the dry environment to the equipment. Dynamic dehumidification was pioneered and refined during the 1930s. At the end of World War II, dehumidification was used to preserve (or "mothball") some 3000 merchant and naval vessels. Dehumidification was also used extensively to preserve and protect equipment stored in warehouses. This practice continues today, and one of the main reasons the refit of the Battleships Iowa and Missouri proceeded on time (and under budget) was the corrosion was not perceptible within the sealed envelope of the ship[22].

Dynamic dehumidification can be accomplished through the use of heating, refrigeration or desiccants. During heating of the air, the moisture content (absolute humidity) and dew point (the temperature at which moisture condenses out) remain unchanged. To maintain acceptable RH levels by heating, the air in the room must be heated well in excess of the outside ambient temperature in the summer and winter. Using heat there is risk that the temperature of the materials will lag behind the temperature of the surrounding air and condensation (and corrosion) will form on the material. Heating is also very expensive and therefore, not practical for most applications.

Refrigeration can also be used to dehumidify the air. In this process moisture is actually condensed out. Refrigeration, however is most effective in hot, humid conditions where a relative humidity of 65-70% is desired. If a lower RH level is needed (45-50% for example), or if the refrigeration equipment must operate at ambient temperatures of 45 degrees F - 50 degrees F, this method is not practical or cost-effective.[23]

Dynamic dehumidification through the use of desiccants is another method used to control relative humidity and prevent corrosion and moisture related damage from occurring. Moisture removal occurs by passing air over substances which have a strong afinity for moisture. These substances are known as desiccants and are capable of extracting moisture directly from the air.

Traditional desiccant dehumidification equipment has been successfully used in military and commercial applications since World War II. Such equipment has

proven effective in certain operational functions and large scale storage facilities. This equipment, which is of a granular or liquid type, has proved to be cost-effective and has been shown to reduce the relative humidity and dew point of air, thereby eliminating corrosion and its negative impact. Wide-spread use of traditional dehumidification equipment, however, has been limited to select applications due to its large size, weight, complexity, energy consumption and high life cycle and maintenance support costs.

STATE-OF-THE-ART DESICCANT WHEEL (DEW) DYNAMIC DEHUMIDIFICATION

The Technology

In Scandinavia, corrosion problems due to high relative humidities, pollution and salt air have long caused difficulty for the military and industry. Driven by military necessity, proximity to potential adversaries, and the need to reduce logistics support costs for materials, equipment and weapon systems, Sweden adopted and further developed state-of-the-art DEW dynamic dehumidification technology. They set as their preservation and corrosion prevention requirements such parameters as:

- Effective dehumidification in all climates
- Low investment cost
- Low operating cost
- Simple installation
- Simple maintenance and supervision
- High reliability
- Rugged, light-weight and compact (24)

To meet these requirements, a unique and cost effective dehumidification technology was developed. DEW technology utilized a desiccant impregnated honeycombe-construction wheel. Unlike traditional dehumidifiers that use a "bed" or chamber filled with granular or liquid desiccants that can spill, settle, cake and disperse into the air, the DEW method employs a unique Honeycombe constructed media impregnated with desiccant to eliminate the problems inherent with "beds" or chambers. This allows the DEW Honeycombe wheel to operate on either a vertical or horizontal plane, unlike traditional desiccant dehumidifiers which are generally relegated to horizontal operations to maintain the desiccant in place. The Honeycombe DEW construction also allows for light weight and compact design and thus reduced power requirements. Operating on a rotary principle, air is dehumidified in one section of the wheel while the desiccant is simultaneously dried and reactivated in another section. These developments included portability (reduced size), improved maintainability and reliability due to few moving parts, and simple operation with minimal training.

Expanding Technology Applications

While the technology has been effective in all traditional applications, it is interesting to note that new applications have also been developed that capitalize on its size and capability advantages. For example, significant strides have been made with this technology in the area of vehicle preservations. Recent evaluation by the Federal Republic of Germany (FRG) Bundeswehr and the U.S. Army on the use of DEW technology dehumidification in association with flexible plastic covers may revolutionize the methods by which vehicular equipment is stored and maintained.

In Bundeswehr evaluations of DEW technology, M48-A2 main battle tanks were overhauled and then placed into flexible plastic covers connected to these dehumidifiers. The evaluations began in the summer of 1976. The method, using flexible plastic covers and DEW dehumidifiers, is referred to as the Enclosed Dry Air Method (EDAM). The M48-A2 tanks were stored, without any maintenance whatsoever being performed, for a period of 11 years and 3 months. Upon removal in October, 1987, the tanks were tested, driven and weapons fired. The results verified that the vehicles were totally free of corrosion, fully operational and in a condition equal to or better than similar equipment in every day use.(25) Based on these results and other data inputs, the Bundeswehr is reportedly going to "lay-up" and preserve one-third of their forces using this technique on a rotating basis. It is important to note that energy costs for this technique are extremely low and the storage package (flexible cover and DEW dehumidifier) required minimal attention and maintenance during the 11 year study.

Similarly, evaluations conducted by the U.S. Army 21st Support Command in Europe also indicated that the use of DEW technology with flexible plastic covers was the most cost-effective method to store war reserve materials (specifically, tracked vehicles were evaluated).(26) The 21st Support Command evaluations included most known storage techniques. For practical and economic reasons, three methods were selected for final evaluation. These methods, selected for final evaluation, were (a) building controlled humidity warehouse (CHW), (b) DEW technology dehumidifiers in combination with flexible plastic covers, and (c) maintaining the status quo (routine maintenance--no humidity control). Results demonstrated that the DEW plastic cover method provided the benefits of a CHW at a fraction of the total cost. In fact, the system had distinct advantages over CHW in that it was portable and could be easily transported to wherever the equipment was going. Analysis also indicated that this EDAM technique was only slightly more expensive than the status quo option. A primary difference was that the vehicles protected against atmospheric corrosion and moisture related faults with DEW technology were maintained at readiness levels close to 99%, while those receiving the standard maintenance were at readiness levels below 50%.

DEW technology is also currently used by Scandinavian, European and NATO forces to control moisture-induced aircraft failures and corrosion. Requiring no modification to aircraft, dehumidifiers are connected directly to aircraft propulsion systems (through air intakes) and routed through existing environmental control ducts to airframe cavities, avionics, radar, fire control and life support systems.

Test results in Sweden demonstrated that aircraft connected to portable DEW equipment while on the ground achieved significant improvement in system Mean-Time-Between-Failure (MTBF). The MTBF for radar and cockpit instrument systems of the dehumidified aircraft improved nearly 300% in relation to aircraft which were not dehumidified.(27) While this dramatic improvement was achieved and quantified on radar and cockpit instrument systems, the propulsion, air frame and associated systems also benefitted.

The one year test, conducted by the Swedish Air Force in 1981, was expanded and repeated in 1985. Results confirmed aircraft which were not receiving DEW deteriorated while those receiving DEW showed continued improvement. The bottom line of this test was a 5% increase in absolute availability, resulting in another 1.2 aircraft "put on the line" for the typical 24 aircraft fighter squadron. This gain was achieved in a cost effective manner. Savings in manpower and materiel quickly offset initial investment costs and later contributed to continued lower support costs. Five dollars was saved every year for each dollar spent on the initial procurement of DEW dehumidification equipment. Operation and support costs were reduced 20%, increasing the productivity of maintenance manpower. DEW equipment has also improved overall system reliability and performance and has reduced system fault indications by up to 65%.

In another test on installed J79 engines, similarly impressive results were achieved. The Danish Air Force found that circulating Dry Air through installed engines eliminated engine corrosion. Upon tear down, test engines were found to have no corrosion or heat generating residue from burned preservative oil. DEW solved the problems long associated with salt corrosion. Engine performance and condition were improved and crack formation in engine parts was prevented. Also, fresh water rinses and the need for preservation oil were eliminated. In addition, engine tear-down is now easier and consumes fewer man hours. The Danish Air Force estimated that DEW has saved well over $5,000,000 since full scale implementation. Furthermore, it is now generating savings of approximately $1,000,000 annually on engine related maintenance alone.(28)

The U.S. Navy is now leading a Tri-Service evaluation of DEW technology application to U.S. Military aircraft. This evaluation will include aircraft in all operating environments. It is anticipated that the technology will be implemented on a broad scale and result in significant logistics and operational benefits.

To address significant moisture-induced corrosion problems in ammunition storage sites in Europe, the U.S. Air Force is considering large-scale application of the DEW technology plastic cover approach. Ammunition containers have corroded to a state where they afford no protection to the stored 30mm aircraft ammunition. Inventory losses running about 1.5% per year amount to some $12+M. Estimates to refurbish the containers or to procure new ones ranged from $200 - $300 per container (for some 100,000 containers), and even this approach would not totally prevent inventory loss due to moisture damage. The solution being considered is to place the containers (in their current state) into flexible plastic covers, with continual dehumidification provided by DEW technology equipment. Additionally, this option results in the least disruption to ammunition storage sites and offers continuing ammunition inventory protection, reducing inventory shrinkage due to moisture-related corrosion to virtually zero.

In the above example, flexible plastic covers will be used with the DEW technology equipment to achieve the dehumidified environment. Existing buildings can, however, be dehumidified in a cost-effective manner using this same DEW technology equipment. Converting warehouses to controlled humidity warehouses involves simple sealing of cracks, vents, doors and other areas of air infiltration. This method can be as simple as stapling polyvinyl plastic sheets over such openings as well as using simple sealing material around doors, windows etc. DEW technology equipment can be sized to ensure that the proper environment is maintained. Through the establishment of a slight overpressurization of the space to be dehumidified, the "dry air" finds any remaining air egress routes, and thus maintains the RH at the desired levels. Installation of this technology equipment is relatively simple and straight-forward. It can be installed inside or outside (requires no protection) and can be adapted to existing air ducting or merely provide the "dry air" through flexible conduits or tubing.

In summary, U.S. Military use of this new technology is increasing steadily. The equipment has been used to prevent corrosion in such varied applications as ICBM missile silos, munitions storage facilities, test and evaluation chambers, Trident and Polaris submarines, Naval vessels, maritime prepositioned ships, Strategic Defense Initiative, commissaries and the Space Shuttle, to name just a few. Considering the high cost of moisture-induced corrosion (4.2% of GNP - $170B Annual Cost in 1988), there appear to be few areas that cannot benefit from this state-of-the-art corrosion control technology.

REFERENCES

1. L. Bennett, J. Kruger, R. Parker, E. Passaglia, C. Reimann, A. Ruff, H. Yakowitz, "Economic Effects of Metallic Corrosion in the United States," National Bureau of Standards, U.S. Dept. of Commerce Publication NBS.511-1.

2. Rainer Rosch, "Effect of Weather on the Rusting of Bright Steel," Wire World International, Vol. 24, March/April 1982.

3. Francisco Corvo Perez, "Atmospheric Corrosion of Steel in a Humid Tropical Climate--Influence of Pollution, Humidity, Temperature, Solar Radiation and Rainfall," Corrosion-NACA, National Association of Corrosion Engineers, 1984.

4. S. R. Dunbar, W. Showak, "Atmospheric Corrosion of Zinc and Its Alloys," Atmospheric Corrosion, Chapter 37, Wiley-Interscience, New York, NY 1982.

5. Rainer Rosch, "Effect of Weather on the Rusting of Bright Steel.

6. "The Dehumidification Handbook," Cargocaire Engineering Corporation, Amesbury, Massachusetts, 1982.

7. W. H. J. Vernon, "First and Second (Experimental) Report to the Atmospheric Corrosion Research Committee (British Non-Ferrous Metal Research Association)." Transactions of the Faraday Society, Number 19, 1923-1924, Pages 839-934, and Number 23, 1927, Pages 113-204.

8. S. Tosto, B. Brusco, "Effect of Relative Humidity on the Corrosion Kinetics of HSLA Steel and Low Carbon Steels." The Journal of Science and Engineering of the National Association of Corrosion Engineers, Volume 40, No. 10, October 1987.

9. D. W. Rice, R. J. Cappell, P. Peterson, "Indoor Atmospheric Corrosion of Copper, Silver, Nickel, Cobalt, and Iron." Atmospheric Corrosion, Chapter 46, W. H. Ailor, Wiley-Interscience, New York, NY 1982.

10. Unknown Author, "Factors Affecting the Corrosion of Metals in the Atmosphere." Atmospheric Corrosion, Chapter 37, W. H. Ailor, Wiley-Interscience, New York, NY 1982.

11. IBID.

12. S. R. Dunbar, W. Showak, "Atmospheric Corrosion of Zinc and Its Alloys."

13. Rainer Rosch, "Effect of Weather on the Rusting of Bright Steel."

14. Alfred Milch, Pedro Tagaro, "The Stability of Tellurium Films in Moist Air; A Model for Atmospheric Corrosion," Journal of the Electrochemical Society, April 1980.

15. D. W. Rice, P. B. P. Phipps, R. Tremoureux, "Atmospheric Corrosion of Cobalt," Electrochemical Science and Technology, September 1979.

16. D. W. Rice, R. J. Cappell, W. Kinsolving, J. J. Laskowski, "Indoor Corrosion of Metals," Solid-State Science and Technology, April 1980.

17. "Controlled Humidity (CH) Criteria Evaluation." U. S. Army Material Command, Project Report AMC 32-89, May 1986.

18. "Long Term Storage--Ordinance Material Report," U. S. Army, W-36-038-ORD-3771.

19. Susan Dreiband, "Corrosion Prevention and Control." Army Research, Development and Acquisition Bulletin, November-December 1987.

20. IBID.

21. L. E. Helwig, "Temporary Rust-Preventive Compounds for Sheet Steel," Materials Performance, National Association of Corrosion Engineers, December 1984.

22. Lewis G. Harriman, III, "Prevention of Metallic Corrosion in Storage Areas," proceedings of the 1985 International Symposium on Moisture and Humidity, April 1985.

23. Gunnar Asker, Thomas Urdahl, "Ship Dehumidification Systems," presented at the International Institute of Refrigeration Meeting, June 20, 1957.

24. Rolf Hammarstedt, "Control of Humid Environment and Drying of Material Using the Munters Dehumidifier," September 15, 1976.

25. "Edam Test Results--Long Term Storage of Tanks," Bundeswehr (FRG), October 1987.

26. OACSRM, "Determination of the Most Efficient Method for Long Term Storage of Combat Vehicles," 21st Support Command, U. S. Army Europe, April 1986.

27. Stig Hjulstrom, "The Driest Air Force of the World." Swedish Defense Material Administration, TIFF No. 3, 1986.

28. J. Nieport, Lecture Presented at Vaerlose Airbase, Denmark, March 1977.

THE USAF MATERIALS DATA BASE PROGRAM

James J. McNeely
Deputy Director
Chemical/Biological Information
Analysis Center (C/BIAC)
Aberdeen Proving Ground, Maryland 21040
(301) 676-9030

Edward R. Zamejc
Information and Engineering Systems Department
Battelle Columbus Division
505 King Avenue
Columbus, Ohio 43201-2693
(614) 424-4967

Keith J. Johanns
Defense Systems Department
Battelle Columbus Division
505 King Avenue
Columbus, Ohio 43201-2693
(614) 424-5804

Timothy M. Miller
Information Systems Department
Battelle Columbus Division
505 King Avenue
Columbus, Ohio 43201-2693
(614) 424-3232

Fred Meyer, Jr.
USAF Materials Data Base
Project Manager
AFWAL/MLSA
Wright-Patterson AFB, Ohio 45433-6533
(513) 255-5108

Chemical warfare (CW) agents and the attendant decontaminants degrade aircraft and ground support equipment materials. Degradation may include the compromise of mechanical, chemical, optical and electrical properties which result in an inability of a system to perform an intended function. In order to address this vulnerability, personnel will benefit by having access to a comprehensive technical data base detailing the interaction between materials of construction and chemical warfare agents, decontaminants and chemical agent simulants. Design engineers will then be able to minimize accessibility of the critical components or material. The Aeronautical Systems Division (ASD), through Battelle Columbus Division (BCD),

has accomplished the initial development of the U.S. Air Force Materials Data Base which contains information on materials degradation caused by exposure to decontaminants and CW agents. A prototype version has been distributed to a select number of aerospace contractors and government agencies.

OBJECTIVES

The objectives of this program were to collect, organize, and develop an automated mechanism for handling data describing the effects of chemical warfare agents, simulants and decontaminants upon materials and systems.

APPROACH

In order to develop a data base which best meets the user's needs, users were given a choice in determining how the data base was constructed. Representative aerospace contractors and government personnel were invited to a workshop in which a Strawman of the data base was presented. The users then recommended revisions for the approach that would lead to the development of a data base that is more useful to them. A prototype of the data base was designed incorporating user's comments, and a second workshop was held to demonstrate the data base. Additional user comments were obtained during the demonstration and subsequently integrated into the data base design. The prototype was then released to a select group of aerospace contractors and government agencies. A discussion of the data base features and operational requirements is provided as follows.

DATA BASE CONTENT

The data base contains information on literature documents relevant to the material effects of CW agents, decontaminants, and simulants. The data base is relational, menu driven, and can be manipulated to search for desired information on chemicals, materials, components, and degradation effects. Help screens are available throughout the data base. There are six major categories of information in the data base as described below and illustrated in Figure 1.

(1) Bibliographic Tables
(2) Degradation Tables
(3) Test Facility Tables
(4) Community Members Tables
(5) Synonym Tables
(6) Chemical Properties Tables.

Representative screen displays of data base records are presented in Figures 2-5.

The bibliographic records contain the following information: assigned data base reference number, title, authors, performing organization, sponsoring organization, associated report numbers, publication date, contract number, document classification, availability, and government accession number. Each of these records has associated keyword and subject area fields for each reference. Selected documents include an abstract describing the referenced report.

The degradation data records contain technical information regarding specific experiments performed in the referenced documents. The degradation records are divided into specification tables and levels of interaction data (Levels 1-3). The specification tables include the material specification, component specification, test specification, and rating criteria.

Level 1 of the interaction data summarizes the effects between a selected material/chemical or component/chemical interaction. Level 2 describes the test conditions associated with Level 1 data and includes the test temperature, test exposure, number of samples, etc. Level 3 describes a summary of the material property being tested provides the detailed data for a test including the test values, time values, percent change from the control, percent deviation from control, etc.

The test facility records contain information regarding laboratories licensed to test with chemical surety materiel (CSM). The information includes the address of the laboratory, a point of contact, and description of the facility.

The community member records contain organizational information regarding personnel who are involved in materials testing, design engineering, and the chemical defense community. The synonym records contain information regarding synonyms, acronyms, ASTM codes, and tradenames used to describe various chemicals, materials, and properties. These records are meant to standardize the terminology of the data base and aid in search routines.

The chemical property records contain physical property information regarding the CW agents, decontaminants, and simulants referenced in the data base. These records are useful to identify specifics of the chemical threat and for general information on the chemicals.

HARDWARE/SOFTWARE REQUIREMENTS

An IBM® XT, AT or 100% compatible computer equipped with at least one floppy disk drive and 640K RAM memory is required to access the data base. The data base itself is stored on a 20 megabyte capacity Bernoulli cartridge which requires a Bernoulli Box (20 megabyte by 20 megabyte) for operation. An internally fixed disk for the computer would not be allowed for the classified version unless security requirements can be met. A color monitor and an IBM compatible printer are recommended.

In terms of software, a computer operating system such as MS-DOS or PC-DOS is required. The relational data base management system used for operation of the data base is Microrim's RBase® System V. The estimated cost of the hardware and software is about $7,000.

SECURITY REQUIREMENTS

The data base is available in unclassified and classified (SECRET/NOFORN) versions. Therefore, certain hardware and facility security requirements must be met for the classified version. The unclassified version of the data base does not require the hardware and facility requirements by Defense Investigative Service (DIS). However, the program sponsor does request each agency maintain a controlled access for each unclassified version.

DIS approval must be obtained prior to operating the classified data base version by providing them with a Standard Practice Procedure Document. In general, the major requirements of DIS can be satisfied by either buying TEMPEST hardware, fabricating or buying shielded enclosures, employing red and black engineering, or establishing control space. The most cost effective means is through the use of control space in which there must be at least 30 meters from the system to any point of possible undetected interception of data. There must also be a one meter area around the system in which no pipes, phone lines, or power lines are present. No communication devices or fixed hard disks are allowed on the system. Cartridges and printed information from the data base are considered classified information and must be treated as such according to DoD 5200.1R/AFR 205-1.

DISTRIBUTION

The data base will be distributed to users by the U.S. Air Force. Initially, a small group of users are being provided with a prototype of the data base and will be asked to make recommendations of the format, ease of use, etc. After the initial issue has been reviewed and modified as needed, the data base will be made available to other government facilities and to a select broader group of major manufacturers and contractors who have a need to know. Others with a need to know may access the information contained in the data base through the Chemical/Biological Information Analysis Center (C/BIAC) located in Edgewood, MD. The data base cartridge will come with a User's Guide describing system operations.

CONCLUSIONS

This program is intended to provide equipment designers with the information needed to ensure the chemical warfare (CW) survivability of aircraft and ground support equipment. This program includes organizing and disseminating existing information as well as developing a standardized structure for generating data needed in the future.

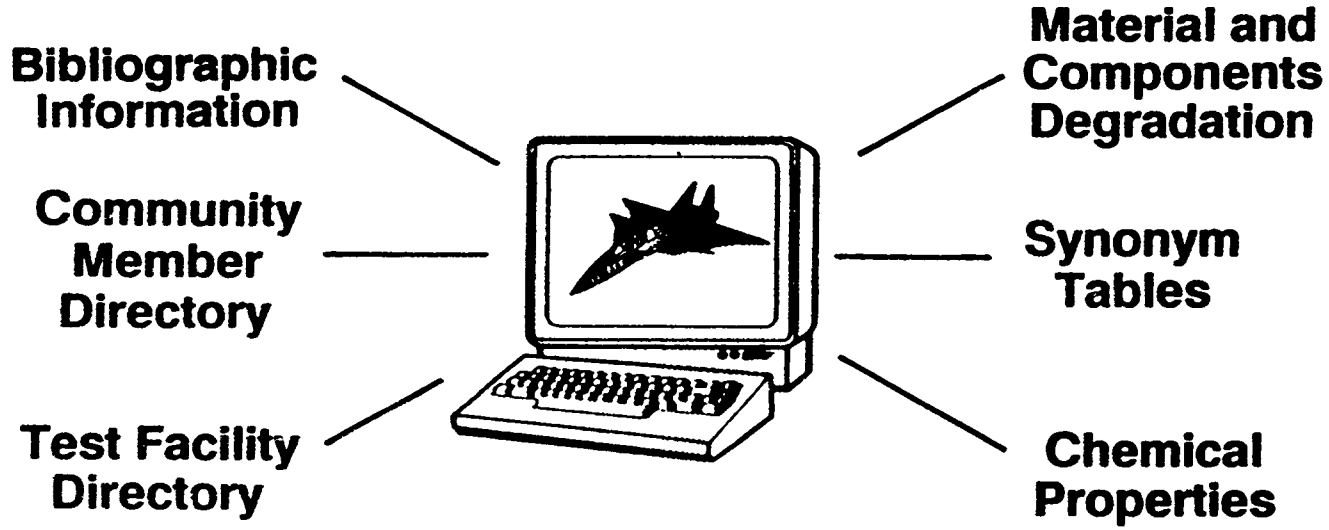

FIGURE 1. USAF MATERIALS DATA BASE RECORDS

BIBLIOGRAPHIC TABLE Page 1 of 2

UNCLASSIFIED

Reference Number: 1
Title: (U) Interaction of Chemical Warfare Agent with Polymers of Military Interest
Author: Pfau, J.P.; Sharpe, R.E.; Jewett, S.K.; Huggins, R.L.; Dick, R.J.
Performing Organization: Battelle Columbus Division, Tactical Technology Center, Columbus, Ohio 43201
PO Number: BATT-CSL-48-1
Sponsoring Organization: Chemical Systems Laboratory, Aberdeen Proving Ground, MD 21010
SO Number: ARCSL-CR-82039
Contract Number: DAAH01-81-C-A277, MIPR No. 1.38199
Publication Date: 82/03/00
Publication Classification: UNCLASSIFIED
Availability: LIMITED-C
Government Number: ADB06851L

Press Enter for next Box, PgDn or PgUp for pages, ESC, for menu

BIBLIOGRAPHIC TABLE Page 1 of 2

BIBLIOGRAPHIC TABLE Page 2 of 2

UNCLASSIFIED

Subject Areas: Vulnerability; Material Susceptibility

Key Words: Degradation Data, Materials, Agents

Abstract: (U) The principal objective of this program was to develop and verify a test procedure for determining whether liquid chemical warfare (CW) agent has an effect on polymeric materials of military interest. The test procedure developed proved to be very effective for detecting significant changes (95% confidence level or greater) in the mechanical property.

Press Enter for next Box, PgDn or PgUp for pages, ESC, for menu

FIGURE 2. BIBLIOGRAPHIC TABLE EXAMPLE OUTPUT

DEGRADATION DESCRIPTIVE SUMMARY TABLE - LEVEL 1

UNCLASSIFIED

Reference Number: 1
Material Code: MQ Extension: 0
Chemical Code: GD Extension: 0
Component Name: -0-
Test Type Number: 1
Test Indicator: MODERATE
Rating Confidence: HIGH
General Remarks: (U) Moderate interaction rating due to major effects on tensile strength at 300% elongation, with the other properties varying at 6.85 and 68.5 g/m**2 concentration.

Component Remarks: -0-
Chemical Remarks: (U): NS
Material Remarks: (U): GD beaded on MQ - poor wetting
Test Remarks: (U): NS

Press Enter for next Box, PgDn or PgUp for pages, ESC, for menu

DEGRADATION DESCRIPTIVE SUMMARY TABLE - LEVEL 1
CONDITIONAL SUMMARY TABLE - LEVEL 2

UNCLASSIFIED

Reference Number: 1
Material Code: MQ Extension: 0
Chemical Code: GD Extension: 0
Component Name: -0-
Test Type Number: 1
Test Number: 1
Exposure State: LIQUID
Exposure Units: G/SQM
Test Temperature: 23.
Conditional Rating: MAJOR
Number of Samples: 7
Total Time: 24.

Remarks: (U): Major rating due to severe effects on maximum elongation, major effects on tensile strength properties and toughness, and the others, neglig.

Press Enter for next Box, PgDn or PgUp for pages, ESC, for menu

FIGURE 3. EXAMPLE OF OUTPUTS OF MATERIAL DEGRADATION TABLES (LEVELS 1 THROUGH 2)

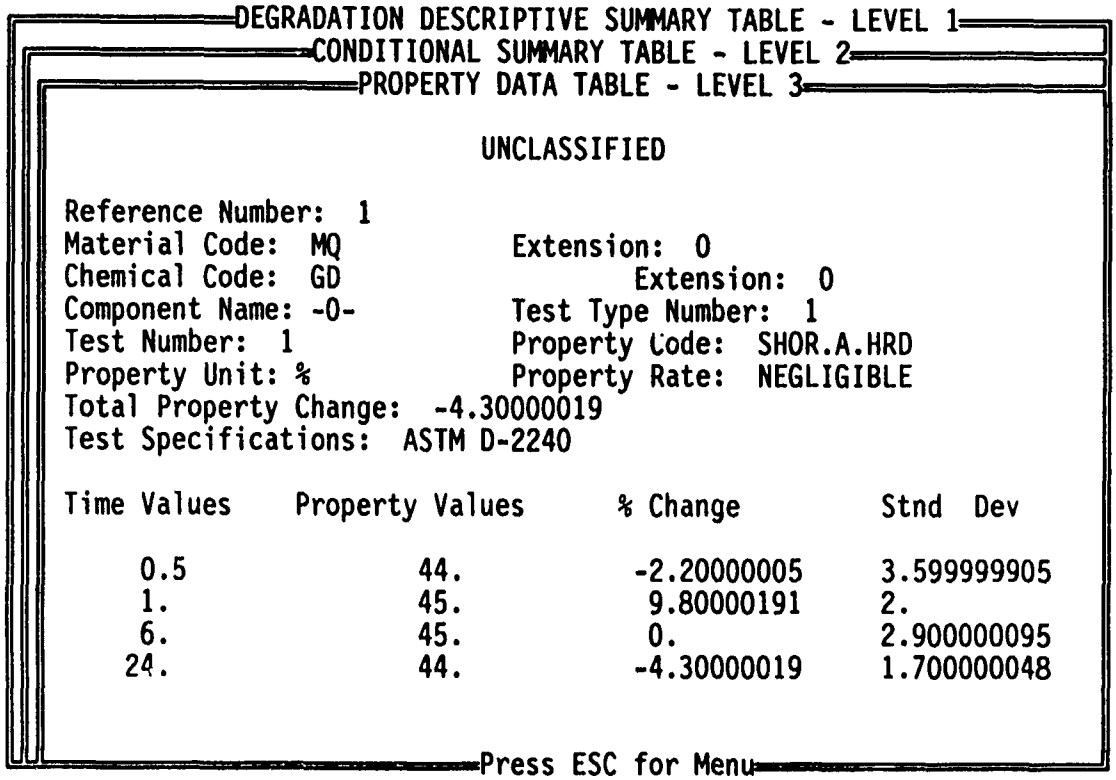

FIGURE 4. EXAMPLE OF OUTPUTS OF MATERIAL DEGRADATION TABLES

CHEMICAL SYNONYM TABLE

UNCLASSIFIED

Chemical Code: STB

Common Name: SUPER TROPICAL BLEACH

Chemical Classification: DECONTAMINANTS

Chemical Type: NA
Chemical Name: NS
Chemical Form: NS
Chemical Composition: BLEACHING POWDER CONSISTING PRIMARILY OF DOUBLE SALTS Ca(OCL)2-2Ca(OH)2 AND CaC12-Ca(OH)2-H2O WITH Ca ADDED AS A DESICCANT. NORMALLY DISSOLVED IN WATER: 566 GRAMS STB.

Other Names: CHLORINATED LIME, BLEACHING POWER

Press Enter for next Box, PgDn or PgUp for pages, ESC, for menu

MATERIAL SYNONYM TABLE

UNCLASSIFIED

Material Name: WROUGHT ALUMINUM ALLOW 2024

Material Code: A92024

Material Category: METALS

Material Family: ALUMINUM

Material Trade Names: NS

Press Enter for next Box, PgDn or PgUp for pages, ESC, for menu

FIGURE 5. EXAMPLE OUTPUTS OF SYNONYM TABLES

AUTHOR INDEX